Titre: Title:	A Numerical Investigation of the Seismic Response of Tailings Impoundments Reinforced with Waste Rock Inclusions
Auteur: Author:	Behnam Ferdosi
Date:	2014
Type:	Mémoire ou thèse / Dissertation or Thesis
Référence: Citation:	Ferdosi, B. (2014). A Numerical Investigation of the Seismic Response of Tailings Impoundments Reinforced with Waste Rock Inclusions [Thèse de doctorat, École Polytechnique de Montréal]. PolyPublie. https://publications.polymtl.ca/1605/

UNIVERSITÉ DE MONTRÉAL

A NUMERICAL INVESTIGATION OF THE SEISMIC RESPONSE OF TAILINGS IMPOUNDMENTS REINFORCED WITH WASTE ROCK INCLUSIONS

BEHNAM FERDOSI

DÉPARTEMENT DES GÉNIES CIVIL, GÉOLOGIQUE ET DES MINES

ÉCOLE POLYTECHNIQUE DE MONTRÉAL

THÈSE PRÉSENTÉE EN VUE DE L'OBTENTION

DU DIPLÔME DE PHILOSOPHIAE DOCTOR

(GÉNIE MINÉRAL)

DÉCEMBRE 2014

UNIVERSITÉ DE MONTRÉAL

ÉCOLE POLYTECHNIQUE DE MONTRÉAL

Cette thèse intitulée:

A NUMERICAL INVESTIGATION OF THE SEISMIC RESPONSE OF TAILINGS IMPOUNDMENTS REINFORCED WITH WASTE ROCK INCLUSIONS

présentée par : FERDOSI Behnam

en vue de l'obtention du diplôme de : Philosophie Doctor

a été dûment acceptée par le jury d'examen constitué de :

M. SILVESTRI Vincenzo, Ph. D., président

M. JAMES Michael, Ph. D., membre et directeur de recherche

M. AUBERTIN Michel, Ph. D., membre et codirecteur de recherche

M. LI Li, Ph. D., membre

M. DUHAIME François, Ph. D., membre

DEDICATION

To my loves, Vila and Rozhina

ACKNOWLEGEMENTS

I would like to express my special appreciation and thanks to my advisors Prof. Michael James and Prof. Michel Aubertin, you have been tremendous mentors for me. I would like to thank you for encouraging my research. Your advice has been priceless.

A special thanks to my family. Words cannot express how grateful I am to my mother and father for all of the sacrifices that they've made on my behalf. I would like to thank my brother-in-law, Farzad, for his support during my studies in Canada. I would also like to thank all of my friends who supported me during my studies, especially Pejman Nekoovaght and Vahid Marefat. I would like to express appreciation to my beloved wife Vila for her unyielding support and sacrifice during my studies in Iran and Canada. I would also like to thank my lovely daughter Rozhina whom I could not spend more time with during my studies, she is a marvel and lights up my life.

RÉSUMÉ

La fréquence de rupture des digues de parcs à résidus miniers est beaucoup plus élevée, par un facteur de 10, que celle des ouvrages de retenue d'eau conventionnels, avec 2 à 3 événements majeurs se produisant annuellement surtout le monde. Une des conséquences de ces ruptures (avec brèche) est l'écoulement de résidus liquéfié. Ces écoulements (ou épanchements) sont responsables de pertes de vie, de dommages à l'environnement et de coûts financiers considérables; ils représentent à cet égard un des principaux risques liés aux opérations minières.

Les résidus miniers produits par les mines en roches dures sont particulièrement susceptibles à la liquéfaction (i.e. un perte quasi-complète de résistance due à un chargement dynamique ou statique), pouvant alors causer une rupture (p. ex. durant un séisme) ou être une conséquence de la rupture (p. ex. suite à une défaillance de la fondation qui réduit le confinement).

Aubertin et al. (2002b) ont proposé d'ajouter des inclusions de roches stériles dans les parcs à résidus, conjointement avec la déposition des rejets de concentrateur, afin d'améliorer leur performance environnementale et géotechnique. La roche stérile est ainsi placée de façon à créer des inclusions continues le long des orientations prédéfinies dans le parc. Il a alors été postulé que ces inclusions pourraient induire divers bénéfices, notamment en accélérant la consolidation des résidus et en agissant comme renforcement pour mieux résister aux sollicitations statiques et sismiques.

James (2009) a réalisé une série d'essais cycliques en cisaillement simple sur des résidus miniers, sur une gamme de contraintes de confinement et de contraintes en cisaillement cycliques. Il a ensuite montré que le modèle constitutif UBCSAND (Beaty and Byrne 1998) pouvait bien représenter le comportement dynamique de ces résidus. James (2009; voir aussi James et Aubertin, 2010, 2012) a aussi utilisé un modèle numérique pour simuler la réponse sismique d'un parc à résidus miniers conceptuel, construit sans et avec des inclusions de roches stériles (IRS). Ces résultats ont montré que de telles inclusions pouvaient grandement améliorer la réponse sismique de ce parc à résidus.

Un des essais cycliques en cisaillement simple réalisé par James (2009) sur des résidus miniers a été simulé avec le modèle UBCSAND (version of 904aR). Les résultats présentés ici, dans cette

thèse, indiquent que le modèle simulé bien les déformations en cisaillement, la génération des pressions interstitielles en excès, et la liquéfaction induites par de telles conditions.

A l'étape suivante, la capacité du modèle UBCSAND, implanté dans le code numérique FLAC (Itasca, 2008), a été évaluée pour simuler le comportement sismique des résidus miniers soumis à des essais sur un table sismique, tels que menés par Pépin et al. (2012a, 2012b). Deux de ces essais (nos. 3 and 7) réalisés sur des résidus seuls et avec un mur de sable ont été simulés. Les résultats de ces modélisations numériques ont montré que le modèle UBCSAND peut prédire correctement la génération de pressions interstitielles dans des résidus soumis à de tels essais, avant ou sans inclusion.

Les parcs à résidus miniers peuvent aussi céder après un événement sismique, en raison de la dissipation des surpressions en excès. Pour représenter ce comportement de façon réaliste, il faut reproduire la consolidation post-sismique (avec dissipation des surpressions). Deux approches ont été utilisées ici pour modéliser cet aspect. La première consiste à ajouter un cap (Vermeer, 1980) au modèle UBCSAND (version 904aR). Le modèle ainsi modifié a été utilisé pour simuler des essais (fictifs) de compression isotrope et œdométrique, et pour analyser la liquéfaction de résidus déposés en surface. Des résultats encourageants ont été obtenus, mais le modèle avec un cap a conduit à des instabilités numériques (possiblement dues à une singularité sur la surface limite). Une autre approche a alors été considérée. Avec cette seconde approche, les valeurs des modules élastiques des résidus miniers ont été mises à jour sur la base de la courbe de consolidation de résidus lâches. Cette approche combine la méthode proposée par Sento et al. (2004) avec le modèle UBCSAND, ce qui permet de reproduire le comportement post-sismique avec le tassement de résidus et la dissipation des surpressions. Les simulations ont alors montré que cette approche prédit correctement les tassements observés lors des essais sur table sismique. Cette approche a aussi été appliquée au cas du tassement post-sismique des dépôts du sable et de résidus en surface, et les résultats concordaient bien avec ceux obtenus de la relation empirique proposée par Wijewickreme et Sanin (2010).

Après ces vérifications relatives aux simulations du comportement sismique et post-sismique des résidus miniers, le modèle UBCSAND a été utilisé pour simuler numériquement le comportement d'un parc à résidus (basé sur le cas d'un site minier situé au Nouveau-Brunswick), auquel on a ajouté des inclusions de roches stériles. Le parc avec diverses configurations

d'inclusions a été soumis à des sollicitations sismiques, avec divers niveaux d'énergie et fréquences dominantes. Les résultats de ces analyses numériques ont montré que le parc à résidus (sans inclusions) pouvait subir des déformations excessives et une rupture sous les chargements sismiques considérés. Les résultats des simulations du parc renforcé ont montré que les inclusions de roches stériles pouvaient réduire considérablement les déformations de la pente aval et ainsi prévenir une rupture. La réponse du parc a aussi été évaluée sur la base de déplacements horizontaux moyens normalisés (AR_x), le long de la pente aval et pour les IRS seules. La performance du parc à résidus pour différentes configurations des inclusions (largeur et espacement) a été classifiée sur la base de ces valeurs du AR_x à la fin du chargement cyclique. Des graphiques montrent la valeur du AR_x (globale et pour les IRS) en fonction de la largeur totale des inclusions, pour diverses configurations. Ces résultats indiquent que dans la majorité des cas, les événements sismiques de basse fréquence produisent des déformations plus grandes que ceux de haute fréquence.

Les effets des IRS sur la réponse d'un parc à résidus ont été analysés numériquement pour le cas d'un autre site minier (situé au Québec). La réponse sismique a de nouveau été évaluée sur la base de la valeur du ARx (globale et des IRS) et aussi en fonction du volume de résidus subissant un déplacement critique, pour diverses configurations d'inclusions. Ces résultats montrent comment les IRS peuvent être adaptées pour améliorer la réponse sismique des parcs à résidus. Ces simulations illustrent une approche pour en arriver à une optimisation de la conception des IRS placées dans un parc à résidus, en fonction de sollicitations sismiques particulières.

ABSTRACT

The rate of failure of tailings impoundments is much larger, by a factor of about 10, than that of conventional water retention dams, occurring at a rate of about 2 to 3 per year worldwide. A primary consequence of the failure of a tailings impoundment is the flow of liquefied tailings. Such flows have been responsible for considerable loss of life, environmental damages and economic costs and represent one of the major risks associated with mining. Tailings, specifically those from hard rock mines, are particularly susceptible to liquefaction (a significant loss of shear strength) that can cause failure of the retention dyke and the release of liquefied tailings. Tailings liquefaction can be induced in dynamic loads, such as earthquakes, or static loads, such as dyke raising, erosion (loss of confining stress) or foundation movement.

Aubertin et al. (2002b) considered placing waste rock in tailings impoundments in tandem with tailings deposition to improve the environmental and geotechnical performance of the impoundments. The waste rock would be placed to create relatively narrow, continuous inclusions along planned routes in the impoundment. It was postulated that these waste rock inclusions would provide a number of benefits, particularly by accelerating the consolidation of the tailings and acting to reinforce the impoundment with respect to static and seismic loads.

James (2009) conducted a series of cyclic simple shear tests on tailings over a range of confining stresses and cyclic stress ratios. Then, using numerical simulations, he showed that the UBCSAND model (Beaty and Byrne 1998) can predict well the cyclic behavior of tailings. James (2009) used numerical analyses to simulate the seismic response of a conceptual tailings impoundment with and without waste rock inclusions. It was shown that the use of such waste rock inclusions (WRI) could considerably improve the seismic response of an impoundment.

One of the cyclic simple shear tests performed by James (2009) on tailings was simulated using the UBCSAND model (version of 904aR). The results of the simulation, presented in this thesis, indicate that the model can represent well the shear strain, excess pore water pressure generation, and initiation of liquefaction under these conditions.

In the next step, the capability of the UBCSAND model, as implemented in FLAC (Itasca, 2008), to simulate the seismic behavior of tailings in seismic table tests was evaluated using tests conducted by Pépin et al. (2012a, 2012b). The two tests (Nos. 3 and 7) were conducted on lightly

tamped tailings without and with a sand wall inclusion. The results of modeling showed that the UBCSAND model can predict fairly well the generation of excess pore water pressure in seismic table testing of tailings with and without an inclusion.

Tailings impoundments may fail after earthquake shaking due to the dissipation of excess pore water pressures. To model this phenomenon realistically, one can simulate post-shaking consolidation (excess pore water pressure dissipation). Two approaches were used to do so. In the first approach, a cap (Vermeer, 1980) was added to the UBCSAND model (version 904aR). The modified model was tested by simulating hypothetical isotropic compression tests, oedometer tests and level ground liquefaction of tailings. Reasonable results were obtained, but the UBCSAND model with a cap developed some mathematical instabilities (possibly due to a singularity on the yield surface). Therefore, another approach was used. In this second approach, the values of the elastic moduli of the tailings were updated in the model based on the consolidation curve of loose tailings. This approach combines the Sento et al. (2004) methods and the UBCSAND model to predict the post-shaking settlement of tailings due to pore water pressure dissipation. The simulations showed that this approach can predict well post-seismic settlement in seismic table testing.

The capability of this model to simulate the post-shaking settlement of level ground liquefaction in tailings was also compared with the empirical relationships of Wijewickreme and Sanin (2010) and the results were encouraging.

After verifying that the UBCSAND model can simulate the seismic and post-seismic behavior of tailings, the seismic response of a tailings impoundment (based loosely on an actual site located in New Brunswick), with and without waste rock inclusions was simulated numerically. The impoundment with various configurations of inclusions was subjected to earthquake loads of various energy contents and with different predominant frequencies. The results of the numerical analyses showed that the tailings impoundment without waste rock inclusion undergoes excessive deformation and failure under the seismic loads considered. The results of simulations with inclusions showed that WRI can significantly decrease the deformation of the downstream slope and prevent failure of the impoundment. Additionally, the response of the tailings impoundment was evaluated based on the average normalized horizontal displacements (AR_x) of the downstream slope and of only the WRI. The performance of the tailings impoundment with

different configurations of WRI (width and center-to-center spacing) was classified based on the AR_x values at the end of shaking. Graphs that show the AR_x (total and WRI) values as a function of the total width of different configurations are presented. These graphs can be used to obtain (preliminary) optimum configurations of WRI for the seismic loads considered. The results also indicate that in most cases, the low frequency ground motions produce significantly more deformation than the high frequency ground motions.

The effect of WRI on the seismic response of a tailings impoundment was further evaluated using numerical simulations of another tailings impoundment (based on a mine site in western Quebec, Canada). The seismic response of the tailings impoundment was again evaluated using AR_x (total and WRI) and the critically displaced volume of tailings at the end of shaking, for different configurations of the inclusions. The results show how the WRI configuration can be adapted to enhance significantly the seismic response of tailings impoundments. These simulations provide preliminary guidelines for the optimum design of WRI placed in tailings impoundments for the seismic loads considered.

TABLE OF CONTENTS

LIST OF TABLES

LIST OF FIGURES

LIST OF SYMBOLS AND ABBREVIATIONS

Symbols

A_{loop}	area of the hysteresis loop
a_{max}	maximum horizontal acceleration
a_h	horizontal pseudostatic acceleration
a_v	vertical pseudostatic acceleration
a, b, x_0	non-dimensional parameters
B	elastic bulk modulus (kPa)
B^e	elastic bulk modulus
B_f	fluid bulk modulus
C_c	compression index (-)
C_{cr}	recompression index
C_N	factor to normalize N_m to a common reference effective overburden stress (kPa)
C_E	correction for hammer energy ratio
C_B	correction for the borehole diameter
C_R	correction for rod length
C_S	correction factor for samples with and without liners
C_Q	normalizing factors for cone penetration resistance
C_r	correction factor
c_U	coefficient of uniformity

D	closest horizontal distance to the fault rupture (km)
D_r	relative density
D_{10}	size of grain that 10% of the grains by weight are smaller that
D_{50}	grain size of 50% passing by mass
E	Young's modulus
e	void ratio
e_0	initial void ratio (-)
$\bar{E}_r$	rebound modulus
F	yield function
f	frequency of applied load
G	shear modulus
G_{sec}	secant shear modulus
G_{tan}	tangent shear modulus
G_s	specific gravity
G_{max}	maximum shear modulus
G_{ur}	secant modulus of unloading-reloading
G_{OF}	low amplitude shear modulus
G^e	elastic shear modulus
I_D	density Index
I_h	Arias intensity in two orthogonal horizontal direction (m/s)

I_x	Arias intensity in x horizontal direction (m/s)
I_y	Arias intensity in y horizontal direction (m/s)
K	elastic bulk modulus (kPa)
K_e	coefficient represents elastic absorption (-)
k_{sat}	saturated hydraulic conductivity
k_0	coefficient of lateral stress
k_2	shear modulus coefficient
$(K_2)_{max}$	constant
k_c	ratio of effective vertical stress to effective horizontal stress
K_α	initial shear stress correction factor
K_σ	initial normal stress correction factor
k_h	horizontal coefficient of permeability
k_v	vertical coefficient of permeability
k_g^e	elastic shear modulus number (-)
k_B^e	elastic bulk modulus number (-)
k_G^p	plastic modulus number
k_{sat}	saturated hydraulic conductivity (m/s)
L	logarithmic strain (-)
N	number of applied stress cycles
N_l	cumulative number of cycles required

$(N_1)_{60}$	corrected number of blows in SPT test
N_m	measured standard penetration resistance
ne	modulus exponent (-)
me	modulus exponent (-)
m_{v3}	coefficient of volume compressibility
m_v	coefficient of volumetric compressibility (1/kPa)
m_p	plastic bulk modulus exponent
M_w	moment magnitude
n	porosity
P	exceedance probability
PI	plasticity Index
p_a	atmospheric pressure (kPa)
p_c	preconsolidation pressure
p_0	existing effective vertical overburden pressure
p'	mean effective stress (kPa)
q_c	cone penetration tip resistance
q_{ss}	shear strength under steady state
r_d	stress reduction factor
R_F	failure ratio
r_u	excess pore water pressure ratio

S_u	undrained shear strength
S_{su}	steady sate shear strength
S_{u-pc}	post cyclic maximum shear strength
s'	effective confining stress (kPa)
t	maximum shear stress (kPa)
T_s	fundamental period of the sliding mass
u_g	excess pore water pressure generated by the cyclic shear stress
V_s	shear wave velocity
V_{S1}	overburden-stress corrected shear wave velocity
V_{S1}^*	limiting upper value of V_{S1}
w_D	dissipated energy
w_s	maximum strain energy
x	exponent (-)
γ_d	dry unit weight
ρ	density
ϕ'	drained friction angle
c'	cohesion
γ_w	unit weight of water
μ_w	dynamic viscosity
τ_c	shear stress

γ_c	shear strain
σ_1'	maximum effective principal stress
σ_2'	intermediate effective principal stress
σ_3'	minor effective principal stress
τ_{oct}	octahedral shear stress
σ_m'	mean principal effective stress
γ_r	shear strain at peak point of loading loop
σ_v'	vertical effective stress
ξ_{max}	maximum damping ratio
ξ	damping ratio
Δu	excess pore water pressure
Δt	shear stress increment
$\Delta s'$	normal stress increment
σ_{3c}'	minor effective consolidation stress
γ_t	threshold shear strain
σ'	effective confining stress
ψ_L	angle of flow liquefaction surface
τ_{static}	initial static shear stress
σ_{v0}'	effective vertical stress
σ_{h0}'	effective horizontal stress

τ_{cyc}	cyclic shear stress
γ_{cyc}	cyclic shear strain
ϵ_v	volumetric strain
Φ	standard normal cumulative distribution function
$d\varepsilon_{ij}^{p}$	incremental plastic strain
σ_{ij}	total stress component
$\Delta\varepsilon^{p}$	increment of plastic strain
$\{\sigma\}$	state of stress
$\{\Delta\sigma'\}$	vector of total effective stress increment
$\{\Delta\varepsilon\}$	incremental total stress
σ_n	normal stress
ψ	dilation angle
η	stress ratio
$d\varepsilon_v$	incremental volumetric strain
$d\varepsilon_p$	incremental shear strain
ϕ_{cv}	constant volume friction angle
ν	Poisson's ratio
η_f	stress ratio at failure
ϕ_f	friction angle at failure
ϕ_d	developed friction angle

η_d	developed stress ratio
$\Delta\varepsilon_v^p$	incremental plastic volumetric strain
$\Delta\gamma_s^p$	incremental plastic shear strain
ψ_d	developed friction angle
λ^s	scalar plastic multiplier
G_i^p	initial plastic shear modulus
G_i^*	normalized initial plastic shear modulus
Δk^s	cone mechanism hardening parameter
$\Delta\varepsilon_1^{ps}$	increment of major plastic strain
$\Delta\varepsilon_3^{ps}$	increment of minor plastic strain
σ^c	cap pressure
k_β^p	plastic modulus number
η	stress ratio (-)
$d\varepsilon_v$	volumetric strain increment (-)
ρ_d	dry density
ϕ'	friction angle (°)
σ'_{vc}	initial vertical effective stress (kPa)
σ'_m	mean effective stress (kPa)
σ'_v	effective vertical stress (kPa)
ψ_d	angle of dilation

Abbreviations

AR_x	average normalized horizontal displacement of downstream slope of tailings impoundment
CPT	cone penetration test
CSR	cyclic stress ratio
CRR	cyclic resistance ratio
CSL	critical state line
CDSS	cyclic direct simple shear test
DMT	dilatometer test
FC	fine content
epwp	excess pore water pressure
FLS	flow liquefaction surface
MSF	magnitude scaling factor
Mxdis	maximum horizontal displacement of downstream slope of impoundment
OCR	over consolidation ratio
PGA	peak ground acceleration
PMT	pressuremeter test
SPT	standard penetration test

LIST OF APPENDICES

INTRODUCTION

Hard rock mining produces two primary types of quasi-solid waste: waste rock and tailings. These wastes often contain contaminants such as heavy metals and chemical agents used in ore processing. If they contain sulphides, they may also produce acid mine drainage. The safe disposal of tailings, which exceed the mass of the extracted economically-viable minerals by factors varying from about 4 for iron ore typical quality to 1,000,000 for gold, is a primary concern for the mining industry. During the last 50 years, more than 30 tailings impoundments have failed as a result of seismic activity, causing significant loss of life as well as environmental and economic damage (ICOLD 2001; Aubertin et al. 2002b; WISE 2104). Therefore, the evaluation of the seismic stability of tailings impoundments and methods of improving their seismic stability are priorities.

Stone (gravel) columns may be used in naturally occurring soils to either prevent liquefaction or control its effects (Sasaki and Tanighuchi, 1982; Barksdale et al. 1983; Ledbetter, 1985; Sonu et al., 1993; Adalier et al., 2003). In sands, liquefaction may be prevented by the dissipation of excess pore water pressures through the vertical columns as they are generated during earthquake shaking. Additionally, the rigid columns provide reinforcement that reduces shear strains and thus deformation and the tendency for excess pore water pressure generation. In silts, the drainage effect of the columns during earthquake shaking is negligible due to the relatively low hydraulic conductivity of such fine-grained soils. However, the reinforcement effect results in a stiffer response that can reduce the rate of generation of excess pore water pressure during earthquake shaking and significantly reduce deformation, while helping to dissipate the pressures after the event.

Expanding on this concept, Aubertin et al. (2002a) suggested a new co-disposal method involving waste rock and tailings. In this method, waste rock is placed inside of tailings (waste rock inclusions) to improve the seismic stability of tailing impoundments. Aubertin et al. (2002b) theorized that the addition of waste rock inclusions in tailings impoundments would increase the consolidation rate of the tailings during deposition (as confirmed by Jaouhar et al., 2011, 2013; L. Bolduc and Aubertin, 2013, 2014) and provide shear resistance to static and dynamic loads.

James (2009) conducted numerical analyses of the behavior of a conceptual tailings impoundment without and with waste rock inclusions subjected to a range of earthquake loadings. The simulations were conducted with version 5 of the FLAC finite difference software program (Itasca, 2006). The elasto-plastic Mohr-Coulomb model was used to simulate the behavior of the waste rock inclusions and the UBCSAND model (version 904a; Beaty and Byrne 1998) was used to simulate the behavior of the tailings. The applicability of the model to tailings was verified through numerical simulations of cyclic simple shear testing of the tailings. The analysis showed that the presence of waste rock inclusions resulted in a significant improvement in seismic performance and in some cases prevented failure of the impoundment.

Pépin et al. (2012a, 2012b) used seismic table testing to evaluate the effect of rigid, draining, or rigid-draining inclusions on the dynamic behavior of tailings. The testing demonstrated the ability of such inclusions to reduce the rate of excess pore water pressure generation and deformation.

Despite these preliminary results, some gaps and uncertainties remain; these can be summarized as follows

- Capabilities of available constitutive laws have not been evaluated to predict the seismic response of tailings submitted to complex loading conditions, as in seismic table tests.
- The available models usually cannot predict correctly the post seismic settlement of tailings due to pore water pressure dissipation.
- The seismic response of an actual tailings impoundment has only been evaluated partially, and many important situations and conditions have not yet been assessed.
- The effect of seismic loads on critically displaced volumes of tailings has not been evaluated nor used to assess the response of impoundments.
- There is no guideline to optimize the design of waste rock inclusions in tailings impoundment with respect seismic response.

Objectives

The objectives of this research can be summarized as follows:

- Verifying and calibrating the UBCSAND model for the simulation of the pore water pressure generation during seismic table tests performed on tailings by Pépin et al. (2012a, 2012b).
- Developing the required FISH routine(s) to allow the UBCSAND model to better represent the tailings behavior post-shaking, specifically the volumetric plastic strains due to isotropic compression or when the loading direction is on or parallel to yield surface or in direction that does not intersect the yield surface (as when tailings are consolidating during the dissipation of excess pore water pressures after shaking). "FISH" is an internal programming language used in the finite difference code FLAC (Itasca, 2008) which is used here for the numerical simulations.
- A numerical investigation of the seismic response of two tailings impoundments with and without waste rock inclusions, based (loosely) on their general characteristics and considering critical seismic loadings.
- Determining the effect of waste rock inclusion configuration on the seismic performance of the subject tailings impoundments.
- Developing a path to preliminary guidelines for the design of tailings impoundments reinforced with waste rock inclusions with respect to seismic stability.

Scope and content

Chapter 1 of this thesis reviews the state of art and practice literature review. It contains:

- A description of wastes produced by hard rock mining and waste disposal methods.
- Geotechnical concerns related to tailings impoundments, specifically regarding seismic stability.
- A summary of the hydro-geotechnical properties of tailings and waste rock.
- Description of the dynamic behavior of tailings and waste rock.
- An overview of methods for improving the seismic stability of tailings impoundments.
- Constitutive models for the numerical modeling of the dynamic behavior of tailings.
- Numerical modeling of conceptual tailings impoundment reinforced with waste rock inclusion.

Chapter 2 presents the organization and outline of the thesis. It also explains the connections between the different chapters and briefly describes their content; this thesis mainly consists of three papers submitted to peer-reviewed journals.

Chapter 3 presents numerical simulations of the seismic and post-seismic behavior of tailings, conducted with FLAC (Itasca, 2008). It describes the numerical simulations of cyclic simple shear tests and seismic table tests performed on tailings using the UBCSAND model version 904aR (Beaty and Byrne, 2011). In this chapter, a new approach is introduced for simulating the post-liquefaction behavior of tailings due to excess pore water pressure dissipation. In this approach, the modulus of tailings is updated based on the consolidation curve of loose tailings.

Chapter 4 presents a numerical investigation of the effects of waste rock inclusions on the seismic stability of an upstream-raised tailings impoundment. The seismic response of an actual tailings impoundment without and with waste rock inclusions was targeted here, based loosely on the site conditions at a tailings impoundment located in New Brunswick, Canada. In situ data such as CPT, SPT and shear wave velocity were used to estimate the properties of the tailings. The simulations have been performed for unconsolidated and consolidated tailings. The results of unconsolidated tailings are presented in this chapter and the results obtained for consolidated tailings are presented in Appendix C.

Chapter 5 presents the results of an investigation of the effect of waste rock inclusions on the seismic response of a tailings impoundment located in the Abitibi region of Quebec, Canada (but with conditions somewhat different than those at the mine site). The UBCSAND and Mohr-Coulomb elasto-plastic models were used respectively to simulate the tailings and waste rock (with FLAC). The effects of frequency content and intensity of the seismic loads and of the inclusions configuration on the deformation of the downstream slope of the impoundment and critically displaced volume of tailings were investigated in this chapter. Preliminary guidelines for optimizing waste rock inclusions with respect to the applied seismic loads are also included in this chapter.

Chapter 6 presents a summary and a general discussion with the limitations of this research.

Finally the main conclusions of this research are recalled and recommendations for further research are presented.

Additional details on the dynamic numerical simulations of tailings impoundments conducted for this research are presented in the appendices.

CHAPTER 1: LITERATURE REVIEW

The seismic stability of tailings impoundments is a concern. During the last 50 years, more than thirty tailing impoundments have failed as a result of seismic activity, particularly due to tailings liquefaction (ICOLD 2001; Aubertin et al. 2002b; WISE 2014).

Aubertin et al. (2002b) suggested the use of waste rock inclusions to increase the seismic stability of tailings impoundments. Afterwards, James (2009), James and Aubertin (2010, 2012), and Pépin et al. (2012a, 2012b) investigated the behavior and stability of tailings and tailings impoundments with inclusions, experimentally and numerically. The results of these studies indicate that the presence of waste rock inclusions can improve the seismic performance of tailings impoundments and retard and/or reduce the excess pore water pressure generation in tailings during the seismic loading.

Although comprehensive research has been done to model a conceptual upstream-raised tailings impoundment reinforced with waste rock inclusions (James, 2009), an actual upstream-raised impoundment reinforced with the waste rock inclusions has not been simulated numerically. Guidelines for the design of tailings impoundments with waste rock inclusions have not yet been proposed. This project aims at using comprehensive dynamic numerical modeling to achieve these goals. Additionally, the above-mentioned results identified certain limits of the UBCSAND model (Naesgaard, 2011) which will be addressed as part of this work.

This chapter summarizes a literature review on the seismic stability of tailings impoundments without and with waste rock inclusions, and reviews some using existing constitutive models.

1.1 Mine waste

1.1.1 Tailings

Separating valuable minerals from ore produces a concentrate of the valuable minerals and tailings, a slurry containing fine particles of crushed rock of no economic value. Vick (1990) classifies tailings into four categories; soft-rock tailings, hard-rock tailings, fine tailings, and coarse tailings, based on their geological origin and general engineering behavior:

- Soft-rock tailings are derived from fine coal refuse, trona, and potash among others. They are combinations of fines (particles less than 0.075 mm) and sands (particles between 0.075 mm and 4.75 mm) with the fines portion often called “slimes” being a greater portion of the mass and highly active (plastic). The engineering behavior of soft rock tailings is thus dominated by slimes and is somewhat similar to that of plastic silt or clay.
- Hard-rock tailings are produced from base and precious metals such as lead-zinc, copper, gold-silver, molybdenum, and nickel. Hard-rock tailings are combinations of sand and slime where the slimes are nonplastic and overall behavior of these types of tailings is characterized by inter-granular friction with little or no cohesion.
- Fine tailings are produced from phosphatic clays, bauxite red muds, taconite, and slime from oil sands mines among others. These types of tailings consist mainly of fines and their engineering behaviors, such as the sedimentation-consolidation, are comparable to those of highly plastic clays.
- Coarse tailings are produced from tar sands, uranium, gypsum, coarse tactonite, and phosphate mines. They are mostly composed of sand-sized particles with little fines and behave similarly to coarse-grained sands.

This research is focused on hard rock tailings. However, many of the findings may be applicable to other types of tailings as well.

Hard rock tailings particles may contain significant concentrations of sulphide minerals such as pyrite, pyrrhotite, and arsenopyrite (Aubertin et al., 2002a; Bussiere, 2007) as well as trace metals. The presence of these substances may be problematic from an environmental viewpoint as described later in this document.

1.1.2 Waste rock

Extraction of ore in a mining operation requires that rock be excavated, either in an open pit or an underground mine, to reach the ore body or to provide service openings. This excavated material is known as “waste rock” and has no economic value. Waste rock typically consists of angular particles of rock varying from sand to boulder in size. The maximum particle size, typically 0.5 to 1.0 m, is determined by the characteristics of the parent rock (i.e. fractures and

joints), the method excavation (i.e. blasting method and pattern) and, in underground mines, the need to transport the waste rock to the surface for disposal.

According to Aubertin et al. (2002a), the ratios of dry weight of waste rock to tailings in Canada for open-pit and underground mines are about 9:1 and 3:1, respectively.

As with tailings, waste rock from hard rock mines may contain significant concentrations of sulphide minerals such as pyrite, pyrrhotite, and arsenopyrite (Aubertin et al., 2002a; Bussiere, 2007) as well as trace metals. Waste rock from hard rock mines tends to consist of hard, angular particles. The durability of the particles is variable; waste rock particles containing sulfides may be subject to physical degradation due to chemical reactions.

1.1.3 Waste water

The mineral extraction process often includes crushing and grinding of the ore and the addition of water to facilitate chemical extraction or to create flowable slurry for transport of the ore resulting particles through the plant. Once the valuable minerals are extracted, the resulting waste may be divided into tailings slurry and waste water that may contain chemicals used in the ore extraction process or metals leached from the rock particles.

1.2 Management of mine wastes

Mine wastes should be deposited and treated in a manner that avoids environmental damage and geotechnical instability. Selection of a suitable disposal area and design and construction of the disposal site should be included in the mine wastes management process. Wastes management is one the most important aspects of mining and of geotechnical engineering because mine wastes can create various environmental and geotechnical problems. Many publications on mine wastes management have been issued by different researchers and practitioners such as Vick (1990), Aubertin et al. (2002a), and Bussiere (2007), Blight (2010). In the following sections, a brief review of the published works, specifically Bussiere, (2007) is recalled.

1.2.1 Tailings management

1.2.1.1 Conventional methods of tailings disposal

Tailings are usually transported as slurry and deposited in dedicated areas, called tailings impoundments (Bussiere, 2007). The impoundments are retained, partly or completely by dykes, and the natural topography. These impoundments may contain tailings and waste water. The location of tailings impoundments depends on different parameters based on geological, topographical, geotechnical, hydro-geological, environmental, and operational considerations. The materials used for the construction of the retention dykes are the tailings (coarse fraction), waste rock or borrow soils.

Most impoundments are constructed in stages. Typically, an initial stage capable of retaining the tailings deposition for the first few years of mine operation is constructed using a starter dyke composed of borrow material and subsequent stages composed of the coarse fraction of the tailings (or waste rock or borrow material) are added to increase the height of the dyke and the thus the capacity of the impoundment as needed. Three different methods are commonly used to raise the retention dykes; upstream, downstream, and centerline (Vick, 1990).

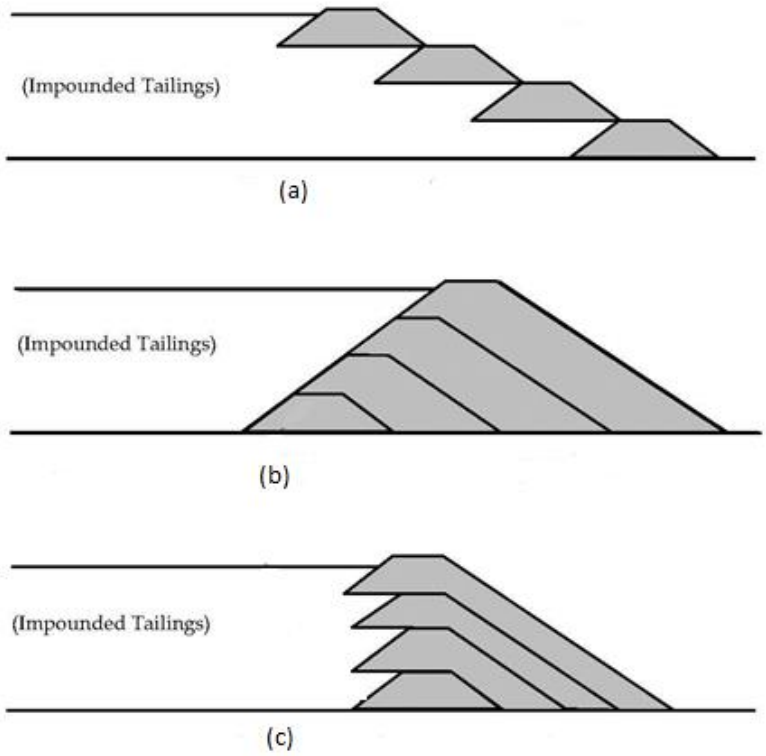

Figure 1-1: Common types of raised embankments; a) upstream-raised impoundment b) downstream-raised impoundment c) centerline-raised impoundment (modified from Vick, 1990)

1.2.1.2 Densified tailings

A vast majority of tailings are deposited hydraulically as slurry in tailings impoundments and allowed to consolidate under their own weight. As a result, the tailings may be highly susceptible to liquefaction and flow (in the event of a rupture of the retention dyke) which can lead to considerable adverse consequences (to be discussed later). Additionally, a significant quantity of water in the form of free water and pore water is stored in the impoundment.

To reduce the risk of liquefaction and flow of tailings and to reduce the water load of mining operations in areas of scarcity, tailings may be by the removal of a portion of the pore water prior to deposition. The technologies employed in the densification of tailings, thickened tailings, paste tailings and filtered tailings, offer interesting operational alternatives for tailings deposition and are described briefly below.

Thickened tailings

The thickened tailings (TT) method was proposed by Robinsky (1975) to reduce environmental risks associated with conventional tailings impoundments. The TT technology minimizes the requirement for retaining dykes and eliminates the pond formed on the surface of most impoundments by creating a self-supporting homogenous mass of tailings. In this method, the tailings are densified by thickeners to a solids content of 50% to 70%. Thickened tailings behave like a viscous fluid. The thickened tailings are discharged downhill into a valley or from a tower on flat terrain. The yield stress of these types of tailings is 10 to 300 Pa. The TT are relatively homogenous. The risk of stability problems associated with tailing impoundments is reduced. Desiccation in natural climatic conditions may increase consolidation and the strength of TT. These tailings are initially partially saturated and their susceptibility to liquefaction is not yet clear. In area with high levels of seismicity, stability of TT under seismic loading is of concern.

Paste tailings

Paste tailings (PT) are a mixture of tailings and water and occasionally a binding agent such as cement. Segregation usually does not occur in the dense tailings. Paste tailings are tailings that are thickened using a thickener and filter discs. A suitable paste is then made by adding water to achieve a solids content of 70% and 85% (Martin et al. 2006). Paste tailings create self-supporting homogenous tailings stacks that do not require retention dykes. The undrained shear strength of PT varies between 5 and 60 kPa and may be higher due to desiccation in arid regions. PT do not segregate during deposition; therefore tailings keep their homogeneity. Binders may also be added to PT to increase the shear strength and water-retention properties and decrease the hydraulic conductivity. There are, however, a number of uncertainties regarding the long term and seismic behavior of paste tailings.

Filtered tailing

Filtered tailings (FT) are produced using high pressure filters to increase the solids content to 80% to 90%. They form a cake that can be handled using conventional earth moving equipment (Davies and Rice 2001). FT have high in situ density and low water content. Therefore, their geotechnical characteristics are better than those of conventional (slurry) tailings.

The cost of filtering and transporting tailings are relatively high. However, in dry climatic regions, water recovery is important and is Artic climates, slurry transport is problematic. Therefore, uses of FT under these conditions lead to important advantages (Davies and Rice 2001).

1.2.1.3 Co-disposal of tailings and waste rock

Mine waste co-disposal is "the simultaneous or alternate deposition of tailings and waste rock in the same surface facility" (Bussiere, 2007). Co-disposal methods include: co-mixing, layering and waste rock inclusions in tailings impoundments. Co-disposal of mine wastes aims to achieve better properties relative to tailings alone.

Co-mixing

Waste rock and tailings can be combined prior to deposition. In this method the tailings fill the voids between the coarser waste rock. Co-mixing results in increased shear strength, lower hydraulic conductivity and improved water retention (Wilson et al. 2000, 2002, and 2003). Wickland and Wilson (2005) showed that co-mixing produces dense, high strength, and low hydraulic conductivity materials that are less prone to physical instability relative to conventional tailings. Application of this method in the field requires further study and research.

Layering co-disposal

Another method for co-disposal of tailings and waste rocks is to add layers of tailings within waste rock piles. Tailings layers may reduce oxygen flux and water infiltration (Lamontage et al. 1999; and Fala et al. 2003; Bussiere 2007). Although layering co-disposal reduces oxygen flux and water infiltration, it cannot completely eliminate the potential for acid mine drainage (AMD) (Bussiere 2007). Co-disposal by layering is also in the conceptual stage and more research is needed to evaluate its application in the field.

1.2.2 Waste rock management

As mentioned in section 1.1.2, waste rocks are commonly placed in purpose built waste rock piles. There are different methods of constructing waste rock piles: dumping, push dumping, free dumping, and drag line (Aubertin et al. 2002a). Waste rock piles are designed using different

configurations such as valley-fill, ridge, cross-valley, heaped, and side-hill to form, waste rock piles. Surface disposal of waste rock may cause environmental and geotechnical problems, such as acid mine drainage or instability (Aubertin et al. 2002a).

1.3 Environmental and geotechnical concerns of tailings impoundments

As mentioned in section 1.2, the most common method for managing tailings is to store them in surface impoundments. Environmental and geotechnical concerns should be considered in the design of tailings impoundments. Hard rock tailings are capable of producing acid (Aubertin et al., 2002a; Bussire, 2007) and may contain concentrations of heavy metals and chemicals used in ore processing. This is potentially dangerous for the environment. In addition to such environmental concerns, the geotechnical stability of tailings impoundments is another issue that is very important in their design and construction. According to Davies (2002), failure of tailings impoundments is ten times more likely than for water retention dams. Some of the environmental and geotechnical concerns are described in the following sub-sections.

1.3.1 Environmental concerns and solutions

As previously noted, hard rock tailings may contain significant concentrations of sulphide minerals such as pyrite, pyrrhotite, and arsenopyrite (Aubertin et al., 2002a; Bussiere, 2007) as well as trace metals. The exposure of sulphide minerals to oxygen and water can produce acid. The resulting acid mine drainage (AMD) is one of the primary environmental concerns for tailings impoundments. Bussiere (2007) reported different methods of preventing or reducing AMD:

- Limiting water infiltration by the construction of a low saturated hydraulic conductivity cover. These covers are configured like those that have been developed for the isolation of domestic and hazardous wastes (Aubertin and Chapuis 1991; Daniel and Koerner, 1993; Rowe et al., 2004).
- Covers utilising capillary barrier effects can be effective in limiting water infiltration in arid climates (Williams et al., 1997; Zhan et al., 2001; Alberight et al., 2004).

- Another method for limiting AMD is submerging the tailings under water to prevent the entry of oxygen (Amyot and Vezina, 1997; Julien et al., 2004). This is a very common method.
- Oxygen consuming materials such as wood waste, straw mulch, or other organic residues can be used as a cover to to consume oxygen in the air before it reaches the tailings (Tasse et al., 1997; Cabral et al., 2000).
- Covers with capillary barrier effects can be used to create a low oxygen diffusion layer to limit oxygen migration (Nicholson et al., 1989; Aubertin et al., 1995; Bussiere et al., 2003).

Other environment contaminants in tailings are heavy metals in the water as well as residual compounds from ore processing, such as sodium cyanides used in gold extraction. Such heavy metals and chemical compounds can have adverse environmental impacts if released from the impoundments through seepage (or failure of the impoundment). If the foundations of the impoundment are not sufficiently impervious, a liner must be added to prevent groundwater contamination. The liner can be made from clay or a composite system.

1.3.2 Geotechnical stability concerns

From a geotechnical point of view, the design of tailings impoundments, specifically the retention dykes, is somewhat different from that of water-retention dams. According to CDA (2010), unique aspects of tailing dams that should be taken into account in geotechnical design include: the applied load from tailings on dam, an elevated phreatic surface, the potential for AMD, seepage pathways and internal erosion due to freezing or deterioration of decant pipes, and hydro-mechanical interactions with other infrastructure.

According to Davies (2002) there are more than 3,500 tailings dam worldwide. Several of these dams have experienced significant failure over the years. There were 238 reported of tailings dams failure between 1917 and 2014 (ICOLD, 2001; WISE, 2014). Some 26 of the 238 incidents were due to seismic loading. Based on ICOLD (1996a; 1996b), the five most frequent causes of failure of tailings dams are: slope of foundation instability, internal erosion, surface erosion, overtopping, and decantation structure malfunction.

Davies (2002), Davies et al. (2002a, 2002b) suggested that static liquefaction is frequently associated with tailings impoundment failure. Static liquefaction is the reduction of the shear strength due to increased pore water pressures (reached at steady state point). The conditions that can trigger of static liquefaction are (Davies et al., 2002b):

- Increased pore water pressure as a result of a raised phreatic surface.
- Rapid raising of the impoundment.
- Loss of confinement (e.g. removal of toe due to overtopping, erosion, etc.).
- Foundation failure that creates undrained loading in the tailings.

Tailings may also undergo liquefaction as a result of dynamic loading. This phenomenon is described in detail in Section X.

Notable failures of tailings impoundments around the world due to static of dynamically-induced liquefaction include:

- Barahona tailings dam, a 61-meter-high structure, located at the El Teniente copper mine in Chile failed due to liquefaction during an earthquake with a magnitude of 8.2 in October 1928. Approximately 4 million tons of liquefied tailings were released as a result of the failure (Ishihara et al., 1980; ICOLD, 2001).
- On March 28, 1965 multiple tailings dam failures occurred due to seismically induced liquefaction in northern Chile. Failure of the El Cobre tailings impoundment released 2 million tons of tailings and 200 lives were lost (Dobry and Alvarz, 1967; Davies and Lighthall, 2001; WISE, 2014).
- In 1968, tailings dam failed in Hokkaido, Japan due to seismically induced liquefaction. The magnitude of earthquake was 7.9. Failure released 90,000 cubic meters of tailings that traveled 150 meters downstream (WISE, 2014).
- In 1969 in Spain, a tailings dam failed after heavy rain due to static liquefaction. Failure released 115,000 cubic meters of tailings and caused major downstream damage and loss of life (WISE, 2014).

- In 1970 in Mufulira, Zambia, a tailings impoundment failed due to static liquefaction and about 1 million tons of liquefied tailings were released. The tailings flowed into underground mine works and 89 miners lives were lost (WISE, 2014).
- On 15 January, 1978 in Japan, two tailings dams failed due to seismically induced liquefaction. That released tailings severely damaged the environment downstream. The magnitude of the earthquake was 7 (Ishihara, 1984).
- On 13 October 1980, in New Mexico, USA, a tailings dam failed due to static liquefaction. The dam was breached due to pore water pressure build up as a result of rapid raising of the dam. The failure released 2 million m^3 of tailings. The tailings flowed 8 km downstream and damaged farmlands (WISE, 2014).
- In March 1985, the Cerro Negro No.4 and Veta de Agua No. 1 Tailings Impoundments (Chile) failed during a magnitude 7.8 earthquake due to seismically induced liquefaction in Chile. The failures released 500,000 and 280,000 cubic meters of tailings, respectively, which flowed as much as 8 km downstream (WISE, 2014).
- The Stava Tailings Dam in Italy failed on July, 1985. Approximately 240,000 m^3 liquefied tailings were released. The tailings flowed at speeds of up to 60 km/h and destroyed the village of Stava and also caused some damages at the village of Tesero. The reason for failure was the decrease in effective stress due to an increase in the phreatic surface. The decreasing effective stress created a stress path that reached the failure surface triggering static liquefaction (Davies et al., 2002a).
- A tailings impoundment at the Sullivan Mine in Canada failed due to static liquefaction on August of 1991. The dam was constructed on a foundation of older tailings. Shear strain increased after construction of dam resulting in increasing pore water pressure that led to static liquefaction. The failure was brittle and indications of liquefaction such as sand boils were observed on site (Davies et al., 2002a).
- The Tapo Canyon tailings dam in southern California failed due to seismically induced liquefaction on 17 January, 1994 (Harder and Stewart, 1996).

- Merriespruit Harmony Mine Tailings Impoundment failed due to overtopping on February 22, 1994 in South Africa. After overtopping and erosion of toe, the local slope increased to 2:1(H:V) and static liquefaction and flow sliding were initiated. Over 600,000 m^3 and 90,000 m^3 of tailings and water were released, respectively (Davies et al., 2002a).
- On 12 November 1996, an upstream-type tailings impoundment failed following a magnitude 6.4 earthquake in Peru. Failure released 300,000 cubic meters of liquefied tailings materials that flowed 600 meters and entered a river (WISE, 2014).
- Los Frailes (Azancollar) Tailings Dam failure in 1998 in Spain is probably the most publicized tailing dam failure to date. Due to a foundation failure, static liquefaction was triggered that exerted a thrust to the dam that resulting in relatively rapid progression and large lateral displacement of a section of the retention dyke (Davies et al., 2002a).

According to Azam and Li (2010), 14% of tailings dam failures were due to seismic liquefaction before 2000. After 2000, no failure due to seismic liquefaction was reported. There are many existing and abandoned tailings impoundments in the world that are susceptible to failure due to liquefaction of the retained tailings.. Aubertin et al. (2002b), James (2009), James and Aubertin (2010, 2012) showed that reinforcing tailings impoundments with waste rock inclusions can improve the stability of tailings impoundments under static and seismic conditions and control the effects of liquefaction of the tailings. This technique will be reviewed further later in thesis.

1.4 Hydro-geotechnical properties of hard rock tailings and waste rock

Geotechnical stability is an important concern in the design, construction, operation, and closure of tailings impoundments. Static and dynamic liquefaction have been identified as an important cause of failure for tailing impoundments (e.g. Ishihara, 1984; Davies et al., 2002a; Davies et al., 2002b; Davies, 2002). Evaluation of the static and seismic stability requires adequate knowledge of the hydro-geotechnical properties of the material to be retained and of the material to be used to construct the dam (or dyke). This section presents a summary of the properties of tailings and waste rock reported by various sources (Bussière, 2007; James, 2009).

1.4.1 Hydro-geotechnical properties of hard rock tailings

1.4.1.1 Index properties and mass-density relationships

Gradation – The gradation of hard rock tailings varies from fines (particles less than 0.075 mm in size) to fine sand (particles between 0.075 and 0.425 mm in size) with the fines fraction generally being the larger of the two.

The gradation of tailings samples taken from a mill (prior to deposition) is usually different from that of samples taken from a tailings impoundment (after deposition). The reason for this difference is grain size segregation of particles by during hydraulic deposition as slurry (Bussière, 2007). Segregation can also result in thin layers of relatively finer and coarser particles. The finer lenses have very little sand and are often referred to as "tailings slimes" while the coarser lenses may be predominated sand and are often referred to as "tailings sands."

Specific Gravity – The specific gravity (relative density, D_r) of tailings is dependent on the mineral content. Hard rock mine tailings often contain heavy minerals such as pyrite and metals that result in specific gravities somewhat higher than those typically associated with natural soils ($\geq$ 2.6 to 2.7).

For hard rock mine tailings, Vick (1990) indicates a specific gravity range of 2.6 to 3.0. Aubertin et al. (1996) measured specific gravities of 2.78 to 2.87 for four homogenized samples from four different sites. Qiu and Sego (2001) gives specific gravities of 2.75 for copper tailings and 3.17 for gold tailings. Wijewickreme et al. (2005a) showed, based on 20 samples of copper-gold-zinc tailings, specific gravities varying between 3.36 and 4.42. Bussière (2007) stated that for gold mines where the ore is mined from quartz veins, specific gravity values ranged from 2.6 to 2.9. He also noted that for sulphide tailings, the specific gravity is between 2.9 to 4.5.

James (2009) measured the specific gravity of tailings samples from the Laronde Mine in western Quebec and found and average value of 3.88. The sulphide content was noted as the reason for this high value.

Plasticity Index - According to Vick (1990), Aubertin et al. (1996, 2002), Qiu and Sego (2001), Wijewickreme et al. (2005a), Bussière (2007), James (2009), and James et al. (2011), hard rock tailings are nonplastic to very low plasticity. Aubertin et al. (1996) showed that tailings plasticity

indices are close to zero. Qiu and Sego (2001) showed that copper and gold tailings are nonplastic. Wijewickreme et al. (2005a) reported that copper-gold-zinc tailings were nonplastic and their plasticity index was around 2. Bussière (2007) mentioned that the plastic limit of tailings is close to zero.

Classification – According to the Unified Soil Classification System (Holtz and Kovacs, 1981), the tailings are non-plastic silts (ML), or silty sands (SM) for the coarser fraction.

In-place Dry Unit Weight – The in-place dry density is a function of the specific gravity, degree of consolidation and effective stress and can thus vary significantly with depth and time.

1.4.1.2 Shear strength parameters

Bussière (2007) reported that the drained friction angle,ϕ', of hard rock mine tailings varies between 30^o and 42^o and that the cohesion (c') is close to zero.

Vick (1990) indicates that drained friction angle $\phi'$of tailings is up to 6^o higher than natural sand or silt because tailings particles tend to be more angular and stronger. Vick (1990) also indicated that the undrained friction angle ϕ of tailings(slims) is typically between 14^o and 25^o, and the undrained cohesion, c, varies between 0 and 100 kPa.

Based on direct shear testing of Laronde Gold Mine tailings samples prepared as slurry and normally consolidated to stresses of 100 to 400 kPa, James (2009) found that the drained friction angle ϕ' was 36.6° (without cohesion) and was little affected by the variation of the confining stress. Poncelet (2012) used undrained triaxial compression testing of Canadian Malartic Mine tailings and found an undrained friction angle of 35.9° and no cohesion.

1.4.1.3 Hydrogelogic properties

The hydraulic conductivity of tailings varies significantly due to segregation. The horizontal hydraulic conductivity is usually much larger greater than the vertical hydraulic conductivity. The values given below are usually for homogenized tailings.

According to Bussière (2007), saturated hydraulic conductivity of fine grained tailings (ML) is between 1×10^{-4} and 1×10^{-6} cm/s and the value for coarse grained tailings (SM) is between 1×10^{-2} and 1×10^{-4} cm/s. Also James et al. (2011) estimated the values of k_{sat} by

consolidation test for Laronde Gold Mine tailings; k_{sat} was varies between 3.3×10^{-6} and 2.7×10^{-5} cm/s.

Aubertin et al. (1996) and Chapuis and Aubertin (2003) showed that Hazen and Kozeny-Carman relationship for estimating saturated hydraulic conductivity is not well suited for tailings. Aubertin et al. (1996) proposed the following formula for estimating of k_{sat} of tailings.

$$k_{sat} = 1962\frac{e^{5.16}}{1+e}C_U^{1/3}D_{10}^2 \quad (1.1)$$

Where the constant 1962 is the ratio between the unit weight of the fluid and the dynamic viscosity, multiplied by a material parameter that is approximately 0.02 for hard rock tailings. e is void ratio, C_U is uniformity coefficient ($\frac{D_{60}}{D_{10}}$), D_{60} and D_{10} are diameters corresponding to 60% and 10% passing on the cumulative grain-size distribution curve (cm), respectively.

Mbonimpa et al. (2002) generalized formula (1.1) for estimating of k_{sat} of a variety of soils and tailings as follows:

$$k_{sat}[^{cm}/_{S}] = C_G\left(\frac{\gamma_w}{\mu_w}\right)\left(C_U^{1/3}D_{10}^2\right)\left(\frac{e^{3+x}}{1+e}\right) \quad (1.2)$$

For this equation, C_G is a constant equal to 0.1, γ_w is the unit weight of water (9.81 KN/m^3), μ_w is the dynamic viscosity of water (1×10^{-3}Pa), e is the void ratio, x is a parameter equal to 2.0 for soils low plasticity, C_U is the coefficient of uniformity of the soil (= $\frac{D_{60}}{D_{10}}$), and D_{10} is size of grain that 10% of the grains by weight are smaller that.

James et al. (2011) showed that the estimated hydraulic conductivity of tailings using the above formula (1.2) is in the range that measured in the laboratory.

1.4.1.4 Consolidation properties

According to Bussière (2007) the value of the compression index (C_c) is typically between 0.05 to 0.1 for sand tailings and between 0.2 to o.3 for slimes (see also Vick, 1990). The value of the recompression index (C_{cr}) is between 0.003 and 0.03. The value of the coefficient of consolidation (c_v) for coarse grain tailings (classified as SP by the USCS classification) varies between 10^2 and 10^{-1} cm^2/s and is between 10^{-1} and 10^{-3} cm^2/s for fine grain tailings (SM and ML).

1.4.2 Hydro-geotechnical properties of waste rock

1.4.2.1 Particle size

Particle size distribution influences seepage and stability of waste rock (McLemore et al., 2009). Gamache-Rochette (2004) and McLemore et al. (2009) showed typical grain size distributions of waste rock in piles from around the world. According to McLemore et al. (2009) the percentage of gravel, sand, and fines in mine waste rock are from 5 to 70%, 20 to 53%, and 0 to 42%, respectively. Waste rock may be classified as "sandy gravel with cobbles" (Leps 1970; Robertson 1985; Quine 1993; and Hawley 2001).

1.4.2.2 Density and specific gravity

Williams (2000) indicated the density of waste rock varies from 1.6 to 2.2 t/m^3 and higher. The specific gravity, G_s, for a copper-zinc mine varied between 2.6 and 4.8 (Kesimal et al. 2004). McLemore et al. (2009) showed that the value of specific gravity varies from 1.81 to 2.84 for the site studies in their research.

1.4.2.3 Shear strength

Sherard et al. (1963) cited by James (2009) showed that the angle of internal friction of "loosely dumped" rock fill is between 40^o and 45^o. This value for compacted rock fill is somewhat higher. Leps (1970) indicated by triaxial tests that the average friction angle is between 37^o and 55^o. McLemore et al. (2009) showed that internal friction angle varies from 21^o to 55^o.

The friction angle of rockfill (e.g. waste rock) is dependent on the hardness of the rock, the shape of the particles, the confining stress, and the gradation of the rockfill. Given that waste rock from

hard rock mines tends to be hard, angular and well graded, the friction angle is expected to vary from about 55° under low confining stresses to about 40° under high confining stresses.

1.5 Dynamic behavior of tailings and waste rock

As noted previously, seismic loads can have significant detrimental effects on tailings impoundments. Some of these effects are caused by the dynamic behavior of the retained tailings. There are fundamental characteristics of the dynamic behavior of tailings, including the initial shear modulus, shear modulus reduction and damping with shear strain, excess pore water generation, potential for liquefaction, and post liquefaction strength, that are important in the evaluation of their response to seismic loads and the possible effects on the retention structure. The dynamic characteristics of tailings and similarly behaving soils are described and discussed in this section.

1.5.1 Shear modulus, and dynamic damping

When a sample of soil is subjected to cyclic loading, the stress-strain behavior exhibits a hysteresis loop for each cycle of loading (Kramer, 1996). Two important parameters of this loop are its inclination and its breadth. Its inclination depends on stiffness and may be defined at any point by a tangent shear modulus, $G_{tan,}$ defined as the ratio of the applied shear stress to the induced shear strain. The value of G_{tan} varies but its average value can be approximated by the secant shear modulus, G_{sec} (Kramer, 1996).

$$G_{sec} = \frac{\tau_c}{\gamma_c} \tag{1.3}$$

where τ_c and γ_c, are the shear stress and shear strain at a given point respectively; G_{sec} and τ_c have same units (typically kPa) and γ_c is dimensionless. The area of the loop is related to the energy dissipation during cyclic loading, which may be described by the damping ratio, ξ (Kramer, 1996).

$$\xi = \frac{W_D}{4\pi W_s} = \frac{1}{2\pi}\frac{A_{loop}}{G_{sec}\gamma_c^2} \quad (1.4)$$

Where W_D, W_s and A_{loop} are the dissipated energy, the maximum strain energy, and the area of the hysteresis loop, respectively. W_D, W_s, A_{loop}, and G_{sec} have consistent units.

The shear modulus G and damping ratio ξ are the primary characteristics used in ground response analysis (Seed and Idriss, 1970b; Kramer, 1996). The magnitude of the shear modulus (secant modulus) and damping ratio varies with the maximum shear strain induced. Several tests can be used to measure the shear modulus and the damping ratio (Seed and Idriss, 1970b; Seed et al., 1984; Kramer, 1996; Ishihara, 1996, Towhata, 2008), including:

- Direct determination of stress-strain relationships (cyclic triaxial compression tests, cyclic simple shear tests, cyclic direct shear tests, and cyclic torsional shear tests).
- Forced vibration tests.
- Free vibration tests.
- In situ measurement of shear wave velocities.
- Analysis of ground response during earthquake ground motions.

1.5.1.1 Shear modulus

Shear modulus of sandy soils

The secant shear modulus of soils tends to decrease with increasing shear strain. The locus of points corresponding to the tips of hysteresis loops is called the backbone curve. The slope of the backbone curve at the origin corresponds to the highest value of shear modulus, G_{max}, and is known as the maximum or low-strain shear modulus. As the shear strain increases the modulus ratio $\frac{G_{sec}}{G_{max}}$ decreases from an initial value of 1.0 and progressively approaches 0. The variation of modulus ratio relative to shear strain is described by modulus reduction curve. The backbone and modulus reduction curves can be obtained based on drained and undrained tests (Kramer, 1996).

Seed and Idriss (1970b), proposed the following formula for estimating the maximum shear modulus of soil.

$$G_{max} = 14760 \times \frac{(2.973 - e)^2}{1 + e} (OCR)^a (\sigma_m^{'})^{\frac{1}{2}} \quad (1.5)$$

Where G_{max} , e, *OCR* are maximum shear modulus (psf[1]), void ratio, overconsolidation ratio; 'a' is a parameter that depends on plasticity index of the soil (as shown in Table 1.1), and $\sigma_m^{'}$ is mean principle effective stress in psf.

Table 1.1: Parameter 'a' for various values of the plasticity index PI (after Hardin and Drenvich, 1972)

PI	a
0	0
20	0.18
40	0.30
60	0.41
80	0.48
≥100	0.50

The secant modulus value, G, at any strain level, γ, can be calculated based on following formula (Hardin and Drenvich, 1972)

$$G = \frac{G_{max}}{1 + {}^{\gamma}/_{\gamma_r}} \quad (1.6)$$

where

$$\gamma_r = \frac{\tau_{max}}{G_{max}} \quad (1.7)$$

with

$$\tau_{max} = \left\{ \left(\frac{1+K_0}{2} \sigma_v^{'} sin\phi^{'} + c^{'} cos\phi^{'} \right)^2 - \left(\frac{1+K_0}{2} \sigma_v^{'} \right)^2 \right\}^{1/2} \quad (1.8)$$

[1] Psf – Pounds per square foot.

Where K_0, $\sigma_v^{'}$, $c^{'}$, $\phi^{'}$ are the coefficient of lateral stress at rest, vertical effective stress, effective cohesion, and effective friction angle, respectively. All parameters have consistent units. An alternative empirical formula for maximum shear modulus of sand (psf) is as follows (Seed and Idriss, 1970b)

$$G_{max} = 1000K_{2,max}(\sigma_m^{'})^{0.5} \tag{1.9}$$

Where values of $K_{2,max}$ are determined from the void ratio and density index (D_r) and are given in Table 1.2. According to Idriss et al. (1984), the values of $K_{2,max}$ for gravels are in the range of 80 to 180. For fine-grained soils values of G_{max} can be estimated from Table 1.3.

Table 1.2: Estimation of $K_{2,\ max}$ for sand (after Seed and Idriss, 1970b)

e	$K_{2,max}$(psf)	D_r(%)	$K_{2,max}$(psf)
0.4	70	30	34
0.5	60	40	40
0.6	51	45	43
0.7	44	60	52
0.8	39	75	59
0.9	34	90	70

Table 1.3: Values of G_{max}/S_u (for clayely soils) where S_u is undrained shear strength (after Weiler, 1988)

Plasticity Index	Overconsolidation Ratio, OCR		
	1	2	3
15-20	1100	900	600
20-25	700	600	500
35-45	450	380	300

Typical results of cyclic triaxial tests obtained on “Touyoura” sand can be represented by straight line as follows (Ishihara, 1996)

$$G_{max} = AF(e)\left(\sigma_0^{'}\right)^n \tag{1.10}$$

Where *F(e)* is a function of the void ratio. G_{max} and $\sigma_0^{'}$ (initial mean effective stresses) are in kPa. The values of A and n are dependent to the shear strain amplitude. For sufficiently small strain of $\gamma \leq 10^{-5}$, G_{max} is as follows (Ishihara, 1996)

$$G_{max} = 8400 \times \frac{(2.17 - e)^2}{1 + e}(\sigma_m^{'})^{\frac{1}{2}} \tag{1.11}$$

where G_{max} and $\sigma_m^{'}$ are in kPa.

Kokusho (1987) summarized empirical formulae for estimating G_{max}. As shown in Table 1.4, the value of n (eq. 1.10) is usually equal to 0.5 and A can take different values based on the variability of the shear modulus for individual sands.

Table 1.4: Constants A, n in proposed empirical equation (1.10) for the small strain modulus (after Kokusho, 1987)

	References	A	$F(e)$	n	Soil material	Test method
Sand	Hardin–Richart (1963)	7000	$(2.17-e)^2/(1+e)$	0.5	Round grained Ottawa sand	Resonant column
		3300	$(2.97-e)^2/(1+e)$	0.5	Angular grained crushed quartz	Resonant column
	Shibata–Soelarno (1975)	42000	$0.67-e/(1+e)$	0.5	Three kinds of clean sand	Ultrasonic pulse
	Iwasaki *et al.* (1978)	9000	$(2.17-e)^2/(1+e)$	0.38	Eleven kinds of clean sand	Resonant column
	Kokusho (1980)	8400	$(2.17-e)^2/(1+e)$	0.5	Toyoura sand	Cyclic triaxial
	Yu–Richart (1984)	7000	$(2.17-e)^2/(1+e)$	0.5	Three kinds of clean sand	Resonant column
Clay	Hardin–Black (1968)	3300	$(2.97-e)^2/(1+e)$	0.5	Kaolinite, etc.	Resonant column
	Marcuson–Wahls (1972)	4500	$(2.97-e)^2/(1+e)$	0.5	Kaolinite, $I_p^{**}=35$	Resonant column
		450	$(4.4-e)^2/(1+e)$	0.5	Bentonite, $I_p=60$	Resonant column
	Zen–Umehara (1978)	2000 ~ 4000	$(2.97-e)^2/(1+e)$	0.5	Remolded clay, $I_p=0\sim50$	Resonant column
	Kokusho *et al.* (1982)	141	$(7.32-e)^2/(1+e)$	0.6	Undisturbed clays, $I_p=40\sim85$	Cyclic triaxial

*σ_0' : kPa, G_0 : kPa, **I_p : Plasticity Index

In situ tests may also be used to estimate the maximum shear modulus. Kramer (1996) summarized some of the more widely used formulae for estimating of the maximum shear modulus of soils (see Table 1.5).

Troncosco and Garces (2000) investigated the effect of ageing on the shear modulus of tailings based on in situ testing at four closed tailings impoundments in Chile. The proposed formula for computing the increase in the shear modulus with time is expressed as follow:

$$G_{max} = \sigma_v^{0.5} \times 117.24 t^{0.67} \tag{1.12}$$

Where G_{max}, σ_v, and t are maximum shear modulus (kg/cm^2), vertical effective pressure (kg/cm^2), and time (year) respectively.

Shear modulus of gravelly soils

Seed et al. (1984) showed that for most practical purposes, the following formula can be used for computing the shear modulus of gravelly soils

$$G = 1000K_2(\sigma_m^{'})^{0.5} \quad (1.13)$$

K_2 is a shear modulus coefficient and is function of the grain size distribution, relative density and shear strain of the soil. Typical values of K_2 for gravels are 1.35 to 2.5 times K_2 of sands (Seed et al., 1984). The value of G_{max} is calculated based on the value of $K_{2,max}$. Seed et al. (1984) proposed the following formula for computing the $K_{2,max}$

$$K_{2,max} = 20(N_1)_{60}^{1/3} \quad (1.14)$$

Where $(N_1)_{60}$ is the corrected value of the standard penetration test (SPT) blow count. The values of $K_{2,max}$ for very loose sand and very dense sand are about 30 and 70, respectively.

Table 1.5: Empirical relationships between G_{max} and in-situ test parameters (after Kramer, 1996)

In situ test	Relationship	Soil Type	References	Comments
SPT	$G_{max} = 20000(N_1)_{60}^{0.333}(\sigma'_m)^{0.5}$	Sand	Ohata and Goto (1976), Seed et al. (1986)	$G_{max}\ and\ \sigma'_m$ in lb/ft2
SPT	$G_{max} = 325N_{60}^{0.68}$	Sand	Imai and Tonouchi (1982)	G_{max} in kips/ft2
CPT	$G_{max} = 1634(q_c)^{0.25}(\sigma'_v)^{0.375}$	Quartz Sand	Rix and Stokoe (1991)	$G_{max}, q_c\ and\ \sigma'_v$ in kPa; Based on field tests in Italy and on calibration chamber tests
CPT	Figure available in Baldi et al. (1986)	Silica sand	Baldi et al. (1986)	$G_{max}, q_c\ and\ \sigma'_v$ in kPa; Based on field tests in Italy
CPT	$G_{max} = 406(q_c)^{0.695}e^{-1.130}$	clay	Mayne and Rix (1993)	$G_{max}, q_c\ and\ \sigma'_v$ in kPa; Based on field tests in worldwide sites
CPT	Figure available in Robertson and Campanella (1996)	Normaly consolidated,uncemented quartz sand	Robertson and Campanella (1996)	$G_{max}, q_c\ and\ \sigma'_v$ in kPa
DMT	$G_{max}/E_d = 2.72 \pm 0.59$	Sand	Baldi et al. (1986)	Based on calibration chamber tests
DMT	$G_{max}/E_d = 2.2 \pm 0.7$	Sand	Belloti et al. (1986)	Based on field tests
DMT	$G_{max} = \frac{530}{(\sigma'_v/p_a)^{0.25}} \frac{\gamma_D/\gamma_w - 1}{2.7 - \gamma_D/\gamma_w} K_0^{0.25}(p_a\sigma'_v)^{0.5}$	Sand, silt, clay	Hryciw (1990)	$G_{max}, q_c\ and\ \sigma'_v$ in same units; γ_D is dilatometer based unit weight of soil; based on field tests
PMT	$3.6 \leq \frac{G_{max}}{G_{ur,c}} \leq 4.8$	Sand	Belloti et al. (1986)	$G_{ur,c}$ is corrected unloading-reloading modulus from cyclic PMT
PMT	$G_{max} = \frac{1.68}{\alpha_p} G_{ur}$	Sand	Byrne et al. (1991)	G_{ur} is secant modulus of unloading-reloading portion of PMG; α_p is factor that depends on unloading-reloading stress conditions; based on theory and field test data

where SPT=Standard Penetration Test, CPT=Cone Penetration Test, DMT=Dilatometer Test, PMT= Pressuremeter Test.

Ishihara (1996) summarized different parameters based on eq. 1.10 for the estimation of G_{max} of gravel (proposed by several researchers; refer to Table 1.6).

Table 1.6: Constants in proposed empirical formulae of initial shear modulus for gravels, eq. 1.10 (after Ishihara, 1996)

Reference	A	$F(e)$	n	Material	Sample size	Test method
Prange (1981)	7 230	$(2.97 - e)^2 / 1+e$	0.38	Ballast D_{50} = 40 mm, U_c = 3.0	Dia.: 100 cm Length: 60 cm	Resonant column
Kokusho and Esashi (1981)	13 000	$(2.17 - e)^2 / 1+e$	0.55	Crushed rock D_{50} = 30 mm, U_c = 10	Dia.: 30 cm Length: 60 cm	Triaxial
Kokusho and Esashi (1981)	8 400	$(2.17 - e)^2 / 1+e$	0.60	Round gravel D_{50} = 10 mm, U_c = 20	Dia.: 30 cm Length: 60 cm	Triaxial
Tanaka *et al.* (1987)	3 080	$(2.17 - e)^2 / 1+e$	0.60	Gravel D_{50} = 10 mm, U_c = 20	Dia.: 10 cm Length: 20 cm	Triaxial
Goto *et al.* (1987)	1 200	$(2.17 - e)^2 / 1+e$	0.85	Gravel D_{50} = 2 mm, U_c = 10	Dia.: 30 cm Length: 60 cm	Triaxial
Undisturbed						
Nishio *et al.* (1985)	9 360	$(2.17 - e)^2 / 1+e$	0.44	Gravel D_{50} = 10.7 mm, U_c = 13.8	Dia.: 30 cm Length: 60 cm	Triaxial

In Table 1.6, ‘A’ is a constant and ‘n’ is an exponent.

Kokusho and Tanaka (1994) used ground freezing and push-tube sampling to recover undisturbed samples for measurement of the shear modulus sandy gravel. They investigated the effect of effective confining pressure on the initial shear modulus, G_{max} sandy gravel. They showed that the initial shear modulus tends to increase with increasing confining pressure. They also assessed the effect of the void ratio on the maximum shear modulus of undisturbed gravelly soils. They showed that the maximum shear modulus decreases with increasing void ratio. This effect is more pronounced at lower confining stresses.

1.5.1.2 Modulus reduction

Seed and Idriss (1970b) analyzed the modulus reduction of coarse and fine-grained soils. They confirmed that the shear modulus of soils decreases with increasing shear strain. Other researchers investigated the effects of various parameters such as plasticity, confining pressure, void ratio, and grain size on the modulus reduction of different soils. Zen et al. (1978) (cited by Kramer (1996)) and Kokushu et al. (1982) showed the influence of plasticity index on the shape of the modulus reduction curve. According to their work, the shear modulus of low plasticity soils degrades faster than that of highly plastic soils. Dobry and Vucetic (1987) and Sun et al. (1988) showed that the effect of the plasticity index on modulus reduction is more important than that of the void ratio. Ishibashi (1992) studied the effect of confining pressure on the modulus reduction of soil. He showed that the effect of confining pressure is significant in non-plastic soils and much less significant in highly plastic soils.

Ishibashi and Zhang (1993) presented the following formula for predict the modulus reduction behavior.

$$\frac{G}{G_{max}} = K(\gamma, PI)(\sigma_m^{'})^{m(\gamma,PI)-m_0} \tag{1.15}$$

where

$$K(\gamma, PI) = 0.5\left\{1 + tanh\left[ln\left(\frac{0.000102+n(PI)}{\gamma}\right)^{0.492}\right]\right\} \tag{1.16}$$

$$m(\gamma, PI) - m_0 = 0.272\left\{1 - tanh\left[ln\left(\frac{0.000556}{\gamma}\right)^{0.4}\right]\right\}\exp(-0.0145PI^{1.3}) \tag{1.17}$$

$$n(PI) = \begin{cases} 0.0 & for\ PI = 0 \\ 3.37 \times 10^{-6} PI^{1.404} & for\ 0 < PI \leq 15 \\ 7.0 \times 10^{-7} PI^{1.976} & for\ 15 < PI \leq 70 \\ 2.7 \times 10^{-5} PI^{1.115} & for\ PI > 70 \end{cases} \tag{1.18}$$

Where G, G_{max}, γ, PI, and $\sigma_m^{'}$ are shear modulus, maximum shear modulus, shear strain, plastic index, and effective normal stress respectively. G, G_{max}, *and* σ_m' have consistent units (typically kPa).

Kokusho (1980) investigated the behavior of gravelly soils by preparing reconstituted samples from crushed rock and round gravel. According to these results, modulus reduction occurs more rapidly in crushed rock than in soils.

Troncoso and Verdugo (1985) investigated the effect of silt content on the shear modulus of tailings sands. They found that the shear modulus reduction at a given level of shear strain increased with increasing silt content.

James (2009) used cyclic simple shear test results to estimate the shear modulus of tailings from the Laronde Mine in eastern Quebec. The tests were conducted at different mean principle effective stresses. The results show a good agreement with the G/G_{max} curve proposed by Seed et al. (1984) for clean sand.

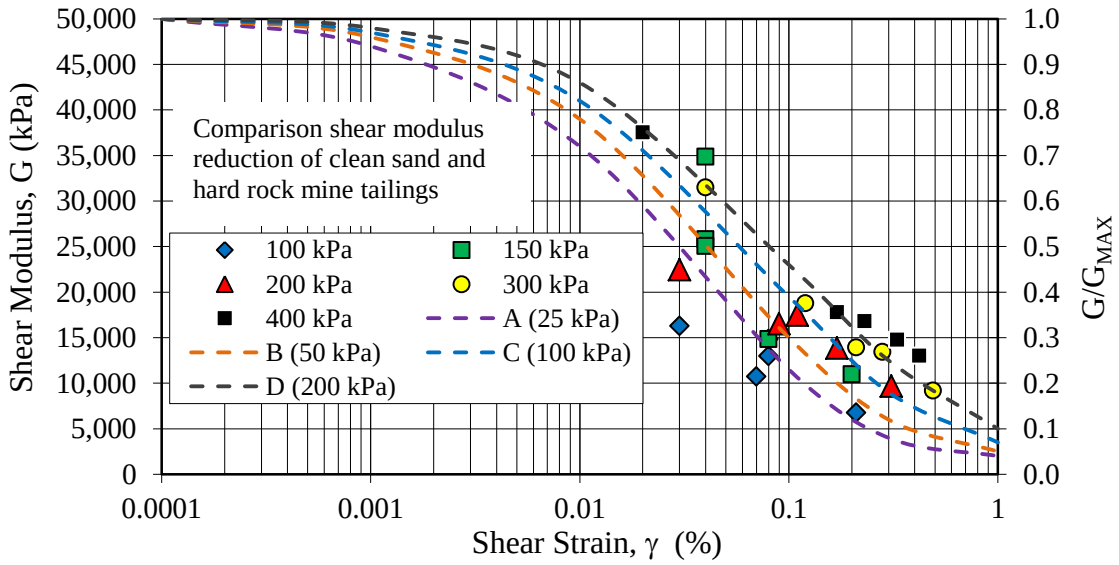

Figure 1-2: Shear moduli from CSS testing (data grouped by consolidation stress) and G/G_{MAX} curves from Seed et al. (1984) for mean effective stresses of 25, 50, 100, and 200 kPa (modified after James, 2009)

1.5.1.3 Damping ratio

Energy is dissipated during unloading-reloading cycles as a result of the permanent deformation and friction between grains of soil. This dissipated energy can be represented by the damping ratio, defined above. Energy transmission from an element to the next is reduced by the effect of damping (Kramer, 1996).

Hardin and Drnevich (1972) proposed the following relationship for the damping ratio;

$$\xi = \frac{\xi_{max} \cdot \gamma/\gamma_r}{1 + \gamma/\gamma_r} \tag{1.19}$$

where ξ_{max} is maximum damping ratio at very large strains, γ_r is calculated by eq. 1.7, and γ is shear strain. This relationship is very similar to that proposed by the same authors for the shear modulus reduction. The typical values of ξ_{max} for different soils, in percent, are given in Table 1.7.

Table 1.7: Values of ξ_{max} (after Hardin and Drnevich, 1972)

Soil type	Values of ξ_{max}
Clean dry sands	$33 - 1.5logN$
Clean saturated sands	$28 - 1.5logN$
Saturated Lick Creek silt	$26 - 4\sigma_m^{\frac{1}{2}} + 0.7f^{\frac{1}{2}} - 1.5logN$
Various saturated cohesive soils including Rhodes Creek Clay	$31 - (3 + 0.03f)\sigma_m^{\frac{1}{2}} + 1.5f^{\frac{1}{2}} - 1.5logN$

Where N is equal to number of loading cycles; f is the frequency of the applied load in cycles per second; and σ_m is mean principal effective stress in kg/cm^2.

Theoretically, there is no damping below a threshold shear strain (Kramer, 1996). However, according to experimental evidence, damping exists even at very low strains. This damping increases with increasing shear strain.

Ishibashi and Zhang (1993) presented a formula for estimating the damping ratio of plastic and non-plastic soils, which can be expressed as follows.

$$\xi = 0.333\frac{1+\exp(-0.0145PI^{1.3})}{2}\left[0.586\left(\frac{G}{G_{max}}\right)^2 - 1.547\frac{G}{G_{max}} + 1\right] \quad (1.20)$$

Where the value of $\frac{G}{G_{max}}$ is computed by equation (1.15).

Ishihara (1996) compared the effect of shear strain on damping ratio of undisturbed and reconstituted samples of gravel. These tests indicated the damping ratio of undisturbed samples was higher than that of the reconstituted samples at the same level of strain.

1.5.2 Pore water pressure generation due to cyclic loading

Seed and Lee (1966), cited by Holtz and Kovacs (1981), performed cyclic undrained triaxial testing to investigate pore water pressure generation in loose and dense sands due to cyclic loading. They prepared two samples of Sacramento River sand, one loose and the other dense. The loose sample (contractive) was isotropically consolidated to an effective confining stress of 100 kPa resulting in an initial void ratio, e_0, of 0.87 (a density index of 38%). The cyclic undrained triaxial test was done using a deviatoric stress of 39 kPa. The results of this test are shown on Figure 1-3. As shown in Figure 1-3(a), significant axial strain was not generated until the 9th cycle; between the 9th and 10th cycles, the axial strain increased dramatically, to approximately 10 percent. The pore water pressure (Figure 1-3(b)) increased gradually until the 9th cycle and then dramatically in the tenth cycle. After a few more cycles, the magnitude of the pore water pressure was equal to the effective confining stress; at this point the effective stress became zero. By this time, the axial strain exceeded 20%.

The dense sample (dilative) had an initial void ratio of 0.71 (a density index of 78%). Cyclic undrained triaxial testing was performed under an effective confining pressure of 100 kPa and a deviatoric stress of 70 kPa. The results of this test are shown on Figure 1-4. Significant axial strain did not develop until the 10th cycle or so and the pore water pressure increased gradually during this phase of the loading. After the 10th cycle, the pore water pressure increased dramatically but axial strain still increased gradually. At the 16th cycle pore water pressure reaches the initial confining pressure. As shown in Figure 1-4 (a), the value of axial strain after 20 cycles is about 5%.

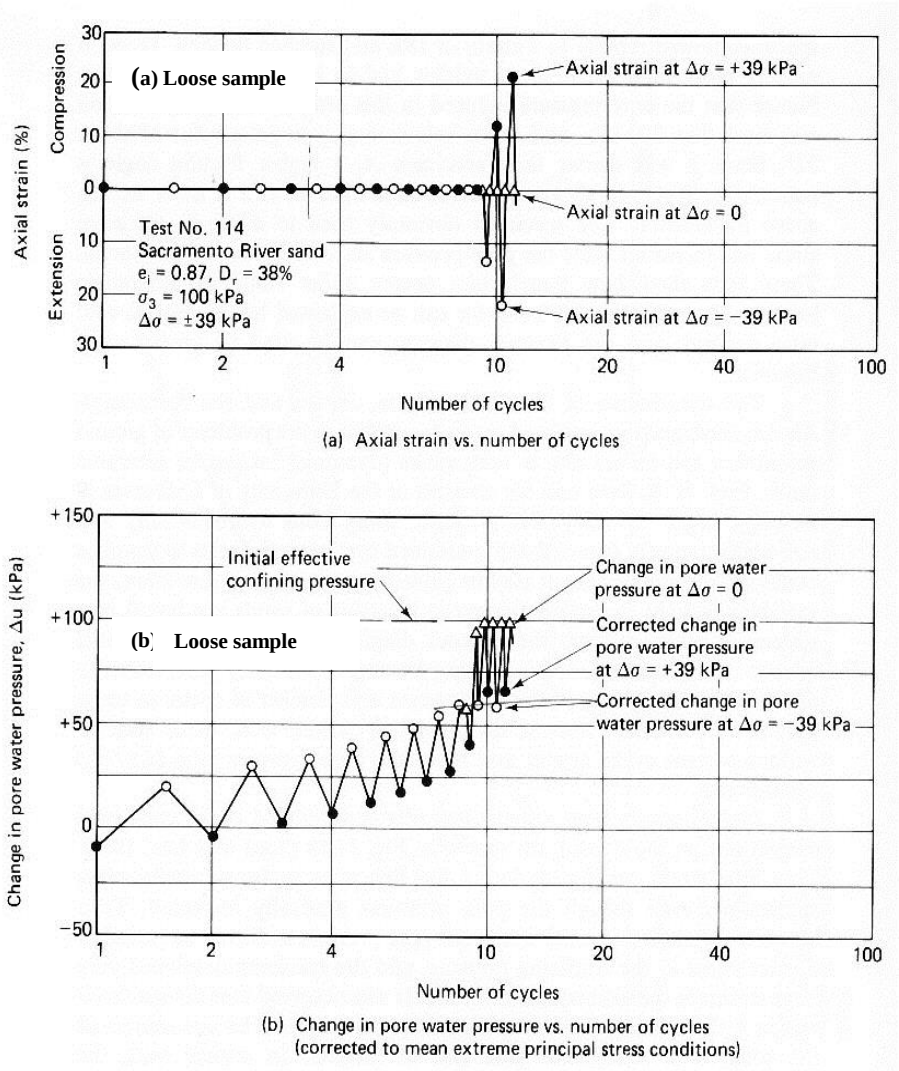

Figure 1-3: Typical cyclic triaxial compression test results on a sample of contractive sand (a) axial strain versus number of cycles (b) excess pore water pressure versus number of cycles (modified after Holtz and Kovacs, 1981)

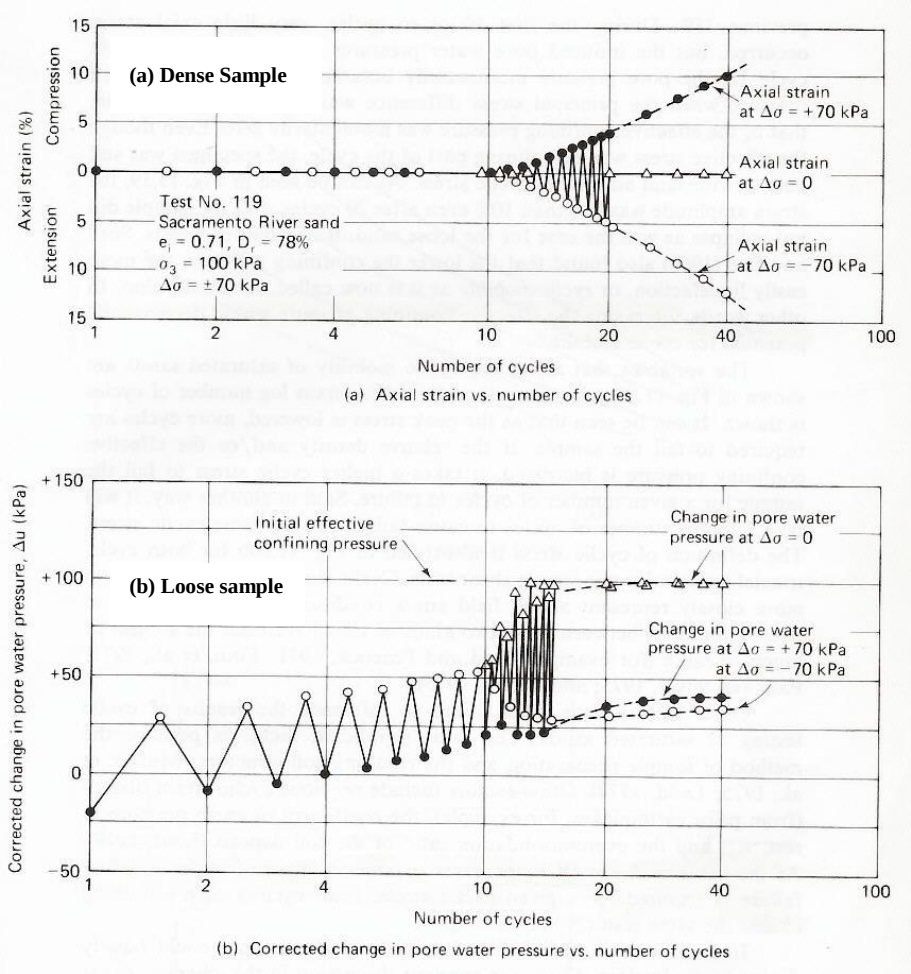

Figure 1-4: Typical cyclic triaxial compression test results on a sample of dilative sand (a) axial strain versus number of cycles (b) excess pore water pressure versus number of cycles (modified after Holtz and Kovacs, 1981)

Many researchers have developed formulas for predicting excess pore water generation due to cyclic loading. Pioneering work in this field was done by DeAlba et al. (1975). Using cyclic triaxial testing, they developed the following relationship for predicting excess pore water pressure in soils prone to liquefaction.

$$r_u = \frac{1}{2} + \frac{1}{\pi} sin^{-1}\left(2\left(\frac{N}{N_l}\right)^{1/\alpha} - 1\right) \tag{1.21}$$

Where r_u, N, and N_l are the excess pore water pressure ratio, the number of applied stress cycles, the cumulative number of cycles required to cause liquefaction respectively. Exponent α is function of the soil properties and test conditions and its average value is equal to 0.7. The excess pore water pressure ratio, r_u is equal to $\frac{\Delta u}{\sigma_{3c}^{'}}$ where $\sigma_{3c}^{'}$ is minor effective consolidation stress and Δu is excess pore water pressure generated during undrained cyclic triaxial loading.

Dobry et al. (1982) developed a relationship between the shear strain amplitude and the excess pore water pressure ratio. They performed cyclic, strain-controlled, triaxial tests on samples using different preparation methods and different initial confining pressures. Although the sample preparation methods and initial confining pressure were different, a unique relationship between the shear strain amplitude and the excess pore water pressure was obtained.

Troncoso and Verdugo (1985) showed the effect of silt content on the generation of pore water pressure in tailings sands (> 0.075 mm). According to their tests, the excess pore water pressure increases more rapidly in silty sands than in the clean sands. Also they showed that for the same excess pore water pressure increase, much larger axial deformation occurred in the silty sands relative to clean sands. In this case, the presence of silt had a significant effect on the dynamic behavior of the tailings.

Dobry and Swiger (1979), cited by Chang et al. (2007), showed that the threshold shear strain in sand is dependent on the isotropic confining effective stress (the threshold shear strain is the level of shear strain at which excess pore water pressure is initiated during cyclic loading):

$$\gamma_t = 1.33 \times 10^{-5}(\sigma^{'}) \qquad (1.22)$$

Where $\gamma_t$is in percent and $\sigma^{'}$ is in Pascals. The value of threshold shear strain based on this formula is between 0.01 and 0.04% for initial effective confining stresses between 25 and 200 kPa, respectively. The value of the threshold shear strain at 100 kPa is close to 0.01% (NRC 1985).

Chang et al. (2007) developed a field test method for predicting the in situ excess pore water pressure generation in sand due to the cyclic loading. The main feature of this method is to

capture the coupled response of the induced shear strain and generated pore water pressure due to dynamic loading. In this testing method, a vibroseis truck applies vibration vertically on a circular foundation. This vibration produces stress waves (shear, compression, and Rayleigh-type surface waves). These stress waves propagate through the instrumented area. Embedded instruments (geophones) measure the particle velocity short-time histories and miniature pore-pressure transducers measure excess pore water pressure-time histories.

A relationship between excess pore water pressure ratio (r_u), shear strain (γ), and number of loading cycles (N) was obtained from in situ measurement. According to the results of these tests, the threshold shear strain for excess pore water generation is between 3×10^{-3} and 5×10^{-3}%. This value of threshold shear strain is smaller than the typical value of 0.01% for confining pressure of 101 kPa given by Chang et al. (2007).

Chang et al. (2007) also compared the results of in situ tests with the results of strain-controlled cyclic triaxial tests performed by Dobry et al. (1982). The comparison showed that the threshold shear strain measured in situ is lower than that obtaining from the laboratory testing. Also the excess pore water pressure was generated more rapidly in the in situ tests than during the laboratory tests.

Chang et al. (2007) also compared the results of in situ testing with the relationship presented by Seed et al. (1975), and the results of strain-controlled cyclic simple shear testing on reconstituted specimens. The results of these comparisons showed that the trend of excess pore water pressure generation during the in situ testing is similar to that measured in strain-controlled cyclic testing. However, both differ significantly from the results of stress-controlled cyclic testing by Seed et al. (1975).

1.5.3 Liquefaction

After the 1964 earthquakes in Alaska USA and at Niigata in Japan, liquefaction became one of the most important research subjects in geotechnical earthquake engineering. Since then, a great deal of research has been conducted with respect to liquefaction. Although many important questions have been answered, there remain significant areas of uncertainty (Kramer, 1996).

1.5.3.1 Liquefaction and cyclic mobility

The term "liquefaction" is commonly used to refer to two related phenomena, flow liquefaction and cyclic mobility. These are described and defined below. James (2009) presented the following definitions for liquefaction and cyclic mobility that are close to other researchers' definitions, such as Holtz and Kovacs (1981), Seed and Idriss (1982), Kramer (1996), and Youd et al. (2001). According to James (2009), liquefaction can be defined as:

> "The generation of excess pore water pressure within saturated, contractive, cohesionless soil due to static or dynamic loading, sufficient to bring the soil to the steady state condition or a condition of zero (or very low) effective stress that could result in excessive deformation under gravity or external loading."

Cyclic mobility is defined as (James, 2009):

> "The generation of excess pore water pressure and limited deformation within a saturated, dilative, cohesionless soil caused by dynamic loading."

Based on Idriss and Boulanger (2011), following four conditions are associated with liquefaction:

- An excess pore water ratio,r_u, that reaches 100%.
- Shear strains that exceed a specific amount (3%, 7.5%, etc.).
- Manifestations like settlements, cracking, spreading, or boiling are observed at the surface.
- The shear stresses are more than shear strength required for static stability.

In this research, the term "liquefaction" will refer to the occurrence of flow liquefaction in contractive tailings, and "cyclic mobility" will refer to the development of excess pore water pressures in dilative tailings.

1.5.3.2 Liquefaction susceptibility

There are different methods for evaluating liquefaction susceptibility potential. Two main methods (pedological and state criteria) are described in the following (Kramer, 1996):

Pedological criteria

In the past, it was considered that only sands were susceptible to liquefaction. However, it has been shown that silts and clays of very low plasticity (as defined by plasticity index) are also susceptible to liquefaction (Kramer, 1996). Clays with sufficient plasticity (high cohesion) are not susceptible to liquefaction, though they may be susceptible to softening under seismic loads (Kramer, 1996).

Most gravels are not subject to liquefaction, but may undergo cyclic mobility (Coulter and Migiaccio, 1966, Kramer, 1996).

State criteria

Casagrande (1936), performed drained static, triaxial tests on loose and dense specimens of sand. He showed that when specimens of loose (contractive) and dense (dilative) sand are sheared under the same constant effective confining stress, the specimens reach a condition where the volumes and the shear stresses are both constant and the strain is unlimited. Under this condition, the void ratios of the specimens were approximately the same. The value of the void ratio under this condition is known as the critical void ratio, e_c. This state where the specimens underwent "unlimited" strain at a constant shear stress, constant volume and constant effective confining stress is known as the steady state condition, or the critical state condition (Castro, 1975; Castro and Polous, 1977). For a given soil, the void ratio and the shear stress associated with the steady state condition vary with the effective confining stress. The locus of these points (steady state points) in three-dimensional space e-p'-q is called the steady state line (SSL) (Kramer, 1996).

The initial state of a soil (initial stresses and density) is an important factor in evaluating its susceptibility to liquefaction or cyclic mobility. Soils that are susceptible to liquefaction based on pedological criteria may not be susceptible to liquefaction based on state criteria. These soils are, however, susceptible to cyclic mobility.

The potential for the occurrence of liquefaction or cyclic mobility depends on the initial state of the soil. Therefore any susceptibility criterion must consider the initial state of the soil.

The liquefaction susceptibility of a soil may be evaluated using the steady state line (SSL line) criterion. If the initial state of a soil is above the SSL (usually expressed in the e-log p' plane,

where p' is mean effective stress) it is susceptible to liquefaction but if its initial state is below the SSL, it is susceptible to cyclic mobility. The location and slope of the SSL are dependent on the gradation and angularity of a soil (Kramer, 1996).

1.5.4 Post liquefaction strength of soils

Accurate estimation of shear strength of liquefied soil is necessary for evaluating liquefaction induced instability. In the following, three different methods for estimating the steady state shear strength of soil will be described. One of the methods is based on undisturbed sampling of soil and determination of the steady state shear strength in the laboratory. The second method is based on in situ testing and the third method is based on a normalized strength approach. More details are provided by Kramer (1996) and Idriss and Boulanger (2008).

1.5.4.1 Laboratory testing approach: steady-state strength.

According to Idriss and Boulanger (2008), "The term 'critical state' refers to the conditions that exist in sand when it is being sheared continuously and no further changes in volume or stress are occurring; it is described by the critical-state line (CSL), which represents all possible combinations of void ratio and confining stress at the critical state. The term 'steady state' refers to the critical-state condition with the additional requirement of a constant rate of deformation". The steady state of soil is function of its density. Other parameters, such as the stress path, affect steady state but the effect of density is the most important. Therefore, sampling of cohesionless soil for laboratory determination of the steady state relationship of soils should be done with a minimum amount of disturbance. After sampling of the cohesionless soil, samples are consolidated in the laboratory to a stress states equivalent to the in situ conditions. The samples are then subjected to undrained static triaxial testing to determine the steady state shear strength of soil (S_{su}). Due to sampling, transportation, handling, and consolidation, it is virtually impossible to obtain completely undisturbed samples. Therefore, Poulos et al. (1985) proposed a procedure for correcting the steady state shear strength of soil measured in the laboratory (Kramer, 1996).

1.5.4.2 In situ testing approach: residual strength.

Seed and Harder (1990) and Stark and Mesri (1992) recommend using the back calculation method for the steady state shear strength of soil based on SPT testing. In the SPT test, a standard hammer is driven to earth at the bottom of a borehole, 30 to 40 blows per minute with a 63.6 kg hammer released from a height of 76 cm. The number of blows required to drive the sampler 30 cm in a soil is defined as the standard penetration resistance, N. N value is often normalized to overburden pressure of 1 ton/m^2 (100 kPa) and is corrected to an energy ratio 60% (named $(N_1)_{60}$) and other factors. SPT also is corrected to consider the effect of fines as follows (Kramer, 1996):

$$(N_1)_{60-cs} = (N_1)_{60} + N_{corr} \tag{1.23}$$

Where the value of N_{corr} can be taken from Table 1.8. The residual undrained shear strength is computed from Figure 1-5 based on equivalent clean sand SPT.

Table 1.8: Recommended Fines Correction for Estimation of Residual Undrained Strength by Seed-Harder and Stark-Mesri Procedures (after Kramer, 1996)

	N_{corr}(blows/ft)	
Percent Fines	Seed-Harder	Stark-Mersi
0	0	0
10	1	2.5
15	---	4
20	---	5
25	2	6
30	---	6.5
35	---	7
50	4	7
75	5	7

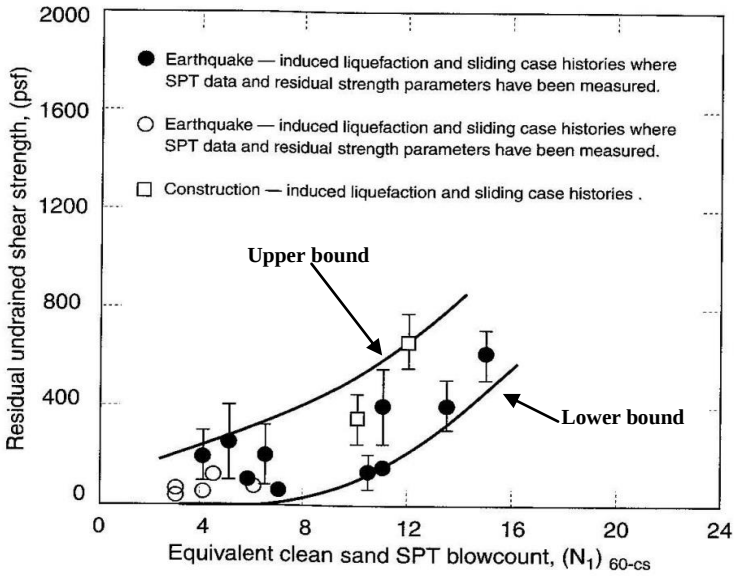

Figure 1-5: Relationship between residual strength and corrected SPT resistance. (modified after Seed and Harder, 1990)

1.5.4.3 Normalized strength approach: residual strength ratio.

Different researchers presented different formula for computing the residual shear strength (S_r), the value of soil strength in steady state condition, from the initial effective in situ strength of soil :

Vasquez-Herrera et al. (1990), proposed the following formula for computing the residual shear strength of reconstituted silty sand from Lower San Fernando Dam.

$$\frac{S_r}{\sigma_{v0}^{'}} \approx 0.12 \qquad (1.24)$$

where S_r is the residual shear strength and $\sigma_{v0}^{'}$ is the initial vertical effective stress.

Byrne et al. (1993) proposed the following formula for estimating the residual shear strength based on frozen and cored samples from the Duncan Dam site.

$$\frac{S_r}{\sigma_{v0}^{'}} \approx 0.21 \tag{1.25}$$

Castro and Troncoso (1989) used vane shear testing to measure the residual shear strength of very loose slimes (I_P=20 to 22) at three different tailing dams in Chile:

$$\frac{S_r}{\sigma_{v0}^{'}} \approx 0.07, 0.11, and\ 0.08 \tag{1.26}$$

The above mentioned values are for different tailings.

Finn et al. (1991) measured the residual shear strength of a clayey silt in the foundation of Sardis Dam by vane shear testing:

$$\frac{S_r}{\sigma_{v0}^{'}} \approx 0.075 \tag{1.27}$$

Stark and Mesri (1992) presented the following formula for computing residual shear strength of soil using the corrected, clean sand SPT blow count:

$$\frac{S_r}{\sigma_{v0}^{'}} = 0.0055(N_1)_{60-cs} \tag{1.28}$$

Ishihara (1993) stated that if loose sand with a large initial confining pressure is sheared, after the peak, the behavior changes from contractive to dilative. This point is called phase transformation point. The mobilized shear strength of the soil at this point is less than its steady state strength. This is called quasi-steady state point (QSS). If loose sand is brought to the QSS point during seismic loading, it may undergo large deformations. Therefore, the shear strength at

QSS may be considered to be equivalent to the residual shear strength (S_r) for the stability analysis in practical problems (Ishihara, 1993).

Wijewickreme et al. (2005a) conducted cyclic direct simple shear tests on undisturbed and reconstituted samples of tailings from copper-gold-zinc mine. The results of testing show that $S_{u\text{-}PC}/\sigma'_{vc}$ (ratio of post cyclic maximum shear strength to effective normal stress) varies between 0.130 to 1.070 with an average value of 0.343.

Using post-cyclic testing of five samples of non-plastic tailings from a gold mine in the province of Quebec, James et al. (2011) measured $S_{u\text{-}PC}/\sigma'_{vc}$ values of approximately 0.11.

Idriss and Boulanger (2008) proposed the following formula for computing the normalized residual shear strength of sands and silty sands based on the SPT values for two different conditions. According to Idriss and Boulanger (2008), the first condition assumes that the void redistribution does not occur after shaking. For this condition, the formula based on the SPT is as follows:

$$\frac{S_r}{\sigma'_{v0}} = exp\left(\frac{(N_1)_{60cs-Sr}}{16} + \left(\frac{(N_1)_{60cs-Sr} - 16}{21.2}\right)^3 - 3.0\right) \times \left(1 + exp\left(\frac{(N_1)_{60cs-Sr}}{2.4} - 6.6\right)\right) \leq tan\phi' \quad (1.29)$$

Where S_r, σ'_{vc}, and ϕ' are residual shear strength, effective normal stress, and effective friction angle respectively. The value of $(N_1)_{60cs-Sr}$ is computed as follows

$$(N_1)_{60cs-Sr} = (N_1)_{60} + \Delta(N_1)_{60-Sr} \quad (1.30)$$

Where $(N_1)_{60}$ is the corrected value of SPT. The value of $\Delta(N_1)_{60-Sr}$ is computed from Table 1.9.

Table 1.9: Values of $\Delta(\mathrm{N_1})_{60-\mathrm{Sr}}$ recommended by Seed (1987) (after Idriss and Boulanger, 2008)

Fine content	$\Delta(N_1)_{60-Sr}$
10	1
25	2
50	4
75	5

Void redistribution occurs after an earthquake when pore water dissipation cannot occur because sometime a non-permeable layer of soil overlies the liquefied soil layer and prevents pore water pressure dissipation. Therefore water stays between these two layers and causes a void redistribution. The formula for computing the normalized residual shear strength of sands and silty sands for conditions that void redistribution occurs after an earthquake is:

$$\frac{S_r}{\sigma_{v0}^{'}} = exp\left(\frac{(N_1)_{60cs-Sr}}{16} + \left(\frac{(N_1)_{60cs-Sr} - 16}{21.2}\right)^3 - 3.0\right) \leq tan\phi^{'} \qquad (1.31)$$

where all the parameters are the same as for formula (1.29).

1.6 Evaluation of liquefaction resistance of granular soil

Fundamental work on the evaluation of the liquefaction resistance of soils was done by Seed and his collaborators at the University of California, Berkley after severe earthquakes caused extensive damage in Alaska (U.S.) and Niigata (Japan) in 1964. Over the years, different methods have been developed for the evaluation of liquefaction. The most important techniques are the *cyclic stress approach* and *cyclic strain approach.* These two techniques, like other techniques, have their advantages and disadvantages and are explained in the following sections.

In the following sections, liquefaction evaluation methods explained by Kramer (1996), Youd et al. (2001), Idriss and Boulanger (2008) and other researchers have been summerized.

1.6.1 Cyclic stress approach

Pioneering work on the evaluation of the initiation of liquefaction and the determination of the liquefaction susceptibility of soils was performed by Seed and Lee (1966) and Seed and Idriss (1971), who developed the cyclic stress approach. In this method, the initiation of liquefaction is related to uniform cyclic shear stress amplitude and an equivalent number of cycles of loading. Liquefaction is initiated when the cyclically-induced excess pore water pressure is equal to the initial effective stress in soil, i.e an excess pore water pressure ratio, $r_u(=\frac{\Delta u}{\sigma_v'})$, of 1.0 (Seed and Lee, 1966).

1.6.1.1 Characterization of earthquake loading.

Earthquake-induced shear stresses have irregular patterns, while most liquefaction evaluations assume uniform cycles of shear stress, making direct comparison of the two loadings difficult. For comparison, the earthquake-induced irregular shear stresses are assumed to be equivalent to uniform cyclic stresses with an equivalent number of cycles of loading. For the sake of this conversion, the amplitude of the equivalent cyclic stresses is assumed to be equal to 65% of the maximum shear stress induced by the earthquake and the number of equivalent cycles is a function of the earthquake magnitude, as shown in Figure 1-6.

For a level or gently sloping ground, the equivalent uniform cyclic shear stress is computed as follows (Seed and Idriss, 1971).

$$\tau_{cyc} = 0.65\frac{a_{max}}{g}\sigma_v r_d \tag{1.32}$$

Where a_{max}, g, σ_v, and r_d are the peak (horizontal) ground acceleration, the acceleration due to gravity, the total vertical stress, and the stress reduction factor, respectively. Idriss and Boulanger (2008) explained the reason for selecting of 0.65 τ_{max} as amplitude of the uniform shear stress cycles, "The choice of 0.65 to represent a reference stress level is somewhat arbitrary, but it was selected in the beginning of the development of liquefaction evaluation procedures in 1966 and has been in use ever since. More importantly, the overall liquefaction evaluation procedure

would be essentially unaffected by the choice of a different reference stress ratio, provided that the adjustment factors for the duration of shaking and the empirically derived liquefaction correlations were all derived for that reference stress."

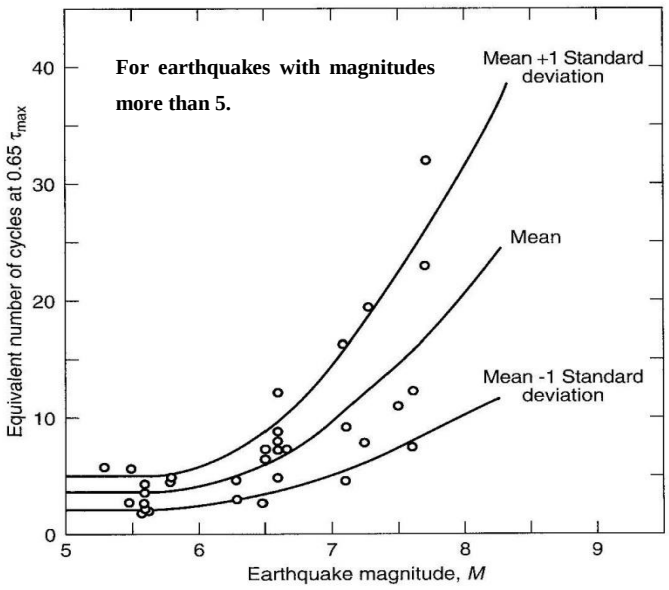

Figure 1-6: Number of equivalent uniform stress cycles, N_{eq}, for earthquakes of different magnitudes (Richter) (modified after Seed et al., 1975)

If the soil column above depth z is considered as a rigid body, the maximum shear stress at the base of this column is defined as product of its mass ($\frac{\gamma.z}{g}$) and maximum horizontal surface acceleration (a_{max}). where γ is unit weight of the soil and g is gravity acceleration. This maximum shear stress can thus be expressed as follows (Idriss and Boulanger, 2008)

$$(\tau_{max})_r = \frac{\gamma.z}{g} a_{max} \tag{1.33}$$

where subscript 'r' means rigid column. In reality, the soil column behaves as a deformable body. Therefore, the maximum shear stress at the base of the column is different from the maximum shear stress at the base of a rigid column. The ratio of maximum shear stress at base of

a deformable column to maximum shear stress at the base of a rigid body is defined as a shear stress reduction coefficient (r_d), which can be defined as follows (Idriss and Boulanger, 2008)

$$r_d = \frac{(\tau_{max})_d}{(\tau_{max})_r} \tag{1.34}$$

Youd et al. (2001) recommended the following formula proposed by Liao and Whitman (1986) for computing r_d

$$r_d = 1.0 - 0.00765z \ \ for\ z \leq 9.15\ m \tag{1.35a}$$

$$r_d = 1.174 - 0.0267z \ \ for\ 9.15 < z \leq 23\ m \tag{1.35b}$$

where z is equal to depth below ground surface in meters.

Seismic load is also characterized using the CSR (cyclic stress ratio) defined as the ratio of uniform cyclic shear stress (τ_{cyc}) to initial effective normal stress (σ'_{v0}). CSR is used to represent the dynamic loading of earthquake and cyclic laboratory tests.

1.6.1.2 Characterization of liquefaction resistance

Characterization based on laboratory tests.

The proposed relationship between the CSR in triaxial and the CSR in simple shear testing is (Seed et al. 1975):

$$(CSR)_{ss} = c_r(CSR)_{tx} \tag{1.36}$$

Where c_r is an empirical correction factor and its value may be estimated from Table 1.10, where K_0 is the ratio of the vertical and horizontal effective consolidation stresses applied in triaxial testing (at rest condition).

According to Seed et al. (1975), the CSR required in the field to produce initial liquefaction is 90% of the CSR from unidirectional cyclic shear tests; therefore:

$$(CSR)_{field} = \frac{\tau_{cyc}}{\sigma'_{v0}} = 0.9\ (CSR)_{ss} = 0.9 c_r (CSR)_{tx} \quad (1.37)$$

Table 1.10: Values of CSR Correction Factor, c_r (see eq. 1.37)(after Kramer, 1996)

References	Equation	$C_r\ for$:	
		$K_0 = 0.4$	$K_0 = 1.0$
Finn et al. (1971)	$C_r = (1 + K_0)/2$	0.7	1.0
Seed and Peacock (1971)	Varies	0.55-0.72	1.0
Castro (1975)	$C_r = 2(1 + 2K_0)/3\sqrt{3}$	0.69	1.15

The cyclic stress ratio that causes liquefaction in a specified numbers of cycles is defined as the cyclic resistance ratio of the soil (CRR). Boulanger and Idriss (2004) and Idriss and Boulanger (2008) proposed a the relationship between CRR and number of equivalent uniform cycles of loadings, N, expressed as follows

$$CRR = a.N^{-b} \quad (1.38)$$

where ‘a’ is equivalent to the cyclic shear stress ratio that causes liquefaction with one cycle. Factors like the method of deposition, density index, overconsolidation, and ageing affect the value of ‘a’ (Idriss and Boulanger, 2008).

James et al. (2011) reported that “a lower ‘b’ value (constants in equation 1.38) indicates that the cyclic shear resistance is more strongly influenced by larger amplitude cycles” (Boulanger and Idriss, 2004). The value of exponent ‘b’ for clean sand is typically close to 0.34 and close to 0.14 for clay (Idriss and Boulanger, 2008).

Laboratory characterization of the liquefaction resistance of hard rock tailings

Several researchers, such as Mittal and Morgenstern (1975), Ishihara et al. (1980, 1981), Garga and Mckay (1984), Troncoso and Verdugo (1985), Troncoso (1986), Wijewickreme et al. (2005a), Al-Tarhouni (2011), and James et al. (2011), have evaluated the cyclic resistance of tailings based on cyclic direct simple shear or cyclic triaxial tests. These investigations are described in the following section.

Ishihara et al. (1980, 1981) performed cyclic triaxial tests on undisturbed tailings samples from 7 different tailings impoundments in Japan and Chile (Quartz slime, El Cobre old dyke slime, El Cobre No.4 dyke, Disuputada in Chile, Michikoshi skime, Kosaka slime, Fukutobe). All the samples (fine and coarse grain) were retrieved using a thin-walled tube sampler to obtain relatively undisturbed samples. After performing cyclic triaxial tests on these samples, the samples were blended with water and then poured to a mould to prepare reconstituted samples. Then cyclic triaxial test was conducted on the reconstituted samples. The results of these showed that the cyclic shear resistance of the reconstituted samples is smaller than that of the undisturbed samples.

Garga and McKay (1984) collected the results of the cyclic testing on samples from 20 tailings and 13 non-tailings materials from Canada, Chile, Japan, and the USA. The materials were classified as tailings sands, tailings slimes, non-tailings natural sands, and non-tailings natural fines. They plotted the cyclic shear stress (CSR) versus the number of required cycles to cause liquefaction. For the sake of comparison, they normalized the CSR of the tailings sands and the non-tailings sands to the cyclic stress ratio of sand with a density index I_D of 50% percent. However, according to ASTM standard, if more than 12% of the sand consists of fines, the concept of relative density (density index) is not relevant (Garga and McKay, 1984). In this case, it was used for tailings with up to 40% fines. Garga and McKay (1984) explained the reason for using the relative density for tailings sands with up to 40% fines:

- The origin, grain shape, texture, and hardness of the fine tailings are similar to coarse grain tailings.
- The plasticity index of tailings with fine percent of up to 40% is approximately zero (or negligible).

Garga and McKay (1984) included the following observations from the results of the collected data on the tailings and non-tailings samples.

- Tailings sands have a narrow range of cyclic shear strength behavior, when normalized to a relative density I_D= 50%. A relatively small scatter is seen for non-tailings sands. The results showed that the cyclic shear strength of non-tailings sands is larger than that of tailings sands. Also, the cyclic shear strength of reconstituted samples is less than that of undisturbed samples.
- As mentioned in above, the cyclic shear strength of non-tailings sands is more than that of tailings sands. Also a wide range of strength is shown for these types of tailings due to the wide range of origin, grain size, structure, and stress history.
- There is no appreciable difference between the cyclic shear strength of tailings slimes and non-tailings fine materials (although the clay fraction can change this result).

Garga and McKay (1984) showed that fine sands with a D_{50} (size corresponding to 50% passing by mass) from 0.1 to 0.3 mm generally exhibit the lowest cyclic shear strength behavior. Also in the fine sand range (D_{50} from 0.1 to 0.3 mm), non-tailing sands have a greater cyclic shear strength than that of tailings sands.

Troncoso and Verdugo (1985) and Troncoso (1986) investigated the effect of silt content on the cyclic shear resistance and critical state of tailings materials, using triaxial compressive and cyclic triaxial testing. They showed that for tailings with the same void ratio, increasing the silt content decreases the cyclic shear resistance. Also at the same confining stress and void ratio, the cyclic shear resistance of clean tailings sand was 2.7 times greater than tailings with 30 percent silt content.

Additionally, tailings sands with higher silt contents have lower liquefaction resistance relative to clean tailings sands (no fines). The effect of silt on the liquefaction susceptibility of sands will be discussed in details in the following sections.

Wijewickreme et al. (2005a) performed constant volume cyclic direct simple shear testing on samples from fine-grained laterite, copper-gold, and copper-gold-zinc tailings. The samples of laterite and copper-gold tailings were undisturbed but the samples of copper-gold-zinc tailings were both undisturbed and reconstituted. Fine-grained laterite samples consisted of silts and

clayey silts with relatively high specific gravities and plasticity indices compared to the copper-gold and copper-gold-zinc tailings. After consolidation of the samples to vertical effective stresses higher than the vertical in situ effective stresses, the cyclic sinusoidal shear loads were applied at uniform cyclic stress ratio amplitudes, at a load frequency of 0.1 Hz. They postulated that liquefaction was triggered at a shear strain equal to 3.75% in CDSS (cyclic direct simple shear) testing, which is equivalent to 2.5% axial strain in cyclic triaxial testing.

The results of CDSS tests on laterite tailings for two different confining stresses, 100 and 200 kPa, showed that the cyclic shear resistance of laterite tailings increases with the effective confining stress. This is contrary to test results that have been obtained by others (e.g. Seed, 1983; Marcuson et al., 1990; Boulanger and Idriss, 2004; Idriss and Boulanger, 2008).

The results of CDSS testing on the samples from copper-gold-zinc tailings indicate that the effective confining stress and initial relative density do not significantly influence the cyclic shear strength of these tailings.

James et al. (2011) performed CDSS testing on samples from a gold hard rock mine located in western Quebec. The samples, non-plastics silt and sand, were prepared as slurries and then consolidated to vertical effective stresses of 100 to 400 kPa. The CDSS tests were performed with cyclic stress ratios, CRS, values between 0.075 and 0.15.

The samples were loaded by symmetrical, unidirectional, and sinusoidal cyclic shear stress with frequency of 0.1 Hz under constant-volume conditions. The CRR values of the samples were based on a shear strain of 3.75% for the initiation of liquefaction.

The results of these tests indicated that the behavior of the specimens under CDSS test is consistent with saturated, cohesionless, contractive sands under cyclic loading (James et al., 2011). Also they showed that for a given value of CSR, the cyclic shear resistance is not affected significantly by a variation of the confining effective. The effect of confining stress on the cyclic shear resistance of tailings and soils will be reviewed in the following sections.

Based on test results, James et al. (2011) developed the following relationship for CRR (cyclic shear resistance) and number of cycles for liquefaction initiation, N:

$$CRR = 0.15N^{-0.19} \tag{1.39}$$

Also, James et al. (2011) showed that tailings with a high percentage of fines or made entirely of fines have a cyclic shear resistance that is comparable with the cyclic shear resistance of clean sands of similar density index.

Al-Tarhouni et al. (2011) performed CDSS tests on two types of specimens prepared by wet and dry-wet methods. The samples were of thickened gold tailings. The CDSS tests were done under constant-volume conditions with sinusoidal shear stresses. The amplitude of shear stress varied between 0.075 and 0.15. Like James et al. (2011) and Wijewickreme et al. (2005a), they considered 3.75% shear strain as initiation of liquefaction.

The results of their tests show that the effective consolidation stress did not have a significant influence on the CRR of these types of tailings. Also, the CRR of these tailings was dependent to the void ratio after consolidation.

Al-Tarhouni et al. (2011) also showed that the desiccation and shrinkage of tailings can increase the in CRR. This may be due to overconsolidation caused by matric suction. Based on their results, when the samples are dried beyond the shrinkage limit, the CRR did not increase probably because there was no further increase in the effect of matric suction (Al-Tarhouni et al., 2011). They showed that the samples made by the dry-wet method were more resistant to liquefaction than those prepared by the wet method (dry and wet sample preparation techniques are described by Ishihara 1996). Also, they showed that dried samples with water contents of 13, 16, and 19% had similar cyclic resistance ratio.

Characterization based on tield tests.

Laboratory testing is not completely representative of the in situ behavior of soils and tailings, in part because the retrieval of samples causes disturbance. To obtain undisturbed samples, special methods like freezing should be used, but these techniques are expensive and they are not commonly used except for critical projects. To avoid the above mentioned difficulties, methods to evaluate the liquefaction potential based on in situ testing have become state-of-practice (Youd et al., 2001). These main methods are described in below (based on Youd et al., 2001).

Several methods, commonly used are based on the standard penetration test (SPT), the cone penetration test (CPT), the shear wave velocity measurement (V_s) . The primary advantages and disadvantages of each method are given in Table 1.11.

Table 1.11: Comparison of advantages and disadvantages of various field tests for assessment of liquefaction resistance (After Youd et al., 2001)

	Test Type		
Feature	SPT	CPT	V_s
Past measurements at liquefaction sites	Abundant	Abundant	Limited
Type of stress-strain behavior influencing test	Partially drained, large strain	Drained, large strain	Small strain
Quality control and repeatability	Poor to good	Very good	Good
Detection of variability of soil deposits	Good for closely spaced tests	Very good	Fair
Soil types in which test is recommended	Nongravel	Nongravel	All
Soil sample retrieved	Yes	No	No
Test measures index or engineering property	Index	Index	Engineering

Standard penetration test (SPT).

The SPT test is the most common field test that is used for the evaluation of liquefaction. Figure 1-7 shows the value of CRR versus $(N_1)_{60}$ for sands with different fines content for a reference earthquake of magnitude 7.5. $(N_1)_{60}$ is the SPT blow count normalized to an overburden pressure of approximately 100 kPa, a hammer energy ratio of 60% and other factors. The points above the plotted curves show the region where liquefaction is likely. In the region below these curves, liquefaction is unlikely. The curve of CRR versus $(N_1)_{60}$ for fines content <5% is called the "SPT clean-sand base curve".

The CRR for earthquakes of different magnitudes is corrected by a scaling factor that will be defined later.

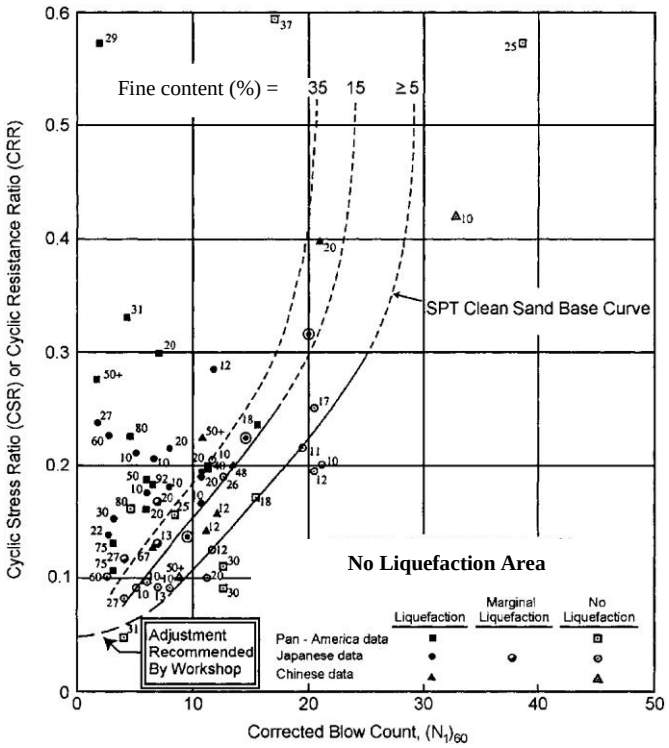

Figure 1-7: SPT Clean-Sand base curve for magnitude 7.5 earthquakes with data from liquefaction case histories (taken from Youd et al., 2001- modified from Seed et al., 1985)

SPT clean-sand base curve.

The initial SPT clean-sand base curve proposed by Seed et al. (1985) passed through origin in Figure 1-7. Youd et al. (2001) modified this curve to intersect the CRR axis at 0.05 as shown in Figure 1-7. This change represents a limit the CSR below which liquefaction is not likely to occur.

Youd et al. (2001) recommended the following formula for the clean-sand base curve:

$$CRR_{7.5} = \frac{1}{34 - (N_1)_{60}} + \frac{(N_1)_{60}}{135} + \frac{50}{[10.(N_1)_{60} + 45]^2} - \frac{1}{200} \qquad (1.40)$$

This equation is valid for $(N_1)_{60}$ <30. Equation (1.40) is the solid curve in Figure 1-7. For large N values, the sand is considered to be too dense and does not liquefy (Youd et al., 2001).

Influence of fines content.

Much research has been done on the effect of the fines content on the liquefaction resistance of soils. As mentioned in previous sections, Troncoso and Verdugo (1985) and Troncoso (1986) showed that at the same initial void ratio the cyclic resistance ratio decreases with increasing silt content. Seed et al. (1985) showed that the cyclic resistance of soil increases with fines content. These research results, along with results of others, show seemingly contradictory results (Kuerbis et al., 1988; Koester, 1994; Thevanayagam and Mohan, 1998; Thevanayagam et al., 2000; Naeini and Baziar, 2004; Chien et al., 2002, James et al., 2011).

Polito and Martin (2001) suggested that choosing different bench marks like void ratio, relative density, penetration resistance, and sand skeleton void ratio for comparison is the reason behind this apparent contradiction. They performed 300 undrained cyclic shear tests on specimens of sands, nonplastic silty sands, and nonplastic silts. Based on their test results, there is critical silt content beyond which cyclic behavior of silty sands changes. Up to this limit, the cyclic behavior is controlled by sand to sand interaction, beyond this limit the cyclic resistance of the soil is controlled by the density index and is independent from silt content. The effect of the density index is then significantly reduced. The cyclic shear strength of the soil with sand to sand interaction is greater than that of soil with silt to silt interaction at the same relative density. Additionally, the presence of silt tends to decrease the penetration resistance (Seed and Idriss, 1970a). More research is required with respect to the relationship between the fines content, nature of fine content (plastic or non-plastic), the liquefaction resistance, and penetration resistance.

Seed et al. (1985) developed CRR curves for different fines content as shown in Figure 1-7. Youd et al. (2001) recommended a method developed by I. M. Idriss with assistance of R. B. Seed for considering influence of fines on the CRR. The method corrects the value of $(N_1)_{60}$ to an equivalent clean sand value, $(N_1)_{60cs}$, as follows:

$$(N_1)_{60-cs} = \alpha + \beta(N_1)_{60} \quad (1.41)$$

Where α and β are coefficients that are determined from

$$\alpha = 0 \; for \; FC \leq 5\% \quad (1.42a)$$

$$\alpha = \exp\left[1.76 - \left(\frac{190}{FC^2}\right)\right] \quad for \; 5\% < FC < 35\% \quad (1.42b)$$

$$\alpha = 5.0 \; for \; FC \geq 35\% \quad (1.42c)$$

$$\beta = 1.0 \; for \; FC \leq 5\% \quad (1.43a)$$

$$\beta = \left[0.99 + \left(\frac{FC^{1.5}}{1000}\right)\right] \; for \; 5\% < FC < 35\% \quad (1.43b)$$

$$\beta = 1.2 \; for \; FC \geq 35\% \quad (1.43c)$$

where FC in above formulae shows fine content. Based on Ulrich and Hughes (1994) and James (2009), it can be I inferred that hard rock tailings behave like clean sands with respect to their shear strength and penetration resistance. Therefore applying correcting factor for considering the effect of fine content may result in over-estimation of cyclic resistance of tailings (James et al., 2011).

Other corrections.

Table 1.12 shows several factors that influence the value of SPT.

Table 1.12: Corrections to SPT (Modified from Skempton 1986) as listed by Robertson and Wride (1998)

Factor	Equipment variable	Term	Correction
Overburden pressure	—	C_N	$(P_a/\sigma'_{vo})^{0.5}$
Overburden pressure	—	C_N	$C_N \leq 1.7$
Energy ratio	Donut hammer	C_E	0.5–1.0
Energy ratio	Safety hammer	C_E	0.7–1.2
Energy ratio	Automatic-trip Donut-type hammer	C_E	0.8–1.3
Borehole diameter	65–115 mm	C_B	1.0
Borehole diameter	150 mm	C_B	1.05
Borehole diameter	200 mm	C_B	1.15
Rod length	<3 m	C_R	0.75
Rod length	3–4 m	C_R	0.8
Rod length	4–6 m	C_R	0.85
Rod length	6–10 m	C_R	0.95
Rod length	10–30 m	C_R	1.0
Sampling method	Standard sampler	C_S	1.0
Sampling method	Sampler without liners	C_S	1.1–1.3

The following equation incorporates the available factors (Table 1.12) as follows (Youd et al., 2001)

$$(N_1)_{60} = N_m C_N C_E C_B C_R C_S \tag{1.44}$$

Where N_m, C_N, C_E, C_B, C_R, C_s are the measured standard penetration resistance, a factor to normalize N_m to a common reference effective overburden stress (of 100 kPa), a correction for the hammer energy ratio, a correction factor for the borehole diameter, a correction factor for rod length, and a correction factor for samplers with or without liners, respectively.

The measured value of N in the SPT test increases with an increase of the effective overburden pressure. Therefore an overburden correction factor must be applied to the value of *N* (Seed and Idriss, 1982). Youd et al. (2001) recommend using the formula proposed by Liao and Whitman (1986) for the overburden correction factor:

$$C_N = (P_a/\sigma'_{vo})^{0.5} \tag{1.45}$$

Where C_N normalizes the N_m to an effective overburden pressure equal to 100 kPa (P_a). According to Youd et al. (2001), the value of C_N should not be more than 1.7. Kayen et al. (1992) proposed the following formula for C_N

$$C_N = \frac{2.2}{1 + \sigma'_{vo}/P_a} \tag{1.46}$$

Based on this formula, the value of C_N is limited to 1.7. The σ'_{vo} should be the value of effective overburden pressure in the time of drilling (Youd et al., 2001).

According to Youd et al. (2001), Equation (1.45) is suitable for use to overburden pressure of up to 200 kPa. For an effective overburden pressure equal to 300 kPa, they suggest using Equation (1.46). They do not recommend Equations (1.45) and (1.46) for an effective overburden pressures greater than 300 kPa. This pressure corresponds to a depth greater than the depth whose the simplified method is applicable.

A correction factor for hammer energy is also applied. For all U.S. testing practice, the average of 60% is generally accepted by all researchers (Youd et al., 2001).

Magnitude scaling factor (MSF).

All the liquefaction evaluation methods described above (SPT, CPT, and V_s) are for an earthquake with a magnitude of 7.5. For scaling the cyclic resistance of the soils for earthquakes of other magnitudes, Seed and Idriss (1982) introduced the scaling factor (MSF), based on the CSR:

$$MSF = \left(\frac{CSR}{CRR_{7.5}}\right) \tag{1.47}$$

where CSR is the calculated cyclic shear stress ratio generated by the earthquake shaking of interest, and $CRR_{7.5}$ is the cyclic resistance ratio for a magnitude 7.5 earthquake (computed based on the methods discussed in previous sections).

Various researchers have proposed different formulae for computing the scaling factor (Youd and Noble, 1997). Values of these scaling factors are shown in Table 1.13 respectively.

Youd et al. (2001) recommended the new MSF proposed by Idriss (column 3 in Table 1.12) as a lower bound for earthquakes with magnitude smaller than 7.5. They also recommended the MSF proposed by Andrus and Stokoe (column 7 in Table 1.12) as an upper bound. Also, for magnitudes >7.5, they recommended new MSF proposed by Idriss (column 3 in Table 1.12).

Table 1.13: Magnitude scaling factor (MSF) values defined by various investigators (after Youd and Noble 1997)

Magnitude, M	Seed and Idriss (1982)	Idriss[a]	Ambraseys (1988)	Arango (1996) Distance based	Arango (1996) Energy based	Andrus and Stokoe (1997)	Youd and Noble (1997b) $P_L < 20\%$	Youd and Noble (1997b) $P_L < 32\%$	Youd and Noble (1997b) $P_L < 50\%$
5.5	1.43	2.20	2.86	3.00	2.20	2.8	2.86	3.42	4.44
6.0	1.32	1.76	2.20	2.00	1.65	2.1	1.93	2.35	2.92
6.5	1.19	1.44	1.69	1.60	1.40	1.6	1.34	1.66	1.99
7.0	1.08	1.19	1.30	1.25	1.10	1.25	1.00	1.20	1.39
7.5	1.00	1.00	1.00	1.00	1.00	1.00	—	—	1.00
8.0	0.94	0.84	0.67	0.75	0.85	0.8?	—	—	0.73?
8.5	0.89	0.72	0.44	—	—	0.65?	—	—	0.56?

Note: ? = Very uncertain values.
[a]1995 Seed Memorial Lecture, University of California at Berkeley (I. M. Idriss, personal communication to T. L. Youd, 1997).

James et al. (2011) used the Boulanger and Idriss (2004) relationship for computing magnitude scaling factor (MSF) for tailings; this can be expressed as follow:

$$MSF = \frac{CRR_M}{CRR_{M=7.5}} = \left[\frac{N_{M=7.5}}{N_M}\right]^b \tag{1.48}$$

where CRR_M is cyclic resistance ratio associated with a magnitude 'M' earthquake, $CRR_{M=7.5}$ is cyclic resistance ratio associated with magnitude 7.5, $N_{M=7.5}$ is the number of equivalent loading cycles associated with an earthquake of magnitude 7.5, N_M is the number of equivalent loading cycles associated with earthquake of magnitude 'M', and 'b' is obtained from formula (1.38).

The values of *MSF* calculated by James et al. (2011) are different from the values recommended by Idriss and Boulanger (2008). James et al. (2011) attributed this difference to cyclic shear response of tailings as indicated by the 'b' value in equation (1.38).

Correction factor for high overburden stress, static shear stresses.

Seed (1983) proposed the following formula for effect of initial shear stress and effective confining pressure:

$$\left(CRR_{field}\right)_{\alpha,\sigma} = \left(CRR_{field}\right)_{\alpha=0,\sigma<1\ ton/ft^2} K_\alpha K_\sigma \tag{1.49}$$

where $\alpha = \tau_{h,static}/\sigma_{v0}^{'}$ and K_α and K_σ are calculated based explained procedures by Harder and Boulanger (1997) and Youd et al. (2001).

As discussed previously, different researchers studied the effect of high overburden stress on cyclic shear resistance of the soils. Cyclic testing by Wijewickreme et al. (2005b), James et al. (2011), and Al-Tarhouni et al. (2011) indicates that CRR is not dependent on changing of the confining pressure for slurry deposited and normally consolidated tailings. Therefore, they suggested K_σ should be considered equal to 1 for slurry deposited tailings.

1.6.2 Cyclic strain approach

Seed (1976) showed that a number of complex factors influence the liquefaction resistance of soils. These factors should be evaluated carefully for determination of liquefaction characteristics of soils. For this reason, some researchers, like Dobry and Ladd (1980) and Dobry et al. (1982 presented methods on the basis of cyclic shear strain rather than cyclic shear stress for determining earthquake-induced cyclic shear strain and liquefaction resistance. Researchers such as Silver and Seed (1971) and Youd (1972), showed that cyclic shear strain controls the densification (volumetric strain) of sand. Therefore they presented methods that are based on cyclic shear strain (Kramer, 1996).

In the cyclic shear strain approach, the irregular strain time history induced by an earthquake can be converted to cycles of uniform amplitude and an equivalent number of cycles (similar to the

cyclic shear stress approach). The time history of cyclic shear strain is computed by ground response analysis. The amplitude of uniform shear strain at an equivalent number of cycles corresponding to earthquake magnitude on basis of cyclic shear stress can be estimated by the methods proposed by Dobry et al. (1982) (Kramer, 1996):

$$\gamma_{cyc} = 0.65 \frac{a_{max}}{g} \frac{\sigma_v r_d}{G(\gamma_{cyc})} \tag{1.50}$$

$G(\gamma_{cyc})$ is shear modulus of soil at $\gamma = \gamma_{cyc}$. As γ_{cyc} is on both side of the equation (1.50), its value should be computed with iterative methods. For computing value of γ_{cyc} , $G_{\max}$ and $G(\gamma_{cyc})$ are computed from the appropriate modulus reduction curves (section 1.5). Then γ_{cyc} is computed from equation (1.50). If value γ_{cyc} is greater than the threshold shear strain of the soil (the threshold shear strain is the level where excess pore water pressure is generated), liquefaction can occur (Kramer, 1996). This approach is not used as commonly as the stress approach.

1.7 Methods for improving the seismic stability of tailings impoundments

1.7.1 An overview

James and Aubertin (2010, 2012) reviewed the some methods for improving the dynamic stability of tailings impoundments such as buttressing, lowering water table level in the dyke and impoundment, improving the properties of tailings and dyke using methods such as reducing initial water content, and densification of tailings, and using inclusions as draining and reinforcing system in the tailings and near the dyke.

The reinforcement and draining system may consist of gravel and sand drains, stone columns, and high modulus columns. These methods are used for the mitigation of liquefaction in sands, non-plastic silts, and silty sands. Different researchers such as Sasaki and Taniguchi (1984), Adalier et al. (2003), and Martin et al. (2004) have performed tests, numerical simulations and

site investigations for evaluating the performance of such system (especially stone columns) for the mitigation of liquefaction in sand and non-plastic silt deposits. L.Bolduc and Aubertin (2014) investigated numerically the influence of waste rock inclusions on tailings consolidation. These methods are described briefly in the following.

1.7.2 Stone columns and gravel drains

Stone columns can mitigate liquefaction in deposits of silt and sand. Adalier et al. (2003) explained the possible benefits of stone columns:

- Densification of the soil (depending on the method of installation).
- Dissipation of excess pore water pressure during earthquake shaking. The dissipation of pore water pressure during the seismic loading depends to saturated hydraulic conductivity of sand or silt.
- Increasing the stiffness of the soil, thereby reducing shear strains during earthquake shaking and reducing or preventing of generation of excess pore water pressure.

The benefits of stone columns and gravel drains have been investigated by several researchers. Seed and Booker (1977) developed a method for stabilizing potentially liquefiable sand deposits using gravel drains. This method relies on the ability of gravel drains to dissipate excess pore water pressures generated during and after vseismic loading. Sasaki and Taniguchi (1984) investigated the effects of gravel drains in the mitigation of liquefaction in sand deposits using shaking table tests. Adalier et al. (2003) investigated the performance of stone columns in the reinforcement of non-plastic silts through centrifuge testing. Also Martin et al. (2004) investigated the effect of jet grouting (high modulus columns) in the mitigation of liquefaction during the 1999 Kocaeli Earthquake in Turkey. The results of these studies are discussed below.

Seed and Booker (1977) developed a method for designing gravel drains for dissipating excess pore water pressures during the seismic loading. In this method, effective radius and distance of the gravel drains are calculated in such way that excess pore water pressure does not increase from a considered limiting value for design during the seismic event. The details of this method are available in Seed and Booker (1977).

Sasaki and Tanighuchi (1984) performed large scale shaking table tests for evaluating gravel drains as a liquefaction countermeasure. The size of model (box) was 12 m in length, 3 m in depth, and 2 m in width. These tests were performed for evaluating the effect of gravel drains as liquefaction countermeasure for stabilizing of a half-buried type road model. In addition to shaking table tests, cyclic laboratory tests and finite element modeling were performed. The results of their research are as follows:

- The increase in pore water pressure near the gravel drain was smaller than that in other areas during the excitation. The gravel drains decreased the generation of excess pore water pressures within a distance of 50 cm.
- After cyclic loading, the gravel drains helped to dissipation of excess pore water pressures.
- The gravel drains installed below half buried type road model remarkably reduced the uplift pressure due to excess pore water pressure generation.
- If gravel drains are designed correctly, they would be effective as liquefaction countermeasures in sandy ground around buried structures.
- Reasonable results were obtained by modeling of excess pore water pressure generation using the two dimensional finite element program "SADAP".

Adalier et al. (2003) performed four separate centrifuge tests for evaluating the effect of stone columns as a liquefaction countermeasure in non-plastic silts. They focused on the stiffening effect of stone columns rather than the drainage effect. The dimensions of the model for all tests were 0.254 m high, 0.458 m long and 0.254 m wide. Test No.1 and No.2 were performed with gravitational values of 50 g and Test No.3 and 4 were performed with gravitational values of 63g. The test No. 1 was performed to evaluate the liquefaction of non-plastic silts without any reinforcement (stone columns), whereas Test No. 2 was performed to investigate the effect of stiffening by stone columns on the response of non-plastic silts under seismic loads. The liquefaction of non-plastic silts without any reinforcement was investigated with Test No. 3. Finally, Test No. 4 was performed to evaluate the effect of stone columns and surcharge loads on the liquefaction of the non-plastic silts.

The non-plastic silt had an effective friction angle of 25^o at an I_D of 65%. Uniformly graded, subrounded, clean "Nevada No 120" sand with D_{50} of 0.15 mm was used to model the stone columns (friction angle 37^o at density index of 65%). The hydraulic conductivity of the sand was 600 times greater than that of the silt. For gravitational values of 50g and 63g, the prototype hydraulic conductivities of sand were estimated to be 2.6×10^{-3} m/s and 3.3×10^{-3} m/s, respectively.

The comparison of the results of Test (model) 1 and 2 showed that the generation of excess pore water pressure was retarded in model 2 relative to model 1. While model 1 was liquefied at the end of the 12th cycle, just top-half of model 2 was liquefied at the end of the shaking (20^{th} cycle). The increase in the liquefaction resistance of reinforced model 2 relative to model 1 was attributed by Adalier et al. (2003) to the increased stiffness of model 2 by the stone columns.

In model 2, the top-half of model liquefied due to seismic loading. Adalier et al. (2003) explained that sufficient vertical stress or confining pressure might be required for preventing liquefaction in this area and such pressure should be more than 45 kPa.

The comparison of models 3 and 4 showed that the foundation settlement in model 4 was 50% less than model 3. Also the generation of excess pore water pressure (epwp) was retarded in model 4 relative to model 3 and its value was less than the epwp in model 3. The epwp in model 4 dissipated faster than that in model 3.

In general, the models with stone columns showed stiffer responses to shaking. Also the excess pore water generation due to shaking was retarded by the use of stone columns and the settlement in these models was less than in the unreinforced models (Adalier et al., 2003).

Martin et al. (2004) investigated the performance of high-modulus columns (jet-grouting) at a shopping center under construction, where a parking that had been remediated was subjected to the 1999 Kocaeli Earthquake (M=7.4). Herein a brief of their works are explained.

The results of the study showed that the jet grouted area did not experience any damage during or after the Kocaeli 1999 earthquake, which produced a horizontal acceleration of 0.24g. However, non jet-grouted areas with stone columns (jet grouted columns) experienced 10-12 cm of settlement. Martin et al. (2004) suggested that stone columns increased the stiffness of the foundation and therefore decreased shear strains. Thus, the value of the shear strains was less

than or close to the threshold shear strain (0.01% according to NRC, 1985). Hence, excess pore water pressure did not develop during the earthquake. The parking and Lot C areas experienced 10 to 12 cm settlement as mentioned before. According to Martin et al. (2004), wick drains did not prevent excess pore water pressure development and surcharges slightly increased the liquefaction resistance of the underlying layers of soils.

Some important points summarized by Martin et al. (2004) were

- The replacement ratio of stone columns in the silty sand was 7% whereas in other layers it was 2% because the design process assumed that just the silty sands were vulnerable to liquefaction. However, after the earthquake, it was seen that other layers like the ML/CL or CH showed liquefaction-type behavior.
- Application of 3.3 m height surcharge increased the liquefaction resistance only slightly.
- Wick drains installed in the parking and Lot C areas did not decrease the excess pore water pressure generation during the earthquake but may cause uniform settlement of the parking and Lot C areas during post-liquefaction reconsolidation.
- The reason the significant settlement in the CH layer could not explain. It was postulated that loss of strength and softening of the CH layer due to the earthquake shaking and shear distortion due to the overlying fill was the reason for this settlement.
- The high modulus stone columns (jet grouting) increased the stiffness of the foundation. Therefore, shear strains remained below the threshold shear strain value (1%). Thus, excess pore water pressures did not develop in the reinforced area.

Finally, according to the above mentioned research on the performance of stone columns in soils of low permeability, stone columns mainly serve to increase the stiffness of the soils and decrease the shear strains. Therefore they prevent or retard excess pore water pressure generation and mitigate liquefaction in these types of soils. Stone columns do not provide significant drainage of excess pore water pressures in situ for these fine grained soils during shaking.

1.7.3 Waste rock inclusions

Aubertin et al. (2002a) recommended the co-disposal of tailings and waste rocks in surface impoundments. They suggested placement of the waste rock on the upstream faces of dams, at

the base of the impoundment and inside the impoundments. According to Aubertin et al. (2002a), co-disposal of waste rock and tailings has the following advantages

- Waste rock inclusions accelerate drainage and increase the consolidation rate of tailings. Stability of tailings impoundments increases due to consolidation.
- Waste rock inclusions can mitigate the effect of liquefaction of tailings impoundments.
- Placing of waste rock inside tailings may decrease the potential for Acid Mine Drainage (AMD) from the waste rock.

Shaking table tests and numerical modeling were performed to assess the performance of waste rock inclusions as a liquefaction countermeasure. In the following, this work is briefly summarized.

Pépin et al. (2009, 2012a, 2012b) conducted 11 shaking table tests for evaluating the performance of sand inclusions in tailings under seismic loading. The physical model was a box with 1-m-square area and with a height of 75 cm. One test was conducted on sand with three different acceleration and the others on tailings with and without inclusions. The applied seismic load was a sinusoidal loading with frequency of 1 Hz. Table 1.14 shows a summary of the shaking table tests. The shaking table test on the sand was performed with 3 peak ground accelerations (PGA) of 0.12g, 0.17g, and 0.35g, whereas for all tests on tailings the PGA was equal to 0.12g. Table 1.15 shows the summary of materials properties used for the shaking table tests.

In general, inclusions decreased the value of pore water pressure relative to the tests without inclusions (Pépin et al. 2009, 2012a, and 2012b). Also the rate of excess pore water pressure in the physical models with inclusions was less than that in models without inclusions. Test 9 as shown in Table 1.14, is a physical model with a wall type inclusion and layer of coarse sand on the bottom of the model. Inclusions in Test 9 were more effective relative to other tests. Test 7 with a wall inclusion was also effective. The model with a rigid/non-drainage column (Test 5) was effective only in the bottom part of the model. The results of this test are fairly similar to the results of Adalier et al. (2003) obtained by centrifuge test for evaluating the performance of stone columns as liquefaction countermeasure in non-plastic silt.

Table 1.14: Summary of shaking table tests (after Pépin et al., 2012b)

Test	Material	Conditions	Density index, I_D (%)	Peak acceleration (g)
1	Sand*	—	31	0.12, 0.17, 0.35
2	Tailings	Loose, no inclusion	65	0.12
3	Tailings	Consolidated, no inclusion	>80	0.12
4	Tailings	Rigid column with sand	76	0.12
5	Tailings	Rigid column	77	0.12
6	Tailings	Sand column	80	0.12
7	Tailings	Sand wall	82	0.12
8	Tailings	Consolidated, no inclusion	83	0.12
9	Tailings	Sand wall and bed	83	0.12

*Results not presented here (see Pépin 2010).

Table 1.15: Summary of materials properties (after Pépin et al., 2012b)

Characteristics	Tailings	Sand
USCS classification	ML	SP
Solid grain relative density	3.39	2.67
Maximum dry unit weight (kN/m^3)	22.41	N.A.
Hydraulic conductivity, k_{sat} (cm/s)	2.2×10^{-5}	1.4×10^{-2}
Void ratio, e	0.62	0.62
Maximum void ratio, e_{max}	1.46	—
Minimum void ratio, e_{min}	0.48	—
D_{10} (mm)	0.005	0.21
D_{50} (mm)	0.040	0.40
D_{60} (mm)	0.048	0.42

Note: D_i, soil particle diameter at which i% of the mass of the soil specimen is finer; ML, nonplastic silt; SP, poorly graded sand; USCS, Unified Soil Classification System (ASTM 2006).

James (2009) evaluated the dynamic response of tailings impoundments with and without waste rock inclusions using numerical modeling. He used the UBCSAND model developed by Beaty and Byrne (1998) for modeling the behavior of tailings. After calibrating of model with results of cyclic simple shear tests, he simulated conceptual reinforced and conventional tailings impoundments. The results of analyses showed that waste rock inclusions enhance seismic performance of tailings conceptual tailings impoundments.

1.8 Methods of seismic analysis of tailings impoundments

One of the important requirements for designing safe tailings impoundments with respect to seismic loadings is selecting suitable seismic analysis methods. Jibson (2011) classified the methods for assessing the seismic stability into three main types:

- Pseudostatic analysis
- Permanent-displacement analysis
- Stress-deformation analysis

In the following sections, the above mentioned methods are briefly described and their advantages and disadvantages are discussed (based on Kramer, 1996; Beikae, 1997; Seid-Karbasi and Byrne, 2004; Bray and Travasarou, 2007; Psarropolous and Tsopanakis, 2008; James, 2009; James and Aubertin, 2010; Jibson, 2011).

Canadian Dam Association (CDA) (2007) recommended the following progressive methodology for seismic stability analysis of embankment dams:

- Screening level
- Pseudo-static method
- Permanent deformations- Simplified methods
- Simple liquefaction assessment
- Dynamic analysis- Linear equivalent approach
- Dynamic analysis- Effective stress approach

1.8.1 Pseudostatic analysis

Pseudostatic seismic analysis has been used to evaluate the seismic stability slopes and dams since the 1920s (Kramer, 1996). This method consists of a limit equilibrium analysis with horizontal and vertical inertial forces added to static forces acting on the mass of the slopes a dam to simulate earthquake loading. These inertial forces are defined as (Kramer, 1996):

$$F_h = \frac{a_h W}{g} = k_h W \qquad (1.51a)$$

$$F_h = \frac{a_v W}{g} = k_v W \qquad (1.51b)$$

where a_h and a_v are horizontal and vertical pseudostatic accelerations, respectively; W is the weight of a potential failure mass; k_h and k_v are dimentionless horizontal and vertical pseudostatic coefficients, and g is acceleration of due to gravity. The vertical pseudostatic coefficient is not usually considered in the computing of the factor of safety.

According to Kramer (1996) and Jibson (2011), pseudostatic analysis are not precise because it does not consider the effect of the load-history of the earthquake, deformation, or other dynamic effects. Pseudostatic methods are not applicable in cases where pore water pressure may develop or when there is a significant strength loss due to earthquake loading. Table 1.16 (Seed ,1979) shows cases where the computed safety factor by the pseudostatic method indicated stability, yet failure occurred due to seismic loading.

Table 1.16: Results of pseudostatic analysis of earth dams that failed during earthquake (after Seed, 1979)

Dam	k_h	FS	Effect of Earthquake
Sheffield Dam	0.10	1.2	Complete failure
Lower San Fernando Dam	0.15	1.3	Upstream slope failure
Upper San Fernando Dam	0.15	~2–2.5	Downstream shell, including crest slipped about 6 ft downstream
Tailings dam (Japan)	0.20	~1.3	Failure of dam with release of tailings

Nonetheless, this method is easy to apply and commonly used in professional practice. The value of k_h is based on assumption, regional practice, and engineering judgment. Table 1.17 shows recommended value for the pseudostatic coefficient. As shown in this table, the values vary considerably. Most of these values were obtained based on calibration for earth dams in which one meter displacement is considered acceptable. These values are often used for natural slopes. However, in natural slopes the acceptable value of displacement is generally between 5 and 30 cm (Wieczorek et al. 1985; Blake et al., 2002; Jibson and Michael, 2009). According to Jibson

(2011), based on the California Division of Mines and Geology (1997), the common value of k_h that is used in practice is equal to 0.15 with a safety factor more than 1.1. This value was calibrated based on results of earth dams with an acceptable displacement of one meter (Jibson, 2011).

Table 1.17: Pseudostatic coefficients from various studies (after Jibson, 2011)

Pseudostatic coefficients from various studies.

Investigator	Recommended pseudostatic coefficient (k)	Recommended factor of safety (FS)	Calibration conditions
Terzhagi (1950)	0.1 (R-F = IX) 0.2 (R-F = X) 0.5 (R-F>X)	>1.0	Unspecified
Seed (1979)	0.10 (M = 6.50) 0.15 (M = 8.25)	>1.15	<1 m displacement in earth dams
Marcuson (1981)	0.33–0.50 × PGA/g	>1.0	Unspecified
Hynes-Griffin and Franklin (1984)	0.50 × PGA/g	>1.0	<1 m displacement in earth dams
California Division of Mines and Geology (1997)	0.15	>1.1	Unspecified; probably based on <1 m displacement in dams

R-F is Rossi-Forel earthquake intensity scale.
M is earthquake magnitude.
PGA is peak ground acceleration.
g is acceleration of gravity.

To use Hynes-Griffin and Franklin (1984) method for Pseudostatic analysis in soils that exhibit small pore water pressure generation during the seismic loading, 80 percent of the undrained strength should be considered as “dynamic yield strength” (Jibson, 2011). These soils are clayey materials, dry or partially saturated cohesionless soils, or very dense saturated cohesionless materials (Hynes-Griffin and Franklin, 1984).

Different researchers, like Bray and Rathje (1998) and Bray and Travasarou (2009), have proposed methods for computing the value of pseudostatic coefficient.

1.8.2 Permanent-displacements methods

Newmark (1965) proposed a method for evaluating the stability of slopes during seismic loading. This method considers the volume as a rigid block that slides on an inclined plane. A certain amount of acceleration is required to overcome the basal resistance. This acceleration is called yield or critical acceleration. After selecting a ground motion acceleration time history, the parts of this acceleration time history that are larger than the critical acceleration are integrated for

obtaining a velocity-time history. Then, the velocity time history is integrated for computing the permanent displacement due to the ground motion (Jibson, 2011).

Makdisi and Seed (1978) revised Newmark`s method, considering the block as deformable mass. They produced charts for computing the permanent displacement based on geometry, earthquake magnitude, the ratio of yield acceleration to peak acceleration, and initial fundamental frequency of the structure. They calibrated their model according to a small number of strong-motion records (Jibson, 2011). This method is classified as decoupled permanent-displacement methods, because the dynamic response and the plastic displacement are computed independently.

Another permanent-displacement method is based on coupled stability analysis. In this method, the dynamic response of the sliding mass and the permanent displacement are modeled together. Different researchers, like Lin and Whitman (1983), and Rathje and Bray (1999, 2000), have used the coupled method for computing permanent displacement. They also compared the results of the coupled methods with the decoupled and rigid block methods. Lin and Whitman (1983) pointed out that the decoupled method produces an error in computed permanent displacement. The computation time with the coupled method is larger than the rigid block and the decoupled method. The coupled method is considered more sophisticated relative to other permanent-displacement methods (Jibson, 2011).

Bray and Travasarou (2007) proposed a simplified procedure for estimating seismic-induced deviatoric slope displacements. This method is semi-empirical. It requires yield coefficient (k_y), initial fundamental period of the sliding mass in second (T_s), spectral acceleration of the input ground motion at a period of $1.5T_s$ in the unit of g ($S_a(1.5T_s)$), peak ground acceleration (PGA), and earthquake magnitude (M). This model computes the probability of the negligible “zero” displacement and likely amount of the nonzero displacement.

This methods is applicable for soils which their strength or stiffness are not decreased during the seismic loading (Bray and Travasarou, 2007).

1.8.3 Stress-deformation analysis

Different stress-deformation analysis methods have been used for the seismic stability analysis of earth dams and natural slopes. These methods are based on calculations with the finite-element, finite-difference, discrete-element, distinct-element methods. The distinct-element is usually

used for stability analysis of fractured rock mass and other blocky media, whereas the discrete-element (particle flow) is usually used for granular media. For stress-deformation in soil, finite-element and finite-difference methods are more commonly applied. For example, two widely used softwares, PLAXIS and FLAC that are based on finite-element and finite-difference, respectively, are often used for stress-deformation analysis in geotechnical engineering (Itasca, 2008, Plaxis, 1998). To obtain acceptable results from stress-deformation analyses, representative material properties must be obtained from laboratory and field testing or suitable published data. Also the geometry and boundary conditions of the problem must be defined correctly and appropriate constitutive models should be selected. Therefore, stress-deformation analyses may be costly and time consuming.

Stress-deformation analysis is a powerful approach because it can model the actual geometry of problem as well as non-linear stress-strain behavior, water flow, excess pore water pressure development, shear modulus degradation, and dynamic damping during dynamic loading. Other methods, such as the pseudostatic or permanent displacement, are based on several simplifying assumptions that omit most of these phenomena.

For the seismic modeling of natural slopes or earth dams, with excess pore water generation during seismic loading, different constitutive laws have been proposed by Dafalias (1986), Prevost (1989), Zienkiewics et al. (1990), Bryne et al. (1995), Beaty and Byrne (1997), Elgamal et al. (1999), Kramer and Arduino (1999), Jefferies and Been (2006), and Adrianopolos et al. (2006).

According to Jibson (2011), although stress-deformation analysis is powerful method but the following conditions must be provided to obtain acceptable results

- For obtaining the correct material properties, undisturbed samples should be provided or field tests should be performed. Also extensive laboratory test should be performed.
- A suitable ground motion should be selected.
- It needs accurate constitutive laws that can predict excess pore water pressure development as well as stress and strain.
- Computational requirements.

1.9 Constitutive models for the numerical modeling of dynamic behavior of tailings

As mentioned in section 1.8, there are different methods for stability analysis of tailings impoundments. The pseudostatic analysis is not suitable for the seismic stability analysis of reinforced tailings impoundment, because they cannot predict and simulate excess pore water pressure generation during the seismic analysis. Also, permanent-displacement methods cannot be used in cases in which soil loses its strength or stiffness during the seismic loading (Bray and Travasarou, 2007). In tailings impoundments excess pore water pressures increase during seismic loading and tailings lose strength and stiffness because, therefore, pseudostatic analysis and permanent displacement methods are not suitable for stability analysis of reinforced tailings impoundments. The stress-deformation analysis is suitable for seismic analysis of liquefaction in tailings impoundments.

Suitable constitutive laws should be chosen to obtain reasonable results from dynamic numerical modeling of tailings impoundments. In recent years, some researchers such as Seid-Karbasi and Byrne (2004), and James (2009) have applied the UBCSAND model, to tailings material. The model was calibrated for tailings based on cyclic simple shear testing. After calibrating the model, they carried out seismic numerical modeling of tailings impoundments.

1.9.1 UBCSAND model

The UBCSAND model was developed by Byrne et al. (1995) at the University of British Columbia (UBC) to model the liquefaction of sand. Then, Puebla et al. (1997) and Puebla (1999) later developed the UBCSAND model for predicting and modeling static liquefaction in the CANLEX (Canadian Liquefaction Experiment) project. Later, Beaty and Byrne (1998) and Beaty (2001) further developed the model for seismic modeling of sand and sand-like material. The model was distributed in 2002 as "UBCSAND904a" for use in dynamic modeling. Beaty and Byrne (2011) modified the model, now distributed as "UBCSAND90aR".

Many researchers like Bryne et al. (2003), Seid-Karbasi and Byrne (2004), Byrne et al. (2004), James (2009), Naesgaard et al. (2011), have used the UBCSAND model to simulate the dynamic behavior of sand and tailings in dams and impoundments. In the following sections, the fundamentals and development of the UBCSAND model are discussed.

1.9.1.1 UBCSAND model for meismic loading

Beaty and Byrne (1998), and Beaty (2001) developed the UBCSAND model for dynamic analysis of sand and sand like material. The fundamental formulation of the UBCSAND model for seismic analysis is the same as the UBCSAND model for static liquefaction developed by Puebla et al. (1997) and Puebla (1999). However, the hardening behavior of the UBCSAND models for static and dynamic liquefaction is different. Furthermore, the UBCSAND model for seismic liquefaction does not have a cap mechanism.

The UBCSAND model for seismic liquefaction was distributed in 2002 and is used by many researchers for the seismic analysis of earth dams and tailings impoundments. Figure 1-8 show stress ratio history, incremental stress ratio versus plastic shear strain for the UBCSAND904a and UBCSAND904aR. Figure 1-8 (a) shows stress ratio history showing loading, unloading, and reloading, Figure 1-8(b) shows incremental stress ratio versus plastic shear strain for cone mechanism for UBCSAND904a, and Figure 1-8(c) shows incremental stress ratio versus plastic shear strain for cone mechanism for UBCSAND904aR. Beaty and Byrne (2011) showed that this version of UBCSAND model does not work properly when there is initial shear stress bias (non-level ground condition). The UBCSAND904a model behaves elastically during the unloading-reloading cycles as shown in Figure 1-8(b). Also as long as direction of stress ratio (η) does not change, cycles of unloading-reloading are elastic as shown in Figure 1-8 (a) and (b). Therefore, plastic volumetric strains are not produced during these cycles. It means that this model cannot predict excess pore water pressure built up when there are significant initial shear stresses.

Also Beaty and Byrne (2011) analysed the Success Dam project using the UBCSAND904a model and showed that size of the excess pore water pressure zone beneath the upstream shell of the dam was smaller than measured zone size. Figure 1-9 indicates the predicted shear stress beneath upstream shell of Success Dam using UBCSAND version 904a. As shown in this figure, there are significant cycles that pore waster pressures are not generated due to them using the UBCSAND model version of 904a.

Beaty and Byrne (2011) revised the UNBCSAND model for solving the above mentioned problem. They changed the unloading-reloading response from elastic to elastic response in unloading and plastic response in reloading as shown in Figure 1-8(c). The stiffness of the

reloading is several times larger than the initial stiffness during the first loading. This model was called UBCSAND904aR. This model is isotropic hardening. This model can predict plastic strains and excess pore water pressures when there is initial shear stress bias (non-level ground condition). For example, as shown in Figure 1-9, three big cycles shown inside of green oval are considered as unloading and reloading in the UBCSAND model. The UBCSAND904a behaves elastically during these three cycles, and then it cannot capture plastic strains due to these cycles. Therefore, excess pore water pressures are not produced due to these cycles. The UBCSAND904aR considers reloading as non-linear behavior, and then it can capture plastic strains and excess pore water pressure due to these three cycles shown in green oval.

This model does not predict plastic strains when the loading is isotropic compression or stress path is in the direction of constant stress ratio line. Therefore, a model that can predict plastic strains under isotropic triaxial compression or when the stress path is in the direction of constant stress ratio should be developed.

In following sections, the elastic and plastic shear response of the UBCSAND model is briefly recalled based on Puebla et al. (1997), Puebla (1999).

Elastic response

The elastic response of sand is assumed to be isotropic and incrementally linear elastic. For plane strain conditions, the relationship between increments of strains and increments of stresses is expressed

$$\{\Delta\varepsilon^e\} = [C^e]\{\Delta\sigma'\} \tag{1.52}$$

where $[C^e]$ is the compliance matrix. The bulk B^e and shear G^e moduli can be computed in terms of the Young's modulus and Poisson's ratio

$$B^e = \frac{E}{3(1-2v)} \tag{1.53}$$

$$G^e = \frac{E}{2(1+v)} \tag{1.54}$$

Pubela et al. (1997) postulated that these elastic parameters are stress dependent and can be expressed as

$$G^e = k_G^e P_a \left(\frac{s'}{P_a}\right)^{me} \tag{1.55}$$

$$B^e = \frac{2G^e(1+\upsilon)}{3(1-2\upsilon)} \tag{1.56}$$

where $k_G^e, P_a,$ me, $s' = \frac{\sigma_1' + \sigma_3'}{2}$, υ are the elastic shear modulus, the atmospheric pressure, the elastic shear modulus exponent, the effective confining pressure, and Poisson's ratio, respectively.

Plastic shear response

Failure and yield function of the UBCSAND model

It is assumed that the ultimate strength is based on a Mohr-Coulomb type failure criterion. This failure criterion is a line with slope equal to $\sin\phi_f$ (where ϕ_f is the value of the friction angle at failure). This failure criterion is expressed in terms of effective principle minor (σ_3') and major (σ_1') stresses as

$$f_f = \sigma_1' - \sigma_3' N_{\phi f} = 0 \tag{1.57}$$

$$N_{\phi f} = \frac{1 + sin\phi_f}{1 - sin\phi_f} = \frac{1+\eta_f}{1-\eta_f} \tag{1.58}$$

where η_f is the stress ratio at failure ($\eta = (\sigma_1 - \sigma_3)/(\sigma_1' + \sigma_3')$). Puebla et al. (1997) and Puebla (1999) defined the yield loci during loading according to Poorooshasb et al. (1966) and Ishihara et al. (1975)

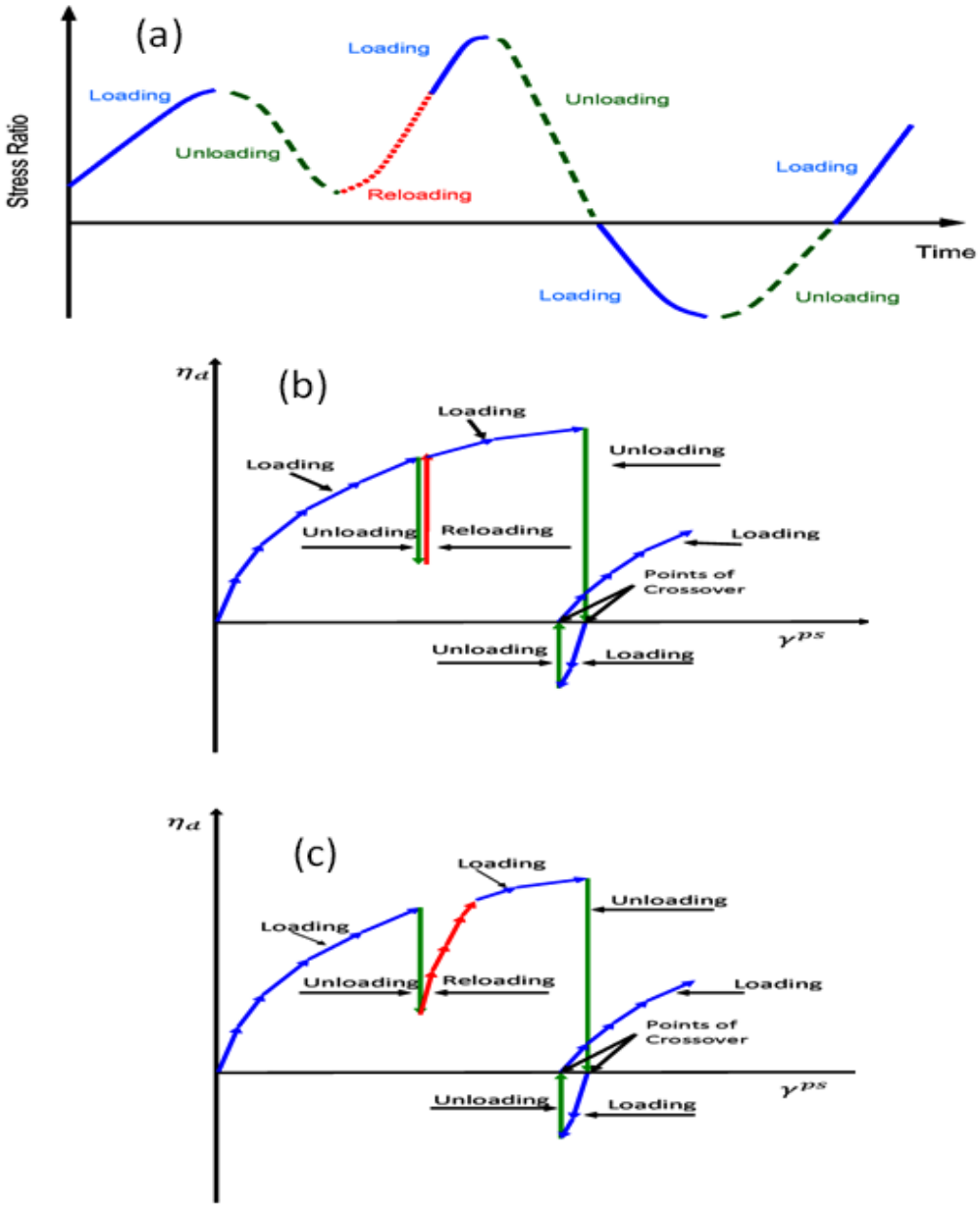

Figure 1-8: (a) Stress ratio history showing loading, unloading, and reloading (after Beaty and Byrne, 2011). (b) Incremental stress ratio versus plastic shear strain for cone mechanism for UBCSAND904a. (c) Incremental stress ratio versus plastic shear strain for cone mechanism for UBCSAND904aR

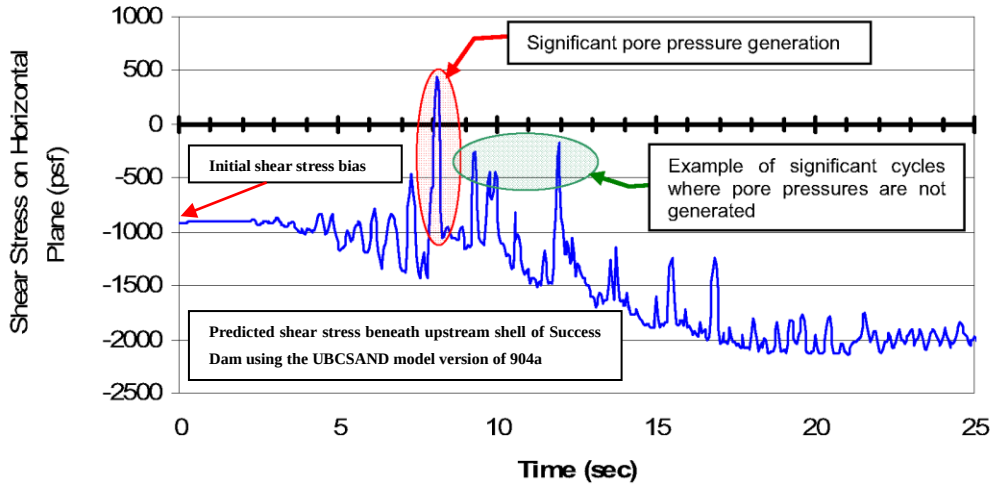

Figure 1-9: Example of predicted shear stress beneath upstream shell of Success Dam using UBCSAND version 904a (modified after Beaty and Byrne, 2011)

$$f^s = \sigma_1' - \sigma_3' N_{\phi d} = 0 \tag{1.59}$$

$$N_{\phi d} = \frac{1 + sin\phi_d}{1 - sin\phi_d} = \frac{1 + \eta_d}{1 - \eta_d} \tag{1.60}$$

$$\eta_d = \frac{t}{s'} = sin\phi_d \tag{1.61}$$

where η_d and ϕ_d are the developed stress ratio and friction angle respectively and $t = (\sigma_1' - \sigma_3')/2$, $s' = (\sigma_1' + \sigma_3')/2$, and σ_3' and σ_1' are effective principal stresses.

Flow rule and plastic potential of the UBCSAND model

According to Puebla (1999), the directions of plastic shear strains are computed based on a non-associated flow rule. Derivation of the relationship between the increments of plastic shear strain and plastic volumetric strain is similar to the derivations presented by Taylor (1948), Rowe (1962), Schofield and Wroth (1968), and Matsuoka and Nakai (1977). This relationship is

$$\Delta\varepsilon_v^{ps} = (sin\psi_d)\Delta\gamma^{ps} \tag{1.62}$$

where $\Delta\varepsilon_v^{ps}$ is the volumetric plastic strain and $\Delta\gamma^{ps}$ is the plastic shear strain, ψ_d is the dilation angle. The relationship between ψ_d, the constant friction angle ϕ_{cv}, and the developed friction angle ϕ_d is

$$sin\psi_d = (sin\phi_{cv} - sin\phi_d) \tag{1.63}$$

Equation 1.62 is based on non-associated flow rule because the direction of incremental of plastic shear strain is not perpendicular to the yield loci. Equation 1.63 shows that if the developed friction angle (ϕ_d) be less than the constant volume friction angle (ϕ_{cv}), then the sand contracts under shear loading. If the developed friction angle is greater than the constant volume friction angle, then the sand dilates under shear loading.

The plastic potential function, based on the non-associated flow rule, can be written as

$$g^s = \sigma_1' - \sigma_3' N_{\psi d} = 0 \tag{1.64}$$

$$N_{\psi d} = \frac{1 + sin\psi_d}{1 - sin\psi_d} \tag{1.65}$$

The plastic strain increments $\Delta\varepsilon_{ij}^{ps}$ can be calculated according to plasticity theory flow rule as follows

$$\Delta\varepsilon_{ij}^{ps} = \lambda^s \left(\frac{\partial g^s}{\partial \sigma_{ij}'}\right) \tag{1.66}$$

Hardening rule for the UBCSAND model

The incremental stress ratio can be related to an increment of plastic shear strain as follows

$$\Delta\gamma^{ps} = \left(\frac{1}{G^*}\right)\Delta\eta_d \tag{1.67}$$

where G^* is the normalized tangent plastic shear modulus and calculated from following relationship

$$G^* = k_G^p \left(\frac{s'}{P_A}\right)^{np-1}\left[1 - \left(\frac{\eta_d}{\eta_f}\right)R_F\right]^2 \tag{1.68}$$

where R_F, η_f, η_{ult}, k_G^p, and np are the failure ratio=η_f/η_{ult}, the stress ratio at failure, the ultimate stress ratio from the best fit hyperbola, the plastic shear modulus number, and the plastic shear modulus exponent.

Undrained response

An element of soil under undrained loading conditions is shown on the left side of Figure 1-10. This element can be represented by an equivalent fluid that occupies the total volume of the element. Therefore pore water pressure can be computed from the following formula (Puebla, 1999).

$$\Delta u = \left(\frac{B_f}{n}\right)\Delta\varepsilon_v \tag{1.69}$$

where B_f, n, and $\Delta\varepsilon_v$ are the fluid bulk modulus, the porosity of soil element, and the volumetric strain increment, respectively.

The equation 1.69 can be written in matrix format as follows

$$\{\Delta u\} = \left[D_f\right]\{\Delta\varepsilon\} \tag{1.70}$$

where $\{\Delta u\}$, $\left[D_f\right]$, and $\{\Delta\varepsilon\}$ are the vector of pore water pressure, the equivalent stiffness matrix, and the vector of the strain increments respectively.

Also, the relationship between the increments of total effective stresses due to the elastic and plastic responses with the increments of strains is:

$$\{\Delta\sigma'\} = \left[[D'^e] + [D'^p]\right]\{\Delta\varepsilon\} \tag{1.71}$$

where $\{\Delta\sigma'\}$ is the vector of total effective stress increments, D'^e is constitutive elastic matrix, D'^p is constitutive plastic matrix, and $\Delta\varepsilon$ is the vector of total strain increments which can be written as:

$$\{\Delta\varepsilon\} = \{\Delta\varepsilon^e\} + \{\Delta\varepsilon^p\} = \{\Delta\varepsilon^e\} + \{\Delta\varepsilon^{ps}\} \tag{1.72}$$

where $\{\Delta\varepsilon^e\}$, $\{\Delta\varepsilon^p\}$, and $\{\Delta\varepsilon^{ps}\}$ are the vector of elastic strain increments, the vector of the plastic strain increments, and the vector of plastic strain increments of the cone shear mechanism, respectively.

By adding Equation 1.70 to 1.71, the relationship between total stresses and strains can be written as (Puebla, 1999):

$$\{\Delta\sigma\} = \left[[D'^e] + [D'^p] + \left[D_f\right]\right]\{\Delta\varepsilon\} \tag{1.73}$$

The above equation indicates that the UBCSAND model is a fully-coupled, effective stress model.

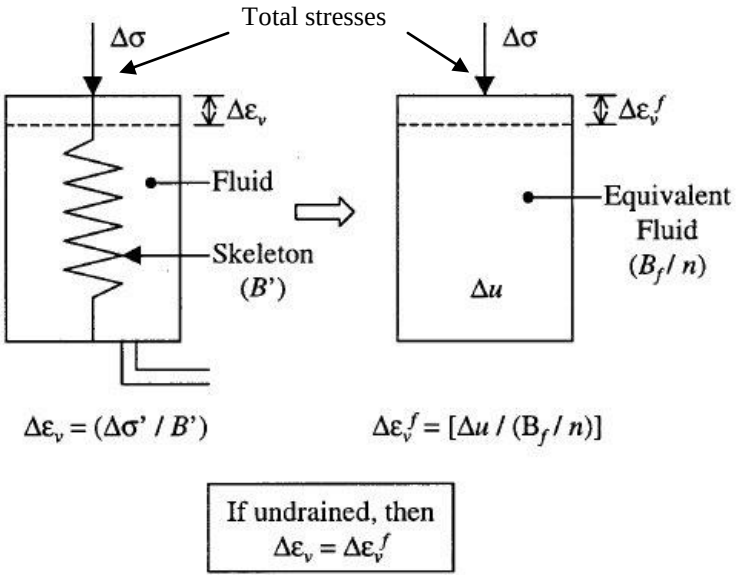

Figure 1-10: Soil element and equivalent fluid models (modified after Puebla, 1999)

1.9.1.2 Material properties required for applying the UBCSAND model

The required material properties to apply the UBCSAND model are the corrected standard penetration blow count, $(N_1)_{60}$, (blows per 0.3 m); the constant volume friction angle, ϕ_{cv}, in degrees; the anisotropic factor, f_{ani}; the total density, ρ_{TOTAL}, in Mg/m^3; and the porosity, n.

The elastic shear modulus number, k_G^e, and elastic bulk modulus number, k_B^e, can be estimated from the following formula respect to $(N_1)_{60}$ (Beaty and Byrne, 2011)

$$k_G^e = 21.7 * 20 * (N_1)_{60}^{0.333} \tag{1.74}$$

$$k_B^e = 0.7 \cdot k_G^e \tag{1.75}$$

The elastic shear modulus exponent in eq. 1-55, *me*, is considered equal to 0.5 (Beaty and Byrne, 2011).

The failure angle (peak friction angle), ϕ_f, can be estimated based on the constant volume friction angle, ϕ_{cv}, as follows (Beaty and Byrne, 2011)

$$\phi_f = \phi_{cv} + \frac{(N_1)_{60}}{10.0} \tag{1.76}$$

The constant volume friction angle can be estimated based on laboratory testing and its value often varying from 30 to 33° for sandy soils (Puebla et al., 1997) and 35.6° for hard rock mine tailings in western Quebec (James, 2009).

The plastic shear modulus number, k_G^P, can be estimated based on the elastic shear modulus number, k_G^e, and $(N_1)_{60}$ as follows (Beaty and Byrne, 2011)

$$k_G^P = 0.003 \cdot k_G^e \cdot (N_1)_{60}^2 + 100 \tag{1.77}$$

The failure ratio, R_F, can be calculated based on $(N_1)_{60}$ as follows

$$R_F = 1.0 - (N_1)_{60}/100 \tag{1.78}$$

R_F is often between 0.5 and 0.99.

CHAPTER 2: ORGANIZATION AND OUTLINE

Background information on the topic of this thesis, with the objectives, scope and content of the thesis are presented in the Introduction.

Chapter 1, Literature Review, presents a state of the art and practice on tailings and waste rock, tailings impoundments and their seismic behavior; the use of waste rock inclusions to improve the seismic stability of tailings impoundments is also introduced.

The main part of this thesis is made of three manuscripts that have been submitted to peer-reviewed journals for publication. These manuscripts constitute Chapters 3 through 5:

- Chapter 3: "Numerical simulations of the seismic and post-seismic behavior of tailings," submitted to the Canadian Geotechnical Journal on Aug, 2014.
- Chapter 4: "Effect of waste rock inclusions on the seismic stability of an upstream raised tailings impoundment: a numerical investigation," submitted to the Canadian Geotechnical Journal on Oct, 2014.
- Chapter 5: "Investigation of the effect of waste rock inclusions configuration on the seismic response of a tailings impoundment," submitted to the Journal of Geotechnical and Geological Engineering on Nov, 2014.

In summary, these chapters include the followings:

Chapter 3 presents numerical simulations of dynamic laboratory testing, physical modelling and tailings liquefaction under level ground (standard) conditions. One of the cyclic simple shear tests conducted by James (2009) was modeled using the UBCSAND model (version of 904aR). The results showed that this model can predict very well the shear strain, generation of excess pore water pressure, and initiation of liquefaction in tailings. Afterwards, two seismic table tests conducted by Pépin et al. (2012a, 2012b) have been simulated numerically. One test specimen consisted of lightly tamped tailings and the other test consisted of lightly tamped tailings with a sand wall inclusion. The simulations showed encouraging results. These simulations served for validation and calibration of the UBCSAND model. Subsequently, the post-shaking consolidation of tailings due to excess pore water pressure dissipation in the seismic table testing was simulated using the UBCSAND model adapted using the Sento et al. (2004) method. In this approach, the elastic

moduli of the tailings after shaking were updated using the consolidation curve of the tailings, which was determined from laboratory testing. This approach predicts very well the settlement in the seismic table testing in comparison to the measured values in the laboratory. Also, the settlement of tailings under ground level (horizontal) conditions was simulated numerically and the results were compared with the empirical formulation of Wijewickreme and Sanin (2010). The settlements predicted by numerical simulation were in very good agreement with this expression.

Chapter 4 presents numerical simulations of an actual upstream raised tailings impoundment in New Brunswick, Canada with and without waste rock inclusions. The results of numerical simulation of the impoundment with consolidated tailings are presented. First, the tailings impoundment without WRI was simulated numerically using modified high (Saguenay) and low (Northridge) frequency ground motions. The results of analysis showed that the tailings impoundment undergoes excessive deformation and is unstable. Then simulations were performed for different configurations of WRI using the modified high and low frequency ground motions. Next, the reinforced tailings impoundment with waste rock inclusions was classified based on the average value of horizontal displacements (AR_x) of the downstream slope at the end of shaking for various ground motions. The results showed that some arrangements of waste rock inclusions can improve significantly the seismic response of tailings impoundment. Also a graph was introduced that shows the average value of horizontal nodal velocity of the downstream slope of the impoundment (Xvel) at the end of shaking as function of AR_x. Based on this graph, when the Xvel is more than 20 cm/s, in most cases, the impoundment fails. Finally, some graphs were presented that show the AR_x (total and WRI) as a function of the total width of inclusions for different configurations. These graphs can be used as a guideline for optimum design of WRI configuration in the tailings impoundment for the ground motions considered.

Chapter 5 presents the numerical simulation of an actual tailings impoundment in western Quebec, Canada. This tailings impoundment is an upstream raised tailings impoundment with dykes composed of waste rock. The starter dyke and dykes raises are composed of the WRI. This tailings impoundment is the first ever in which waste rock inclusions have been constructed. In this chapter, the results of analyses with consolidated tailings in the

impoundment are presented. The results of numerical simulation showed that the tailings impoundment without waste rock inclusion deforms excessively and fails. The effect of ground motion intensity (energy content) and frequency, WRI configuration on the critically displaced volume of tailings, and effect of inclusions configuration on the performance of the tailings impoundment are investigated. The results of the simulations showed that low frequency ground motions tend to induce more deformation than high frequency ground motions. The results also showed that if WRI configurations are selected properly, they can enhance very well the seismic performance of the tailings impoundment and decrease the critically displaced volume of tailings at the end of shaking. The response of tailings impoundment evaluated using the average value of horizontal displacements (AR_x) of downstream slope (total and WRI). Some graphs were presented that showed the AR_x of the downstream slope (total and WRI) as functions of the total width of WRI for different configurations. These graphs can be used as an optimum design guideline of WRI considering earthquakes equivalent to the ground motions applied in the simulation.

It should be noted that the three manuscripts included in this thesis (Chapters 3 to 5) are based on those initially submitted to the journals (with some minor corrections, usually requested by the evaluation committee).Corrections made later (as requested by the Reviewers and Editors, and others), before publication in the Journals, are not included here. The final published papers may thus differ from the versions appearing in the Thesis.

Chapter 6 includes a summary and a general discussion on the results; it also highlights some of the limitations of this research work.

A total of 379 dynamic numerical simulations of tailings impoundments were completed for this work. Details of all of the simulations and other important aspects of the research are presented in the appendices.

Appendix A describes the UBCSAND model with a cap (version 904aR) and shows the corresponding simulations results. It also illustrates and discusses the limitations of the UBCSAND model with a cap.

The subject of Appendix B is numerical simulations of seismic table tests conducted on tailings with and without a sand wall inclusion. The FLAC and UBCSAND model were used again for the simulations.

Appendix C presents the results of numerical simulations of a tailings impoundment based (loosely) on a mine site located in New Brunswick, Canada (with consolidated tailings). Also, some results obtained for unconsolidated tailings that are not presented in Chapter 4 are provided in this appendix.

Appendix D presents the results of numerical simulations of a tailings impoundment (based on a site located in the west of Quebec, Canada) with unconsolidated tailings. Also, some results obtained for consolidated tailings are presented in this appendix.

CHAPTER 3: ARTICLE 1-NUMERICAL SIMULATION OF THE SEISMIC AND POST-SEISMIC BEHAVIOR OF TAILINGS

Behnam Ferdosi*, Michael James, and Michel Aubertin

Submitted to Canadian Geotechnical Journal

Department of Civil, Geological and Mining Engineering, École Polytechnique de Montréal

C.P. 6079, Centre-ville, Montréal, QC, Canada, H3C 3A7

* Corresponding author: Behnam Ferdosi, Phone 514-340-4711 ext 3751; fax 514-340-4477
Email: behnam.ferdosi@polymtl.ca

Abstract

Several tailings impoundments have failed as a result of earthquakes in the last few decades. A majority of these failures were due to direct seismic loading, tailings liquefaction during shaking, or the post-seismic behavior of the tailings as it relates to the dissipation of excess pore water pressures that were generated during shaking. Previous work has indicated that the UBCSAND model (Byrne et al. 1995) is capable of simulating the cyclic simple shear testing response of low plasticity tailings over a range of consolidation stresses and cyclic shear ratios. However, the ability of the model to simulate the dynamic and subsequent behavior of such tailings for other conditions, such those induced by shakings table tests, has not yet been evaluated. In this regard, it is known that the main components of the UBCSAND model cannot realistically simulate some specific responses, including the post-seismic volumetric strains related to excess pore water pressure dissipation. This paper presents numerical modeling results of the dynamic behavior of tailings from hard rock mines. It introduces a method for simulating their post-seismic behavior by including an updating scheme for the elastic moduli into the UBCSAND model. The results of cyclic simple shear testing, seismic table testing and complementary experimental relationships were used to calibrate and validate the model with its new component. The simulated response of tailings during cyclic simple shear testing and for a complete seismic table test shows that the proposed approach simulates the experimental observations well. Level ground, seismically-induced liquefaction and post-seismic behavior of a 15-m-thick tailings

deposit are also simulated, leading to post-liquefaction settlements that are in agreement with empirical relationships.

Keywords: Tailings, Liquefaction, Settlement, Numerical modeling, Seismic behavior, Post-seismic behavior, Cyclic tests, Shaking table tests

3.1 Introduction

In the last 50 years, more than thirty tailings impoundments have failed due to seismic activity. Many of these failures have been attributed to liquefaction of the retained tailings or of tailings used to construct the retention dykes (ICOLD 2001; Aubertin et al. 2002; WISE 2014). Liquefaction of the retained tailings leads to additional loads on the retention dykes and liquefaction of tailings used to construct these dykes produces a loss of stiffness and shear strength that may lead to rupture. In at least one instance, tailings impoundment failure occurred hours after the end of earthquake shaking and was attributed to the redistribution and dissipation of excess pore water pressures that had been generated during shaking (Ishihara 1984). In recognition of the potential for post-seismic failure, analysis of the post-seismic stability of tailings impoundments is increasingly included in the design and evaluation processes (e.g. James and Aubertin, 2010; CDA, 2014). Post-seismic stability analyses generally consist of the application of the limit equilibrium method with reduced material strengths to account for excess pore water pressure generation or liquefaction (Byrne et al., 2004). However, this method may not fully consider the potentially destabilizing effects of excess pore water pressures, the associated stiffness and strength reduction and corresponding deformations. Alternatively, dynamic numerical analysis is increasingly used in the evaluation of the seismic response and stability of tailings impoundments (e.g. Lo et al. 1988; Seid-Karbasi and Byrne; 2004; Psarropoulos and Tsompanakis, 2008; Roberto et al. 2008; D'Appolonia 2009; James, 2009; James and Aubertin, 2012). To consider the effects of excess pore water pressures and their dissipation, the constitutive and numerical models must adequately simulate the seismic and post-seismic response of tailings.

Some constitutive models of material behavior currently available are capable of realistically simulating the dynamic and, by extension, the seismic behavior of tailings, particularly excess

pore water pressure generation and liquefaction. The UBCSAND model, developed by Byrne et al. (1995) and later revised and extended by others, including Puebla et al. (1997), Beaty and Byrne (1998, 2011), and Naesgaard (2011), can realistically simulate excess pore water pressure generation in sands due to cyclic loading, up to liquefaction. James (2009) showed that the UBCSAND model is also capable of simulating the behavior of low plasticity tailings from hard rock mines during cyclic simple shear testing under a range of consolidation stresses and cyclic stress ratios. However, the ability of the UBCSAND model to simulate other loading conditions such as seismic table testing of tailings has not yet been evaluated.

Seid-Karbasi and Byrne (2004) and James (2009) also used the UBCSAND model to simulate the seismic behavior of tailings in the evaluation of the seismic stability of tailings impoundments. Recent calculations have shown however that the basic form of this model cannot accurately simulate the post-dynamic settlement (reconsolidation) of tailings during excess pore water pressure dissipation (Ferdosi et al. 2013).

One of the limitations is that the plasticity (Coulomb) criterion used in the UBCSAND model does not have a cap (i.e. it is open on the positive side of the stress plane). Hence, a stress path that is parallel or that remains below the stress ratio $\eta = t/s'$ (where $t = (\sigma_1' - \sigma_3')/2$ and $s' = (\sigma_1' + \sigma_3')/2$), where σ_1' and σ_3' are principal maximum and minimum effective stresses, with units in kPa) does not meet the yield surface. Therefore, the soil usually behaves elastically during reconsolidation associated with excess pore water pressure dissipation. As a result, calculations with the UBCSAND model can give post-liquefaction volumetric strains that are often significantly lower than reality. Hence, the model may underestimate deformations in or near the retention dyke during the post-shaking behavior of a tailings impoundment. This can lead to a non-conservative assessment of performance and stability.

The numerical simulations presented in this paper aim at reproducing cyclic simple shear tests performed by James (2009) and seismic table tests conducted by Pépin et al. (2012a; 2012b) on low plasticity tailings. The simulations were conducted using version 904aR of the UBCSAND model implemented in FLAC (Version 6.0). These are used to validate and calibrate the model with respect to the dynamic behavior of tailings.

The simulations are conducted with a modified version of the UBCSAND model, which was implemented to improve the post-dynamic behavior. With the approach adopted here, an

experimental consolidation curve was used to update the values of shear and bulk moduli in the UBCSAND model to simulate the initially small but increasing stiffness of the material during excess pore water pressure dissipation and post-liquefaction volumetric strains.

The calculated settlement obtained with this approach are compared with seismic table tests results obtained by Pépin et al. (2012a, 2012b) and empirical relationships presented by Wijewickreme and Sanin (2010). The post-liquefaction reconsolidation settlement was used to assess, in a preliminary manner, the ability of the modified UBCSAND model to simulate the post-liquefaction behavior. Simulations results for laboratory tests and from field scale calculations indicate that the model can realistically simulate the behavior of tailings under seismic loading.

3.2 Validation of the UBCSAND model based on laboratory testing

James (2009) conducted 25 cyclic direct simple shear tests on specimens of tailings from a gold mine in western Quebec. The tailings were characterized as nonplastic silt (ML) with a small amount of fine-grained sand. The samples were prepared as slurry and consolidated anisotropically (K_0 conditions) to vertical effective stresses varying from 100 to 400 kPa. Dynamic loading consisted of cyclic shear stresses (cyclic stress rations varied from 0.075 to 0.15) applied under constant volume conditions at a frequency of 1 Hz (see also James et al. 2011).

James (2009) used FLAC (version 5) and the UBCSAND model (version 904A) to simulate the cyclic direct shear tests. The numerical calculations demonstrated the ability of the model to simulate the dynamic behavior of these tailings reasonably well, particularly pore water pressure generation and shear strain. A key finding of the tests simulations was that the corrected, clean sand standard penetration test blow count, $(N_1)_{60\text{-}cs}$, and the constant volume friction angle, ϕ_{cv}, of the tailings, two key parameters of the UBCSAND model, were independent of the consolidation stress.

In this current research, version 904aR of the UBCSAND model was calibrated based on a single cyclic direct simple shear test performed by James (2009) where the sample was anisotropically consolidated under a stress of 100 kPa, with cyclic loading consisted of a CSR of 0.10 at a frequency of 1 Hz.

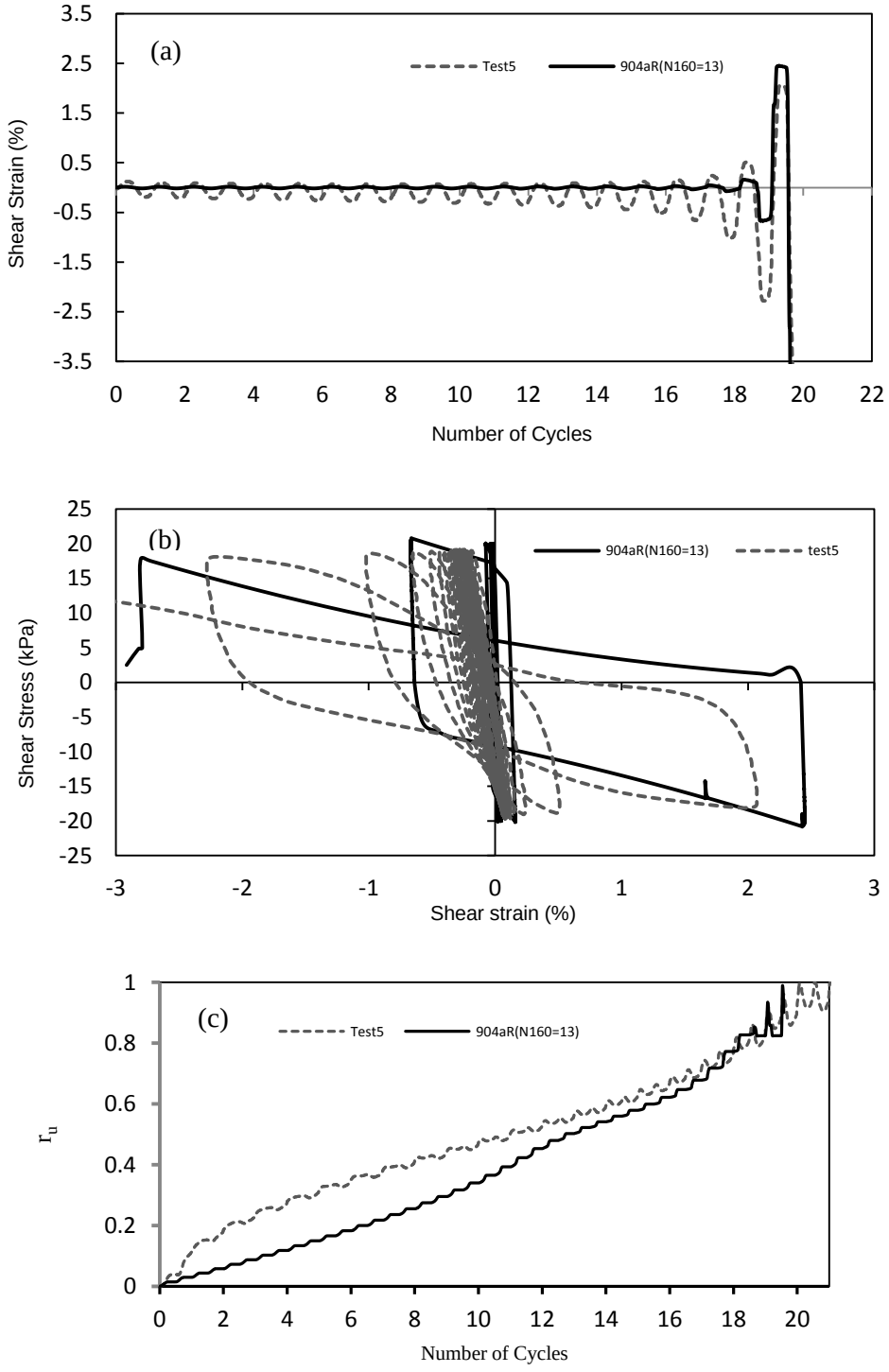

Figure 3-1: (a) Shear strain versus number of cycles for a CDSS (cyclic direct simple shear test) test on tailings, and FLAC modeling, (b) Shear stress versus shear strain for a CDSS test on tailings, and FLAC modeling, (c) Development of the excess pore water pressure ratio, r_u (ratio of excess pore water pressure to initial effective stress), during CDSS testing and simulation

The properties of the sample were based on the results of conventional laboratory testing, including the constant volume friction angle, ϕ_{cv}, which equaled 35.6°. The corrected standard penetration resistance, $(N_1)_{60\text{-}cs}$ was found iteratively (using the UBCSAND model) such that the behavior of the simulated sample was similar to that of the laboratory test with respect to the general stress-strain behavior and the number of cycles to cause liquefaction (assumed to occur at a shear strain of 3.75%). This lead to a $(N_1)_{60\text{-}cs}$ value of 13 (blows/30 cm). The results of the actual test and simulation are shown on Figure 3-1. The calculations shown here complement those performed by James (2009) for different ranges of cyclic shear stress ratios and confining effective stresses. As can be seen in Figure 3-1, there is a good agreement between the simulations and experimental results.

3.3 Updating of the shear and bulk moduli based on the consolidation curve

Previous work performed by Tokimatsu and Seed (1987), Thomas (1992), Sento et al. (2004), Hydes et al. (2007), Higuchi and Ejiri (2012), and Ziotopoulou and Boulanger (2013) indicated that the post-liquefaction reconsolidation of soils is dependent on the initial void ratio, e_0 (or density index or relative density), accumulated (or maximum) shear strain at the end of cyclic loading, effective confining stress, and initial shear stress.

Using the conventional Terzaghi consolidation solution, Sento et al. (2004) proposed a model to predict the post-shaking reconsolidation behavior of sand, considering the effect of the above mentioned parameters. Higuchi and Ejiri (2012) successfully used this model to predict ground settlement due to liquefaction. A similar approach is used here to represent the post-liquefaction behavior of low plasticity tailings.

Based on this approach, the relationship between volumetric strain increments and mean effective stress can be expressed as (Sento et al., 2004):

$$d\varepsilon_v = \frac{0.434 C_c}{1 + e_0} \frac{dp'}{(p' + p_0 \times 10^{-x})} \tag{3.1}$$

where $d\varepsilon_v$ is the volumetric strain increment; C_c is the compression index; e_0 is the initial void ratio; p' is the mean effective stress; p_0 is the initial mean effective stress; exponent x is computed based on the density index (or relative density) and accumulated shear strain. Sento et al. (2004) presented a graph (based on tests results) that gives a relationship between exponent x, cumulated shear strain and relative density of Toyoura sand; the value of x varies between 2 and 8 for a shear strain of up to 400%, at a relative density of 65%.

Rearranging the formula proposed by Sento et al. (2004) gives the coefficient of volumetric compressibility m_v:

$$m_v = \frac{d\varepsilon_v}{dp'} = \frac{0.434C_c}{1+e_0}\frac{1}{(p' + p_0 \times 10^{-x})} \tag{3.2}$$

Application of this relationship to tailings is supported by pre- and post-liquefaction consolidation tests performed by Thevanayagam and Martin (2001) who showed that silt, silty sand and sand often have a comparable (same order of magnitude) compressibility (m_v) at similar effective stresses. Additionally, Thevanayagam and Martin (2001) and Hyde et al. (2007) showed that the pre- and post-liquefaction consolidation curves of loose silts are parallel to each other in the *e-p'* plane (i.e. same value of C_c). Other testing results also showed that low plasticity tailings from hard rock mines behave as sandy soils in many ways (e.g. James, 2009; James et al. 2011). These observations thus tend to suggest that the model proposed by Sento et al. (2004) can be used to compute the coefficient of volume change (m_v) of tailings during post-shaking reconsolidation.

The value of Young's modulus at each level of effective stress can then be obtained from the following relationship (e.g. Bowles 1996):

$$E = \frac{(1+v)(1-2v)}{(1-v)m_v} \tag{3.3}$$

where υ is Poisson's ratio. These relationships have been added to the FISH version of the UBCSAND model to update the values of the elastic shear (*G*) and bulk (*B*) moduli of tailings as a function of the effective stress during the post-shaking analysis.

Consolidation curves obtained from compression column tests on tailings slurry conducted by L. Bolduc (2012), Essayad (2014) and by the first author were used to calibrate the model, using the method proposed by Sento et al. (2004).

Figure 3-2 shows the comparison between one of the consolidation curves, from a representative test result, and the curve given by equation (3.1). As shown in this figure, there is very good agreement between the results of the test and the calculated curve. In this case, it was determined that the value of the compression index C_c = 0.07 (based on the test results), for an initial void ratio (e_0) of 0.99; the value of x was set at 2 for the simulations; additional calculations indicated that the results are not very sensitive to this value (for the range of values mentioned above). It should be mentioned that other parameters such as C_c, and e_0 are independent of parameter x. The results in Figure 3-2 indicate that the model of Sento et al. (2004) can be used to represent the consolidation behavior of the tailings.

Post-shaking reconsolidation of seismic table testing by Pépin et al. (2012a, 2012b) was then simulated and the calculated settlements were compared with measured values; these results are presented below. Subsequently the simulated post-shaking settlement of a level ground tailings deposit will be compared with values estimated by the method of Wijewickreme and Sanin (2010).

3.4 Shaking table test simulation

3.4.1 Material properties

To assess the validity of the above described approach for cyclic loading conditions, simulated results are compared with experimental testing data. Pépin et al. (2012a, 2012b) conducted seismic table tests to investigate the dynamic behavior of tailings with and without draining or rigid inclusions. One of these tests was on lightly tamped, saturated homogeneous tailings. The density index of the tailings was about 80%. The dimensions of the rigid box used for the testing was 107-cm-square in plan and 75 cm in height. The tailings were placed in the box to a height of 51 cm. Basic properties of the tailings are given in Table 3.1.

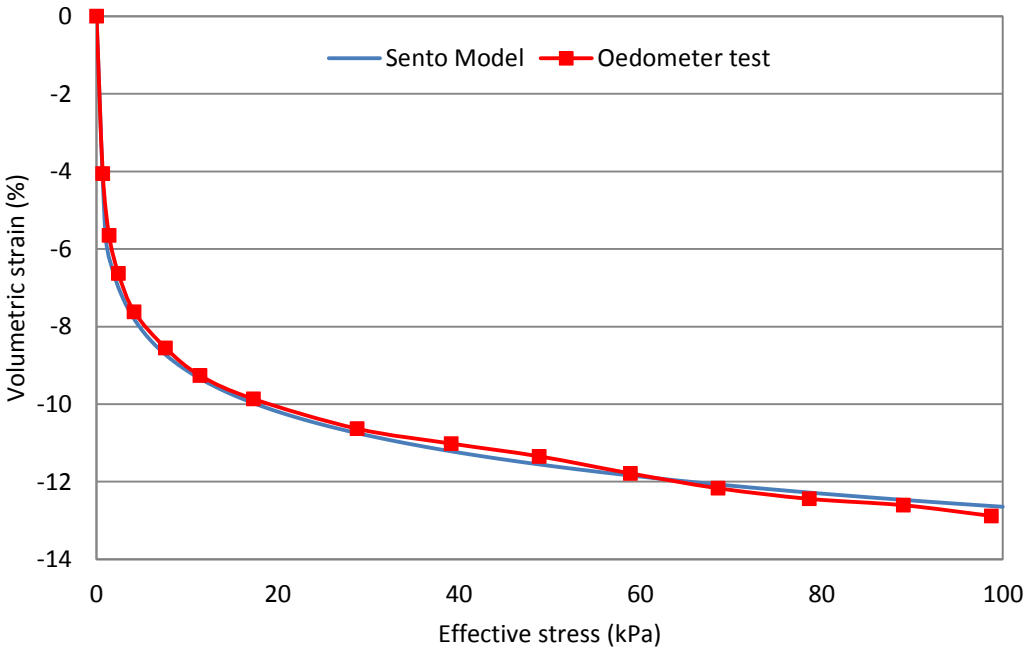

Figure 3-2: Comparison between the measured consolidation curve and the curve given by the by Sento et al. (2004) model

Table 3.1: Summary of tailings characteristics for test 3 on the shaking table (after Pépin et al. 2012b)

Characteristics	Property
USCS Classification	ML
Solid grain relative density	3.39
Initial void ratio, eo	0.62
Maximum void ratio, emax	1.46
Minimum void ratio, emin	0.48
D10 (mm)	0.005
D50 (mm)	0.04
D60 (mm)	0.048

The UBCSAND model was used to simulate the behavior of tailings. Input parameters are shown in Table 3.2. In this model, the stress dependent elastic shear and bulk moduli were defined as follows:

$$G = k_g^e P_A \left(\frac{p'}{P_A}\right)^{ne} \tag{3.4}$$

$$B = k_B^e P_A \left(\frac{p'}{P_A}\right)^{me} \tag{3.5}$$

where k_g^e and k_B^e are the elastic shear and bulk modulus numbers, *ne* and *me* are modulus exponents, and P_A is atmospheric pressure in kPa .

Table 3.2: Input parameters used to simulate shaking table testing on tailings (test 3)

$(N_1)_{60}$	Density (kg/m^3)	ϕ_{cv}° (measured)	Initial porosity (n)	Shear modulus number k_g^e	Bulk modulus number k_B^e
30	2200	35.6º	0.39	110*	261*

ϕ_{cv}°= constant volume friction angle

* details are available in section 3.4.1

Based on results taken from the literature (e.g. Liang and Elias 2010; Jaouhar et al. 2011; Ormann et al. 2011) and from various tests conducted on similar types of (relatively dense) tailings (L. Bolduc, 2012; Essayad, 2014), it has been established that the value of Young's modulus is usually between 3000 to 10000 kPa. An average value of 7000 kPa was adopted for the initial simulations, with a Poisson ratio ν equal to 0.31 (typical for such materials). The corresponding values of the shear and bulk moduli then become *G* = 2671 kPa and *B* = 6140 kPa.

The maximum mean effective stress (static) in the tailings during the shaking table test was about 5.3 kPa. Applications of equations (3.4) and (3.5) used in the UBCSAND model leads to (rounded) values of the shear k_g^e and bulk k_B^e modulus numbers of 110 and 260, respectively. These values were used in all of the simulations of seismic table tests.

A saturated hydraulic conductivity k_{sat} of 1x10^{-8} m/s was used for the tailings in the simulation. This value of k_{sat} is in the lower range given by Mbonimpa et al. (2002) and Bussière (2007) for hard rock tailings; additional measurements on somewhat similar tailings recently gave k_{sat} values between 1x10^{-8} and 2x10^{-7} m/s (Essayad, 2014).

The UBCSAND model often tends to underestimate the value of damping at low shear strains and overestimate the value of the damping at high shear strains (Beaty and Byrne, 2011). A

minor value of stiffness proportional Rayleigh damping was thus initially applied to the tailings and then removed once the shear strain value reached 0.015%. A FISH function was written to monitor the shear strain in each element; when the value of shear strain reached 0.015%, Rayleigh damping was removed from that element. This threshold value 0.015% for the shear strain was selected based on the simulations results of cyclic simple shear tests of sand and comparison of predicted and measured value of damping reported by Beaty and Byrne (2011).

3.4.2 Boundary conditions

The shaking table test (No 3) was conducted using a sinusoidal dynamic loading with theoretical peak horizontal acceleration of 0.1 g and a frequency of 1 Hz. Five piezometers were installed at heights of 6.4, 14.4, 19.4, 30.4, and 39.4 cm from the top of the tailings, as shown in Figure 3-3, to measure the excess pore water pressure during the seismic loading.

Since a rigid box was used on the seismic table, the dynamic load was applied at the base and on both sides of the model. The dynamic load was applied as horizontal velocity based on integration of the acceleration function. Figure 3-3 shows the mechanical boundary conditions, horizontal velocity seismic loads and the position of the piezometers inside of the rigid box.

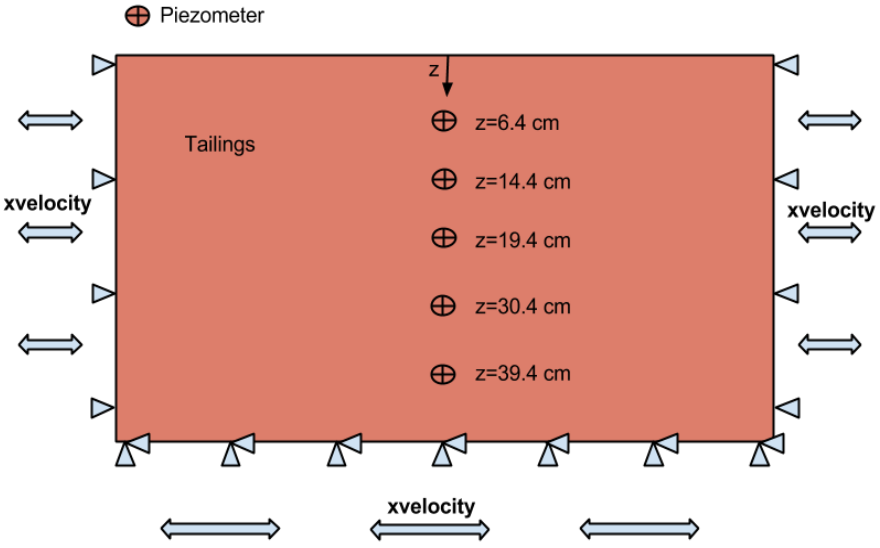

Figure 3-3: Boundary conditions imposed to the model and piezometric measurement locations

3.4.3 Simulation results during shaking

The numerical simulation corresponding to the results shown here was performed with the small value of 0.015% for the stiffness proportional damping for zones in which the shear strain was below the threshold value of 0.015%. Figure 3-4 shows that calculations with this stiffness proportional damping, for a predominant frequency of 1 Hz, lead to a very good agreement between the simulated excess pore water pressures and those of measured in the test for depths of 6.4, 14.4, and 19.4 cm. This figure also indicates that the EPWP generation rates at depths of 30.4 and 39.4 cm is somewhat higher than those of the actual testing, but there is nonetheless a good agreement between the final values of the excess pore water pressures measured during testing and calculated with FLAC. Additional simulations results obtained without considering stiffness proportional damping are presented by Ferdosi et al. (2014); the latter give a poorer agreement than the one shown in Figure 3-4.

The differences between some of the predicted and measured pore water pressures, particularly the rate of pore water pressure development, can be attributed, at least partly, to the limitation of a 2D plain strain numerical modeling which cannot perfectly simulate 3D physical phenomena.

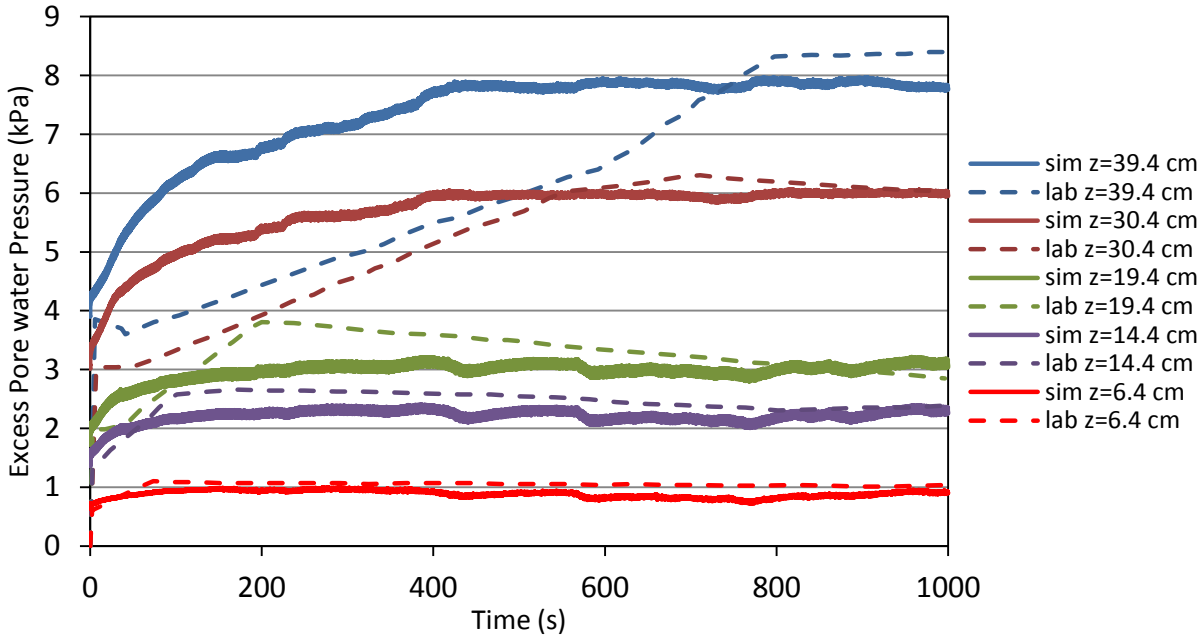

Figure 3-4: The results of the generated excess pore water pressure measured (test 3) and predicted by the UBCSAND model, considering a small value of stiffness proportional damping for zones in which shear strain is less than 0.015%

3.4.4 Post-shaking settlement

After shaking stopped during the test, the surface of the tailings specimen experienced 9.9 mm of settlement due to excess pore water pressure dissipation.

Calculations made for this part of the test were performed using the UBCSAND model with updating of the shear and bulk moduli, as described above, to simulate the post-shaking behavior of the tailings.

A compression index, C_c, of 0.095 was adopted for the liquefied tailings, based on values obtained by L. Bolduc (2012) and Essayd (2014) (see also Bussière, 2007). The value of x = 2 (Eq. 2) used in these calculations correspond to the lowest value reported by Sento et al. (2004) for sand, for relevant conditions. A sensitivity analysis performed with x equal to 3 to 7 indicated that this value had little effect on the post-shaking settlement. Again, the Poisson's ratio was 0.31.

During the post-shaking phase of the simulation, the value of m_v changes with the variation of the effective stress due to excess pore water pressure dissipation. This is required to capture the observed response of the tailings as indicated by Figure 3-2. The values of m_v and of the elastic moduli were computed using Equations 3.2, 3.3, 3.4, and 3.5 (details are available in section 3.3).

The simulation leads to a surface settlement due to excess pore water pressure dissipation of 10.3 mm. There is thus a good agreement with the measured value of 9.9 mm for the settlement in seismic table test No.3. The post-liquefaction settlement of the seismic table test was also simulated with the original UBCSAND model for constant (without updates) shear and bulk moduli numbers, leading to a settlement less than 1 mm. There is thus a major influence of this modification to the model, which is required to bring the simulation results closer to the experimental data.

3.5 Post-liquefaction settlement of a level ground model

To evaluate the above mentioned approach under more realistic conditions, a 15-m deep tailings deposit underlain by 2 m of dense till and then by hard rock was simulated with FLAC (based on a model analyzed by James, 2009, which was itself loosely based on a real case).

3.5.1 Geometry and boundary conditions

The model as shown in Figure 3-5 is 130-m-wide and 18 m-high. The surface of the tailings was assumed to be flat with imposed level ground conditions and the groundwater table positioned at the surface.

The seismic load was applied as input motion (acceleration) to the bottom of model as shown in Figure 3-5. Ground motion record S-16T of the 1988 Saguenay earthquake (moment magnitude 5.9; NRC, 2003), was applied at the base of the model to simulate the occurrence of an earthquake. Also, the free field boundary condition was considered for along sides of the model as shown in Figure 3-5 in yellow.

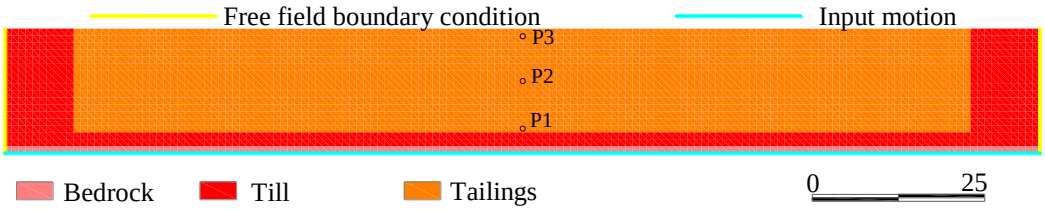

Figure 3-5: Geometry and boundary condition of the FLAC model used to seismic analysis of level ground condition

3.5.2 Material properties

The material properties used for the tailings were the same as those used above for the cyclic simple shear tests. Typical published values were used for the till and bedrock as shown in Table 3.3 (James 2009).

The corrected value of $(N_1)_{60}$was 13, based on the value that has been obtained from calibration of the model using the simple cyclic shear test. The initial void ratio was 0.62.

3.5.3 Simulation results

As a result of seismic loading, excess pore water pressures were generated and liquefaction developed throughout the tailings deposit. A post-shaking analysis was done using coupled mechanical-fluid analysis, to assess consolidation due to excess pore water pressure dissipation,

Table 3.3: Material properties of Bedrock and Glacial till (taken from James, 2009) for simulations of the tailings impoundment

Material Properties	Bedrock	Glacial Till
Model	Mohr	Mohr
Dry density ρd , (kg/m3)	2,200	2,000
Friction angle, φ (°)	40	36
Cohesion, c (kPa)	50,000	250
Dilation angle, φ_d(°)	15	10
Porosity, n	0.10	0.15
Shear modulus, G (MPa)	7.69×10^{4}	360
Bulk modulus, B (MPa)	1.67×10^{4}	780
Hydarulic conductivity, k (m/s)	1.0×10^{-8}	1.0×10^{-7}

using the Sento et al. (2004) approach. The model was run for three different values of the compression index, C_c = 0.07, 0.18, and 0.3. The value of x in Equation 3.2 (for varying moduli) was set at 2.

Figure 3-6 shows the variation of the r_u (ratio of excess pore water pressure to initial effective stress) during the seismic loading at the bottom, middle, and top of the model. As shown in this figure, the PWPs tend to increase progressively during seismic loading, until they reach a plateau at different times (depending on their depth). All zones reached r_u > 0.9 in this case. The average value of the excess pore water pressure ratio, r_u, in the central part of the model at the end of shaking was about 0.94.

According to an analysis presented by Naesgaard and Byrne (2007) and Naesgaard (2011), zones with a value of r_u more than 0.7 during the seismic loading and between 0.5 and 0.7 at the end of seismic loading may be considered as having liquefied; such critical values of r_u agree with relationships presented by Idriss and Boulanger (2008).

A FISH function was written in FLAC to compute the maximum value and final value of r_u during and at the end of the seismic loading. When the value of r_u is more than 0.7 during the seismic load and more than 0.6 at the end of loading, the simulations uses the proposed method (i.e. adjustment of elastic moduli based on the Sento et al. 2004 approach) with the UBCSAND model to compute the post-shaking consolidation of tailings.

The numerical simulations performed with three values of C_c, i.e. 0.07, 0.18, and 0.3 (considering updated values for the elastic moduli, given by Eq. 2 and 3), predicted settlements of the ground surface equal to 31, 48, 56 cm, respectively. These results for the post-shaking settlements are in good agreement with the estimated values from the empirical method of Wijewickreme and Sanin (2010) that vary from 24 to 40 cm. Hence, the modeling approach adopted here appears to represent quite well the response of tailings during and after seismic loading.

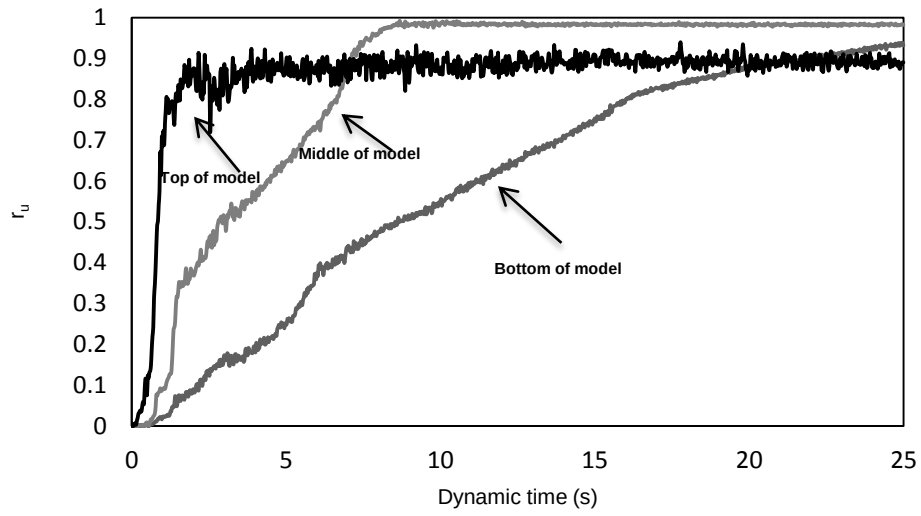

Figure 3-6: Variation of excess pore water pressure ratio r_u with time during seismic loading in the bottom, middle, and top of the model (P1, P2, and P3 points as shown in Figure 3-5) for level ground using UBCSAND

3.6 Discussion

3.6.1 Alternative model with a cap

As an alternative to the modified stiffness approach presented above, the UBCSAND model was modified by adding a cap to the yield surface (based on the model describe by Puebla et al, 1999) to capture volumetric plastic strains (Ferdosi et al. 2013). This approach has some advantages over the one used here, including the possibility of producing strain hardening of the tailings. However, the UBCSAND model with a cap tended to develop numerical errors in FLAC, which prevented completion of the simulations. These errors may be attributed to numerical

singularities that exist at the intersection of the cap with the shear yield surface. More work would be required on this aspect to use it for the analysis of tailings impoundments.

3.6.2 Limitations and ongoing work

Although the results presented above are very encouraging, some limitations should be kept in mind. For instance, the results of the numerical simulation of shaking table test showed that the rate of pore water pressure generation near the bottom of the model is higher than measured values reported by Pépin et al. (2012a, 2012b). As mentioned above, the differences in the rate of generation of excess pore water pressure may be due, at least in part, to the inability of the plane strain model to simulate all of the mechanisms involved in the dynamic loading of a specimen in a relatively narrow rigid box. Also, the value of $(N_1)_{60}$ = 30 used in these simulation seems somewhat high for tailings with a relative density of 80%. However, simulations with different values of $(N_1)_{60}$ (of 15, 20, and 25) did not provide a better match with the measured pore water pressures. Hence, this aspect may require additional work.

Also, a sensitivity analysis was performed with additional strain values of 0.01%, 0.02%, 0.025%, and 0.03% as the threshold to remove the stiffness proportional damping during the simulation. The results of this analysis showed that the value of 0.015% yields better results for tailings submitted to a shaking table test. Additional work is also underway to simulate other conditions related to the response of tailings and tailings impoundments, including the presence of waste rock inclusion (James et al. 2013; L. Bolduc and Aubertin, 2014).

3.7 Conclusion

The liquefaction of tailings in cyclic simple shear test and seismic table test were simulated by the UBCSAND model implemented in FLAC. The results show that this model can predict well the pore water pressure generation measured during CDSS and seismic table tests. However, the model had to be modified to simulate the post-shaking settlement of tailings observed during seismic table tests. To do so, the method of Sento et al. (2004) was combined with the UBCSAND model to update the elastic moduli and calculate the post-shaking settlement of tailings. The simulations results obtained with this approach were compared with the measured settlement after a shaking table test and with predicted values from an empirical method for a large scale tailings impoundment. The comparisons show an encouraging agreement in both

cases. These results are being used to further advance the analysis of the seismic performance of tailings impoundments.

3.8 Acknowledgements

This research work is being supported by the Natural Sciences and Engineering Research Council of Canada (NSERC), the partners of the Industrial NSERC Polytechnique-UQAT Chair (2006-2012) and those of the Research Institute on Mines and the Environment (RIME UQAT-Polytechnique; www.rime-irme.ca)

3.9 References

Aubertin, M., Bussiere, B., and Chapuis, R. 1996. Hydraulic conductivity of homogenized tailings from hard rock mines. Canadian Geotechnical Journal, 33(3):470-482.

Aubertin, M., Mbonimpa, M., Jolette, D., Bussiere, B., Chapuis, R.P., James, M., Riffon, O. 2002. Stabilité géotechnique des ouvrages de retenue pour les résidus miniers: problèmes persistants et méthodes de contrôle. Défis & Perspectives : Symposium 2002 sur l'environnement et les mines, Rouyn-Noranda, 3-5 novembre 2002. Développement Économique Canada/Ministère des Ressources Naturelles du Québec/CIM. Comptes-Rendus sur CD-ROM.

Bardet, J.P. 1997. Experimental soil mechanics, Prentice-Hall, Upper Saddle River, NJ.

Beaty, M. and Byrne, P. M. 1998. An effective stress model for predicting liquefaction behavior in sand. Proceedings of Geotechnical Earthquake Engineering and soil dynamic III, Seattle, Washinton, USA. ASCE Special Publication. 75(1):766-777.

Beaty, M.H. and Byrne, P.M. 2011. UBCSAND constitutive model Version 904aR. Document report: UBCSAND Constitutive Model on Itasca UDM Web site: http://www.itasca-udm.com/pages/continuum.html.

Bowles, J. E. (1996). Foundation analysis and design (5th edition). New York, USA : McGraw-Hill College.

Bussière, B. 2007. Hydro-Geotechnical properties of hard rock tailings from metal mines and emerging geo-environmental disposal approaches. Canadian Geotechnical Journal, 44(9): 1019-1052.

Byrne, P.M., Roy, D., Campanella, R.G., and Hughes, J., 1995. Predicting liquefaction response of granular soils from pressuremeter tests, ASCE National Convention, San Diego, USA; ASCE Geotechnical Special Publication 56.

Byrne, P.M., Park, S., Beaty, M., Sharp, M., Gonzalez, L., and Abdoun, T. 2004. Numerical modeling of liquefaction and comparison with centrifuge tests, Canadian Geotechnical Journal, 41(2):193-211.

Canadian Dam Association (CDA). (2014). Application of dam safety guidelines to mining dams. Edmonton AB: Canadian Dam Association.

D'Appolonia Engineering. 2009. Engineering and Design Manual – Coal Refuse Disposal Facilities. 2nd Edition, Mine Safety and Health Administration (MSHA), Pittsburgh, PA, USA.

Essaayd, K. 2014. Master Thesis (to be completed), Ecole Polytechnique de Montreal.

Ferdosi, B., James, M., and Aubertin, M. 2013. Numerical modeling of the post-liquefaction consolidation of tailings, Proc. GeoMontreal 2013, Montreal, Qc, Canada. Canadian Geotechnical Society. 7 pages.

Ferdosi, B., James, M., and Aubertin, M. 2014. Numerical modeling of seismic table testing of tailings with and without inclusion, GeoRegina 2014, Regina, Saskatchewan, Canada. Canadian Geotechnical Society. 6 pages.

Geremew, A.M., Yanful, E.K. 2013. Dynamic properties and influence of clay mineralogy types on the cyclic strength of mine tailings. International Journal of Geomechanics, 13(4):441-453.

Higuchi, S. and Ejiri, J. 2012. Influence of the earthquake motion characteristics on the ground settlement behavior due to liquefaction. Proceedings of the International Symposium on Engineering Lessons Learned from the 2011 Great East Japan Earthquake, March 1-4, Tokyo, Japan.,1:789-800.

Hyde, A., Higuchi, T., Yasuhara, K. 2007. Postcyclic recompression, stiffness, and consolidated cyclic strength of silt. Journal of Geotechnical and Geoenvironmental Engineering, ASCE, 133(4):416-423.

ICOLD. 2001. Tailings dams – risk of dangerous occurrences – lessons learnt from past experiences. International Commission on Large Dams and United Nations Environmental Program (ICOLD), Paris. Bulltin No. 121.

Ishihara, K. 1984. Post-earthquake failure of a tailings dam due to liquefaction of the pond deposit. Proceedings of the International Conference on Case Histories in Geotechnical Engineering, Rolla, Missouri, USA. University of Missouri. 1:1129-1143.

James, M. 2009. The use of waste rock inclusions to control the effect of liquefaction in tailings impoundments . Ph.D. Thesis, Ecole Polytechnique de Montreal, Montreal QC, Canada.

James M. and Aubertin, A. 2010. On the dynamic response of tailings and the stability of tailings impondments for hard rock mines. Geotechnical News 23(3), 39-43.

James, M., Aubertin, M., Wijewickreme, D., Ward Wilson, G. 2011. A laboratory investigation of the dynamic properties of tailings. Canadian Geotechnical Journal, 48(11): 1587–1600.

James, M., Aubertin, M. 2012. The use of waste rock inclusions to improve the seismic stability of tailings impoundments. GeoCongress 2012, Okland USA. American Society of Civil Engineers. 1: 4166-4175.

James, M., Aubertin, M., Bussière, B. 2013. On the use of waste rock inclusions to improve the performance of tailings impoundments. Proc.18th Int. Conf. Soil Mechanics and Geotechnical Engineering, Paris 2013, ISSMGE, pp. 735-738.

Jaouhar, E.M., Aubertin, M. , and James, M. 2011, Effect of mine waste rock inclusions on the consolidation of tailings. Proc. Pan-Am CGS Conference, Toronto, Canada. Canadian Geotechnical Society. 8 pages.

L. Bolduc, F. 2012. Une étude sur l'utilisation des roches stériles comme inclusions drainantes dans les résidus miniers, MScA Thesis, Ecole Polytechnique de Montréal, Montreal QC, Canada.

L. Bolduc, F., Aubertin, M. 2013. Analysis the effect of waste rock inclusions on tailings consolidation: Laboratory and modeling of the large scale in situ behavior, Proc. GeoMontreal 2013, Montreal, Qc, Canada. Canadian Geotechnical Society. 7 pages.

L. Bolduc, F., Aubertin, M. (2014). Numerical investigation of the influence of waste rock inclusions on tailings consolidation. Canadian Geotechnical Journal.Vol. 51, (to be published),12 pages.

Liang, J. Z., Elias, D. 2010. Seismic evaluation of tailings storage facility. Proc. Australian Earthquake Engineering Society 2010 Conference, Perth, Western Australia. Australian Earthquake Engineering Society. 8 pages.

Lo, R.C., Klohn, E.J., Finn, and W.D.L. 1988. Stability of hydraulic sandfill tailings dams. Hydraulic Fill Structures. ASCE. p.549-572.

Mbonimpa, M., Aubertin, M., Chapuis, R. P., and Bussiere, B. 2002. Practical pedotransfer functions for estimating the saturated hydraulic conductivity. Geotechnical and Geological Engineering, 20(3): 235-259.

Mosquera, J., Hamade, T., Mitri, H. 2013. Comparative stability analysis of tailings storage facilities. 23rd World Mining Congress, 11-15 August, Montreal, Canada. Canadian Institute of Mining and Metallurgical. Paper 566.

Naesgaard, E. 2011. A Hybrid Effective Stress-total stress procedure for analyzing embankments Subjected to potential liquefaction and flow. PhD. Thesis, The University of British Coulombia, Vancouver BC, Canada.

Naesgaard, E., Byrne, M. 2007. Flow liquefaction simulation using a combined effective stress-total stress approach. Proc. OttawaGeo2007, Ottawa, Ontario, Canada. Canadian Geotechnical Society. pp. 943-950.

Natural Resources Canada (NRC). 2003. Processed ground motions records of the 1988 Saguenay earthquake. Website accessed on June 16, 2003. http://www.seismo.nrcan.gc.ca/nwfa/index_e.php

Ormann, L., Zardari, M.A., Mattson, H., Bjelkevik, A., Knutsson, S. 2011. Numerical analysis of curved embankment of an upstream tailings dam. Electronical Journal of Geotechnical Engineering, 16(1):931-944.

Pépin, N., Aubertin, M., James, M., Leclerc, M. 2012a. Seismic simulator testing to investigate the cyclic behavior of tailings in an instrumented rigid box. Geotechnical Testing Journal, 35(3): 469-479.

Pépin, N., Aubertin, M., James, M. 2012b. Seismic table investigation of the effect of inclusions on the cyclic behavior of tailings. Canadian Geotechnical Journal, 49(4): 416-426.

Psarropoulos, P.N. et Tsompanakis, Y. 2008. Stability of tailings dams under static and seimic loading. Canadian Geotechnical Journal, 45(5): pp.663-675.

Puebla, H. 1999. A constitutive model for sand and the analysis of the CanLex embankments. Ph.D. Thesis. University of British Columbia, Vancouver BC, Canada.

Puebla, H., Byrne, P.M., and Phillips, R. 1997. Analysis of CANLEX liquefaction embankments: prototype and centrifuge models. Canadian Geotechnical Journal, 34(5): 641-657.

Roberto, M., Marco, DF., Erica, B., and Erica, Z. 2008. Dynamic slope stability analysis of mine tailings deposits: the case of Raibl mine. Seismic Engineering Conference Commemorating the 1908 Messina and Reggio Calabria Earthquake, Reggio Calabria Italy. American Institute of Physics. 1: 542-549.

Seid-Karbasi, M., Byrne, P. M. 2004. Embankment dams and earthquakes. Hydropower and Dams, 11(2): 96-102.

Sento, N., Kazama, M., Uzuoka, R., Matsuya, A., Ishimaru, M. 2004. Liquefaction-induced Volumetric Change During Re-consolidation of Sandy Soil Subjected to Undrained Cyclic Loading Histories. Proceedings of the International Conference on Cyclic Behavior of Soils and Liquefaction Phenomena, Bochum, Germany. Balkemas. 1:199-206.

Thevanayagam, S. and Martin, G.R., 2001. Liquefaction and Post-liquefaction Dissipation / Densification Characteristics of Silty Soils, MCEER Annual Report for Research Year 1, FHWA Contract # DTFH61-98-C-00094.

Thomas, J. 1992. Static, cyclic and post-liquefaction undrained behavior of fraser river sand, Msc. Thesis, The University of British Coulombia, Vancouver BC, Canada.

Tokimatsu, K., and Seed, H. B. 1987. Evaluation of settlements in sands due to earthquake shaking, American Society of Civil Engineers, Journal of Geotechnical Engineering, 113(8): 861-878.

Wijewickreme, D. and Sanin, M.V. 2010. Post-cyclic Reconsolidation Strains in Low-plastic Fraser River Silt due to Dissipation of Excess Pore Water Pressures. ASCE Journal of Geotechnical and Geoenvironmental Engineering, 136(10): 1347-1357.

Wise Uranium Project (WISE). 2014. Chronology of major tailings dam failures. Consulted on May 15,2014. www.antenna.nl/wise/uranium/mdaf.html.

Ziotopoulou, K. and Boulanger, W. 2013. Numerical modeling issues in predicting post-liquefaction reconsolidation strains and settlements. Proc. 10th International Conference on Urban Earthquake Engineering. March 1-2, 2013, Tokyo, Japan. Tokyo Institute of Technology. pp. 469-475.

CHAPTER 4: ARTICLE 2- EFFECT OF WASTE ROCK INCLUSIONS ON THE SEISMIC STABILITY OF AN UPSTREAM RAISED TAILINGS IMPOUNDMENT: A NUMERICAL INVESTIGATION

Behnam Ferdosi*, Michael James, and Michel Aubertin

Submitted to Canadian Geotechnical Journal

Department of Civil, Geological and Mining Engineering, École Polytechnique de Montréal

C.P. 6079, Centre-ville, Montréal, QC, Canada, H3C 3A7

* Corresponding author: Behnam Ferdosi, Phone 514-340-4711 ext 3751; fax 514-340-4477
Email: behnam.ferdosi@polymtl.ca

Abstract

Over the years, seismic activity has been a relatively common cause of tailings impoundment failure. The flow of liquefied tailings from such ruptures can result in very severe consequences including loss of life and environmental damage. A co-disposal technique consisting of placing waste rock inclusions in tailings impoundments prior to and during tailings deposition was proposed by the authors. The waste rock is placed to create continuous inclusions within the impoundment, which provide a number of environmental and geotechnical benefits, particularly with respect to seismic stability. The results of numerical simulations previously performed have shown that the UBCSAND model can predict the seismic response of tailings. This constitutive model was used to conduct simulations to evaluate of the use of waste rock inclusions to improve the seismic stability of a tailings impoundment. The evaluation consists of numerical analyses of an actual impoundment, with and without waste rock inclusions, subjected to earthquake loads of various energy contents and with different predominant frequencies. The analyses were conducted in static, seismic and post-shaking phases. The displacement of the surface of downstream slope of the tailings dyke was recorded during the analyses. The results indicate that the presence of waste rock inclusions can significantly improve the seismic behavior of the impoundment by reducing the displacements of the surface of the downstream slope and the extent of potential failure zones. Also, the results show that in most cases, the influence of a low

frequency earthquake on the displacement of the downstream slope of the tailings dyke is more important than that of a high frequency earthquake. The performances of the tailings impoundment with different configurations of waste rock inclusions (varying width and center-to-center spacing) were classified based on the average normalized horizontal displacement of the downstream slope (AR_x) for a range input ground motions. Charts were then developed to show how the AR_x is influenced by the total width of inclusions, their spacing, and the input ground motions.

Keywords: Tailings, Impoundment, Liquefaction, Seismic analysis, Post-seismic analysis, Waste rock inclusion

4.1 Introduction

The seismic response of tailings impoundments may be significantly influenced by the behavior of the retained tailings as they can exert large forces on the retaining dykes during earthquake shaking, particularly if the tailings undergo strength loss (or liquefaction) as a result of excess pore water pressure generation. Following shaking, the excess pore water pressures developed in the tailings tend to dissipate through the available free surfaces (including the downstream slopes of the tailings impoundment), creating seepage pressures that may act to reduce stability. There are many examples of seismically-induced tailings impoundment failure, including for instance: the Barahona and Cerro Negro tailings impoundments in Chile during earthquakes in 1928 and 1985, respectively, which were attributed to seismically-induced liquefaction of the tailings retained by and forming the dykes (Dobry and Alvarez 1967; ICOLD 2001); the failure of Dykes Nos. 1 and 2 of the tailings impoundment at the Mochikohi Gold Mine in Japan during the 1978 Izu-Ohshim-Kinkai earthquake, which were respectively attributed to tailings liquefaction and the development of de-stabilizing seepage pressures caused by the post-shaking dissipation of excess pore water pressures (Isihara 1984); and the Tapo Canyon tailings dam during the Northridge earthquake on January 17, 1994, where liquefaction occurred in the retained tailings and portions of the dam constructed of tailings (Harder and Stewart 1996; Davis and Lighthall, 2001).

Secure storage of tailings is a very important issue for the mining industry. To help in this regard, Aubertin et al. (2002) proposed a new co-disposal method involving waste rock and

tailings. With this method, waste rock inclusions (WRI) are placed in tailings impoundments forming continuous structures having controlled width and spacing. Such WRI accelerate the consolidation of tailings and may therefore increase their shear resistance (L. Bolduc and Aubertin, 2014). James and Aubertin (2010, 2012) numerically investigated the effect of waste rock inclusions on the seismic performance of tailings impoundments. These preliminary results indicated that WRI can significantly improve the seismic response of impoundments during and after an earthquake. Pépin et al. (2012a, 2012b) conducted seismic table testing of tailings with an inclusion which showed that the presence of inclusions can reduce or retard pore water pressure generation during shaking. There are thus potential benefits in using WRI to improve the seismic stability of tailings impoundments. However, this aspect has not yet been evaluated in detail.

In this investigation, a numerical model was used to assess the effect of waste rock inclusions on the seismic performance of a tailings impoundment, based on an actual impoundment located in New Brunswick (referred to as the NBM tailings impoundment). The simulations were conducted with the UBCSAND and Mohr-Coulomb models for the tailings and the waste rock inclusions, respectively. The simulations are used here to determine the effect of WRI on the performance of the impoundment for earthquakes with different intensities and frequency contents.

The seismic response of the impoundment without waste rock inclusions (the unreinforced impoundment) was simulated using high and low frequency ground motions. The results of these simulations indicate that the impoundment may undergo large deformations due to these ground motions. The response of the tailings impoundment with waste rock inclusions (the reinforced impoundment) was then simulated using these same seismic loadings and with WRI of different widths and center-to-center spacing in the downstream slope. The effect of the waste rock inclusions was evaluated using the average horizontal displacement of the downstream slope of the tailings. The WRI configurations were then classified based on these displacements. Post-shaking stability analyses were also performed. The results include charts that show the average normalized horizontal displacements of the downstream slope of the impoundment as a function of the total width of the WRI within the downstream slope of the impoundment.

4.2 Review of related work

The tailings and waste rock co-disposal technique proposed by Aubertin et al. (2002), and described in more details by James (2009), includes various features aimed at improving the geotechnical and environmental response of mine wastes disposal sites. This technique consists of placing a layer of waste rock on the bottom and sides of the tailings impoundment and then rows of waste rock within the impoundment, which are progressively raised prior to each stage of filling. The rows of waste rock would be placed along pre-determined routes to create continuous inclusions that extend the depth of the tailings, dividing the impoundment into partly interconnected cells.

The placement of such waste rock inclusions (WRI) in tailings impoundments is expected to have a number of beneficial effects on the environmental and geotechnical performance of the impoundments. Briefly, the inclusions accelerate consolidation of the tailings, compartmentalize the tailings into cells, reduce or eliminate the quantity (and exposure of reactive) waste rock to be disposed of at a separate facility, and improve the static and seismic stability of the impoundment (James, 2009; James and Aubertin, 2010; James et al. 2013). Simulations results reported by Jaouhar et al. (2011, 2013) and L. Bolduc and Aubertin (2013, 2014) have demonstrated how the presence of such waste rock inclusions can accelerate pore water pressure dissipation during and after tailings placement.

The WRI technique considered here differs significantly from other co-disposal methods in that the waste rock and tailings are placed separately in the impoundment, rather than layered or mixed together to form a relatively homogenous material (e.g. Williams 1996; Wickland and Wilson 2005; Bussière, 2007; Khalili et al. 2010; Wijewickreme et al. 2010). The existing technique most similar to the one analysed here is the use of sand or gravel columns to control liquefaction in soil deposits (Barksdale, 1983; Aubertin et al. 2002; Adalier et al. 2003; Jaouhar, 2011). There are however key differences between the use of WRI in tailings impoundments and of such circular columns in soil deposits; these can be summarized as follows: a) the inclusions are linear structures instead of the more commonly used isolated circular (vertical) elements; b) the WRI are placed in tandem with the tailings rather than installed after tailings deposition; c) the inclusions improve the seismic stability mainly by providing reinforcement during

earthquake shaking; and d) the inclusions provide additional benefits other than improved stability, as noted above and in the following.

Work conducted on somewhat similar techniques was nonetheless considered when initiating this investigation. For instance, Adalier et al. (2003) conducted seismic table testing of non-plastic silt with and without vertical gravel columns. Their results showed that these columns retarded and reduced the pore water pressure generation within the silt during cyclic loading. This reduction was attributed to the increased rigidity of the mass which reduced shear strains. The effect of drainage via the stone columns during cyclic loading was minimal due to the relatively low hydraulic conductivity of the silt and fairly short duration of loading. This suggests that although waste rock inclusions in tailings impoundments can improve long term drainage during tailings deposition (as shown by L. Bolduc and Aubertin, 2013, 2014), their main role during a seismic event is to provide reinforcement; this assumption was confirmed by simulations conducted by James (2009; see also James and Aubertin 2012).

Pépin et al. (2012a, 2012b) conducted nine seismic shaking table tests on tailings including five tests with an inclusion consisting of a more rigid and/or more pervious material (see also Pépin 2010). The experimental results indicated that such inclusions can reduce and/or retard excess pore water pressure generation during cyclic loading (similarly to observations by Adalier et al., 2003).

The risk of migration of the fine tailings particles into the waste rock inclusions, particularly during placement and consolidation also needs to be considered; this feature has been documented for granular soil columns placed in fine soils deposits (Jaouhar, 2011). Ongoing observations at an actual mine site (with WRI) have shown however that this potential problem can be controlled by appropriate deposition measures (L. Bolduc and Aubertin, 2014). It is also noted that the improvement in seismic stability would not be directly affected by this phenomenon, because it is mainly due to the rigidity and strength of the inclusions rather than their drainage capacity (James, 2009). Nonetheless, when they remain highly pervious, the WRI can also accelerate the dissipation of excess pore water pressure during the post-shaking phase. Their contribution to the consolidation of tailings can thus increase their strength not only during deposition, but also in a post-shaking phase.

With these considerations in mind, a series of numerical simulations have been conducted to investigate the seismic response of a representative tailings impoundment, without and with WRI. These are described in the following.

4.3 Methods of Analysis

The numerical analyses were conducted in three phases: i) static; ii) dynamic; and, when failure did not occur during the dynamic analysis, iii) post-shaking.

Static analyses were conducted to evaluate the state of stresses, strains and pore water pressures within the models under a condition of mechanical and hydraulic equilibrium, i.e. the state prior to earthquake shaking.

In the dynamic analyses, earthquake ground motions were applied to simulate the occurrence of seismic loadings of known intensities. During these simulations, mechanical, hydraulic and dynamic equilibrium equations were solved simultaneously. This approach was extended to the post-shaking analysis.

Two actual earthquake ground motion records were modified for use in the simulations. The first was record S16T of the Saguenay earthquake which occurred on November 25, 1988 in the province of Quebec, Canada and had a moment magnitude of 5.9 (NRC, 2003). The epicentral distance of this ground motion record was 43 km. The second was record P9023 of the Northridge earthquake which occurred on January 17, 1994 near Los Angeles, California, USA and had a moment magnitude of 6.7 (PEER, 2014). The epicentral distance of this ground motion was 31 km.

The Saguenay (S16T) and the Northridge records (P0923) were scaled to have Arias intensities of earthquakes having magnitudes of 6.5, 7.0, and 7.5 and a fault to site distance of 30 km, and also with a magnitude of 7.0 and with a fault to site distance of 20 km. These seismic loadings were selected for the simulations based on an empirical relationship proposed by Lo and Klohn (1995). This relationship indicates that an earthquake with a magnitude of 6.5 (or larger) and a fault to site distance of 30 km could induce a “potential problem” for a typical impoundment (see also James, 2009).

The numerical simulations were conducted using version 6 of the FLAC (Fast Lagrangian Analysis of Continua) two-dimensional finite difference software program (Itasca Consulting

Group, Minneapolis, Minnesota, USA), under plane strain conditions. The large-strain mode was used to accommodate the potential for significant deformation of the impoundment. Other information on the modeling approach can be found in James (2009) and Appendix C.

4.4 Characteristics of the NBM Tailings Impoundment

The impoundment considered for this study was used for the disposal of tailings from a hard rock mine that primarily produced zinc concentrates. The impoundment is a ring-type structure that was progressively raised in the upstream direction (James and Leahy, 2010). Tailings were deposited hydraulically from the perimeter dykes. Such hydraulically deposited tailings are known to be particularly susceptible to liquefaction (Vick, 1990; Wijewickreme et al. 2005; James et al. 2011), while upstream-raised tailings impoundments may be highly vulnerable to seismically-induced rupture (Vick, 1990; Davies, 2002; Davies et al. 2002).

The exact location of the NBM tailings impoundment is undisclosed. This particular tailings impoundment was selected for this study because in situ testing data (SPT, CPT, piezometers, and shear wave velocity measurements) were available, and also because it has been deemed potentially susceptible to seismically induced liquefaction and rupture (James and Leahy, 2010).

It should be noted however that the seismic loadings used to evaluate the impoundment in this study do not correspond to the design earthquake ground motion (DEQM) parameters of the actual site. The seismic loads used here were developed to conduct a comparative assessment of the seismic behavior of a “typical” tailings impoundment without and with waste rock inclusions of various sizes and spacings. There are no WRI in the actual impoundment.

The NBM tailings impoundment has a maximum height of about 40 m. A representative cross-section of the impoundment was developed for this study, and is shown in Figure 4-1. At the selected cross-section, the impoundment consists of a compacted glacial till starter dyke with a height of 5.5 m. Tailings were hydraulically deposited from the crest of this starter dyke. Subsequently, the impoundment was raised in the upstream direction using compacted coarse tailings and deposition continued. Based on in situ testing data (CPT), the depth of the compacted tailings on the downstream slope forming the retaining dyke is estimated to be 5 m. The average inclination of the downstream slope is about 5.5:1 (H:V).

Tailings deposition and raising of the dyke occurred over a period of nearly 40 years.

The phreatic level in the impoundment was determined through piezometric measurements and is controlled by the pond level.

The in situ testing data (CPT, SPT) indicated that the tailings were under-consolidated (in the context of this thesis, the term under-consolidated means that the tailings have not yet reached the equilibrium pore water pressures, as excess PWP still remain due to the addition of tailings, i.e. not yet fully consolidated under imposed loads) at the time of testing. Analysis of the data is indicative of the stratification typical of hydraulically deposited tailings.

Subsurface conditions below the impoundment consisted of a 2-m-thick layer of medium dense glacial till underlain by moderately fractured, hard bedrock.

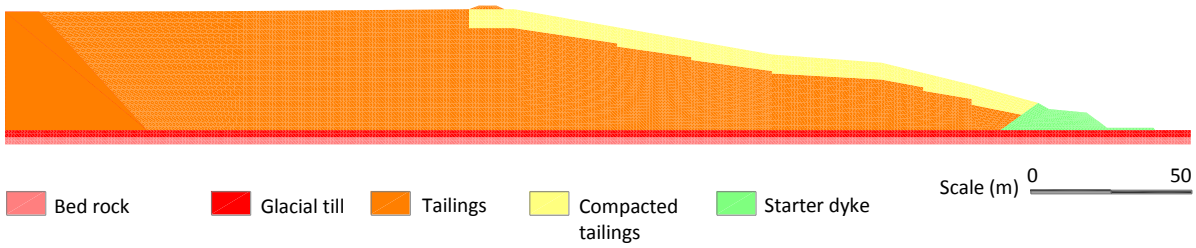

Figure 4-1: Typical section of the NBM tailings impoundment with the external dyke

4.5 Simulations of the impoundment response

The tailings impoundment, without and with WRI, was simulated numerically to evaluate its seismic performance under a series of earthquake ground motions. As a first step, the seismic performance of the impoundment without waste rock inclusion was evaluated using ground motions based on the 1988 Saguenay (Quebec) earthquake and 1994 Northridge (California) earthquakes. The impoundment with various configurations of WRI was then evaluated using the same modified ground motions. Inclusion widths of 8, 12, 16, and 25 m were considered and the center-to-center spacings of the inclusions varied from 3 to 12 times the inclusion width. For all configurations of WRI, the right corner of the first inclusion was located at x=300 m as shown in Figure 4-2(a) and the last inclusion was below the crest of the tailings dyke as shown in Figure 4-2(b).

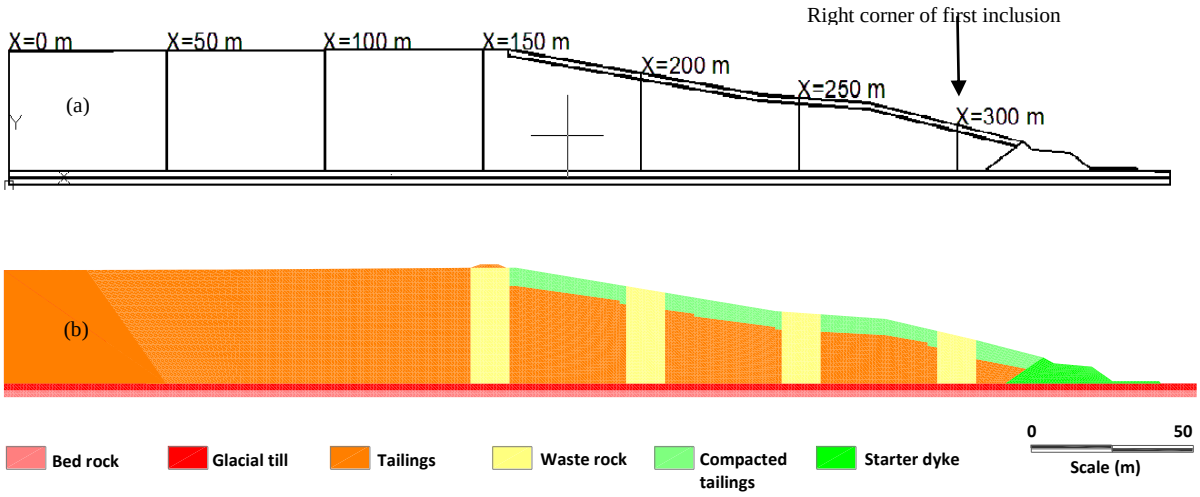

Figure 4-2: Cross section of the tailings impoundment with WRI a) schematic cross-section with locations of some points on the surface of the impoundment were simulations results are extracted; b) a typical cross section of tailings dyke reinforced by WRI

4.5.1 Constitutive Models of Material Behavior

Two constitutive models were used to represent material behavior, the Mohr-Coulomb elastic-plastic model (Itasca, 2008) and the UBCSAND model (Byrne et al. 1995; Puebla et al.1997; Beaty and Byrne1998, 2011; Puebla1999; Naesgaard 2011). The latter model was applied to the retained and compacted tailings, while the Mohr-Coulomb model was used for all other materials.

The UBCSAND model was developed to simulate the static and dynamic behavior of sandy soils (Byrne et al. 2003). This model was successfully used to simulate (and complement) conventional and large-scale dynamic laboratory testing and to conduct case histories (Puebla et al. 1997; Seid-Karbasi and Byrne, 2004; Byrne et al. 2004; Castillo et al. 2006). The UBCSAND model has also been shown to represent well the pore water pressures, shear strains development, and liquefaction of tailings (James 2009).

The material properties used by the UBCSAND model include the followings:

i. Corrected, clean-sand, standard penetration test blow count, $(N_1)_{60\text{-}cs}$, in blows per 300 mm.

ii. Constant volume friction angle, φ'_{cv}.

iii. Dry density, ρ_d.

iv. Hydraulic conductivity, k.

v. Porosity, n.

Parameters $(N_1)_{60\text{-}CS}$ and φ'_{cv} are used within the UBCSAND model to evaluate other properties required to conduct the numerical analyses.

The constant volume friction angle, φ'_{cv} defines the stress ratio $\eta = t/s'$ (where $t = (\sigma'_1 - \sigma'_3)/2$ and $s' = (\sigma'_1 + \sigma'_3)/2$), where σ'_1 and σ'_3 are principal maximum and minimum effective stresses, with units in kPa) for which plastic shear strains do not cause further plastic volumetric strains (i.e. critical state condition). This angle may be obtained from laboratory testing or from correlations with the internal peak friction angle, ϕ', and $(N_1)_{60}$ (Byrne et al. 2004).

The applicability of the UBCSAND model to the tailings was evaluated earlier in this investigation by using the model (with FLAC) to simulate the dynamic behavior of tailings submitted to cyclic simple shear testing and comparing this behavior with the results of actual tests. These simulations confirmed that the numerical model could represent well the dynamic behavior of the low plasticity tailings (James, 2009). More recently Ferdosi et al. (2013, 2014) used the UBCSAND model to simulate (with FLAC) pore water pressure generation during seismic table tests performed on tailings by Pépin et al. (2012a, 2012b), with and without a sand wall inclusion. The results of the simulations showed that the UBCSAND model can predict well the tailings behavior with and without the inclusion.

The Mohr-Coulomb model implemented in FLAC is an elasto-plastic formulation that uses a shear yield function with a tension cut off defined by the cohesion divided by the tangent of the internal friction angle. The shear flow rule is non-associated and the tension flow rule is associated (Itasca 2008).

4.5.2 Combined effective stress-total stress approach for post shaking analysis

Naesgaard and Byrne (2007) proposed a combined effective stress-total stress approach for flow liquefaction simulation. In this approach, the value of the pore pressure ratio (r_u) is monitored in all zones during shaking using a FISH function written for this purpose. This function finds and saves the maximum value of the pore pressure ratio (r_{umax}) in each zone during shaking. Another function was written using FISH to calculate the value of the pore pressure ratio ($r_{ucurrent}$) at the end of shaking (Ferdosi, 2014). Based on the criteria proposed by Naesgaard (2011), a zone is considered as having liquefied if the value of r_{umax} exceeds 0.7 and the value of $r_{ucurrent}$ is more than 0.6 (see details in Naesgaard, 2011).

Following the dynamic calculations, one of two methods may be employed for the post-shaking analysis in FLAC. The first method, selected here, is a total stress approach in which the UBCSAND model is replaced by the Mohr-Coulomb model, with a liquefied (residual) undrained shear strength assigned to liquefied zones. In the non-liquefied zones, the Mohr-Coulomb model is applied with the corresponding strength parameter (ϕ). The water bulk modulus is set to zero to prevent pore water pressure change during this analysis. The values of the shear and bulk moduli in the Mohr-Coulomb model are equal to their values at the end of shaking. The model is run in the dynamic mode under gravimetric loading only. If the displacements do not increase during the post-shaking phase, the tailings impoundment is deemed to be stable; if displacements increase, the impoundment is deemed to become unstable. The continuing displacements occur because the driving forces exceed the resisting forces and the model is not in equilibrium.

The second method, not used here, consists of a continuation of the coupled effective stress analysis (see details in Seid-Karbasi and Byrne, 2007).

4.5.3 Material Properties

Properties for the materials used in the construction of the NBM tailings impoundment were selected from data provided by James (2009) and James and Leahy (2010). . The report from James and Leahy (2010) includes values for the saturated hydraulic conductivity based on field investigation and experience with similar soils. Values for the hydraulic conductivity of the

tailings and compacted till were taken from James (2009; see also Chapuis and Aubertin, 2003; Bussière, 2007). Table 4.1 shows the values that have been used in the numerical simulations.

Table 4.1: Hydraulic Conductivity of the different materials (after James and Leahy, 2010)

Material	Saturated Hydraulic Conductivity (m/s)
Till core	5.0×10-7
Granular fill	1.0×10-5
Coarse granular fill	1.0×10-4
Rockfill	1.0×10-3
In-situ Glacial Till	5.0×10-7
Bedrock	5.0×10-6
Tailings horizontal hydraulic conductivity	2.25×10-6
Tailings vertical hydraulic conductivity	4.5×10-7
Compacted till	1.0×10-7
Horizontal hydraulic conductivity of compacted tailings	2.25×10-7
Vertical hydraulic conductivity of compacted tailings	4.5×10-8

Table 4.2 gives other material properties for the tailings, compacted tailings, starter dyke (compacted till), glacial till, and bedrock. This table indicates that the corrected SPT value, $(N_1)_{60}$, measured in 1997 was between 1 and 5 (blows/300 mm). More recently, James and Leahy (2010) gave $(N_1)_{60}$ = 3 from the tailings surface to a depth of 30 m (based on additional field testing). This normalized value of 3 was used here for the retained tailings.

The method adopted here for the post-shaking analyses requires the value of the liquefied undrained shear strength of the tailings. This value can be estimated using an experimental relationship defined by James et al. (2011), based on laboratory testing of tailings from a gold mine in western Quebec:

$$\frac{S_{u-PC}}{\sigma'_{vc}} = 0.11 \tag{4.1}$$

Where S_{u-PC} and σ'_{vc} (kPa) are the post-liquefaction undrained shear strength and initial vertical effective stress respectively.

The elastic moduli of the waste rock inclusions were computed based on the relationship proposed by Seed and Idriss (1970) and Rollins et al. (1998):

$$G_{max} = 1000(K_2)_{max}(\sigma'_m)^{0.5} \quad (4.2)$$

Table 4.2: Material properties (adapted from James 2009 and James and Leahy, 2010)

Properties	Tailings	Compacted Tailings	Starter Dam (Compacted till)	Glacial Till	Bedrock
Dry unit weight, γ_{dry} (Mg/m3)	2.35	2.4	2.4	1.95	2.2
Effective friction angle, $\emptyset'$ (deg)	36.6	36.6	35	36	40
Effective cohesion, c' (kPa)	0	0	0	0	48000
Dilation angle, ψ_d(deg)	Varied[1]	Varied[1]	10	10	10
Porosity, n	0.4	0.35	0.35	0.3	0.1
Modulus elasticity, E (MPa)	Varied[2]	Varied[2]	250	940	35000
Poisson's ratio, ν	-	-	0.3	0.3	0.3
SPT $(N_1)_{60-cs}$ blows/300 mm	P1: 1-5(*) P2: 3(*)	12	-	-	-

Notes:

-P1 is based on values measured in 1997;

-P2 is an estimation of the expected values for the present conditions;

[1] In the UBCSAND model, the dilation angle is computed based on the constant volume friction angle (φ'_{cv}) and developed friction angle (φ_d). φ'_{cv} =35.6° for tailings (based on James et al. 2011)

[2] In the UBCSAND model, the shear and bulk moduli are computed based on the corrected value of SPT and mean effective stress (see Byrne et al. 2004)

where σ'_m is effective mean stress (in lb/ft^2), The value of $(K_2)_{max}$ (dimensionless) is 30 for loose sand and 75 for dense sand. Rollins et al. (1998) reported that $(K_2)_{max}$ for gravel is 1.35 to 2.5 times higher than that for sands. Assuming a Poisson's ratio of 0.3 and a coefficient of earth pressure at-rest (K_0) of 0.4, and converting equation (4.2) to SI, the aforementioned relationship for the shear (G) and bulk (K) moduli (kPa) of waste rock inclusions becomes (James 2009):

$$G = 55000(0.6\sigma_v')^{0.5} \quad (4.3)$$

and

$$K = 2.3833G \quad (4.4)$$

where σ_v' is the effective vertical stress (kPa). A FISH program was written and included in FLAC to assign the values of shear and bulk moduli to waste rock inclusions according to the effective vertical stresses (Ferdosi, 2014).

The (fluid) bulk modulus for pure water at room temperature is 2×10^9 Pa, but because of dissolved air or air bubbles in water, the actual bulk modulus of water is usually less (Itasca, 2008). Based on Chaney (1978), this modulus can be considered an order of magnitude smaller than the bulk modulus of pure water for an air/water mixture at 99% saturation in compacted sand (Itasca, 2008). Therefore, water bulk modulus of 2×10^8 Pa was used for these analyses.

4.5.4 Damping parameters

The model constructed to represent the NBM tailings impoundment includes five materials: bedrock, glacial till, compacted till (starter dyke), retained tailings, and the compacted tailings used to raise the dyke. As stated above, the elasto-plastic Mohr-Coulomb model was used for the bedrock, glacial till, compacted till, dyke and the UBCSAND model was used for the impounded tailings and compacted tailings.

Rayleigh damping was assigned for the bedrock. The damping ratio and the center frequency of the Rayleigh damping were adjusted so that the recorded acceleration-time history at the top of the bedrock was the same as the input acceleration-time history at the base of the model. The corresponding damping ratio and center frequency for Rayleigh damping in the bedrock obtained in this manner are 0.01 and 5 Hz, respectively.

The Hysteretic Sigmoidal model-sig3 (Itasca, 2008) was used for the glacial till and compacted till. This approach leads to an asymptotic shape function that can be used to represent the degradation curve for the shear modulus *G*. This Sigmoidal model is expressed as (Itasca, 2008):

$$G_s = \frac{a}{1 + exp\left(-\frac{(L - x_0)}{b}\right)} \tag{4.5}$$

where G_s is the secant modulus, L is logarithmic strain, and a, b, and x_0 are non-dimensional parameters that are determined by fitting this function to a specific shear modulus degradation curve. The required parameters for this equation are provided by Itasca (2008) for sand and clay. The authors have used the shear modulus degradation curves presented in Seed et al. (1984) for dense sand; the corresponding parameters a, b, and x_0 (Eq. 4.5) were estimated to be 1.014, -0.4792, and -1.249, respectively. These were used for the glacial till.

The Sigmodial model-sig3 was also applied to the waste rock. The required parameters for waste rock were obtained by fitting Eq. 4.5 to the degradation curve of a gravely soil provided by in Rollins et al. (1998). Calibration of a single element model test using FLAC gave values of parameters a, b, and x_0, which were calculated to be 1.02, -0.698, and -1.45, respectively. Figures 4-3 and 4-4 show the modulus reduction and the corresponding damping ratio curves obtained from the tests results. As shown in these figures, there is good agreement between the results from the numerical simulations using of a single element and the testing results reported by Rollin et al. (1998).

Beaty and Byrne (2011) noted that the UBCSAND model often tends to underestimate the damping at low strains and overestimates the damping for large strains (see also Boulanger et al., 2011; Bray and Dashti, 2012). A number of authors (e.g. Naesgaard et al. 2004; Armstrong et al. 2010; Boulanger et al. 2011; Fung et al. 2011; Dashti and Bray 2012; Ziotopoulou et al. 2012) have mentioned that a small value of stiffness proportional Rayleigh damping is necessary for the elastic response under high frequency motions, to prevent the effect of numerically generated noise on the results. Itasca (2008) also noted that adding a small amount of damping often helps remove residual numerical oscillations without affecting the solution. Therefore, a value of stiffness proportional damping of 0.2%, with the predominant frequency of the input motion, was assigned to the tailings, compacted tailings and waste rock; this provided more stable numerical calculations.

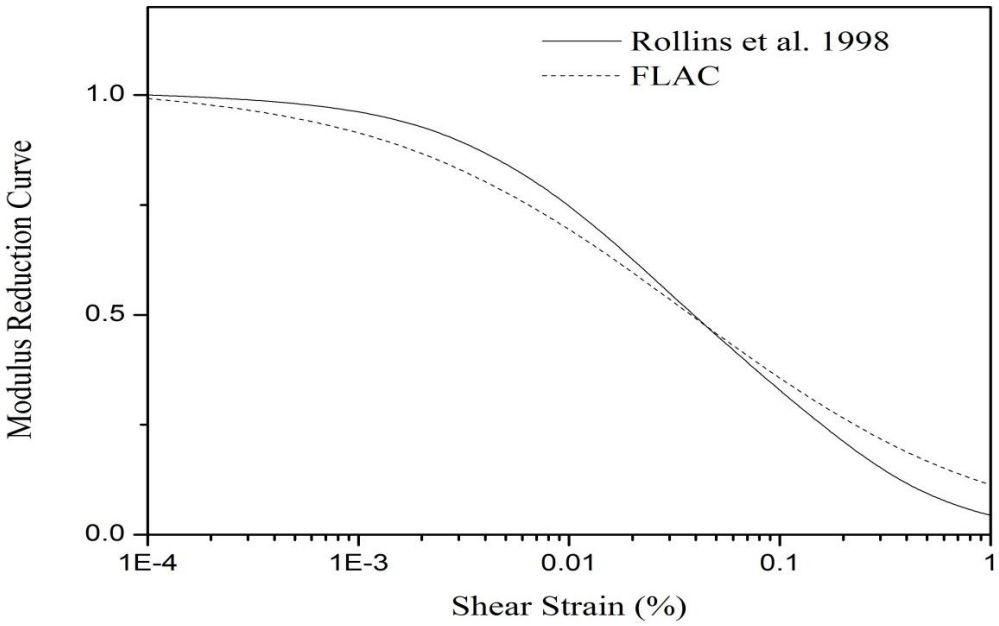

Figure 4-3: Shear modulus reduction curves for gravel soil presented by Rollins et al. (1998) (blue curve) and calculated by FLAC (red curve) for waste rock

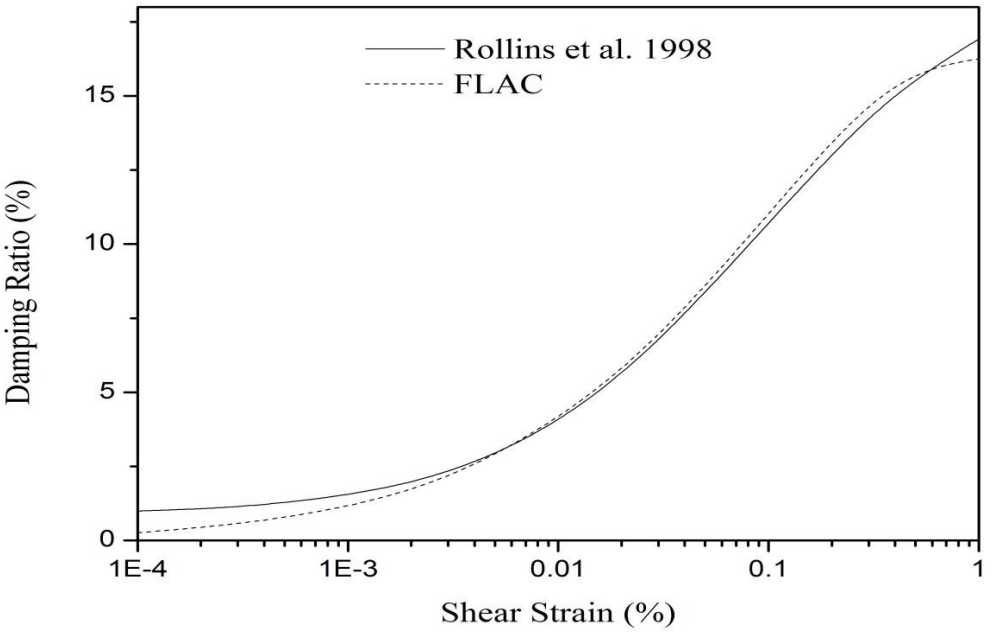

Figure 4-4: Damping ratio curves for gravel soil presented by Rollins et al. (1998) (blue curve) and calculated by FLAC (red curve) for waste rock.

4.5.5 Earthquake ground motions

A series of ground motions (with horizontal acceleration) were developed for evaluating the response of the tailings impoundment. The Saguenay 1988 (record S16T) and Northridge 1994 (record P0923) were selected to define the earthquake ground motions. These ground motions have similar peak ground acceleration and energy content but different frequency contents. The S16T record was chosen from the 11 available records for the seismic analysis based on relatively high value of Arias intensity and close epicentral distance (James, 2009). The Saguenay earthquake ground motion is characterized by fairly high frequencies that are considered to be typical of east coast ground motions (NRC, 2003). The Northridge earthquake ground motion, though of almost similar peak acceleration and energy content (Arias intensity), is characterized by relatively low frequencies, typical of west coast events.

To scale the ground motions to the assumed magnitudes and epicentral distances, the Arias intensity, I_h, was first computed for earthquakes with different magnitudes. The Arias Intensity is defined with the method of Wilson (1993) as presented in Kramer (1996):

$$logI_h = M_w - 2logR - k_eR - 3.990 + 0.365(1 - P) \qquad (4.6)$$

where: I_h is the Arias intensity in two orthogonal horizontal direction; $I_h = I_x + I_y$.

Distance R (km) is defined as: $R = \sqrt{D^2 + h^2}$

where D is the closest horizontal distance to the fault rupture (in km) and h is a correction factor with a default value of 7.5.

Coefficient k_e represents elastic absorption with a default value of zero; P is the exceedance probability that was taken as 0.5.

Conlin (1987) and Lo and Klohn (1995) presented an empirical relationship between the epicentral distance and the local earthquake magnitude (M_L) for tailings impoundments. Based on this graphical relationship and assuming an epicentral distance equal to 30 km, it was assumed that an operating impoundment could show unsatisfactory performance for an earthquake having a magnitude of 6.5 or greater (James, 2009). The intensities were computed

for three values of earthquake magnitudes, i.e. 6.5, 7.0, and 7.5, for an epicentral distance of 30 km.

The bracketed durations for different earthquake magnitudes (for the epicentral distance of 30 km) were computed based on a graph proposed in Chang and Krinitzsky (1977) (reported in Kramer, 1996). Table 4.3 gives the corresponding earthquake ground motion parameters. The values of peak ground acceleration PGA have been extracted from the scaled records of the Saguenay S16T, for earthquake magnitudes of 6.5, 7.0, and 7.5. The Arias Intensity (I_h) based on Eq. (4.6) was calculated for two dimensional shaking. The value is first halved for one dimensional shaking and then increased by 20 % to account for the effect of the second horizontal dimension (e.g. Pyke et al., 1974; Boulanger and Seed, 1995).

Table 4.3: Earthquake ground motion parameters

Identification of Earthquake	Magnitude (Mw), Source to site distance (km)	Arias intensity Ix(m/s)	PGA (g)	Duration (seconds)
E1-sag	6.5, 30	0.309	0.173	25
E3-sag	7.0, 30	0.977	0.295	27.5
E5-sag	7.5, 30	3.091	0.434	40
E1-north	6.5, 30	0.309	0.173	20
E3-north	7.0, 30	0.977	0.295	22
E5-north	7.5, 30	3.091	0.434	32

After computing the Arias intensities (I_x) for the different earthquake magnitudes at an epicentral distance of 30 km, the Saguenay (S16T) and the Northridge (P0923) records have been adjusted in such way that their scaled Arias intensities were equal to the computed Arias intensities given in Table 4.3. Figure 4-5 (a,b) shows the scaled acceleration time history of the Saguenay (S16T) and the Northridge (P0923) earthquake records for an earthquake with M_w = 7.0. This figure indicates that both events have approximately the same peak horizontal ground acceleration (PGA) and Arias intensity. However, they have different frequency contents.

Six ground motions (E_1-sag, E_3-sag, E_5-sag, E_1-north, E_3-north, and E_5-north), with 3 magnitudes, were used for the seismic analyses of the NBM tailings impoundment.

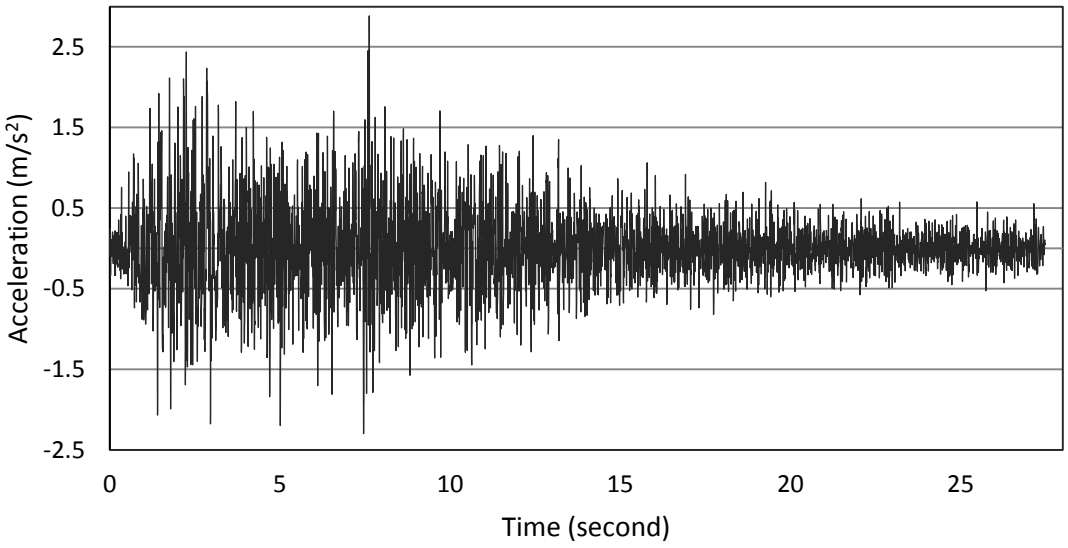

Figure 4-5a: Earthquake ground motion E_3-sag based on the S16T record, Mw=7.0; PGA=0.295g (see Table 4.3)

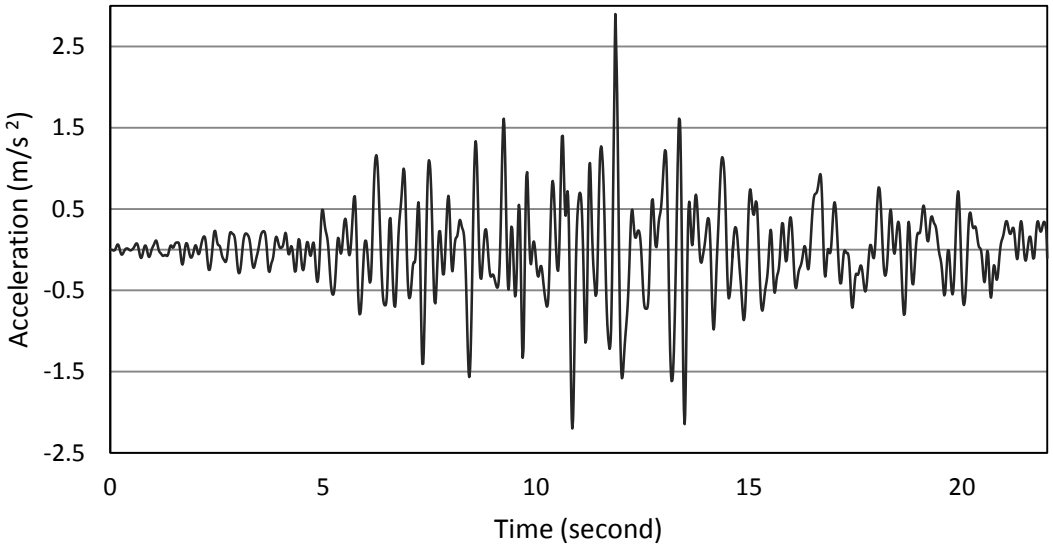

Figure 4-5b: Earthquake ground motion E_3-north based on the Northridge record, Mw=7.0, PGA=0.295g (see Table 4.3)

4.6 Static numerical analysis of the tailings impoundment

A static analysis was conducted to establish the stresses and pore water pressures (PWP) distributions in the impoundment prior to dynamic analyses. The simulation was done assuming instantaneous construction of the impoundment, and was brought to equilibrium using a coupled fluid-mechanical analysis. The PWP distribution with the phreatic surface in the tailings impoundments are shown in Figure 4-6. The simulated PWP are virtually identical to those reported by James and Leahy (2010) based on piezometric measurements in the impoundment.

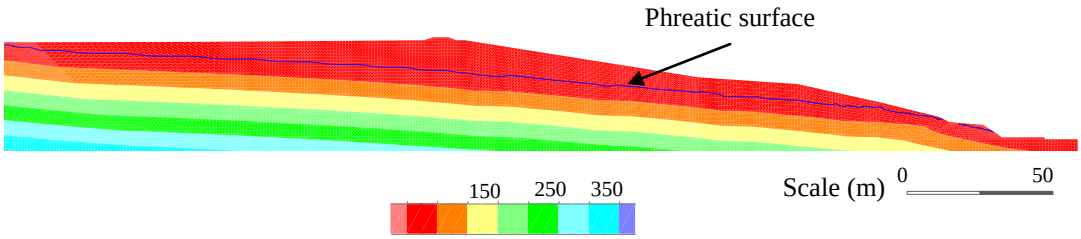

Figure 4-6: Distribution of pore water pressures in the impoundment under static condition

4.7 Dynamic numerical analysis of the tailings impoundment

A series of more than 50 dynamic numerical analyses were conducted to evaluate the seismic performance of the tailings impoundment without and with waste rock inclusions (considering various widths and spacing). The calculations were performed for under-consolidated and normally consolidated tailings, with the Saguenay and Northridge ground motions scaled to three magnitudes.

The geometric model of the tailings impoundment cross-section would be 2000 m long if the entire impoundment was included. To limit the number of elements to a manageable value, the cross-section was thus terminated at a preselected (shorter) distance from the crest. Also, the compressible nature of the tailings leads to excessive deformation during the dynamic phase of the analysis when a free-field boundary is imposed at the left side of the model. To prevent this, a (fictitious) buttress of glacial till was included on the left side of the model. The distance of 150 m from the crest to this buttress was sufficiently large so it does not affect the deformations in the area of concern along and near the downstream slope.

The dynamic analyses consisted of a shaking phase where seismic loads were applied. These were followed by a post-shaking phase where equilibrium was evaluated using the liquefied undrained strength of the tailings (where liquefaction occurred).

The key results are presented in terms of the value of horizontal displacement at each node on the downstream slope of the tailings impoundment at the end of shaking, normalized by the initial height of each node; this gives the normalized horizontal displacement of that each point (R_x). The values of R_x at the end of the shaking are given for different widths and center-to-center spacing of the inclusions to illustrate the effect of WRI on the tailings response.

4.7.1 Dynamic analyses of the impoundment without inclusions

The unreinforced tailings impoundment was analyzed to evaluate its seismic performance. This provided a basis for comparison to determine the relative effect of the waste rock inclusions. The model parameters are given in Tables 1 to 3. The value of $(N_1)_{60}$ for the unconsolidated tailings is 3 blows/300 mm. The scaled seismic loads for the Saguenay S16T earthquake with magnitudes 6.5 and 7.0 were applied to the tailings impoundment. The two simulations results indicate that the tailings impoundment becomes unstable during shaking. For instance, Figure 4-7 shows the displacements of the tailings in the downstream direction for a seismic event with a magnitude of 7.0 and epicentral distance of 30 km; the displacements exceed 10 m due to this earthquake. The model developed an unsolvable geometry after reaching this excessive value of the displacement before end of shaking.

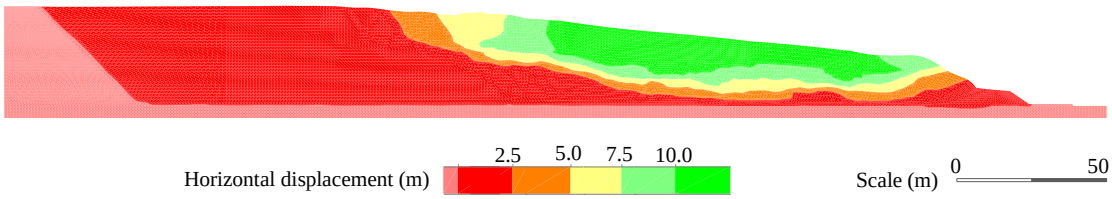

Figure 4-7: Horizontal displacements iso-contours (m) in the tailings impoundment due to E_3-sag earthquake record (M_w=7.0 and d=30 km)

4.7.2 Dynamic analyses of the reinforced tailings impoundment

Seismic stability of reinforced tailings impoundments (with WRI) were performed for 56 combinations of widths, W, and center-to-center spacings, S, of waste rock inclusions. The effect

of these inclusions on the seismic performance of the impoundments and comparison with the results without inclusions are illustrated here using a simulation performed with 12-m-wide inclusions and center-to-center spacing of 42 m (Figure 4-8). The Saguenay (S16T) earthquake record with magnitude of 7.0 (epicentral distance of 30 km) was used as the seismic load in this case. Figure 4-9 shows the horizontal displacement iso-contours at the end of shaking. As seen in this figure, the maximum horizontal displacement on the surface of downstream slope of the tailings impoundment is less than 1 m, compared to more than 10 m for the case without inclusions shown in Figure 4-7. Figure 4-9 shows that maximum horizontal displacements occurred in the tailings between adjacent waste rock inclusions.

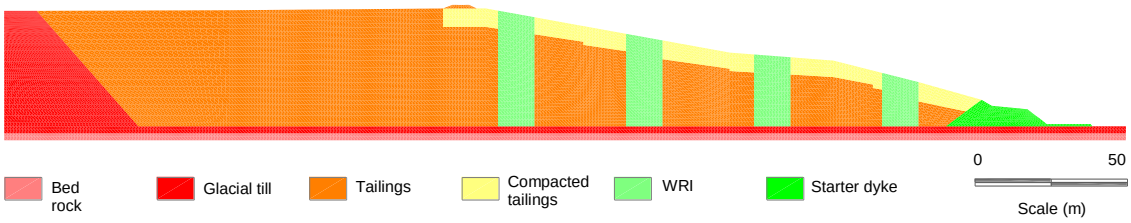

Figure 4-8: Positions of the WRI in the reinforced tailings impoundment, with a width of W= 12 m and center-to-center spacing S= 42 m

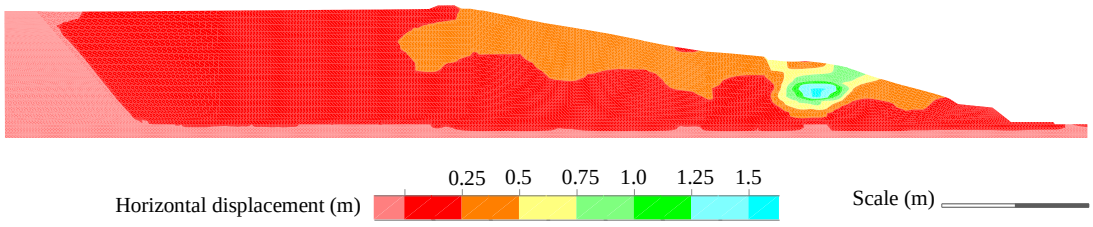

Figure 4-9: Horizontal displacements iso-contours (m) in the reinforced tailings impoundment (with WRI) for W= 12 m and S= 42 m, E_3 earthquake record (M_w=7.0, d=30 km)

4.7.3 Performance and classification of the reinforced tailings impoundment

The seismic analyses were performed on the impoundment with WRI for different combinations of widths and center-to-center spacing, using the scaled Saguenay and Northridge ground motions (E_1-sag, E_3-sag, E_5-sag, with M_w = 6.5, 7.0, and 7.5, respectively; E_1-north, E_3-north, and E_5-north, also with M_w = 6.5, 7.0, and 7.5). A total of 56 simulations were conducted for under-consolidated tailings, $(N_1)_{60} = 3$; additional simulations were also performed for

consolidated tailings, with $(N_1)_{60}$ = 8, but these results are not presented here (see Appendix C for details). As it is not possible to show the results of all these analyses, an overview is presented using the average values of R_x (horizontal displacement normalized by initial height) at the end of shaking. A FISH function was written in FLAC to compute the value of R_x at 156 locations along the downstream slope of the impoundment dyke and to evaluate the average value of normalized horizontal displacements (AR_x) by averaging the calculated values of R_x. The computed AR_x values are given in Table 4.4. The first column in this table represents the range of the average value of R_x in increments of 5%. The second column gives the different arrangements of the WRI; the first number is the width W of the inclusions (in meters) and the second number is the center- to-center spacing S (in meters). E_1, E_3 and E_5 are the earthquake records for the 3 magnitudes considered. SAG and NOR identify the high (Saguenay, S16T) and low (Northridge, P0923) frequency earthquake records, respectively.

The results shown in Table 4.4 indicate that the size and spacing of the waste rock inclusions can have a significant effect on the performance of the impoundment (in terms of the relative displacements R_x). Table 4.4 indicates that the WRI can improve markedly the seismic response of tailings impoundment when a proper configuration (arrangement) is chosen. For example, for the E_1-sag ground motion, the arrangement 8-56 (i.e. W= 8 m, S = 56 m) leads to AR_x < 5%; increasing the center-to-center spacing from 56 to 64 (arrangement 8-64) lead to AR_x > 30%. Hence, increasing the spacing between the WRI beyond certain distance may significantly reduce their positive effects. Other factors, such as the positions of the WRI, affect the results of seismic analysis. Is appears that displacement of the WRIs in some instances prevents local failure or the expansion of failure zones.

Results from these analyses also show that upstream raised tailings impoundments can be stabilized against strong ground motion using well designed WRI. For example, for the E_5-sag strong ground motion (Mw=7.5 and epicentral distance of 30 km), the arrangement 16-40 leads to ARx < 5%, while the arrangements 16-56 and 25-100 gives ARx between 5% and 10%. Therefore, choosing an appropriate arrangement is key to decreasing the displacements to an acceptable range and also to prevent failure.

Such results can thus be very helpful to optimize the design of the WRI with respect to the seismic stability of the impoundment.

Table 4.1: Classification of the reinforced tailings impoundments with waste rock inclusions based on the average value of R_x (AR_x) for the downstream slope at the end of shaking; various earthquakes with unconsolidated tailings

Average value of R_x on the slope of tailings impoundment (AR_x)	Widths W and Center-to-center Spacings S of WRI*		
0-5%	8-48-E1-SAG	12-42-E3-SAG	16-48-E5-SAG
	8-56-E1-SAG	12-36-E5-SAG	16-48-E3-SAG
	8-40-E1-NOR	12-108-E1-SAG	16-48-E3-NOR
	8-32-E3-SAG	16-80-E1-SAG	16-40-E5-SAG
	8-32-E1-NOR	16-64-E1-SAG	25-75-E3-SAG
	12-60-E1-NOR	16-64-E1-NOR	25-112.5-E1-NOR
	12-48-E3-SAG	16-56-E3-SAG	25-100-E1-SAG
	12-48-E1-NOR	16-56-E1-SAG	----------
5-10%	8-28-E3-NOR	12-42-E3-NOR	16-56-E5-SAG
	8-28-E5-SAG	12-42-E5-SAG	16-80-E1-NOR
	8-48 -E1-NOR	12-48-E3-NOR	25-100-E5-SAG
	8-56-E1-NOR	12-60-E1-SAG	25-125-E1-NOR
	8-64-E1-NOR	12-72-E1-NOR	
10-15%	8-96-E1-NOR	16-48-E5-NOR	16-80-E3-NOR
	12-96-E1-NOR	16-64-E3-NOR	25-112.5-E3-NOR
	16-112-E1-NOR	16-64-E3-SAG	25-125-E3-NOR
	16-128-E1-NOR		----------
15-20%	8-48-E3-NOR	12-60-E3-NOR	----------
20-25%	16-112-E3-NOR	----------	----------
25-30%	16-128-E3-NOR	25-112.5-E1-SAG	----------
>30%	8-64 -E1-SAG	12-96-E1-SAG	----------
	12-48-E5-NOR	16-112-E1-SAG	----------

*First number is the width W (m), second number is the center-to-center spacing S of inclusions; E1 to E5 indicate the earthquake records for SAG (high frequency, Saguenay) and NOR (the low frequency, Northridge) events.

4.7.4 Post-shaking analyses of the reinforced impoundment

Post-shaking analyses considering unconsolidated and consolidated tailings have also been performed. The average of the normalized horizontal displacements (AR_x) and the horizontal velocities (Xvel) along the downstream slope of the tailings impoundment at the end of shaking were used to present the main results; these were then analyzed to evaluate if these parameters could be used to assess the post-shaking response. A FISH function was written to compute the average value of the horizontal velocities at the end of shaking (Ferdosi, 2014).

The numerical models were run using the total stress approach described above to evaluate stability immediately after shaking, for cases where the impoundment did not fail during the earthquake. A stable condition was considered if the model rapidly returned to a state of static equilibrium (with minimal nodal velocities); the impoundment was considered unstable if it did not return to equilibrium, i.e. when there are ongoing nodal displacements after shaking.

Figure 4-10 shows the average horizontal nodal velocities on the downstream slope of the impoundment at the end of shaking (i.e. end of seismic analysis) versus the average value of R_x (AR_x). On this figure, diamonds represent stable WRI configurations (defined in Table 4.A, in appendix) and the triangles represent WRI configurations that became unstable during the post-shaking phase. The results of these analyses show that about 90% of the simulated cases with WRI which were stable during seismic loading remained stable post-shaking. This figure also shows that when the average velocity along the slope is more than about 20 cm/s, instability occurred for a large majority of the cases. For most of these unstable cases, the ratio of the center-to-center spacing to inclusion width (S/W) was more than about 8. For such unstable cases, the width of the inclusions is relatively narrow and the center-to-center spacing of the inclusions is relatively large.

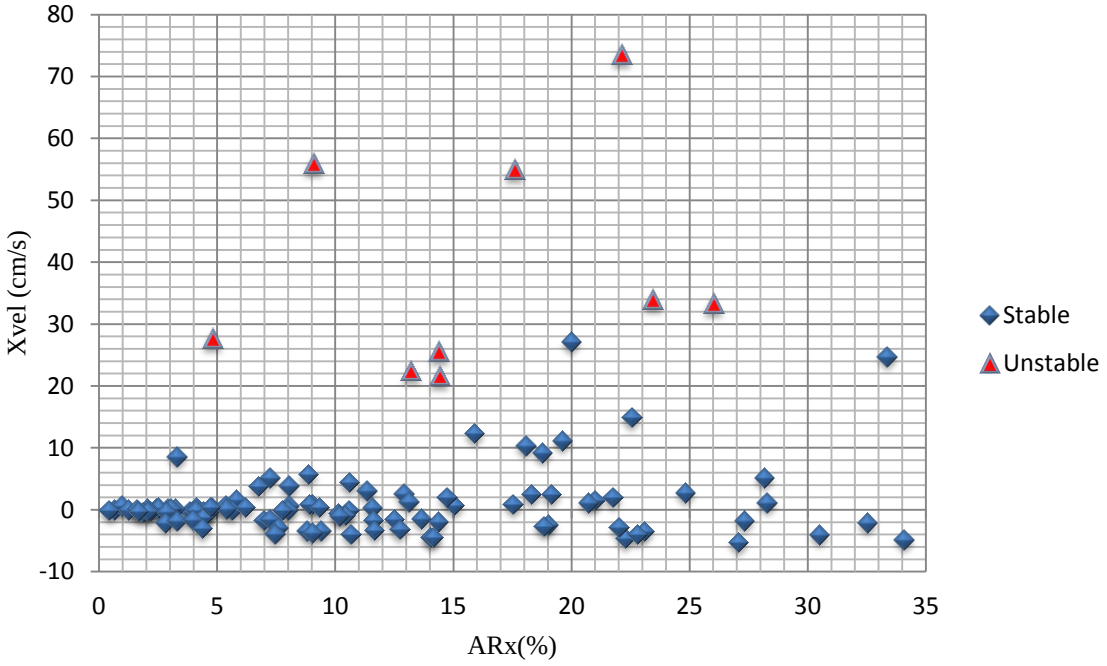

Figure 4-10: The average horizontal nodal velocities (X_{vel}) along the external dyke slope at the end of shaking versus the average normalized horizontal displacement (AR_x) for different combinations of widths W and center-to-center spacings S of the WRI (see details in Table 4.A), the definitions of "stable" and "unstable" are defined in Section 4.7.4.

4.8 Complementary analyses and discussion

Many factors may affect the stability of the tailings impoundment. Some of these were assessed above, while others are briefly discussed in the following.

4.8.1 Effect of the frequency content

The influence of the frequency content of the seismic events was also evaluated specifically for the reinforced impoundment. This aspect is illustrated here using the Saguenay and the Northridge ground motions for a magnitude of 6.5 and an epicentral distance of 30 km (E_1 records). Figure 4-11 shows the value of the R_x along the downstream slope of the tailings dyke for these high (Saguenay) and low (Northridge) frequency ground motions. In this figure, the left vertical axis represents the value of R_x. The solid and dashed curves correspond to the results obtained using the Saguenay and Northridge ground motions, respectively.

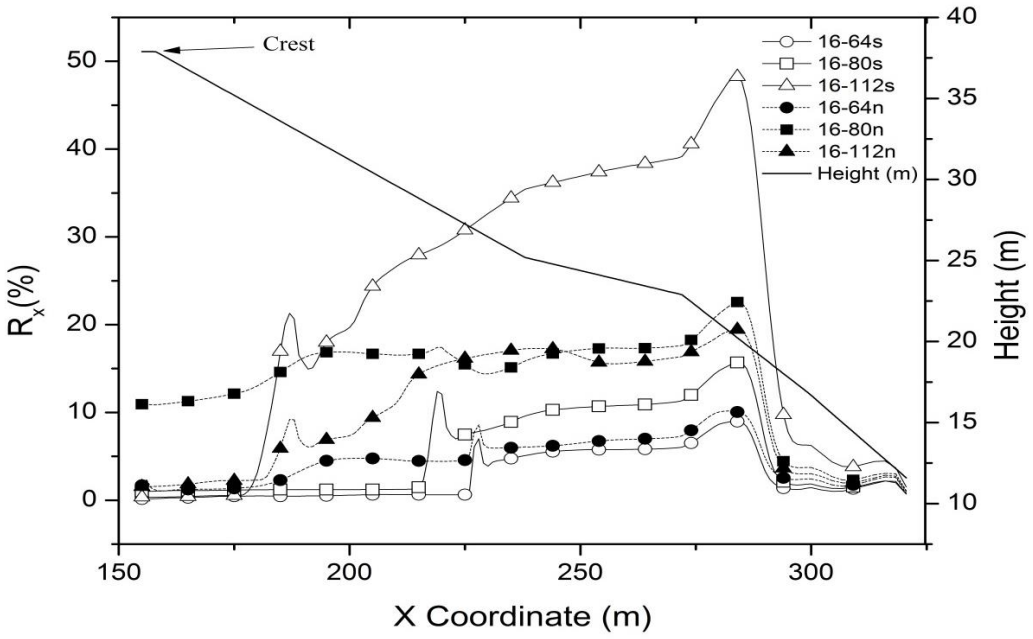

Figure 4-11: Values of R_x at different locations X (and height) along the external slope of the tailings dyke due to E_1 earthquake record. At top right: the first number is the width W (m) of the inclusions, the second number is the center-to-center spacing S (m); "s" and "n" identify the high (Saguenay) and low (Northridge) frequency ground motions, respectively.

Results in Figure 4-11 show that when the center-to-center spacing, S, of the WRI is relatively small, the value of R_x on the surface of the slope for the Northridge ground motion is greater than that produced by the Saguenay ground motion. However, when S increases, the relative displacements R_x produced by the high frequency ground motion become larger than those due to the low frequency ground motion. (Recall that both earthquakes have been scaled so that they have the same Arias intensity and peak horizontal ground acceleration). For example, the value of R_x along the surface of the slope for 16-m-wide inclusions spaced at 64 m (16-64) is the same for both earthquakes. However, for S= 80 m, the value of R_x for the low frequency event is greater than that due to the high frequency event. Increasing of inclusion spacing, S, to 112 m produces a reverse tendency, with the high frequency ground motion generating more displacements than the low frequency even; for configuration 16-112, the high frequency (Saguenay, E_1) event produced significantly more displacements than the low frequency event (Northridge, E_1). There is thus a major effect of the predominant frequency content on the response of the reinforced tailings impoundments, particularly for relatively thin and widely

spaced WRI. This factor must thus be taken into account when analyzing the response of an impoundment.

4.8.2 Effect of the WRI configuration

The geometrical arrangement of the WRI is another key influence factor. Figure 4-12 (a, b) shows the averages of R_x along on the slope of the reinforced impoundment as a function of the total width of WRI, for the E_1-sag and E_1-north ground motions (with M_w=6.5). Figure 4-12(a) indicates that for inclusions with a total width of 24 meters (three 8-m-wide inclusions), the arrangement of 8-56 shows the lowest value of AR_x while the arrangement 8-64 leads to the largest average displacement. For a total width of 32 meters, the arrangement of 8-48 shows the best performance, with the lowest AR_x, while the arrangement 16-80 leads to largest AR_x. For a total width between 48 and 50 meters, all the configurations offer the same performance except for the arrangement 25-125, which gives a larger value of AR_x. In this latter case, the WRI are not displaced much, but the tailings between successive inclusions are displaced much more relative to the other arrangements.

These results indicate that the spacing between the waste rock inclusions should not exceed a critical value, beyond which the inclusions tend to lose their positive effect on the deformation of the downstream slope.

Figure 4-12(a) also shows that all the WRI arrangements considered for the high frequency event (Saguenay) lead to stable conditions, thus improving the seismic performance of the tailings impoundment. Figure 4-12(b), illustrating the response under the low frequency ground motion (Northridge), shows that all arrangements with a total width between 24 and 50 m show a satisfactory performance, with AR_x less or around 5% for the external dyke slope and WRI. Arrangement 16-80 however leads to AR_x > 10% for the slope. This result confirms that increasing spacing of the WRI beyond a critical value may produce a drastic loss of their efficiency.

Figure 4-13 (a, b) shows the averages of R_x along on the downstream slope (dyke) of the reinforced impoundment as function of the total width of WRI for E_3-sag and E_3-north ground

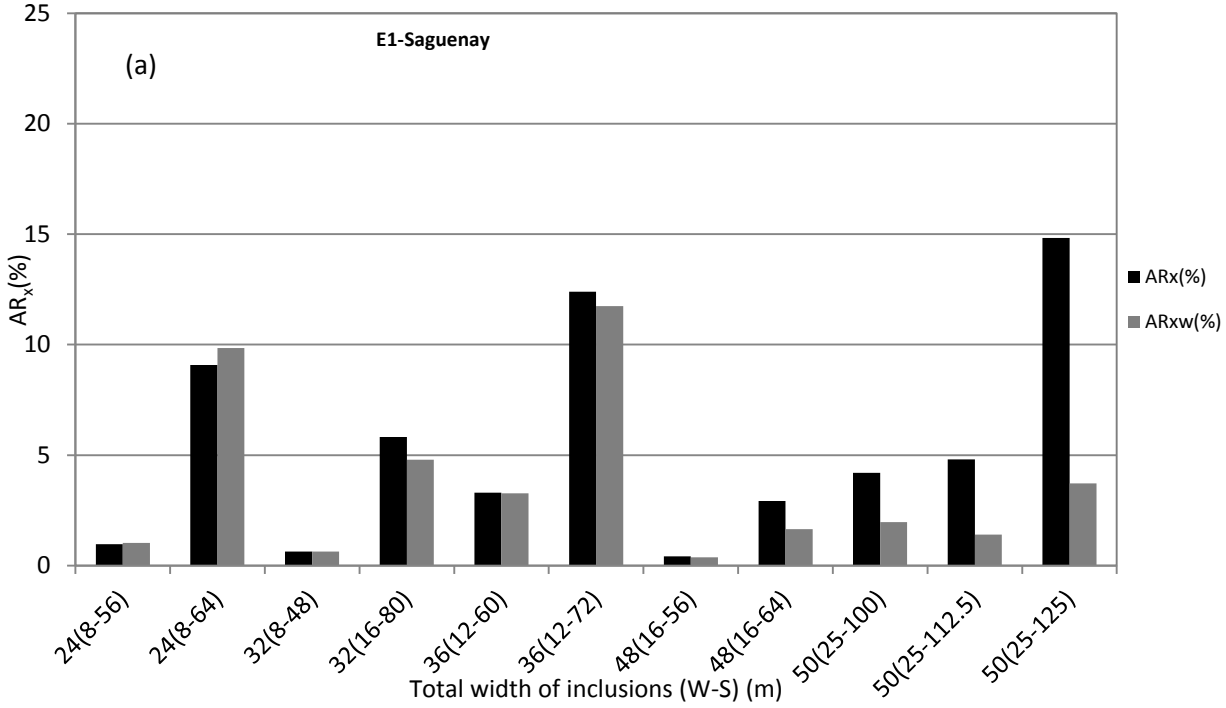

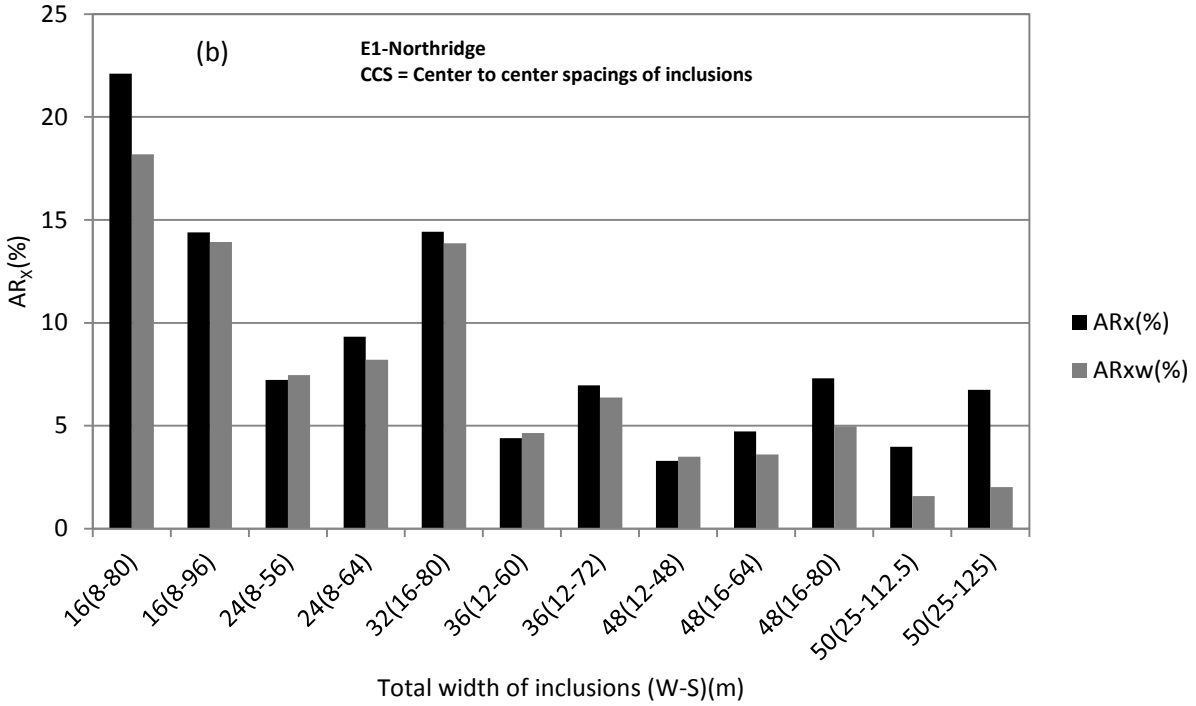

Figure 4-12: Average normalized horizontal displacements AR_x of the external slope of the dyke for reinforced impoundments versus total widths of the WRI placed in the tailings , for different local width and spacing (M_w=6.5) (a) E_1-sag, (b) E_1-north ground motions

motions (with M_w= 7.0). Figure 4-13(a) indicates that the WRI with a total width of 48 meters (i.e. arrangements 8-32, 12-42, 12-48, and 16-56) show the lowest values of AR_x in comparison to the arrangements 16-64 (with the same total width of 48 meters) and 25-75 (with a total width of 75 meters). These results indicate that the arrangements 16-64 and 25-75 don't enhance the seismic performance of the impoundment as effectively as arrangements 8-32, 12-42, 12-48, and 16-56. Although the width of each inclusion and the total width of the inclusions are larger for arrangement 25-75, compared with other arrangements (i.e. 8-32, 12-42, 12-48, and 16-56), the performance of the former is not as good as that of the latter. This further illustrates how an increase of the spacing between inclusions may eliminate their beneficial effect on the seismic performance of tailings impoundment.

Figure 4-13(b) shows that the arrangements with a total width between 48 and 50 meters lead to the same performance under low frequency ground motion E3-north (i.e. same value of AR_x). This figure also indicates that all the arrangements with a total width of 32 meters lead to the same performance; in these cases however, the efficiency of the WRI is limited, with AR_x >15%. Such WRI have narrow widths or wide spacing.

Comparison between results shown in Figure 4-13 (a) and (b) further indicates that the low frequency ground motions produce larger displacements of the tailings than the high frequency motions, as was also observed from the results presented above.

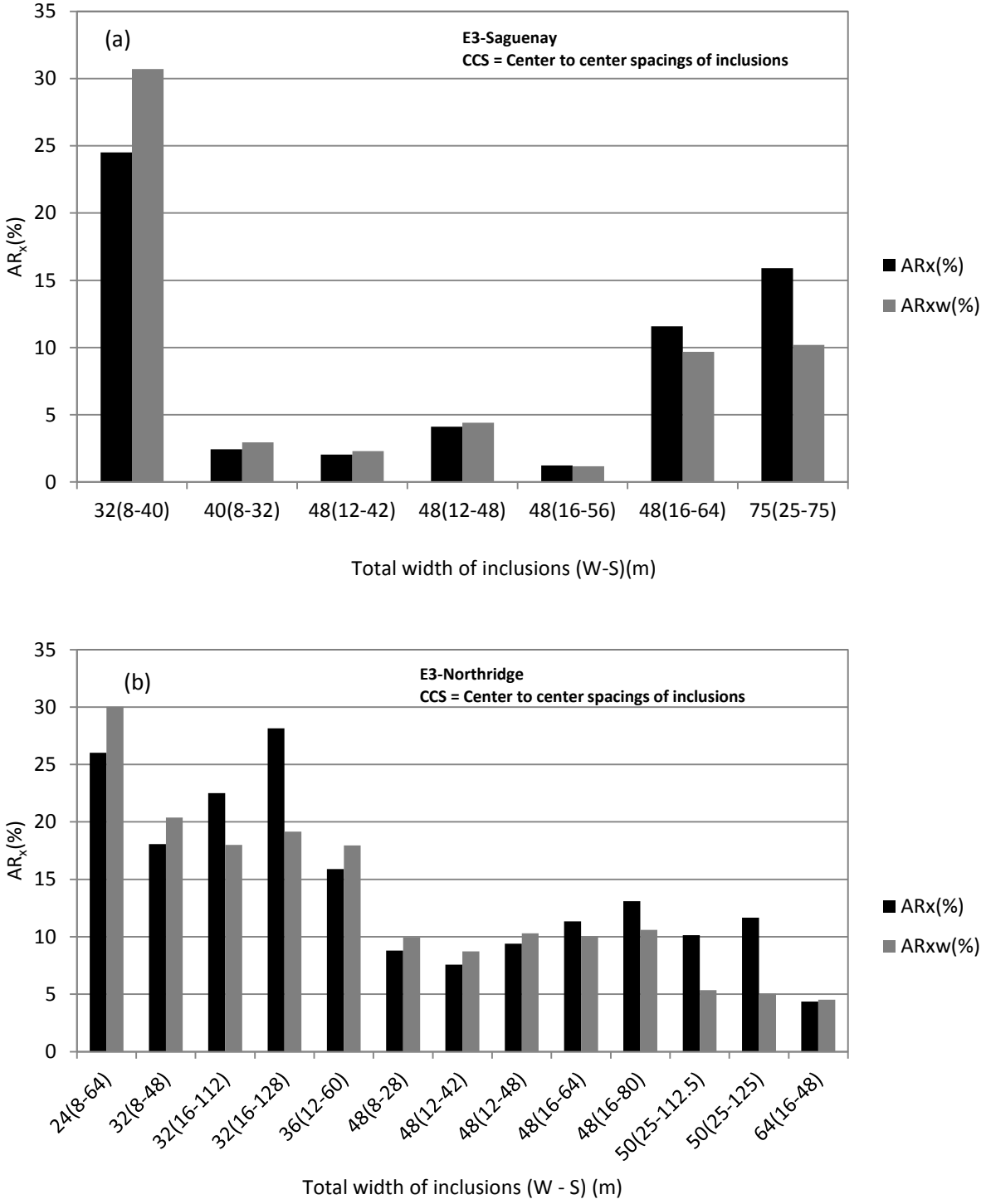

Figure 4-13: Average normalized horizontal displacements AR_x of the external slope of the dyke for reinforced impoundments versus total widths of the WRI placed in the tailings , for different local width and spacing (M_w=7.0) (a) E_3-sag, (b) E_3-north ground motions

4.8.3 Consolidated tailings

Additional simulations have been conducted on the unreinforced impoundment with consolidated tailings, $(N_1)_{60} = 8$, blows/30 cm. The results, presented in Appendix C, indicate that the impoundment is stable when subjected to the E_1-sag, E_3-sag, E_1-north, and E_3-north ground motions; the unconsolidated tailings impoundment was unstable against the same ground motions (as shown above).

The unreinforced consolidated tailings impoundment becomes unstable in the simulations for larger magnitude earthquakes, for both types of ground motions. These analyses clearly indicate that consolidation (and strength gain) enhances the seismic performance of tailings impoundment.

Fifty three analyses were performed for the consolidated tailings impoundment reinforced with different configuration of WRI, for M_w > 7.0. The same trends described above for the unconsolidated tailings have been obtained for the consolidated cases, but with a better resistance of the impoundment to seismic loadings (Appendix C). There is thus an additional advantage to the use of WRI as these can accelerate the consolidation of the tailings.

Inclusions can also be used to evacuate water outside the impoundment and lower the position of the water table in the tailings, which can then become more easily unsaturated. Recent results presented by Narvaez et al. (2014) show that unsaturated tailings can have a much larger strength, due to apparent cohesion. This gain can improve the seismic response of tailings; this aspect is now being investigated further. The ongoing investigation also considers other WRI configurations, including cases where the inclusions are located well within the impoundment (not only along the external slope).

4.9 Conclusion

The effect of waste rock inclusions configuration, in term of their width and center-to-center spacing, on the seismic performance of a tailings impoundment was evaluated numerically. An actual tailings impoundment was modeled numerically with different configurations of WRI, considering unconsolidated tailings. The results of analyses show that the presence of such inclusions can significantly improve the seismic performance and stability of a tailings impoundment. The simulations also indicate that the width and center-to-center spacing of the

inclusions have an important effect on the seismic performance of the impoundment. The response of the different configurations are classified based on the average normalize horizontal displacements AR_x of the downstream slope of impoundment. The results show how to best use WRI to stabilize the upstream raised tailings impoundment against different ground motions.

The effect of the high and the low frequency ground motions was also evaluated using Saguenay (S16T) and the Northridge (P0923) earthquakes records after scaling the records to represent earthquakes of known magnitudes and epicentral distances. The results show that in most cases, low frequency earthquakes cause larger displacements of the tailings near the edge of the impoundment than high frequency earthquakes. There are cases however, depending on WRI configuration, where the displacements of the downstream slope of the tailings impoundment can be larger for the high frequency ground motion. The predominant frequency content of the ground motion is thus an important parameter that must be taken into account for the seismic analysis of tailings impoundments.

Post-shaking analyses were also performed for different WRI configurations. A chart was developed to show the relationship between the post-shaking stability of stable impoundments with the AR_x and horizontal velocity x_{vel} at the end of the seismic analysis. The results of these analyses indicate that a horizontal velocity $x_{vel} > 20$ cm/s at the end of shaking leads to an unstable condition in the post-shaking stage.

4.10 Acknowledgements

This research is being supported by the Natural Sciences and Engineering Research Council of Canada (NSERC), the partners of the Industrial NSERC Polytechnique-UQAT Chair (2006-2012) and those of the Research Institute on Mines and the Environment (RIME UQAT-Polytechnique; www.rime-irme.ca).

4.11 References

Adalier, K., Elgamal, A., Meneses, J., and Baez J. I. 2003. Stone columns as liquefaction countermeasure in non-plastic silty soils. Soil Dynamics and Earthquake Engineering, 23(7): 571-584.

Armstrong, R. J., Boulanger, R. W., and Beaty, M. H. 2010. Nonlinear numerical modeling of centrifuge test results for embankments underlain by liquefied soil. In Proceedings, Collaborative Management of Integrated Watersheds, 30th Annual United States Society on Dams Conference, Sacramento, 12-16 April 2010. United States Society on Dams, pp. 201-215.

Aubertin, M., Mbonimpa, M., Jolette, D., Bussiere, B., Chapuis, R.P., James, M., Riffon, O. 2002. Stabilité géotechnique des ouvrages de retenue pour les résidus miniers: problèmes persistants et méthodes de contrôle. Défis & Perspectives : Symposium sur l'environnement et les mines, Rouyn-Noranda, Développement Économique Canada/Ministère des Ressources Naturelles du Québec/CIM. Comptes-Rendus sur CD-ROM.

Barksdale, R.D., and Bachus, R.C. 1983. Design and construction of stone columns volume I. Report FHWA-RD-83-026, National Technical Information Service, Springfield, VA.

Beaty, M. and Byrne, P. M. 1998. An effective stress model for predicting liquefaction behavior in sand. Proceedings of Geotechnical Earthquake Engineering and soil dynamic III, Seattle, Washinton, USA. ASCE Special Publication. 75(1):766-777.

Beaty, M.H. and Byrne, P.M. 2011. UBCSAND constitutive model Version 904aR. Document report: UBCSAND Constitutive Model on Itasca UDM Web site: http://www.itasca-udm.com/pages/continuum.html.

Boulanger, R. W. and Seed, R. B. 1995. Liquefaction of sand under bidirectional monotonic and cyclic loading. Journal of Geotechnical and Geoenvironmental Engineering, 121(12), 870-878.

Boulanger, R. W., Kamai, R., and Ziotopoulou, K. 2011. Numerical modeling of liquefaction effects. In Proceeding of the Effects of Surface Geology on Seismic Motion, 4th IASPEI / IAEE International Symposium, University of California, Santa Barbara, CA., 23-26 August 2011.

Bray, J.D., Dashti, S. 2012. Liquefaction-Induced Building Movements, Invited Keynote Paper, Proceedings of the International Conference on Performance-Based Design Earthquake Geotechnical Engineering, Taormina, Italy.

Bussière, B. 2007. Hydro-Geotechnical properties of hard rock tailings from metal mines and emerging geo-environmental disposal approaches. Canadian Geotechnical Journal, **44**(9): 1019-1052.

Byrne, P. M., Park, S. S. and Beaty, M. 2003. Seismic liquefaction: centrifuge and numerical modeling. *In* Proceedings of the Third International Symposium on FLAC and FLAC3D Numerical Modelling in Geomechanics, Sudbury ON, 22-24 October. Balkema Publishers, Lisse NL, Balkema, pp. 321-331.

Byrne, P. M., Park, S.S, Beaty, M., Sharp, M., Gonzalez, L., and Abdoun, T. 2004. Numerical modeling of liquefaction and comparison with centrifuge tests. Canadian Geotechnical Journal, 41, 193-211.

Byrne, P.M., Roy, D., Campanella, R.G., and Hughes, J., 1995. Predicting Liquefaction Response of Granular Soils from Pressuremeter Tests, ASCE National Convention, San Diego, 23-27 October 1995, ASCE, Geotechnical Special Publication 56, pp. 122-135.

Castillo, J., Hallman, D., Byrne, P., and Parra, D. 2006. Non-linear dynamic analysis of heap leach pad under high phreatic levels. *In* Proceedings of FLAC and Numerical Modeling and Geomechanics, Mardrid, Spain, 29-31 May 2006. Itasca Consulting Group, Inc., Minneapolis MN, pp. 187-194.

Chang, F.K., Krinitzsky, E.L. 1977. State-of-the-art for assessing earthquake hazards in the united states. Report 8. Duration, Spectral Content, and Predominant Period of Strong Motion Earthquake Records fromWestern United States, United States.

Chaney, R. C. 1978. Saturation effects on the cyclic strength of sands. In Proceedings of the Geotechnical Engineering Division Specialty Conference, Pasadena, California, 19-21June 1978. ASCE, pp. 342-358.

Chapuis, R.P., Aubertin, M. 2003. On the use of the Kozeny-Carman equation to predict the hydraulic conductivity of soils. Canadian Geotechnical Journal, **40**(3): 616-628.

Conlin, B. 1987. A review of the performance of mine tailings impoundments under earthquake loading conditions. Proceedings of Earthquake Geotechnique, Vancouver, May 1987. BiTech Publishing.

Dashti, S., Bray, J.D. 2012. Numerical Insights into Liquefaction-Induced Building Settlement, Proceeding of the 2012 Geo-Congress, Geo-Institute, Oakland, CA. 25-29 March 2012, ASCE, pp.1660-1669.

Davies, M. P. 2002. Tailings impoundment failures: are geotechnical engineers listening? Geotechnical News, **20**(3): 31-36.

Davies, M. P. and Lighthall, P. C. 2001. Geotechnical aspects of several recent mine tailings impoundment failures. In Proceedings of the 54th Canadian Geotechnical Conference, Calgary, AB. Canada Geotechnical Society, pp. 321-326.

Davies, M.P., Lighthall, P.C., Rice, S. and Martin, T.E. 2002. Keynote Address: Design of tailings dams and impoundments, In Proceedings 2002 SME Annual Meeting, Phoenix, Arizona, 25–27 February 2002. Society for Mining, Metallurgy, and Exploration, Inc., Littleton, Colorado SME, AGM, Phonix.

Dobry, R. and Alvarez, L. 1967. Seismic Failures of Chilean Tailings Dams. Journal of the Soil Mechanics and Foundations Division, 93(SM6): 237-260.

Ferdosi, B. 2014. Ongoing Ph.D thesis, Department of Civil, Geological and Mining Engineering, Ecole Polytechnique de Montreal, Montreal, QC.

Ferdosi, B., James, M., and Aubertin, M. 2013. Numerical modeling of the post-liquefaction consolidation of tailings, Proc. GeoMontreal 2013, Montreal, Qc, October 2013. Canadian Geotechnical Society, 7 pages.

Ferdosi, B., James, M., and Aubertin, M. 2014. Numerical modeling of seismic table testing of tailings with and without inclusion, GeoRegina 2014, Regina, Saskatchewan, October 2014. Canadian Geotechnical Society, 6 pages.

Fung, G., Parra, E.P., Sully, J.P., Kerr, J.R., and Akins, K.P. 2011. Seismic modeling of a reinforced slope, 2011 Pan-Am Canadian Geotechnical Society Conference, Toronto, On., October 2011. Canadian Geotechnical Society, 7 pages.

Harder, L. F. Jr. and Stewart, J. P. 1996. Failure of Tapo Canyon tailings dam. Journal of Performance of Constructed Facilities, ASCE, 10(5): 109-114.

ICOLD. 2001. Tailings dams – risk of dangerous occurrences – lessons learnt from past experiences. International Commission on Large Dams and United Nations Environmental Program (ICOLD), Paris. Bulltin No. 121.

Ishihara, K. 1984. Post-Earthquake Failure of a Tailings Dam due to Liquefaction of the Pond Deposit. Proceedings of the International Conference on Case Histories in Geotechnical Engineering, St-Louis, 1984. University of Missoiuri Rolla, Missouri, pp. 1129-1143.

Itasca Consulting Group, Inc. (Itasca). 2008. FLAC – Fast Lagrangian Analysis of Continua. Version 6.00. [computer software and user manual]. Minneapolis MN: Itasca Consulting Group, Inc.

James, M. 2009. The use of waste rock inclusions to control the effect of liquefaction in tailings impoundments . Ph.D. Thesis, Department of Civil, Geological, and Mining Engineering, Ecole Polytechnique de Montreal, Montreal, QC.

James M. and Aubertin, A. 2010. On the dynamic response of tailings and the stability of tailings impondments for hard rock mines. Geotechnical News, **23**(3), 39-43.

James, M., Aubertin, M. 2012. The use of waste rock inclusions to improve the seismic stability of tailings impoundments. GeoCongress 2012, Okland, 22-25 March 2012. American Soceity of Civil Engineers, pp. 4166-4175.

James, M., Aubertin, M., Bussière, B. 2013. On the use of waste rock inclusions to improve the performance of tailings impoundments. In Proceeding of the 18th International Conference Soil Mechanics and Geotechnical Engineering, 2-6 September 2013. ISSMGE, pp. 735-738.

James, M., Aubertin, M., Wijewickreme, D., Ward Wilson, G. 2011. A Laboratory Investigation of the Dynamic Properties of Tailings. Canadian Geotechnical Journal, **48**(11)*:* 1587–1600.

James, M., Leahy, D. 2010. Phase 1 tailings dam stability study of Mine No.12 site, Final report, SNC.LAVALIN Company, Montreal, QC.

Jaouhar, E.M., Aubertin, M. and James, M. 2011. Effect of waste rock inclusions on the consolidation of mine tailings. In Proceedings of 2011 CGS Geotechnical Conference, Toronto ON, 2 – 6 October 2011. Canadian Geotechnical Society.

Jaouhar, E.M., Aubertin, M., and James, M. 2013. The effect of tailings properties on their consolidation near waste rock inclusions. In GeoMontreal 2013:Geosciences for Sustainability, Proceedings of the 66th CGS Conference, October 2013, Montreal, QC. Canadian Geotechnical Society, 8 Pages.

Khalili, A., Wijewickreme, D. and Wilson, G.W. 2010. Mechanical response of highly gap-graded mixtures of waste rock and tailings. Part I: Monotonic shear response. Canadian Geotechnical Journal, 47(5): 552-565.

Kramer, S. L. 1996. Geotechnical Earthquake Engineering. Prentice-Hall Inc., Upper Saddle River, N.J.

L. Bolduc, F., Aubertin, M. 2013. Analysis the effect of waste rock inclusions on tailings consolidation: laboratory and modeling of the large scale in situ behavior, GeoMontreal 2013, Montreal, QC, October 2013. Canadian Geotechnical Society.

L. Bolduc, F., Aubertin, M. 2014. A numerical investigation of the influence of waste rock inclusions on tailings consolidation, Canadian Geotechnical Journal, **51**(9): 1021-1032.

Lo, R.C., Klohn, E. L. 1995. Design Considerations for Tailings Dams, Proceedings of the 5th International Conference on Tailings and Mine Waste '96, Fort Collins CO, 1995. Taylor and Francis, London, pp. 113-121.

Naesgaard, E. 2011. A Hybrid Effective Stress-Total Stress Procedure for Analyzing Embankments Subjected to Potential Liquefaction and Flow. PhD. Thesis, Civil Engineering Department, The University of British Coulombia, Vancouver, B. C.

Naesgaard, E., Byrne, P.M. 2007. Flow liquefaction simulation using a combined effective stress – total stress model, 60th Canadian Geotechnical Conference, Ottawa, On, October 2007. Canadian Geotechnical Society, pp. 943-950.

Naesgaard, E., Yang, D., Byrne, P., and Gohl, B. 2004. Numerical analysis for the seismic safety retrofit design of the immeresed-tube George Massey tunnel, 13th World Conference on Earthquake Engineering, Vancouver, B.C., 1-6 August 2004. Canadian Association for Earthquake Engineering.

Narvaez, B., Aubertin, M., Saleh-Mbemba, F. 2014. Application of a predictive model to estimate the tensile strength of unsaturated tailings, GeoRegina 2014, Regina, Saskatchewan, October 2014. Canadian Geotechnical Society, 7 pages.

Natural Resources Canada (NRC). 2003. Processed Ground Motions Records of the 1988 Saguenay Earthquake. Website accessed on June 16, 2003. http://www.seismo.nrcan.gc.ca/nwfa/index_e.php.

Pacific Earthquake Engineering Research Center (PEER). 2014. P0923 : Earthquake and station details. Consulted on February, 2011. http://peer.berkeley.edu/svbin/Detail?id=P0923.

Pépin, N. 2010. Étude du comportement cyclique de résidus miniers avec inclusions drainantes par des essais sur table sismique. M.Sc. A. Thesis, École Polytechnique de Montréal, Montréal, Quebec.

Pépin, N., Aubertin, M., James, M., Leclerc, M. 2012a. Seismic simulator testing to investigate the cyclic behavior of tailings in an instrumented rigid box. Geotechnical Testing Journal, **35**(3): 469-479.

Pépin, N., Aubertin, M., James, M. 2012b. Seismic Table Investigation of the Effect of Inclusions on the Cyclic Behavior of Tailings. Canadian Geotechnical Journal, **49**(4): 416-426.

Puebla, H. 1999. A constitutive model for sand and the analysis of the CanLex Embankments. Ph.D. thesis, Civil Engineering Department, University of British Columbia, Vancouver, B. C.

Puebla, H., Byrne, P.M., and Phillips, R. 1997. Analysis of CANLEX liquefaction embankments: prototype and centrifuge models. Canadian Geotechnical Journal, 34(5): 641-657.

Pyke, R., Chan, C. K., and Seed, H. B. 1974. Settlement and liquefaction of sands under multi-directional shaking. Report No. EERC 74-2, Earthquake Engineering Research Center, Berkeley, CA.

Rollins, K.M., Evans, M.D., Diehl, N.B. and Daily, W.D. III. 1998. Shear modulus and damping relationships for gravels. Journal of Geotechnical and Geoenvironmental Engineering. 124(5): 396-405.

Seed, H. B., Idriss, I. M. 1970. Soil moduli and damping factors for dynamic response analyses. Report No. EERC 70-10, Earthquake Engineering Research Center, Berkeley, CA.

Seed, H.B., Wong, R.T., Idriss, I.M. and Tokimatsu, K. 1984. Dynamic moduli and damping factors for dynamic analysis of cohesionless soils. Report No. UCB/EERC-84/14, Earthquake Engineering Research Center, Berkeley, CA.

Seid-Karbasi, M. and Byrne, P. M. 2004. Embankment dams and earthquakes. Hydropower and Dams, 2: 96-102.

Seid-Karbasi, M. and Byrne, P. M. 2007. Seismic liquefaction, lateral spreading, and flow slides: a numerical investigation into void redistribution. Canadian Geotechnical Journal, 44(7): 873-890.

Vick, S. G. 1990. Planning, design and analysis of tailings dams. Vancouver, BC: BiTech Publishers Ltd.

Wickland, B.E. and Wilson, G.W. 2005. Self-weight consolidation of mixtures of mine waste rock and tailings. Canadian Geotechnical Journal, **42**(2): 327-339.

Wijewickreme, D., Sanin, M. V. and Greenaway, G. 2005. Cyclic shear response of fine-grained mine tailings. Canadian Geotechnical Journal, 42(5): 1408-1421.

Wijewickreme, D., Khalili, A. and Wilson, G.W. 2010. Mechanical response of highly gap-graded mixtures of waste rock and tailings. Part II: Undrained cyclic and post-cyclic shear response, Canadian Geotechnical Journal, **47**(5): 566-582.

Williams, D.J. 1996. Broadening the options — innovative tailings disposal concepts and practices. Proceedings of the 3rd International and 21st Annual Minerals Council of Australia Environmental Workshop, Newcastle, 14–18 October 1996. pp. 264–278.

Wilson, R.C. 1993. Relation of Arias intensity to magnitude and distance in California. Open-file report 93-556, U.S. Geological Survey, Reston, Virginia, 42pp.

Ziotopoulou, K. and Boulanger, W. 2013. Numerical modeling issues in predicting post-liquefaction reconsolidation strains and settlements. 10th International Conference on Urban Earthquake Engineering, Tokyo, 1-2 March 2013, Tokyo Institute of Technology, Tokyo, Japan.

4.12 Appendix

Table 4.A: Values of the average normalized horizontal displacement (AR_x) and average horizontal velocity (x_{vel}) of the impoundment dyke for different WRI configurations and input ground motion.

Configuration*	AR_x (%)	Xvel (cm/s)	Configuration	AR_x(%)	Xvel (cm/s)
8-48 -E1-Sag-SPT3	0.64	0.087	8-32-E1-North-SPT3	2.79	-2.047
8-56 -E1-Sag-SPT3	0.96	0.67	8-40-E1-North-SPT3	4.41	-1.01
8-64 -E1-Sag-SPT3	9.08	55.94	8-48-E1-North-SPT3	5.38	0.19
12-60 -E1-Sag-SPT3	3.3	8.59	8-56-E1-North-SPT3	7.23	5.22
12-96 -E1-Sag-SPT3	17.59	55	8-64-E1-North-SPT3	9.33	0.47
12-108 -E1-Sag-SPT3	20.99	1.55	8-80-E1-North-SPT3	22.11	73.57
16-56 -E1-Sag-SPT3	0.41	-0.022	8-96-E1-North-SPT3	14.39	25.6
16-64 -E1-Sag-SPT3	2.92	0.17	12-48-E1-North-SPT3	3.29	-1.74
16-80 -E1-Sag-SPT3	5.82	1.7	12-60-E1-North-SPT3	4.4	-1.16
16-112 -E1-Sag-SPT3	23.45	34	12-72-E1-North-SPT3	6.97	-1.63
25-100 -E1-Sag-SPT3	4.2	0.052	12-96-E1-North-SPT3	13.21	22.44
25-112.5 -E1-Sag-SPT3	4.8	27.7	16-64-E1-North-SPT3	4.72	0.46
8-32 -E3-Sag-SPT3	2.43	0.3	16-80-E1-North-SPT3	14.42	21.62
12-42 -E3-Sag-SPT3	2.03	0.24	16-112-E1-North-SPT3	10.6	4.49
12-48 -E3-Sag-SPT3	4.12	0.32	16-128-E1-North-SPT3	11.61	-1.62
16-48 -E3-Sag-SPT3	1.23	0.019	25-112.5-E1-North-SPT3	3.97	-1.6
16-56-E3-Sag-SPT3	2.51	0.37	25-125-E1-North-SPT3	6.75	3.81
16-64 -E3-Sag-SPT3	11.56	0.32	8-28-E3-North-SPT3	8.8	-3.35
25-75 -E3-Sag-SPT3	1.59	0.14	8-48-E3-North-SPT3	18.06	10.43
8-28 -E5-Sag-SPT3	9.03	0.9	8-64-E3-North-SPT3	26.01	33.38
12-36-E5-Sag-SPT3	4.41	-0.2	12-42-E3-North-SPT3	7.58	-2.9
12-42-E5-Sag-SPT3	8.03	0.69	12-48-E3-North-SPT3	9.39	-3.33
16-40-E5-Sag-SPT3	2.92	-0.36	12-60-E3-North-SPT3	15.9	12.44
16-48-E5-Sag-SPT3	3.84	-0.23	16-48-E3-North-SPT3	4.36	-2.93
16-56-E5-Sag-SPT3	8	0.012	16-64-E3-North-SPT3	11.33	3.1

Table 4.A: Values of the average normalized horizontal displacement (AR_x) and average horizontal velocity (x_{vel}) of the impoundment dyke for different WRI configurations and input ground motion (continued).

Configuration*	ARx (%)	Xvel (cm/s)	Configuration	ARx(%)	Xvel (cm/s)
25-100-E5-Sag-SPT3	7.75	-0.0475	16-112-E3-North-SPT3	22.54	14.98
8-28 -E4-Sag-SPT8	4.77	0.363	16-128-E3-North-SPT3	28.15	5.21
8-48 -E4-Sag-SPT8	3.23	0.19	25-112.5-E3-North-SPT3	10.14	-0.57
8-56 -E4-Sag-SPT8	8.9	0.97	25-125-E3-North-SPT3	11.66	-3.31
8-64 -E4-Sag-SPT8	18.75	9.24	12-48-E5-North-SPT3	32.51	-2.03
8-80 -E4-Sag-SPT8	18.29	2.48	16-48-E5-North-SPT3	13.64	-1.425
8-88 -E4-Sag-SPT8	24.81	2.74	8-40-E1-North-SPT8	20.7	1.17
12-42 -E4-Sag-SPT8	1.85	-0.32	12-36-E1-North-SPT8	7.44	-3.81
12-48 -E4-Sag-SPT8	2.17	-0.2	12-42-E1-North-SPT8	10.66	-3.9
12-84 -E4-Sag-SPT8	15.02	0.76	12-48-E1-North-SPT8	14.03	-4.45
12-96 -E4-Sag-SPT8	21.75	2.07	12-60-E1-North-SPT8	19.02	-2.34
16-56-E4-Sag-SPT8	2.06	-0.19	16-56-E1-North-SPT8	9.02	-3.7
16-64 -E4-Sag-SPT8	5.37	0.8	16-64-E1-North-SPT8	14.14	-4.41
16-80 -E4-Sag-SPT8	8.04	3.97	16-80-E1-North-SPT8	19.6	11.18
16-112 -E4-Sag-SPT8	28.28	1.16	16-112-E1-North-SPT8	22.29	-4.58
16-144 -E4-Sag-SPT8	33.35	24.72	16-128-E1-North-SPT8	27.06	-5.27
25-75 -E4-Sag-SPT8	1.65	-0.22	12-36-E3-North-SPT8	12.49	-1.52
25-112.5-E4-Sag-SPT8	3.04	0.16	12-42-E3-North-SPT8	18.82	-2.66
25-125 -E4-Sag-SPT8	17.52	0.93	12-48-E3-North-SPT8	23.08	-3.4
8-24 -E5-Sag-SPT8	5.62	-0.05	12-60-E3-North-SPT8	27.33	-1.75
8-32 -E5-Sag-SPT8	4.7	-0.07	16-40-E3-North-SPT8	10.42	-0.87
8-40 -E5-Sag-SPT8	8.86	5.74	16-48-E3-North-SPT8	10.16	-0.92
8-48 -E5-Sag-SPT8	19.98	27.18	16-56-E3-North-SPT8	14.36	-1.89
12-42 -E5-Sag-SPT8	3.95	-0.298	16-64-E3-North-SPT8	22.01	-2.835
12-48-E5-Sag-SPT8	6.2	0.45	16-112-E3-North-SPT8	30.5	-4
12-60-E5-Sag-SPT8	14.73	2.05	16-128-E3-North-SPT8	34.08	-4.77
16-56-E5-Sag-SPT8	4.1	-0.04	25-100-E3-North-SPT8	12.73	-3.1
16-64-E5-Sag-SPT8	12.9	2.647	25-125-E3-North-SPT8	22.77	-3.96

Table 4.A: Values of the average normalized horizontal displacement (AR_x) and average horizontal velocity (x_{vel}) of the impoundment dyke for different WRI configurations and input ground motion (continued).

Configuration*	ARx (%)	Xvel (cm/s)	Configuration	ARx(%)	Xvel (cm/s)
25-112.5-E5-Sag-SPT8	10.57	-0.054	----	----	----
25-125-E5-Sag-SPT8	19.14	2.54	----	----	----

*First number is the width W (m), second number is the center-to-center spacing S of inclusions; E1 to E5 indicate the earthquake records for Sag (high frequency, Saguenay) and North (the low frequency, Northridge) events, SPT3 and SPT8 indicate the under-consolidated and consolidated tailings, respectively.

CHAPTER 5: ARTICLE 3- INVESTIGATION OF THE EFFECT OF WASTE ROCK INCLUSIONS CONFIGURATION ON THE SEISMIC RESPONSE OF A TAILINGS IMPOUNDMENT

Behnam Ferdosi*, Michael James, and Michel Aubertin

Submitted to Journal of Geotechnical and Geological Engineering

Department of Civil, Geological and Mining Engineering, École Polytechnique de Montréal

C.P. 6079, Centre-ville, Montréal, QC, Canada, H3C 3A7

* Corresponding author: Behnam Ferdosi, Phone 514-340-4711 ext 3751; fax 514-340-4477
Email: behnam.ferdosi@polymtl.ca

Abstract

Waste rock inclusions can improve the seismic response of tailings impoundments, mainly through their reinforcing effect. Preliminary simulations of reinforced impoundments illustrated how such inclusions can be beneficial for impoundments subjected to earthquake loadings. This paper presents new results of numerical analyses of the seismic performance of a tailings impoundment with different configurations of waste rock inclusions (i.e. various widths and center-to-center spacings). The simulations were conducted using two base ground motion records, one characterized by high frequencies typical of the east coast of North America and the other characterized by low frequencies typical of the west coast. Both ground motions were scaled to obtain the same Arias intensity and peak horizontal ground acceleration. The seismic response of the tailings impoundment was evaluated using (i) the deformation of the downstream slope at the end of shaking, with respect to the energy content and predominant frequency of the applied ground motions, as well as the configuration of the inclusions, (ii) the critically displaced volume of tailings at the end of shaking. A total of 108 dynamic numerical simulations were conducted and evaluated. The main results presented here show that waste rock inclusions can enhance significantly the seismic performance of a tailings impoundment when appropriate configurations are considered. These also indicate that the low frequency ground motions tend to produce larger deformations and critically displaced volumes of tailings in comparison to the

high frequency ground motions. These simulations results provide preliminary guidelines to determine optimum configurations of waste rock inclusions for different seismic loadings.

Keywords: Tailings, Impoundment, Liquefaction, Seismic analysis, Waste rock inclusion

5.1 Introduction

Tailings impoundments are susceptible to failure due to seismic activity. Such failures often result in the release of the retained tailings, with severe consequences in terms of loss of life, environmental damage and costs (ICOLD 2001; Aubertin et al. 2002; WISE 2014).

Vertical columns are sometimes used to control the effects of seismic loading and liquefaction in silty soils of low hydraulic conductivity, having properties fairly similar to tailings. For instance, Adalier et al. (2003) conducted seismic table testing of non-plastic silt with and without stone columns. The results showed that the columns retarded pore water pressure generation within the silt and reduced soil deformation during cyclic loading. Martin et al. (2004) investigated the seismic response of a site underlain by sand and stiff silty clay where some areas had been remediated by the installation of relatively rigid grouted columns. The site was affected by the 1999 Kocaeli earthquake (M_w=7.4). Post-earthquake comparison of remediated areas with untreated areas indicated that the presence of the columns reduced shear strains and the generation of excess pore water pressures. Pépin et al. (2012a, 2012b) conducted seismic table tests on tailings; some of these included a vertical inclusion consisting of a more rigid and/or more pervious material. The results showed that circular or linear inclusions can reduce or retard excess pore water pressure generation during cyclic loading. The improved seismic performance was mainly due to the stiffening effect of the inclusions that act to reduce shear strain of the mass. The drainage effect of pervious inclusions was not significant during shaking due to the low hydraulic conductivity of the tailings, but they helped with the dissipation of the excess pore water pressures at the end of cyclic loading.

Considering the potential advantages of vertical rigid columns (e.g. Barksdale 1983, 1987), Aubertin et al. (2002) proposed using waste rock in tailings impoundments to improve their geotechnical and environmental performance (see also James and Aubertin 2009, 1010). This tailings and waste rock co-disposal method involves the installation of a thin layer of waste rock on the bottom and sides of an impoundment and the addition of continuous rows of waste rock

placed along predetermined routes in the impoundment prior to and during tailings deposition. These rows (inclusions) of waste rock, raised with each stage of impoundment construction, are the object of this investigation.

The fact that waste rock inclusions (WRI) are more rigid and more permeable than the tailings leads to a number of benefits. Two of the most significant advantages are accelerated consolidation of the tailings and improved seismic performance of the impoundments (James et al. 2013). The accelerated consolidation has been studied using numerical modeling (L.-Bolduc and Aubertin, 2014) and physical modeling (Saleh-Mbemba 2015). This behavior is also being monitored at a large tailings impoundment being constructed in western Quebec, Canada; this is the first mine site where waste rock inclusions have been installed. The improved seismic performance has been studied using numerical modelling of a conceptual tailings impoundment by James (2009). The preliminary simulation results demonstrated that the presence of WRI resulted in significantly reduced deformation of the retention dyke during seismic loading, which in some instances may prevent failure of the impoundment. The improved performance was due to the rigidity and strength of the inclusions. The higher hydraulic conductivity of the waste rock was not a factor during seismic loading due the short duration of the events, but the WRI accelerate and direct the dissipation of excess pore water pressures in the tailings during the post shaking phase.

This paper presents dynamic numerical analyses of a tailings impoundment loosely based on an actual site located in Quebec, Canada. The impoundment was modeled with and without waste rock inclusions; it should be noted that the simulated WRI differ from those actually built at the mine site. In this investigation, the location and configuration (width and center-to-center spacing) of the inclusions was varied to assess the effect of these characteristics. The model was subjected to seismic loadings of various intensities with ground motion characteristics similar to high and low frequency earthquakes typical of North America. The results of the simulations are then used to evaluate the seismic response and performance of the impoundment with respect to the WRI configuration and the intensity and frequency characteristics of the ground motion. Presentations of the results include indications for their optimal design and application.

5.2 Methods of analysis and evaluation

The numerical modeling was conducted using version 6 of FLAC (Itasca 2008). The model was first applied to simulate the hydro-geotechnical response and assess pore water pressures and initial stresses under static conditions. Then, seismic numerical analyses were conducted. Seismic loads with different Arias intensities and frequency contents were applied to the tailings impoundment model and its performance was evaluated for each loading.

The performance of the tailings impoundment was evaluated at the end of seismic loading based on the horizontal displacements of nodal points on the downstream slope of the impoundment normalized by the nodal height leading to a relative displacement R_x and also using the critically displaced volume of tailings in this area.

5.3 The tailings impoundment

The final height of the simulated tailings impoundment is 40 m. The external dykes are constructed using the upstream method. The starter dyke and dykes raises are composed of waste rock. Each dyke raise is 2 m high. The crest width is 15 m and side slopes are 2.5:1 (H:V), as shown schematically on Figure 5-1. Each subsequent dyke raise overlaps the preceding dyke raise by 6 m. A geotextile (not shown) is used to provide filter protection between the tailings and the waste rock.

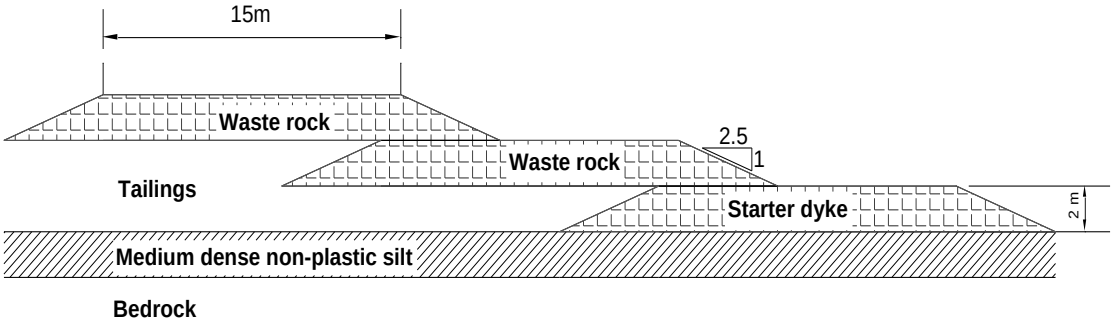

Figure 5-1: Cross section of the external dyke after three construction steps

Site investigation (Golder Associates, 2011) indicates that a 2-meter-thick layer of medium dense to dense silt underlies the impoundment. Moderately fractured, hard bedrock lies beneath the silt layer.

5.4 Numerical modeling of the tailings impoundment

5.4.1 Constitutive models

The UBCSAND model was used to simulate the seismic response of the tailings. This constitutive model was developed by Byrne and his collaborators (Byrne et al. 1995; Puebla 1999; Puebla et al.1997; Beaty and Byrne 1998, 2011; Naesgaard 2011) to simulate the cyclic behavior of granular saturated sand. James (2009) showed that the UBCSAND can predict quite well the excess pore water pressure, shear strain and number of cycles to the initiation of liquefaction in tailings submitted to simple cyclic shear testing, for different confining effective stresses and cyclic stress ratios. Ferdosi et al. (2013, 2014a, 2014b) have recently showed that the UBCSAND model can also predict fairly well the generation of pore water pressures during seismic table testing of tailings with and without a sand wall inclusion (using experimental data from Pépin et al. 2012a,b). Following these encouraging results, the UBCSAND model was used to simulate the dynamic response of tailings and of the non-plastic silt underlying the tailings impoundment.

The elasto-plastic Mohr-Coulomb model as implemented in FLAC was used for the waste rock and other materials.

5.4.2 Model geometry

Figure 5-2 shows a typical cross section of the tailings impoundment that was considered in the numerical modeling. As the actual tailings impoundment is very large, modeling the extent of the impoundment would be difficult due to the number of elements required; therefore, the model was terminated at a distance of 160 m from the dyke crest. Also, as tailings are very soft (deformable), the use of a free field boundary at the left hand side of the model would result in excessive deformation during seismic analysis (i.e. bad geometry error before the end of shaking). Therefore, a buttress composed of a stiff glacial till was used at the left hand side of the model and a free field boundary conditions was applied to the left and right hand sides of the

model. The distance of this buttress from the crest is sufficiently large (160 m) that it does not affect the results of the simulations along and near the downstream slope (dyke) of the impoundment. A total of 12618 quadrilateral elements with maximum size of 1 m by 1 m were used to create the mesh of the model. The large strain option in FLAC was used in the simulations.

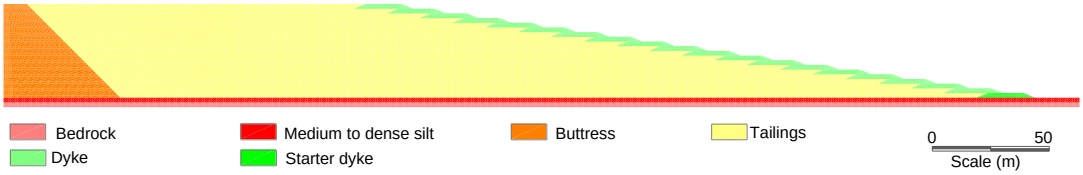

Figure 5-2: Model of the tailings impoundment used for the numerical simulations

5.4.3 Material properties

James (2009) conducted cyclic simple shear testing of tailings from a nearby mine (see also James et al. 2011). The specimens were prepared as slurry, anisotropically consolidated to vertical effective confining stresses from 100 to 400 kPa, and tested with cyclic stress ratios (CSR) of 0.075 to 0.15. Subsequently, the tests were simulated numerically with FLAC using the UBCSAND model. The simulations showed an acceptable agreement with the laboratory testing for a corrected SPT value, $(N_1)_{60}$, of 11 blows/30 cm for all levels of confining stress. Therefore, $(N_1)_{60} = 11$ was adopted here for consolidated tailings in the impoundment. The effective friction angle of these tailings was found to be 36.6° based on direct shear testing at confining stresses of 100 to 500 kPa (James 2009). The average dry unit weight of the tailings is about 17 kN/m^3 over vertical effective confining stresses of 100 to 400 kPa. Table 5.1 presents the material properties used in the simulations. These properties were obtained from laboratory tests and numerical analysis performed by James (2009) and in-situ data reported by Golder Associates (2011).

The shear and bulk moduli of the waste rock (inclusions and dykes raises) were computed from the following formulas, developed by James (2009):

$$G = 55000(0.6 \cdot \sigma_v')^{0.5} \quad (5.1)$$

and

$$K = 2.3833 \cdot G \quad (5.2)$$

where σ_v' is the effective vertical stress in kPa; the shear modulus G and bulk modulus K are also expressed in kPa. A FISH routine was written in FLAC to assign the values of the shear and bulk moduli for the dykes and WRI using Eq. (5.1) and (5.2).

5.4.4 Damping parameters

Rayleigh damping was applied in the bedrock to account for the natural damping of the rock mass. The damping ratios for Rayleigh damping for high and low frequency earthquake records were adjusted so that the acceleration at the top of the bedrock was the same as the input acceleration record. The Rayleigh damping ratios for the bedrock for the high and low frequencyearthquake ground motions were found to be 0.03 and 0.02, respectively, with center frequencies of 5 Hz for both records.

The sigmoidal hysteretic damping model “sig3” (Itasca 2008) was applied to the waste rock (dykes and inclusions) and buttress. The model parameters were obtained using the procedure described in Itasca (2008) (see details in Ferdosi et al. 2014c, which deals with a different mine site, without WRI). The simulated shear modulus reduction and damping curves were adjusted to the experimental results reported by Rollins et al. (1998) for gravelly soils.

The UBCSAND model tends to underestimate damping at low shear strains (Beaty and Byrne 2011). Various authors, such as Naesgaard et al. (2004), Boulanger et al. (2011), Fung et al. (2011), Bray and Dashti (2012), Dashti and Bray (2012), and Ziotopoulou et al. (2012), used a small value of stiffness proportional Rayleigh damping to compensate for this underestimated damping at low shear strains. A small value of, 0.2% was used here for stiffness proportional damping, with the center frequency of the input motion for the tailings and foundation soils. Itasca (2008) also suggested assigning such a small value of stiffness proportional damping to materials simulated with the hysteretic damping model. This damping was assigned here to remove low amplitude waves with high frequency content that are numerical artifacts (Itasca

2008). According to Itasca (2008), a damping ratio of 0.2% is appropriate and it does not affect the analysis.

Table 5.1: Material properties (adapted from James 2009, Golder Associates 2011)

Properties	Tailings	Medium to dense non-plastic silt	Dyke (waste rock)	Glacial Till	Bedrock
Dry unit weight, ρ_{dry} (kN/m3)	17.0	16.20	20.0	19.5	22.0
Effective friction angle, $\emptyset'$ (°)	36.6	32	45	36	40
Effective cohesion, c' (kPa)	0	0	0	0	48000
Dilation angle, ψ_d (°)	varied[1]	varied[1]	10	10	10
Porosity, n	0.4	0.4	0.25	0.3	0.1
Modulus of elasticity, E (MPa)	varied[2]	varied[2]	Varied[3]	940	35000
SPT $(N_1)_{60-cs}$ (blows/300 mm)	11	32	NA*	NA*	NA*
Hydraulic conductivity (m/s)	5.8×10^{-8}	2.5×10^{-7}	10^{-3}	5×10^{-7}	1×10^{-8}

[1] In UBCSAND model, the dilation angle is computed based on the constant volume friction angle (φ'_{cv}) and developed friction angle (φ_d). φ'_{cv} is considered 35.6° for the tailings (James et al. 2011) and 30° for the silt (Lambe and Whitman, 1969).

[2] In UBCSAND model, the shear and bulk modulus are computed based on the corrected value of SPT and mean effective stress (see Byrne et al. 2004).

* Not applicable

[3] See Eqs. (1) and (2).

5.4.5 Seismic loads

The seismic loads applied to the tailings impoundment model were simulated using modified earthquake ground motion records composed of horizontal accelerations at given time steps (e.g.

0.05 seconds). These motions were applied to the bottom of the model to produce one dimensional acceleration time histories.

Record S16T of the 1988 Saguenay (Quebec, Canada) earthquake (M_w=5.9) was used as the base for the high frequency ground motions and record 0923-H1 of the 1994 Northridge (California, US) earthquake (M_w=6.7) was used for the low frequency ground motions (NRC 2003, PEER 2014). Both records were modified by factoring the accelerations and time steps to simulate seismic events of known Arias intensities associated with given magnitudes and epicentral distances. The main characteristics of the original and modified ground motions, for a magnitude M_w = 7.0 and 7.5, are given in Table 5.2. Detailed calculations of the modified ground motions are presented in Ferdosi et al. (2014c). The Arias intensities of the modified ground motions were selected from the preliminary simulations performed by James (2009); these are expected to induce significant deformations or failure of the subject tailings impoundment without waste rock inclusions. The tailings impoundment without inclusions was also analyzed using the modified Saguenay and Northridge ground motions with a magnitude M_w = 6.5 and an epicentral distance of 30 km; the results (not presented here) showed that the consolidated tailings impoundment remained stable, with limited deformations, in these cases.

Table 5.2: Parameters of the base and modified ground motions

Ground Motion		Magnitude (Mw)	Source to site distance (km)	Arias intensity I_x(m/s)	PGA (g)	Duration (seconds)
Saguenay ground motions						
base	S16T	5.9	43	0.17	0.131	25
modified	E_4-sag	7.0	20	2.05	0.378	35
modified	E_5-sag	7.5	30	3.09	0.434	40
Northridge ground motions						
base	0923-H1	6.7	31.2	0.22	0.129	20
modified	E_4-north	7.0	20	2.05	0.378	28
modified	E_5-north	7.5	30	3.09	0.434	32

5.5 Seismic analysis of the unreinforced tailings impoundment

To provide a basis for the evaluation of the effects of waste rock inclusions on the seismic response of the tailings impoundment, analyses of the impoundment without inclusions to the E_4-sag and E_4-north ground motion records were conducted. Figs. 3 and 4 present the deformed geometries and the horizontal displacements of the impoundment at the end of shaking for the E_4-sag and E_4-north ground motions, respectively.

The analyses with the E_4-sag ground motion stopped 32 seconds into the 35-second-long ground motion due to a bad geometry error (excessive deformation of at least one element). At this point, the crest of the impoundment had displaced approximately 7 m in the downstream direction. Continued shaking would have resulted in additional displacements and probably failure of the impoundment. Analysis with the E_4-north ground motion caused 25 m of horizontal displacement of the downstream slope of the tailings impoundment after 25 seconds when the simulation ended due to a bad geometry error. This was also indicative of a probable failure of the impoundment. A FISH function was also written in FLAC to compute the values of the pore water pressure ratio r_u (ratio of excess pore water pressure to initial effective stress) at the end of shaking (or the end of execution). The results indicated that all of the retained tailings liquefied ($r_u > 0.8$) due to the E_4-sag and E_4-north ground motions.

As shown in Figs. 3 and 4, the results of these simulations lead to significant deformations, and possibly failure of the impoundment without inclusions, due to the E_4-sag and E_4-north ground motions.

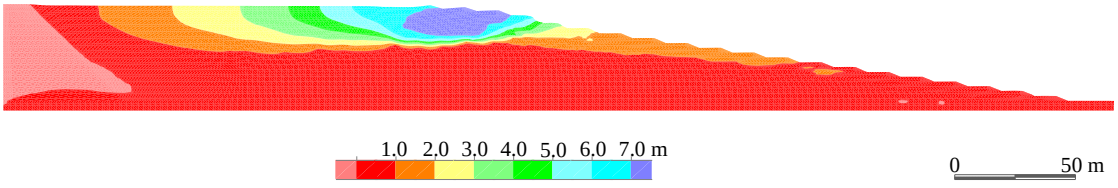

Figure 5-3: Final deformed geometry and horizontal displacements contours due to the E_4-sag ground motion (after 32 seconds)

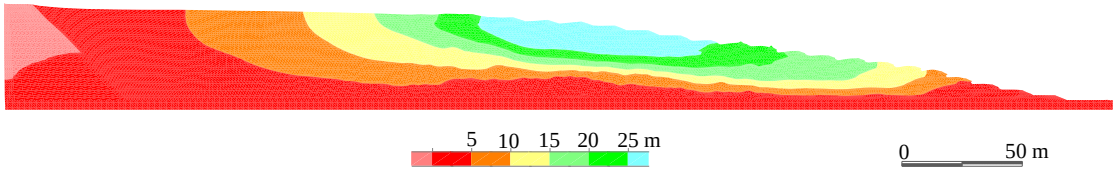

Figure 5-4: Final deformed geometry and horizontal displacements contours due to E_4-north ground motion (after 25 seconds)

5.6 Seismic analysis of the impoundment with waste rock inclusions

The seismic response of the tailings impoundment with waste rock inclusions was evaluated using the four modified ground motion records listed in Table 5.2. The width W (m) and center-to-center spacing S (m) of the inclusions were varied to evaluate the effect of the configuration. The width varied from 8 to 25 m and the spacing varied from 24 to 125 m. The 27 combinations of width and spacing considered are listed in Table 5.3. Each configuration was analyzed using the four modified ground motion records, resulting in 108 simulations. The run time for each simulation varied from 28 to 55 hours. The main results of these analyses are summarized in Tables 5.4 and 5.5.

Table 5.3: Widths and spacing of waste rock inclusions

Width of inclusions (W) (m)	8	12	16	20	25
Configurations (W-S)*	8-24, 8-32, 8-40, 8-48, 8-56, 8-64, 8-72	12-24, 12-36, 12-48, 12-60, 12-72, 12-84, 12- 96	16-32, 16-48, 16-64, 16-80, 16-96	20-40, 20-60, 20-80, 20-100	25-50, 25-75, 25-100, 25-125

*In these configuration, the first number represents the inclusion width "W" and second number is the center-to-center spacing "S" between the inclusions. Units are in meters.

Figure 5-5 shows the tailings impoundment reinforced with WRI, for configuration 12-36 (i.e. width, W, and center-to-center spacing, S, are 12 and 36 m, respectively).

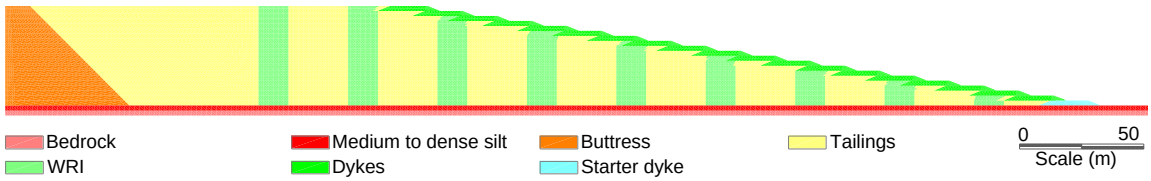

Figure 5-5: A typical model cross section of the tailings impoundment reinforced by WRI, having widths, W, of 12 m and a spacing, S, of 36 m

Figure 5-6 shows the horizontal displacement of the external dyke and impoundment with inclusions (W =12 m and S=36 m) at the end of shaking due to the E4-north ground motion. As shown in this figure, the maximum horizontal displacement at end of shaking is 2.5 m; this displacement value for the unreinforced impoundment (Figure 5-4) is more than 25 m. It is thus seen that the WRI can enhance significantly the seismic response of the impoundment, in this case by decreasing the horizontal displacement by a factor of 10.

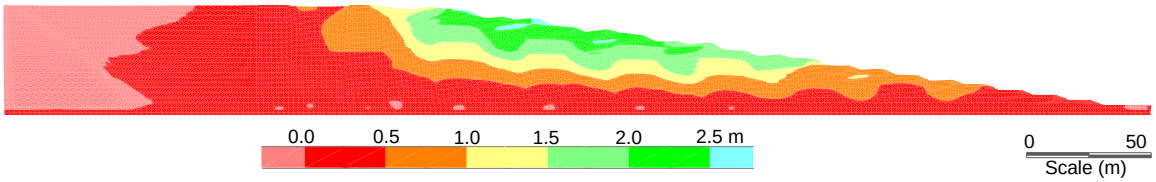

Figure 5-6: Final deformed geometry and horizontal displacement contour due to the E_4-north ground motion (at end of shaking) in the reinforced tailings impoundment (with WRI) for W=12 m and S=36 m

Figure 5-7 shows the pore water pressure ratio (r_u) distribution inside of the reinforced tailings impoundment (with WRI) for configuration 12-36. As indicated by the large values of r_u (> 0.8) in this figure, the tailings between the WRI are liquefied at the end of shaking. Hence, as

expected from the results obtained by James (2009), the simulations indicate that the WRI would not reduce significantly the generation of excess pore water pressures in tailings (except for locations very close to the inclusions), but would rather serve to prevent their deformation and flow due to liquefaction.

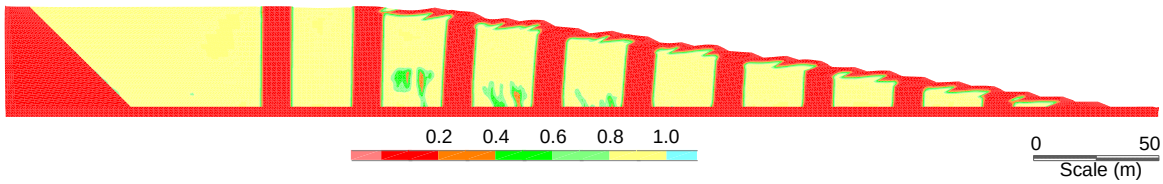

Figure 5-7: Distribution of the pore water pressure ratio (r_u) due to E_4-north earthquake record (at end of shaking) in the reinforced tailings impoundment (with WRI) for W=12 m and S=36 m

To evaluate the results of the simulations, the horizontal displacement at the end of shaking of each nodal point on the downstream slope of the tailings impoundment was divided by its initial height above the original ground surface. This value, called the normalized horizontal displacement, R_x (%), was registered for each simulation. The average value of the normalized horizontal displacement along the downstream slope, AR_x (%), was also calculated.

The simulations results indicate that, in some cases, the horizontal displacements at the top of the WRI were significantly different from those of the tailings between the inclusions. This was particularly evident where the spacing of the inclusions was relatively wide. Therefore, the relative displacements values R_x and AR_x were also evaluated for the inclusions alone. The results are given in Tables 5.4 and 5.5 These show, for instance, that the configuration 25-125 gives an average relative displacement (AR_x total) of 19.12% for the entire impoundment, and an average displacement (AR_x WRI) of 2.82% for the WRI, at the end of shaking for the E_5-sag ground motion (see Table 5.4). This example illustrates a situation where the horizontal displacements at the surface of tailings are much larger than those at the top of WRI.

Tables 5.4 and 5.5 include all the calculated values of AR_x total and AR_x WRI for the simulations conducted with the modified Saguenay and modified Northridge ground motions,

respectively. These tables also give the maximum horizontal displacement at the surface of the downstream slope of the impoundment (Mxdis) for different WRI configurations at end of shaking.

In general, these results indicate that the deformation of the downstream slope (based on the AR_x values) tend to (i) decrease with increasing inclusion width W ; (ii) increase with increasing inclusion spacing S; (iii) increase with increasing seismic loading; and (iv) be more significant for the Northridge than for the Saguenay ground motions.

When analyzing more specifically the individual results, it is seen that for 17 of the 108 simulations conducted, excessive deformation of individual elements near the surface of the impoundment led to an execution ("bad geometry") error that halted the simulation before the specified duration. These incomplete simulations are marked with an asterisk in Tables 5.4 and 5.5. Other characteristics of the simulations results are presented and discussed below.

Table 5.4: Average normalized horizontal displacements (AR_x) of the downstream slope of the impoundment (AR_x total) and of the WRI (AR_x WRI) for various inclusions configurations (modified Saguenay ground motions)

Arrangement		E4-sag			E5-sag		
Width W (m)	Spacing S (m)	ARx total (%)	ARx WRI (%)	Mxdis (m)#	ARx total (%)	ARx WRI (%)	Mxdis (m)#
8	24	1.73	1.67	0.6	3.26	3.26	1.25
	32	2.89	2.63	1.0	5.36	5.21	2.0
	40	3.93	3.2	1.75	7.35	6.47	3.0
	48	3.82	2.73	1.75	9.76	7.83	4.0
	56	4.36	3.38	1.5	8.0	6.76	2.25
	64	5.21	3.7	2.5	22.1*	17.5*	10.0*
	72	4.39	3.07	1.4	15.1	11.36	7.0
12	24	0.96	0.82	0.3	1.65	1.47	0.6
	36	1.92	1.34	0.6	3.17	2.39	1.0
	48	3.08	1.85	1.25	6.2	4.25	2.0
	60	4.06	2.46	2.5	7.5	5.16	3.0
	72	4.01	1.89	1.4	17.65	11.3	8.0
	84	4.6	2.4	1.5	11.95	7.08	6.0
	96	5.02	2.34	2.4	15*	7.19*	10.0*
16	32	0.9	0.64	0.25	1.45	1.07	0.4
	48	2.31	1.3	1.0	3.43	2.18	1.25
	64	3.08	1.38	1.25	6.23	3.11	2.5
	80	3.55	1.47	1.4	7.3*	3.22*	4.0*
	96	3.9	1.38	1.5	16.3*	6.91*	8.0*
20	40	0.91	0.56	0.3	1.48	0.956	0.4
	60	2.41	0.87	1.0	4.0	1.74	2.0
	80	3.0	0.93	1.25	8.02*	2.72*	3.5*
	100	3.9	1.22	1.75	9.8*	3.13*	6.0*
25	50	1.18	0.46	1.75	1.8	0.8	0.6
	75	2.65	0.68	1.25	4.9	1.35	3.0
	100	3.605	0.82	1.75	7.96	1.84	4.5
	125	3.63	0.73	1.5	19.12*	2.82*	8.0*

* Analysis was stopped because of bad geometry error in some elements

maximum horizontal displacement of downstream slope surface of impoundment

Table 5.5: Average normalized horizontal displacements (AR_x) of the downstream slope of the impoundment (AR_x total) and of the WRI (AR_x WRI) for various inclusions configurations (modified Northridge ground motions)

Arrangement		E4-north			E5-north		
Width W (m)	Spacing S (m)	ARx total (%)	ARx WRI (%)	Mxdis (m)#	ARx total (%)	ARx WRI (%)	Mxdis (m)#
8	24	7.98	8.63	3.0	13.04	14.37	6.0
	32	13.47	14.44	6.0	21.08	22.95	9.0
	40	17.85	17.56	7.0	26.74	26.89	11.0
	48	20.81	18.56	8.0	30.6	28.69	12.5
	56	21.26	18.93	8.0	30.4	27.62	12.5
	64	24.96	21.64	9.0	33.48	30.27	12.5
	72	24.56	19.82	9.5	35.58	29.85	15
12	24	2.69	2.73	1.3	4.1	4.2	2.0
	36	6.22	5.43	2.5	9.68	8.67	4.0
	48	12.02	9.85	5.0	17.86	15.18	7.0
	60	16.5	14.3	6.0	23.85	21.05	10.0
	72	19.61	13.63	7.5	28.12	20.85	12.5
	84	24.69	17.13	8.0	31.59	22.3	12.5
	96	24.5	14.62	8.0	35.1	22.3	12.5
16	32	2.22	2.04	1.0	3.46	3.28	1.5
	48	5.68	4.58	2.5	8.5	7.23	3.5
	64	10.77	7.36	5.0	15.58	11.48	6.0
	80	15.57	9.47	6.0	21.44	14.06	8.0
	96	19.06	9.98	8.0	24.1	14.08	9.0
20	40	2.19	1.72	1.0	3.22	2.66	1.5
	60	5.96	3.48	2.5	8.35	5.36	3.5
	80	11.23	5.02	5.0	16.84*	10.5*	6.0*
	100	15.42	7.0	6.0	21.27	10.64	8.0
25	50	2.51	1.36	1.25	3.58	2.07	1.5
	75	7.07	2.42	3.0	9.26	3.76	3.5
	100	9.56*	4.33*	3.5*	18.03	5.65	8.0
	125	18.09*	6.0*	8.0*	12.11*	2.34*	5.0*

* Analysis was stopped because of bad geometry error in some elements

maximum horizontal displacement of downstream slope surface of impoundment

5.6.1 Effect of ground motion intensity and frequency

The results summarized in Tables 5.4 and 5.5 show that for all the configurations, the response of the impoundment, as determined the AR_x total values, was better (i.e. less displacement) for the ground motions of lower Arias intensity (I_h=2.05 m/s) than those of higher intensity (I_h=3.09 m/s) (with details given in Table 5.2). This is an expected outcome that can be quantified with the numerical calculations.

Figure 5-8 presents graphically the AR_x total and AR_x WRI values for the impoundment with 8-meter-wide inclusions and the different center-to-center spacing considered for the modified Saguenay ground motions E4-sag (I_h=2.05 m/s) and E_5-sag (I_h=3.09 m/s). For the E_4-sag ground motion, the AR_x total values vary from 2 to 5 % and the AR_x WRI values vary from 2 to 3.5%. These values indicate that there is a relatively limited deformation of the surface of the downstream slope of the impoundment and that the displacements at the top of the tailings and inclusions were fairly similar. For the E_5-sag ground motion (greater energy content but of similar frequency content), the AR_x total values range from 3% to 22%, generally increasing with increasing spacing, while the AR_x WRI values range from 3% to 17%, also increasing with increasing spacing. For this earthquake, the displacements at the surface of the downstream slope increase significantly with the spacing and become excessive at a spacing, S, of 64 m (AR_x total of 22%).

For the modified Saguenay loadings, an increase in the energy content (intensity) of the loading by about 50% (i.e. E_4 to E_5) also resulted in much larger displacements of the downstream slope. These displacements also increase with increasing spacing of the inclusions. It is worth recalling here that the simulated Mxdis value of the impoundment without WRI due to E_4-sag ground motions is 7 m (see Figure 5-3 above). According to Table 5.4, for the different configurations of WRI, the horizontal displacement of the downstream slope varies between 0.6 and 2.5 m for the E4-sag ground motion. Hence, WRI can improve markedly the seismic response of the tailings impoundment.

Similarly, the response of the impoundment with 8-m-wide inclusions for the modified Northridge ground motions E_4-north and E_5-north (I_h values of 2.05 and 3.09 m/s, respectively) can be interpreted using the AR_x (total and WRI) values shown on Figure 5-9. For the E_4-north ground motion, the AR_x total values vary from 8% for spacing of 24 m to 25% for 72 m; the AR_x

WRI values are fairly similar in magnitude though generally slightly less. The increased intensity of the E_5-north ground motion resulted in AR_x total values of 13% to 36%, increasing with a spacing going from 24 m to 72 m. Again, the AR_x WRI values were typically slightly less, indicating compatible displacements between the top of the inclusions and the surface of tailings.

As shown in Figure 5-4, the unreinforced impoundment displaced horizontally by more than 25 m due to the E_4-north ground motion. As shown on Table 5.5, the Mxdis values for different configurations due to the E_4-north ground motion are between 3.0 m and 9.5 m. This indicates that even relatively narrow WRI, with a width, W, of 8 m, can decrease significantly the maximum displacements, depending on the spacing.

For 8-m-wide inclusions, the displacement of the downstream slope increased considerably with the increase in the energy content of the ground motions used to simulate the earthquake loadings. This was the case for both the high and low frequency ground motions. As indicated by the results summarized in Tables 5.4 and 5.5, this finding is also applicable to all of the other inclusion widths considered (up 25 m).

Tables 5.4 and 5.5 also show that the Mxdis of the tailings impoundment is reduced for configurations with larger widths. For example, the Mxdis due to E_4-north ground motion for W=8 m is between 3.0 m and 9.5 m and for W=20 m it is between 1.0 m and 6.0 m.

Different combinations of width and spacing can lead to fairly similar total displacements, but different performance of the impoundment. For instance, configurations 8-24 and 20-60 lead to Mxdis of 3.0 and 2.5 m, respectively. However, the values of AR_x WRI for these same configurations (8-24 and 20-60) are 8.63% and 3.48%, respectively; the latter configuration (20-60) thus appears to be more stable in comparison. Comparing results presented in Figs. 8 and 9 illustrates the effect of the ground motions, based on the modified Saguenay and Northridge ground motions. These results show that the values of AR_x (total and WRI) due to the E_4-sag ground motion (I_h=2.05 m/s) vary between 2 and 5% for all spacings (Figure 5-8a). For the E_4-north ground motion (I_h=2.05 m/s), the values of AR_x (total and WRI, Figure 5-9a) vary from 8% (24 m spacing) to 25% (72 m spacing).

In these same figures (Figure 5-8b and 5-9b), it is seen that he AR_x total values for the E_5-sag ground motion vary from 3 to 22 % and those for the E_5-north ground motion vary from 13 to

36%. Again, for the same level of earthquake energy, the lower frequency ground motions produce significantly more deformation of the downstream slope of the impoundment for all spacings (from 24 to 72 m).

With 8-m-wide inclusions, the lower frequency modified Northridge ground motions produced significantly more deformation, for all of the spacings and widths (Tables 5.4 and 5.5, and Figure 5-8 and 5-9), than the higher frequency modified Saguenay ground motions (for the same values of Arias intensity).

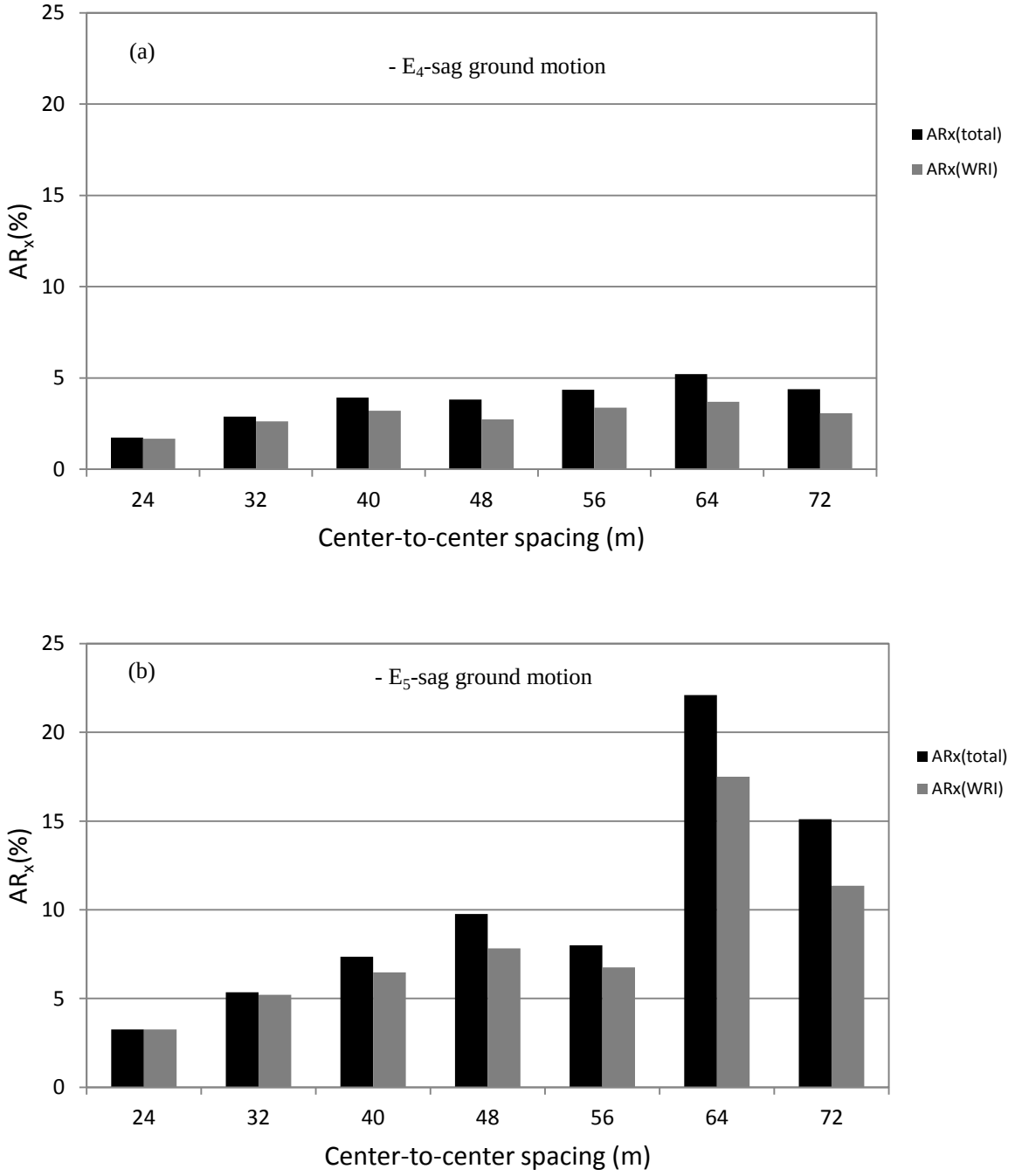

Figure 5-8: Normalized horizontal displacements AR_x for impoundments with 8-meter-wide inclusions (a) E_4-sag ground motions (b) E_5-sag (calculation was stopped for center-to-center spacing of 64 m due to bad geometry error after 33 seconds)

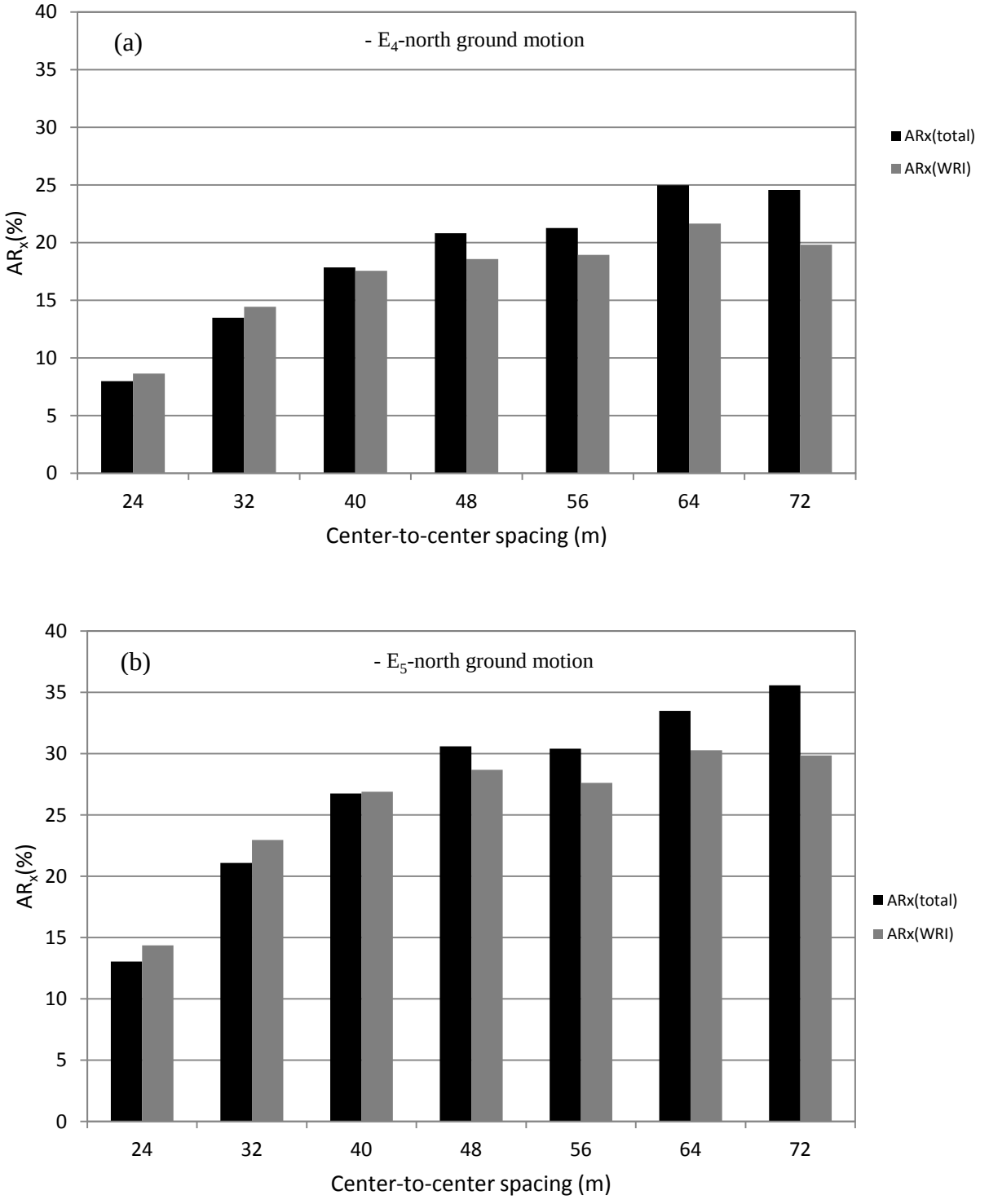

Figure 5-9: Normalized horizontal displacements AR_x for impoundment with 8-meter-wide inclusions (a) E_4-north ground motions; (b) E_5-north

5.6.2 Effect on the WRI configuration on the critically displaced volume of tailings

The effect of WRI configuration on the volume of critically displaced tailings at the end of shaking was also evaluated. Jibson (2011) reported that, based on the California Geological Survey's (2008) guidelines, horizontal displacements of more than 100 cm are prone to cause damaging landslide movement. This value of the displacement of 100 cm is considered here as a threshold to evaluate the effect of WRI configuration on the critically displaced volume of tailings due to seismic events. A FISH function was written in FLAC to delineate the area (volume), if any, in the impoundment (under the downstream slope and upstream of the crest) where the tailings has undergone at least 100 cm of horizontal displacement at the end of shaking. Figure 5-10 shows contours of the areas (or volume, for a unit section in plane strain) of the impoundment that displaced more than 100 cm due to the earthquakes simulated with the E_4-sag and E_4-north ground motion records for various WRI arrangements. Figure 5-10(a), (b), (c), (d), and (e) show the contours of horizontal displacements that exceed 100 cm, for WRI widths of 8, 12, 16, 20, and 25 m respectively. The solid and dashed lines show the results due to the modified Saguenay and Northridge results, respectively. The legends on the right side of the figures show the configurations of the WRI; the first number is the width of the inclusions and the second number is the center-to-center spacing of the inclusions; the subscripts 'sag' and 'north' indicate the high and low frequency records, respectively. It is noted that some arrangements shown in the legend don't correspond to any of the results (contours) shown, indicating that the impoundment with such configuration did not deform more than 100 cm; this is the case for instance for arrangement of 8-24sag, included in the legend of Figure 5-10(a), but not shown in the graphic.

For the relatively high frequency modified Saguenay ground motion (E_4-sag) and all of the WRI configurations considered, the volume of the tailings that deformed more than 100 cm is relatively small (configurations 12-24 and 12-36 for example) and it is generally limited to the tailings below the downstream slope to a maximum depth of about 10 m. For the unreinforced tailings impoundment (Figure 5-3), most of the impoundment downstream slope shows a displacement that exceeds 100 cm.

These results for reinforced tailings are in general agreement with those shown in Figure 5-8(a), where the AR_x (total and WRI) values in these cases vary between 2 and 5 %, indicating

relatively minor displacements of the tailings and waste rock inclusions along the downstream slope of the impoundment. For the lower frequency modified Northridge ground motion (E_4-north), the volume of the tailings that deformed more than 100 cm is always larger than for the E_4-sag ground motion, for all cases shown in Figure 5-10. For instance, for 8-m-wide inclusions spaced 24 to 56 m center-to center (Figure 5-10a), the critically displaced volume extend to more than 80 m upstream of the crest and to a depth of about 35 m below the surface of the downstream slope due to E_4-north ground motion. The simulations results indicate that for this loading, the 8-m-wide inclusions did not significantly improve the performance of the impoundment, regardless of the spacing. Fairly similar observations are seen for 12-m-wide inclusions with 24 m to 96 m spacing, as shown in Figure 5-10(b).

For the E_4-north loading and 16-m-wide inclusions (see Figure 5-10c), the arrangement of 16-32 (width-spacing) limited deformation within the impoundment to less than 100 cm (everywhere), but this may not be a realistic arrangement (at least for inner part of the impoundment). For configuration 16-48, a significant volume of tailings displaced by more than 100 m occurred between locations of 150 to 300 m to a depth of 40 m below the crest (Figure 5-10c). For this width (16 m) and spacings of up to 96 m, critically displaced zones of similar sizes and depths are observed. These results indicate that the ability of 16-m-wide inclusions to limit deformation of the impoundment under this loading (E_4-north) is largely controlled by the spacing; spacings exceeding 32 m lead to significant displacements for such an upstream constructed dyke (Figure 5-10c). Referring to Table 5.5, the AR_x total values with 32-m-spacing is 2.22 %, while the AR_x total values for the 48 to 96-m-spacing varies from 5.68 % to 19.05%, respectively.

There is no zone of critically displaced tailings (> 100 cm) for the 20-40 configuration (Figure 5-10d) due to E_4-north ground motion. For arrangement 20-60, local displacements greater than 100 cm occur between locations of 155 m and 270 m to a depth of about 20 m due to E_4-north ground motion. For arrangement of 20-80, displacements of more than 100 cm occurred below the downstream slope to a depth of about 55 m below the crest. Figure 5-10d further indicates that configuration 20-100 resulted in deformations in excess of 100 cm below the downstream slope and to 60 m upstream of the crest to a depth of about 40 m due to E_4-north ground motion.

For arrangements 25-50, the tailings impoundment subjected to E_4-north ground motions does not deform more than 100 cm (Figure 5-10e). For other configurations, such as 25-75, the

displacements in the lower portions of the impoundment appear to have been limited by the inclusions, resulting in localized areas of critical displacements. This behavior is in accordance with the differences between the AR_x total (7.07%) and AR_x WRI (2.42%) values given in Table 5.5. For configurations 25-100 and 25-125, the simulations resulted in bad geometry errors that occurred within the tailings after 19.5 and 23 seconds, respectively; calculations were automatically stopped by the program. Therefore, it was not possible evaluate their specific condition at the end of the seismic loading, although large displacements can be expected in these cases.

The results of these simulations indicate that the low frequency loadings resulted in much greater volumes of tailings being critically displaced (> 100 cm) for each configuration of WRI than for the high frequency loading. This suggests that, for low frequency events, the construction method used to build the dykes should probably be revised (considering a downstream or center-line method for instance).

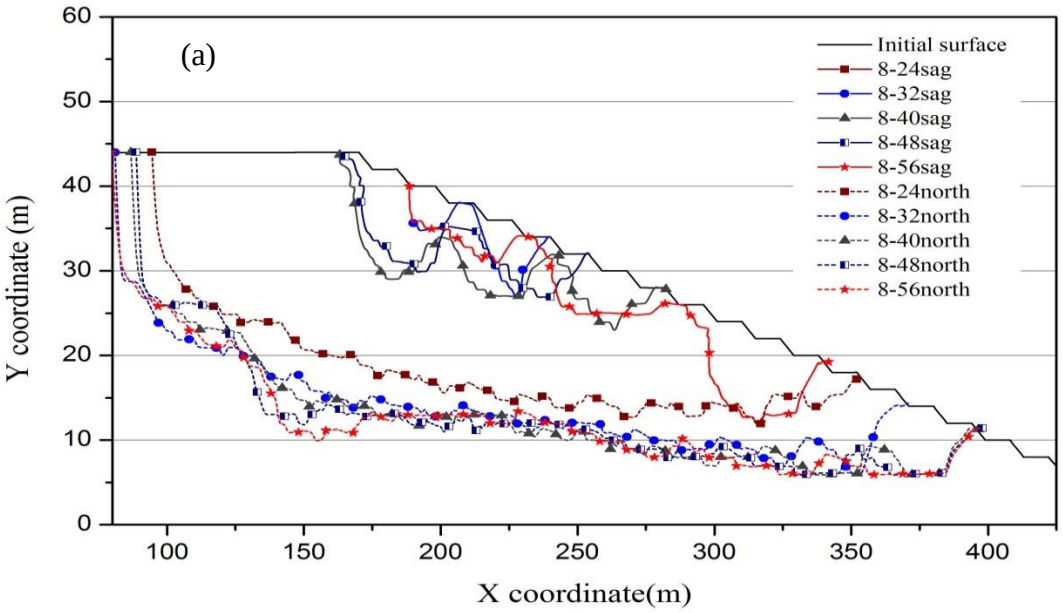

Figure 5-10: Delineation of the zone of the impoundment that is displaced more than 100 cm at the end of seismic loading, for the E4-sag and E4-north ground motions and various WRI configurations, (a) WRI width of 8 m; (b) WRI width of 12 m; (c) WRI width of 16 m; (d) WRI width of 20; (e) WRI width of 25 m

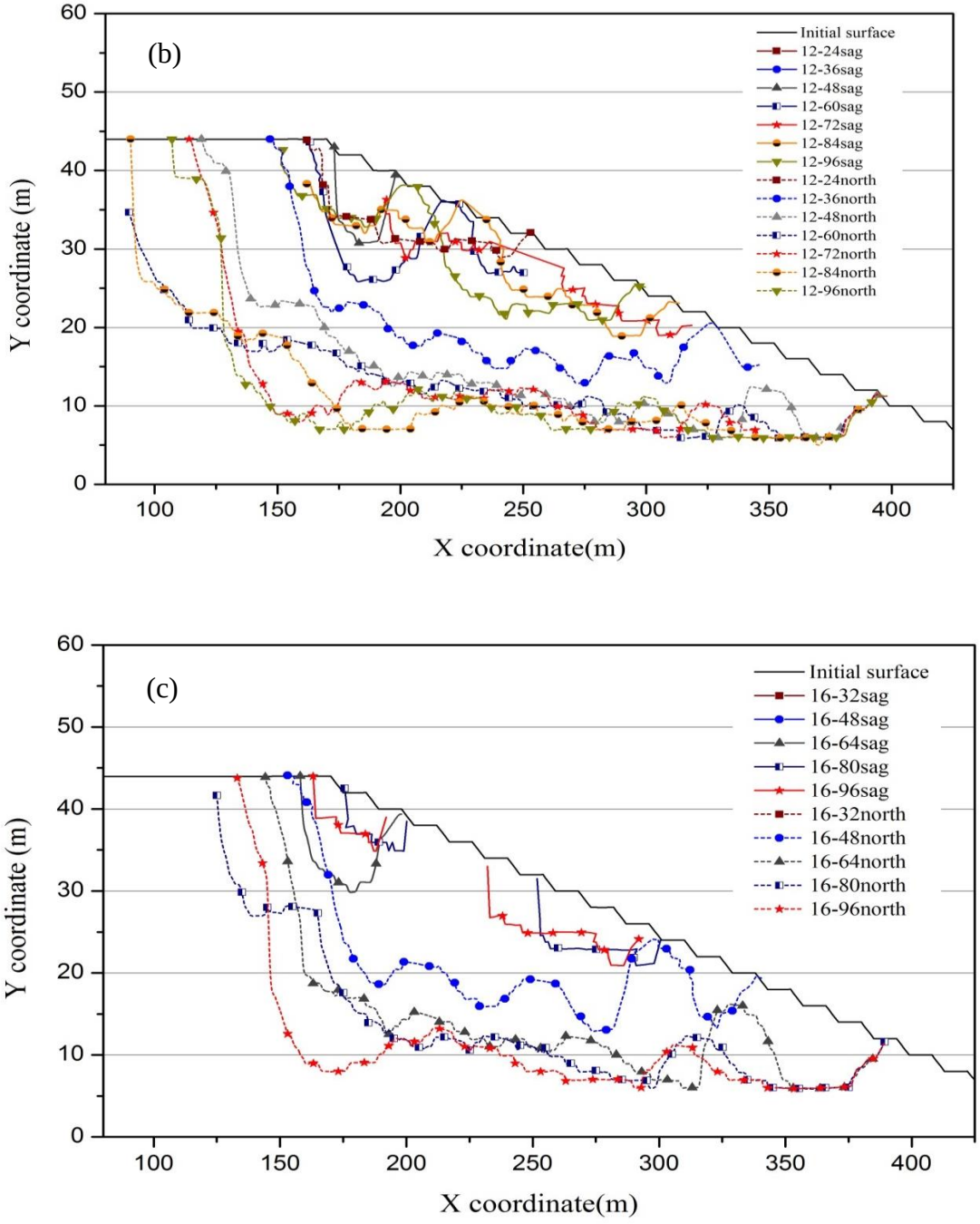

Figure 5-10: Delineation of the zone of the impoundment that is displaced more than 100 cm at the end of seismic loading, for the E4-sag and E4-north ground motions and various WRI configurations, (a) WRI width of 8 m; (b) WRI width of 12 m; (c) WRI width of 16 m; (d) WRI width of 20; (e) WRI width of 25 m (continued)

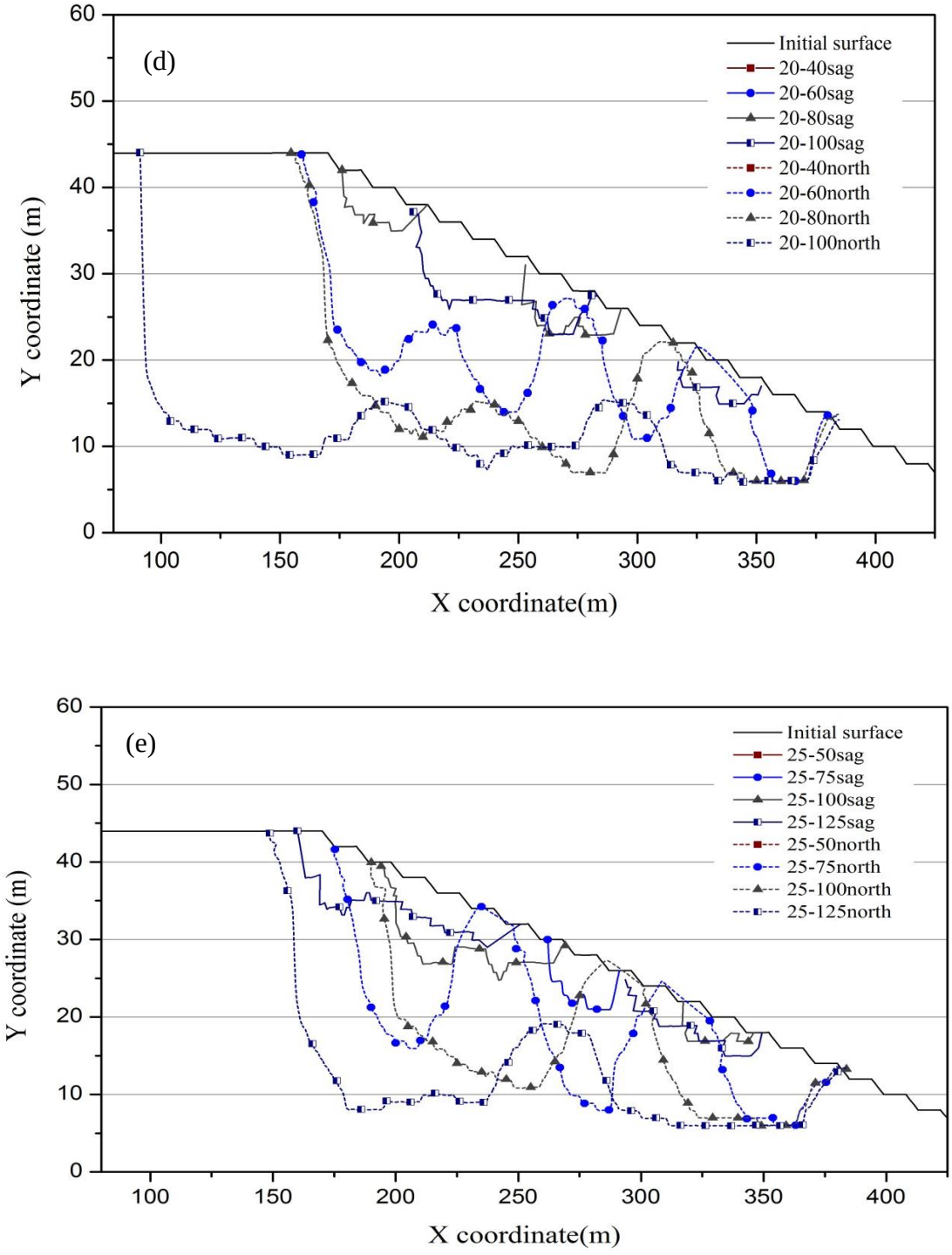

Figure 5-10: Delineation of the zone of the impoundment that is displaced more than 100 cm at the end of seismic loading, for the E_4-sag and E_4-north ground motions and various WRI configurations, (a) WRI width of 8 m; (b) WRI width of 12 m; (c) WRI width of 16 m; (d) WRI width of 20; (e) WRI width of 25 m (continued)

5.6.3 Effect of inclusions configuration on the performance of the tailings impoundment

As indicated above, the performance of the tailings impoundment was evaluated for different earthquakes and configurations. The results are presented here in terms of the average normalized horizontal displacements of the external dyke slope (total and WRI) for different values of the total widths of inclusions (i.e. width of individual inclusions by the number of inclusions, for each configuration). Graphs are presented for each of the modified ground motions records in Figure 5-11a to d. In these figures, the horizontal axes represent the total width of the WRI, with the numbers in the parenthesizes giving the width and center-to-center spacing, respectively. For example, 48 (12-96) means that the total width of inclusions is 48 m, with four 12-m-wide inclusions spaced 96 m center-to-center). The vertical axes represent the AR_x values of the downstream slope of the impoundment (total and WRI). Figs. 11 (a), (b), (c), and (d) show the graphs for E_4-sag, E_5-sag, E_4-north, and E_5-north earthquake records, respectively.

Figure 5-11(a) (E_4-sag) indicates that although the AR_x total values are approximately the same for configurations of 8-48, 12-60, 12-72, and 20-100, having a total WRI width between 56 and 60 m, the AR_x WRI value for configuration 20-100 is significantly less than that for the other ones. This means that this configuration will result in less displacement at the top of the inclusions under this seismic loading.

On Figure 5-11(b) (E_5-sag), it is seen that the 12-60, 12-72 and 20-100 configurations have the same total width of 60 m. Among these, the AR_x total and WRI of configuration 12-60 are between 5 and 10%, while the AR_x total is between 15 and 20% and the AR_x WRI is between 10 and 15% for configuration of 12-72. For configuration of 20-100, the AR_x total and WRI are 10 and 3, respectively. Based on these results, it can be inferred that the configuration of 20-100 would perform better than that the other configurations. Also, the configuration 12-60 shows the lowest AR_x total. These and other results shown in Figure 5-11 (a) and 11 (b) tend to indicate that configurations with larger WRI widths have a better performance compared with the configurations with smaller widths, for the same total width of the inclusions.

Figure 5-11(c) (E_4-north) shows that for WRI with total widths of 48 m, 60 m, 64 m, 72 to 80 m, and 84 to 96 m, the smallest AR_x total are obtained for configuration of 12-96, 20-100, 16-80, 20-80, and 16-48 respectively. This suggests that for a given value of the total WRI width, it is

usually better to use configurations if larger inclusion width. For the cases illustrated in Figure 5-11 (c), the performance of the configurations with W=8 m is not acceptable, as these lead to high values of AR_x.

Figure 5-11 (d) (E_5-north) shows that among the configurations 8-48, 12-60, 12-72, and 20-100 (total WRI width of 56 to 60 m), the AR_x total and WRI for the configuration 20-100 are the smallest. For configurations with a total WRI width of 64 m (i.e. 8-40, 16-80 and 16-96), configuration of 16-80 gives the lowest values of AR_x total and WRI. For configurations with a total WRI width of 72 m to 75 m (i.e. 8-32, 25-100), configuration of 25-100 leads to the lowest values of AR_x total and WRI.

These simulations results confirm that the presence of waste rock inclusions in a tailings impoundment can considerably decrease the displacements at the surface of the downstream slope and the deformation of the tailings within the slope. The seismic performance of the impoundment is largely determined by the width and spacing of the inclusions. As expected, wider inclusions placed closer to each other result in less displacement (of the slope) and deformation (of the tailings). Results such as those shown in Figure 5-11, Tables 5.4 and 5.5 can be used to identify optimum configurations of the waste rock inclusions for a given tailings impoundment with respect to the ground motions considered.

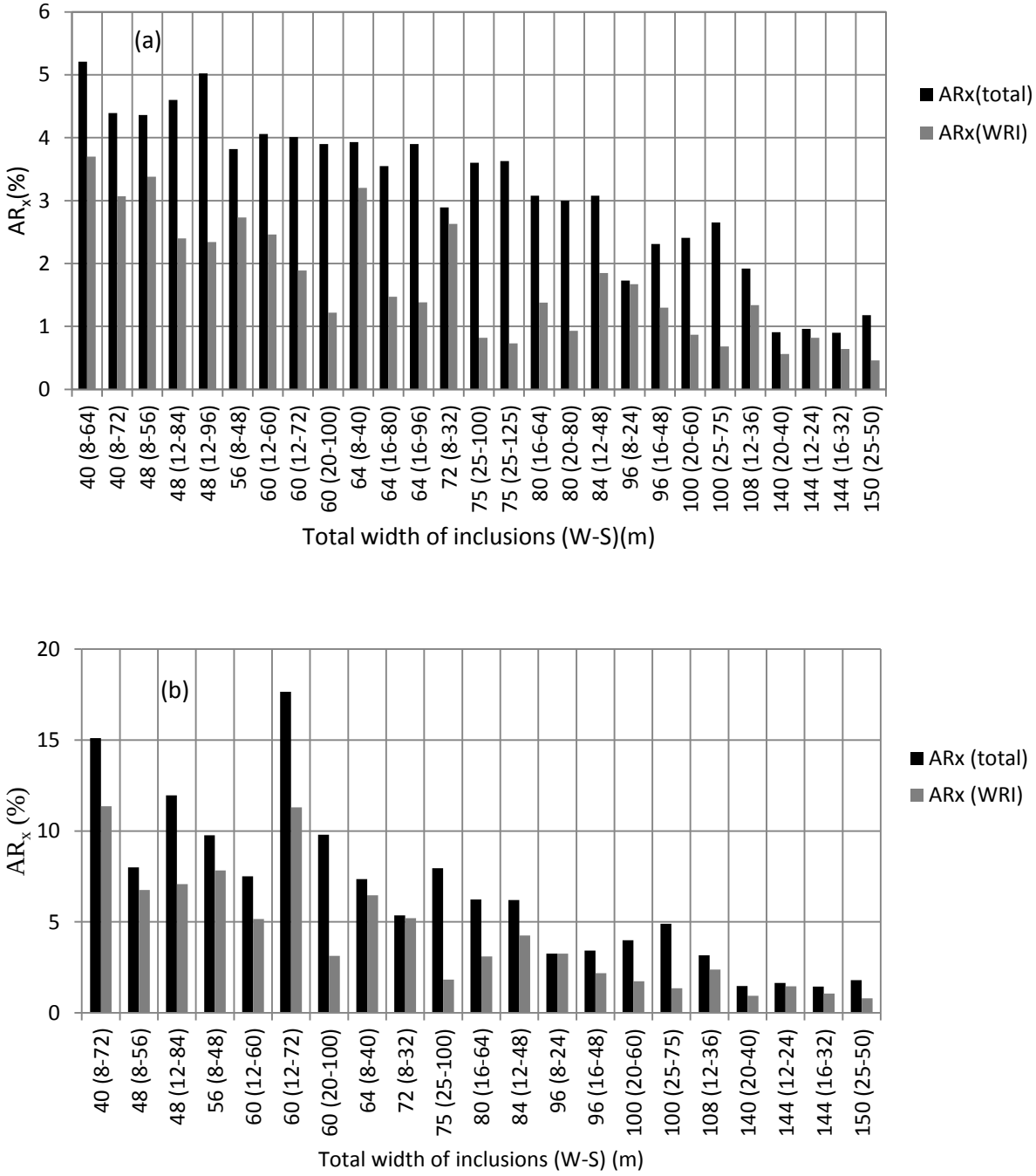

Figure 5-11: Average of normalized horizontal displacements of the downstream slope of the tailings impoundment (ARx total) and of the WRI (ARx-WRI) as function total width of the inclusion, for different configurations (width, spacing) and modified ground motions (a) E4-sag, (b) E5-sag (c), E4-north, and (d) E5-north

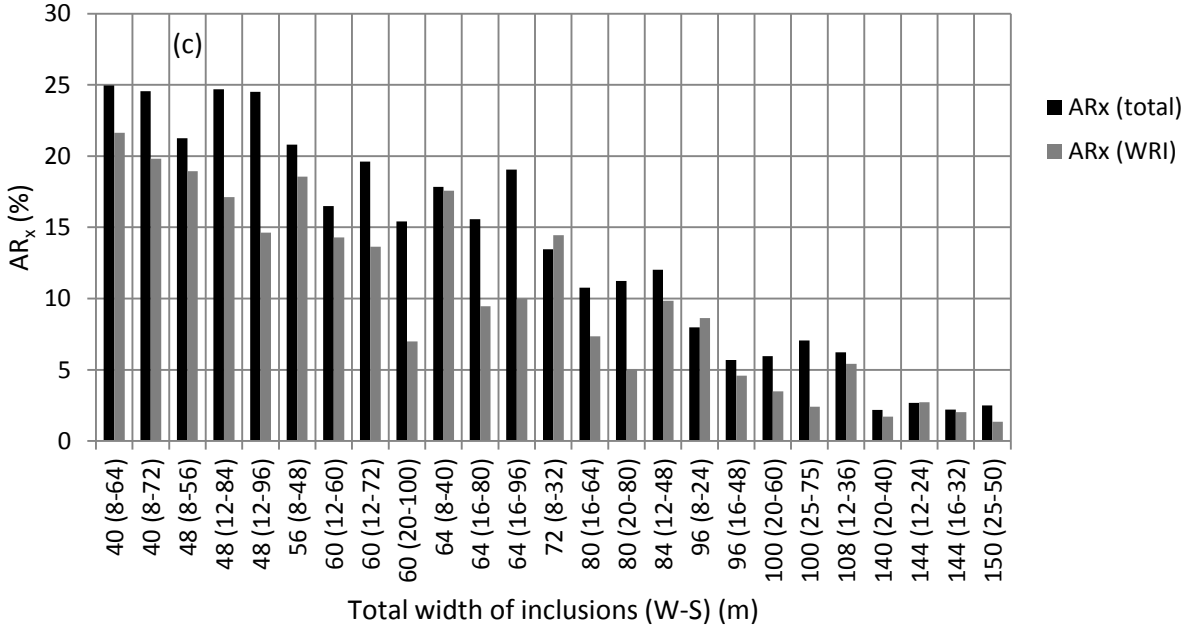

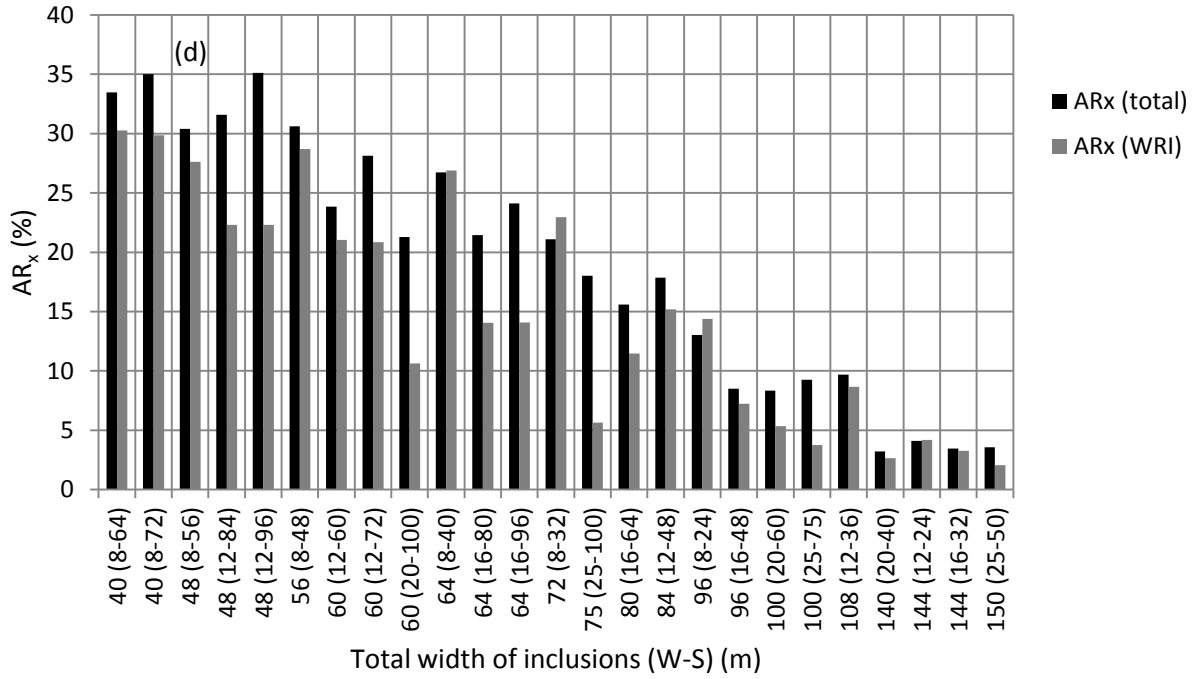

Figure 5-11: Average of normalized horizontal displacements of the downstream slope of the tailings impoundment (AR_x total) and of the WRI (AR_x-WRI) as function total width of the inclusion, for different configurations (width, spacing) and modified ground motions (a) E_4-sag, (b) E_5-sag (c), E_4-north, and (d) E_5-north (continued)

5.7 Complementary remarks

The results presented in this paper were obtained by simulating the response of consolidated tailings in the impoundment. As seismic events can also occur during the operation of an impoundment, it was also deemed necessary to analyze the seismic response of unconsolidated tailings, which is the situation often encountered during their disposal. The results of analyses with unconsolidated tailings (i.e. 162 additional simulations) are presented in Appendix D. The results of these analyses indicate that the simulated impoundment would become unstable for seismic events having a much lower energy than those considered here. The results also show that WRI can enhance the seismic response of the tailings impoundment significantly. A total of 162 runs were completed for unconsolidated tailings and the results are presented in Appendix D of Ferdosi (2014).

Analyses presented above were performed using the modified Saguenay 1988 and Northridge 1994 ground motions. Analyses can also be performed based using other earthquake ground motions, such as those presented in Atkinson (2009) to match the 2005 National Building Code of Canada uniform hazard spectrum.

Various factors have not been considered in this investigation. Among these, the effect of groundwater level on the seismic response of the tailings impoundment is important, and it should be addressed based on the relevant conditions at the site, this aspect may be particularly critical when the ground water level is such that the tailings become unsaturated. The issue is part of ongoing research.

The results of distribution of the excess pore water ratio, r_u, of the tailings at the end of the shaking showed that WRI do not prevent or retard liquefaction in the impoundment. Inclusions limit the deformation and flow of tailings. More details are available in Appendix D.

5.8 Conclusion

The seismic response of a tailings impoundment was simulated numerically. Calculations were made without and with waste rock inclusions, for various configurations, using high and low frequency earthquake ground motion records of known energy content. The impoundment without inclusions was deemed to become unstable under the seismic loads considered here, and which were selected to induce significant deformation and excess pore water pressures.

The seismic response of the impoundment is evaluated using the normalized horizontal displacement of the downstream slope and inclusions, together with the volume of the impoundment displaced beyond a threshold value of 100 cm at the end of shaking.

The evaluation of the results of the 108 simulations presented here indicates that the presence of waste rock inclusions can significantly improve the seismic performance of an impoundment, by reducing the displacement of the downstream slope and the volume of critically displaced tailings. It is also shown that the low frequency ground motions (typical of the west coast of North America) tend to induce significantly larger displacements than the high frequency ground motions (typical of the east coast). Displacements also increase markedly with an increase in the energy content (Arias intensity) for both low and high frequency ground motions. Generally, the displacement of the downstream slope and critically displaced volume of tailings tend to decrease with increasing width of the inclusions, and increase with increasing spacing of the inclusions.

Results are presented graphically to illustrate how to select an optimal configuration of inclusions (width and spacing) with respect to the seismic performance of the tailings impoundment for specific seismic loadings.

5.9 Acknowledgements

This research work is being supported by the Natural Sciences and Engineering Research Council of Canada (NSERC), the partners of the Industrial NSERC Polytechnique-UQAT Chair (2006-2012) and those of the Research Institute on Mines and the Environment (RIME UQAT-Polytechnique; www.rime-irme.ca).

5.10 References

Adalier K, Elgamal A, Meneses J, and Baez J I (2003) Stone columns as liquefaction countermeasure in non-plastic silty soils. Soil Dynamics and Earthquake Engineering, 23(7): 571-584.

Atkinson G M (2009) Earthquake time histories compatible with the 2005 National building code of Canada uniform hazard spectrum. Canadian Journal of Civil Engineering, 36: 991-1000.

Aubertin M, Mbonimpa M, Jolette D, Bussiere B, Chapuis RP, James M, Riffon O (2002) Stabilité géotechnique des ouvrages de retenue pour les résidus miniers: problèmes persistants et méthodes de contrôle. Défis & Perspectives : Symposium sur l'environnement et les mines, Rouyn-Noranda, Développement Économique Canada/Ministère des Ressources Naturelles du Québec/CIM. Comptes-Rendus sur CD-ROM.

Barksdale R D, Bachus RC (1983) Design and construction of stone columns volume I. Report FHWA-RD-83-026, National Technical Information Service, Springfield, VA.

Barksdale R D (1987) Application of the state of the art of stone columns- liquefaction, local bearing failure, and example calculations. Technical Report REMR-GT-7, The Georgia Institute of Technology, 90p.

Beaty M, Byrne P M (1998) An effective stress model for predicting liquefaction behavior in sand. Proceedings of Geotechnical Earthquake Engineering and soil dynamic III, Seattle, Washinton, USA. ASCE Special Publication. **75**(1):766-777.

Beaty M H, Byrne P M (2011) UBCSAND constitutive model Version 904aR. Document report: UBCSAND Constitutive Model on Itasca UDM Web site: http://www.itasca-udm.com/pages/continuum.html.

Boulanger R W, Kamai R, Ziotopoulou K (2011) Numerical modeling of liquefaction effects. In Proceeding of the Effects *of Surface Geology on Seismic Motion, 4th IASPEI / IAEE International Symposium*, University of California, Santa Barbara, CA., 23-26 August 2011.

Bray J D, Dashti S (2012) Liquefaction-Induced Building Movements. Invited Keynote Paper, Proceedings of the International Conference on Performance-Based Design Earthquake Geotechnical Engineering, Taormina, Italy.

Byrne PM, Roy D, Campanella R G, Hughes J (1995) Predicting Liquefaction Response of Granular Soils from Pressuremeter Tests. ASCE National Convention, San Diego, 23-27 October 1995, ASCE, Geotechnical Special Publication 56, pp. 122-135.

Byrne P M, Park S S, Beaty M, Sharp M, Gonzalez L, Abdoun T (2004) Numerical modeling of liquefaction and comparison with centrifuge tests. Canadian Geotechnical Journal, 41, 193-211.

California Geological Survey (2008) Guidelines for evaluating and mitigating seismic hazards in California. California Geological Survey Special Publication 117A. 98 pp.

Dashti S, Bray J D (2012) Numerical Insights into Liquefaction-Induced Building Settlement. Proceeding of the 2012 Geo-Congress, Geo-Institute, Oakland, CA. 25-29 March 2012, ASCE, pp.1660-1669.

Ferdosi B, James M, Aubertin M (2013) Numerical modeling of the post-liquefaction consolidation of tailings. Proc. GeoMontreal 2013, Montreal, Qc, October 2013. Canadian Geotechnical Society, 7 pages.

Ferdosi B, James M, Aubertin M (2014a) Numerical modeling of seismic table testing of tailings with and without inclusion. GeoRegina 2014, Regina, Saskatchewan, October 2014. Canadian Geotechnical Society, 6 pages.

Ferdosi B, James M, Aubertin M (2014b) Numerical simulations of the seismic and post-seismic behavior of tailings. Submitted to Canadian Geotechnical Journal.

Ferdosi B, James M, Aubertin M (2014c) Effect of waste rock inclusions on the seismic stability of an upstream raised tailings impoundment: a numerical investigation. Submitted to Canadian Geotechnical Journal.

Fung G, Parra E P, Sully J P, Kerr J R, Akins K P (2011) Seismic modeling of a reinforced slope. 2011 Pan-Am Canadian Geotechnical Society Conference, Toronto, On., October 2011. Canadian Geotechnical Society, 7 pages.

Rapport Factuel (2011) Investigation géotechnique pour le parc à résidus miniers. Projet Canadian Malartic, Malartic, Québec, Golder Associés, 1001 de Maisonneuve Ouest, Montréal, Sept. 2011.

ICOLD (2001) Tailings dams – risk of dangerous occurrences – lessons learnt from past experiences. International Commission on Large Dams and United Nations Environmental Program *(ICOLD)*, Paris. Bulltin No. 121.

Itasca Consulting Group, Inc. (Itasca) (2008) FLAC – Fast Lagrangian Analysis of Continua. Version 6.00. [computer software and user manual]. Minneapolis MN: Itasca Consulting Group, Inc.

James M (2009) The use of waste rock inclusions to control the effect of liquefaction in tailings impoundments. Ph.D. Thesis, Department of Civil, Geological, and Mining Engineering, Ecole Polytechnique de Montreal, Montreal, QC.

James M, Aubertin M, Wijewickreme D, Ward Wilson G (2011) A Laboratory Investigation of the Dynamic Properties of Tailings. Canadian Geotechnical Journal, **48**(11)*:* 1587–1600.

Jibson R W (2011) Methods for assessing the stability of slopes during earthquakes-A retrospective. Engineering Geology, 122 (2011): 43–50.

L.Bolduc F, Aubertin M (2014) A numerical investigation of the influence of waste rock inclusions on tailings consolidation. Canadian Geotechnical Journal, 51(9): 1021-1032.

Martin J R II, Olgun C G, Mitchell J K, Durgunoglu H T (2004) High-modulus Columns for Liquefaction Mitigation. Journal of Geotechnical and Geoenvironmental Engineering, 130(6): 561-571.

Naesgaard E, Yang D, Byrne P, Gohl B (2004) Numerical analysis for the seismic safety retrofit design of the immeresed-tube George Massey tunnel. 13th World Conference on Earthquake Engineering, Vancouver, B.C., 1-6 August 2004. Canadian Association for Earthquake Engineering.

Naesgaard E (2011) A Hybrid Effective Stress-Total Stress Procedure for Analyzing Embankments Subjected to Potential Liquefaction and Flow. PhD. Thesis, Civil Engineering Department, The University of British Coulombia, Vancouver, B. C.

Narvaez B, Aubertin M, Saleh-Mbemba F (2014) Application of a predictive model to estimate the tensile strength of unsaturated tailings. GeoRegina 2014, Regina, Saskatchewan, October 2014. Canadian Geotechnical Society, 7 pages.

Pacific Earthquake Engineering Research Center (PEER) (2014) P0923 : Earthquake and station details. Consulted on February, 2011. http://peer.berkeley.edu/svbin/Detail?id=P0923.

Pépin N, Aubertin M, James M, Leclerc M (2012a) Seismic simulator testing to investigate the cyclic behavior of tailings in an instrumented rigid box. Geotechnical Testing Journal, **35**(3): 469-479.

Pépin N, Aubertin M, James M (2012b) Seismic Table Investigation of the Effect of Inclusions on the Cyclic Behavior of Tailings. Canadian Geotechnical Journal, **49**(4): 416-426.

Puebla H (1999) A constitutive model for sand and the analysis of the CanLex Embankments. Ph.D. thesis, Civil Engineering Department, University of British Columbia, Vancouver, B. C.

Puebla H, Byrne P M, Phillips R (1997) Analysis of CANLEX liquefaction embankments: prototype and centrifuge models. Canadian Geotechnical Journal, 34(5): 641-657.

Rollins K M, Evans M D, Diehl N B, Daily W D III (1998) Shear modulus and damping relationships for gravels. Journal of Geotechnical and Geoenvironmental Engineering. 124(5): 396-405.

Saleh-Mbemba F (2015) Ongoing Ph.D thesis, Department of Civil, Geological and Mining Engineering, Ecole Polytechnique de Montreal, Montreal, QC.

Wise Uranium Project (WISE) (2014) Chronology of major tailings dam failures. Consulted on May 15,2014. www.antenna.nl/wise/uranium/mdaf.html.

Ziotopoulou K, Boulanger R W, Kramer S L (2012) Site response analysis at liquefiable sites. ASCE Geo-Congress 2012: State of the Art and Practice in Geotechnical Engineering, R D Hryciw, A Athanasopoulos-Zekkos, N Yesiller eds, Geotechnical Special Publication No.225, ASCE Geo-Institute, 1799-1808.

CHAPTER 6: SUMMARY AND GENERAL DISCUSSION

The literature review presented in this Thesis indicated that there remained uncertainties with respect to the seismic analysis of tailings impoundments and effect of waste rock inclusions on the seismic response of tailings impoundments. Some of these uncertainties were addressed in this Thesis, and are briefly discussed below:

- Although the UBCSAND model can represent well the shear strain, pore water pressure generation, initiation of liquefaction, liquefied and post-liquefied strengths of tailings submitted to cyclic simple shear testing (James, 2009). However, the capability of this model (and of other available models) to simulate the dynamic behavior of tailings for other loading conditions, such as for seismic table testing, had not yet been investigated, so some work on this aspect was conducted here.
- The results of previous simulations using the UBCSAND model, conducted by Naesgaard, (2011), showed that it cannot correctly predict post-seismic settlement due to excess pore water pressure dissipation. This aspect is important because it gives an indication of the model ability to simulate the post-seismic properties of the tailings, specifically the "elastic" moduli, which are required for deformation and stability analyses.
- The seismic responses of a conceptual reinforced tailings impoundment and an impoundment retained by an earthfill dyke (based loosely on a real case) were investigated numerically by James (2009). However, the seismic response of an actual impoundment with an upstream-raised tailings dyke and WRI had not yet been investigated.
- The effect of seismic loads on the critically displaced volume of tailings impoundments (reinforced or not) has not yet been investigated either.
- There is no guideline for the analysis and optimum design of WRI as reinforcement against seismic loads. Extensive numerical simulations were conducted here to develop preliminary guidelines for optimizing the configuration of WRI.

To cover these gaps and reach the above mentioned goals, the UBCSAND model was first calibrated and validated (in Chapter 3) using the results of cyclic simple shear and seismic table tests. The study was performed in the following steps:

- The version 904aR of the UBCSAND model was used to validate the ability of the model to capture the dynamic behavior of tailings submitted to cyclic simple shear testing. This version of the UBCSAND model can include the effect of initial shear stress bias, while it considers reloading as a plastic behavior. Therefore it is different from the version 904a that has been widely used in previous research works (mostly on sand). This newer version was used in this Thesis to evaluate the seismic behavior of tailings. Tests results from James (2009) were used for a partial validation.
- The capacity of the UBCSAND model to simulate the dynamic behavior of tailings without and with a rigid/draining inclusion was verified using the numerical simulation of seismic table tests performed by Pépin et al. (2012a, 2012b). This verification serves to confirm the applicability of the system of analysis (the UBCSAND model and FLAC 2D) to the seismic analysis of tailings impoundments with waste rock inclusions. The UBCSAND model implemented in FLAC simulates plane strain condition; accordingly, tests no 3 and 7 of Pépin et al. (2012a, 2012b) were selected as these are compatible with such 2D analyses.
- When the stress path is oriented toward to open side of the yield surface used in the UBCSAND model (without a cap), the model considers that the response is elastic, therefore it cannot capture volumetric plastic strains, even for large mean stresses. To improve the UBCSAND model, the cap component proposed by Vermeer (1980) and adapted by Puebla (1999) was added to version 904aR of the UBCSAND model to better capture post-shaking behavior, specifically consolidation induced by excess pore water pressure dissipation.
- Hypothetical isotropic compression and oedometer tests were simulated using the UBCSAND model without and with a cap to compare the results and evaluate the effect of this cap on the volumetric plastic strains.
- The method of Sento et al. (2004) was used to represent the settlement of tailings based on the results from compression tests performed on loose (slurry) tailings. The results showed that this approach can represent very well the consolidation behavior of tailings.
- The capability of the UBCSAND model to capture post-seismic settlement of tailings was further validated by simulating the post-seismic settlement from the seismic table tests performed by Pépin et al. (2012a, 2012b) on tailings. To do so, the method of Sento

et al. (2004) was added to the UBCSAND model in FLAC. The consolidation curve of tailings, described using the Sento et al. (2004) approach, serves to evaluate the value of Young's modulus for various effective stresses, which are then computed and updated in the UBCSAND model.

- Level ground condition was simulated to validate the ability of the UBCSAND model with a cap and with the Sento et al. (2004) formulation, to capture post-seismic consolidation. The results were successfully compared with the results of an empirical method proposed by Wijewickreme and Sanin (2010).

The above mentioned investigations provided the following results:

- The UBCSAND version of 904aR can represent well the shear strains, excess pore water pressures, and required number of cycles to initiate of liquefaction in Test No. 5 by James (2009).
- The UBCSAND model with a cap can predict fairly well post-seismic settlement of a level ground condition. However, in some cases, the simulation was stopped due to numerical instability, which can be attributed to a mathematical singularity at the intersection of the shear and cap yield surfaces that affects the calculation of the plastic strain.
- The results of simulations with FLAC and the UBCSAND model showed that this model can simulate fairly well the generation of excess pore water pressure in seismic table tests. Two seismic tests performed by Pépin et al. (2012a, 2012b) were simulated. One of the tests was conducted on consolidated tailings without inclusion and another one was performed on these same tailings with a sand wall inclusion.
- Adding the Sento et al. (2004) method to the UBCSAND model for post-seismic conditions leads to good predictions for the settlement of tailings due to the excess pore water pressure dissipation following seismic table testing. The simulated results of level ground condition of tailings using this approach also agree with those given by the empirical relationship proposed by Wijewickreme and Sanin (2010).

After obtaining encouraging results from numerical simulations of the seismic and post-seismic behavior of tailings using the UBCSAND model, a numerical investigation on the effect of waste rock inclusions on the seismic stability of an upstream raised tailings impoundment was

conducted (Chapter 4). A tailings impoundment located in New Brunswick, Canada, was used as a base for the numerical simulations. This impoundment was chosen because of the available laboratory and in situ testing data (SPT, CPT, and shear wave velocity). The effect of different configurations of WRI on the seismic response of the impoundment with unconsolidated or consolidated tailings was investigated. The results of the 56 analyses of unconsolidated tailings are presented in Chapter 4 and the results obtained from 53 analyses for consolidated tailings are presented in appendix C.

The UBCSAND model was used to simulate the tailings and the Mohr-Coulomb model was used to simulate the inclusions and other materials in the model constructed with FLAC. The shear modulus reduction and hysteretic damping curves for waste rock were obtained through numerical analysis of a single-element model of waste rock, by adjusting the model parameters iteratively to match the experimental curves provided by Rollins et al. (1998) for gravelly soils.

Two seismic ground motions were chosen for earthquake loading. The Saguenay 1988 and Northridge 1994 ground motions were selected to represent high (East coast) and low (West coast) frequency seismic events. These two ground motions were scaled so that they have the same energy content and peak ground acceleration. The simulations then show the effect of such frequency content on the seismic response of reinforced tailings impoundments.

Two parameters were introduced to help with the evaluation and comparison of the simulations results. The first one is the average value of the normalized horizontal displacements (AR_x) of the downstream slope; the value of AR_x was calculated to the entire impoundment and for the WRI alone. The second parameter is average horizontal velocity of the downstream slope (Xvel) of the impoundment.

The numerical results can be summarized as follows:

- The reinforced tailings impoundments with WRI were classified based on the average value of the relative horizontal displacements R_x (i.e. AR_x) for the downstream slope at the end of shaking, for various ground motion records. This classification can be used as preliminary guideline to select an optimum WRI configuration to resist seismic loads. More simulations should be performed to further develop this classification for a wider range of seismic loads based on existing requirements (such as the Canadian Dam

Association Guidelines, 2014). This classification is the first of its kind, and it can be used for different impoundments and configurations of the inclusions.

- Based on the post-shaking analyses, a graph was presented to illustrate the relationship between the average values of horizontal nodal velocity (Xvel) and of the average displacements (AR_x) of the downstream slope of the tailings impoundment. The results indicate that when the value of Xvel exceeds 20 cm/s at the end of the seismic analysis, the slope will continue to deform in the post-liquefaction stage, leading to failure in most of the cases. These unstable cases can be related to the WRI configurations for which their width is relatively small or the center-to-center spacing is relatively large. The results of these analyses showed that, in general, WRI having a small width and large center-to-center spacing are much less effective, and thus should not be used for the reinforcement of tailings impoundment.
- The results also showed that if the configurations are selected properly, they can improve significantly and efficiently the seismic response of tailings impoundments.
- Graphs of the AR_x values of the downstream slope of the dyke (total and WRI) as functions of the total width of WRI placed in tailings were also presented for the high and low frequency ground motions. These graphs can be used to identify optimum configurations of WRI for a given tailings impoundment submitted to pre-set seismic loadings.
- The effects of high and low frequency ground motions on the seismic response of the tailings impoundment were also evaluated. The results showed that in most cases, low frequency ground motions cause larger displacements of the tailings than high frequency ground motions. Therefore, seismic analysis of tailings impoundments should be performed for critical loads with different frequency contents, to assess their behavior and performance during seismic events.

After evaluating the effect of WRI on the seismic response of an upstream raised tailing impoundment in New Brunswick, another tailings impoundment located in western Quebec, Canada, was targeted for the next series of simulations (Chapter 5).

The main differences between the two tailings impoundments are related to their geometry and method of construction. The impoundment in New Brunswick was constructed in using the

upstream method with a relatively narrow dyke made of compacted tailings, at an average downstream slope inclination of 5.5:1 (H:V). The second impoundment analyzed is currently being constructed in the upstream direction using 2-m-high, 15-m-wide waste rock raises, with an average downstream slope of 7:1 (H:V). Although this is the first impoundment in which waste rock inclusions are being constructed, the simulated cases are not based specifically on the actual WRI configurations at the site (but rather on alternative options that could be considered).

A total of 270 simulated runs were conducted to investigate the effect of WRI on the seismic response of the tailings impoundment. The following issues were specifically investigated and discussed:

- The effect of ground motion intensity and frequency content on the seismic response of the tailings impoundment. As mentioned before, the Saguenay 1988 and Northridge 1994 ground motions were selected and scaled for hypothetical earthquakes with a magnitude M_w = 6.5, 7.0, and 7.5, and epicentral distance of 30 km; another earthquake with M_w = 7.0 and epicentral distance of 20 km was also used in some calculations. The scaling was performed so that the modified Saguenay and Northridge seismic acceleration time histories have the same energy content and peak ground acceleration.
- The effect of the WRI configuration on the critically displaced volume of tailings. As was the case in the previous chapter, the AR_x total and AR_x WRI were used to evaluate the seismic response of the reinforced tailings impoundment at the end of the shaking. In some cases, failure occurred at relatively low depth in the impoundment, which would limit the damage. The seismic response was also evaluated based on the volume of tailings that displaced horizontally by more than a critical value of 100 cm. This critically displaced volume of tailings is very helpful to evaluate the seismic response of impoundments, and it provides complementary information to the AR_x. A FISH function was written to connect the points inside of tailings impoundment that displace more than 100 cm, and to provide a contour of the corresponding area (volume). This indicator was used to assess the effect of different WRI configurations, and help identify the best solutions for the specific conditions being simulated. The effect of inclusions configuration on the overall response of the tailings impoundment. This effect was evaluated specifically with a series of graphs that show the relationship between AR_x

total, AR_x WRI, and the total width of the inclusions, considering different configurations. The combination of ARx total and AR_x WRI alone helps identify cases where the total displacements may be high even though the WRI remain stable. This happens in a few cases where both the width and center-to-center spacing of inclusions are large; this is the case for instance for configuration 25-125, which gives a high value of AR_x total but a relatively small value of ARx WRI, indicating that the inclusions are stable and would prevent the flow of tailings.

The main results of these analyses are presented in Chapter 5, with detailed results provided in Appendix D. These results can be summarized as follows:

- The average normalized horizontal displacements (AR_x) of the downstream slope of the impoundment (total and WRI) were computed for various WRI configurations, for modified high and low frequency ground motion records. The results showed that certain configurations resulted in significant improvement of the seismic response of the impoundment. The values of AR_x total, AR_x WRI alone, and maximum horizontal displacement of the tailings for different seismic loads were presented in two separate tables for the high and low frequency ground motions.
- The results also showed that the low frequency ground motions critically displaced a greater volume of tailings in comparison to the high frequency ground motions. The critically displaced volume of tailings due to seismic loading can be controlled very well by selecting appropriate WRI configurations. The results also showed that the critically displaced volume of tailings is a good parameter (indicator) to investigate the seismic response of tailings impoundment.
- Additional graphs were presented to illustrate the relationships between the AR_x of the downstream slope (total and WRI) and the total width of the inclusions, for different configurations and for the high and low frequency ground motions. Such type of graphs can be used as a preliminary guideline for the optimum design of WRI.

Although important results were obtained from this research, there are some limitations that should be considered when analyzing and using the simulations outputs; the main ones can be identified as follows:

- The UBCSAND model with a cap showed some errors during analysis, which prevented completion of the post-seismic simulations. These errors are attributed to the numerical instabilities related to the singularity that exists at intersection of the cap and the shear yield surfaces. Other formulations for such a cap may help prevent these errors (e.g. Aubertin and Li, 2004), but more work is required on this aspect.
- Although the simulations results of seismic table tests are encouraging, some important limitations should be recalled. For instance, the rate of pore water pressure generation near the bottom of the seismic table test model is much higher than the actual rate measured by Pépin et al. (2012a, 2012b). These differences may be due, at least in part, to the inability of the plane strain model (FLAC and UBCSAND) to simulate a three dimensional specimen in a rigid box. Also, the value of $(N_1)_{60}$ = 30 blows/30 cm used in the simulations seems somewhat high for tailings with a relative density of 80%. However, simulations with different values of $(N_1)_{60}$ (e.g. 15, 20, and 25 blows/foot) did not provide a better match with the measured excess pore water pressures. Hence, this aspect may require additional work.
- The effect of the ground water level on seismic response of actual tailings should be investigated. When the ground water level is such that the part of tailings become unsaturated, their shear strength may be changed (increased) due to the suction generated in the pores (Narvaez et al. 2014). This may help improve the stability of the tailings and tailings impoundment, but this aspect has not been looked at in this project. Additional work on such issue could thus be useful.
- The UBCSAND model has been developed for the plane strain (2D) condition. Therefore, it may not be capable of capturing all of the important behaviors of a three dimensional structure such as a tailings impoundment. Three dimensional testing and modelling of tailings and tailings impoundment with waste rock inclusions (in a centrifuge, for instance) could be very insightful.
- Naesgaard (2011) reported (based on Dismuke, 2003 and Malvick, 2005) that the post-liquefaction reconsolidation volumetric strains of sand for a zero static stress bias (level ground condition) may be different from cases with a static bias (sloping ground). Therefore, cyclic simple shear and triaxial compression tests with initial anisotropic consolidation should be performed on tailings. Post-liquefaction reconsolidation curves

of tailings should also be evaluated more systematically. These curves can be used for updating the Young's modulus of tailings in the UBCSAND model, to improve the analysis of post-seismic response of flat and sloping grounds.

- Seismic and post-seismic analyses should be performed for cases where there are less pervious interlayers in the tailings (which often show such layering). Malvick et al. (2008) showed that these layers can have an effect on pore water pressure dissipation in sand. As a thin water film may then form locally, and localization of shear deformation can occur, causing instability. This issue has not yet been investigated for tailings impoundment, but it may play a role in some cases.

CONCLUSION AND RECOMMENDATIONS

Conclusion

The review of the state of knowledge and current practices with respect mine wastes behavior and disposal, and the seismic evaluation of tailings impoundments has shown that major concerns exist in this field. For instance, the rate of failure of tailings impoundments is unacceptably high, and a significant percentage of failures are by seismic activity. To help improve the situation, a method for the design and construction of tailings impoundments using waste rock was proposed by Aubertin et al., (2002). Preliminary numerical analysis conducted by James (2009) has indicated that this method can significantly improve the seismic stability of such impoundments.

After summarizing the content and connections between the different chapters of this Thesis, recently performed numerical simulations of the seismic and post-seismic behavior of tailings are presented. These provide validation and calibration of the numerical modeling methodology. The following results were obtained:

- The UBCSAND model version 904aR can predict well the results of cyclic simple shear tests on tailings (as performed by James, 2009).
- The UBCSAND model can predict well the excess pore water pressure generation in seismic table testing of tailings without and with a sand wall inclusion. However, the rate of excess pore water pressures generation at the bottom of the tailings in the simulation was greater than that in the laboratory.
- The method of Sento et al. (2004) was combined with the UBCSAND model to update the elastic moduli and simulate the post-shaking behavior (consolidation due to pore water pressure dissipation) of tailings. The comparison of the results of the simulation with the measured settlement in the seismic table test (Pépin, et al. 2012a, 2012b) showed an encouraging agreement.
- The dynamic behavior, specifically post-shaking consolidation, of tailings under level ground conditions was simulated using the UBCSAND model with an updated elastic moduli scheme and compared with the results of the empirical formula proposed by Wijewickreme and Sanin (2010). The comparison leads to encouraging results.

- The UBCSAND with a cap can capture reasonably well the volumetric strains during post-shaking consolidation but this version of the model sometimes generates numerical instability, encounters a mathematical singularity.

The obtained results provided for validation and calibration of the numerical modelling methodology, particularly for version 904aR the UBCSAND model with the elastic moduli updating scheme to simulate the seismic behavior of tailings.

The effect of waste rock inclusions configuration on the seismic response of a tailings impoundment was then evaluated, in terms of their width and center-to-center spacing, based on the case of an actual impoundment located in New Brunswick, Canada. The results indicate that:

- The WRI can significantly improve the seismic response and stability of the tailings impoundment, which was unstable without inclusion for the cases considered here.
- The configuration of the WRI has an important effect on the seismic response of the impoundment.
- The responses of the different configurations can be classified based on the average normalized horizontal displacements, AR_x, of the downstream slope of impoundment. Based on these results, an optimum WRI configuration to stabilize the upstream raised tailings impoundment against the assumed ground motions could be obtained.
- Analyses with high and low frequency ground motions show that, in most cases, low frequency earthquakes cause larger displacements of the tailings than high frequency ground motions. However, in some cases, depending on WRI configuration, the displacements of the downstream slope of the tailings impoundment can be larger for the higher frequency ground motion. The predominant frequency content of the ground motion is thus an important parameter that must be taken into account in the seismic analysis of tailings impoundments.
- Post-shaking analyses for different WRI configurations result in a relationship between the post-shaking stability of impoundments with the AR_x and horizontal nodal velocity, Xvel, at the end of shaking. A horizontal nodal velocity, Xvel, greater than about 20 cm/s at the end of shaking typically leads to an unstable condition at the end of shaking.

The seismic response of another tailings impoundment with and without waste rock inclusions, located in the west of Quebec, Canada, was simulated numerically (for conditions that differ from the actual case). Calculations were made for different WRI configurations using high and low frequency earthquake ground motions of known energy content. The followings summarize the main results obtained:

- The impoundment without inclusion became unstable under the seismic loads considered.
- The seismic response of the impoundment was evaluated using the AR_x values of the downstream slope and of the inclusions, together with the volume of the tailings displaced beyond a threshold value of 100 cm at the end of shaking.
- The evaluation of the results of the 108 simulations indicates that WRI can significantly improve the seismic performance of the impoundment, by reducing the displacement of the downstream slope and the volume of critically displaced tailings.
- The low frequency ground motions induce significantly larger displacements than the high frequency ground motions.
- Generally, the AR_x values of the downstream slope of the tailings dyke decrease with an increased width of the inclusions and increase with a larger spacing between the inclusions.
- Generally, the critically displaced volume of tailings decreases with increasing width of the inclusions and increases with increasing spacing between the inclusions.
- The graphs of the ARx total and WRI values can be used to select an optimal configuration of inclusions (width and spacing) with respect to the seismic stability of the tailings impoundment, for specific seismic loadings.

These results confirm that WRI can have a very beneficial effect on the seismic stability of a tailings impoundment.

Recommendations for additional research

The followings recommendations are provided for further research on WRI, with an emphasis on the situation encountered at mine sites located in western Quebec:

- A laboratory investigation of the dynamic behavior of the tailings using cyclic simple shear testing of saturated and unsaturated specimens, anisotropically consolidated under the range of stresses expected in the impoundment.
- A laboratory investigation of the dynamic behavior of the waste rock.
- Physical modeling of a waste rock inclusion with tailings under controlled conditions to quantify interaction between the two materials and the long-term drainage capacity of the inclusion.
- Comprehensive 3D lifecycle numerical analysis of the subject impoundment to determine the effect of WRI on the overall performance of the impoundment under a range of anticipated conditions.
- Instrumentation and monitoring of a waste rock inclusion at mine sites to determine the effects of the inclusion on the consolidation and saturation of the tailings and the effects of tailings intrusion into the inclusion. This could also be used to validate and calibrate some of the other research at on inclusions that has been conducted using numerical and analytical methods.

Additional recommendations are provided for the general use of inclusions:

- Three dimensional modeling of the seismic table testing of tailings performed with by Pépin et al. (2012a, 2012b). For example, the seismic table test of tailings with a vertical circular column of tailings in the middle of the specimen.
- For better validation of seismic response of an actual tailings impoundment, performing dynamic centrifuge modelling of a tailings impoundment without and with inclusions.
- The development of comprehensive guidelines for the design of waste rock inclusions in tailings impoundments.

REFERENCES

Adalier, K., Elgamal, A., Meneses, J., and Baez J. I. 2003. Stone columns as liquefaction countermeasure in non-plastic silty soils. Soil Dynamics and Earthquake Engineering, 23(7): 571-584.

Adrianopoulos, K. I., Papadimitriou, A. G., and Bouckovalas. 2006. Implementation of a bounding surface model for seismic response of sand. Proceedings of the 4th International FLAC Symposium on Numerical Modeling in Geomechanics, Madrid, Spain. (pp. 387-393). Minneapolis: Itasca Consulting Group, Inc.

Alberight, W.H., Benson, C.H., Gee, G.W., Roesler, A.C., Abichou, T., Apiwantragoon, P., Lyles, B.F., and Rock, S.A. 2004. Field water balance of landfill final covers. Journal of Environmental Quality, 33:2317-2332. PMID: 15537955.

Al-Tarhouni, M., Simms, P., and Sivathayalan, S. 2011. Cyclic behavior of reconstituted and desiccated samples of thickened gold mine tailings. Canadian Geotechnical Journal. 48:(7) 1044-1060, 10.1139/t11-022.

Amyot, G., and S. Vézina. 1997. Flooding as a reclamation solution to an acidic tailings pond—The Solbec case. p. 681–696. In Proc. 4th Int. Conf. on Acid Rock Drainage, Vancouver, BC, Canada. 31 May–6 June 1997. Natural Resources Canada-CANMET, Ottawa, ON.

Andrus, R. D., and Stokoe, K. H. II. 1997. Liquefaction resistance based on shear wave velocity. Proc., NCEER Workshop on Evaluation of Liquefaction Resistance of Soils, Nat. Ctr. for Earthquake Engrg. Res., State Univ. of New York at Buffalo, 89–128.

Andrus, R. D., and Stokoe, K. H. II. 2000. Liquefaction resistance of soils from shear-wave velocity. J. Geotech. and Geoenvir. Engrg., ASCE, 126(11), 1015–1025.

Armstrong, R. J., Boulanger, R. W., and Beaty, M. H. 2010. Nonlinear numerical modeling of centrifuge test results for embankments underlain by liquefied soil. In Proceedings, Collaborative Management of Integrated Watersheds, 30th Annual United States Society on Dams Conference, Sacramento, 12-16 April 2010. United States Society on Dams, pp. 201-215.

Atkinson, G. M. 2009. Earthquake time histories compatible with the 2005 National building code of Canada uniform hazard spectrum. Canadian Journal of Civil Engineering, 36: 991-1000.

Aubertin, M., Bussière, B., and Bernier, L. 2002a. Environnement et gestion des rejets miniers [CD-ROM Manual]. Montréal: Presses Internationales Polytechnique.

Aubertin, M., Bussiere, B., and Chapuis, R. 1996. Hydraulic conductivity of homogenized tailings from hard rock mines. Canadian Geotechnical Journal, **33**(3):470-482.

Aubertin, M., Chapuis, R.P. 1991 Considérations hydro-géotechniques pour l'entreposage des résidus miniers dans le nord-ouest du Québec. 2ème Conf Int sur la Réduction des Eaux de Drainage Acides, Tome III, pp. 1-22.

Aubertin, M., Chapuis, R.P., Aachib, M., Bussière, B., Ricard, J.F., and Tremblay, L. 1995 Évaluation en laboratoire de barrières sèches construites à partir de résidus miniers. Final report. MEND 2.22.2a, École Polytechnique de Montréal, CDT project P1622, 185 pages.

Aubertin, M., Mbonimpa, M., Jolette, D., Bussiere, B., Chapuis, R.P., James, M., and Riffon, O. 2002b. Stabilité géotechnique des ouvrages de retenue pour les résidus miniers: problèmes

persistants et méthodes de contrôle. Défis & Perspectives: Symposium sur l'environnement et les mines, Rouyn-Noranda, Développement Économique Canada/Ministère des Ressources Naturelles du Québec/CIM. Comptes-Rendus sur CD-ROM.

Azam, S., and Li, Q. 2010. Tailings Dam Failures: A Review of the last one hundred years, Geotechnical News, December.

Bardet, J.P. 1997. Experimental soil mechanics, Prentice-Hall, Upper Saddle River, NJ.

Barksdale, R.D., and Bachus, R.C. 1983. Design and construction of stone columns volume I. Report FHWA-RD-83-026, National Technical Information Service, Springfield, VA.

Barksdale, R. D. 1987. Application of the state of the art of stone columns- liquefaction, local bearing failure, and example calculations, Technical Report REMR-GT-7, The Georgia Institute of Technology, 90p.

Beikae, M. 1997. A seismic analysis technique for tailings dams. Proceedings of the International Conference on Tailings and Mine Waste '97, Fort Collins, Colorad (pp. 181-191). Rotterdam: Balkema.

Beaty, M. H. 2001. A synthesized approach for estimating liquefaction-induced displacements of geotechnical structures. Ph.D. Thesis. University of British Columbia, Vancouver BC, Canada.

Beaty, M. H., and Byrne, P. M. 1997. Post-liquefaction shear strength of granular soils: theoritical/conceptual issues, Proceedings, Workshop on Post-Liquefaction Shear Shear Strength of Granular Soils, Urbana-Champion, Illinois, USA.

Beaty, M. and Byrne, P. M. 1998. An effective stress model for predicting liquefaction behavior in sand. Proceedings of Geotechnical Earthquake Engineering and soil dynamic III, Seattle, Washinton, USA. ASCE Special Publication. **75**(1):766-777.

Beaty, M.H. and Byrne, P.M. 2011. UBCSAND constitutive model Version 904aR. Document report: UBCSAND Constitutive Model on Itasca UDM Web site: http://www.itasca-udm.com/pages/continuum.html.

Belem T., Benzaazoua, M., Bussière B., and Dagenais A.-M. 2002. Effects of settlement and drainage on strength development within mine paste backfill. Tailings and Mine Waste'02, 27-30 January 2002, Fort Collins, Colorado, Balkema : Rotterdam, pp. 139-148.

Blake, T.F., Hollingsworth, R.A., and Stewart, J.P. 2002. Recommended procedures for implementation of DMG special publication 117-guidelines for analyzing and mitigating landslide hazards in California. Southern California Earthquake Center, Los Angeles, CA. 127 pp.

Blight, G.E. 2010. Geotechnical engineering for mine waste storage facilities. Leiden: Balkema, 322-338; 453-479.

Blight, G. E., Troncoso, J. H., and Fourie, A. B. 2000. Issues in the geotechnics of mining wastes and tailings, In: GeoEng. 2000 Int. Conf. on Geotechnical and Geological Engineering, Melbourne, Australia, Vol. 1, pp. 1253–1285.

Boulanger, R. W., and Idriss, I. M. 2004. Evaluating the potential for liquefaction or cyclic failure of silts and clays. Rep. UCD/CGM-04/01, Center for Geotech. Modeling, Univ. of Calif., Davis, Calif.

Boulanger, R. W., Kamai, R., and Ziotopoulou, K. 2011. Numerical modeling of liquefaction effects. In Proceeding of the Effects of Surface Geology on Seismic Motion, 4th IASPEI / IAEE International Symposium, University of California, Santa Barbara, CA., 23-26 August 2011.

Bowles, J. E. 1996. Foundation analysis and design (5th edition). New York, USA : McGraw-Hill College.

Bray, J.D., and Dashti, S. 2012. Liquefaction-induced building movements, Invited Keynote Paper, Proceedings of the International Conference on Performance-Based Design Earthquake Geotechnical Engineering, Taormina, Italy.

Bray, J.D., and Rathje, E.M. 1998. Earthquake-induced displacements of solid-waste landfills. Journal of Geotechnical and Geoenvironmental Engineering 124, 242–253.

Bray, J.D., and Travasarou, T. 2007. Simplified procedure for estimating earthquake-induced deviatoric slope displacements. Journal of Geotechnical and Geoenvironmental Engineering 133, 381–392.

Bray, J.D., and Travasarou, T. 2009. Pseudostatic coefficient for use in simplified seismic slope stability evaluation. Journal of Geotechnical and Geoenvironmental Engineering 135, 1336-1340.

Brinkgreve, R. B. J. and P. A. Vermeer, editors. 1998. “PLAXIS Finite Element Code for soil and rock analyses Version 7,” Computer Program Manual, A. A. Balkema, Rotterdam, Netherlands.

Bussière, B. 2007. Hydro-Geotechnical properties of hard rock tailings from metal mines and emerging geo-environmental disposal approaches. Canadian Geotechnical Journal, **44**(9): 1019-1052.

Bussière, B., Aubertin, M., and Chapuis, R.P. 2003. The behavior of inclined covers used as oxygenbarriers. Can. Geotech. J. 40(3): 512-535.

Byrne, P.M., Imire, A.S., and Morgenstern, N.R. 1993. Results and implications of seismic response studies- Duncan Dam. Proceeding. 46th Annual Canadian Geotechnical Conference, Saskatoon, Saskatchewan, pp.271-281.

Byrne, P. M., Park, S. S. and Beaty, M. 2003. Seismic liquefaction: centrifuge and numerical modeling. *In* Proceedings of the Third International Symposium on FLAC and FLAC3D Numerical Modelling in Geomechanics, Sudbury ON, 22-24 October. Balkema Publishers, Lisse NL, Balkema, pp. 321-331.

Byrne, P. M., Park, S.S, Beaty, M., Sharp, M., Gonzalez, L., and Abdoun, T. 2004. Numerical modeling of liquefaction and comparison with centrifuge tests. Canadian Geotechnical Journal, 41, 193-211.

Byrne, P.M., Roy, D., Campanella, R.G., and Hughes, J., 1995. Predicting Liquefaction Response of Granular Soils from Pressuremeter Tests, ASCE National Convention, San Diego, 23-27 October 1995, ASCE, Geotechnical Special Publication 56, pp. 122-135.

Cabral, A., Racine, I., Burnotte, F., and Lefebvre, G. 2000. Diffusion of oxygen through a pulp and paper residue barrier. Canadian Geotechnical Journal, 37 : 201-217.

Canadian Dam Association (CDA). 2007. Dam safety guidelines. Edmonton AB: Canadian Dam Association.

Canadian Dam Association (CDA). 2010. Dam safety guidelines. Edmonton AB: Canadian Dam Association.

Canadian Dam Association (CDA). (2014). Application of dam safety guidelines to mining dams. Edmonton AB: Canadian Dam Association.

California Division of Mines and Geology. 1997. Guidelines for evaluating and mitigating seismic hazards in California. California Division of Mines and Geology Special Publication 117. 74 pp.

California Geological Survey, 2008. Guidelines for evaluating and mitigating seismic hazards in California. California Geological Survey Special Publication 117A. 98 pp.

Castillo, J., Hallman, D., Byrne, P., and Parra, D. 2006. Non-linear dynamic analysis of heap leach pad under high phreatic levels. *In* Proceedings of FLAC and Numerical Modeling and Geomechanics, Mardrid, Spain, 29-31 May 2006. Itasca Consulting Group, Inc., Minneapolis MN, pp. 187-194.

Castro, G. 1975. Liquefaction and cyclic mobility of saturated sands. Journal of Geotechnical Engineering, 101(GT6), 551-569.

Castro G, and Poulos S.J. 1977. Factors affecting liquefaction and cyclic mobility. Journal of Geotechnical Engineering Division, ASCE 103(GT6): 501–506.

Castro, G., and Troncoso, J. 1989. Effect of 1989 Chilean earthquake on three tailings dams. Proceeding, 5th Chilean Conference on Seismology and Earthquake Engineering, Santiago, Chile.

Chaney, R. C. 1978. Saturation effects on the cyclic strength of sands. In Proceedings of the Geotechnical Engineering Division Specialty Conference, Pasadena, California, 19-21June 1978. ASCE, pp. 342-358.

Chang, F.K., and Krinitzsky, E.L. 1977. State-of-the-art for assessing earthquake hazards in the united states. Report 8. Duration, Spectral Content, and Predominant Period of Strong Motion Earthquake Records fromWestern United States, United States.

Chang, W.-J., Rathje, E.M., Stokoe, K.H., and Hazirbaba, K. 2007. In Situ Pore Pressure Generation Behavior of Liquefiable Sand, Journal of Geotechnical and Geoenvironmental Engineering, ASCE, 133(8), 921-931.

Chapuis, R.P., and Aubertin, M. 2003. On the use of the Kozeny-Carman equation to predict the hydraulic conductivity of soils. Canadian Geotechnical Journal, **40**(3): 616-628.

Chien, L.K., Oh, Y.N., and Chang, C.H. 2002. Effect of fines content on liquefaction strength and dynamic settlement of reclaimed soil. Canadian Geotechnical Journal, 39, 254-265.

Conlin, B. 1987. A review of the performance of mine tailings impoundments under earthquake loading conditions. Proceedings of Earthquake Geotechnique, Vancouver, May 1987. BiTech Publishing.

Dafalias, Y.F. 1986. Bounding surface plasticity. I: mathematical foundation and the concept of hypoplasticity, Journal of Engineering Mechanics, ASCE, 112 (9), pp. 966-987.

Daniel, D.E., and Koerner, R.M. 1993. Cover systems. In Proceedings of Geotechnical Practice for Waste Disposal, London, UK. Edited by D.E. Daniel. Chapman & Hall. pp. 455-497.

Dashti, S., and Bray, J.D. 2012. Numerical insights into liquefaction-induced building settlement, Proceeding of the 2012 Geo-Congress, Geo-Institute, Oakland, CA. 25-29 March 2012, ASCE, pp.1660-1669.

Davies, M. P. 2002. Tailings impoundment failures: are geotechnical engineers listening? Geotechnical News, **20**(3): 31-36.

Davies, M. P., and McRoberts, E. 2002. Static liquefaction of tailings – fundamentals and case histories, Amec Earth and Environmental: 23.

Davies, M. P. and Lighthall, P. C. 2001. Geotechnical aspects of several recent mine tailings impoundment failures. In Proceedings of the 54th Canadian Geotechnical Conference, Calgary, AB. Canada Geotechnical Society, pp. 321-326.

Davies, M.P., Lighthall, P.C., Rice, S., and Martin, T.E. 2002b. Keynote Address: Design of tailings dams and impoundments, In Proceedings 2002 SME Annual Meeting, Phoenix, Arizona, 25–27 February 2002. Society for Mining, Metallurgy, and Exploration, Inc., Littleton, Colorado SME, AGM, Phonix.

Davies, M. P. and Rice, S. 2001. An alternative to conventional tailing management – dry stack filtered tailings. AMEC Earth & Environmental, Vancouver, Canada: 10.

DeAlba, P., Chan, C. K., and Seed, H. B. 1975. Determination of soil liquefaction characteristics by large-scale laboratory tests. (Report No. EERC 75-14). Berkeley CA: Earthquake Engineering Research Center.

Dobry, R. and Alvarez, L. 1967. Seismic failures of Chilean tailings dams. Journal of the Soil Mechanics and Foundations Division, 93(SM6): 237-260.

Dobry, R. and Ladd, R.S. 1980. Discussion to "Soil liquefaction and cyclic mobility evaluation for level ground during earthquakes," by H.B. Seed and "Liquefaction potential: science versus practice," by R.B. Peck, Journal of the Geotechnical Engineering Division, ASCE, Vol. 106, No. GT6, pp. 720-724.

Dobry, R., Ladd, R.S., Yokel, F.Y., Chung, R.M., and Powell, D. 1982. Prediction of pore water pressure buildup and liquefaction of sands during earthquakes by the cyclic strain method. NBS Building Science Series 138, National Bureau of Standards, Gaithersburg, Maryland, 150pp.

Dobry, R., and Vucetic, M. 1987. Dynamic properties and siesmic response of soft clay deposits. Proceedings, International Symposium on Geotechnical Engineering of Soft Soils, Mexico City, Vol. 2, pp. 51-87.

Elgamal, A.-W., Parra, E., Yang, Z., Dobry, R., and Zeghal M. 1999. Liquefaction constitutive mode, Proceedings, Physics and Mechanics of Soil Liquefaction Symposium, Balkema, Rotterdam, The Netherlands.

Essaayd, K. 2014. Master Thesis (to be completed), Ecole Polytechnique de Montreal.

Fala, O., Aubertin, M., Molson, J., Bussiere, B., Wilson, G.W., and Martin, V. 2003. Numerical modeling of unsaturated flow in uniform and heterogeneous waste rock piles. In Proceedings of 6th International Conference on Acid Rock Drainge (ICARD) : Application and Sustainability of Technologies, Carins, Australia, 14-17 July 2003. Edited by T. Farrell and G. Taylor. Australian Institute of Mining and Metallurgy (AusIMM), Carlton South, Australia. pp. 895-902.

Ferdosi, B., James, M., and Aubertin, M. 2013. Numerical modeling of the post-liquefaction consolidation of tailings, Proc. GeoMontreal 2013, Montreal, Qc, October 2013. Canadian Geotechnical Society, 7 pages.

Ferdosi, B., James, M., and Aubertin, M. 2014a. Numerical modeling of seismic table testing of tailings with and without inclusion, GeoRegina 2014, Regina, Saskatchewan, October 2014. Canadian Geotechnical Society, 6 pages.

Ferdosi, B., James, M., and Aubertin, M. 2014b. Numerical simulations of the seismic and post-seismic behavior of tailings. Submitted to Canadian Geotechnical Journal.

Ferdosi, B., James, M., and Aubertin, M. 2014c. Effect of waste rock inclusions on the seismic stability of an upstream raised tailings impoundment: a numerical investigation. Submitted to Canadian Geotechnical Journal.

Finn, W.D.L. 1991. Assessment of liquefaction potential and post-liquefaction behavior of earth structures : Developments 1981-1991 (State-of-art paper). Proceeding, 2nd International Conference on Recent Advances in Geotechnical Earthquake Engineering and Soil Dynamics, St. Louis, Missouri, Vol.3, pp. 1833-1850.

Fung, G., Parra, E.P., Sully, J.P., Kerr, J.R., and Akins, K.P. 2011. Seismic modeling of a reinforced slope, 2011 Pan-Am Canadian Geotechnical Society Conference, Toronto, On., October 2011. Canadian Geotechnical Society, 7 pages.

Gamache-Rochette, A. 2004. Une Etude de caraterisation en laboratoire et sur le terrain des ecoulements de l'eau dans les roches steriles. M.Sc. Thesis unpublished. Ecole Polytechnique Montréal PQ, Canada.

Garga, V., and McKay, L. D. 1984. Cyclic triaxial strength of mine tailings. Journal of Geotechnical Engineering, *110*(8), 1091-1105.

Gilstrap, S. D., and Youd, T. L. 1998. CPT based liquefaction resistance analyses using case histories. Tech. Rep. CEG-90-01, Dept. Of Civ. and Envir. Engrg., Brigham Young University, Provo, Utah.

Harder, L. F. Jr. and Stewart, J. P. 1996. Failure of Tapo Canyon tailings dam. Journal of Performance of Constructed Facilities, ASCE, 10(5): 109-114.

Hardin, B.O., and Drnevich, V.P. 1972. Shear modulus and damping in soils: Measurement and parameter effects. J. Soil Mech. Found. Div., ASCE, 98 (6), 603- 624.

Hawley, P.M. 2001. Site Selection: Characterization, and assessment. In slope stability in surface mining. Edited by M.K.M.a.D.J.A.v.Z. In: W.A. Hustrulid, Society for Mining Metallurgy. pp. 267-274.

Higuchi, S., and Ejiri, J. 2012. Influence of the earthquake motion characteristics on the ground settlement behavior due to liquefaction. Proceedings of the International Symposium on

Engineering Lessons Learned from the 2011 Great East Japan Earthquake, March 1-4, Tokyo, Japan.,1:789-800.

Holtz, R. D., and Kovacs, W. D. 1981. An introduction to geotechnical engineering. Englewood NJ: Prentice-Hall, Inc.

Hyde, A., Higuchi, T., and Yasuhara, K. 2007. Postcyclic recompression, stiffness, and consolidated cyclic strength of silt. Journal of Geotechnical and Geoenvironmental Engineering, ASCE, **133**(4):416-423.

Hynes-Griffin, M.E., and Franklin, A.G. (1984). Rationalizing the seismic coefficient method. U.S. Army Corps of Engineers Waterways Experiment Station. Miscellaneous Paper GL-84-13, 37 pp.

Idriss, I. M., and Boulanger, R. W. 2008. Soil liquefaction during earthquake, Earthquake Engineering Research Institute, EERI Publication MNO-12.

Idriss, I. M., and Boulanger, R. W. (2011). Workshop : Liquefaction, May 2011.

International Commission on Large Dams (ICOLD). 1996a. Tailings dam and environment, ICOLD, Paris, issn 0534-8293.

International Commission on Large Dams (ICOLD). 1996b. Monitoring of tailings dams, ICOLD, Paris, issn 0534-8293.

International Commission on Large Dams (ICOLD). 2001. Tailings dams – risk of dangerous occurrences – lessons learnt from past experiences. Bulletin No. 121. Paris: Commission Internationale des Grands Barrages.

Ishibashi, I. 1992. Discussion to effect of soil plasticity on cyclic response, by M. Vucetic and R. Dobry. Journal of Geotechnical Engineering. ASCE, Vol. 118, No. 5, pp. 830-832.

Ishibashi, I., and Zhang, X. 1993. Unified dynamic shear moduli and damping ratios of sand and clay. Soils and Foundations, Vol. 33, No. 1, pp. 182-191.

Ishihara, K. 1984. Post-Earthquake failure of a tailings dam due to liquefaction of the pond deposit. Proceedings of the International Conference on Case Histories in Geotechnical Engineering, St-Louis, 1984. University of Missoiuri Rolla, Missouri, pp. 1129-1143.

Ishihara, K. 1993. Liquefaction and flow failure during earthquakes. Geotechnique, 43(3), 351-415.

Ishihara, K. 1996. Soil behavior in earthquake geotechnics. Oxford: Oxford University Press.

Ishihara K., Tatsuoka F., and Yasuda S. 1975. Undrained deformation and liquefaction of and under cyclic stresses. Soils Found;15(No. 1):29–44.

Ishihara, K., Troncoso, J., Kawase, Y., and Takahashi, Y. 1980. Cyclic strength characteristics of tailings materials. JSSMFE, Soils and Foundations, 20(4), 127-142.

Ishihara, K., Sodekawa, M., and Tanaka, Y. 1981. Cyclic strength of undisturbed mine tailings. Proceedings of the International Conference on Recent Advances in Geotechnical Earthquake Engineering and Soil Dynamics, St-Louis USA. (pp. 53-58. New York: ASCE.

Itasca Consulting Group, Inc. (Itasca). 2006. FLAC – Fast Lagrangian Analysis of Continua. Version 6.00. [computer software and user manual]. Minneapolis MN: Itasca Consulting Group, Inc.

Itasca Consulting Group, Inc. (Itasca). 2008. FLAC – Fast Lagrangian Analysis of Continua. Version 6.00. [computer software and user manual]. Minneapolis MN: Itasca Consulting Group, Inc.

James, M. 2009. The use of waste rock inclusions to control the effect of liquefaction in tailings impoundments . Ph.D. Thesis, Department of Civil, Geological, and Mining Engineering, Ecole Polytechnique de Montreal, Montreal, QC.

James M., and Aubertin, A. 2010. On the dynamic response of tailings and the stability of tailings impondments for hard rock mines. Geotechnical News, **23**(3), 39-43.

James, M., and Aubertin, M. 2012. The use of waste rock inclusions to improve the seismic stability of tailings impoundments. GeoCongress 2012, Okland, 22-25 March 2012. American Soceity of Civil Engineers, pp. 4166-4175.

James, M., Aubertin, M., and Bussière, B. 2013. On the use of waste rock inclusions to improve the performance of tailings impoundments. In Proceeding of the 18th International Conference Soil Mechanics and Geotechnical Engineering, 2-6 September 2013. ISSMGE, pp. 735-738.

James, M., Aubertin, M., Wijewickreme, D., and Ward Wilson, G. 2011. A laboratory investigation of the dynamic properties of tailings. Canadian Geotechnical Journal, **48**(11)*:* 1587–1600.

James, M., and Leahy, D. 2010. Phase 1 tailings dam stability study of Mine No.12 site, Final report, SNC.LAVALIN Company, Montreal, QC.

Jaouhar, E.M., Aubertin, M. and James, M. 2011. Effect of waste rock inclusions on the consolidation of mine tailings. In Proceedings of 2011 CGS Geotechnical Conference, Toronto ON, 2 – 6 October 2011. Canadian Geotechnical Society.

Jaouhar, E.M., Aubertin, M., and James, M. 2013. The effect of tailings properties on their consolidation near waste rock inclusions. In GeoMontreal 2013:Geosciences for Sustainability, Proceedings of the 66th CGS Conference, October 2013, Montreal, QC. Canadian Geotechnical Society, 8 Pages.

Jefferies, M.G. and Been, K. 2006. Soil Liquefaction: A critical state approach, Taylor and Francis, Abingdon, ISBN.

Jibson, R.W. 2011. Methods for assessing the stability of slopes during earthquakes-A retrospective. Engineering Geology, 122 (2011): 43–50.

Jibson, R.W., and Michael, J.A. 2009. Maps showing seismic landslide hazards in Anchorage, Alaska. U.S. Geological Survey Scientific Investigations Map 3077. 2 sheets (scale 1:25, 000), 11-p. pamphlet.

Julien, M.R., Lemieux, M., Cayouette, J., and Talbot, D. 2004. Performance and monitoring of the Louvicourt mine tailings disposal area. In Proceedings of 36th Annual Meeting of the Canadian Mineral Processors, Ottawa, Ont., 20-22 January 2004. Canadian Institute of Mining, Metallurgy, and Petroleum. pp. 57-77.

Kayen, R. E., Mitchell, J. K., Seed, R. B., Lodge, A., Nishio, S., and Coutinho, R. 1992. Evaluation of SPT-, CPT-, and shear wave-based methods for liquefaction potential assessment using Loma Prieta data. Proc., 4th Japan-U.S. Workshop on Earthquake-Resistant Des. of Lifeline Fac. and Countermeasures for Soil Liquefaction, Vol. 1, 177–204.

Kesimal, A., Yilmaz, E., and Ercikdi, B. 2004. Evaluation of paste backfill mixtures consisting of sulphide-rich mill tailings and varying cement contents. Cement and Concrete Research, 34(10): 1817-1822.

Khalili, A., Wijewickreme, D., and Wilson, G.W. 2010. Mechanical response of highly gap-graded mixtures of waste rock and tailings. Part I: Monotonic shear response. Canadian Geotechnical Journal, **47**(5): 552-565.

Koester, J. P. 1994. The influence of fines type and content on cyclic strength. Proceedings of Ground Failures under Seismic Conditions, Atlatnta GA, USA, GSP 44. (pp. 17-33). New York: ASCE.

Kokusho, T. 1980. Cyclic triaxial test of dynamic soil properties for wide strain range. Soil and Foundation, Vol. 20, No. 2, pp. 45-60.

Kokusho, T. 1987. In situ dynamic soil properties and their evaluation. Proceedings of the 8th Asian Regional Conference on Soil Mechanics and Foundation Engineering, Kyoto, Vol. 2, pp. 215435.

Kokusho, T., and Tanaka, Y. 1994, Dynamic properties of gravel layers investigated by in situfreezing sampling. Proceedings of the ASCE Specialty Conference on Ground Failures under Seismic Conditions, Atlanta. pp, 12140.

Kokusho, T., Yoshida, Y., and Esashi, Y. 1982. Dynamic properties of soft clay for wide strain range. Soil and Foundation, Vol. 22, No. 4, pp. 1-18.

Kramer, S. L. 1996. Geotechnical earthquake engineering. Prentice-Hall Inc., Upper Saddle River, N.J.

Kramer, S., and Arduino, P. 1999. Constitutive modeling of cyclic mobility and implications for site response, Proceedings, 2nd International Conference on Earthquake Geotechnical Engineering, Balkema, Rotterdam, The Netherlands.

Kuerbis, R., Negussey, D., and Vaid, Y. P. 1988. Effect of gradation and fines content on the undrained response of sand. Proceedings of Hydraulic Fill Structures, Fort Collins CO, USA, SGP(21). (pp. 330-345). New York: ASCE.

L. Bolduc, F., and Aubertin, M. 2013. Analysis the effect of waste rock inclusions on tailings consolidation: laboratory and modeling of the large scale in situ behavior, GeoMontreal 2013, Montreal, QC, October 2013. Canadian Geotechnical Society.

L.Bolduc, F., and Aubertin, M. 2014. A numerical investigation of the influence of waste rock inclusions on tailings consolidation, Canadian Geotechnical Journal, 51(9): 1021-1032.

Lamontage, A., Lefebvre, R., Poulin, R., and Leroueil, S. 1999. Modelling of acid mine drainge physical processes in a waste rock pile with layered co-mingling. In proceedings of the 52nd Canadian Geotechnical Conference, Regina, Sask., 25-27 October 1999. Pp. 479-485.

Ledbetter, R. H. 1985. Improvement of liquefiable foundation conditions beneath existing structures (Technical Report REMR-GT-2). Washington DC: US Army Corps of Engineers.

Leps, T. M. 1970. Review of shearing strength of rockfill (with discussions). Journal of the Soil Mechanics and Foundations Division, SM4, 1159-1170.

Liang, J. Z., and Elias, D. 2010. Seismic evaluation of tailings storage facility. Proc. Australian Earthquake Engineering Society 2010 Conference, Perth, Western Australia. Australian Earthquake Engineering Society. 8 pages.

Liao, S., and hitman, R. V. 1986. Overburden correction factors for SPT in sand. J. Geotech. Engrg., ASCE, 112(3), 373–377.

Lin, J.S., and Whitman, R.V. 1983. Earthquake induced displacements of sliding blocks. Journal of Geotechnical Engineering 112, 44–59.

Lo, R.C., and Klohn, E. L. 1995. Design considerations for tailings dams, Proceedings of the 5th International Conference on Tailings and Mine Waste '96, Fort Collins CO, 1995. Taylor and Francis, London, pp. 113-121.

Makdisi, F.I., and Seed, H.B. 1978. Simplified procedure for estimating dam and embankment earthquake-induced deformations. ASCE Journal of the Geotechnical Engineering Division 104, 849–867.

Marcuson, W. F. III, Hynes, M. E., and Franklin, A.G. 1990. Evaluation and use of residual strength in seismic safety analysis of embankments. Earthquake Spectra, 6, 529-572.

Martin, J. R. II, Olgun, C. G., Mitchell, J. K., and Durgunoglu, H. T. 2004. High-modulus columns for liquefaction mitigation. Journal of Geotechnical and Geoenvironmental Engineering, 130(6): 561-571.

Matsuoka, H., and Nakai, T. 1977. Stress–strain relationship of soil based on the 'SMP'. In: Proc. 9th Int. conf. Soil Mech. Found. Eng., Tokyo, pp. 153–162.

Mbonimpa, M., Aubertin, M., Chapuis, R. P., and Bussiere, B. 2002. Practical pedotransfer functions for estimating the saturated hydraulic conductivity. Geotechnical and Geological Engineering, **20**(3): 235-259.

McLemore, V.T., Fakhimi, A., van Zyl, D., Ayakwah, G.F., Anim, K., Boakye, K., Ennin, F., Felli, P., Fredlund, D., Gutierrez, L.A.F., Nunoo, S., Tachie-Menson, S., and Viterbo, V.C. (2009). Literature review of other rock piles: characterization, weathering, and stability: New Mexico Bureau of Geology and Mineral Resources, , New Mexico Bureau of Geology and Mineral Resources.

Mittal, H.K., and N.R. Morgenstern. 1975. Parameters for the design of tailings dams. Canadian Geotechnical Journal Vol. 13, p. 277-293.

Mosquera, J., Hamade, T., and Mitri, H. 2013. Comparative stability analysis of tailings storage facilities. 23rd World Mining Congress, 11-15 August, Montreal, Canada. Canadian Institute of Mining and Metallurgical. Paper 566.

Naeini, S. A., and Baziar, M. H. 2004. Effects of fines content on steady-state strength of mixed and layered samples of a sand. Soil Dynamics and Earthquake Engineering, Elsevier, 24, 181-187.

Naesgaard, E. 2011. A hybrid effective stress-total stress procedure for analyzing embankments subjected to potential liquefaction and flow. PhD. Thesis, Civil Engineering Department, The University of British Coulombia, Vancouver, B. C.

Naesgaard, E., and Byrne, P.M. 2007. Flow liquefaction simulation using a combined effective stress – total stress model, 60th Canadian Geotechnical Conference, Ottawa, On, October 2007. Canadian Geotechnical Society, pp. 943-950.

Naesgaard, E., Yang, D., Byrne, P., and Gohl, B. 2004. Numerical analysis for the seismic safety retrofit design of the immeresed-tube George Massey tunnel, 13th World Conference on Earthquake Engineering, Vancouver, B.C., 1-6 August 2004. Canadian Association for Earthquake Engineering.

Narvaez, B., Aubertin, M., and Saleh-Mbemba, F. 2014. Application of a predictive model to estimate the tensile strength of unsaturated tailings, GeoRegina 2014, Regina, Saskatchewan, October 2014. Canadian Geotechnical Society, 7 pages.

National Research Center (NRC). 1985. Liquefaction of soils during earthquakes. Washington DC: National Academy Press.

Natural Resources Canada (NRC). 2003. Processed ground motions records of the 1988 Saguenay earthquake. Website accessed on June 16, 2003. http://www.seismo.nrcan.gc.ca/nwfa/index_e.php.

Newmark, N.M. 1965. Effects of earthquakes on dams and embankments. Geotechnique 15, 139–159.

Nicholson, R.V., Gillham, R.W., Cherry, J.A., and Reardon, E.J. 1989. Reduction of acid generation in mine tailings through the use of moisture-retaining cover layers as oxygen barries. Canadian Geotechnical Journal, 26 :1-8.

Olsen, R. S. 1997. Cyclic liquefaction based on the cone penetration test. Proc., NCEER Workshop on Evaluation of Liquefaction Resistance of Soils, Nat. Ctr. for Earthquake Engrg. Res., State Univ. of New York at Buffalo, 225–276.

Olsen, S. M., and Stark, T. 2002. Liquefied strength ratio from liquefaction flow failure case histories. Canadian Geotechnical Journal, 39, 629-647.

Ormann, L., Zardari, M.A., Mattson, H., Bjelkevik, A., and Knutsson, S. 2011. Numerical analysis of curved embankment of an upstream tailings dam. Electronical Journal of Geotechnical Engineering, **16**(1):931-944.

Pacific Earthquake Engineering Research Center (PEER). 2014. P0923 : Earthquake and station details. Consulted on February, 2011. http://peer.berkeley.edu/svbin/Detail?id=P0923.

Pépin, N. 2010. Étude du comportement cyclique de résidus miniers avec inclusions drainantes par des essais sur table sismique. M.Sc. A. Thesis, École Polytechnique de Montréal, Montréal, Quebec.

Pépin, N., Aubertin, M., and James, M. 2009. An investigation of the cyclic behavior of tailings using shaking table tests: effect of a drainage inclusion on pore water development, GeoHalifax2009, pp. 32-39.

Pépin, N., Aubertin, M., James, M., and Leclerc, M. 2012a. Seismic simulator testing to investigate the cyclic behavior of tailings in an instrumented rigid box. Geotechnical Testing Journal, **35**(3): 469-479.

Pépin, N., Aubertin, M., and James, M. 2012b. Seismic table investigation of the effect of inclusions on the cyclic behavior of tailings. Canadian Geotechnical Journal, **49**(4): 416-426.

Polito, C., and Martin, J. R. II. 2001. Effects of nonplastic fines on the liquefaction resistance of sands. Journal of Geotechnical and Geoenvironmental Engineering, 127(5), 408-415.

Poncelet, N. 2012. Élaboration et implément d'un protocole de laboratoire pour l'étude du potential de liquéfaction de résidus miniers. M.Sc. Thesis unpublished. Ecole Polytechnique Montréal PQ, Canada.

Poorooshasb, H.B., Holubec, I., and Sherbourne, A.N. 1966. The yielding and flow of sand in triaxial compression, Canadian Geotechnical Journal, Vol. 3, No. 4, pp. 179-190.

Poulos, S. J., Gonzalo, C., and France, J. W. 1985. Liquefaction evaluation procedure. Journal of Geotechnical Engineering, 111(6), pp. 773-792.

Prevost, J.H. 1989. DYNA1D: A computer program for nonlinear site response analysis, Technical Report NCEER-89- 0025, National Center for earthquake Engineering Research, SUNY at Buffalo, New York, USA.

Psarropoulos, P.N., and Tsompanakis, Y. 2008. Stability of tailings dams under static and seimic loading. Canadian Geotechnical Journal, **45**(5): pp.663-675.

Puebla, H. 1999. A constitutive model for sand and the analysis of the CanLex Embankments. Ph.D. thesis, Civil Engineering Department, University of British Columbia, Vancouver, B. C.

Puebla, H., Byrne, P.M., and Phillips, R. 1997. Analysis of CANLEX liquefaction embankments: prototype and centrifuge models. Canadian Geotechnical Journal, 34(5): 641-657.

Pyke, R., Chan, C. K., and Seed, H. B. 1974. Settlement and liquefaction of sands under multi-directional shaking. Report No. EERC 74-2, Earthquake Engineering Research Center, Berkeley, CA.

Qiu, Y., and Sego, D. C. 2001. Laboratory properties of mine tailings. Canadian Geotechnical Journal, 38(1), 183-190.

Quine, R.L. 1993. Stability and deformation of mine waste dumps in north-central Nevada. M.S. thesis, University of Nevada, Reno.

Rapport Factuel. 2011. Investigation géotechnique pour le parc à résidus miniers, Projet Canadian Malartic, Malartic, Québec, Golder Associés, 1001 de Maisonneuve Ouest, Montréal, Sept. 2011.

Rathje, E.M., and Bray, J.D. 1999. An examination of simplified earthquake-induced displacement procedures for earth structures. Canadian Geotechnical Journal 36, 72–87.

Rathje, E.M., and Bray, J.D. 2000. Nonlinear coupled seismic sliding analysis of earth structures. Journal of Geotechnical and Geoenvironmental Engineering 126, 1002–1014.

Roberto, M., Marco, DF., Erica, B., and Erica, Z. 2008. Dynamic slope stability analysis of mine tailings deposits: the case of Raibl mine. Seismic Engineering Conference Commemorating the 1908 Messina and Reggio Calabria Earthquake, Reggio Calabria Italy. American Institute of Physics. 1: 542-549.

Robertson, A. 1985. Mine waste disposal: an update on geotechnical and geohydrological aspects.

Robertson, P. K., and Campanella, R. G. 1996. Guidelines for Use and Interpretation of Piezometer Cone Penetration Test. University of California, Berkeley, Department of Civil Engineering, Soil Mechanics Series. Berkeley CA: University of California.

Robertson, P. K., Woeller, D. J., and Finn, W. D. 1992. Seismic cone penetration test for evaluating liquefaction potential under cyclic loading. Can. Geotech. J., Ottawa, 29, 686–695.

Robertson, P. K., and Wride, C. E. 1998. Evaluating cyclic liquefaction potential using the cone penetration test. Can. Geotech. J., Ottawa, 35(3), 442–459.

Robinsky, E.I. 1975. Thickened discharge - a new approach to tailings disposal. Canadian Mining and Metallurgical Bulletin, Vol. 68, December 1975, pp. 47-53.

Rollins, K.M., Evans, M.D., Diehl, N.B. and Daily, W.D. III. 1998. Shear modulus and damping relationships for gravels. Journal of Geotechnical and Geoenvironmental Engineering. 124(5): 396-405.

Rowe, P. W. 1962. The stress-dilatancy relation for static equilibrium of an assembly of particles in contact. Proc. R. Sot**.** A269,500-527.

Rowe, R.K., Quigley, R.M., Brachman, R.W.I., and Booker, J.R. 2004. Barrier systems for waste disposal facilities. 2nd ed. Taylor & Francis Group Spon Press, New York. 587 pp.

Saleh-Mbemba, F. 2015. Ongoing Ph.D thesis, Department of Civil, Geological and Mining Engineering, Ecole Polytechnique de Montreal, Montreal, QC.

Sasaki, Y., and Taniguchi, E. 1982. Shaking table tests on gravel drains to prevent liquefaction of sand deposits. JSSMFE - Soils and Foundations, *22*(3), 1-14.

Schofield, A. N., and Wroth, C. P. 1968. Critical state soil mechanics, McGraw-Hill, pp. 310.

Seed H. B. 1976. Some aspects of sand liquefaction under cyclic loading. Proc. of Conf. on Behavior of Offshore Structures, Norwegian Institute of Technology, Oslo, Norway.

Seed, H. B. 1979. Considerations in the earthquake-resistant design of earth and rockfill dams. Geotechnique. 29(3). 215-263.

Seed, H. B. 1983. earthquake-resistant design of earth dams. Proceedings of the Symposium on Seismic Design of Embankments and Caverns, Philadelphia PA, USA (pp. 41-61). New York: ASCE.

Seed, H. B. 1987. Design problems in soil liquefaction, J. Geotechnical Eng., ASCE 113(8), 827–45.

Seed, H.B., and Booker, J.R. 1977. Stabilization of potentially liquefiable sand deposits using gravel drains, Journal of the Geotechnical Engineering Division, ASCE, Vol. 103, No. GT7, pp. 757-768.

Seed, H. B., and Harder, L. F. 1990. SPT-Based analysis of cyclic pore pressure generation and undrained residual strength. Proceedings of the H. Bolton Seed Memorial Symposium, Berkeley CA, USA. (Vol. 2, pp. 351-376). Vancouver BC: Bitech Publishers.

Seed, H. B., and Idriss, I. M. 1970a. A simplified procedure for evaluating soil liquefaction potential (Report No. EERC 70-9). Berkeley CA: Earthquake Engineering Research Center.

Seed, H. B., and Idriss, I. M. 1970b. Soil moduli and damping factors for dynamic response analyses (Report No. EERC 70-10). Berkeley CA: Earthquake Engineering Research Center.

Seed, H. B., and Idriss, I. M. 1971. Simplified procedure for evaluating soil liquefaction potential. Journal of the Soil Mechanics and Foundation Division, ASCE, Vol. 107, No. SM9, pp. 1249-1274.

Seed, H. B., and Idriss, I. M. 1982. Ground motions and soil liquefaction during earthquakes. Berkeley CA: Earthquake Engineering Research Institute.

Seed, H. B., Mori, K., and Chan, C. K. 1975. Influence of sesimic history on the liquefaction characteristics of sands (Report No. ERRC 75-25). Berkeley CA: Earthquake Engineering Research Center.

Seed, H. B., and Lee, K. L. 1966. Liquefaction of saturated sands during cyclic loading. Journal of the Soil Mechanics and Foundation Engineering Division. 92(6). 105-134.

Seed, H. B., Tokimatsu, K., Harder, L. F., and Chung, R. M. 1985. The influence of SPT procedures in soil liquefaction resistance valuations. *J. Geotech. Engrg.*, ASCE, 111(12), 1425–1445.

Seed, H. B., and Peacock, W. H. 1971. Procedures for measuring soil liquefaction characteristics under cyclic loading. (Report No. ERRC 70-8). Berkeley CA: Earthquake Engineering Research Center.

Seed, H.B., Wong, R.T., Idriss, I.M., and Tokimatsu, K. 1984. Dynamic moduli and damping factors for dynamic analysis of cohesionless soils. Report No. UCB/EERC-84/14, Earthquake Engineering Research Center, Berkeley, CA.

Seid-Karbasi, M., and Byrne, P. M. 2004. Embankment dams and earthquakes. Hydropower and Dams, 2: 96-102.

Seid-Karbasi, M., and Byrne, P. M. 2007. Seismic liquefaction, lateral spreading, and flow slides: a numerical investigation into void redistribution. Canadian Geotechnical Journal, 44(7): 873-890.

Sento, N., Kazama, M., Uzuoka, R., Matsuya, A., and Ishimaru, M. 2004. Liquefaction-induced Volumetric Change During Re-consolidation of Sandy Soil Subjected to Undrained Cyclic Loading Histories. Proceedings of the International Conference on Cyclic Behavior of Soils and Liquefaction Phenomena, Bochum, Germany. Balkemas. 1:199-206.

Sherard, J.L., Woodward, R. T., Gizienski, S. F., and Clevenger, W. A. 1963. Earth and earth-rock dams. New York : John Wiley & Sons, Inc.

Sonu, C. J., Ito, K., and Oishi, H. 1993. Harry Seed, Liquefaction and the gravel drain. Civil Engineering Magazine, 63(12), 58-60.

Strachan, C. 2002. Review of tailings dam incident data. Mining Environmental Management. Tailings Management Guide, January, pp. 7-9.

Stark, T.D., and Mesri, G. 1992. Undrained shear strength of sands for stability analysis. Journal of Geotechnical Engineering, ASCE, Vol. 118, No. 11, pp. 1727-1747.

Sun, J.I., Golesorkhi, R., and Seed, H.B. 1988. Dynamic moduli and damping ratios for cohesive soils, Report No. EERC-88/15, Earthquake Engineering Research Center, University of California, Berkeley.

Sykora, D. W. 1987. Creation of a data base of seismic shear wave velocities for correlation analysis. Geotech. Lab. Misc. Paper GL-87-26, U.S. Army Engr. Waterways Experiment Station, Vicksburg, Miss.

Tasse, N., Germain, D., Dufour, C., and Trembly, R. 1997. Organic waste cover over the East Sullivan mine tailings: Beyond the oxygen barrier. In Proceedings of the 4th International Conference on Acid Rock Drainage (ICARD), Vancouver, B.C., 31 May-6 June 1997. Vol. 4, pp. 1627-1642.

Taylor, D. W. 1948. Fundamentals of soil mechanics. John Wiley, New York.

Thevanayagam, S., Fiorillo, M., and Liang, J. 2000. Effect of non-plastic fiens on undrained cyclic strength of silty soils. Soil Dynamics and Liquefaction 2000: Proceedings of sessions of Geo-Denver 2000, Denver CO, USA (pp. 77-91). Reston VA: ASCE.

Thevanayagam, S., and Martin, G.R. 2001. Liquefaction and Post-liquefaction Dissipation / Densification Characteristics of Silty Soils, MCEER Annual Report for Research Year 1, FHWA Contract # DTFH61-98-C-00094.

Thevanayagam, S., and Mohan, S. 1998. Intergranular void ratio - steady state strength relations for silty sands. Proceedings of Geotechnical Earthquake Engineering III, Seattle WA, USA (pp. 349-360). New York: ASCE.

Thomas, J. 1992. Static, cyclic and post-liquefaction undrained behavior of Fraser river sand, Msc. Thesis, The University of British Coulombia, Vancouver BC, Canada.

Towhata, I. 2008. Geotechnical earthquake engineering. Verlag Berlin Heidelberg: Springer.

Tokimatsu, K., and Seed, H. B. 1987. Evaluation of settlements in sands due to earthquake shaking, American Society of Civil Engineers, Journal of Geotechnical Engineering, **113**(8): 861-878.

Troncoso, J. H. 1986. Critical state of tailing silty sands for earthquake loading. Soil Dynamics and Earthquake Engineering, *5*(3), 248-252.

Troncoso J.H., and Garces E. 2000. Ageing effects in the shear modulus of soils. Soil Dynamics and Earthquake Engineering, Vol. 19, No. 8, pp. 595-601(7).

Troncoso, J. H., and Verdugo, R. 1985. Silt content and dynamic behavior of tailings sands. Proceedings of the 11th Intl Conf on Soil Mechanics and Foundation Engineering, San Francisco CA, USA (Vol 3., pp. 1311-1314). New York: ASCE.

Ulrich, B. F., and Hughes, J. M. O. 1994. SPT/CPT correlations for Mine Tailings. Proceedings of the International Conference on Tailings and Mine Waste '94, Fort Collins CO, *USA* (pp. 215-223). Rotterdam: Balkema.

Vaid, Y.P., and Sivathayalan, S. 1996. Static and cyclic liquefaction potential of Fraser Delta sand in simple shear and triaxial tests. Canadian Geotechnical Journal, **33**: 281–289.

Vasquez-Herrera, A., and Dobry, R. 1990. The behavior of undrained contractive sand and its effect on seismic liquefaction flow failure of earth structures. Report to U.S. Army Corps of engineers, Renssalaer Polytechnic Institute, Troy, New York, 510 pp.

Vermeer, P.A. 1980. Formulation and analysis of sand deformation problems. Ph.D. Thesis, Department of Civil Engineering, Delft University, The Netherlands.

Vick, S. G. 1990. Planning, design and analysis of tailings dams. Vancouver, BC: BiTech Publishers Ltd.

Weiler, W.A. 1988. Small strain shear modulus of clay. Earthquake Engineering and Soil Dynamics II – Recent Advances in Ground-Motion Evaluation, Geotechnical Special Publication No. 20, ASCE, p331.

Wickland, B.E., and Wilson, G.W. 2005. Self-weight consolidation of mixtures of mine waste rock and tailings. Canadian Geotechnical Journal, **42**(2): 327-339.

Wieczorek, G.F., Wilson, R.C., and Harp, E.L. 1985. Map showing slope stability during earthquakes in San Mateo County, California. U.S. Geological Survey Miscellaneous Investigations Map I-1257-E, scale 1:62,500.

Wijewickreme, D., Khalili, A., and Wilson, G.W. 2010. Mechanical response of highly gap-graded mixtures of waste rock and tailings. Part II: Undrained cyclic and post-cyclic shear response, Canadian Geotechnical Journal, **47**(5): 566-582.

Wijewickreme, D., and Sanin, M.V. 2010. Post-cyclic Reconsolidation Strains in Low-plastic Fraser River Silt due to Dissipation of Excess Pore Water Pressures. ASCE Journal of Geotechnical and Geoenvironmental Engineering, **136**(10): 1347-1357.

Wijewickreme, D., Sanin, M. V., and Greenaway, G. 2005a. Cyclic shear response of fine-grained mine tailings. Canadian Geotechnical Journal, 42, 1408-1421.

Wijewickreme, D., Sanin, M. V., and Greenaway, G. 2005b. Cyclic shear response of fine-grained mine tailings. Canadian Geotechnical Journal, 42(5): 1408-1421.

Wijewickreme, D., Sriskandakumar, S., and Byrne, P. 2005b. Cyclic loading response of loose aAir-pluviated Fraser river sand for validation of numerical models simulating centrifuge tests. Canadian Geotechnical Journal, *42*, 550-561.

Williams, D.J. 2000. Assessment of embankment parameters. In Slope Stability in Surface Mining, Society for Mining Metallurgy. pp. pp. 275-284.

Williams, D.J., Wilson, G.W., and Currey, N.A. 1997. A cover system for a potentially acid forming waste rock dump in a dry climate. In Proceeding of the 4th International Conference on

Tailings and Mine Waste ’97, Fort Collins, Colo., 13-17 January 1997. A.A. Balkema, Rotterdam, the Netherlands. Pp. 231-235.

Wilson, R.C. 1993. Relation of Arias intensity to magnitude and distance in California. Open-file report 93-556, U.S. Geological Survey, Reston, Virginia, 42pp.

Wilson, G.W., Wickland, B., and Fines, P. 2002. Concept for co-mixing waste rock and tailings. In Syposium 2002 on Mining and the Environment : Challenges and Prospects, Rouyon-Noranda, Que., 3-5 November 2002. Canadian Institute of Mining, Metallurgy, and Petroleum.

Wilson, J.A., Wilson, G.W., and Fredlund, D.G. 2000. Numerical modeling of vertical and inclined waste rock layers. In Proceedings of the 5th International Conference on Acid Rock Drainage (ICARD 2000), Denver, Colo., 21-24 May 2000. Society of Mining Metallurgy and Exploration Inc, Littleton, Colo. Vol, 1. Pp. 257-266.

Wilson, W., Plewes, H.D., Williams, D., and Robertson, J. 2003. Concepts for co-mixing of tailings and waste rock. In Proceeding of 6th International Conference on Acid Rock Drainge (ICARD) : Application and sustainability of Technologies, Carins, Australia, 14-17 July 2003. Edited by T. Farrell and G. Taylor. Australian Institue of Mining and Metallurgy (AusIMM), Carlton South, Australia. Pp. 437-443.

Wise Uranium Project (WISE). 2014. Chronology of major tailings dam failures. Consulted on May 15,2014. www.antenna.nl/wise/uranium/mdaf.html.

Youd, T. L., Idriss, I. M., Andrus, R. D., Arango, I., Castro, G., and Christian, J. T. 2001. Liquefaction resistance of soils: summary report from the 1996 NCEER and 1998 NCEER/NSF

Workshops on Evaluation of Liquefaction Resistance of Soils. Journal of Geotechnical and Geoenvironmental Engineering, 127(10), 817-833.

Youd, T. L., and Noble, S. K. 1997. Magnitude scaling factors. Proc., NCEER Workshop on Evaluation of Liquefaction Resistance of Soils, Nat. Ctr. for Earthquake Engrg. Res., State Univ. of New York at Buffalo, 149–165.

Zhan, G.S., Aubertin, M., Mayer, A., Burke, K., and McMullen, J. 2001. Capillary cover design for a spent leach pad. Proc. CD-ROM 01-137, Denver, Colorado, Feb 2001, AIME.

Zienkiewicz, O.C., Chan, A.H.C., Pastor, M., Paul, D.K., and Shiomi, T. 1990. Static and dynamic behavior of soils: a rational approach to uantitative solutions. Part I: fully saturated problems, Proceedings, Research Society London, A429.

Ziotopoulou, K., and Boulanger, W. 2013. Numerical modeling issues in predicting post-liquefaction reconsolidation strains and settlements. 10th International Conference on Urban Earthquake Engineering, Tokyo, 1-2 March 2013, Tokyo Institute of Technology, Tokyo, Japan.

Ziotopoulou, K., Boulanger, R. W., and Kramer, S. L. 2012. Site response analysis at liquefiable sites. ASCE Geo-Congress 2012: State of the Art and Practice in Geotechnical Engineering, R. D. Hryciw, A. Athanasopoulos-Zekkos, and N. Yesiller eds., Geotechnical Special Publication No.225, ASCE Geo-Institute, 1799-1808.

APPENDICES

APPENDIX A- THE UBCSAND MODEL WITH CAP

A1. Introduction

The UBCSAND model was developed by Byrne et al. (1995) and later revised by others, including Puebla et al. (1997), Beaty and Byrne (1998, 2011), and Naesgaard (2011). They have shown that the UBCSAND model can realistically simulate excess pore water pressure generation in sands due to cyclic loading, up to liquefaction. However, the basic form of this model cannot accurately simulate the post-dynamic behavior of these materials, specifically the reconsolidation of the material due to excess pore water pressure dissipation. This implies that post-dynamic strength, stiffness and deformations are not adequately simulated.

The plastic criterion used in the UBCSAND model does not have a cap (i.e. it is open on the positive side of the stress plane). Hence, the stress path during excess pore water pressure dissipation, which is parallel to the stress ratio $\eta = t/s'$ (where $t = (\sigma_1' - \sigma_3')/2$ and $s' = (\sigma_1' + \sigma_3')/2$), does not meet a yielding surface. Therefore, the soil behaves elastically during reconsolidation associated with excess pore water pressure dissipation. (refer to Figure A1). As a result, the UBCSAND model shows post-liquefaction volumetric strains that are often significantly lower than reality. In terms of the post-shaking behavior of a tailings impoundment, the model may underestimate potentially destabilizing deformations in or near the retention dyke. This may lead to a non-conservative response vis-a-vis stability or performance.

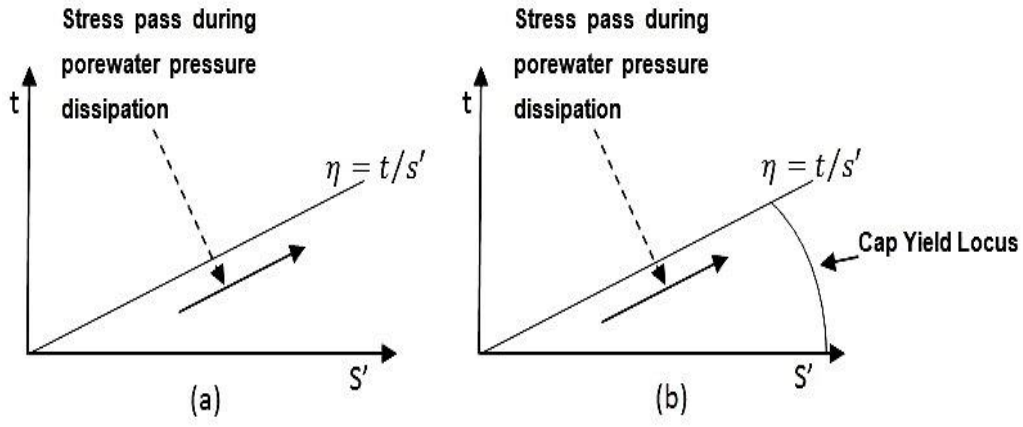

Figure A1: Definition of shear stress ratio in UBCSAND model without cap (a) and with cap (b)

A2. Addition of a cap to the UBCSAND model

As noted before the ability of The UBCSAND model to simulate the post-dynamic response of tailings or sand is limited by the lack of a cap. Therefore, the application of a cap to the model was attamepted.

The cap formulation developed by Vermeer (1980) and adapted by Puebla (1999) was added to version 904aR of the UBCSAND model. The procedure for adding this cap to the model is explained in detail in Puebla (1999).

The yield function of this cap is:

$$f^c = \frac{1}{3}[(\sigma_1')^2 + (\sigma_2')^2 + (\sigma_3')^2] - (\sigma^c)^2 = 0 \qquad (A1)$$

where σ_3', σ_2', and σ_1' are effective principal stresses; σ^c is the isotropic cap pressure (intersection with the p' axis, where $p' = (\sigma_1' + \sigma_3')/2$).

The hardening rule controlling the displacement of the cap is based on the following relationship (Vermeer, 1980; Puebla, 1999):

$$\Delta\varepsilon_v^{pc} = \frac{1}{B^p}\Delta\sigma^c \qquad (A2)$$

where B^p is the plastic bulk modulus, $\Delta\varepsilon_v^{pc}$ is the increment of volumetric plastic strain, and $\Delta\sigma^c$ is the increment of the cap isotropic pressure.

The parameter B^p is defined as:

$$B^p = k_B^p P_A \left(\frac{p'}{P_A}\right)^{mp} \qquad (A3)$$

where k_B^p is the plastic bulk modulus number and *mp* is the plastic bulk modulus exponent, and P_A is atmospheric pressure.

A3. Effect of the cap

The effect of adding the cap was evaluated through comparison of simulated laboratory testing on unit element samples modeled using UBCSAND with and without a cap. As described below, the simulations showed a significant difference in the volumetric strain behavior due to the presence of a cap.

A3.1 Simulation of isotropic compression testing

A plane strain 1-m-square unit element was subjected to isotropic compression at a constant displacement rate of $1x10^{-5}$ m/s. The input parameters are shown in Table A1. The loading was stopped when the mean effective stress, p', reached 500 kPa. An initial cap pressure of 10 kPa was included. As shown in Figure A2, the value of the volumetric strain for the model without a cap when the effective stress reached 500 kPa was 0.4% while it was 1.7% for the model with a cap. The volumetric strain in the model with a cap was thus 4.5 times larger than for the model without a cap. As will be shown below, this larger value appears to be more realistic.

Table A1- Input parameters used to model isotropic compression and oedometer testing

UBCSAND model	$(N_1)_{60\text{-}cs}$	Density (tonnes/m^3)	ϕ_{cv}°	Porosity	Hydraulic conductivity (m/s)	Initial σ_c' (kPa)
with cap	13	2.41	35.6	0.38	4.5e-7	10
without cap	13	2.41	35.6	0.38	4.5e-7	--

ϕ_{cv}°=constant volume friction angle

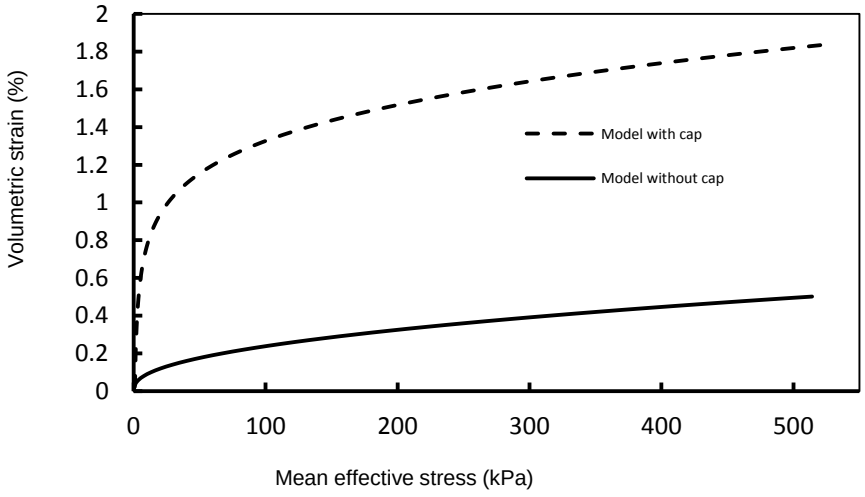

Figure A2 : Volumetric strain versus mean effective stress p' obtained with the UBCSAND model with and without a cap during isotropic compression test simulation

A3.2 Simulation of oedometer testing

A plane strain 1-m-square unit element was subjected to oedometric testing (i.e axial loading with vertical displacement but no lateral displacement). The input parameters were the same as those used for the isotropic compression testing simulation. The upper boundary of the specimen was displaced downwards at a rate of $1x10^{-6}$ m/s to simulate strain-controlled oedometer testing. The test was stopped when the effective mean stress p' reached 50 kPa.

The value of axial strain at the end of the simulated test without a cap was 0.1% while it was 0.9% with a cap (see Figure A3). Again, the presence of a cap (closed yielding surface) resulted in significantly more axial (and volumetric) strain.

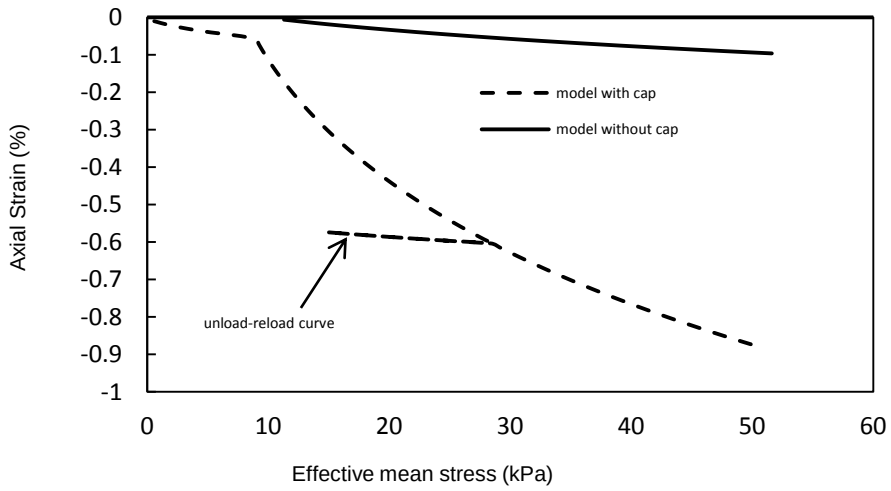

Figure A3: Axial strain versus mean effective stress p' in oedometer test simulations using the UBCSAND model with and without a cap

A3.3 Dynamic numerical modeling of tailings under level ground conditions

To evaluate the UBCSAND model with a cap under more realistic conditions, a 15-m deep tailings deposit underlain by 2 m of dense till and then by hard rock was simulated with FLAC. The mesh was 130-m-wide and 18 m-high, with 1-m-square elements. The surface of the tailings was assumed to be flat to impose level ground conditions. The groundwater table was positioned at the surface of the tailings. The material properties used for the tailings were the same as those used above. Typical published values were used for the till and bedrock (James, 2009).

Ground motion record S-16T of the 1988 Saguenay earthquake (moment magnitude 5.9) (NRC, 2003), was scaled and applied at the bottom of the model to simulate the occurrence of an earthquake that would induce liquefaction throughout the depth of the tailings. As a result of this loading, excess pore water pressures were generated and liquefaction developed throughout the tailings deposit.

Post-shaking analysis was done using the mechanical and fluid analysis modes in parallel and allowing reconsolidation due to excess pore water pressure dissipation.

During early dynamic analyses, the UBCSAND model with a cap developed numerical errors that prevented completion of the analysis. These errors were attributed to numerical singularities that occurred at intersection of the cap with the shear yield surface. Therefore, a high value of the

isotropic cap pressure (σ_c' = 1000 kPa) was assigned for the dynamic analysis to prevent stress paths from reaching the cap.

The post-shaking analysis indicated 32 cm settlement of the surface of the 15-m thick tailings. At the end of shaking, the average excess pore water pressure ratio, r_u, in the zones of the center-column of tailings was 0.94. Given this value the settlement of the tailings was expected to be between 24 and 40 cm based on the empirical method of Wijewickreme and Sanin (2010).

The approach described above ultimately resulted in acceptable results. However, the use of an arbitrary cap pressure to prevent the development of numerical singularities is a fault that belies the ability of this version of the UBCSAND model (with a cap) to realistically simulate post-liquefaction behavior (Ferdosi et la. 2013).

APPENDIX B- NUMERICAL MODELING OF SEISMIC TABLE TESTING OF TAILINGS WITH AND WITHOUT INCLUSION

ABSTRACT

A new co-disposal method consisting of the construction of inclusions made of waste rock in tailings impoundments was proposed by Aubertin et al. (2002) to provide drainage and reinforcement. Research on this innovative disposal method has included intermediate scale physical models and numerical analyses. This paper presents 2D dynamic numerical simulations of instrumented seismic table testing of tailings, with and without inclusion. The goal of the ongoing numerical modelling is to validate and calibrate the use of the UBCSAND model in FLAC using the tests results. The results of the numerical simulations of the seismic table testing indicate that there is an encouraging agreement with the actual experimental data. There are however some differences regarding the rate of excess pore water pressure generation. Key results are presented and briefly discussed in this article.

B1. INTRODUCTION

Impoundments used for storage of hydraulically-deposited tailings may be highly susceptible to statically or seismically-induced liquefaction that can cause failure. There have been several notable failures of tailings impoundments due to the seismic activity that induced excess pore water pressure generation and liquefaction in the retained tailings (Ishihara, 1984; ICOLD, 2001; WISE, 2014). Due to their permanence and the potential for, and effects of, liquefaction of tailings, their dynamic behavior, even in regions of relatively low seismicity, must be considered in stability and performance evaluations.

Several studies , such as Mittal and Morgenstern (1975), Ishihara et al. (1980, 1981), Graga and Mckay (1984), Troncoso and Verdugo (1985), Troncoso (1986), Wijewickreme et al. (2005), Al-Tarhouni (2011), and James et al. (2011), have been conducted using cyclic simple/direct shear or cyclic triaxial testing of tailings, so their dynamic behavior is fairly well understood. Nonetheless, as the vast majority of research has been conducted on the dynamic behavior of naturally occurring soils, the important differences between the behaviors of soils and tailings have raised questions regarding the application of existing methods of analysis and evaluation

(e.g. the simplified method of liquefaction analysis of the UBCSAND model) to the latter, which may require further calibration.

Adalier et al. (2003) conducted seismic table testing of non-plastic silt with and without stone columns (inclusions). It was shown that these columns retarded the pore water pressure generation within the silt during cyclic loading. This reduction was attributed to the increased rigidity of the mass (silt and inclusions) which reduced shear strains. The effect of drainage via the sand columns during cyclic loading was minimal due to the relatively low hydraulic conductivity of the silt and short duration of the tests. Similarly, waste rock inclusions in tailings impoundments are expected to provide drainage during tailings deposition (Bolduc and Aubertin, 2013, 2014) and reinforcement (James and Aubertin 2012) during seismic loading.

The UBCSAND model was developed by Byrne and his collaborators (Byrne et al. 1995; Puebla1995; Puebla et al.1997; Beaty and Byrne1998, 2011; Naesgaard 2011) for simulation of the pore water pressure generation and liquefaction of sandy soils. James (2009) used the UBCSAND model to simulate the cyclic simple shear testing of tailings over a range to confining stresses (100 to 400 kPa) and cyclic stress ratios (0.075 to 0.15) and found reasonably good agreement with respect to excess pore water pressure generation,shear strain development and the number of cycles of loading required to induce liquefaction.

Pépin et al. (2012a, 2012b) conducted nine seismic shaking table tests on tailings including 5 tests with an inclusion consisting of more rigid and/or more pervious material than the tailings (see also Pépin 2010). The results indicate that such inclusions can reduce and/or retard excess pore water pressure generation during cyclic loading. Ferdosi et al. (2013) developed a procedure to model post-seismic consolidation of tailings using updating the shear and bulk moduli of the UBCSAND model based on consolidation tests performed on tailings. The simulations of shaking table testing were in good agreement with the post-shaking settlements measured by Pépin et al. (2012a, 2012b).

To validate and calibrate the use of the UBCSAND model with respect the simulation of the tailings response, two of the seismic table tests reported by Pépin et al. (2012a; 2012b) were modelled numerically in plane strain conditions. One test was conducted on tailings alone and the other was conducted with a relatively thin wall of sand in the center of the rigid box containing the tailings, aligned perpendicularly to the direction of loading.

B2. Numerical modeling of a shaking table test on tailings

Pépin (2010) and Pépin et al. (2012a, 2012b) conducted nine seismic table tests to investigate the dynamic behavior of tailings with and without inclusion. Two tests are the subject of the numerical modeling described herein; a test on tailings without an inclusion and a test on tailings with an inclusion consisting of a sand wall.

Table B1: Summary of tailings characteristics for test 3 (after Pépin et al. 2012b).

Characteristics	Tailings
USCS classification	ML
Relative density, Dr	3.39
Hydraulic conductivity, ksat (cm/s)	2.2×10-5
Void ratio, e	0.62
Maximum void ratio, emax	1.46
Minimum void ratio, emin	0.48
D10 (mm)	0.005
D50 (mm)	0.04
D60 (mm)	0.048

The test without an inclusion was conducted using lightly tamped, saturated tailings (test 3, Table B1). The density index, I_D, of the tailing was about 80%. The internal dimensions of the rigid box used for the testing are 107 cm by 107 cm in plan and 75 cm in height. The tailings were placed in the box to a height of 51 cm. The main characteristics of the tailings are given in Table B1.

This seismic table test was conducted using a sinusoidal dynamic loading with a theoretical peak horizontal acceleration of 0.1 g and a frequency of 1 Hz for duration of 1,000 seconds. Five fluid pressure sensors were installed at depths of 6.4, 14.4, 19.4, 30.4, and 39.4 cm from the top of the tailings to measure excess pore water pressures during the seismic loading, as shown on Figure B1. The excess pore water pressures (EPWP) generated in the tailings during loading is shown by the dashed lines in Figure B2.

Version 904a of the UBCSAND model as implemented in version 5 of FLAC was used to simulate this seismic table test in plane strain. The input parameters used in the numerical calculations are shown in Table B2.

Based on the density index of the tailings (I_D= 80%), a corrected, clean sand standard penetration resistance blow count, $(N_1)_{60\text{-}CS}$, of 30 was considered. In the UBCSAND model, shear and bulk moduli are calculated from following formulas (Puebla et al. 1997)

$$G = k_g^e P_A \left(\frac{p'}{P_A}\right)^{ne} \tag{B1}$$

$$B = k_B^e P_A \left(\frac{p'}{P_A}\right)^{me} \tag{B2}$$

where k_g^e and k_B^e are the elastic shear and bulk modulus numbers, and ne and me are modulus exponents. The values of shear k_g^e and bulk k_B^e modulus numbers were adjusted based on the laboratory test results; these led to k_g^e= 110 and k_B^e = 261. As the test box is rigid, the dynamic load was applied to the bottom and sides of the model as shown in Figure B1. The seismic load was applied as horizontal velocity based on integration of the acceleration function. Mechanical boundary conditions consisted of vertical fixity at the base of the model. The box was considered to be perfectly rigid.

Table B2: Input parameters used to simulate shaking table test 3 on tailings

$(N_1)_{60}$ (blows/30 cm)	30
Density (tonnes/m3)	2.2
ϕ_{cv} (°)	35.6
Porosity, n	0.39
Shear modulus number	110
Bulk modulus number	261

ϕ_{cv}=constant volume friction angle

Figure B2 shows the measured (laboratory) and calculated (numerical modelling) excess pore water pressures generated at different depths z during dynamic loading. As shown, there is reasonable agreement between the laboratory and numerical results, particularly regarding the magnitude of the EPWP at the end of the shaking. However, the simulated excess pore water pressures evolve more rapidly than those measured in the laboratory. Less time is thus required to attain the maximum pore water pressures in the numerical simulation than in the physical modeling, particularly at depths of 30 and 39 cm, though the maximum values at the end of loading are quite close.

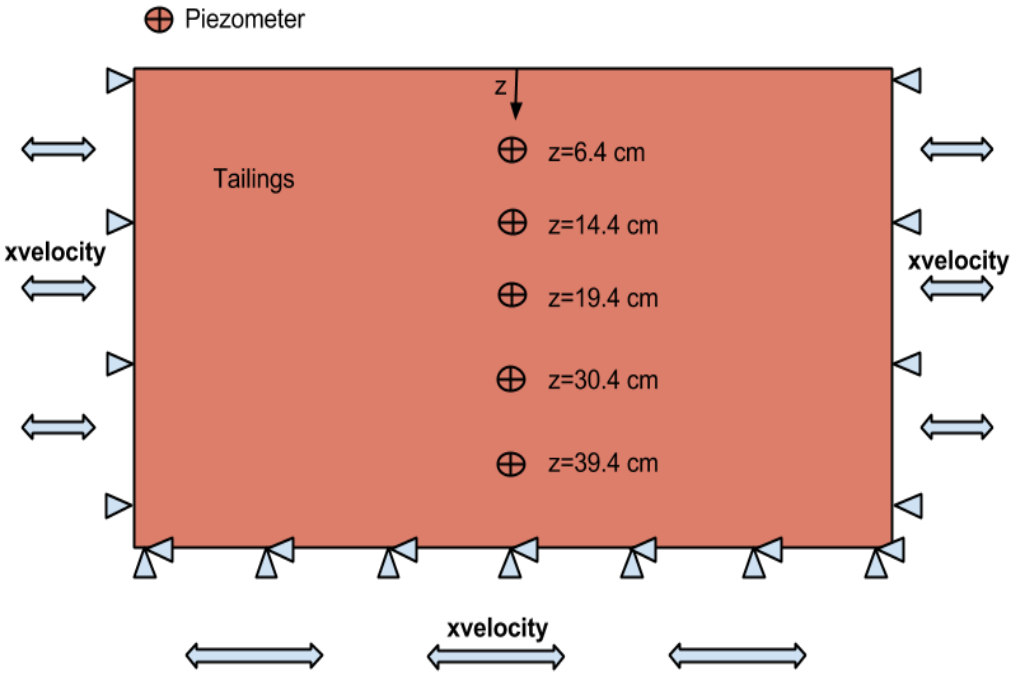

Figure B1: Boundary conditions imposed to the model and piezometric measurement locations

The UBCSAND model is known to underestimate dynamic damping at low levels of shear strain and to overestimate dynamic damping at high levels of shear strains (Beaty and Byrne, 2011). This was considered to be a possible cause for the rapid EPWP development in the numerical simulation shown in Fig. B2, which did not include stiffness proportional damping. Therefore, a minor amount of stiffness proportional Rayleigh damping of 0.05% was assigned to the model during the early phase of calculation. On an element by element basis, the Rayleigh damping was then removed once the shear strain in an individual element reached a threshold value of 0.015%, based on the results of cyclic simple shear testing of sand and comparison of predicted and measured values of damping reported by Beaty and Byrne (2011). Although this value was obtained for sand, it was deemed reasonable for low plasticity tailings (from hard rock mines) given the similarities between these materials (e.g. James et al. 2011). A sensitivity analysis was then conducted with different values of the shear strain threshold (e.g. 0.01%, 0.02%, 0.025%, and 0.03%), which indicated that 0.015% is an appropriate threshold value.

The simulation results obtained with a minor initial value of Rayleigh damping with a threshold shear strain of 0.015% are shown on Figure B3. The addition of the damping slightly alleviated the rapid pore water pressure generation. There is good agreement between the laboratory and

numerical EPWP at all depths, and rates are comparable for sensors located at depths of 6.4, 14.4, and 19.4 cm. However, the rates of EPWP generation in the numerical modelling at depths of 30.4 and 39.4 cm remained significantly higher than those measured.

The good agreement between the maximum values of excess pore water pressures at the end of loading obtained from the physical and laboratory modelling is encouraging, but there is still uncertainty regarding the evolution rate.

It should be recalled here that the 3D rigid box was modelled with FLAC under plane strain conditions. The differences in the rate of generation of excess pore water pressure may be due, at least in part, to the inability of the plane strain model system to simulate all of the mechanisms involved in the dynamic loading of a specimen in a relatively narrow rigid box. Additional work is needed to address this aspect.

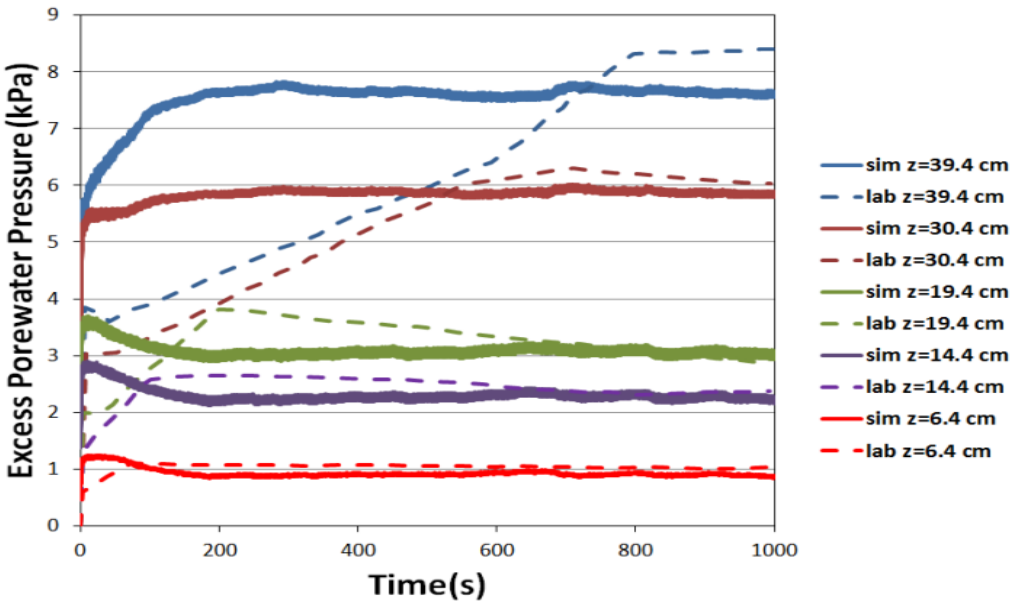

Figure B2: Generated excess pore water pressure measured during test 3 and predicted by the UBCSAND model

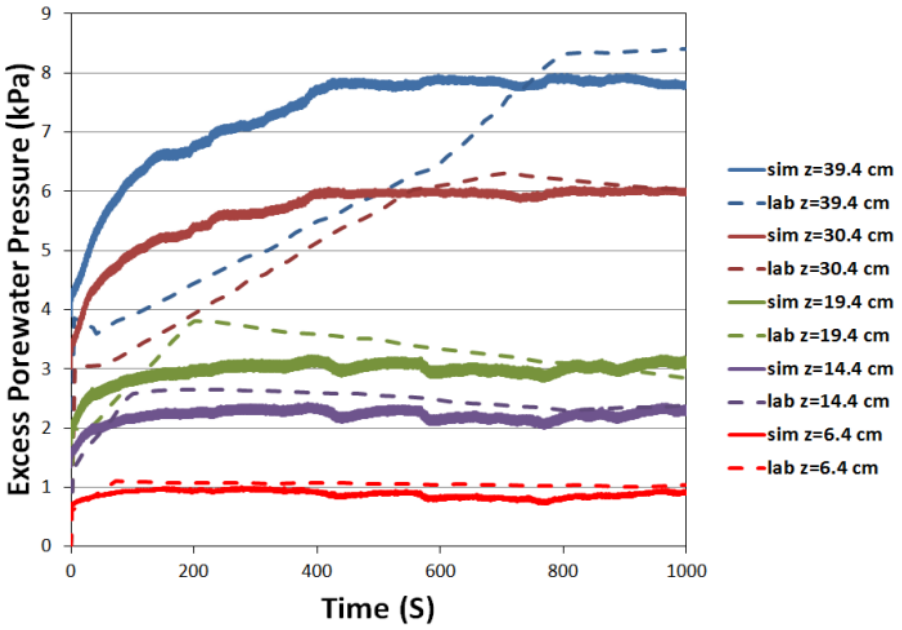

Figure B3: Generated excess pore water pressures measured (test 3) and predicted by the UBCSAND model, considering a small value of stiffness proportional damping for zones in which shear strain is less than 0.015%

B3. Numerical modeling of a shaking table test on tailings with a sand wall

One of the seismic table tests (test 7) conducted by Pépin et al. (2012b) included a sand wall in the tailings. Two aluminium plates were used in the center of the box to construct the sand wall, separating the sand from the tailings. Placement of the sand and tailings was done with the thin plates installed in the box. The deposition of these two materials was done in parallel. The tailings and sand were placed in layers and the former were light tamped to an average density index I_D of about 82%. Then, the aluminium plates were removed slowly from the box. As was the case for all of these tests, the tailings were placed in the box as slurry. The sand was placed in a damp state and then saturated by adding water on top of the model (which was left standing for a few days).

The same cyclic load, characterized by a maximum horizontal acceleration of 0.1g and a frequency of 1 Hz, was applied to the bottom of the box for 1200 seconds. Figure B4 is a schematic of the seismic table test with the tailings and sand wall inclusion; it also shows the

depths of the pore water pressure sensors in the specimen during testing are shown as dashed lines on Figure B5.

In the numerical modelling, the dynamic loading was again applied as velocity time history to the bottom and sides of the model as shown in Figure B4. The material characteristics as presented in Table 3.

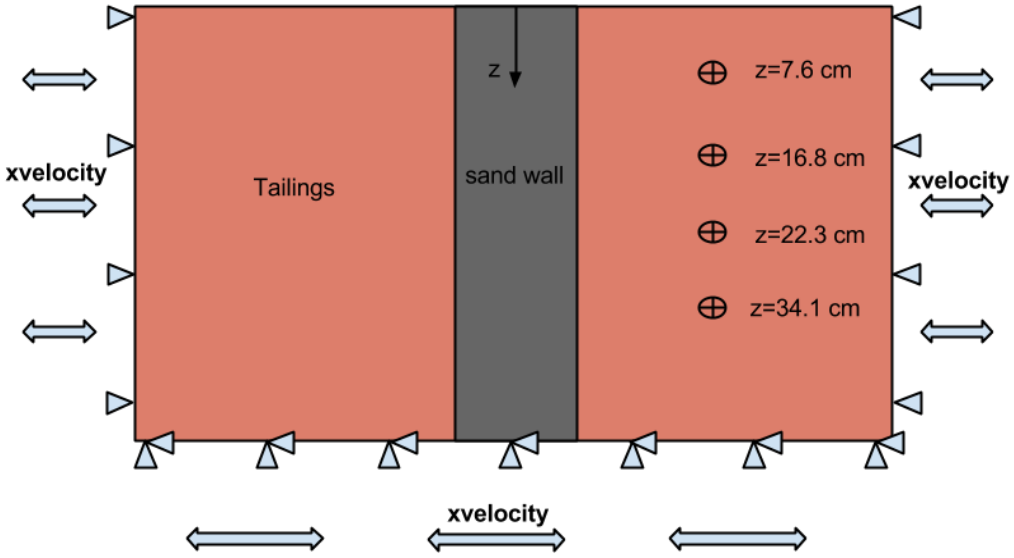

Figure B4: Mechanical boundary conditions with horizontal seismic velocity loads and the position of the piezometers at different depths in the rigid box used for the shaking table test performed on tailings with a sand wall

The numerical simulation of the seismic table test with a sand wall inclusion in the tailings was initially conducted using the same methodology as described above for test 3 without an inclusion. Then a second simulation was conducted in which the finite rigidity of the box was included. The effect of the rigid box was considered as it may have an influence on the rate of pore water pressure generation .This rigidity was taken into account by adding thin elements on the sides of the model. The rigidity (shear G and bulk K moduli) used for these elements was about two orders of magnitude lower than the actual properties of the box; this was still approximately 25 times greater than the stiffness of the tailings. The reduced rigidity was used to reduce computation time, from nearly two months to about one day; this is due to the time step

used in FLAC that can become extremely small when there is a very large contrast in rigidity. This reduced rigidity was nonetheless sufficient for the box to act as a "rigid" body (there was no appreciable deformation at the top of the walls of the box).

Figure B5 presents the results of the laboratory seismic table test with the sand wall (dashed lines) and the results of the numerical modelling. The darker solid lines represent the simulation without consideration of the rigidity of the box and the lighter solid lines represent the simulation when the (reduced) rigidity of the box was taken into account.

As can be seen, consideration of the rigidity of the box had very little effect on excess pore water pressures generation. The EPWP calculated with consideration of the rigidity of the box are slightly lower than those calculated without this consideration, particularly at a depth of 34.1 cm.

Table B3: Input data for the simulation of test 7 on tailings with a sand wall (extracted from Pépin et al. 2012a, 2012b)

Input Parameters	Tailings	Sand (inclusion)
$(N_1)_{60}$	30	40
Dry density (tonnes/m^3)	2.05	1.537
Constant volume friction angle ϕ_{cv} (°)	35.6	35.6
Shear modulus number	110	Computed by the UBCSAND model
Bulk modulus number	261	Computed by the UBCSAND model
Porosity n	0.39	0.425

In Figure B5, the curves identified as '**simu**', '**simR**', and '**test**' show the excess pore water pressures generated during cyclic loading in the model without consideration of the rigidity of the box, with consideration of the rigidity and the actual measurements, respectively.

There is reasonable agreement between the results of the simulations and test for depths 7.6, 16.8, and 22.3 cm as shown in Figure B5. However, at a depth of 34.1 cm the excess pore water pressure generation was much more rapid in the simulations than in the actual test. The pore water pressure values at the end of loading in the simulations are all comparable with those of the actual testing.

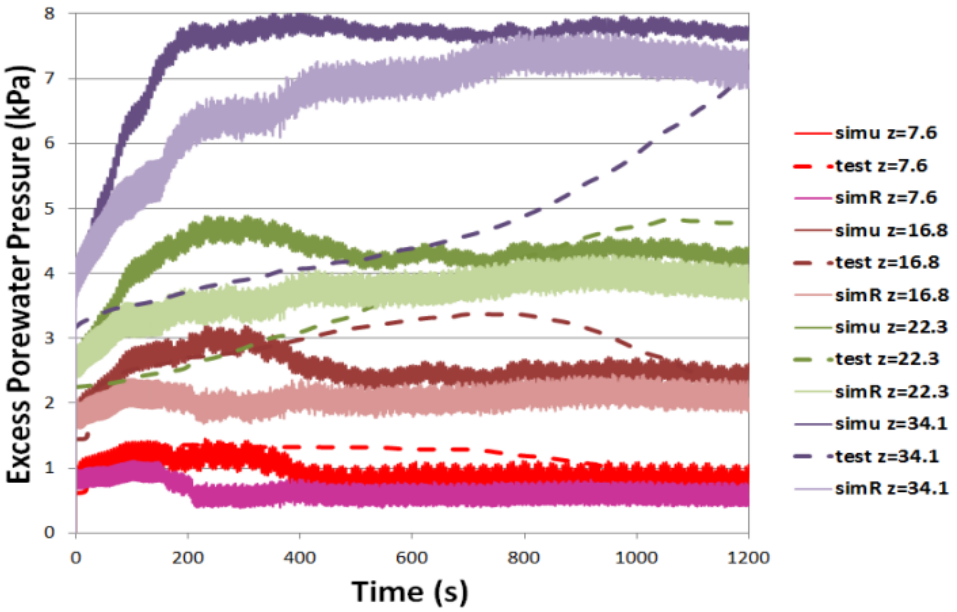

Figure B5: The excess pore water pressures measured during the shaking table test on tailings with a sand wall (test 7); the figure also shows pressured obtained from the simulations of the test with a box of finite rigidity (simR) and without the rigid box (Simu)

Figure B5 also shows that considering the rigidity of the box (but with a reduction by two orders of magnitude) caused a slight decrease in the rate of EPWP generation. The dimensions and rigidity of the box do not permit significant shear strain in the tailings, particularly at bottom of model. Therefore, the rate of pore water generation at the bottom of the tailings specimen should be less than at the top of the model but the simulations results do not show this. This aspect is addressed briefly in the next section.

B4. Discussion

B4.1 Effect of rigid box on pore water pressure generation in shaking table test

A FISH function was written in FLAC to calculate and record the shear strains in the specimen during the simulations. Figures B6 and B7 show the time histories of the shear strains at the bottom and the top of the model with the sand wall inclusion, obtained from the simulations without and with consideration of the relative rigidity of the box, respectively. As shown in Figure B6, the simulated shear strain at the top the model is insignificant relative to that at the bottom of the model.

In reality, because of the finite rigidity of the box and the presence of a free surface at the top, the shear strain at the top should be more than the bottom, as mentioned previously. Therefore, consideration of the rigidity of the box may be an important aspect of the simulation. Figure B7 shows the variation of the simulated shear strains at the bottom and the top of the model for the simulation with consideration of the rigidity of the box. It is seen that the shear strains at the top and bottom of the model are relatively low for the first 200 seconds of loading. However, after 200 seconds the shear strain at the at the top of the model increases in a pseudo-linear manner to the end of loading (1200 second) up to a final value of about 0.17%, while the strain at the top remains almost unchanged.

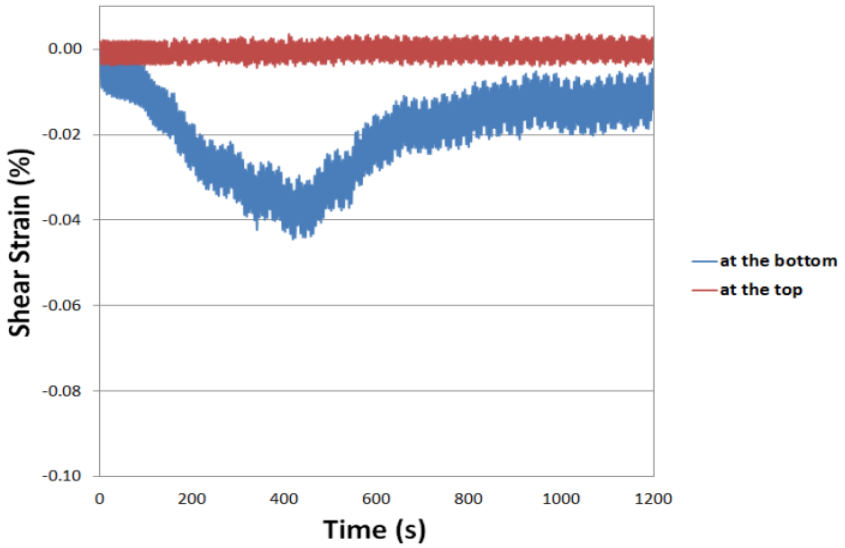

Figure B6: Shear strain histories at the top and bottom of the tailings (test 7) given by simulations without the rigid box

The effect of the relatively rigidity of the box and tailings could partially explain the differences obtained with the simulations (and test) for the rate of excess pore water pressure generation. In the simulations of tailings behavior, without an inclusion, the rigidity of the box was not considered due to the excessive computational time required (approximately one month). Another contributing factor could be the use of plane strain modelling to simulate a three dimensional situation.

DeAlba et al. (1976) demonstrated that the length to width ratio of the specimen box has a significant effect on the generation of excess pore water pressures during seismic table testing. This aspect is not taken into account with FLAC.

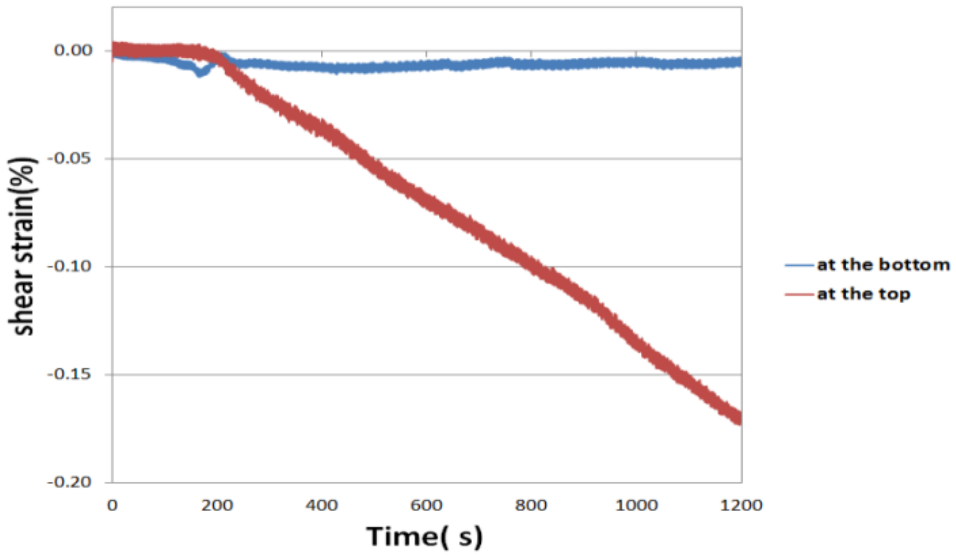

Figure B7: Shear strain histories at the top and the bottom of the tailings (test 7) given by simulations with the rigid box

B4.2 Hydraulic conductivity

Another potentially contributing factor relates to the saturated hydraulic conductivity k_{sat}. As noted above, hydraulic conductivities of $1x10^{-8}$ m/s and $1x10^{-6}$ m/s were used for the tailings and sand for simulation with the rigid box, respectively; for the simulation without the rigid box, hydraulic conductivities of $1x10^{-8}$ m/s and $1x10^{-5}$ m/s were used. Both of these simulations, with and without the rigid box, show reasonable results. The value adopted here for k_{sat} is in the lower range given by Mbonimpa et al. (2002) and Bussière (2007) for hard rock tailings, but it is about an order of magnitude smaller than the value measured by Pépin (2010). As for the sand, the measured value of k_{sat} is $1x10^{-4}$ m/s (Pépin, 2010). As indicated above, the back calculated values for the sand wall are $1x10^{-6}$ and $1x10^{-5}$ m/s for simulations with and without the rigid box, respectively. When the measured value of the hydraulic conductivity is considered for the sand wall, the simulated pore water pressures underestimate the measured values for test 7, and these EPWP dissipate too quickly.

In the actual test, there was no separation between the tailings and the sand. It can be assumed that there was some migration of the finer tailings into the coarse sand during loading. This may explain why the back calculated hydraulic conductivity of the sand wall is lower than the k_{sat} value of the sand.

B4.3 Effect of sand wall on pore water pressure generation in seismic table test

The pore water pressure distribution simulated for the seismic table test performed on the tailings with the sand wall without consideration of the box rigidity, at the end of the shaking, is shown on Figure B8. As the hydraulic conductivity of the sand is one order of magnitude greater than that of the tailings and the sand is stiffer than the tailings, the generated pore water pressure inside of the sand wall is less than in the tailings. The simulated EPWP in the sand are in reasonable agreement with those measured by Pépin (2010).

A comparison of the results of the laboratory seismic table test on the tailings with and without the sand wall inclusion is shown in Figure B9. It is seen that the sand wall inclusion retards the generation of excess pore water pressure in the tailings. This can be attributed mainly to the reinforcing effect of the sand wall (increased rigidity of the tailings/sand mass); drainage through the sand during dynamic loading is expected to have a limited contribution considering the short loading period.

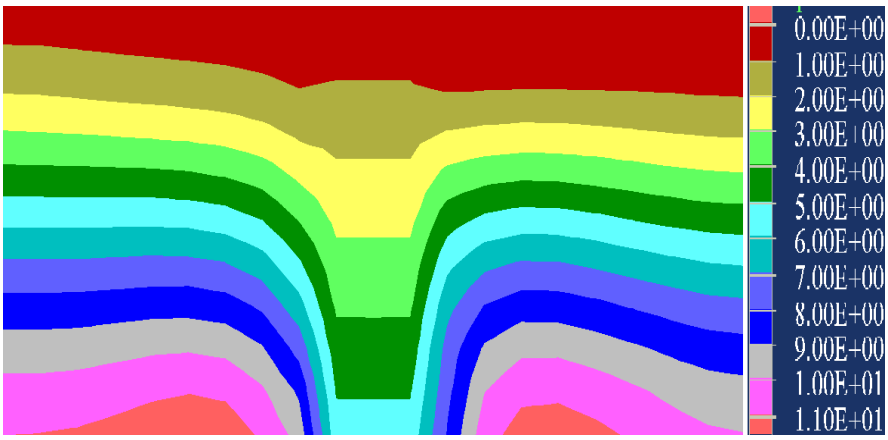

Figure B8: The simulated pore water (kPa) distribution inside of the tailings and sand wall at the end of the seismic loading (test 7)

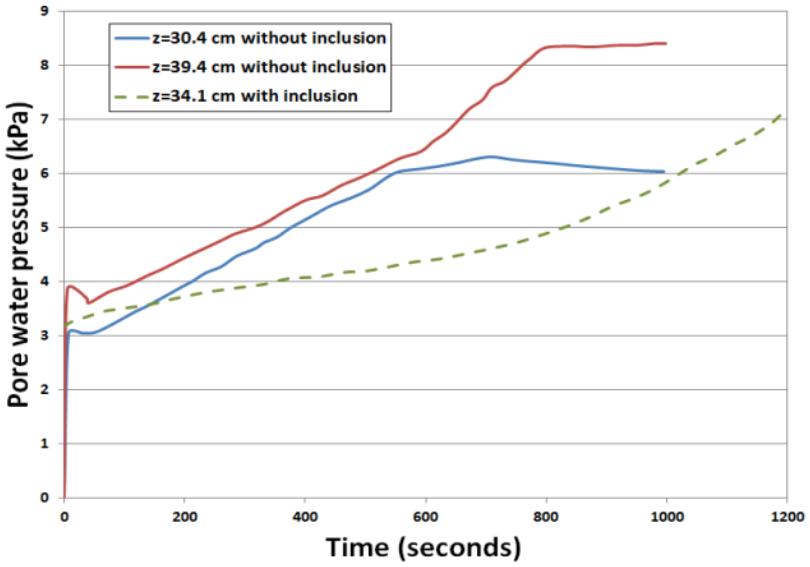

Figure B9: Comparison of the pore water pressures during seismic loading for tests with (test 7) and without (test 3) the sand wall inclusion (extracted from Pépin et al. 2012a)

B5. Conclusion

Seismic table testing of tailings with and without a sand wall inclusion were simulated in FLAC 2D using the UBCSAND model. The results of the simulations show that this method can reasonably reproduce the dynamic behavior, as characterized by the generation of excess pore water pressure of tailings alone and of tailings with a sand wall inclusion under the conditions applied. There are however some discrepancies regarding the rate of EPWP generation at depth in the model. Potential reasons for these differences are discussed briefly in the article.

APPENDIX C-THE RESULTS OF NUMERICAL SIMULATIONS OF A TAILINGS IMPOUNDMENT BASED (LOOSELY) ON A MINE SITE IN NEW BRUNSWICK, CANADA

C1.1 The values of the R_x along the downstream slope of the tailings dyke for the high (Saguenay) and low (Northridge) frequency ground motions

Figure C1 to C39 shows the profile of normalized horizontal displacements of points located along the external slope of the unconsolidated ($(N_1)_{60} = 3$, blows/30 cm) tailings impoundment (R_x) for different arrangements of the waste rock inclusions (WRI) due to the E_1-sag ground motion record (S16T). These figures show the initial profile of the slope of the tailings impoundment. In all the figures shown in this appendix, the arrangements are denoted in the form of wx-dy (where "x" is the width of the inclusion in meters, "y" is the center-to-center spacing of the inclusion in meters); this may be followed by a time (e.g. 19 sec) that indicates the occurrence of an error in the program calculation due to the development of unacceptable geometry in one or more elements.

Figure C1 shows, for instance, that the values of R_x are less than 10% for arrangements w8-d48 and w8-d56. For the w8-d64 arrangement, the value of R_x exceeds 10% for locations between 235 and 305 m. For the other arrangements, the values of R_x are larger than 20% and the model calculations lead to bad geometry in some zones, resulting in computations that were stopped.

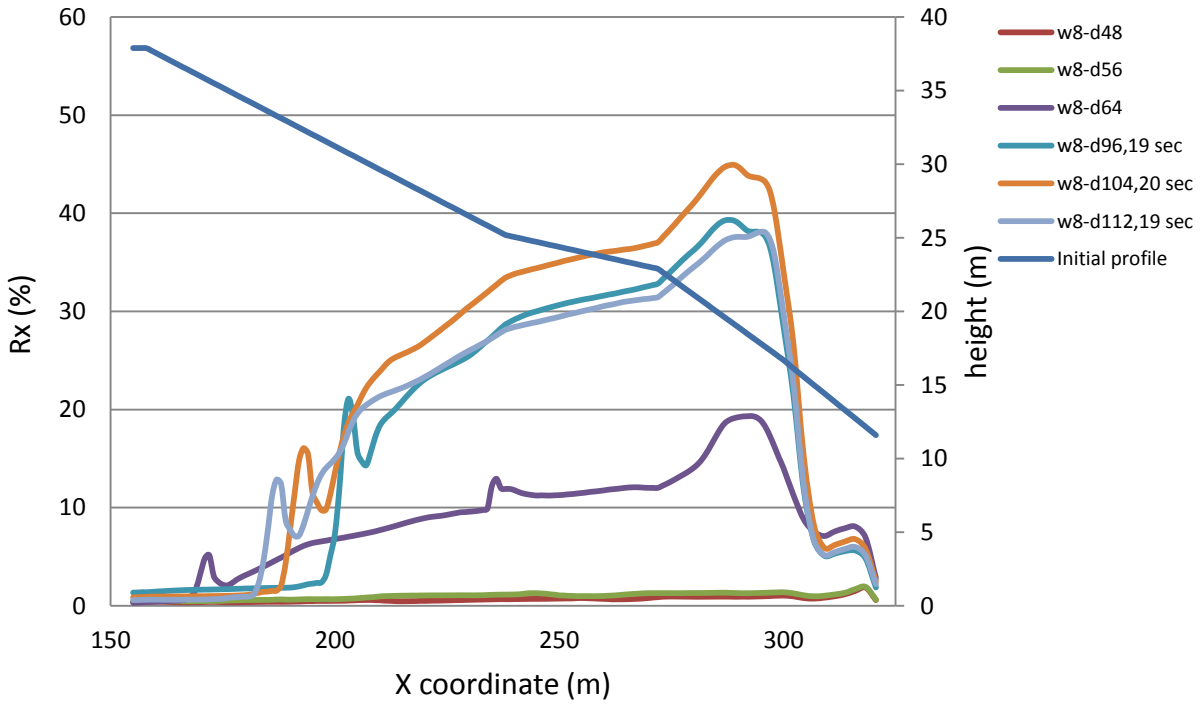

Figure C1: The value of R_x along the slope of the impoundment within unconsolidated tailings ($(N_1)_{60} = 3$, blows/30 cm) due to E_1-sag earthquake record (S16T) for inclusions having a width of 8 meters. In the legend shown at top right, the first number is the width of the inclusions, second number is the center-to-center spacing, and the third number (shown in some cases) represents the time at which the model was stopped due to a bad geometry error

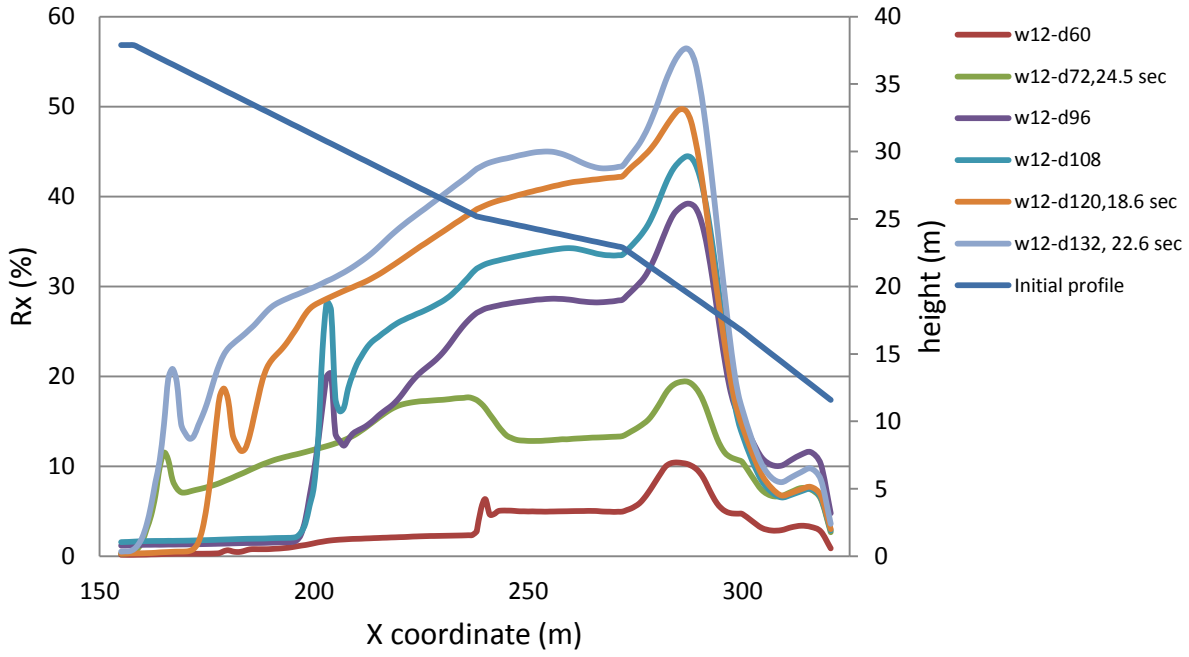

Figure C2: The value of R_x in along the slope of the impoundment within unconsolidated tailings ($(N_1)_{60} = 3$, blows/30 cm) due to E_1-sag earthquake record (S16T) for inclusions with width of 12 meters. In the legend in the right top of the figure, first number is the width of inclusions, second number is center-to-center spacing, and third number in some cases is time that the model was stopped due to bad geometry in a zone

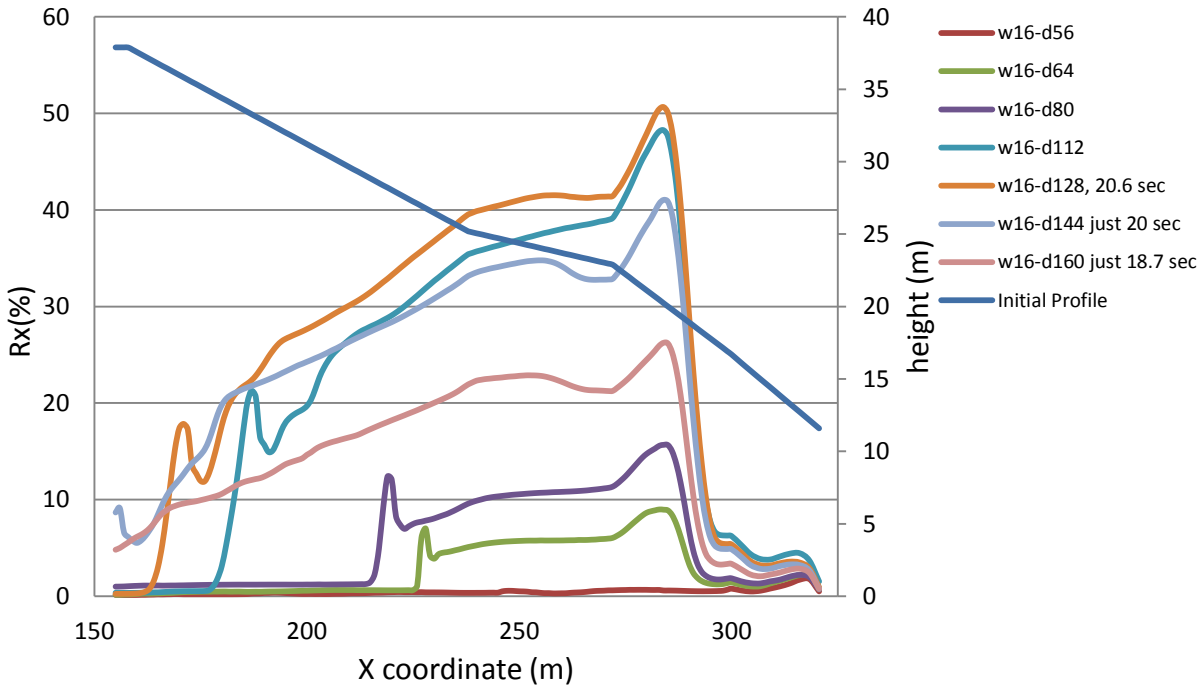

Figure C3: The value of R_x in along the slope of the impoundment within unconsolidated tailings ($(N_1)_{60} = 3$, blows/30 cm) due to E_1-sag earthquake record (S16T) for inclusions with width of 16 meters. In the legend in the right top of the figure, first number is the width of inclusions, second number is center-to-center spacing, and third number in some cases is time that the model was stopped due to bad geometry in a zone

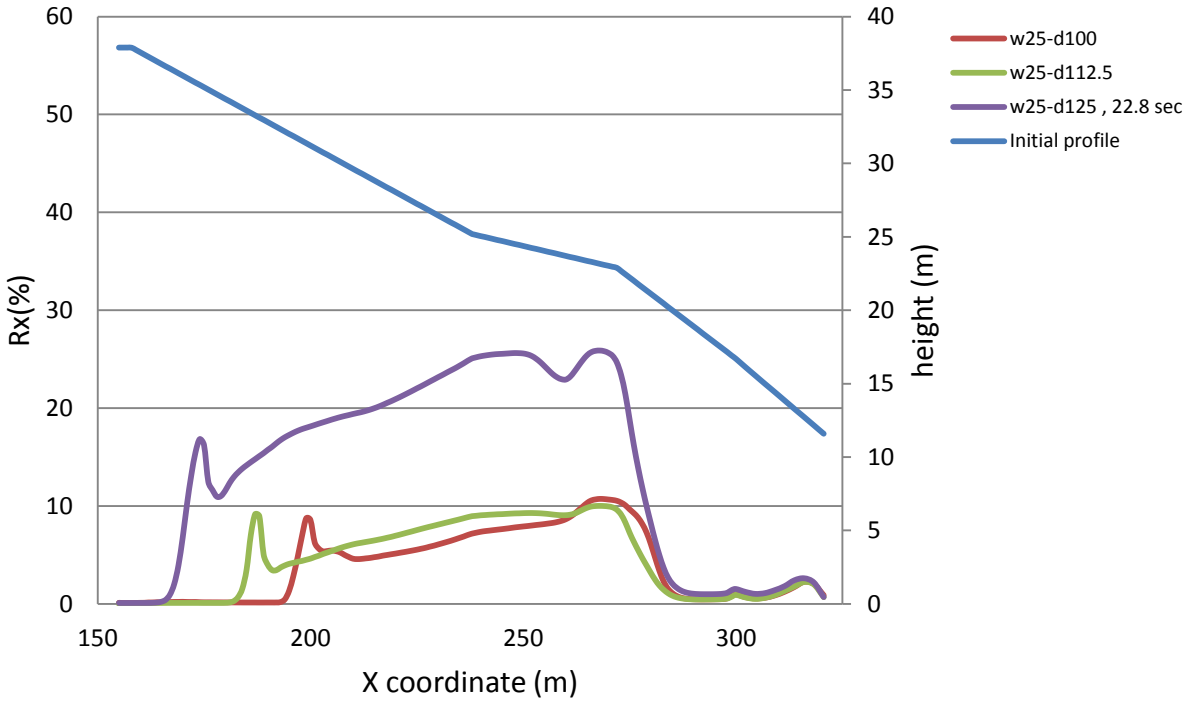

Figure C4: The value of R_x in along the slope of the impoundment within unconsolidated tailings ($(N_1)_{60} = 3$, blows/30 cm) due to E_1-sag earthquake record (S16T) for inclusions with width of 25 meters. In the legend in the right top of the figure, first number is the width of inclusions, second number is center-to-center spacing, and third number in some cases is time that the model was stopped due to bad geometry in a zone

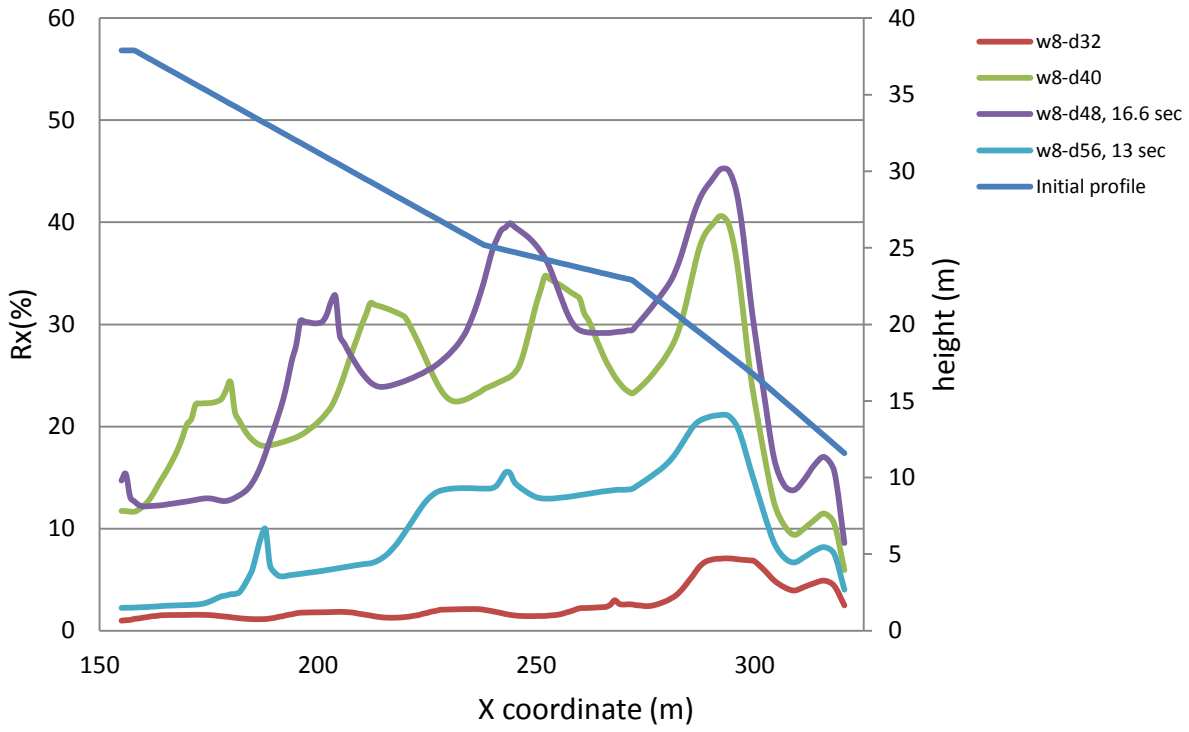

Figure C5: The value of R_x in along the slope of the impoundment within unconsolidated tailings ($(N_1)_{60} = 3$, blows/30 cm) due to E_3-sag earthquake record (S16T) for inclusions with width of 8 meters. In the legend in the right top of the figure, first number is the width of inclusions, second number is center-to-center spacing, and third number in some cases is time that the model was stopped due to bad geometry in a zone

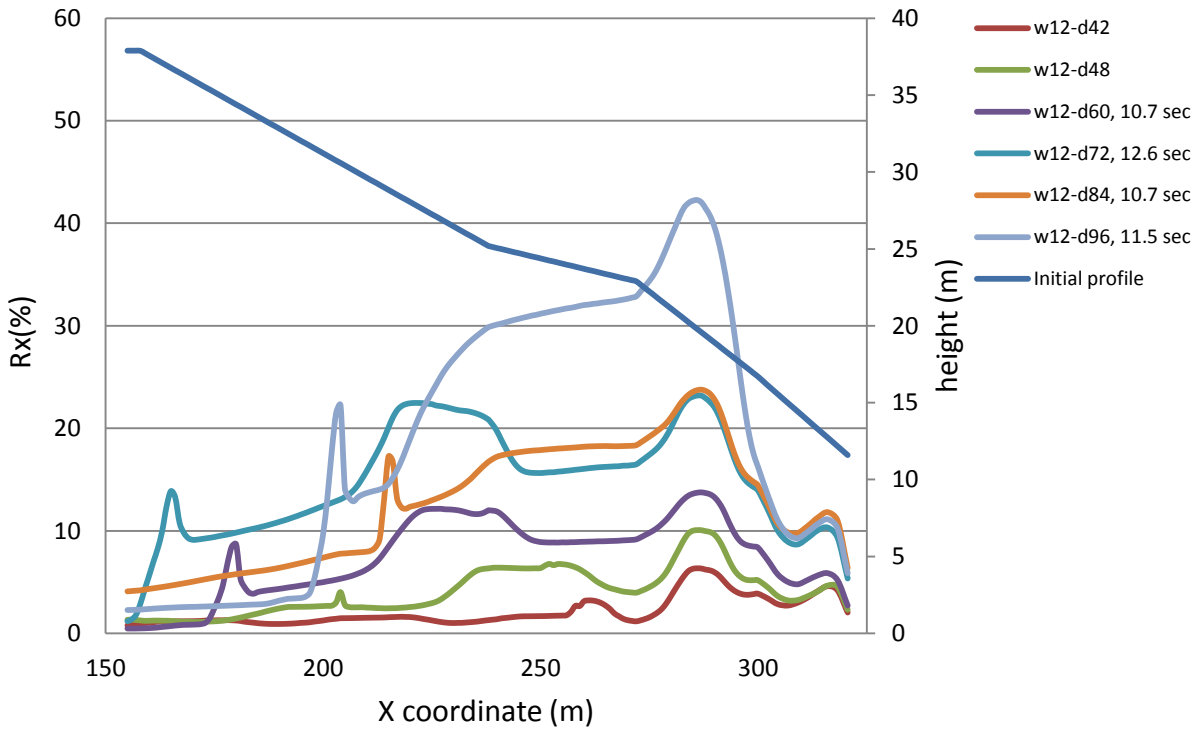

Figure C6: The value of R_x in along the slope of the impoundment within unconsolidated tailings ($(N_1)_{60} = 3$, blows/30 cm) due to E_3-sag earthquake record (S16T) for inclusions with width of 12 meters. In the legend in the right top of the figure, first number is the width of inclusions, second number is center-to-center spacing, and third number in some cases is time that the model was stopped due to bad geometry in a zone

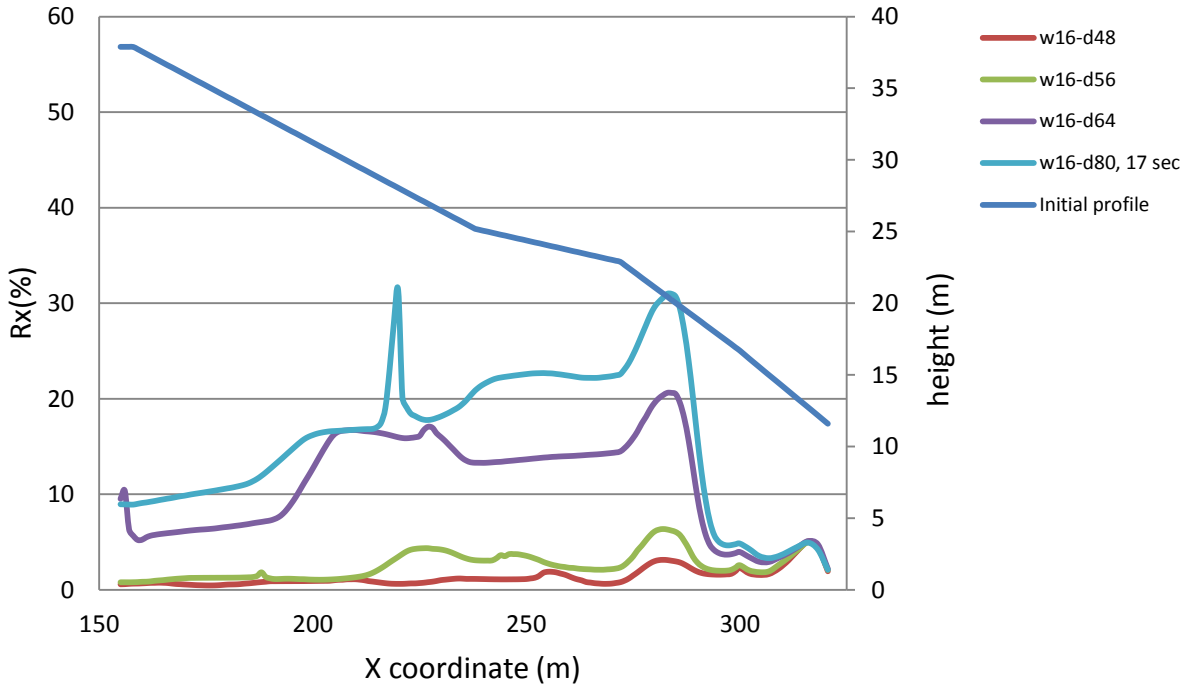

Figure C7: The value of R_x in along the slope of the impoundment within unconsolidated tailings ($(N_1)_{60} = 3$, blows/30 cm) due to E_3-sag earthquake record (S16T) for inclusions with width of 16 meters. In the legend in the right top of the figure, first number is the width of inclusions, second number is center-to-center spacing, and third number in some cases is time that the model was stopped due to bad geometry in a zone

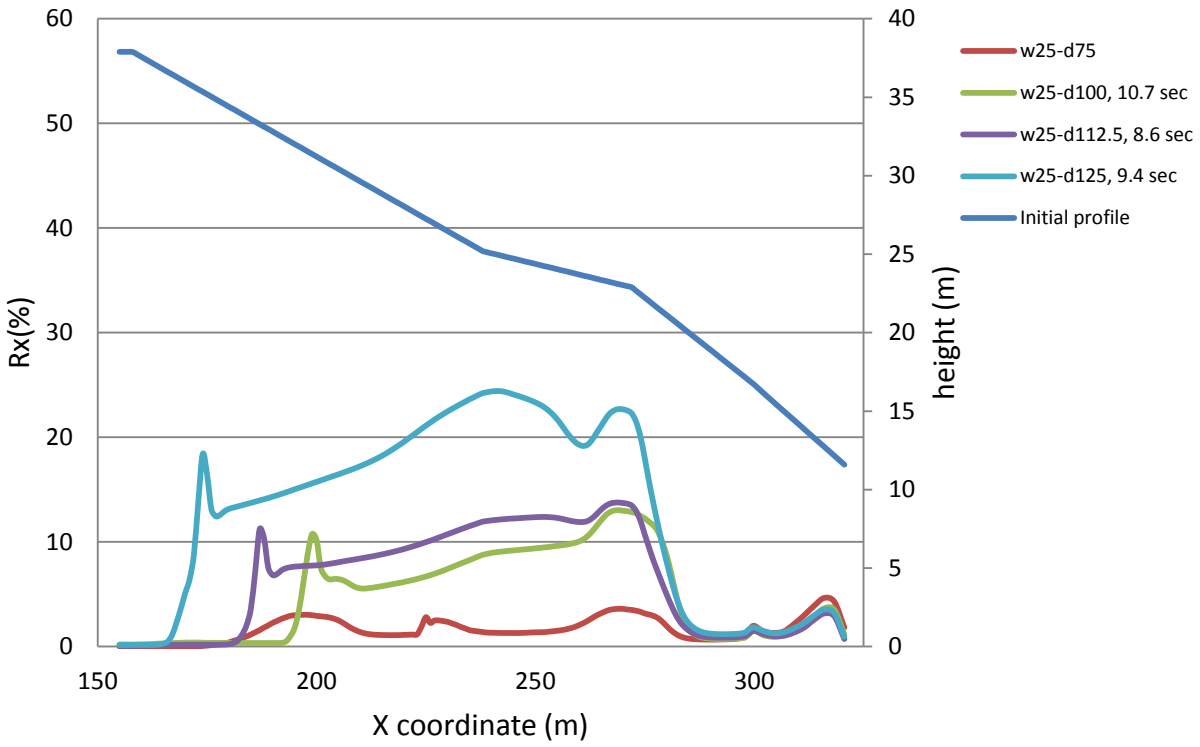

Figure C8: The value of R_x in along the slope of the impoundment within unconsolidated tailings ($(N_1)_{60} = 3$, blows/30 cm) due to E_3-sag earthquake record (S16T) for inclusions with width of 25 meters. In the legend in the right top of the figure, first number is the width of inclusions, second number is center-to-center spacing, and third number in some cases is time that the model was stopped due to bad geometry in a zone

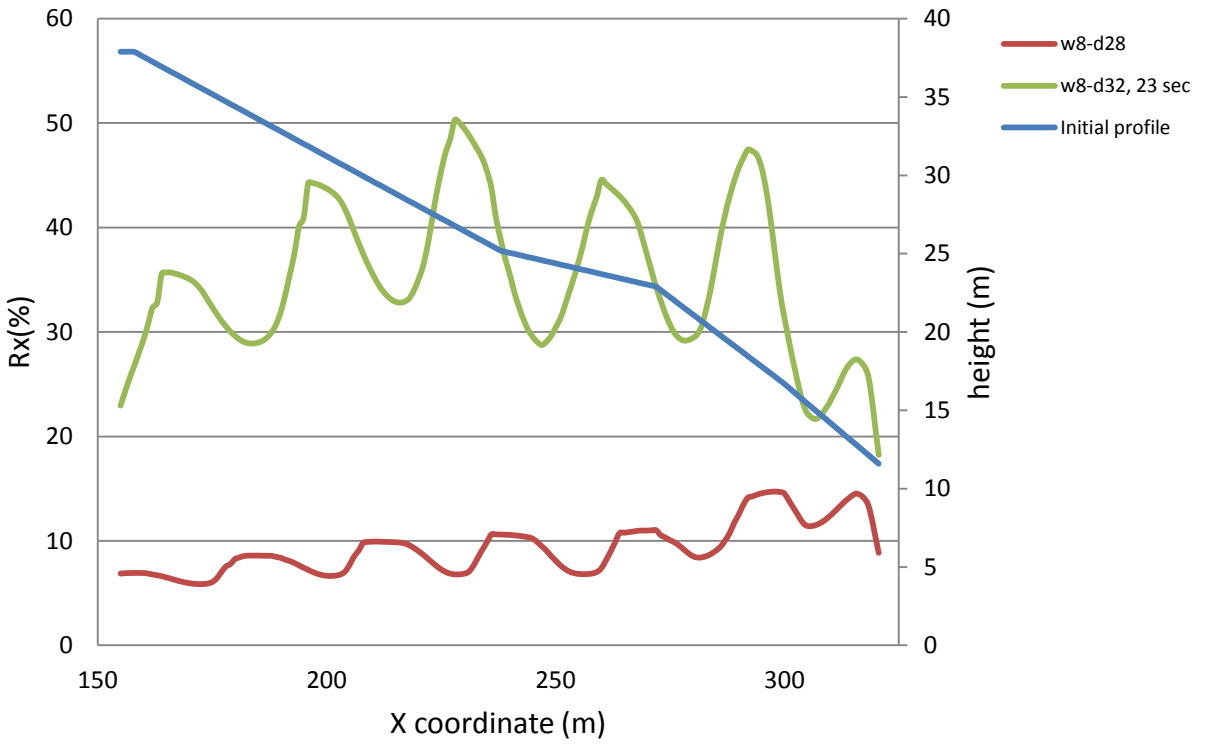

Figure C9: The value of R_x in along the slope of the impoundment within unconsolidated tailings ($(N_1)_{60} = 3$, blows/30 cm) due to E_5-sag earthquake record (S16T) for inclusions with width of 8 meters. In the legend in the right top of the figure, first number is the width of inclusions, second number is center-to-center spacing, and third number in some cases is time that the model was stopped due to bad geometry in a zone

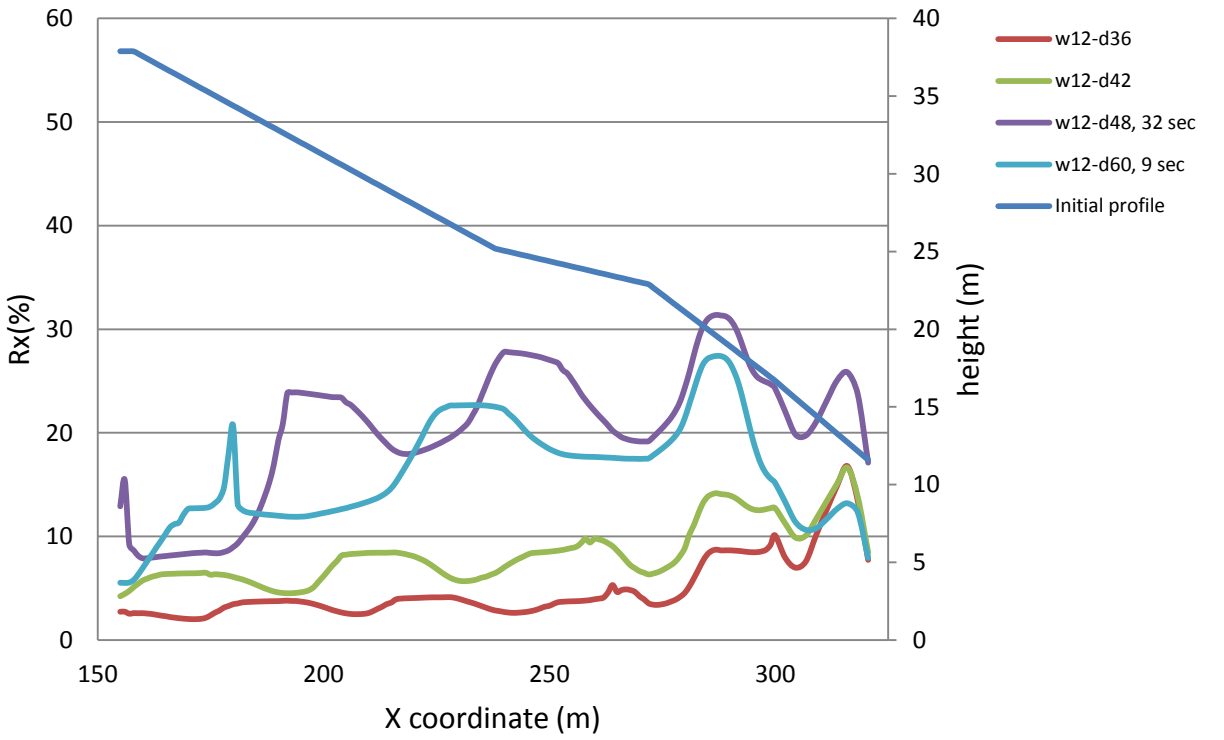

Figure C10: The value of R_x in along the slope of the impoundment within unconsolidated tailings ($(N_1)_{60} = 3$, blows/30 cm) due to E_5-sag earthquake record (S16T) for inclusions with width of 12 meters. In the legend in the right top of the figure, first number is the width of inclusions, second number is center-to-center spacing, and third number in some cases is time that the model was stopped due to bad geometry in a zone

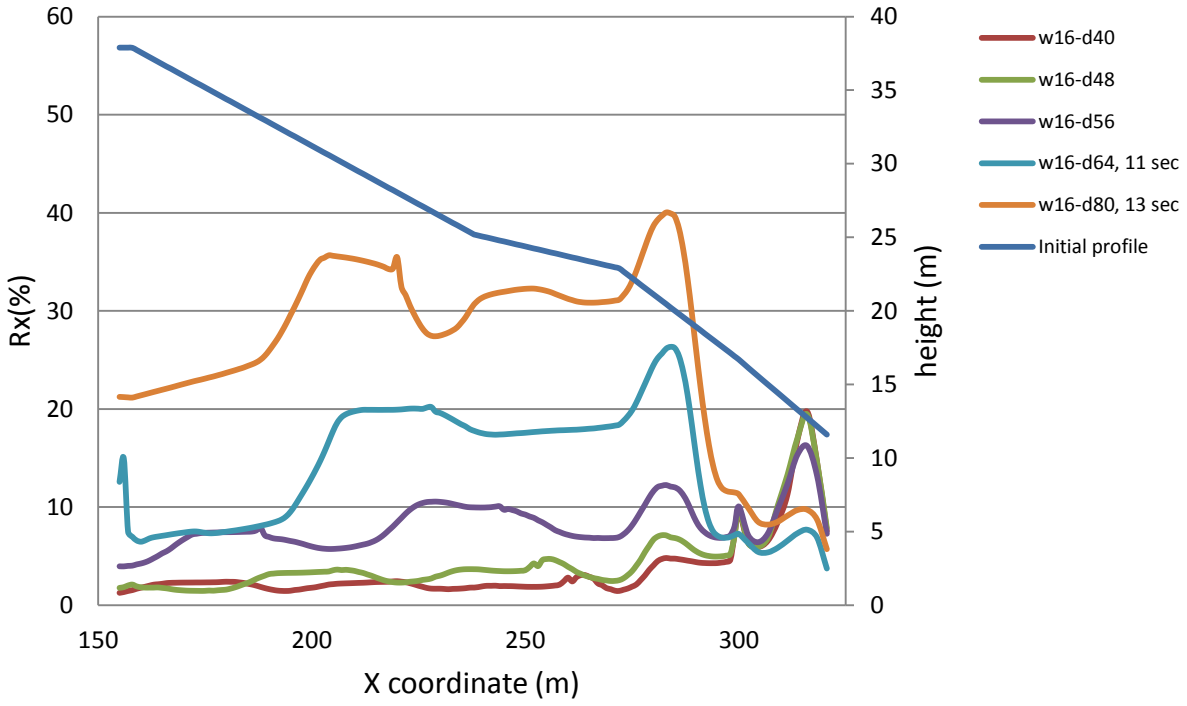

Figure C11: The value of R_x in along the slope of the impoundment within unconsolidated tailings ($(N_1)_{60} = 3$, blows/30 cm) due to E_5-sag earthquake record (S16T) for inclusions with width of 16 meters. In the legend in the right top of the figure, first number is the width of inclusions, second number is center-to-center spacing, and third number in some cases is time that the model was stopped due to bad geometry in a zone

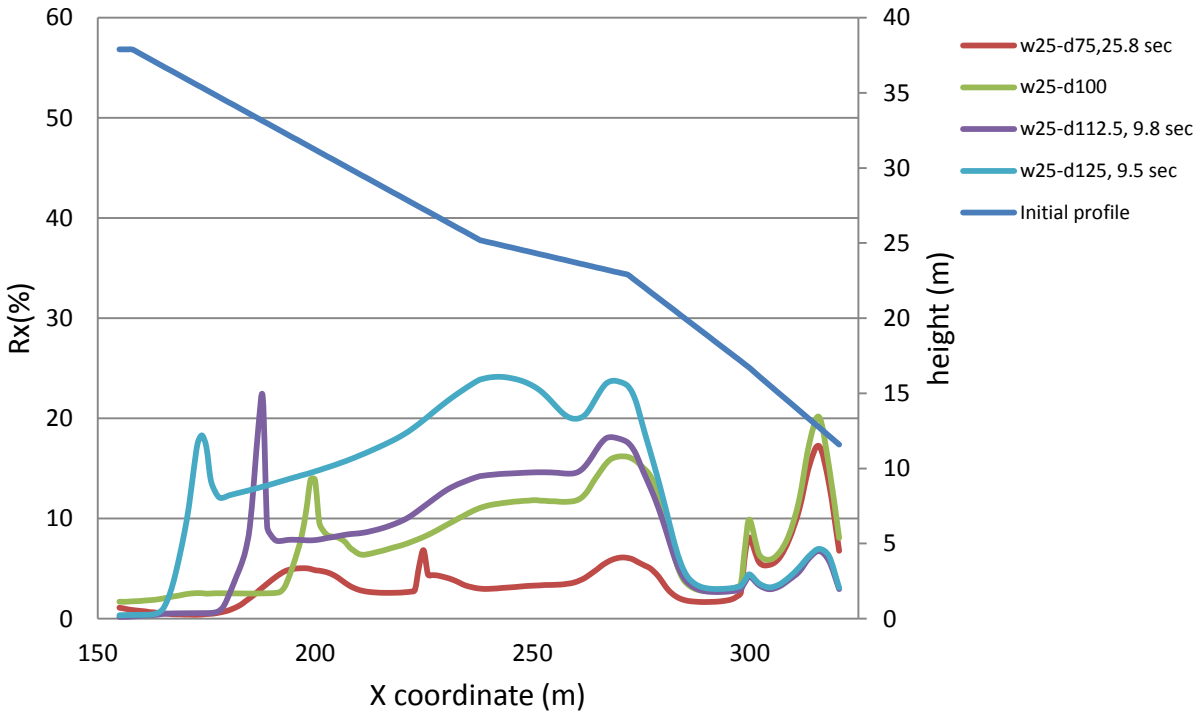

Figure C12: The value of R_x in along the slope of the impoundment within unconsolidated tailings ($(N_1)_{60} = 3$, blows/30 cm) due to E_5-sag earthquake record (S16T) for inclusions with width of 25 meters. In the legend in the right top of the figure, first number is the width of inclusions, second number is center-to-center spacing, and third number in some cases is time that the model was stopped due to bad geometry in a zone

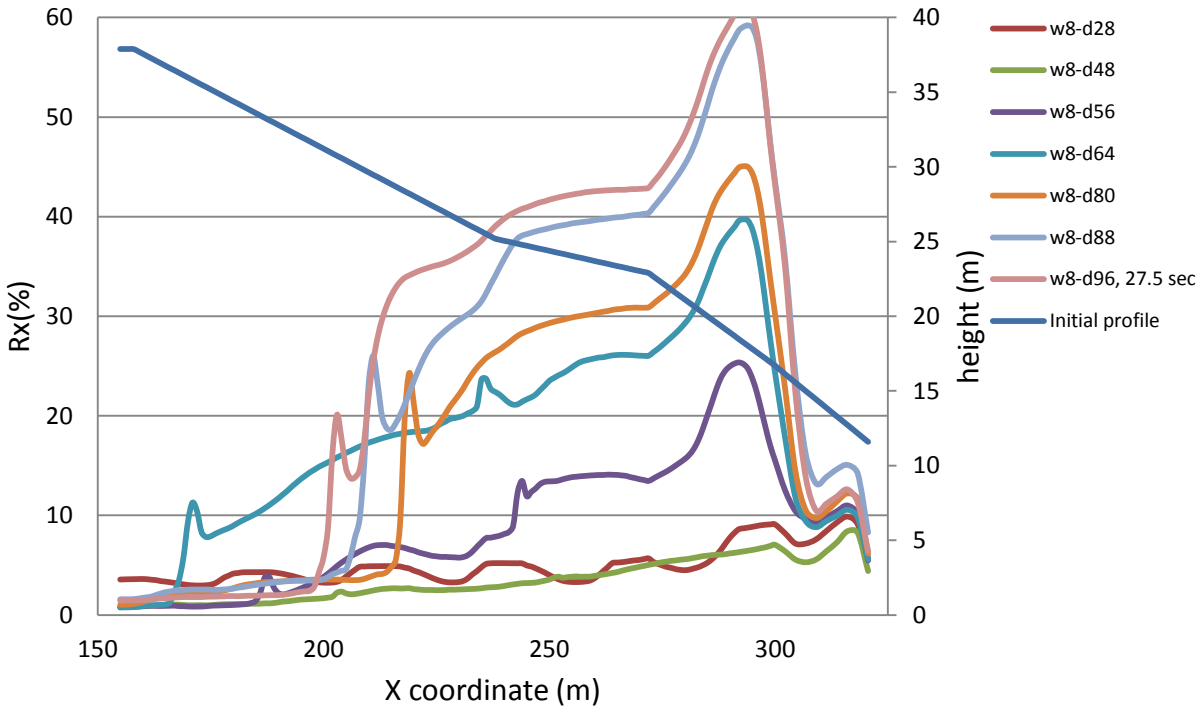

Figure C13: The value of R_x in along the slope of the impoundment within consolidated tailings ($(N_1)_{60} = 8$, blows/30 cm) due to E_4-sag earthquake record (S16T) for inclusions with width of 8 meters. In the legend in the right top of the figure, first number is the width of inclusions, second number is center-to-center spacing, and third number in some cases is time that the model was stopped due to bad geometry in a zone

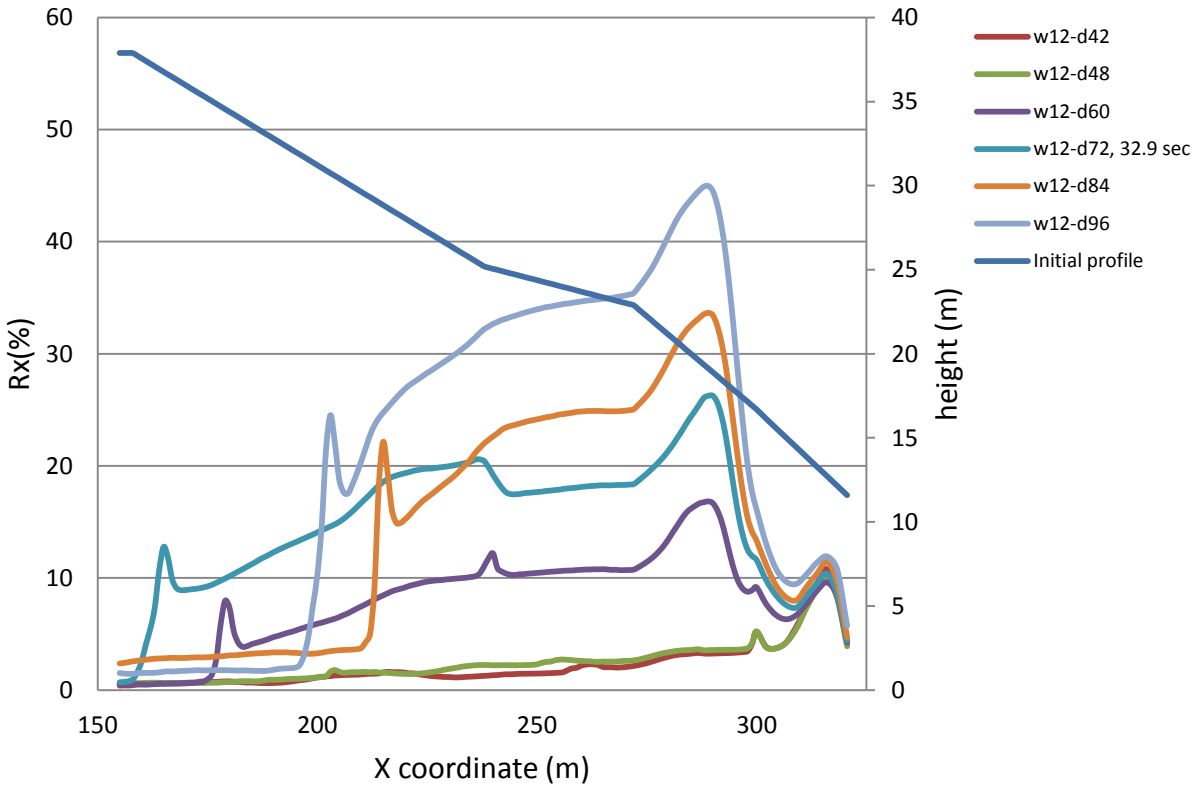

Figure C14: The value of R_x in along the slope of the impoundment within consolidated tailings ($(N_1)_{60} = 8$, blows/30 cm) due to E_4-sag earthquake record (S16T) for inclusions with width of 12 meters. In the legend in the right top of the figure, first number is the width of inclusions, second number is center-to-center spacing, and third number in some cases is time that the model was stopped due to bad geometry in a zone

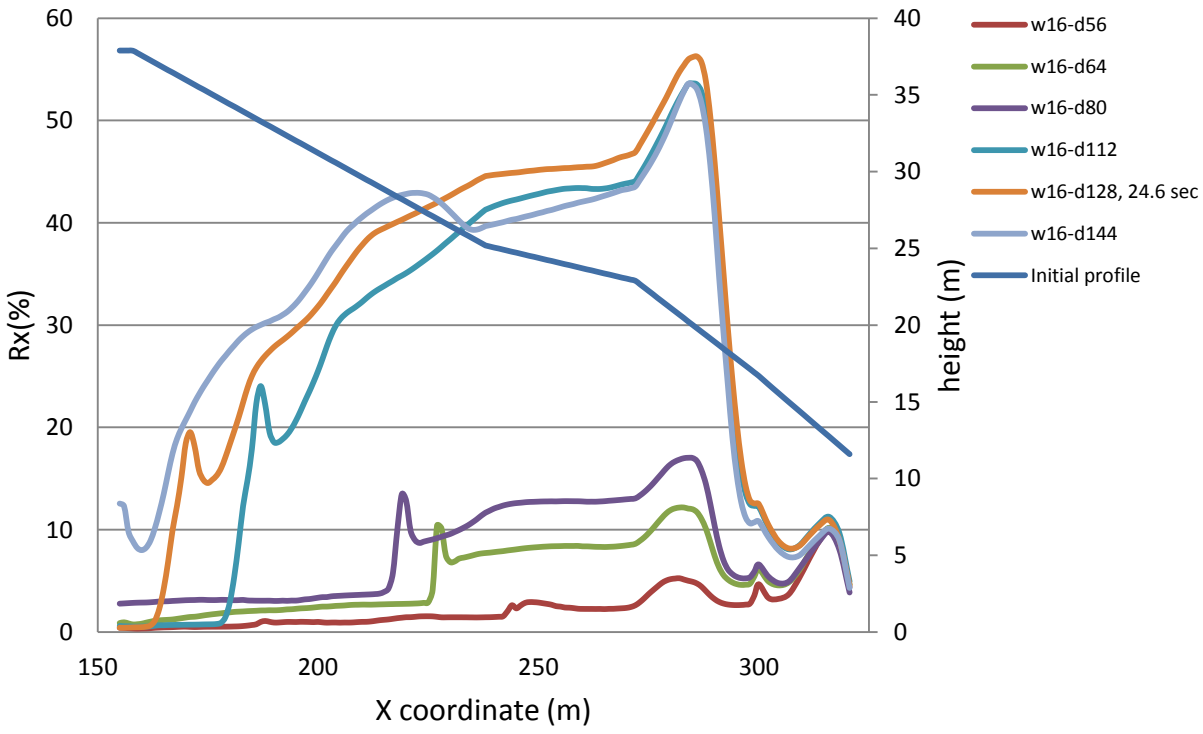

Figure C15: The value of R_x in along the slope of the impoundment within consolidated tailings ($(N_1)_{60} = 8$, blows/30 cm) due to E_4-sag earthquake record (S16T) for inclusions with width of 16 meters. In the legend in the right top of the figure, first number is the width of inclusions, second number is center-to-center spacing, and third number in some cases is time that the model was stopped due to bad geometry in a zone

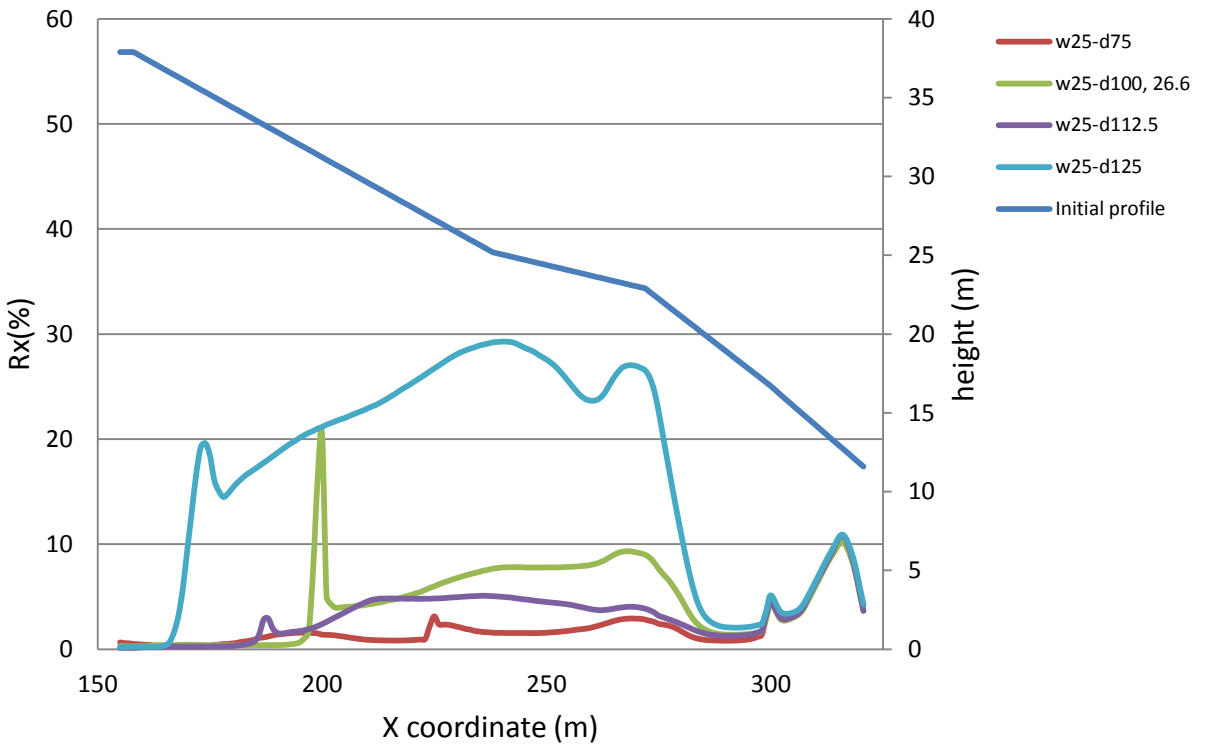

Figure C16: The value of R_x in along the slope of the impoundment within consolidated tailings ($(N_1)_{60} = 8$, blows/30 cm) due to E_4-sag earthquake record (S16T) for inclusions with width of 25 meters. In the legend in the right top of the figure, first number is the width of inclusions, second number is center-to-center spacing, and third number in some cases is time that the model was stopped due to bad geometry in a zone

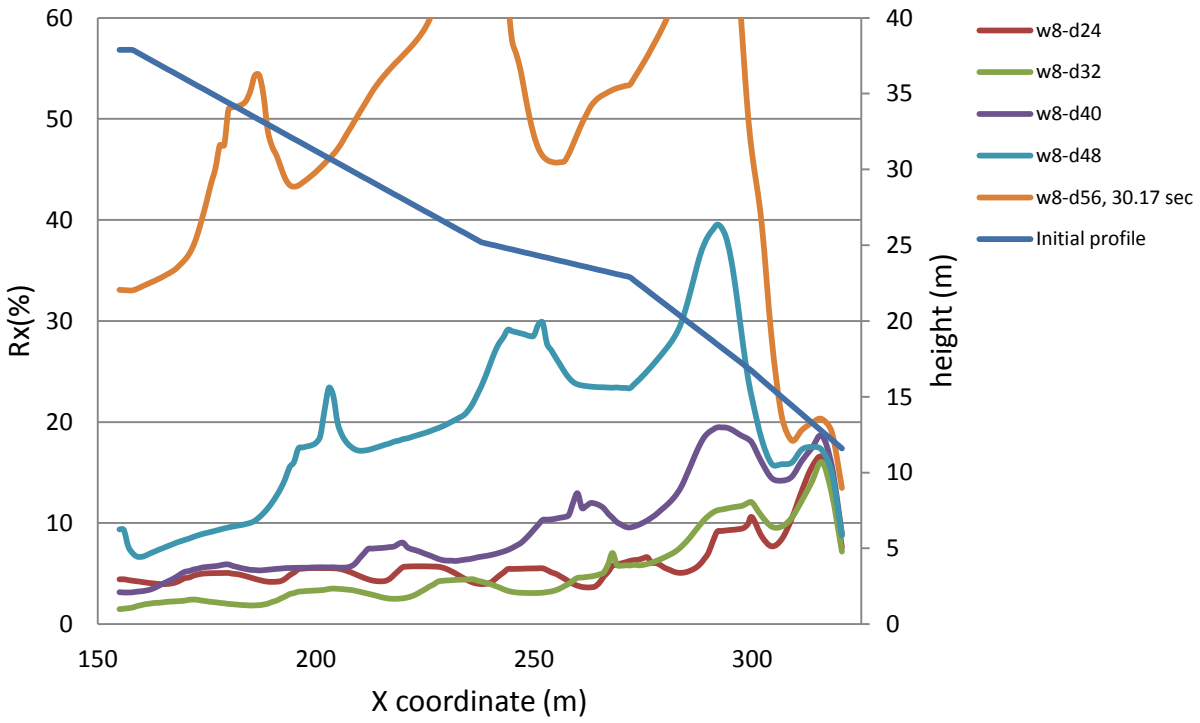

Figure C17: The value of R_x in along the slope of the impoundment within consolidated tailings ($(N_1)_{60} = 8$, blows/30 cm) due to E_5-sag earthquake record (S16T) for inclusions with width of 8 meters. In the legend in the right top of the figure, first number is the width of inclusions, second number is center-to-center spacing, and third number in some cases is time that the model was stopped due to bad geometry in a zone

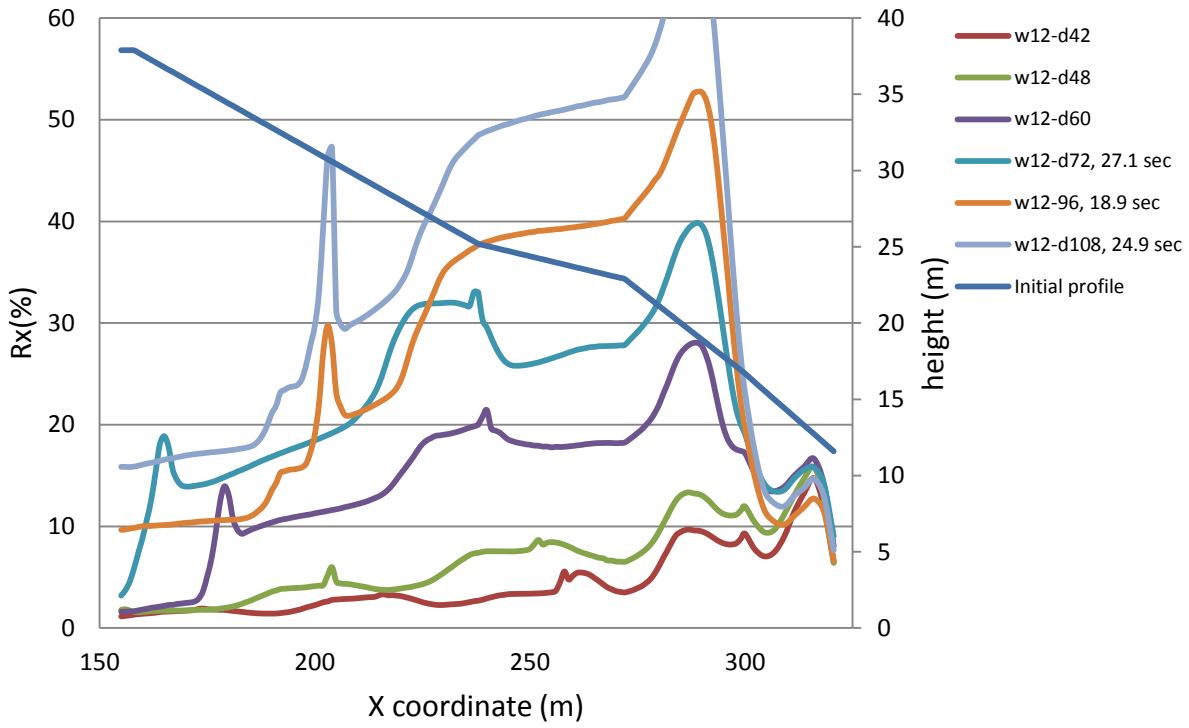

Figure C18: The value of R_x in along the slope of the impoundment within consolidated tailings ($(N_1)_{60} = 8$, blows/30 cm) due to E_5-sag earthquake record (S16T) for inclusions with width of 12 meters. In the legend in the right top of the figure, first number is the width of inclusions, second number is center-to-center spacing, and third number in some cases is time that the model was stopped due to bad geometry in a zone

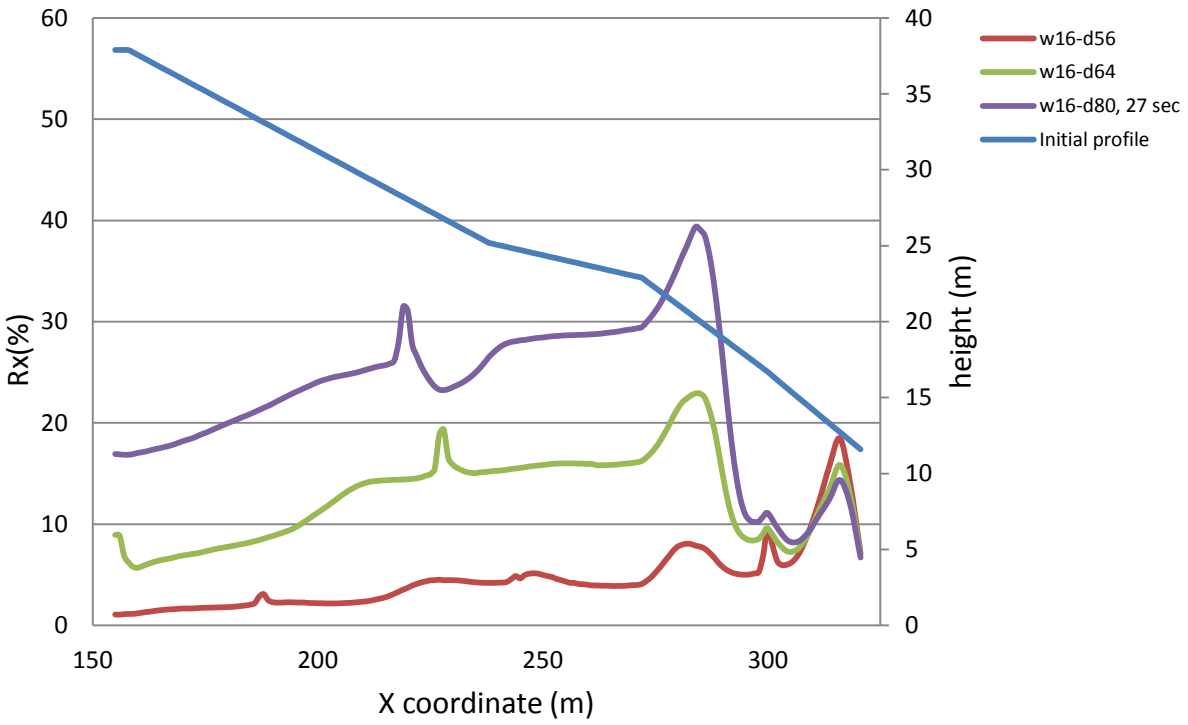

Figure C19: The value of R_x in along the slope of the impoundment within consolidated tailings ($(N_1)_{60} = 8$, blows/30 cm) due to E_5-sag earthquake record (S16T) for inclusions with width of 16 meters. In the legend in the right top of the figure, first number is the width of inclusions, second number is center-to-center spacing, and third number in some cases is time that the model was stopped due to bad geometry in a zone

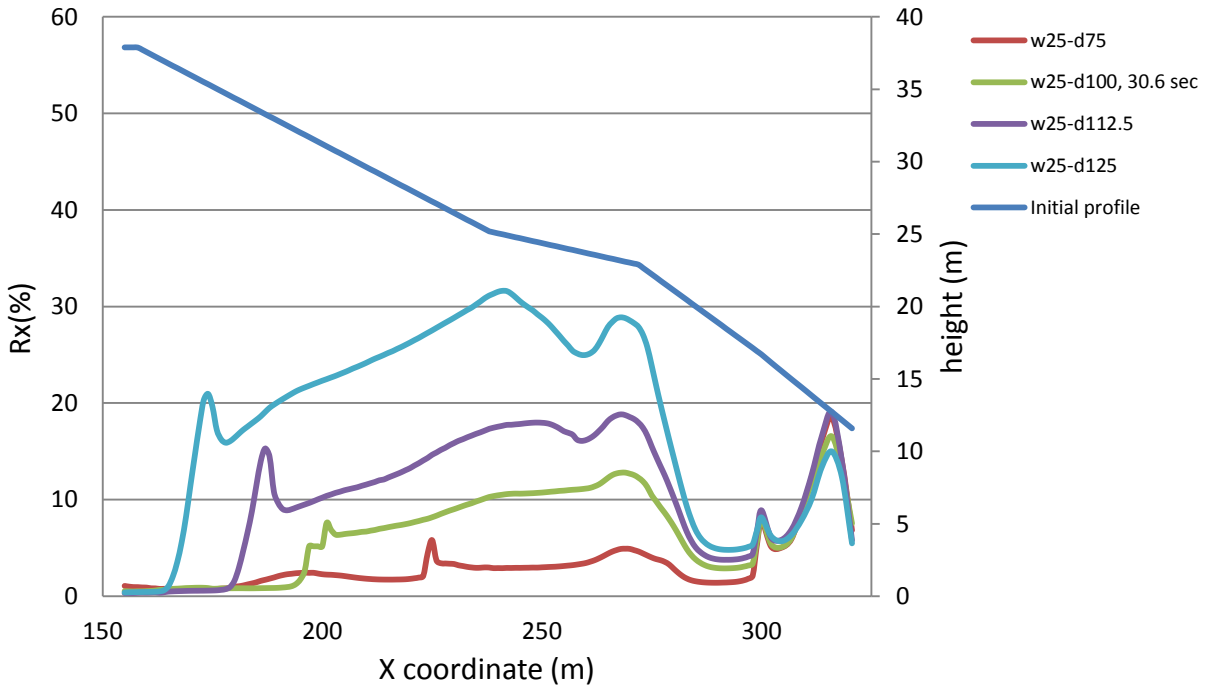

Figure C20: The value of R_x in along the slope of the impoundment within consolidated tailings ($(N_1)_{60} = 8$, blows/30 cm) due to E_5-sag earthquake record (S16T) for inclusions with width of 25 meters. In the legend in the right top of the figure, first number is the width of inclusions, second number is center-to-center spacing, and third number in some cases is time that the model was stopped due to bad geometry in a zone

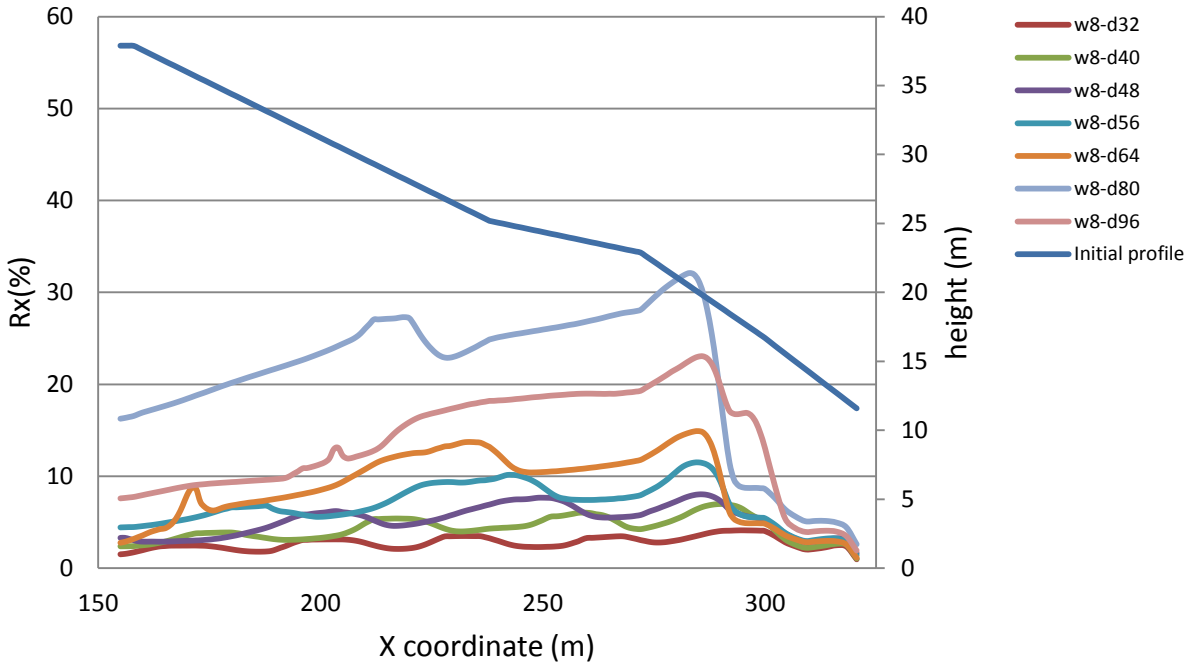

Figure C21: The value of R_x in along the slope of the impoundment within unconsolidated tailings ($(N_1)_{60} = 3$, blows/30 cm) due to the E_1-north earthquake record (Northridge) for inclusions with width of 8 meters. In the legend in the right top of the figure, first number is the width of inclusions, second number is center-to-center spacing, and third number in some cases is time that the model was stopped due to bad geometry in a zone

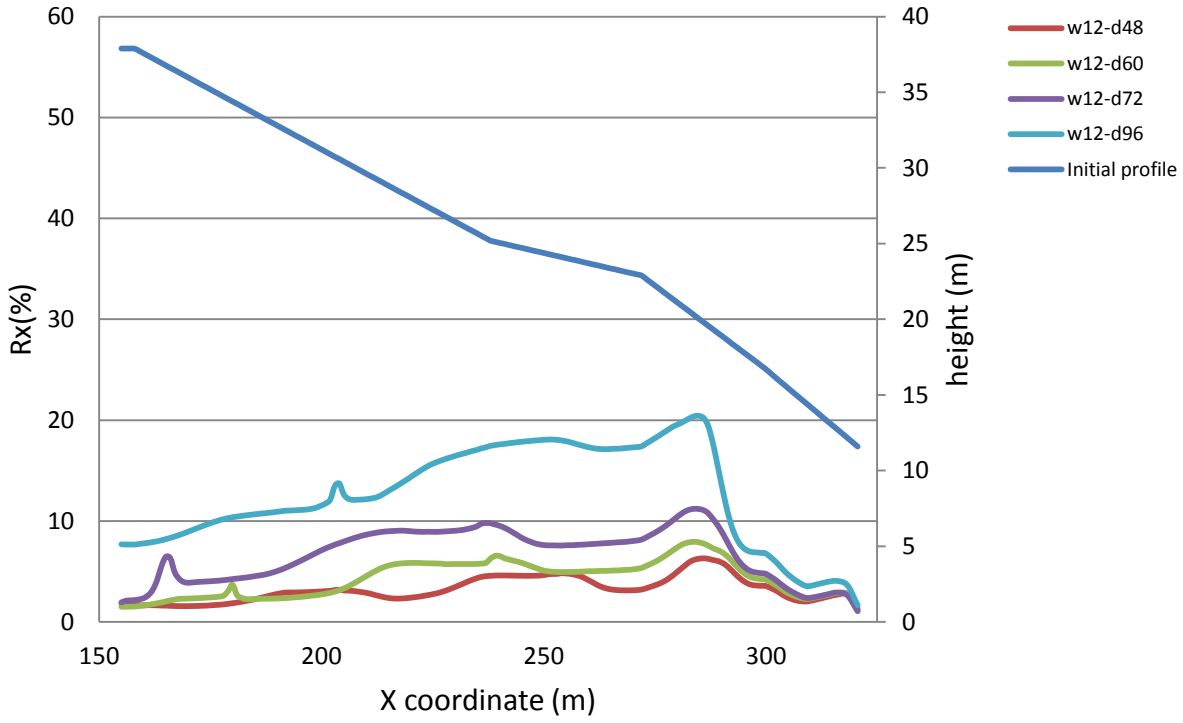

Figure C22: The value of R_x in along the slope of the impoundment within unconsolidated tailings ($(N_1)_{60} = 3$, blows/30 cm) due to the E_1-north earthquake record (Northridge) for inclusions with width of 12 meters. In the legend in the right top of the figure, first number is the width of inclusions, second number is center-to-center spacing, and third number in some cases is time that the model was stopped due to bad geometry in a zone

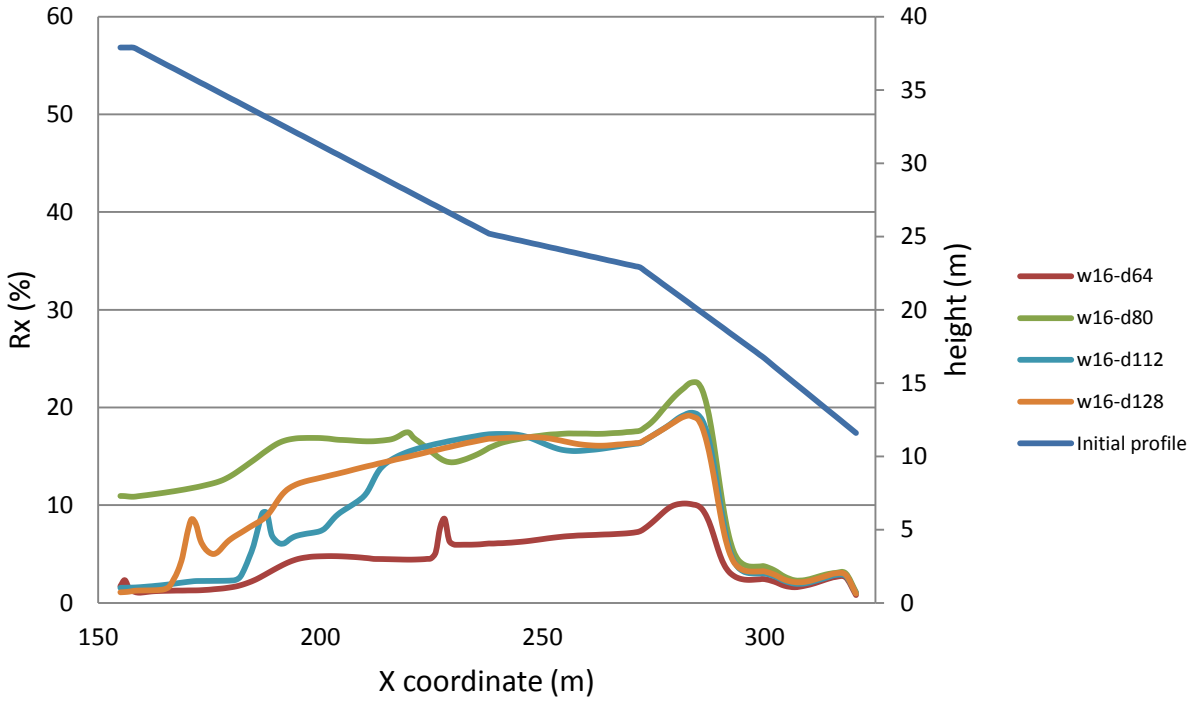

Figure C23: The value of R_x in along the slope of the impoundment within unconsolidated tailings ($(N_1)_{60} = 3$, blows/30 cm) due to the E_1-north earthquake record (Northridge) for inclusions with width of 16 meters. In the legend in the right top of the figure, first number is the width of inclusions, second number is center-to-center spacing, and third number in some cases is time that the model was stopped due to bad geometry in a zone

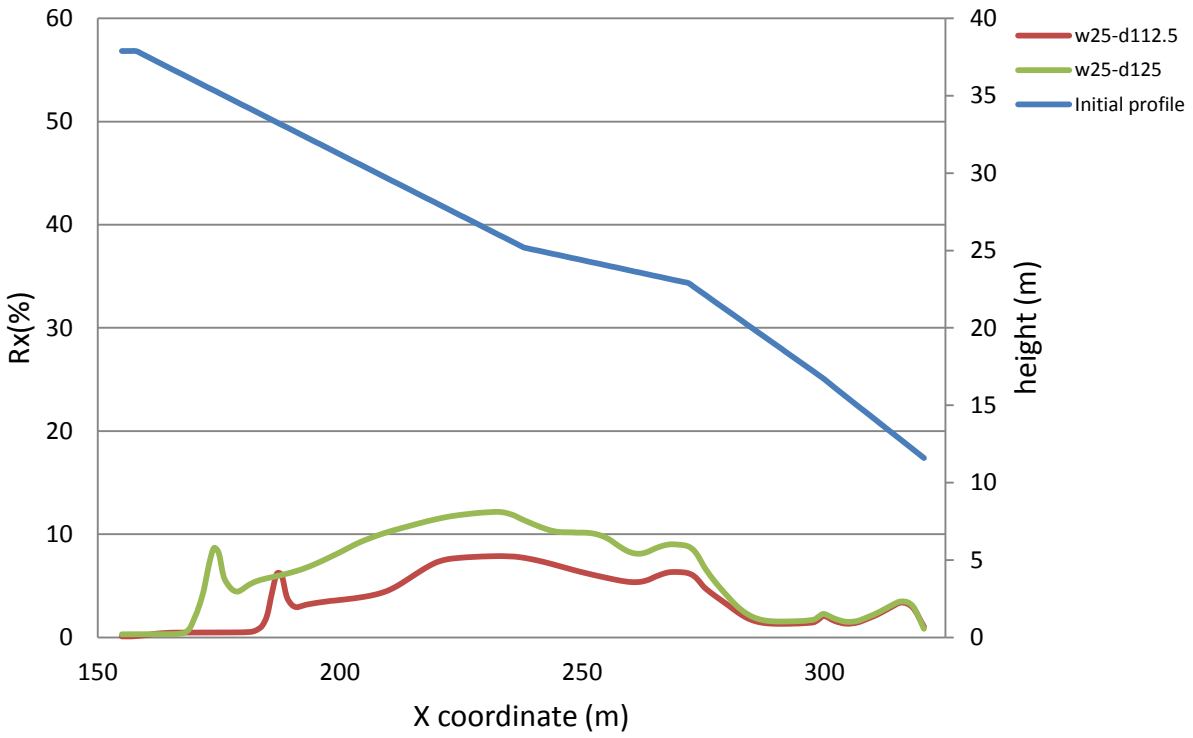

Figure C24: The value of R_x in along the slope of the impoundment within unconsolidated tailings ($(N_1)_{60} = 3$, blows/30 cm) due to the E_1-north earthquake record (Northridge) for inclusions with width of 25 meters. In the legend in the right top of the figure, first number is the width of inclusions, second number is center-to-center spacing, and third number in some cases is time that the model was stopped due to bad geometry in a zone

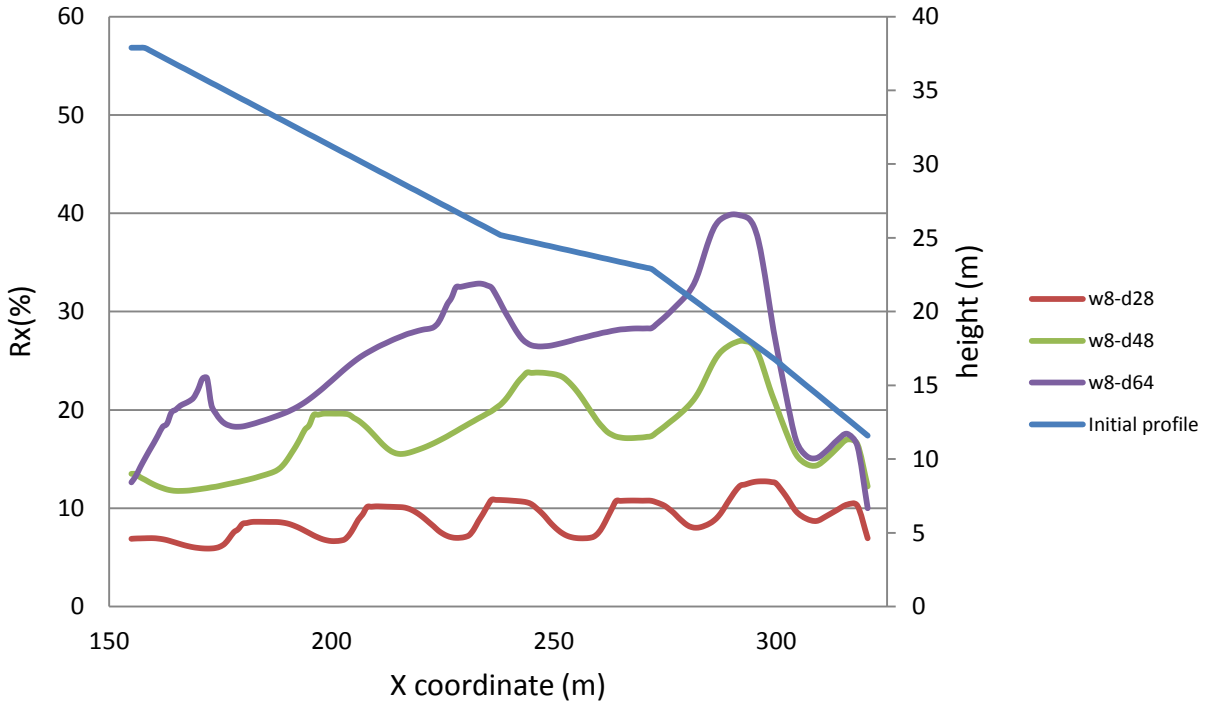

Figure C25: The value of R_x in along the slope of the impoundment within unconsolidated tailings ($(N_1)_{60} = 3$, blows/30 cm) due to the E_3-north earthquake record (Northridge) for inclusions with width of 8 meters. In the legend in the right top of the figure, first number is the width of inclusions, second number is center-to-center spacing, and third number in some cases is time that the model was stopped due to bad geometry in a zone

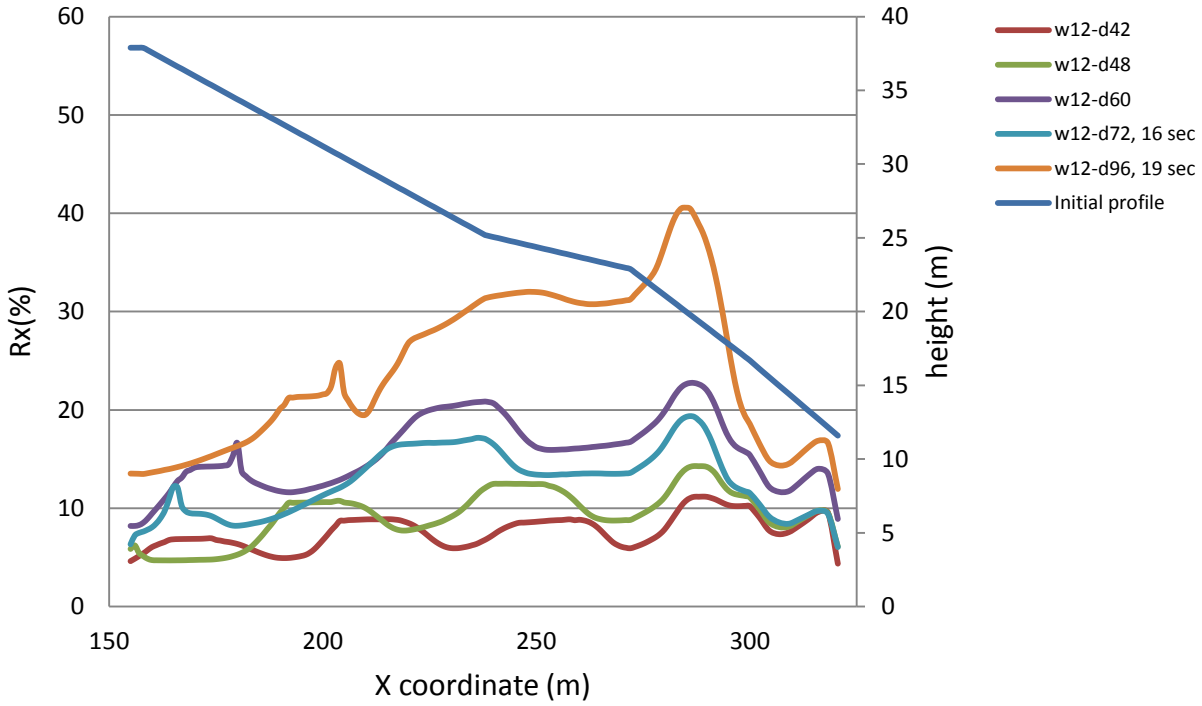

Figure C26: The value of R_x in along the slope of the impoundment within unconsolidated tailings ($(N_1)_{60} = 3$, blows/30 cm) due to the E_3-north earthquake record (Northridge) for inclusions with width of 12 meters. In the legend in the right top of the figure, first number is the width of inclusions, second number is center-to-center spacing, and third number in some cases is time that the model was stopped due to bad geometry in a zone

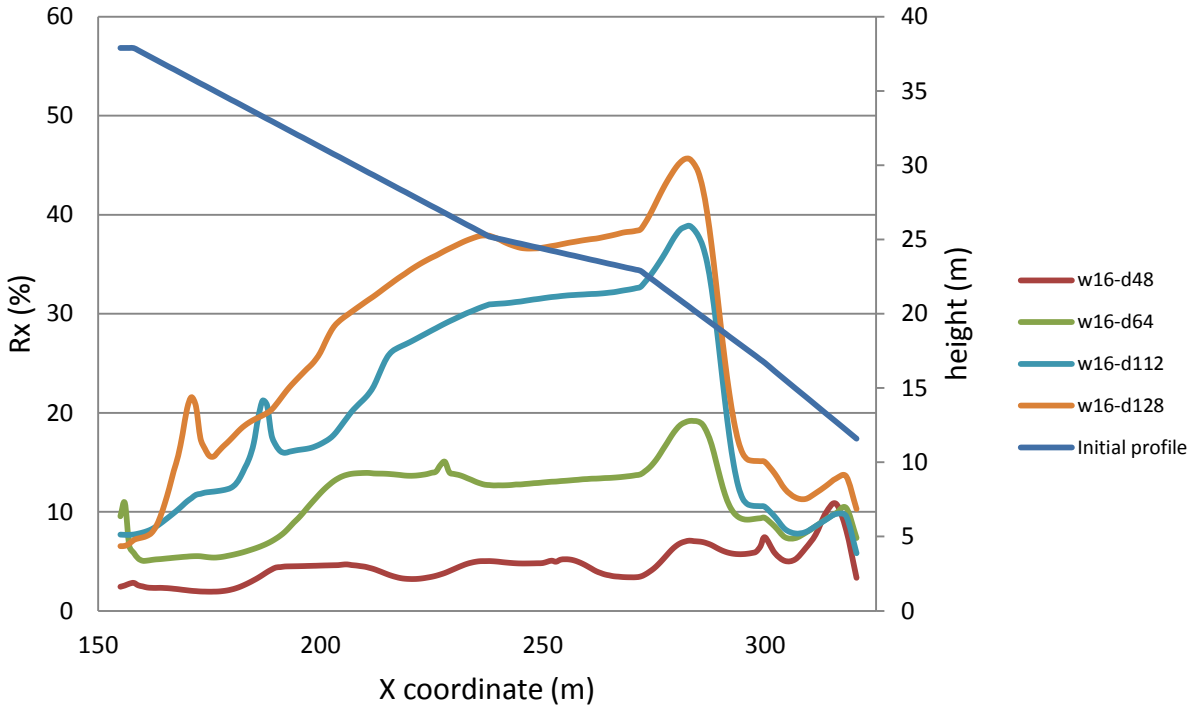

Figure C27: The value of R_x in along the slope of the impoundment within unconsolidated tailings ($(N_1)_{60} = 3$, blows/30 cm) due to the E_3-north earthquake record (Northridge) for inclusions with width of 16 meters. In the legend in the right top of the figure, first number is the width of inclusions, second number is center-to-center spacing, and third number in some cases is time that the model was stopped due to bad geometry in a zone

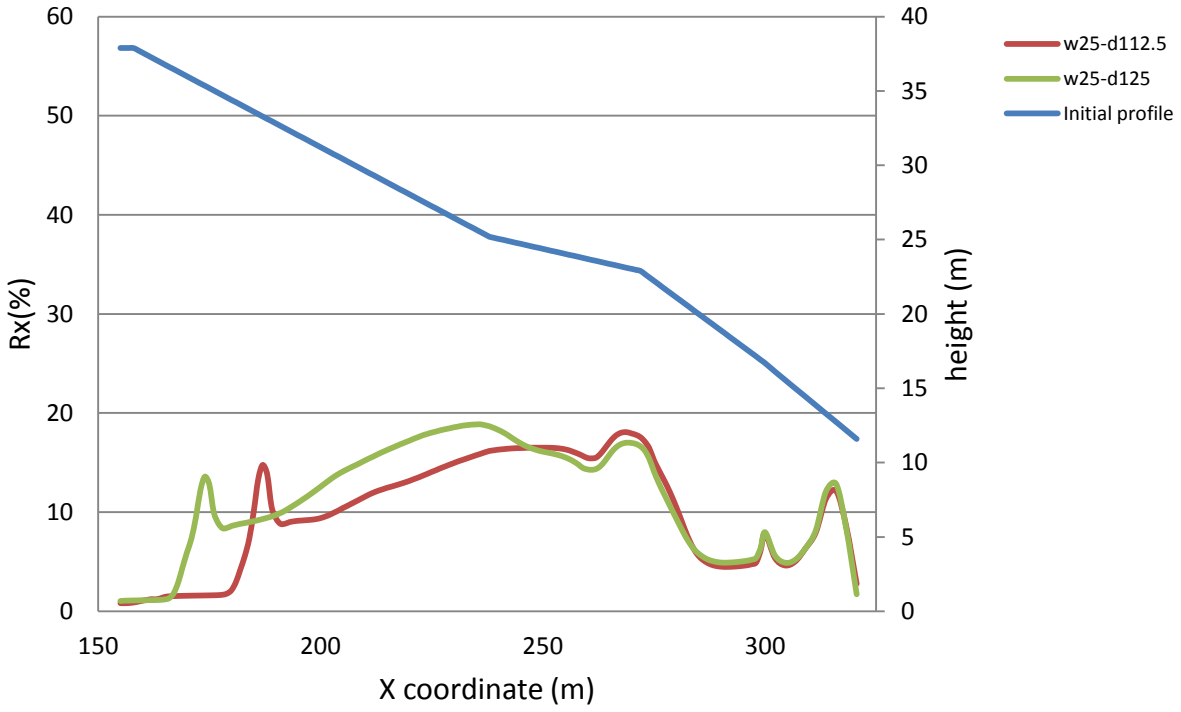

Figure C28: The value of R_x in along the slope of the impoundment within unconsolidated tailings ($(N_1)_{60} = 3$, blows/30 cm) due to the E_3-north earthquake record (Northridge) for inclusions with width of 25 meters. In the legend in the right top of the figure, first number is the width of inclusions, second number is center-to-center spacing, and third number in some cases is time that the model was stopped due to bad geometry in a zone

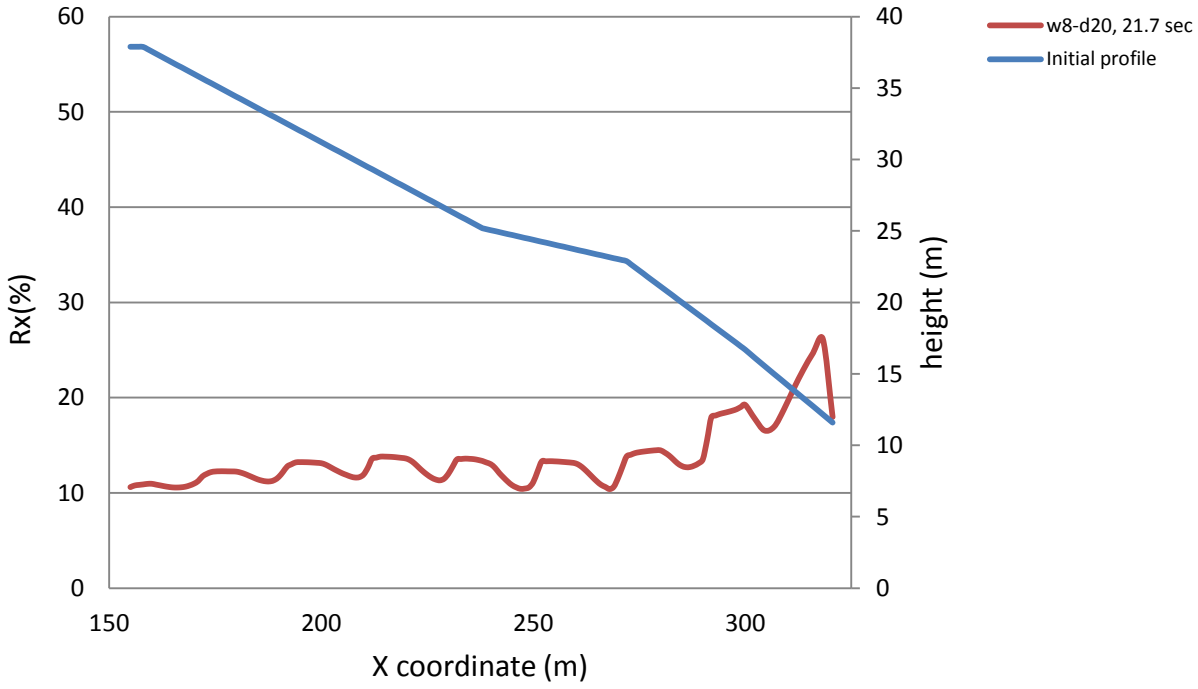

Figure C29: The value of R_x in along the slope of the impoundment within unconsolidated tailings ($(N_1)_{60} = 3$, blows/30 cm) due to the E_5-north earthquake record (Northridge) for inclusions with width of 8 meters. In the legend in the right top of the figure, first number is the width of inclusions, second number is center-to-center spacing, and third number in some cases is time that the model was stopped due to bad geometry in a zone

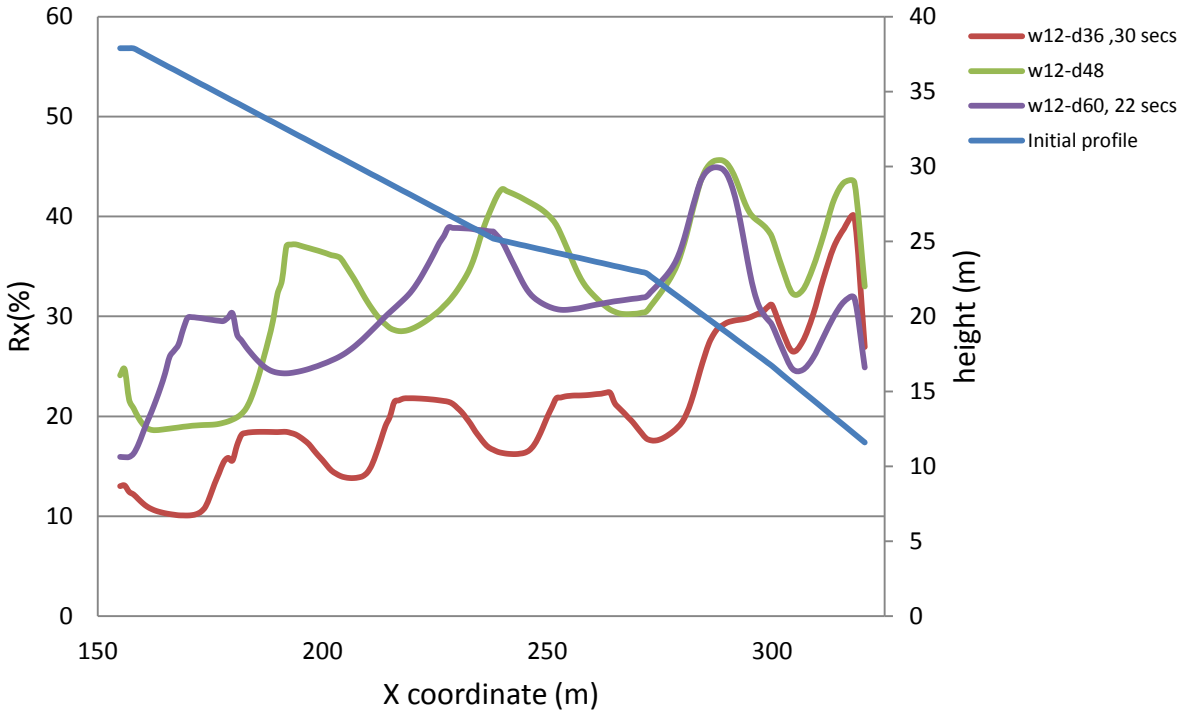

Figure C30: The value of R_x in along the slope of the impoundment within unconsolidated tailings ($(N_1)_{60} = 3$, blows/30 cm) due to the E_5-north earthquake record (Northridge) for inclusions with width of 12 meters. In the legend in the right top of the figure, first number is the width of inclusions, second number is center-to-center spacing, and third number in some cases is time that the model was stopped due to bad geometry in a zone

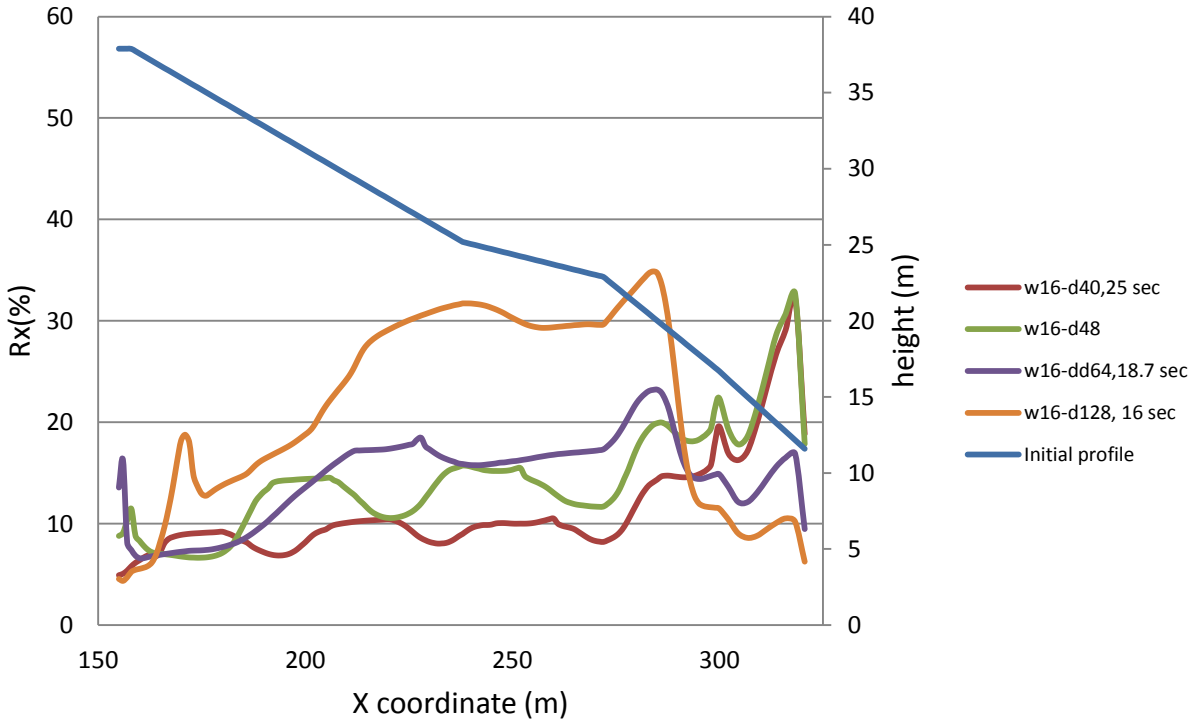

Figure C31: The value of R_x in along the slope of the impoundment within unconsolidated tailings ($(N_1)_{60} = 3$, blows/30 cm) due to the E_5-north earthquake record (Northridge) for inclusions with width of 16 meters. In the legend in the right top of the figure, first number is the width of inclusions, second number is center-to-center spacing, and third number in some cases is time that the model was stopped due to bad geometry in a zone

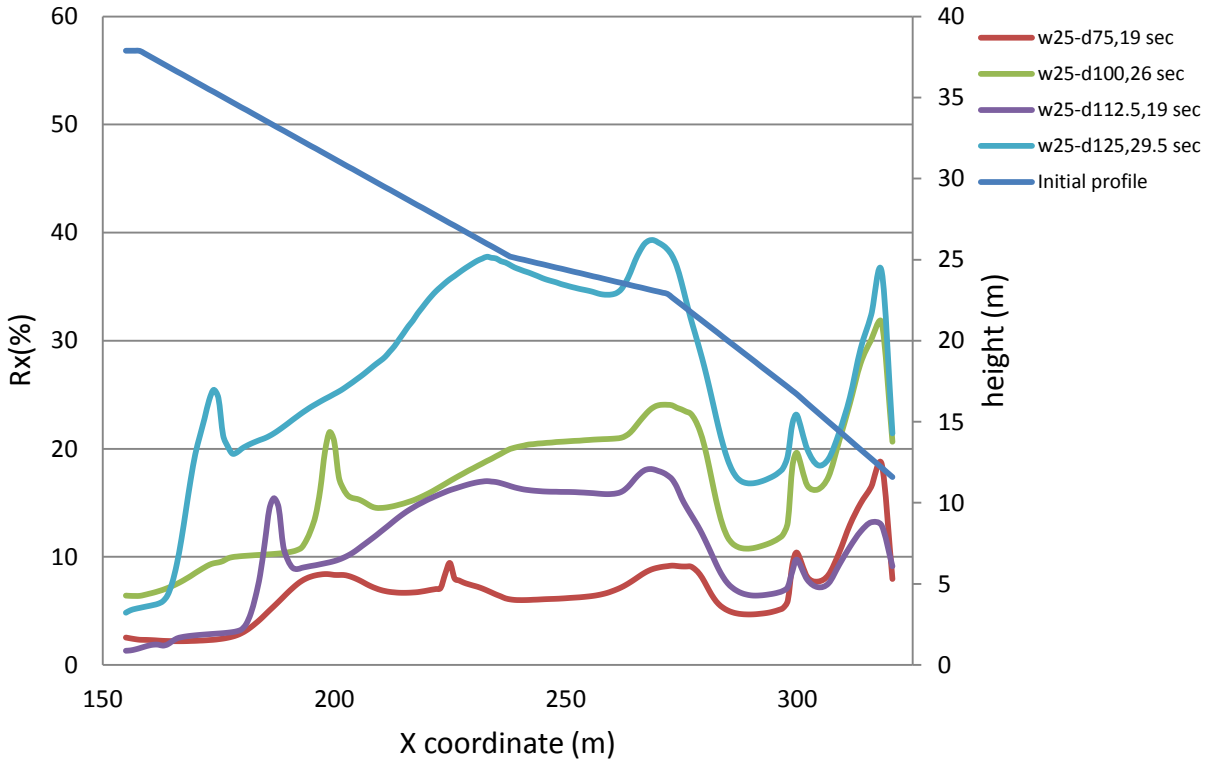

Figure C32: The value of R_x in along the slope of the impoundment within unconsolidated tailings ($(N_1)_{60} = 3$, blows/30 cm) due to the E_5-north earthquake record (Northridge) for inclusions with width of 25 meters. In the legend in the right top of the figure, first number is the width of inclusions, second number is center-to-center spacing, and third number in some cases is time that the model was stopped due to bad geometry in a zone

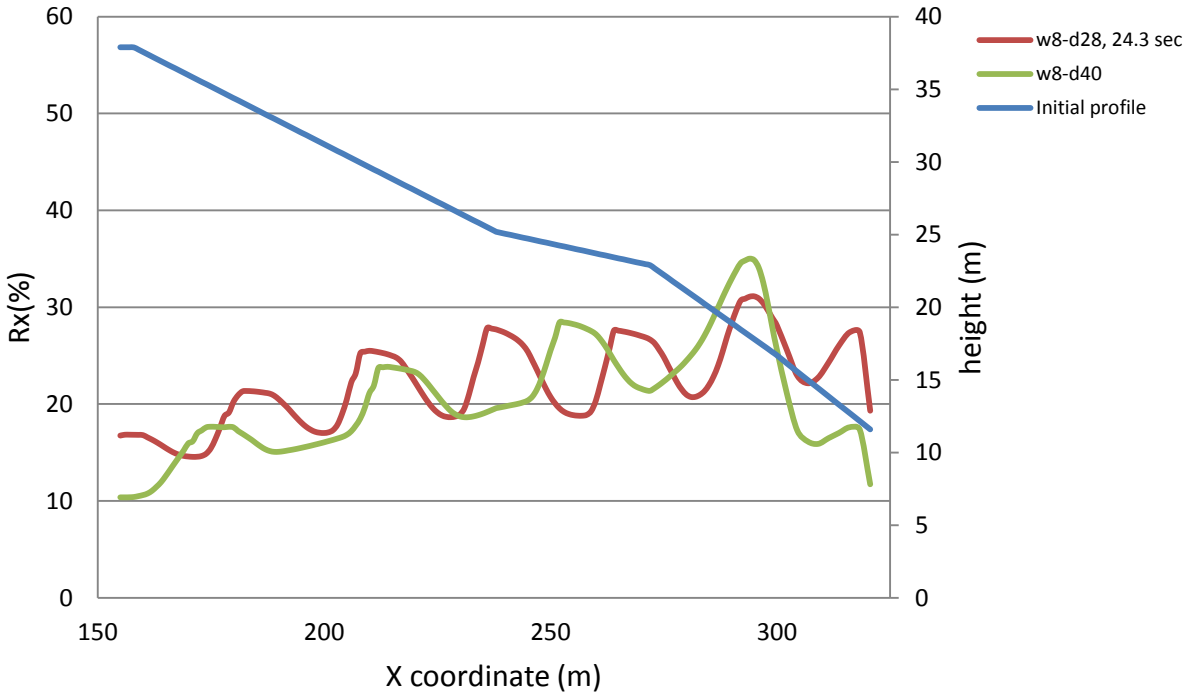

Figure C33: The value of R_x in along the slope of the impoundment within consolidated tailings ($(N_1)_{60} = 8$, blows/30 cm) due to the E_4-north earthquake record (Northridge) for inclusions with width of 8 meters. In the legend in the right top of the figure, first number is the width of inclusions, second number is center-to-center spacing, and third number in some cases is time that the model was stopped due to bad geometry in a zone

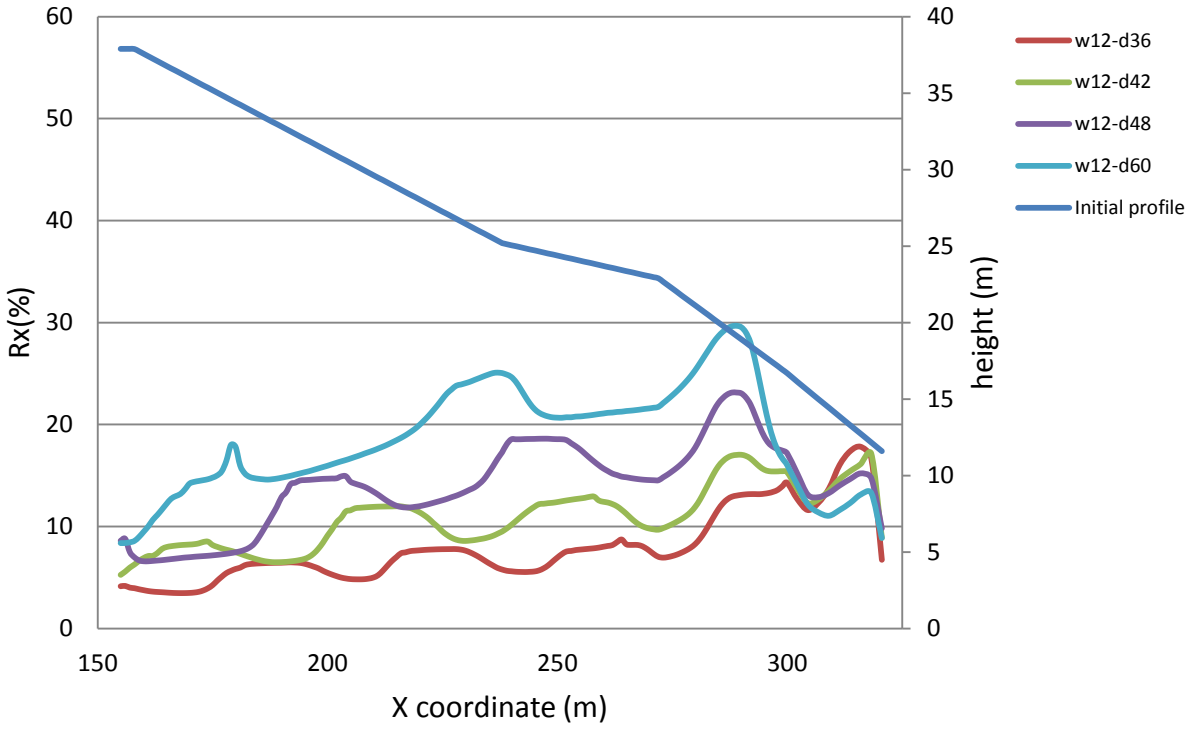

Figure C34: The value of R_x in along the slope of the impoundment within consolidated tailings ($(N_1)_{60} = 8$, blows/30 cm) due to the E_4-north earthquake record (Northridge) for inclusions with width of 12 meters. In the legend in the right top of the figure, first number is the width of inclusions, second number is center-to-center spacing, and third number in some cases is time that the model was stopped due to bad geometry in a zone

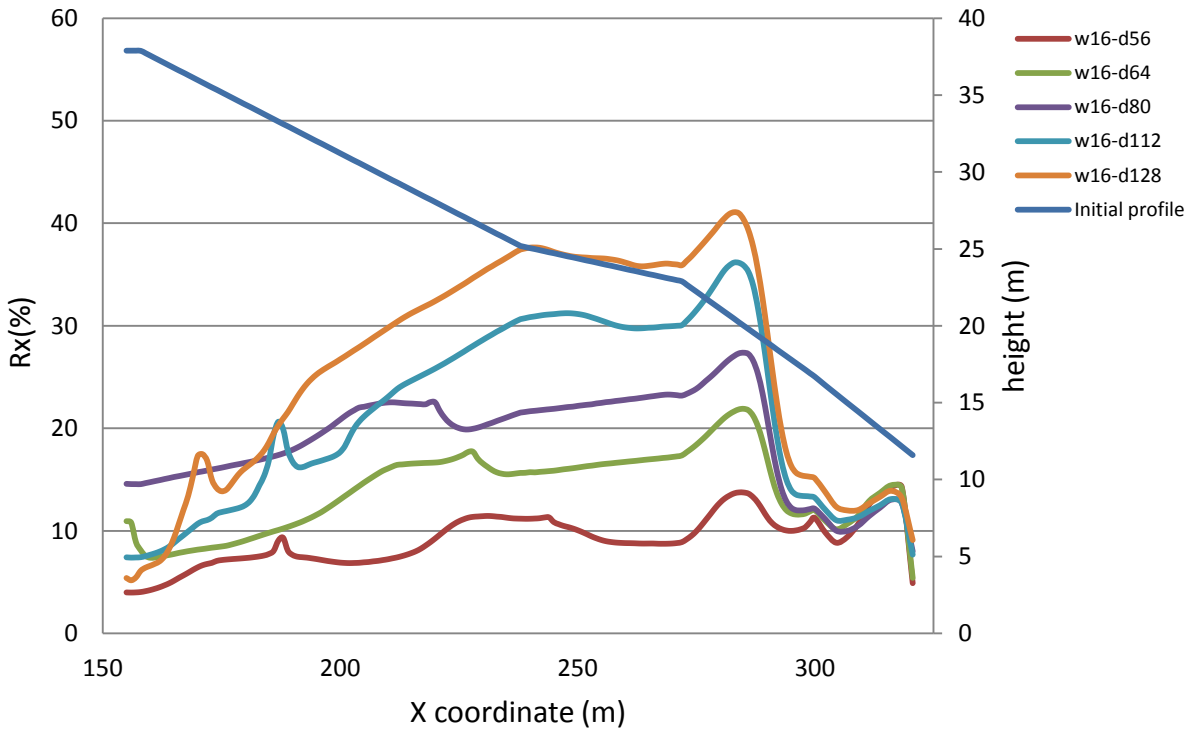

Figure C35: The value of R_x in along the slope of the impoundment within consolidated tailings ($(N_1)_{60} = 8$, blows/30 cm) due to the E_4-north earthquake record (Northridge) for inclusions with width of 16 meters. In the legend in the right top of the figure, first number is the width of inclusions, second number is center-to-center spacing, and third number in some cases is time that the model was stopped due to bad geometry in a zone

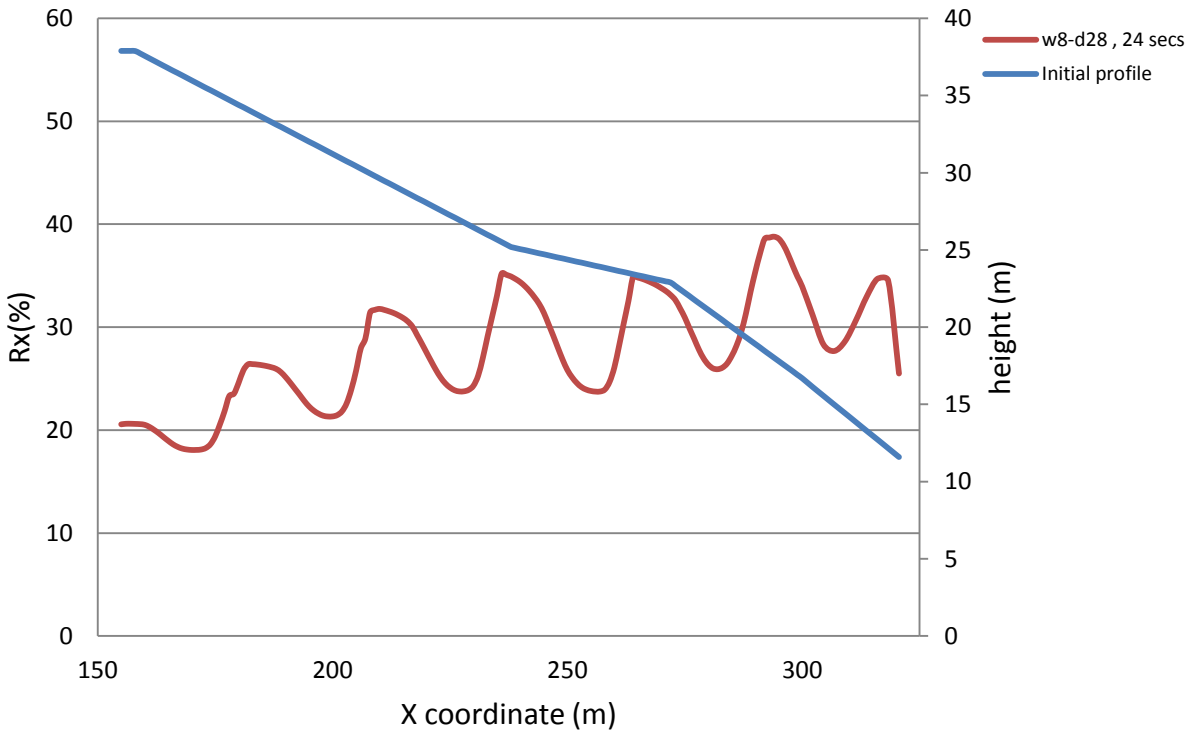

Figure C36: The value of R_x in along the slope of the impoundment within consolidated tailings ($(N_1)_{60} = 8$, blows/30 cm) due to the E_5-north earthquake record (Northridge) for inclusions with width of 8 meters. In the legend in the right top of the figure, first number is the width of inclusions, second number is center-to-center spacing, and third number in some cases is time that the model was stopped due to bad geometry in a zone

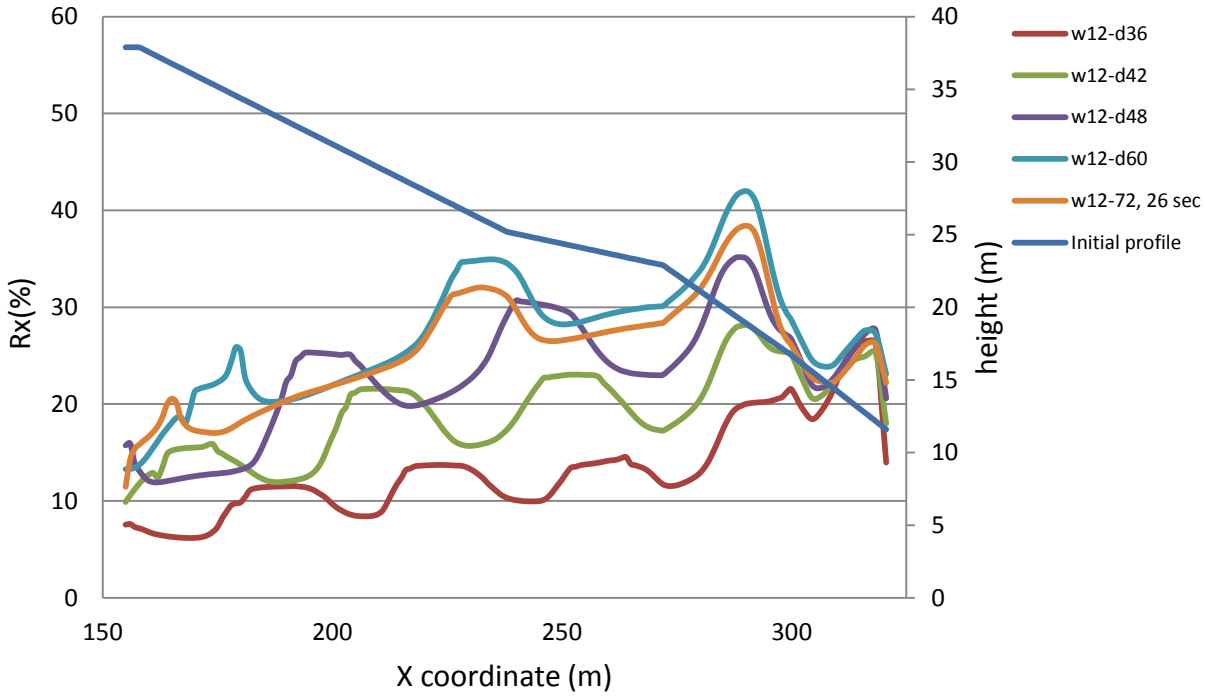

Figure C37: The value of R_x in along the slope of the impoundment within consolidated tailings ($(N_1)_{60} = 8$, blows/30 cm) due to the E_5-north earthquake record (Northridge) for inclusions with width of 12 meters. In the legend in the right top of the figure, first number is the width of inclusions, second number is center-to-center spacing, and third number in some cases is time that the model was stopped due to bad geometry in a zone

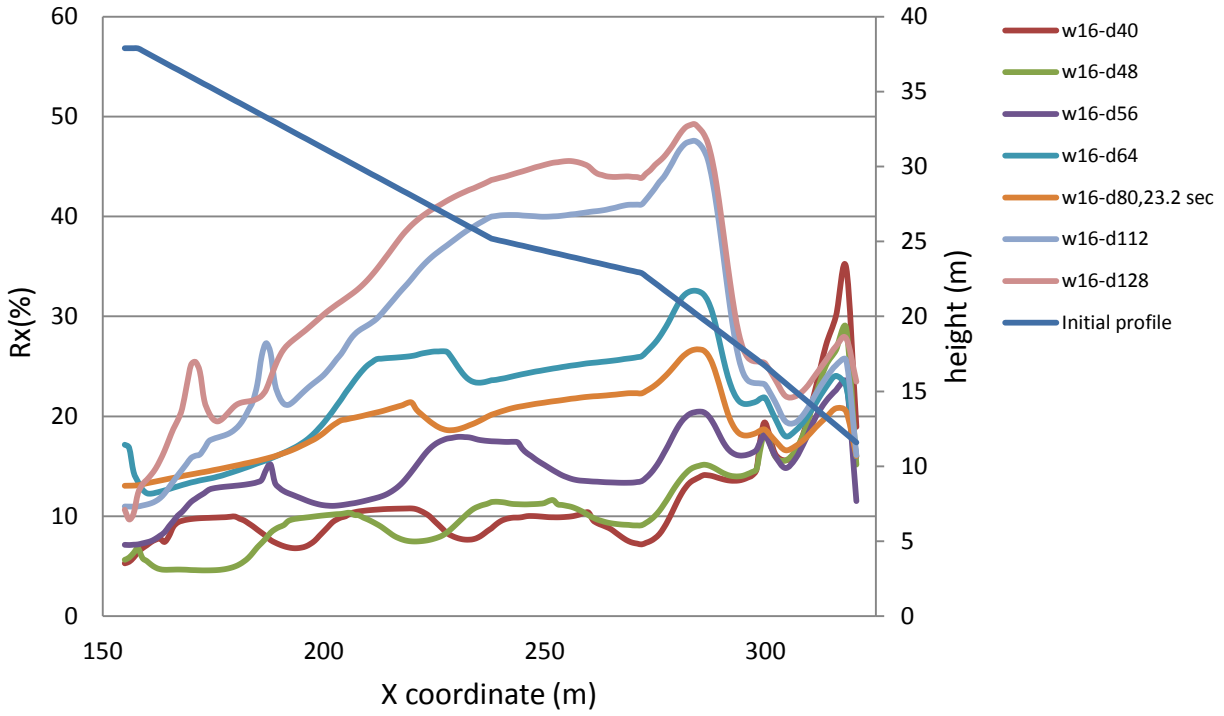

Figure C38: The value of R_x in along the slope of the impoundment within consolidated tailings ($(N_1)_{60} = 8$, blows/30 cm) due to the E_5-north earthquake record (Northridge) for inclusions with width of 16 meters. In the legend in the right top of the figure, first number is the width of inclusions, second number is center-to-center spacing, and third number in some cases is time that the model was stopped due to bad geometry in a zone

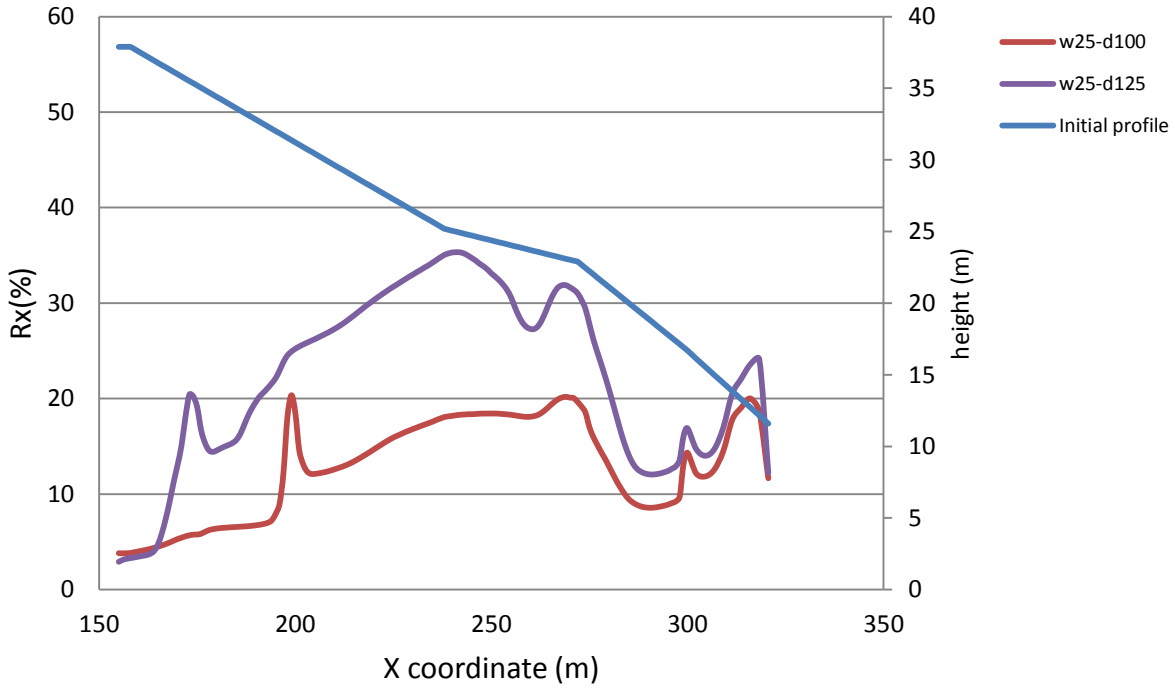

Figure C39: The value of R_x in along the slope of the impoundment within consolidated tailings ($(N_1)_{60} = 8$, blows/30 cm) due to the E_5-north earthquake record (Northridge) for inclusions with width of 25 meters. In the legend in the right top of the figure, first number is the width of inclusions, second number is center-to-center spacing, and third number in some cases is time that the model was stopped due to bad geometry in a zone

C1.2 Effect of inclusions configuration on the performance of the tailings impoundment

Figures C40 to C43 show the average normalized horizontal displacements AR_x of the downstream slope of the impoundment and of the WRI as a function of the total widths of the inclusions in the impoundment for consolidated tailings ($(N_1)_{60} = 8$, blows/30 cm), due to E_4 earthquake record (S16T). The black and gray correspond to the slope of impoundment and the WRI, respectively. Along the horizontal axis, the first number gives the total width of the inclusions; the first number inside the parentheses represents the width of each single inclusion and the second number is the center to center spacing between the inclusions.

Figure C40 shows, for instance, that for arrangements with a total width of 16 and 24 m, the AR_x of the slope and WRI for the arrangement of 8-56 are close to e 10% while these values exceed 20% for other arrangements. For the arrangements with a total width of 32 to 50 meters, the values of AR_x of the slope and WRI for the arrangements of 16-112 are more than 20%; for arrangements 12-84 and 25-125, the AR_x of the slope is more than 10%, while the AR_x of the WRI are usually around 10%. Other arrangements lead to ARx of the slope and WRI smaller than 10%.

The other figures shown here illustrate other cases, for different configurations and loading conditions.

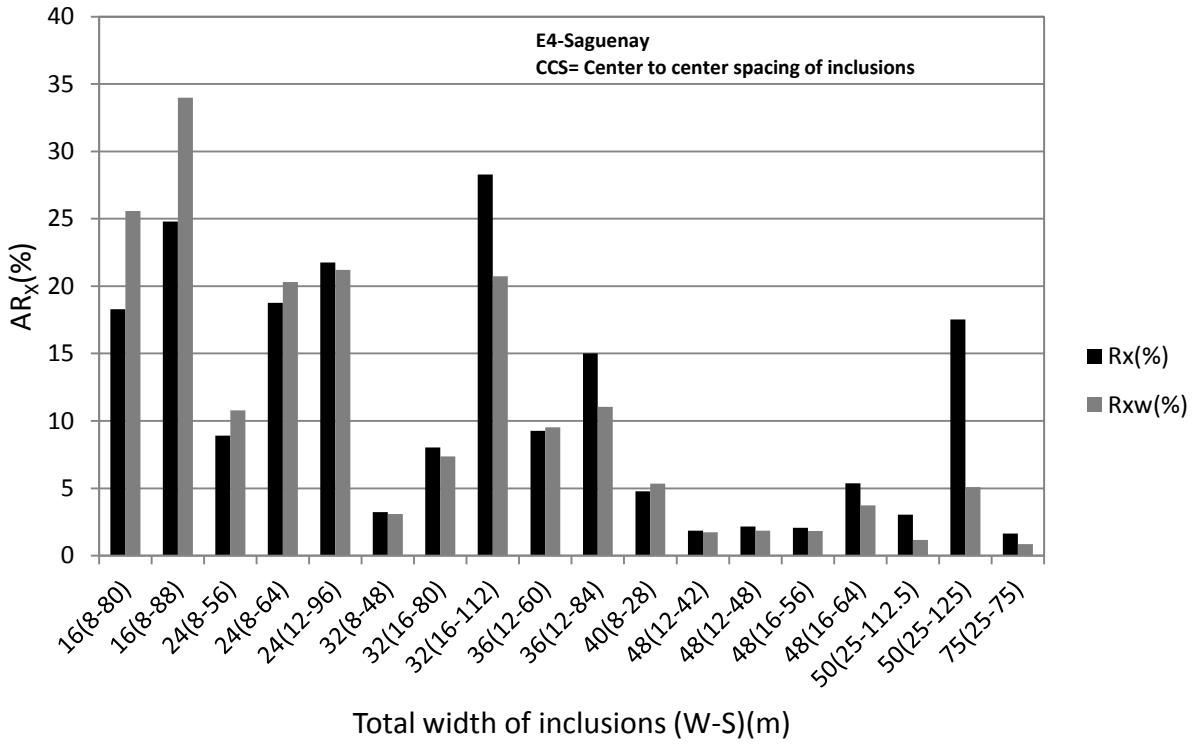

Figure C40: Average normalized horizontal displacements AR_x of the slope of the impoundment and of the WRI as a function of the total widths of the inclusions in the impoundment for consolidated tailings ($(N_1)_{60} = 8$, blows/30 cm), due to the E_4-sag earthquake record (S16T). Along the horizontal axis, the first number is the total width of the inclusions; the first number inside the parenthesis is the width of each single inclusion and the second number is the center to center spacing. Black and Gray bars represent the average normalized horizontal displacements of the slope of the impoundment and of the WRI, respectively

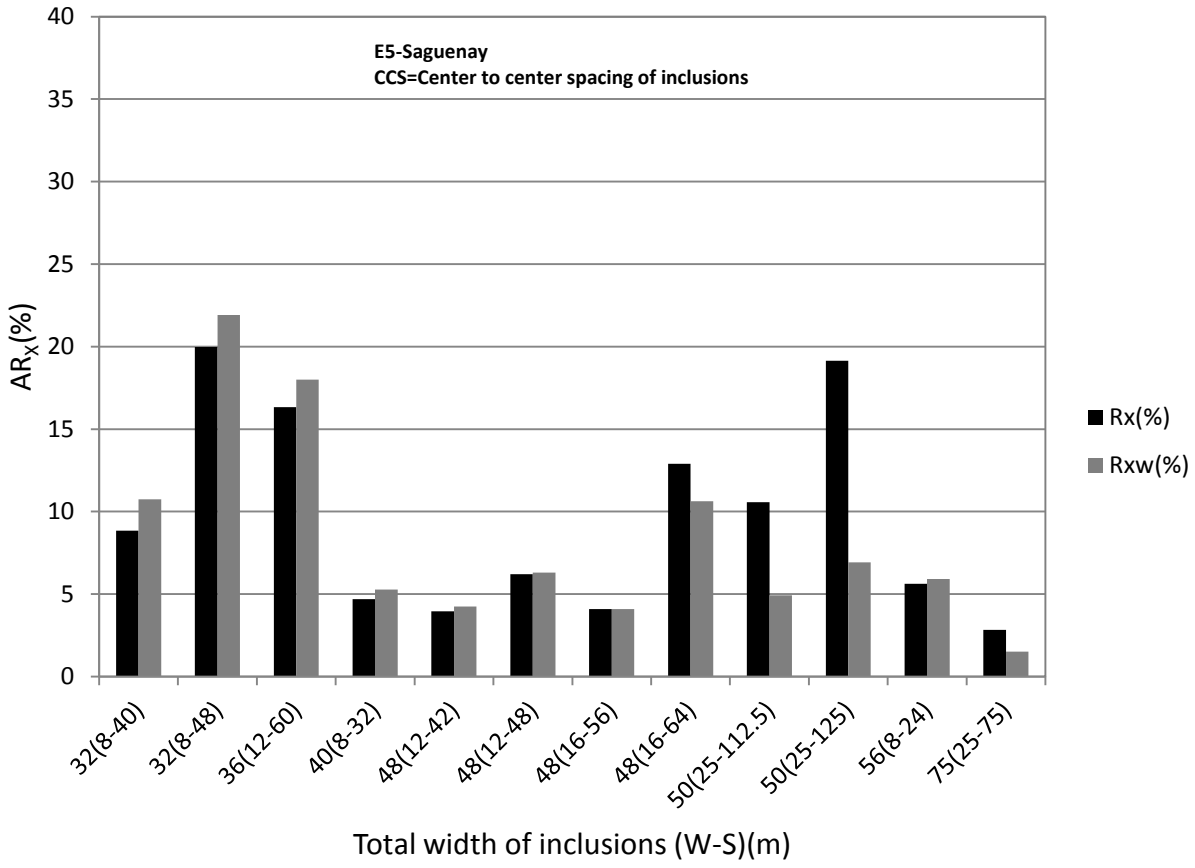

Figure C41: Average normalized horizontal displacements AR_x of the slope of the impoundment and of the WRI as a function of the total widths of the inclusions in the impoundment for consolidated tailings ($(N_1)_{60} = 8$, blows/30 cm), due to the E_5-sag earthquake record (S16T). Along the horizontal axis, the first number is the total width of the inclusions; the first number inside the parenthesis is the width of each single inclusion and the second number is the center to center spacing. Black and Gray bars represent the average normalized horizontal displacements of the slope of the impoundment and of the WRI, respectively

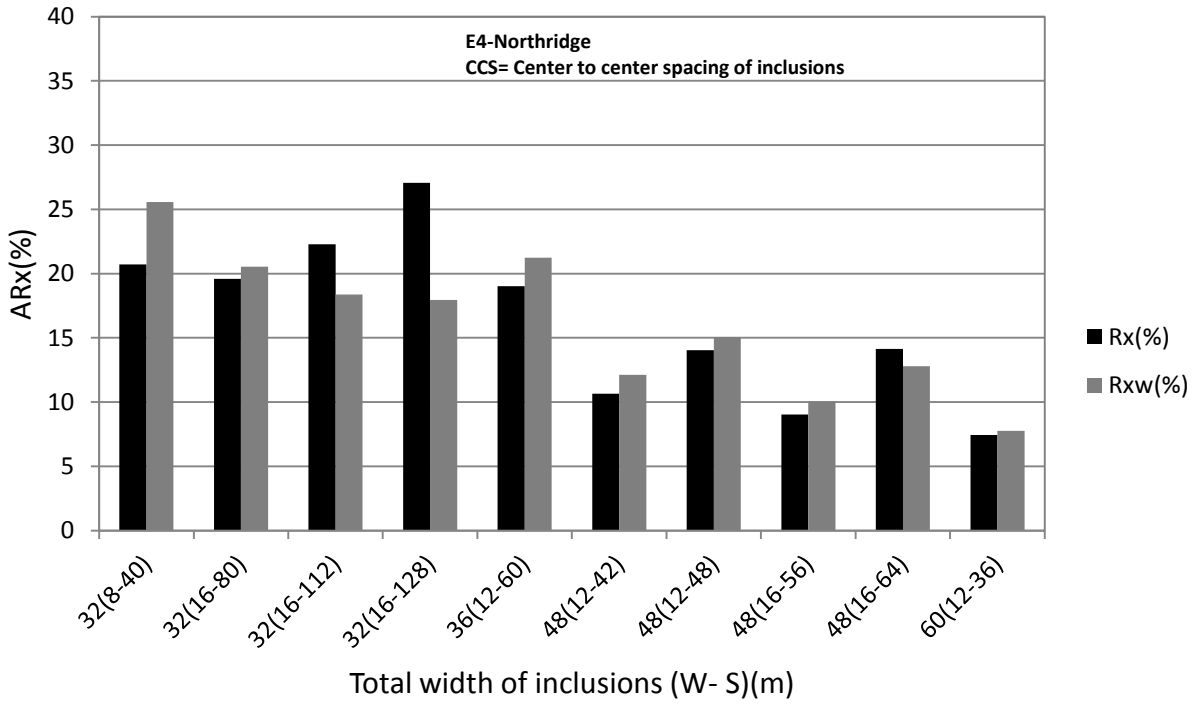

Figure C42: Average normalized horizontal displacements AR_x of the slope of the impoundment and of the WRI as a function of the total widths of the inclusions in the impoundment for consolidated tailings ($(N_1)_{60} = 8$, blows/30 cm), due to the E_4-north earthquake record (Northridge). Along the horizontal axis, the first number is the total width of the inclusions; the first number inside the parenthesis is the width of each single inclusion and the second number is the center to center spacing. Black and Gray bars represent the average normalized horizontal displacements of the slope of the impoundment and of the WRI, respectively

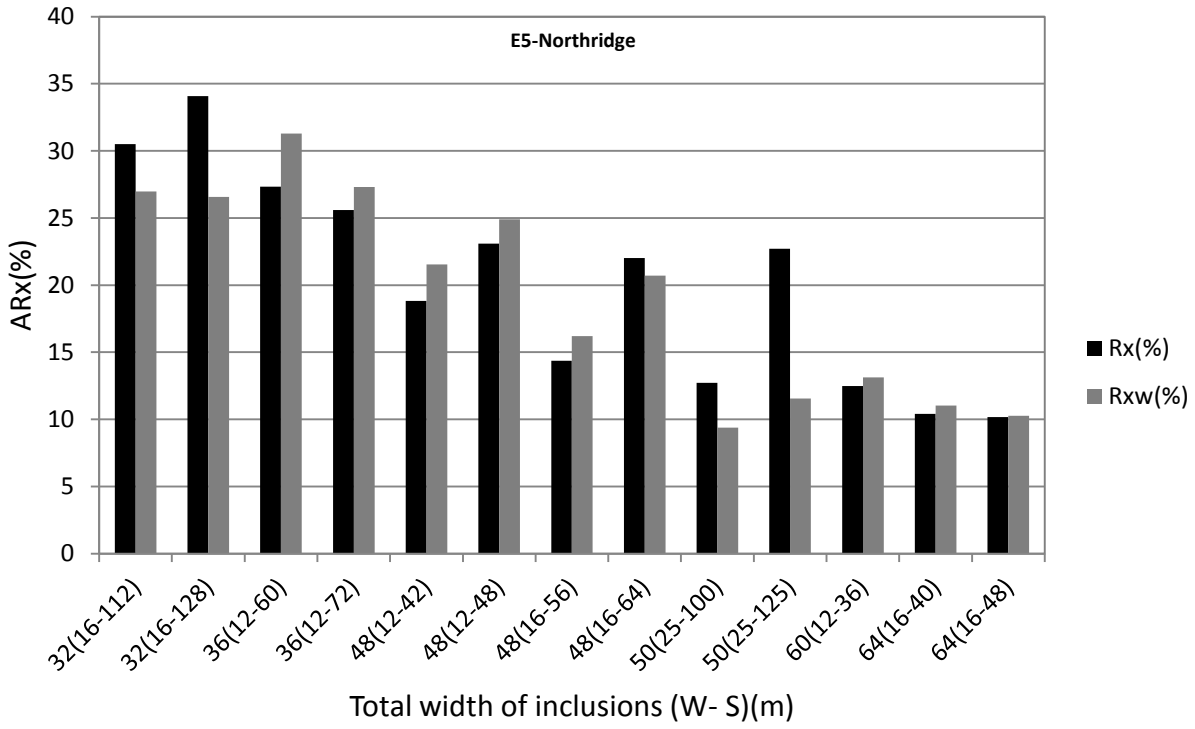

Figure C43: Average normalized horizontal displacements AR_x of the slope of the impoundment and of the WRI as a function of the total widths of the inclusions in the impoundment for consolidated tailings ($(N_1)_{60} = 8$, blows/30 cm), due to the E_5-north earthquake record (Northridge). Along the horizontal axis, the first number is the total width of the inclusions; the first number inside the parenthesis is the width of each single inclusion and the second number is the center to center spacing. Black and Gray bars represent the average normalized horizontal displacements of the slope of the impoundment and of the WRI, respectively

C1.3 Classification of the reinforced (consolidated) tailings impoundment

Table C1 provides a preliminary classification of the reinforced impoundments using the values of AR_x of the external slope at the end of shaking, for various seismic events and consolidated tailings. Seven classes are identified in this table, going from the best performance (0-5%) to the worst response (> 30%)

Table C1 : Classification of the reinforced tailings impoundments with waste rock inclusions based on the average value of R_x (AR_x) for the downstream slope at the end of shaking; various earthquakes with consolidated tailings

Average value of R_x on the slope of tailings impoundment	Different Combinations of Widths and Center to Center Distances of Inclusions*		
0-5%	8-28-E4-SAG	12-42-E4-SAG	25-75-E5-SAG
	8-48-E4-SAG	12-48-E4-SAG	25-75-E4-SAG
	8-32-E5-SAG	16-56-E4-SAG	25-112.5-E4-SAG
	12-42-E5-SAG	16-56-E5-SAG	25-100-E4-SAG
5-10%	8-24 -E5-SAG	12-36-E4-NOR	16-80-E4-SAG
	8-40-E5-SAG	16-56-E4-NOR	
	12-48-E5-SAG	16-64-E4-SAG	
10-15%	12-36-E5-NOR	12-84-E4-SAG	16-64-E4-NOR
	12-42-E4-NOR	16-40-E5-NOR	16-64-E5-SAG
	12-48-E4-NOR	16-48-E5-NOR	25-100-E5-NOR
	12-60-E5-SAG	16-56-E5-NOR	25-112.5-E5-SAG
15-20%	8-48-E5-SAG	12-42-E5-NOR	16-80-E5-NOR
	8-64-E4-SAG	12-60-E4-NOR	25-125-E4-SAG
	8-80-E4-SAG	16-80-E4-NOR	25-125-E5-SAG
20-25%	8-40-E4-NOR	12-96-E4-SAG	25-125-E5-NOR
	8-88-E4-SAG	16-112-E4-NOR	
	12-48-E5-NOR	16-64-E5-NOR	
25-30%	12-60-E5-NOR	16-112-E5-NOR	
	16-112-E4-SAG	16-128-E4-NOR	
>30%	16-128-E5-NOR	16-144-E4-SAG	

*First number shows width of inclusion (m), second number shows center to center distances of inclusions, E4 to E5 show earthquake records, SAG shows high frequency record, NOR shows low frequency records.

C1.4 Damping parameters for the bedrock

Rayleigh damping was assigned for the bedrock. The damping ratio and the center frequency of the Rayleigh damping were adjusted so that the recorded acceleration-time history at the top of the bedrock was the same as the input acceleration-time history at the base of the model. Figure C44 shows acceleration time histories at the top and at the base of this bedrock; this figure indicates that these two acceleration-time histories are virtually identical. The corresponding damping ratio and center frequency for Rayleigh damping in the bedrock obtained in this manner are 0.01 and 5 Hz, respectively. For other ground motions, same results were obtained.

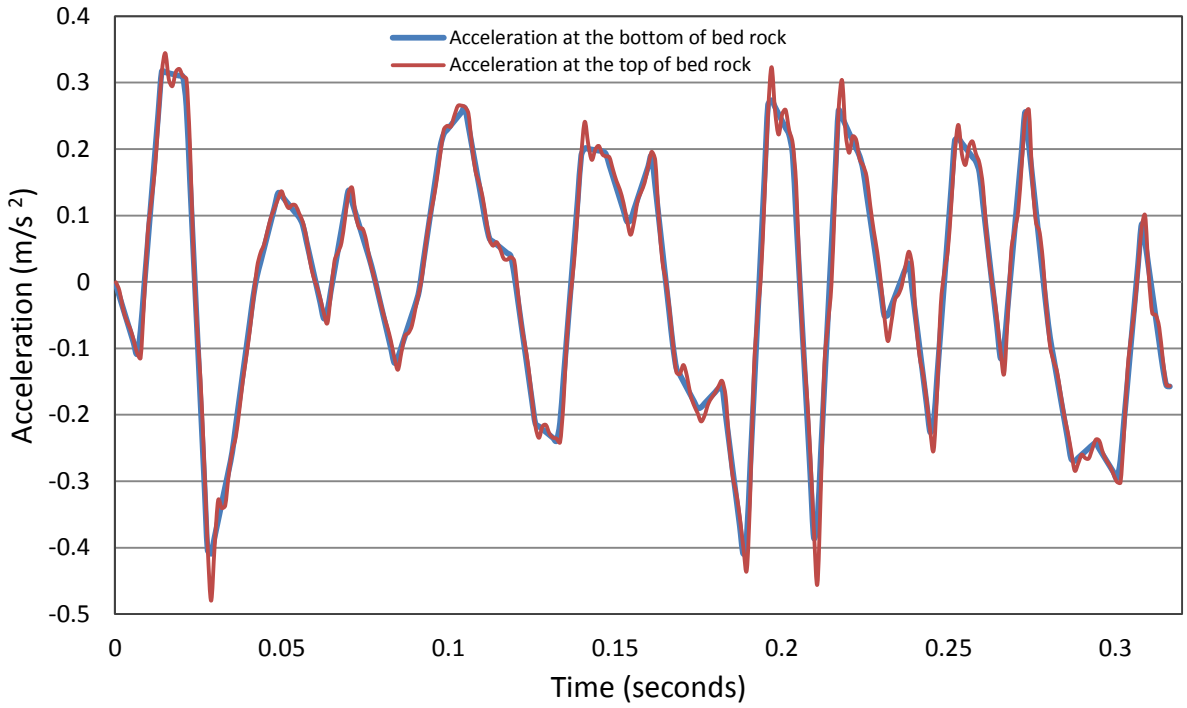

Figure C44: Comparison of input history of scaled Saguenay S16T earthquake acceleration at the base of the bedrock (red curve) and the time history at the top of the bedrock (blue curve)

C1.5 Pore water pressure ratio (r_u)

Figures C45 and C46 show the pore water pressure ratio (r_u) distribution inside the reinforced (unconsolidated) tailings impoundment (with WRI) for configuration 12-42 due to E_3-sag and E_3-north ground motions, respectively. As indicated by the large values of r_u values (> 0.8) in these figures, the tailings between the WRI can be expected to have liquefied at the end of shaking. The simulations indicate that the WRI would not reduce significantly the generation of excess pore water pressures in these tailings (except for locations very close to the inclusions), but would rather serve to prevent their deformation and flow due to liquefaction.

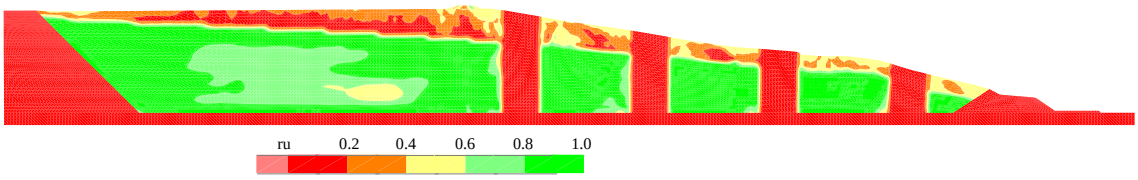

Figure C45: Distribution of the pore water pressure ratio (r_u) due to E3-sag earthquake record (at end of shaking) in the reinforced tailings impoundment (with WRI) for W = 12m and S = 42m for unconsolidated tailings

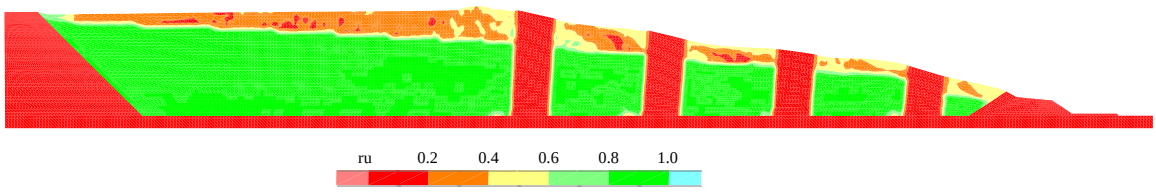

Figure C46: Distribution of the pore water pressure ratio (r_u) due to E3-sag earthquake record (at end of shaking) in the reinforced tailings impoundment (with WRI) for W=12m and S=42m for unconsolidated tailings

Figures C47 and C48 show the pore water pressure ratio (r_u) distribution inside the reinforced (consolidated) tailings impoundment (with WRI) for configuration 12-42 due to E_4-sag and E_4-north ground motions, respectively. As indicated by the large values of r_u values (> 0.8) in these figures, the tailings between the WRI can be expected to have liquefied at the end of shaking. The simulations indicate that the WRI would not reduce significantly the generation of excess pore water pressures in these tailings (except for locations very close to the inclusions), but would rather serve to prevent their deformation and flow due to liquefaction.

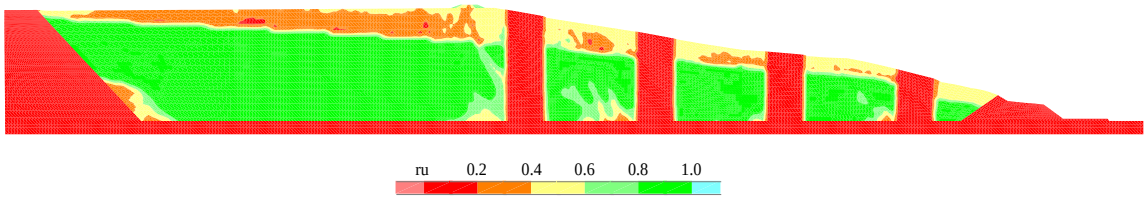

Figure C47: Distribution of the pore water pressure ratio (r_u) due to E4-sag earthquake record (at end of shaking) in the reinforced tailings impoundment (with WRI) for W = 12m and S = 42m for consolidated tailings

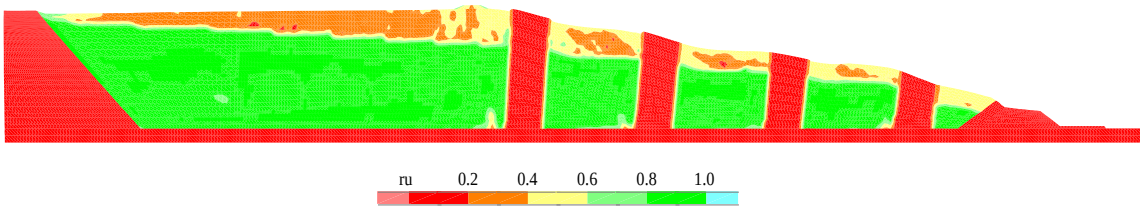

Figure C48: Distribution of the pore water pressure ratio (r_u) due to E4-north earthquake record (at end of shaking) in the reinforced tailings impoundment (with WRI) for W = 12m and S = 42m for consolidated tailings

APPENDIX D- THE RESULTS OF NUMERICAL SIMULATIONS OF A TAILINGS IMPOUNDMENT (BASED ON A SITE LOCATED IN THE WEST OF QUEBEC, CANADA)

D1.1 Values of the relative horizontal displacement R_x along the downstream slope of a tailings impoundment in west of Quebec for the high (Saguenay) and low (Northridge) frequency ground motion

Figures D1 to D50 show the normalized horizontal displacement (R_x) of points located along the slope of the unconsolidated ($(N_1)_{60} = 3$, blows/30 cm) and consolidated ($(N_1)_{60} = 11$, blows/30 cm) tailings impoundment for different configurations of waste rock inclusions (WRI) due to the different ground motion records. These figures show the initial profile of the slope of the tailings impoundment. The configurations are denoted in the form of wx-dy where "x" is the width of the inclusion in meters, "y" is the center-to-center spacing of the inclusion in meters, and may be followed by a time indicated the occurrence of an error in the program due to the development of unacceptable geometry in one or more elements.

Figure D1, for instance, shows that the values of R_x along the slope of impoundment for all configurations are less than 5%. It means that the impoundment with all configurations of WRI is stable due to E_1-sag ground motion

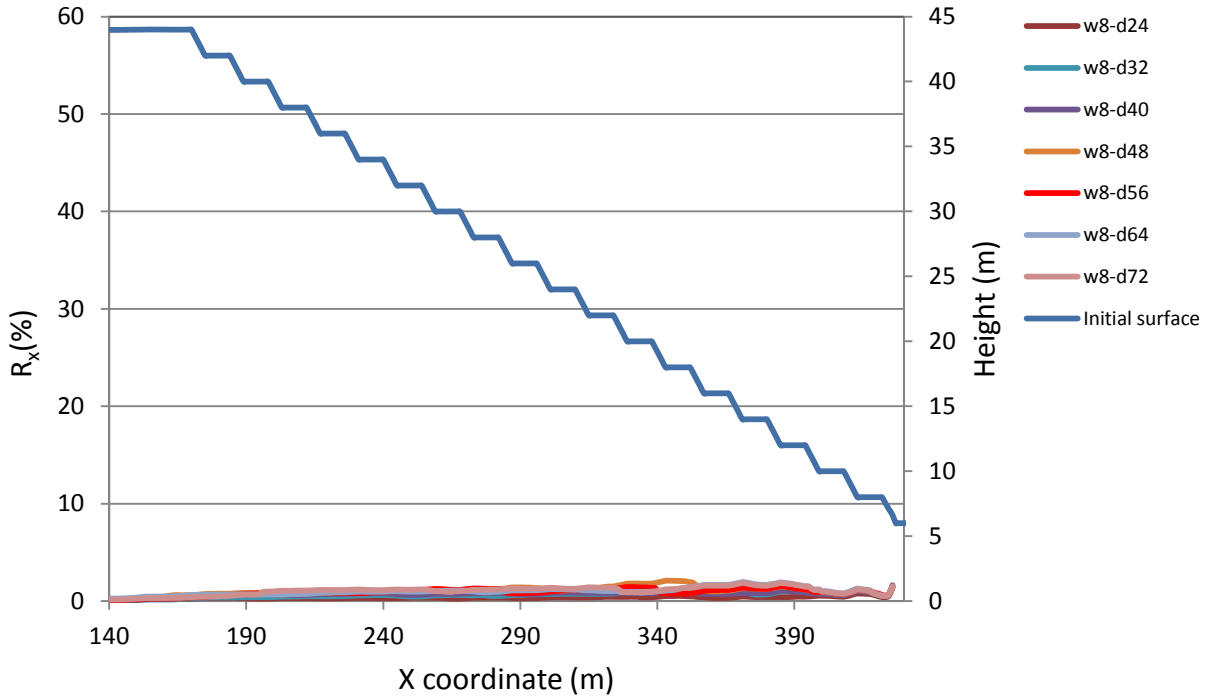

Figure D1: The value of R_x along the slope of the impoundment within unconsolidated tailings ($(N_1)_{60} = 3$, blows/30 cm), due to E_1-sag earthquake record (S16T) for inclusions with width of 8 meters. In the legend in the right top of the figure, first number is the width of inclusions, second number is center-to-center spacing, and third number in some cases is time that the model was stopped due to bad geometry in a zone

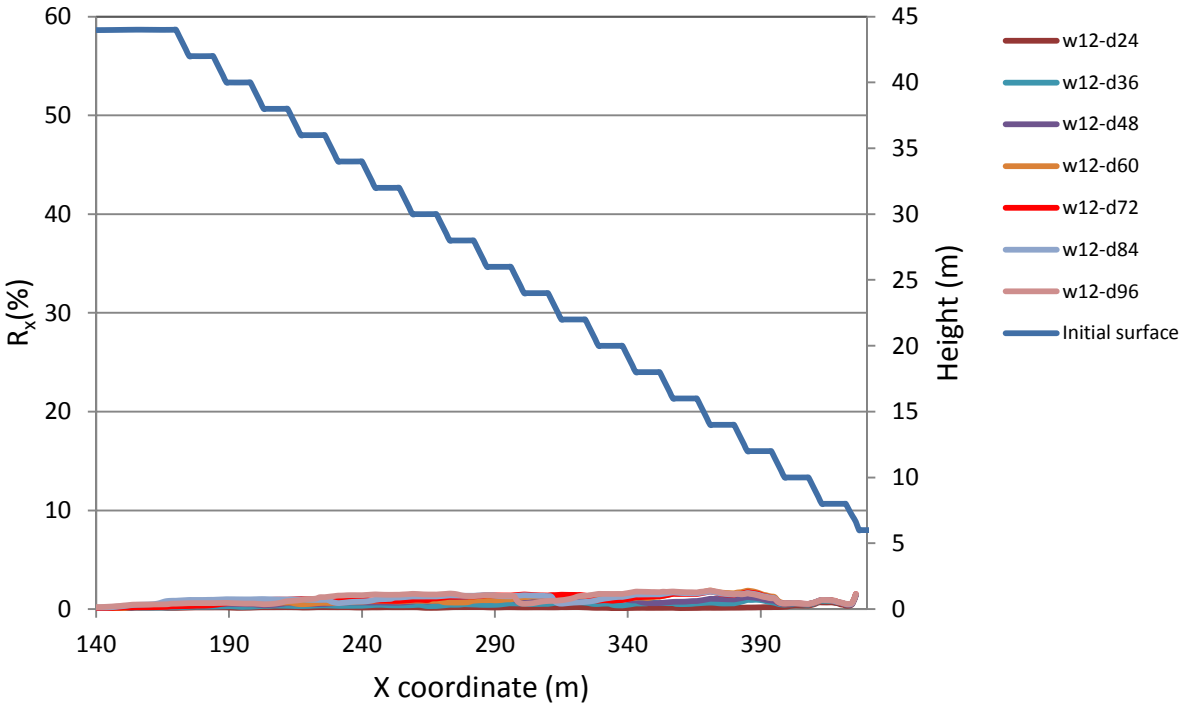

Figure D2: The value of R_x along the slope of the impoundment within unconsolidated tailings ($(N_1)_{60} = 3$, blows/30 cm) due to E_1-sag earthquake record (S16T) for inclusions with width of 12 meters. In the legend in the right top of the figure, first number is the width of inclusions, second number is center-to-center spacing, and third number in some cases is time that the model was stopped due to bad geometry in a zone

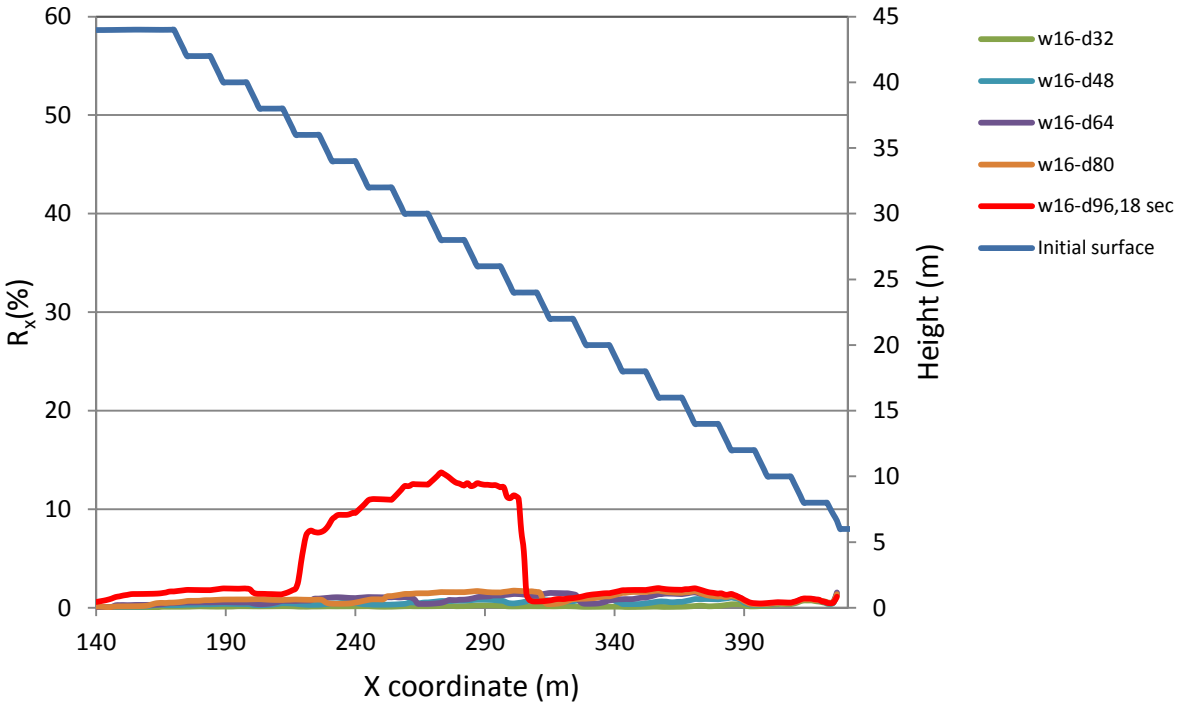

Figure D3: The value of R_x in along the slope of the impoundment within unconsolidated tailings ($(N_1)_{60} = 3$, blows/30 cm) due to E_1-sag earthquake record (S16T) for inclusions with width of 16 meters. In the legend in the right top of the figure, first number is the width of inclusions, second number is center-to-center spacing, and third number in some cases is time that the model was stopped due to bad geometry in a zone

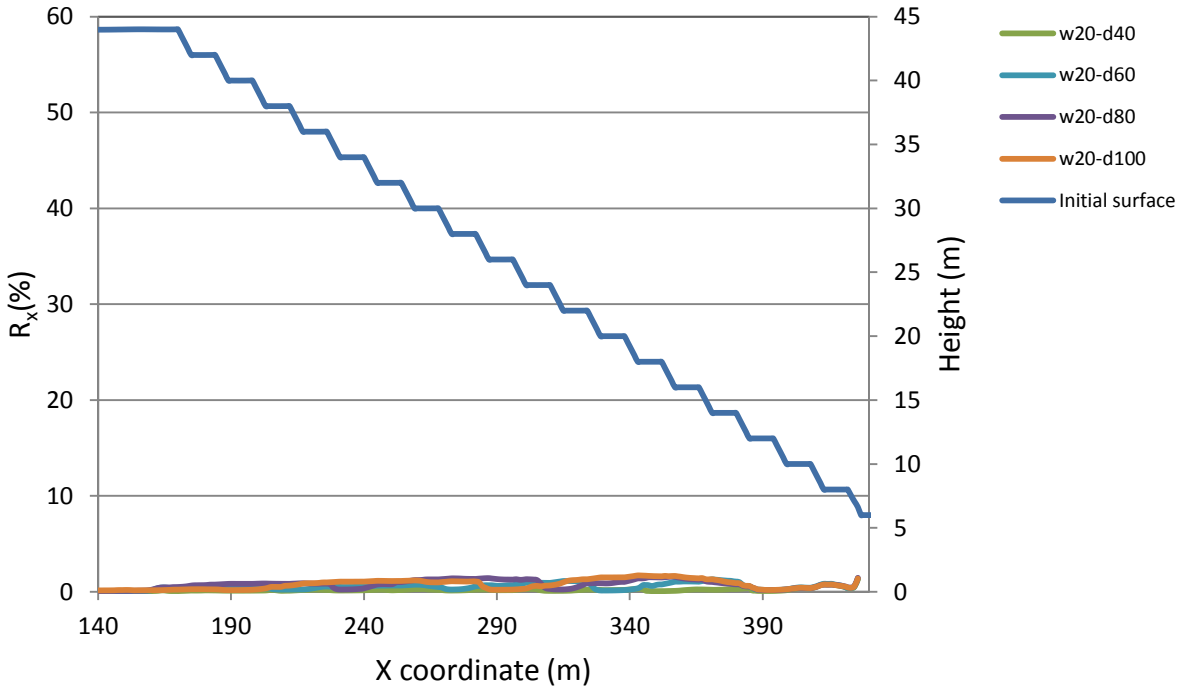

Figure D4: The value of R_x in along the slope of the impoundment within unconsolidated tailings ($(N_1)_{60} = 3$, blows/30 cm) due to E_1-sag earthquake record (S16T) for inclusions with width of 20 meters. In the legend in the right top of the figure, first number is the width of inclusions, second number is center-to-center spacing, and third number in some cases is time that the model was stopped due to bad geometry in a zone

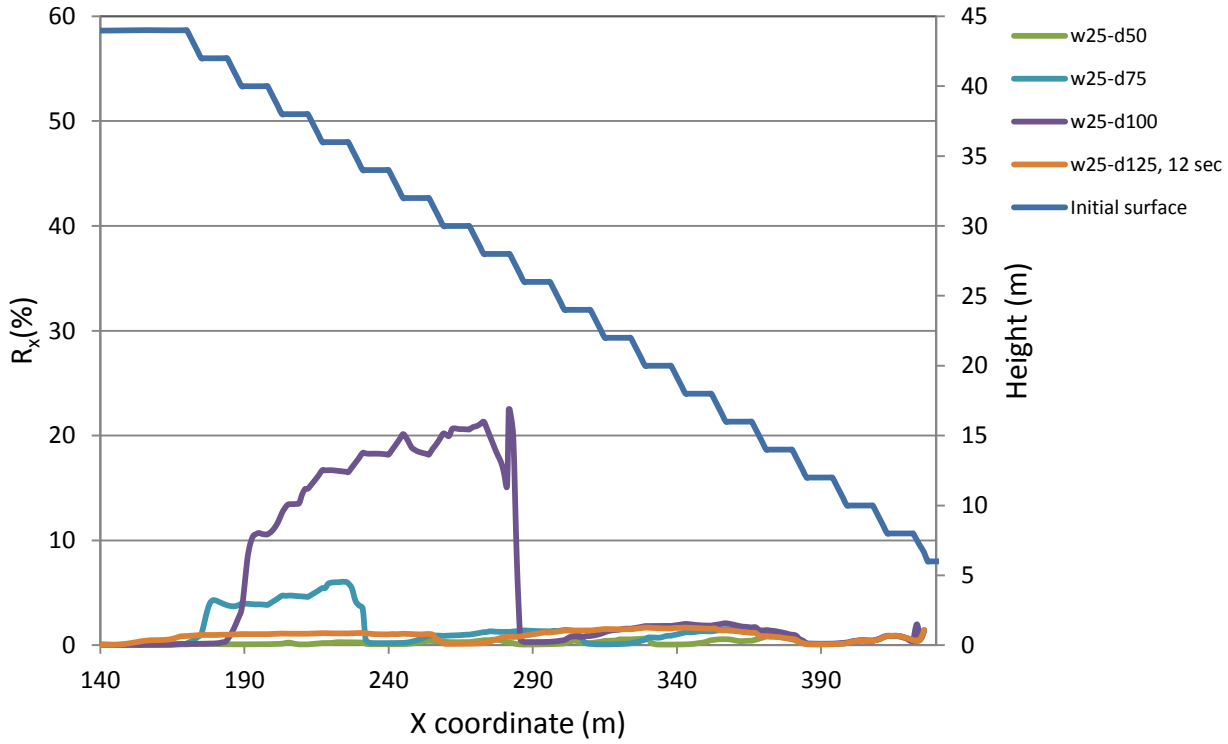

Figure D5: The value of R_x in along the slope of the impoundment within unconsolidated tailings ($(N_1)_{60} = 3$, blows/30 cm) due to E_1-sag earthquake record (S16T) for inclusions with width of 25 meters. In the legend in the right top of the figure, first number is the width of inclusions, second number is center-to-center spacing, and third number in some cases is time that the model was stopped due to bad geometry in a zone

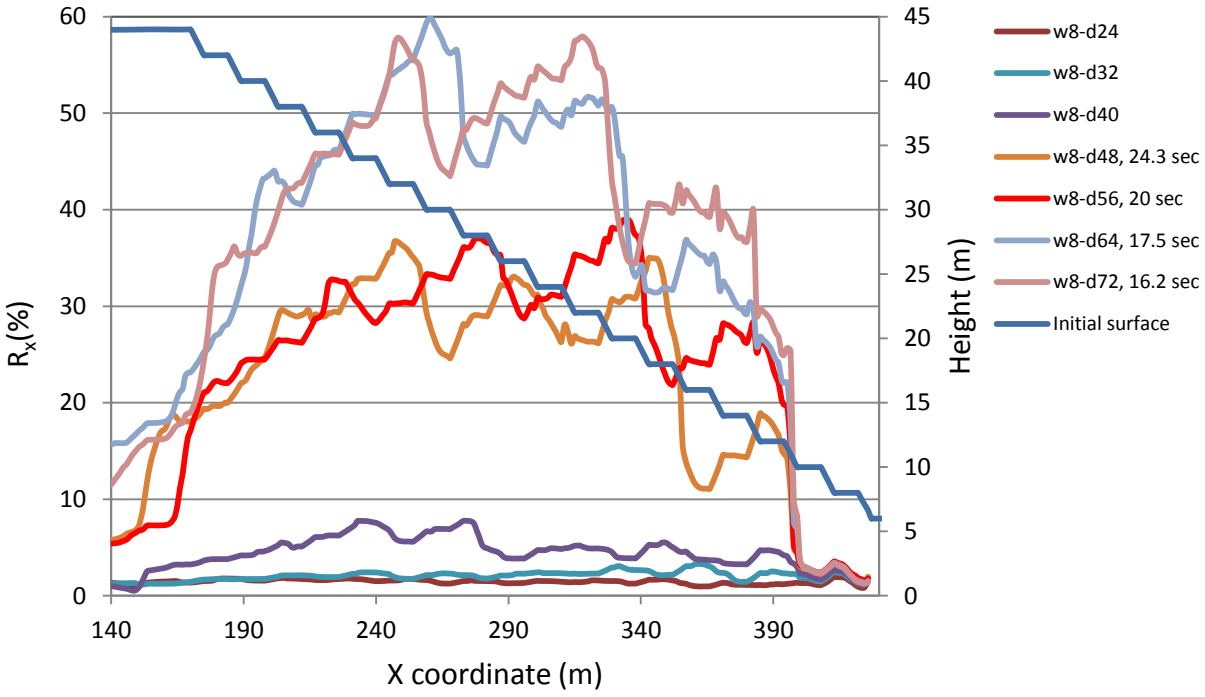

Figure D6: The value of R_x in along the slope of the impoundment within unconsolidated tailings ($(N_1)_{60} = 3$, blows/30 cm) due to E_3-sag earthquake record (S16T) for inclusions with width of 8 meters. In the legend in the right top of the figure, first number is the width of inclusions, second number is center-to-center spacing, and third number in some cases is time that the model was stopped due to bad geometry in a zone

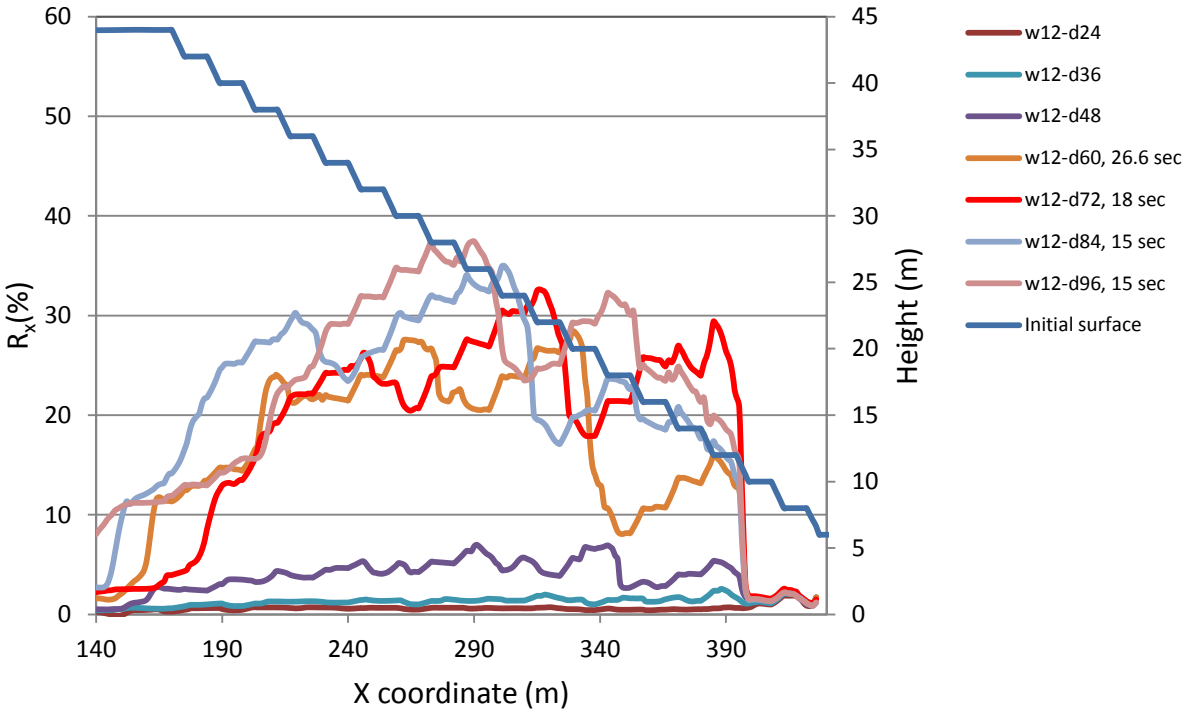

Figure D7: The value of R_x in along the slope of the impoundment within unconsolidated tailings ($(N_1)_{60} = 3$, blows/30 cm) due to E_3-sag earthquake record (S16T) for inclusions with width of 12 meters. In the legend in the right top of the figure, first number is the width of inclusions, second number is center-to-center spacing, and third number in some cases is time that the model was stopped due to bad geometry in a zone

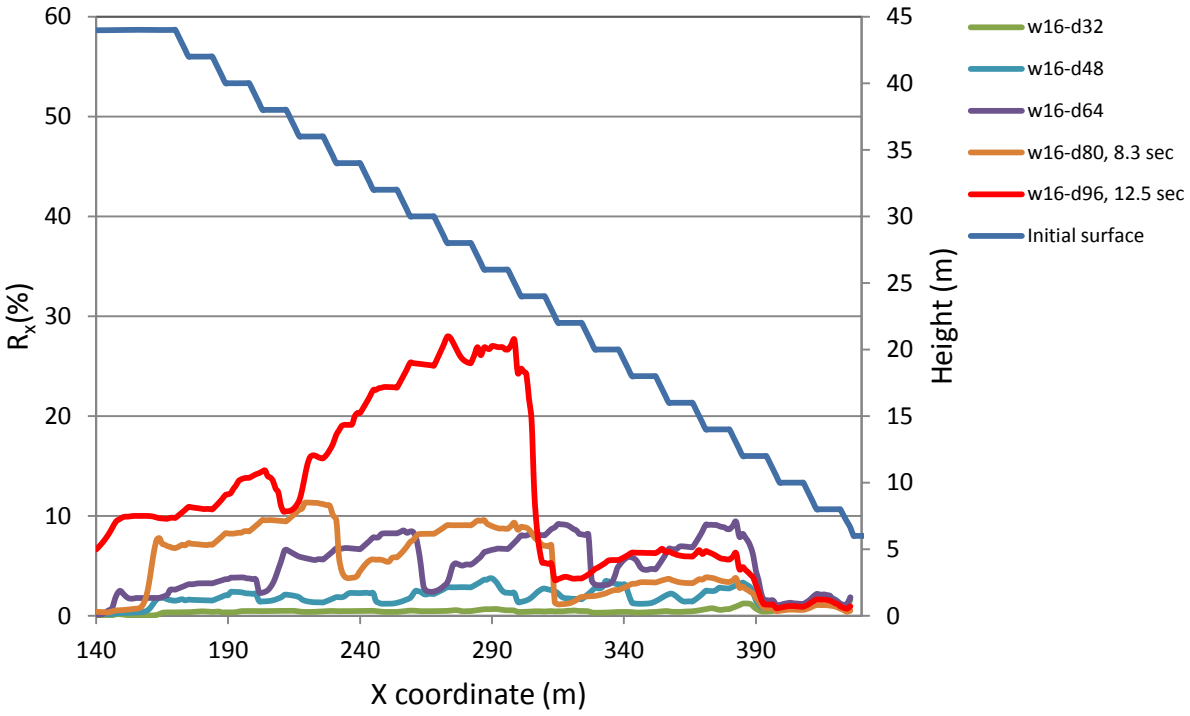

Figure D8: The value of R_x in along the slope of the impoundment within unconsolidated tailings ($(N_1)_{60} = 3$, blows/30 cm) due to E_3-sag earthquake record (S16T) for inclusions with width of 16 meters. In the legend in the right top of the figure, first number is the width of inclusions, second number is center-to-center spacing, and third number in some cases is time that the model was stopped due to bad geometry in a zone

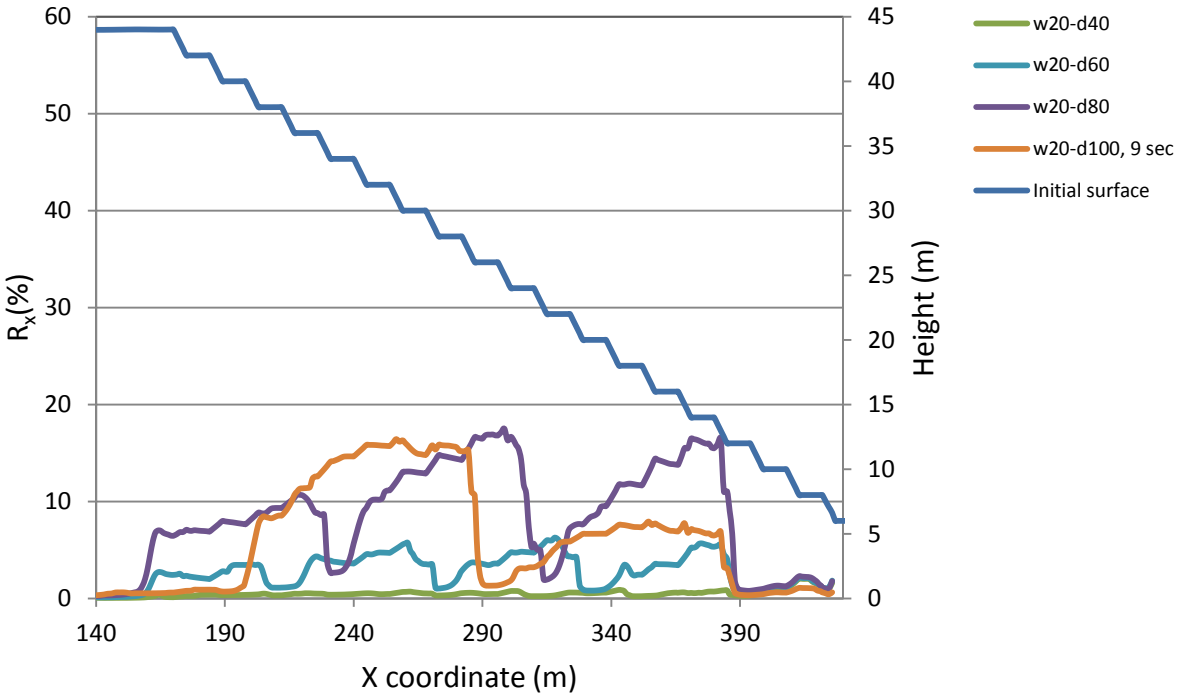

Figure D9: The value of R_x in along the slope of the impoundment within unconsolidated tailings ($(N_1)_{60} = 3$, blows/30 cm) due to E_3-sag earthquake record (S16T) for inclusions with width of 20 meters. In the legend in the right top of the figure, first number is the width of inclusions, second number is center-to-center spacing, and third number in some cases is time that the model was stopped due to bad geometry in a zone

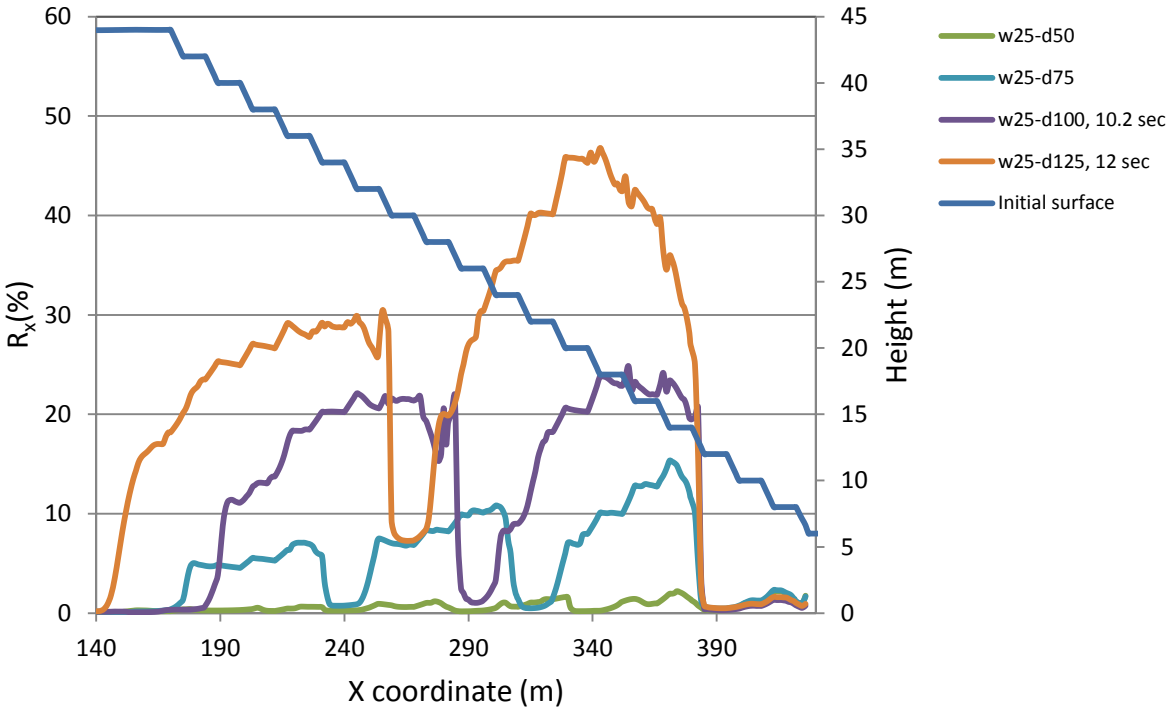

Figure D10: The value of R_x in along the slope of the impoundment within unconsolidated tailings ($(N_1)_{60} = 3$, blows/30 cm) due to E_3-sag earthquake record (S16T) for inclusions with width of 25 meters. In the legend in the right top of the figure, first number is the width of inclusions, second number is center-to-center spacing, and third number in some cases is time that the model was stopped due to bad geometry in a zone

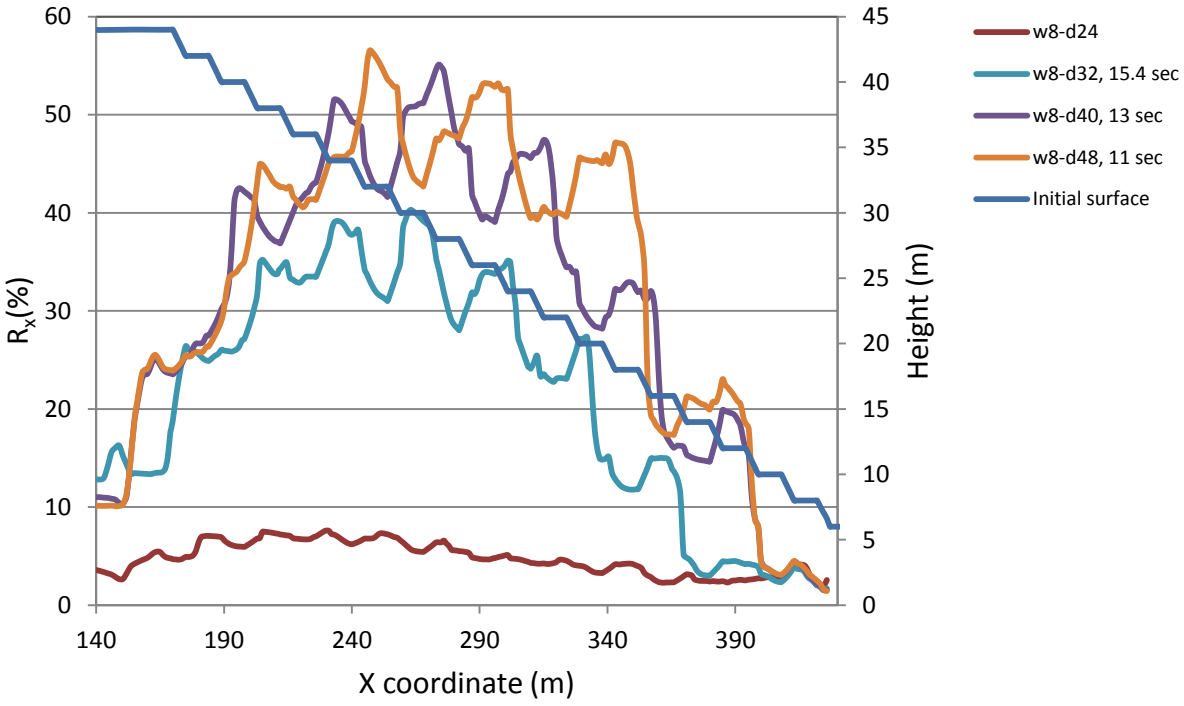

Figure D11: The value of R_x in along the slope of the impoundment within unconsolidated tailings ($(N_1)_{60} = 3$, blows/30 cm) due to E_4-sag earthquake record (S16T) for inclusions with width of 8 meters. In the legend in the right top of the figure, first number is the width of inclusions, second number is center-to-center spacing, and third number in some cases is time that the model was stopped due to bad geometry in a zone

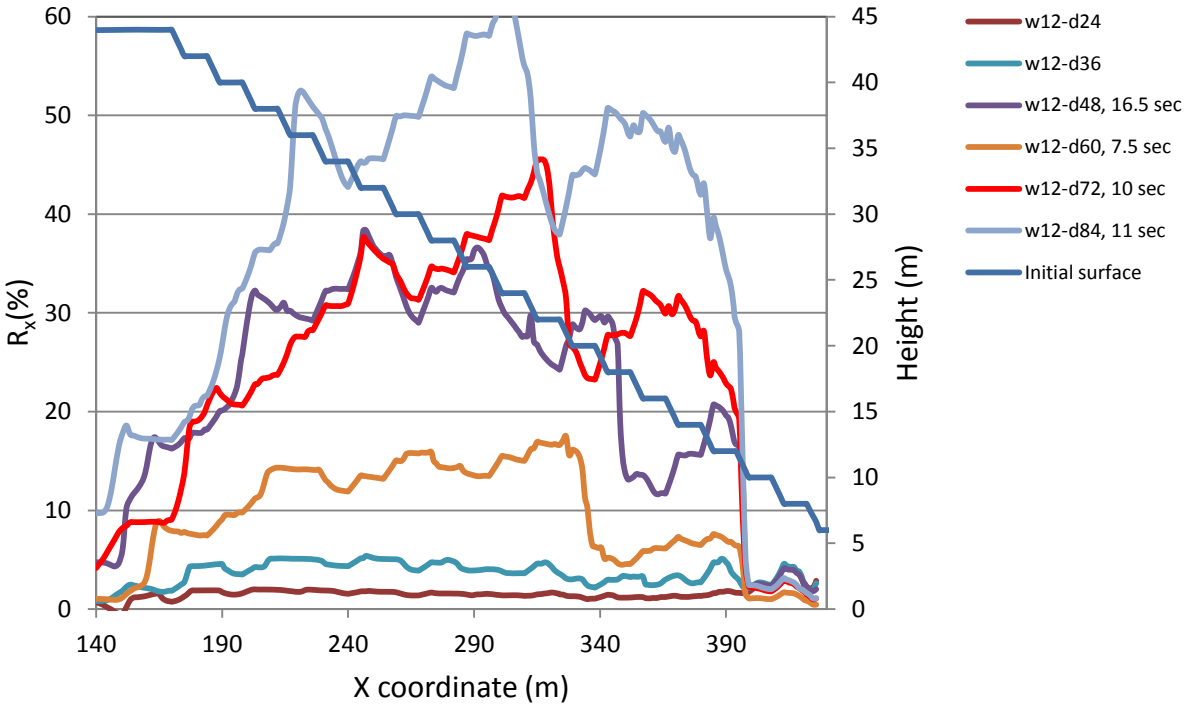

Figure D12: The value of R_x in along the slope of the impoundment within unconsolidated tailings ($(N_1)_{60} = 3$, blows/30 cm) due to E_4-sag earthquake record (S16T) for inclusions with width of 12 meters. In the legend in the right top of the figure, first number is the width of inclusions, second number is center-to-center spacing, and third number in some cases is time that the model was stopped due to bad geometry in a zone

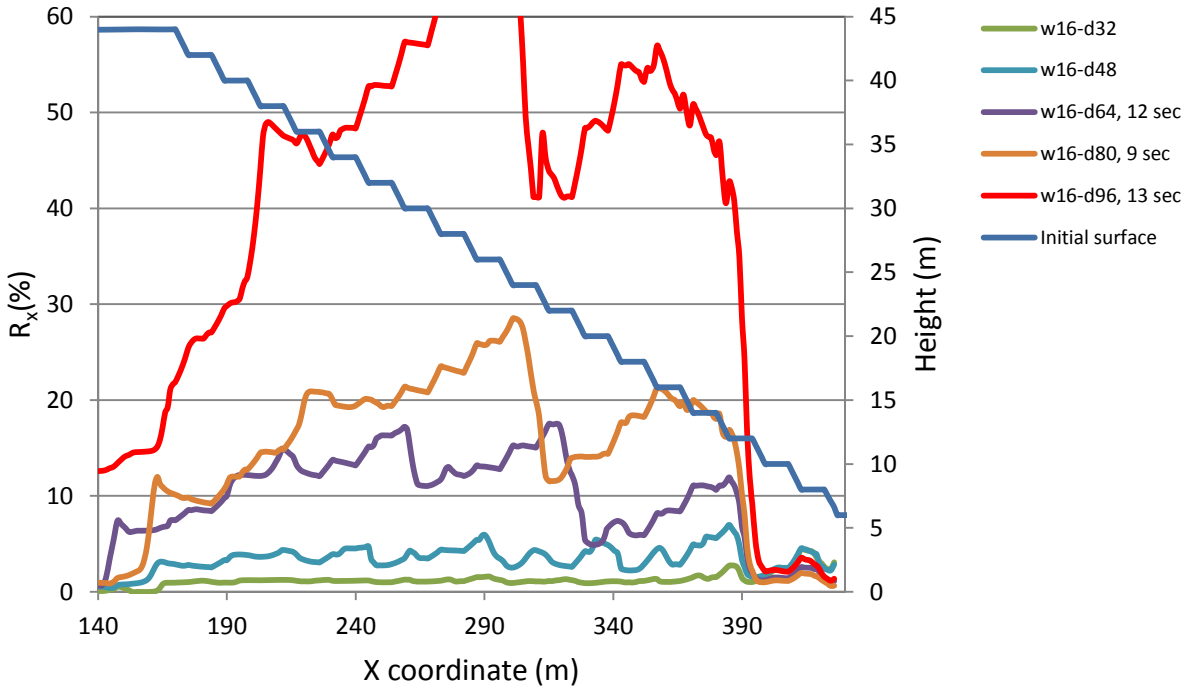

Figure D13: The value of R_x in along the slope of the impoundment within unconsolidated tailings ($(N_1)_{60} = 3$, blows/30 cm) due to E_4-sag earthquake record (S16T) for inclusions with width of 16 meters. In the legend in the right top of the figure, first number is the width of inclusions, second number is center-to-center spacing, and third number in some cases is time that the model was stopped due to bad geometry in a zone

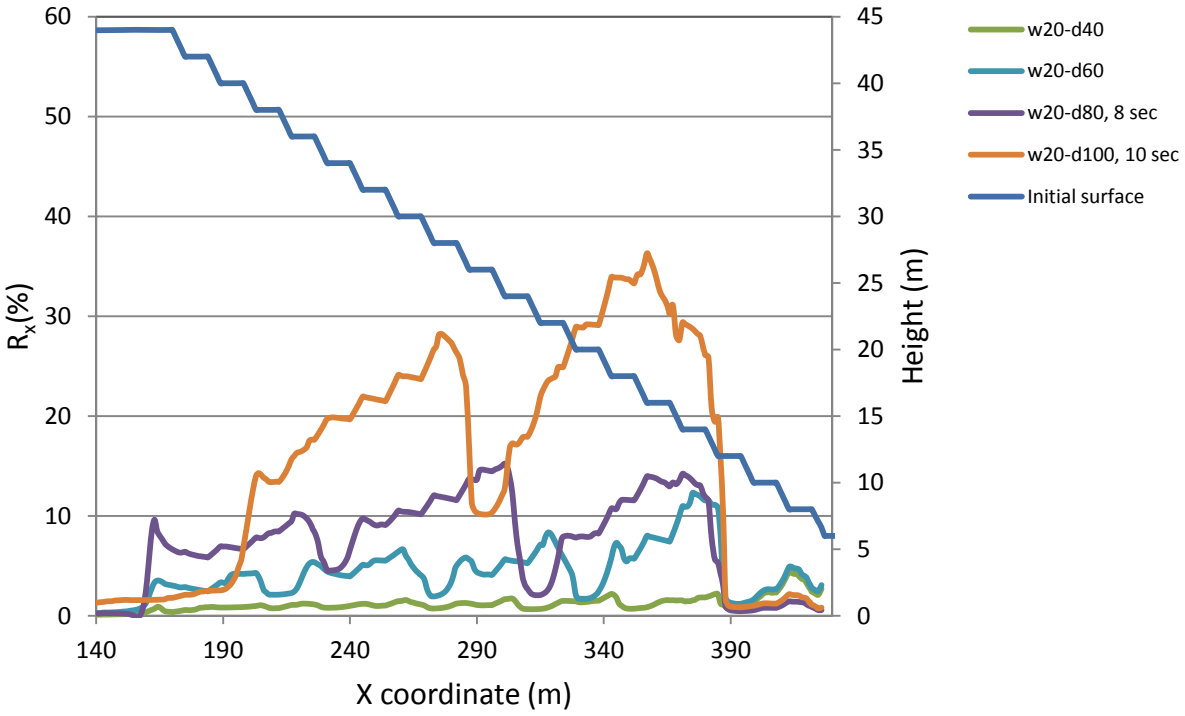

Figure D14: The value of R_x in along the slope of the impoundment within unconsolidated tailings ($(N_1)_{60} = 3$, blows/30 cm) due to E_4-sag earthquake record (S16T) for inclusions with width of 20 meters. In the legend in the right top of the figure, first number is the width of inclusions, second number is center-to-center spacing, and third number in some cases is time that the model was stopped due to bad geometry in a zone

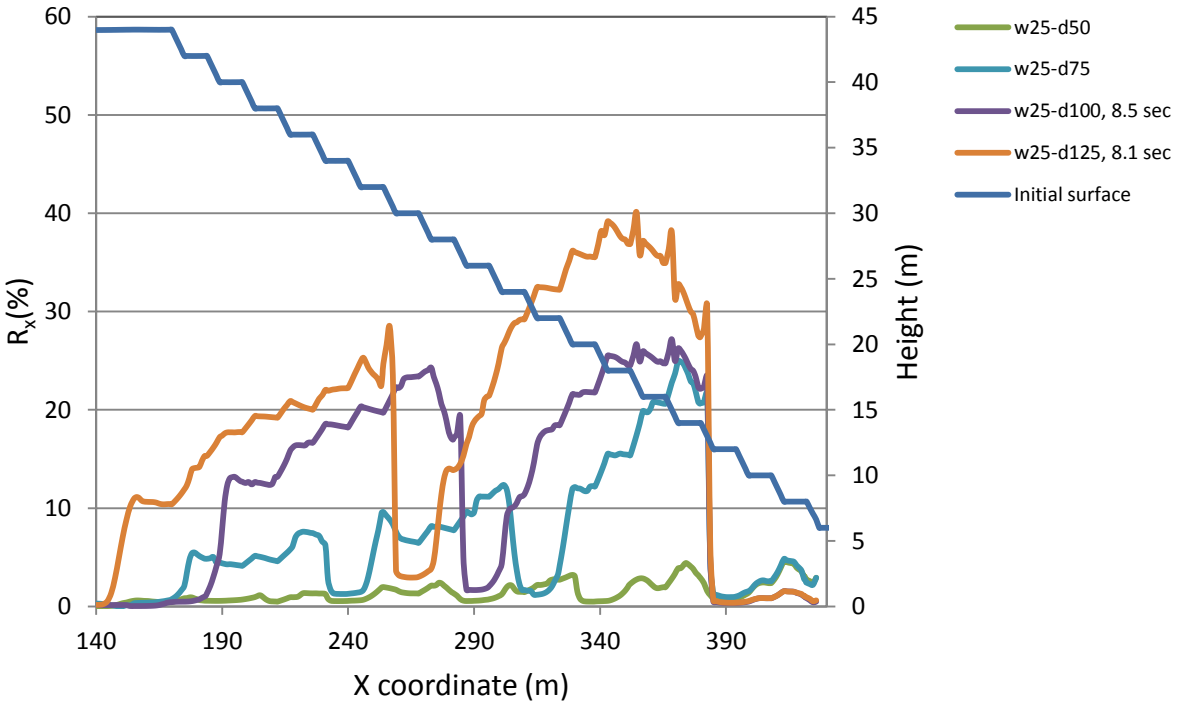

Figure D15: The value of R_x in along the slope of the impoundment within unconsolidated tailings ($(N_1)_{60} = 3$, blows/30 cm) due to E_4-sag earthquake record (S16T) for inclusions with width of 25 meters. In the legend in the right top of the figure, first number is the width of inclusions, second number is center-to-center spacing, and third number in some cases is time that the model was stopped due to bad geometry in a zone

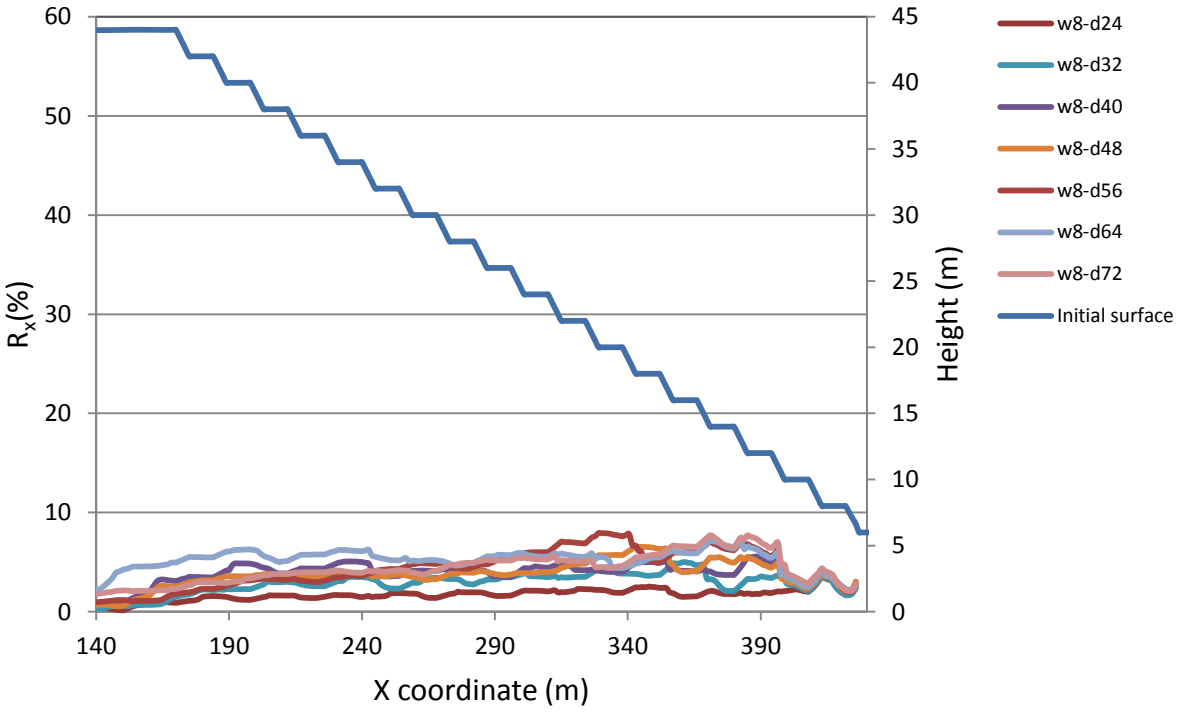

Figure D16: The value of R_x in along the slope of the impoundment within consolidated tailings ($(N_1)_{60} = 11$, blows/30 cm) due to E_4-sag earthquake record (S16T) for inclusions with width of 8 meters. In the legend in the right top of the figure, first number is the width of inclusions, second number is center-to-center spacing, and third number in some cases is time that the model was stopped due to bad geometry in a zone

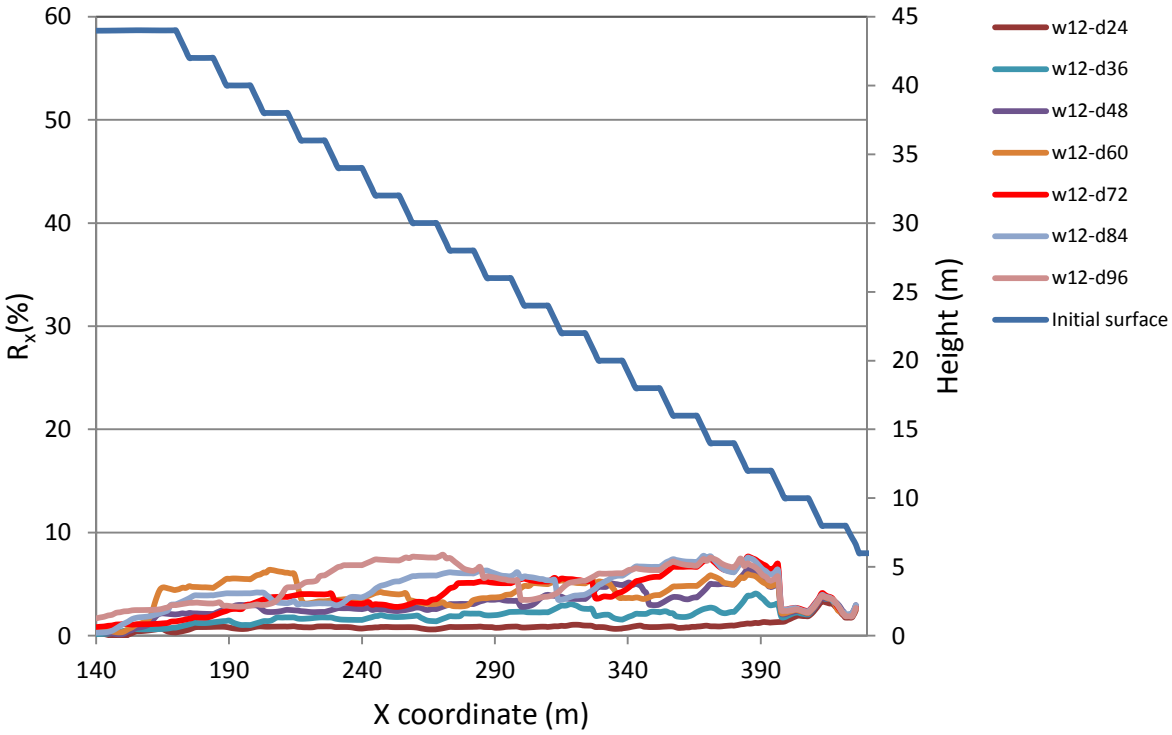

Figure D17: The value of R_x in along the slope of the impoundment within consolidated tailings ($(N_1)_{60} = 11$, blows/30 cm) due to E_4-sag earthquake record (S16T) for inclusions with width of 12 meters. In the legend in the right top of the figure, first number is the width of inclusions, second number is center-to-center spacing, and third number in some cases is time that the model was stopped due to bad geometry in a zone

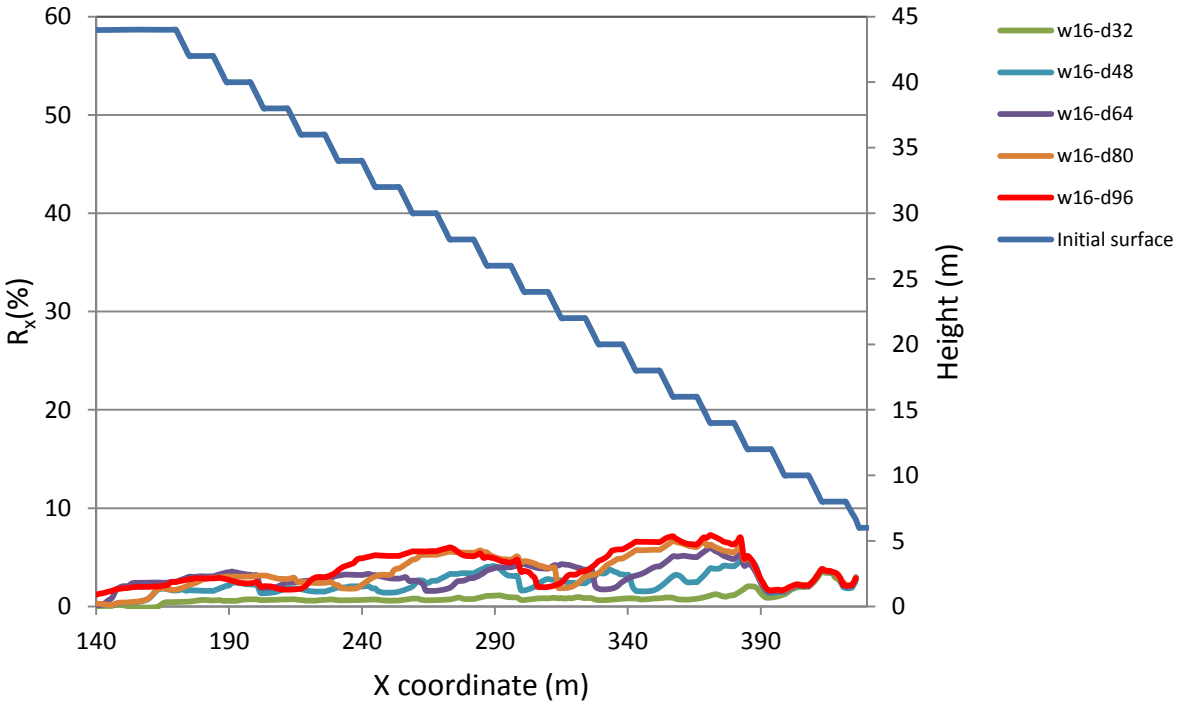

Figure D18: The value of R_x in along the slope of the impoundment within consolidated tailings ($(N_1)_{60} = 11$, blows/30 cm) due to E_4-sag earthquake record (S16T) for inclusions with width of 16 meters. In the legend in the right top of the figure, first number is the width of inclusions, second number is center-to-center spacing, and third number in some cases is time that the model was stopped due to bad geometry in a zone

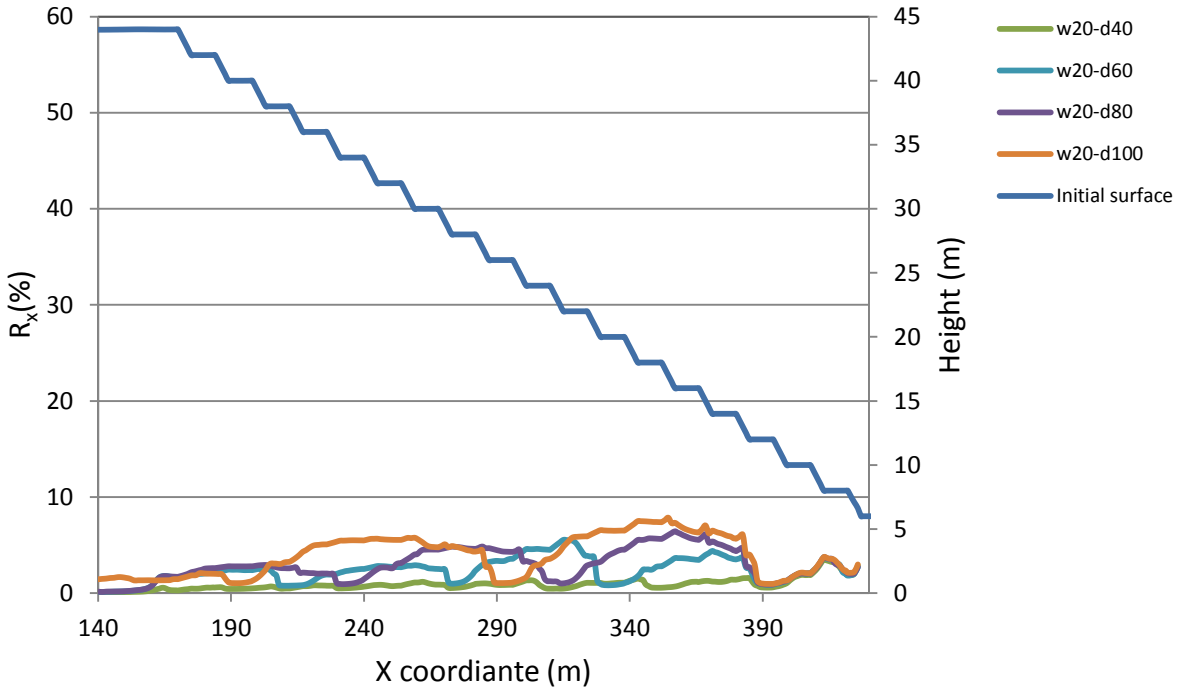

Figure D19: The value of R_x in along the slope of the impoundment within consolidated tailings ($(N_1)_{60} = 11$, blows/30 cm) due to E_4-sag earthquake record (S16T) for inclusions with width of 20 meters. In the legend in the right top of the figure, first number is the width of inclusions, second number is center-to-center spacing, and third number in some cases is time that the model was stopped due to bad geometry in a zone

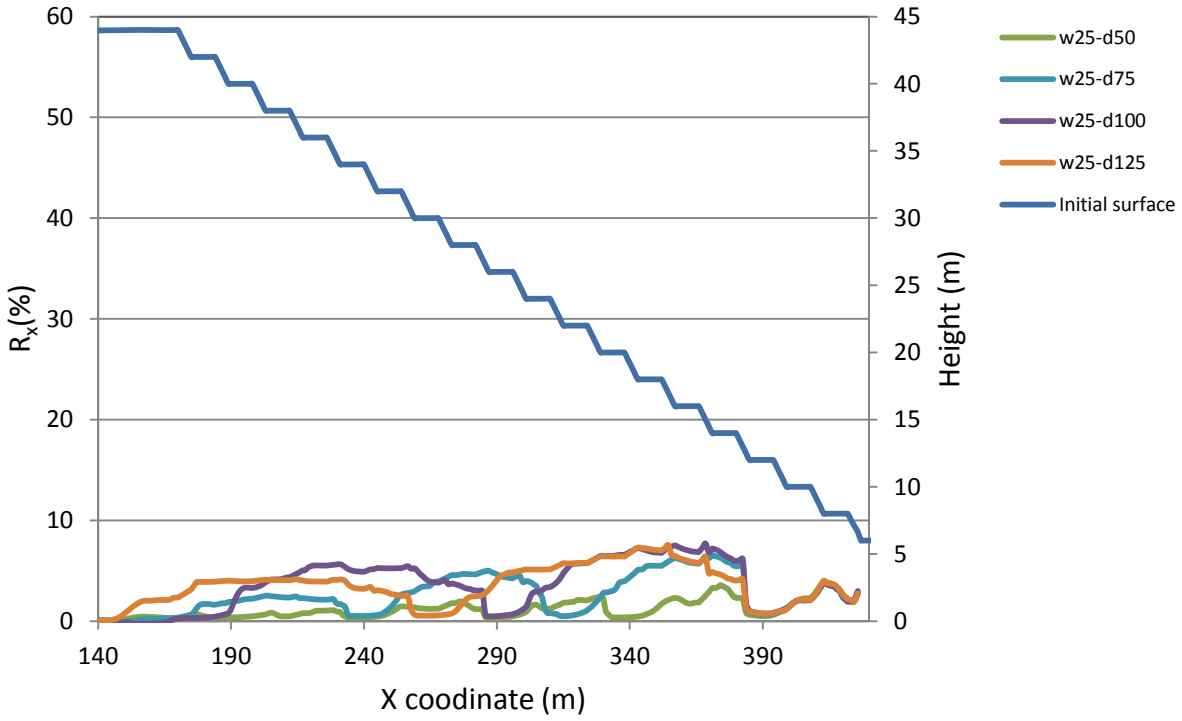

Figure D20: The value of R_x in along the slope of the impoundment within consolidated tailings ($(N_1)_{60} = 11$, blows/30 cm) due to E_4-sag earthquake record (S16T) for inclusions with width of 25 meters. In the legend in the right top of the figure, first number is the width of inclusions, second number is center-to-center spacing, and third number in some cases is time that the model was stopped due to bad geometry in a zone

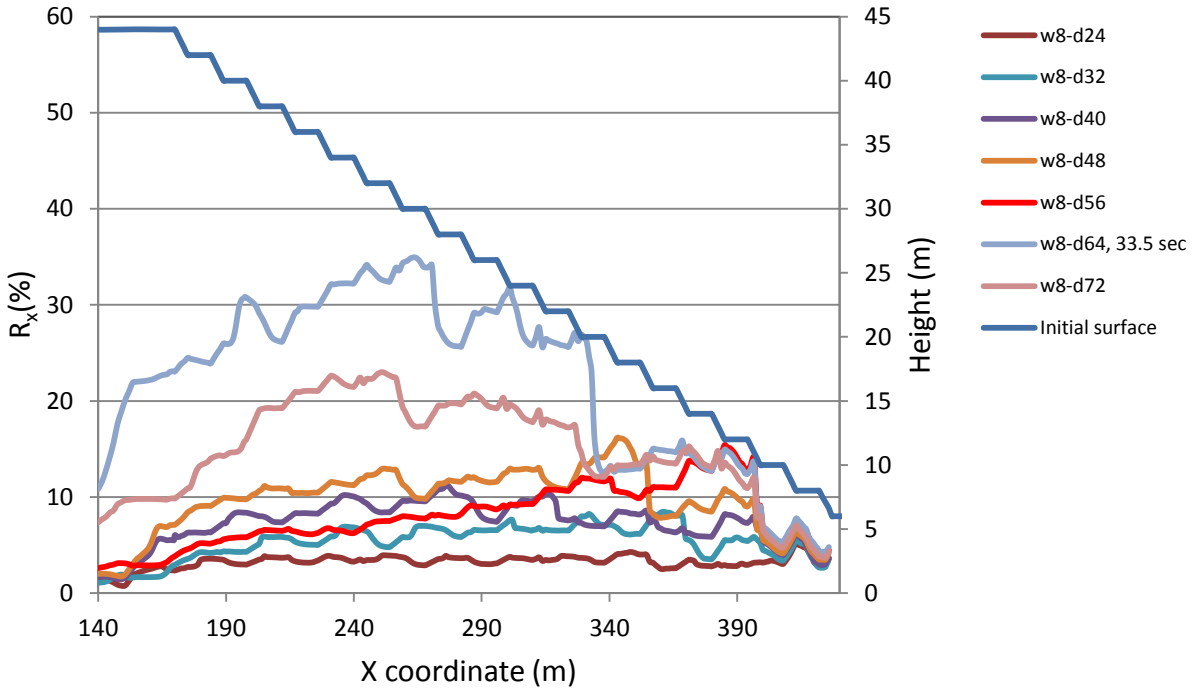

Figure D21: The value of R_x in along the slope of the impoundment within consolidated tailings ($(N_1)_{60} = 11$, blows/30 cm) due to E_5-sag earthquake record (S16T) for inclusions with width of 8 meters. In the legend in the right top of the figure, first number is the width of inclusions, second number is center-to-center spacing, and third number in some cases is time that the model was stopped due to bad geometry in a zone

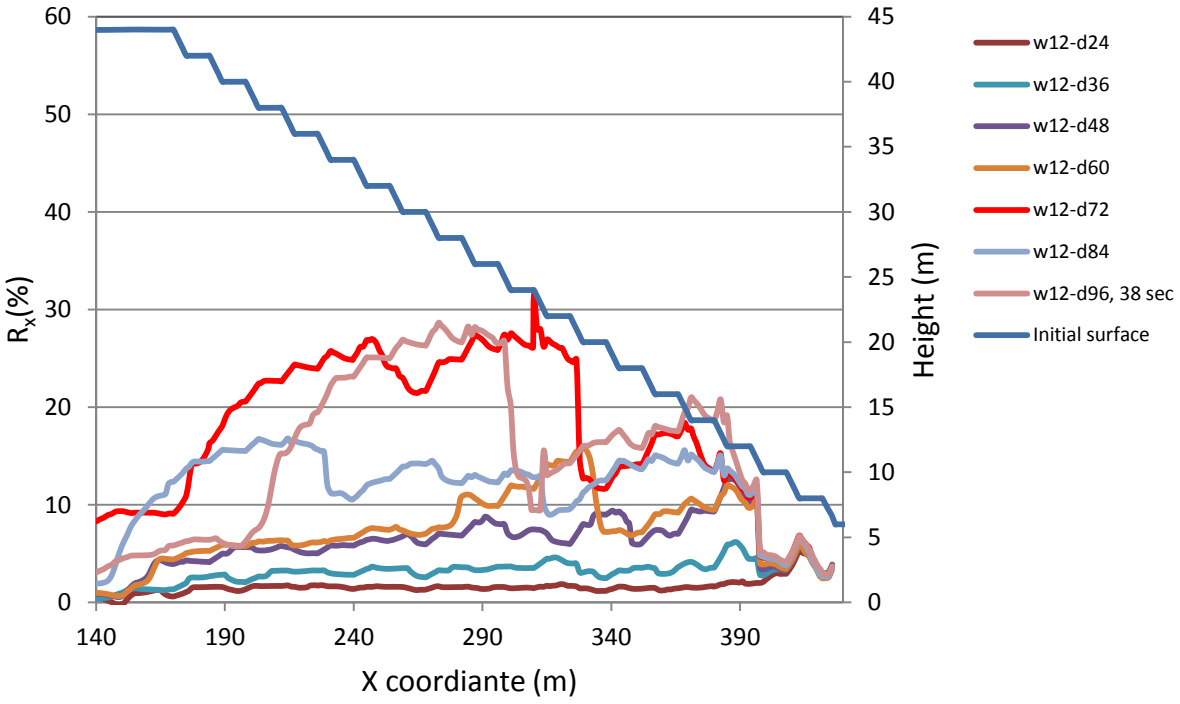

Figure D22: The value of R_x in along the slope of the impoundment within consolidated tailings ($(N_1)_{60} = 11$, blows/30 cm) due to E_5-sag earthquake record (S16T) for inclusions with width of 12 meters. In the legend in the right top of the figure, first number is the width of inclusions, second number is center-to-center spacing, and third number in some cases is time that the model was stopped due to bad geometry in a zone

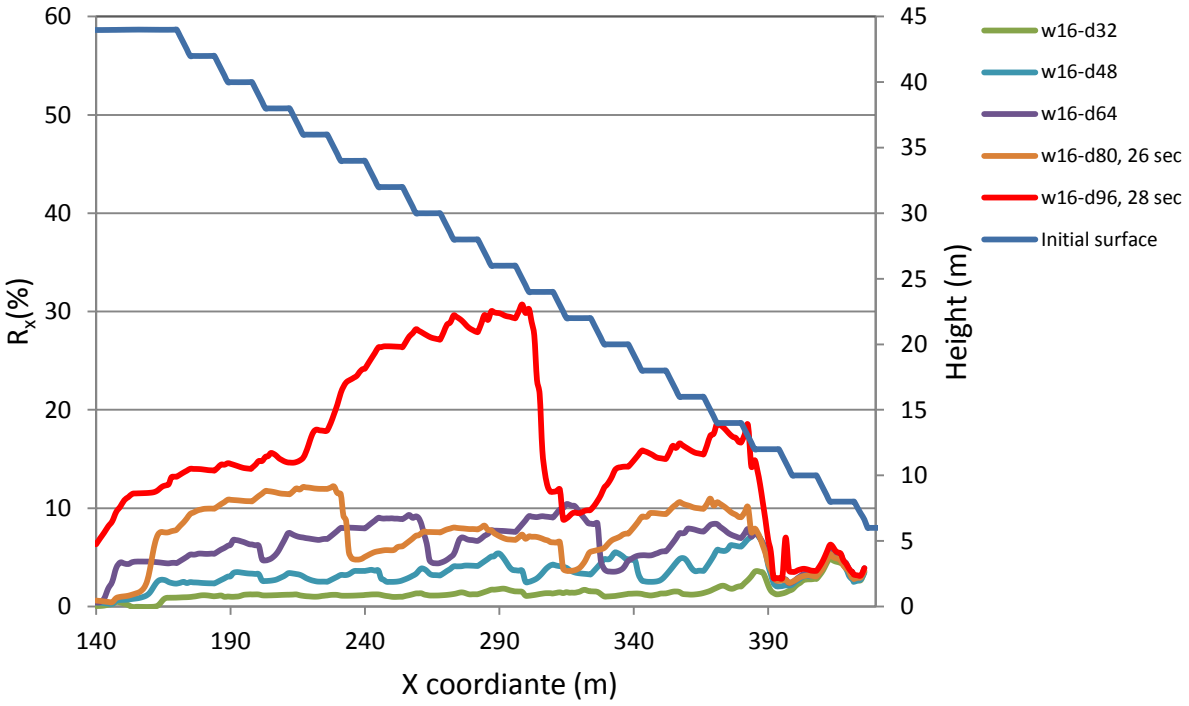

Figure D23: The value of R_x in along the slope of the impoundment within consolidated tailings ($(N_1)_{60} = 11$, blows/30 cm) due to E_5-sag earthquake record (S16T) for inclusions with width of 16 meters. In the legend in the right top of the figure, first number is the width of inclusions, second number is center-to-center spacing, and third number in some cases is time that the model was stopped due to bad geometry in a zone

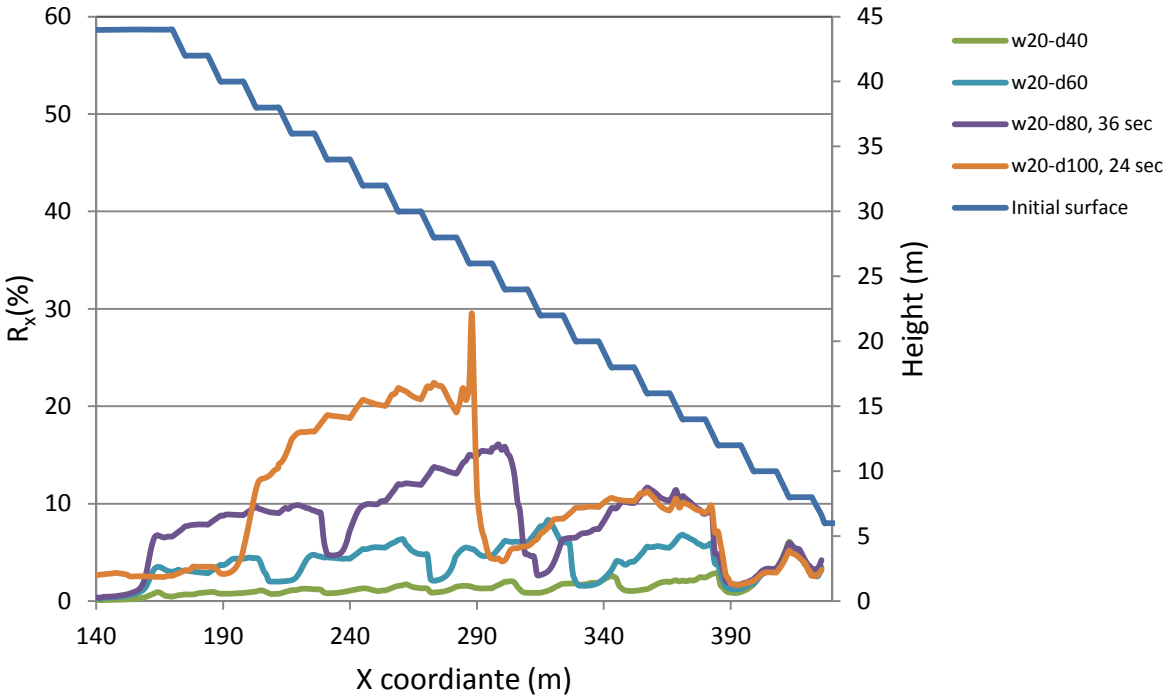

Figure D24: The value of R_x in along the slope of the impoundment within consolidated tailings ($(N_1)_{60} = 11$, blows/30 cm) due to E_5-sag earthquake record (S16T) for inclusions with width of 20 meters. In the legend in the right top of the figure, first number is the width of inclusions, second number is center-to-center spacing, and third number in some cases is time that the model was stopped due to bad geometry in a zone

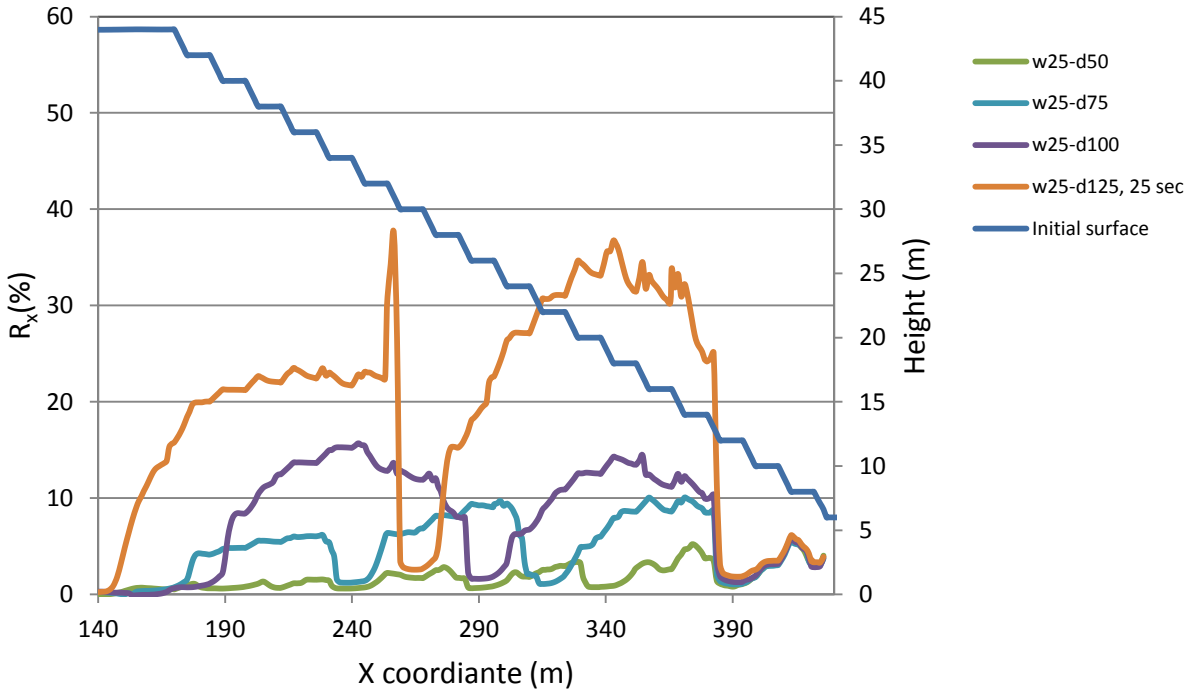

Figure D25: The value of Rx in along the slope of the impoundment within consolidated tailings ($(N_1)_{60} = 11$, blows/30 cm) due to E_5-sag earthquake record (S16T) for inclusions with width of 25 meters. In the legend in the right top of the figure, first number is the width of inclusions, second number is center-to-center spacing, and third number in some cases is time that the model was stopped due to bad geometry in a zone

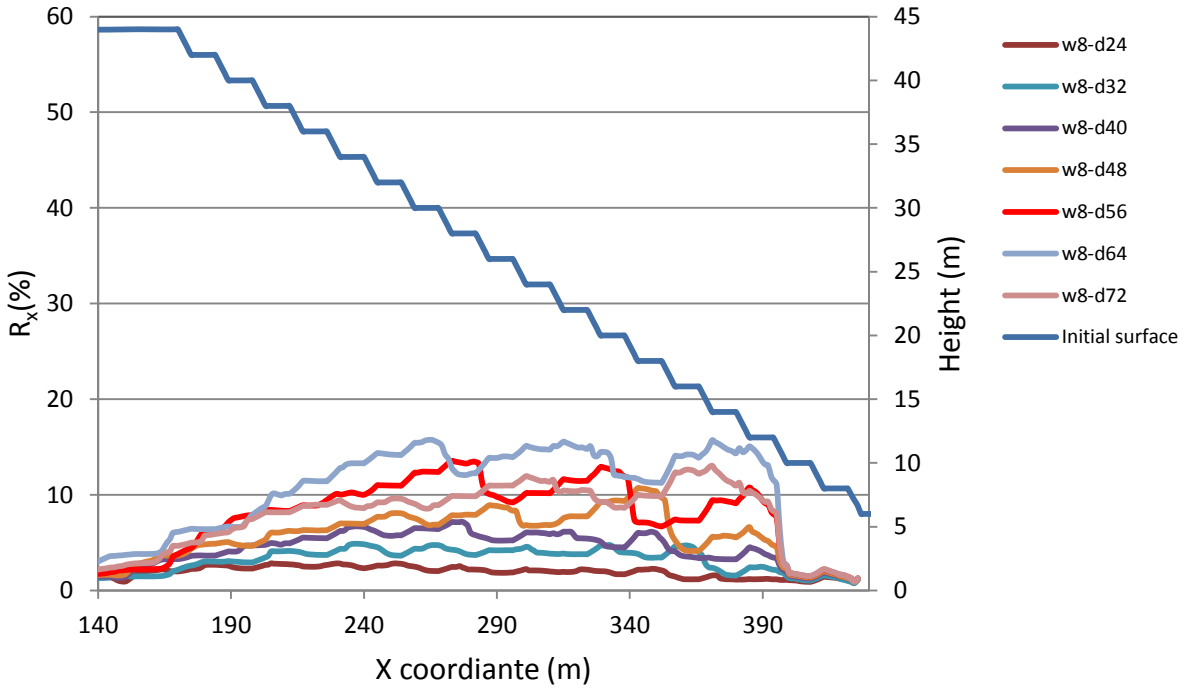

Figure D26: The value of Rx in along the slope of the impoundment within unconsolidated tailings ($(N_1)_{60} = 3$, blows/30 cm) due to E_1-north earthquake record (Northridge) for inclusions with width of 8 meters. In the legend in the right top of the figure, first number is the width of inclusions, second number is center-to-center spacing, and third number in some cases is time that the model was stopped due to bad geometry in a zone

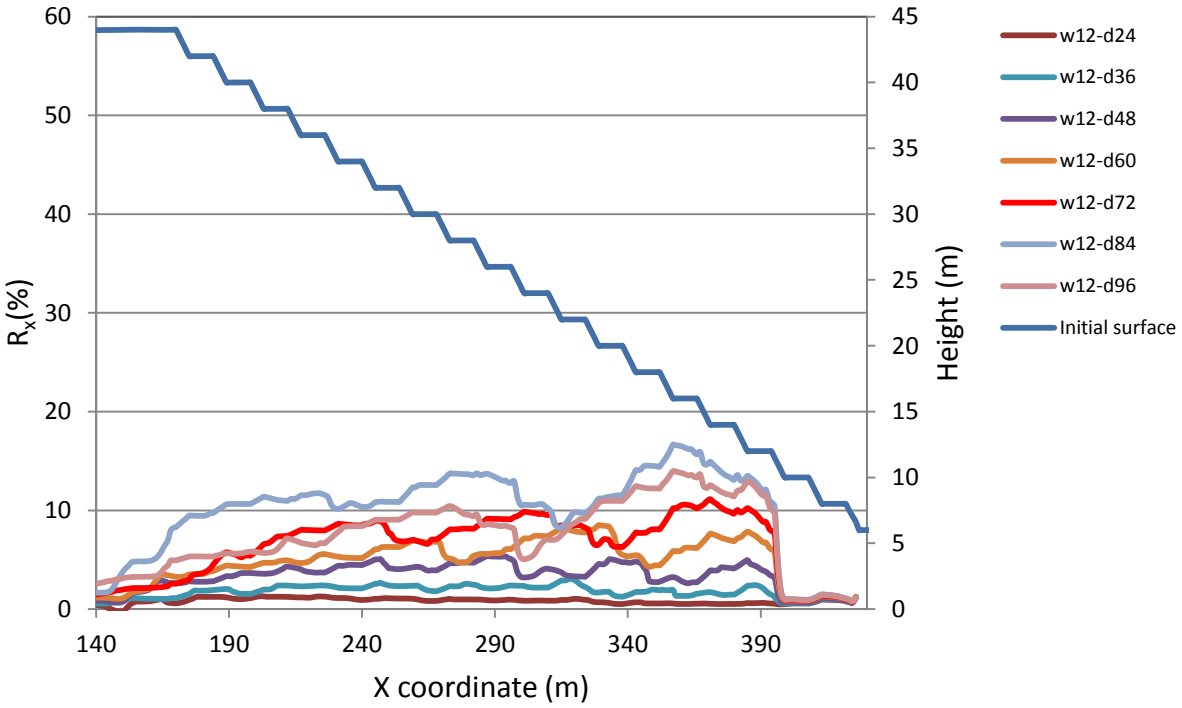

Figure D27: The value of Rx in along the slope of the impoundment within unconsolidated tailings ($(N_1)_{60} = 3$, blows/30 cm) due to E_1-north earthquake record (Northridge) for inclusions with width of 12 meters. In the legend in the right top of the figure, first number is the width of inclusions, second number is center-to-center spacing, and third number in some cases is time that the model was stopped due to bad geometry in a zone

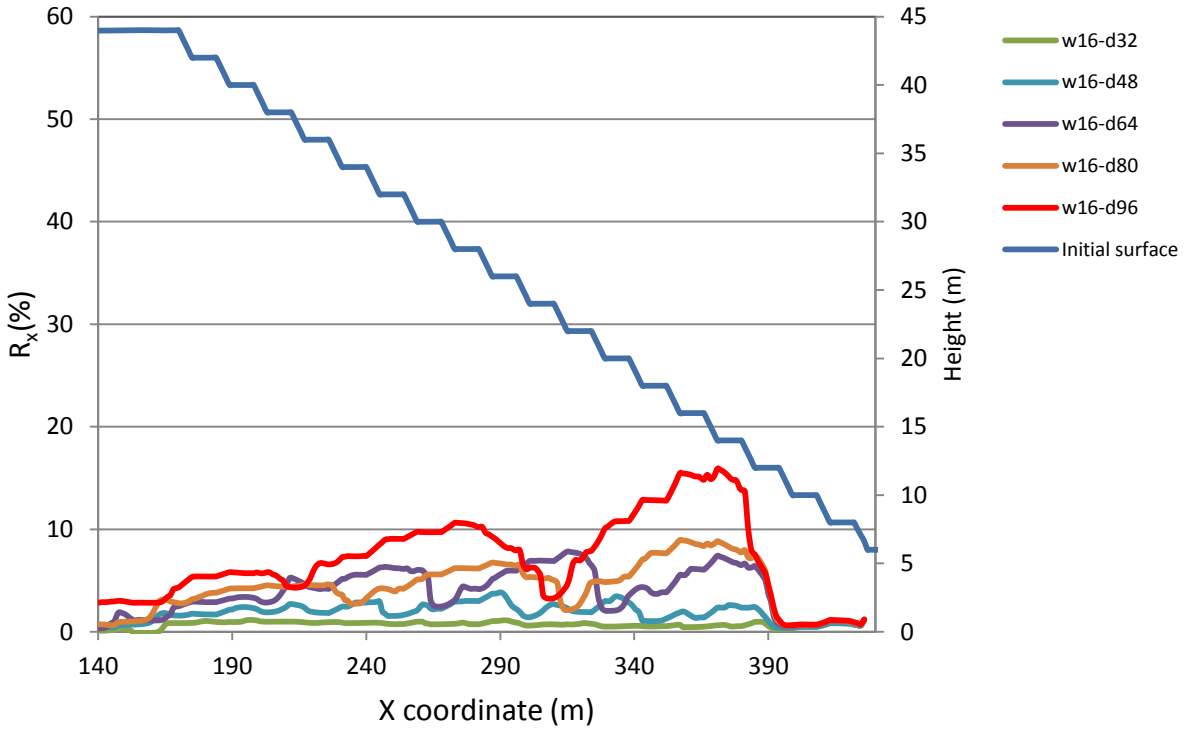

Figure D28: The value of Rx in along the slope of the impoundment within unconsolidated tailings ($(N_1)_{60} = 3$, blows/30 cm) due to E_1-north earthquake record (Northridge) for inclusions with width of 16 meters. In the legend in the right top of the figure, first number is the width of inclusions, second number is center-to-center spacing, and third number in some cases is time that the model was stopped due to bad geometry in a zone

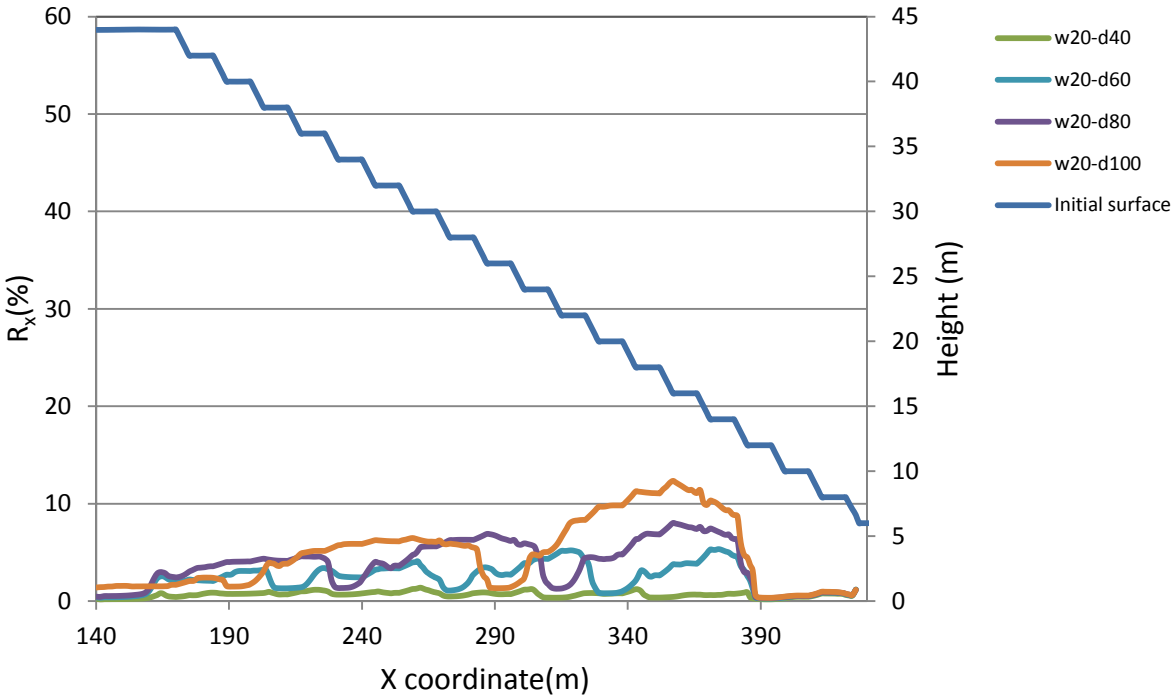

Figure D29: The value of R_x in along the slope of the impoundment within unconsolidated tailings ($(N_1)_{60} = 3$, blows/30 cm) due to E_1-north earthquake record (Northridge) for inclusions with width of 20 meters. In the legend in the right top of the figure, first number is the width of inclusions, second number is center-to-center spacing, and third number in some cases is time that the model was stopped due to bad geometry in a zone

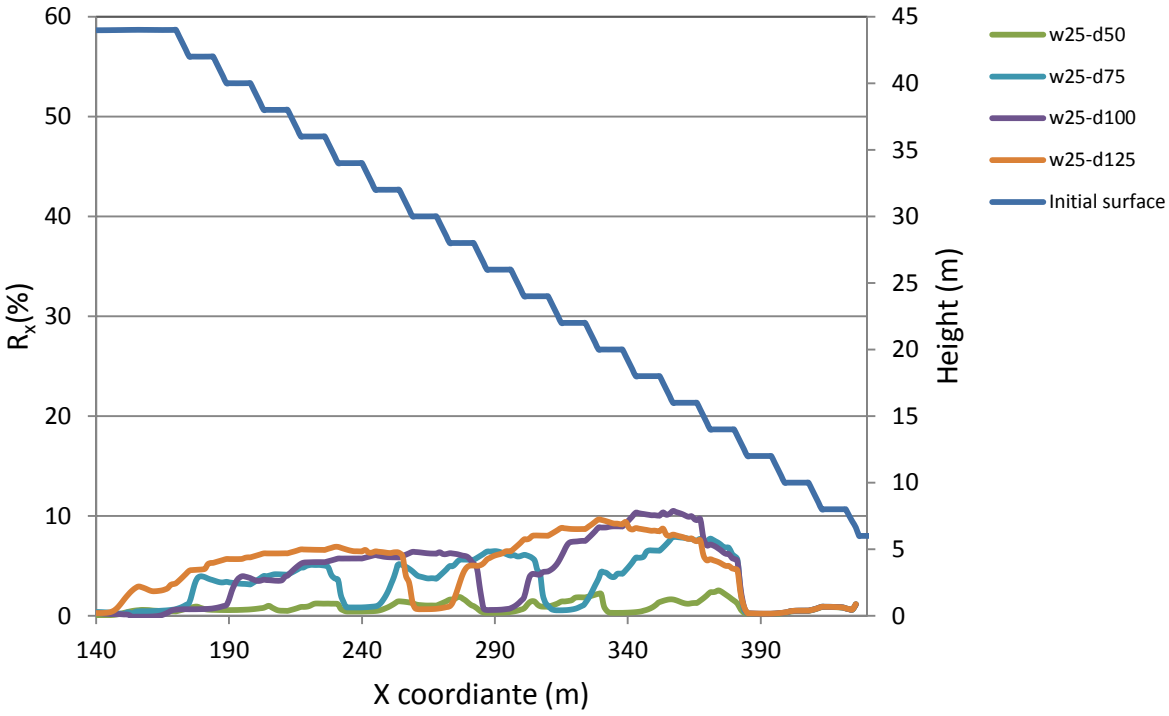

Figure D30: The value of R_x in along the slope of the impoundment within unconsolidated tailings ($(N_1)_{60} = 3$, blows/30 cm) due to E_1-north earthquake record (Northridge) for inclusions with width of 25 meters. In the legend in the right top of the figure, first number is the width of inclusions, second number is center-to-center spacing, and third number in some cases is time that the model was stopped due to bad geometry in a zone

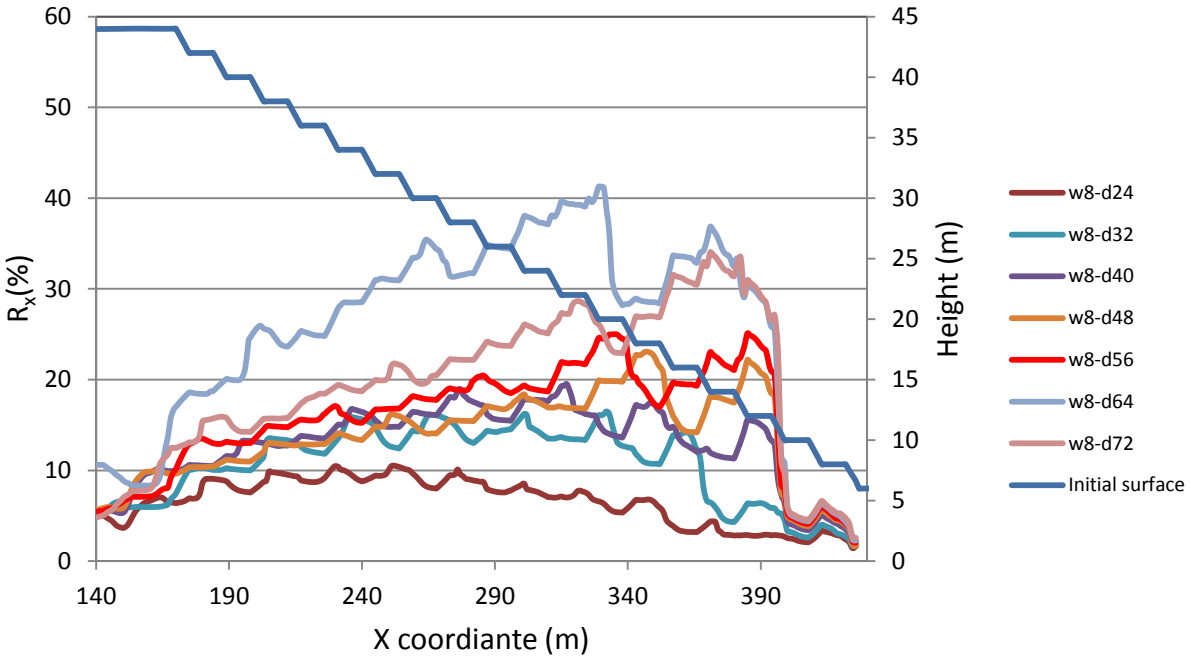

Figure D31: The value of R_x in along the slope of the impoundment within unconsolidated tailings ($(N_1)_{60} = 3$, blows/30 cm) due to E_3-north earthquake record (Northridge) for inclusions with width of 8 meters. In the legend in the right top of the figure, first number is the width of inclusions, second number is center-to-center spacing, and third number in some cases is time that the model was stopped due to bad geometry in a zone

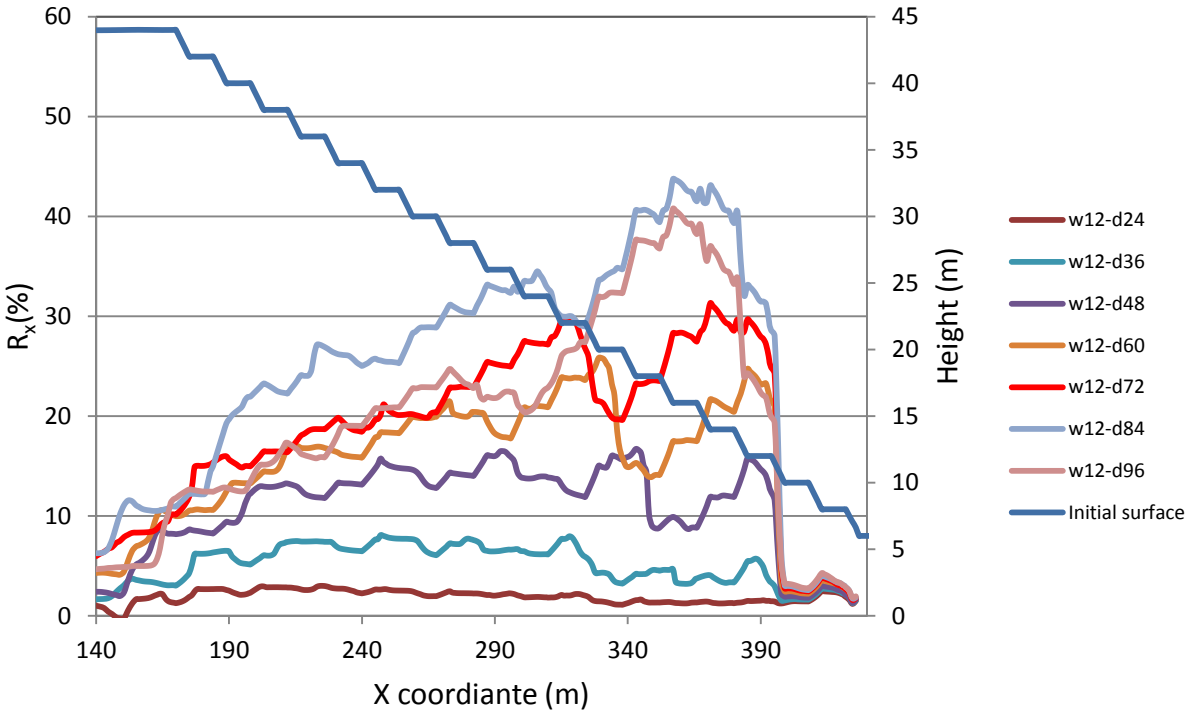

Figure D32: The value of R_x in along the slope of the impoundment within unconsolidated tailings ($(N_1)_{60} = 3$, blows/30 cm) due to E_3-north earthquake record (Northridge) for inclusions with width of 12 meters. In the legend in the right top of the figure, first number is the width of inclusions, second number is center-to-center spacing, and third number in some cases is time that the model was stopped due to bad geometry in a zone

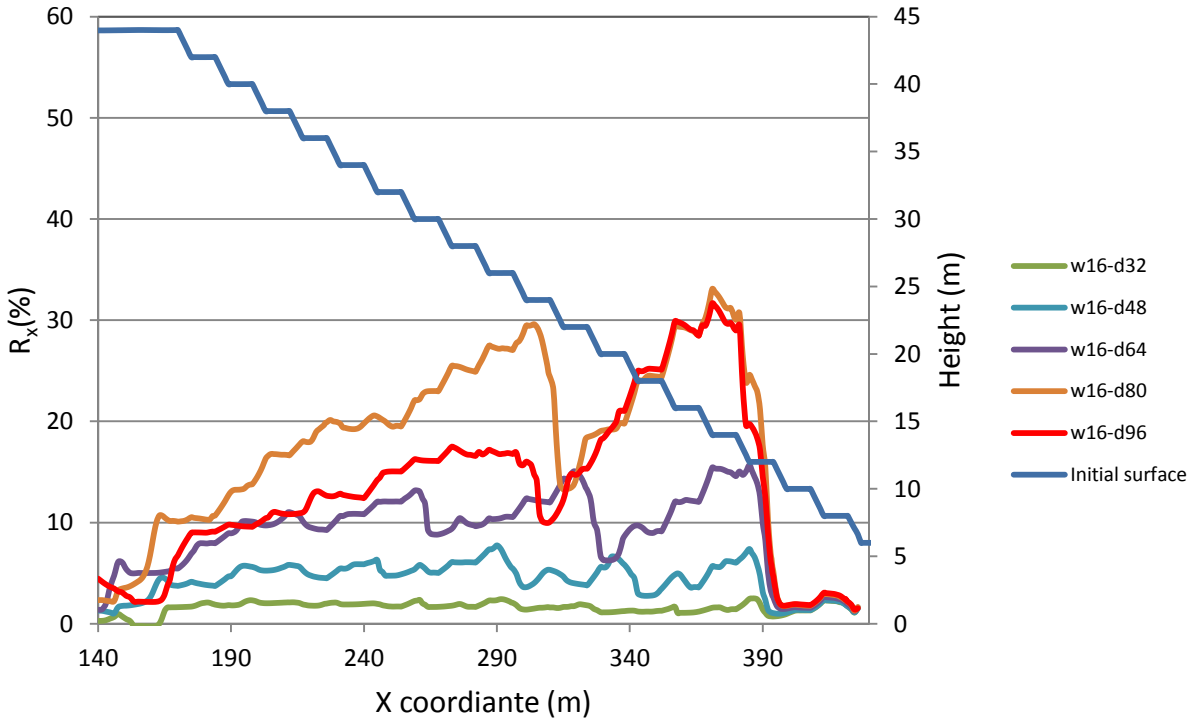

Figure D33: The value of R_x in along the slope of the impoundment within unconsolidated tailings ($(N_1)_{60} = 3$, blows/30 cm) due to E_3-north earthquake record (Northridge) for inclusions with width of 16 meters. In the legend in the right top of the figure, first number is the width of inclusions, second number is center-to-center spacing, and third number in some cases is time that the model was stopped due to bad geometry in a zone

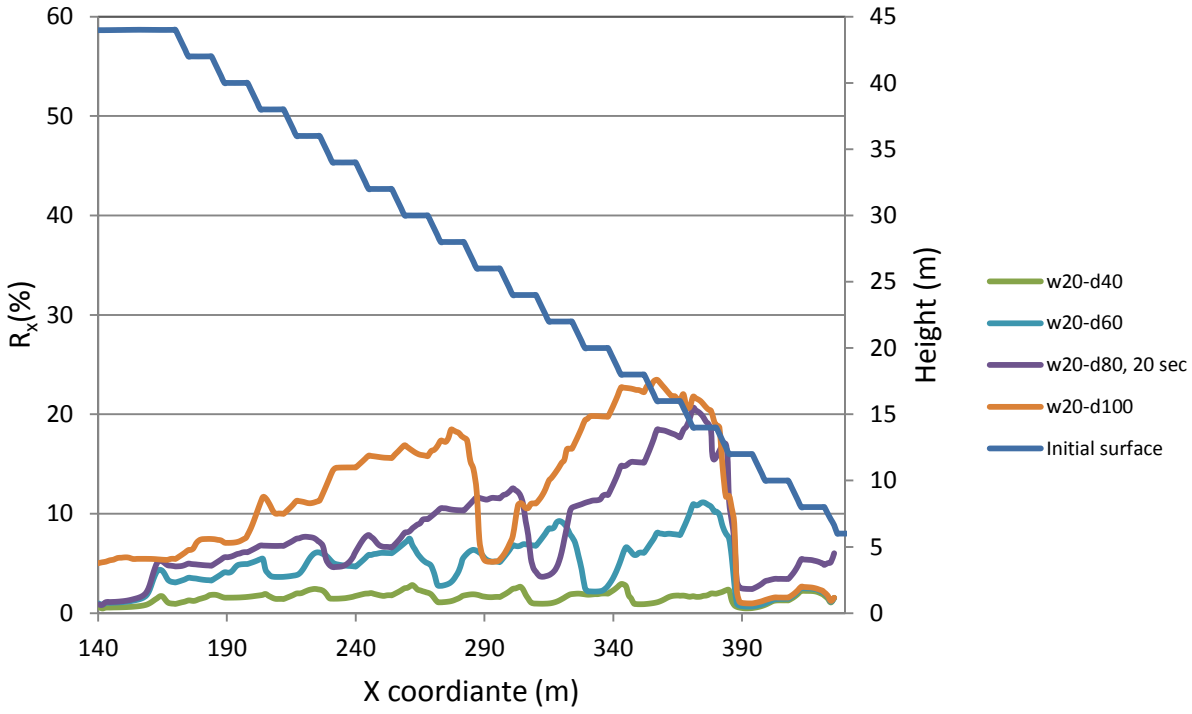

Figure D34: The value of R_x in along the slope of the impoundment within unconsolidated tailings ($(N_1)_{60} = 3$, blows/30 cm) due to E_3-north earthquake record (Northridge) for inclusions with width of 20 meters. In the legend in the right top of the figure, first number is the width of inclusions, second number is center-to-center spacing, and third number in some cases is time that the model was stopped due to bad geometry in a zone

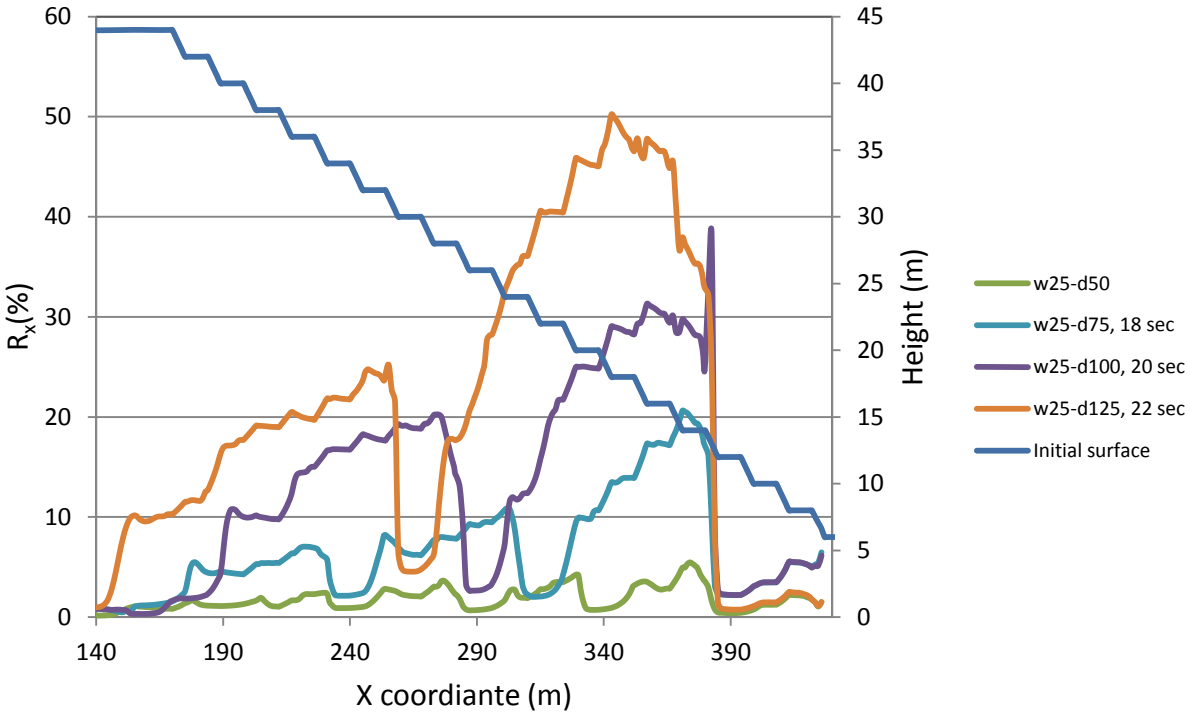

Figure D35: The value of R_x in along the slope of the impoundment within unconsolidated tailings ($(N_1)_{60} = 3$, blows/30 cm) due to E_3-north earthquake record (Northridge) for inclusions with width of 25 meters. In the legend in the right top of the figure, first number is the width of inclusions, second number is center-to-center spacing, and third number in some cases is time that the model was stopped due to bad geometry in a zone

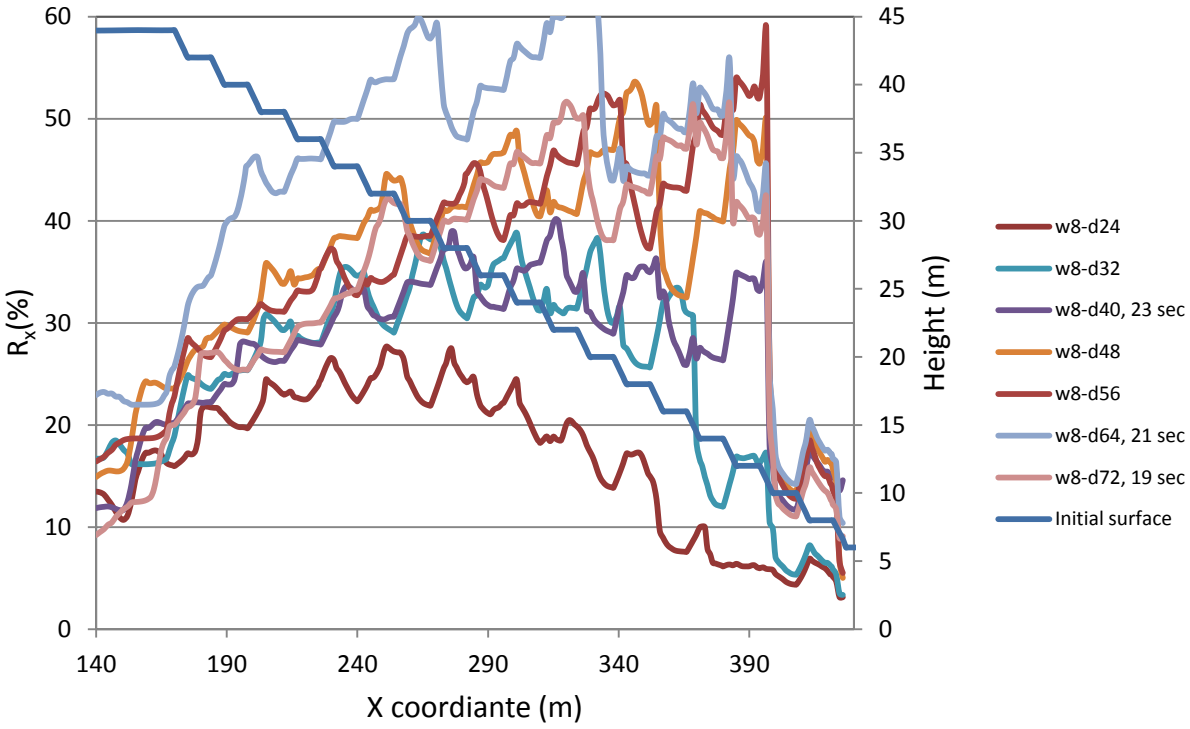

Figure D36: The value of R_x in along the slope of the impoundment within unconsolidated tailings ($(N_1)_{60} = 3$, blows/30 cm) due to E_4-north earthquake record (Northridge) for inclusions with width of 8 meters. In the legend in the right top of the figure, first number is the width of inclusions, second number is center-to-center spacing, and third number in some cases is time that the model was stopped due to bad geometry in a zone

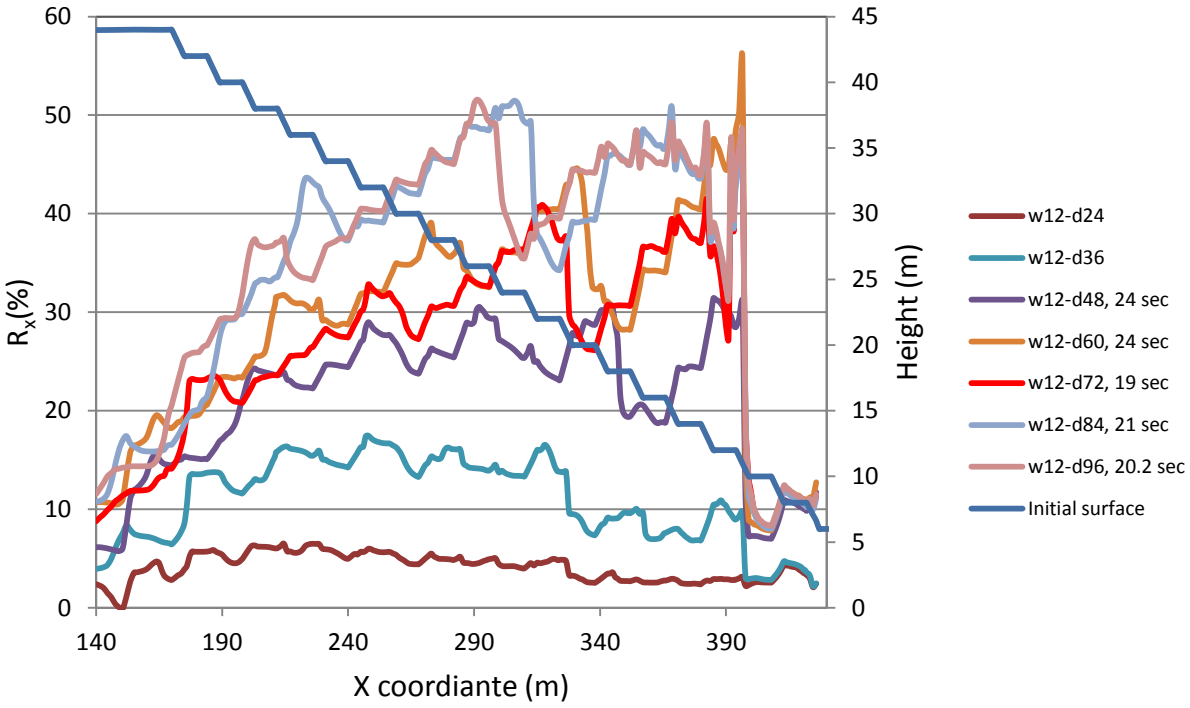

Figure D37: The value of R_x in along the slope of the impoundment within unconsolidated tailings ($(N_1)_{60} = 3$, blows/30 cm) due to E_4-north earthquake record (Northridge) for inclusions with width of 12 meters. In the legend in the right top of the figure, first number is the width of inclusions, second number is center-to-center spacing, and third number in some cases is time that the model was stopped due to bad geometry in a zone

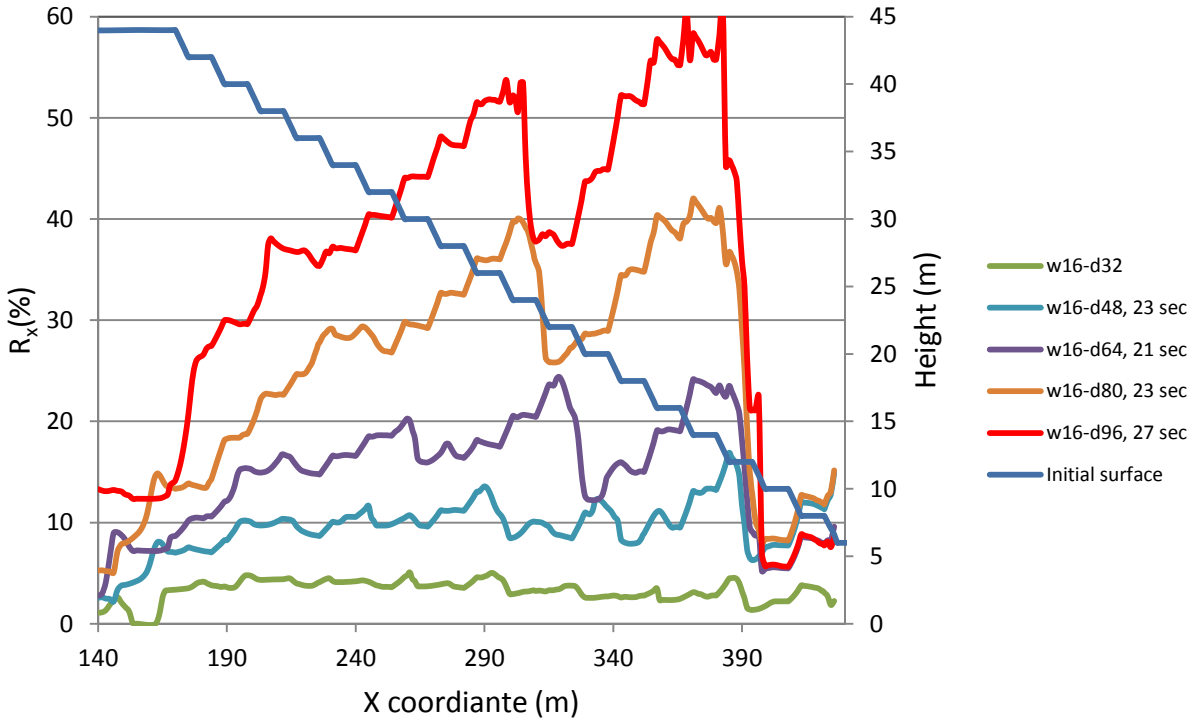

Figure D38: The value of R_x in along the slope of the impoundment within unconsolidated tailings ($(N_1)_{60} = 3$, blows/30 cm) due to E_4-north earthquake record (Northridge) for inclusions with width of 16 meters. In the legend in the right top of the figure, first number is the width of inclusions, second number is center-to-center spacing, and third number in some cases is time that the model was stopped due to bad geometry in a zone

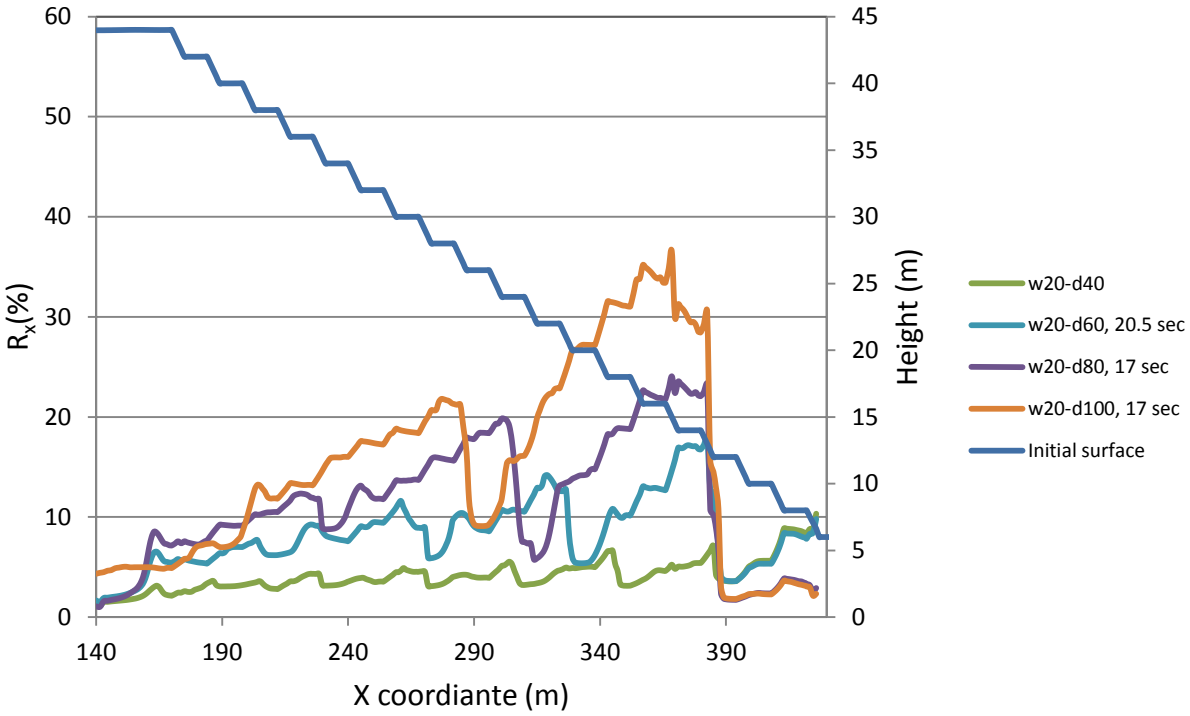

Figure D39: The value of R_x in along the slope of the impoundment within unconsolidated tailings ($(N_1)_{60} = 3$, blows/30 cm) due to E_4-north earthquake record (Northridge) for inclusions with width of 20 meters. In the legend in the right top of the figure, first number is the width of inclusions, second number is center-to-center spacing, and third number in some cases is time that the model was stopped due to bad geometry in a zone

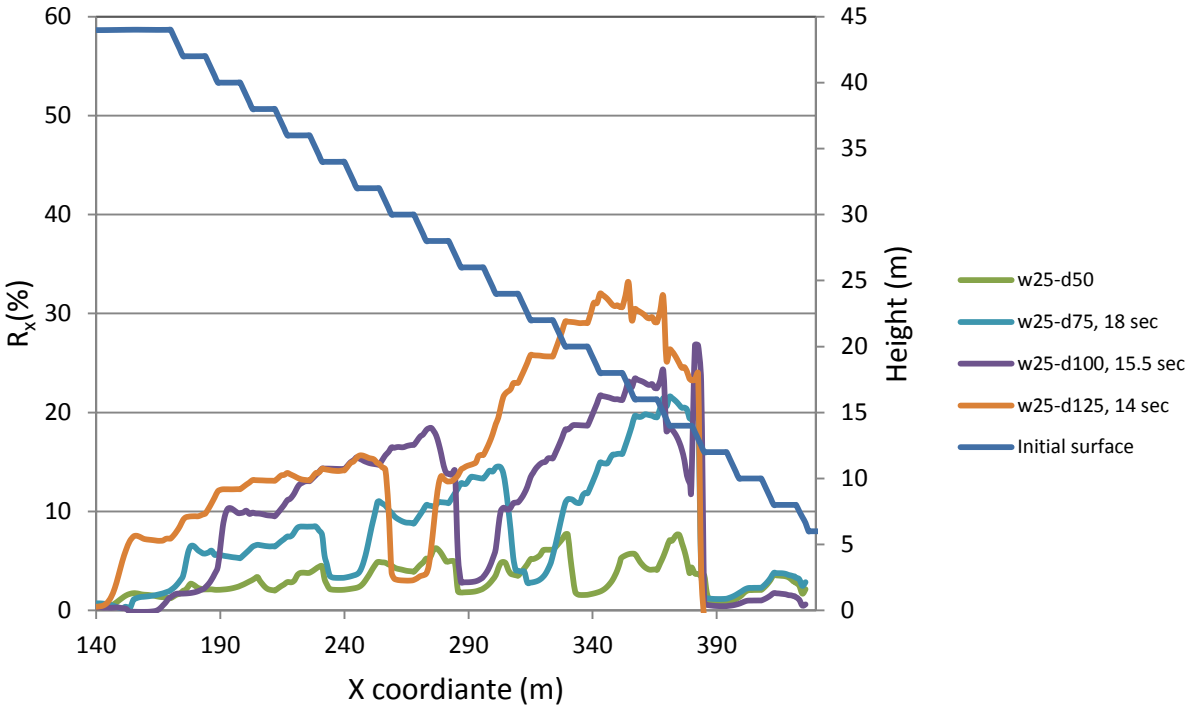

Figure D40: The value of R_x in along the slope of the impoundment within unconsolidated tailings ($(N_1)_{60} = 3$, blows/30 cm) due to E_4-north earthquake record (Northridge) for inclusions with width of 25 meters. In the legend in the right top of the figure, first number is the width of inclusions, second number is center-to-center spacing, and third number in some cases is time that the model was stopped due to bad geometry in a zone

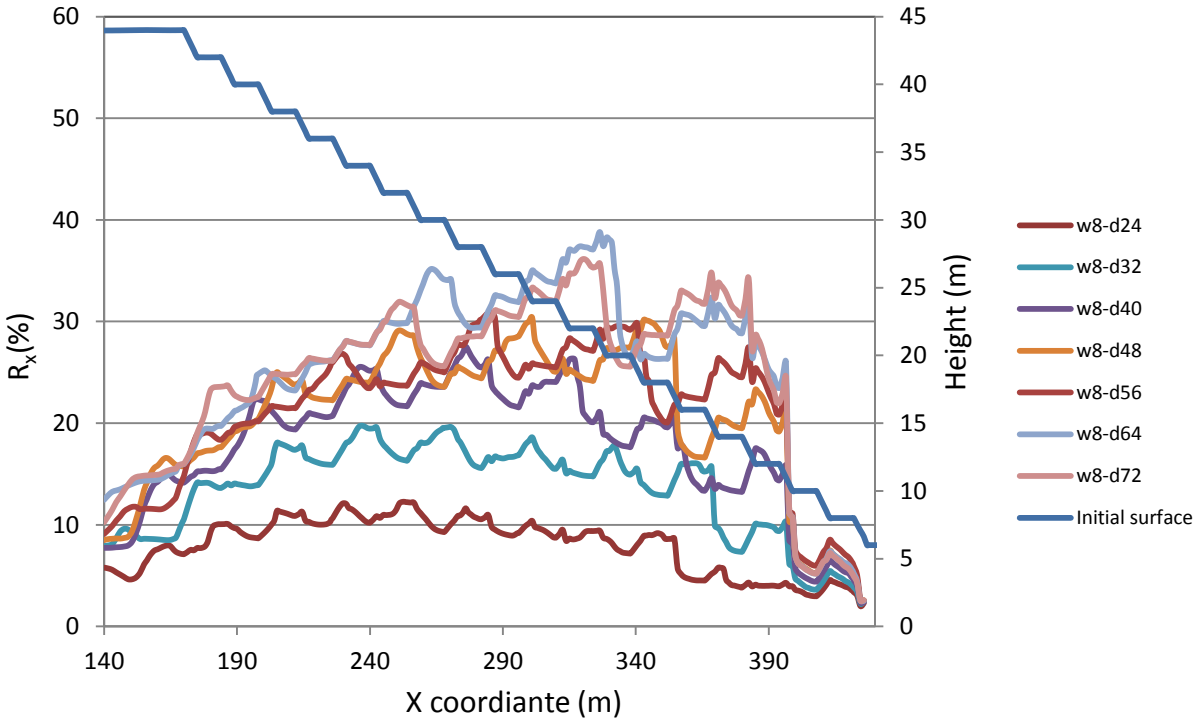

Figure D41: The value of R_x in along the slope of the impoundment within consolidated tailings ($(N_1)_{60} = 11$, blows/30 cm) due to E_4-north earthquake record (Northridge) for inclusions with width of 8 meters. In the legend in the right top of the figure, first number is the width of inclusions, second number is center-to-center spacing, and third number in some cases is time that the model was stopped due to bad geometry in a zone

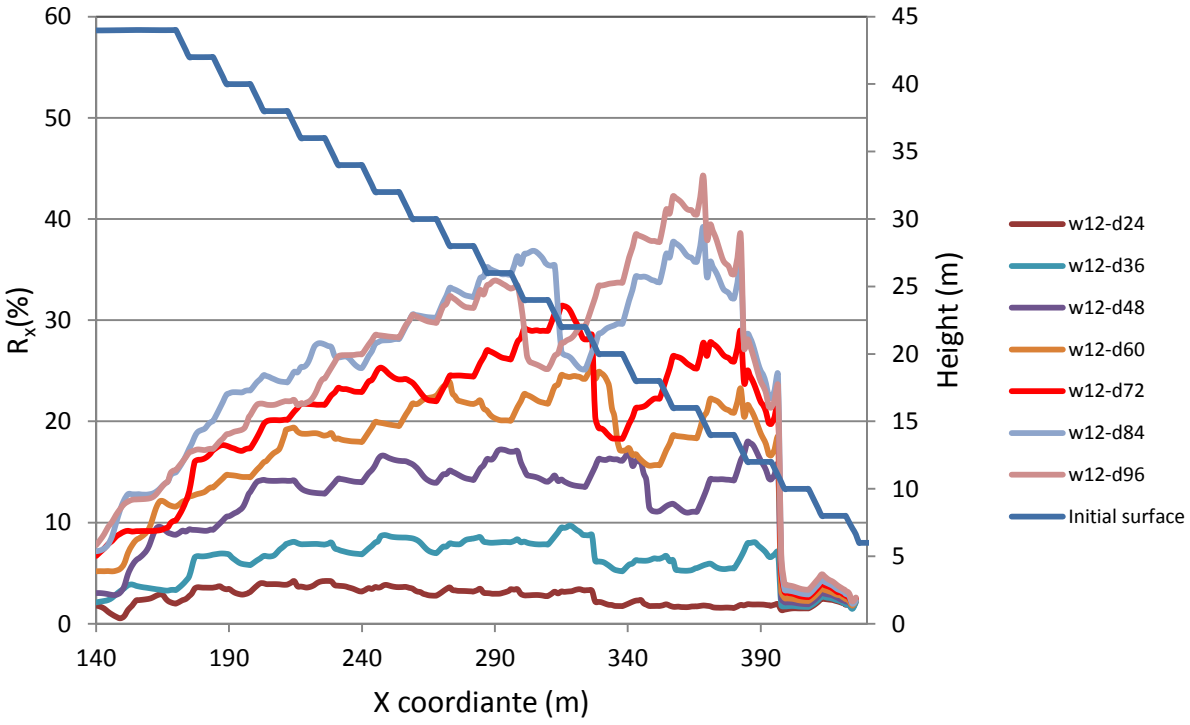

Figure D42: The value of R_x in along the slope of the impoundment within consolidated tailings ($(N_1)_{60} = 11$, blows/30 cm) due to E_4-north earthquake record (Northridge) for inclusions with width of 12 meters. In the legend in the right top of the figure, first number is the width of inclusions, second number is center-to-center spacing, and third number in some cases is time that the model was stopped due to bad geometry in a zone

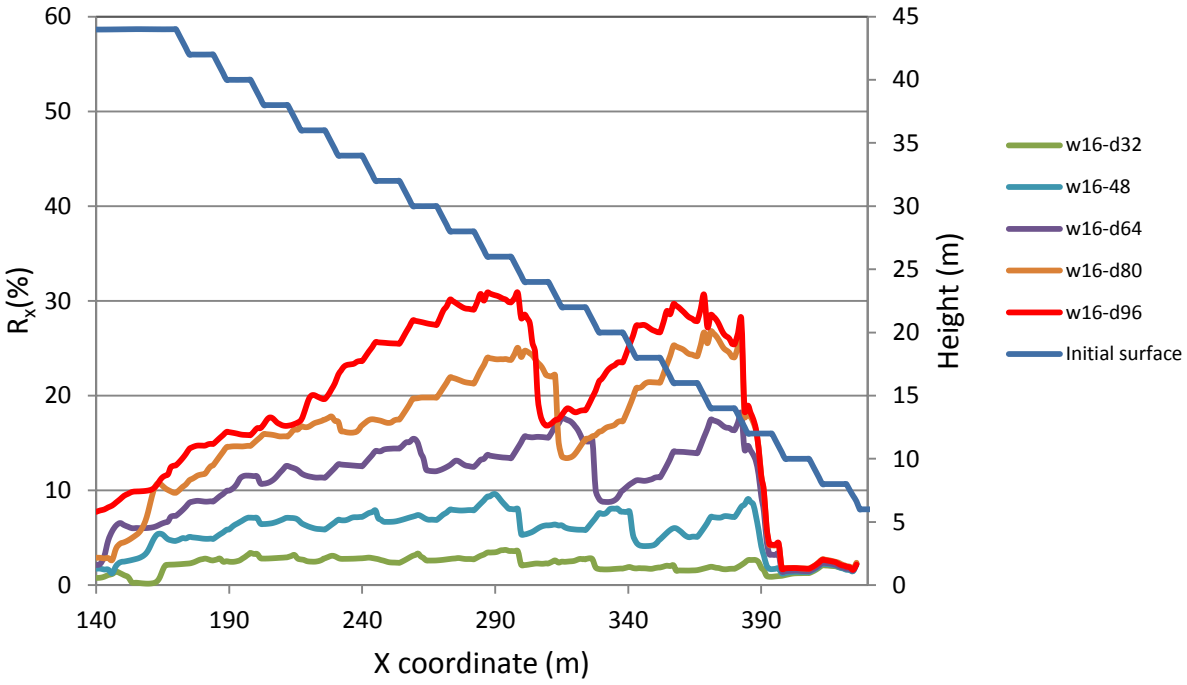

Figure D43: The value of R_x in along the slope of the impoundment within consolidated tailings ($(N_1)_{60} = 11$, blows/30 cm) due to E_4-north earthquake record (Northridge) for inclusions with width of 16 meters. In the legend in the right top of the figure, first number is the width of inclusions, second number is center-to-center spacing, and third number in some cases is time that the model was stopped due to bad geometry in a zone

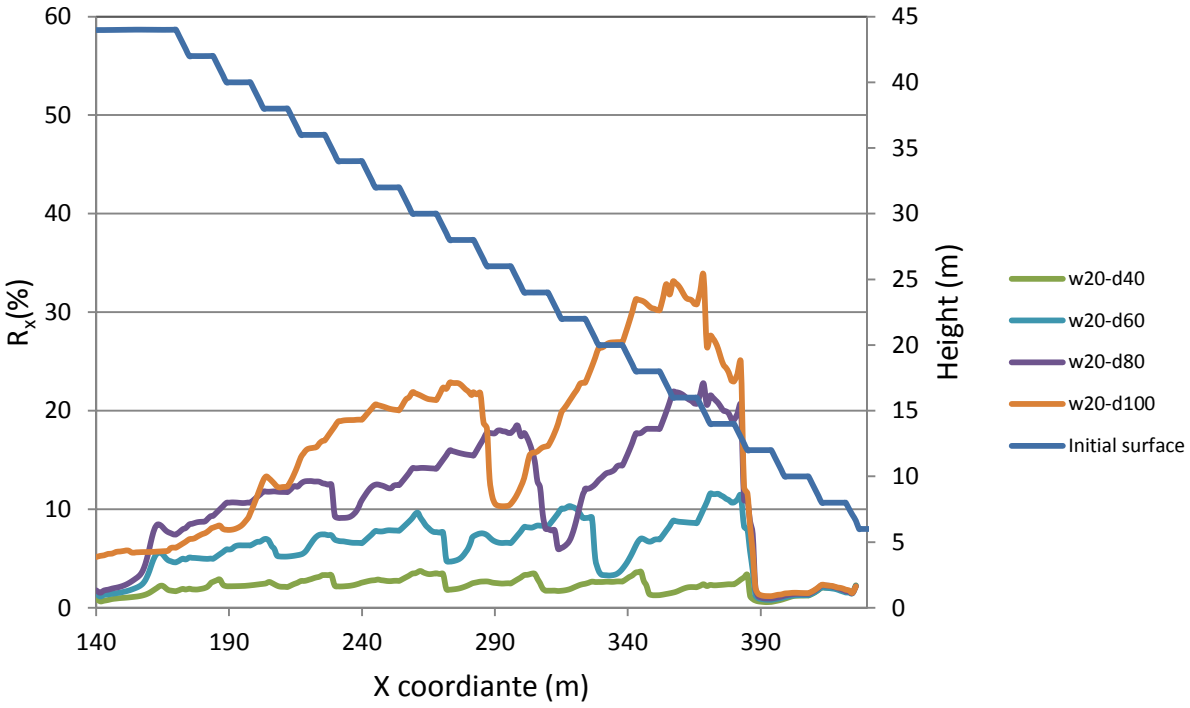

Figure D44: The value of R_x in along the slope of the impoundment within consolidated tailings ($(N_1)_{60} = 11$, blows/30 cm) due to E_4-north earthquake record (Northridge) for inclusions with width of 20 meters. In the legend in the right top of the figure, first number is the width of inclusions, second number is center-to-center spacing, and third number in some cases is time that the model was stopped due to bad geometry in a zone

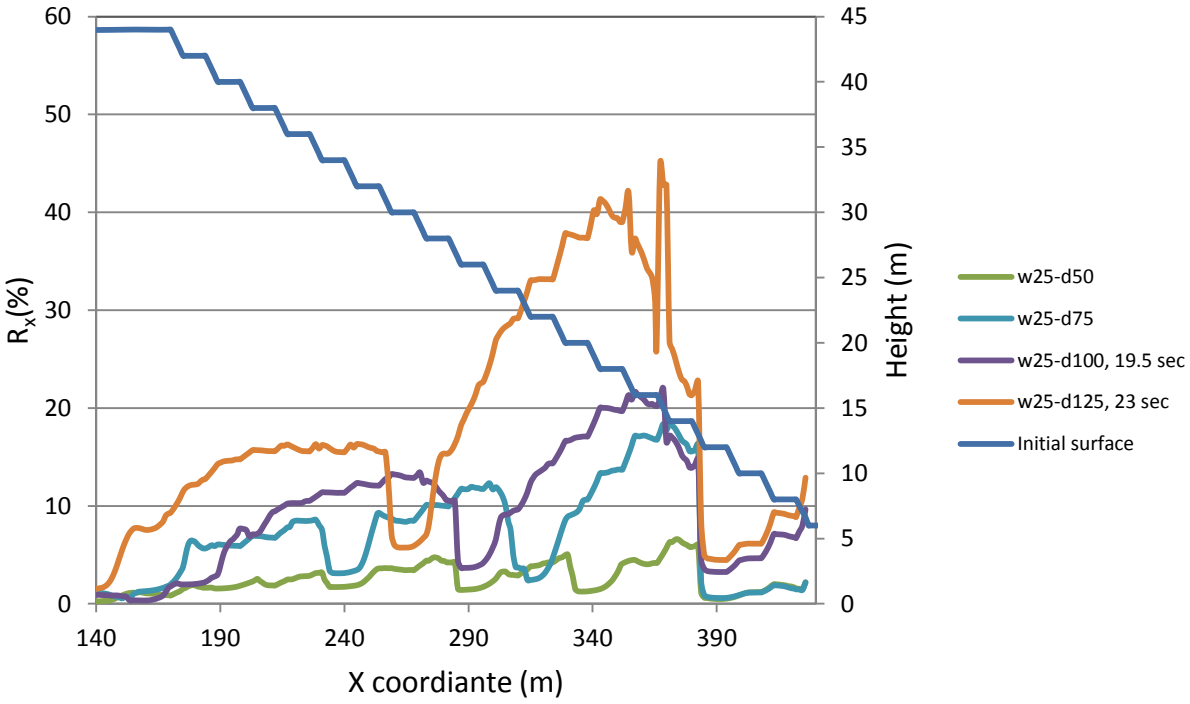

Figure D45: The value of R_x in along the slope of the impoundment within consolidated tailings ($(N_1)_{60} = 11$, blows/30 cm) due to E_4-north earthquake record (Northridge) for inclusions with width of 25 meters. In the legend in the right top of the figure, first number is the width of inclusions, second number is center-to-center spacing, and third number in some cases is time that the model was stopped due to bad geometry in a zone

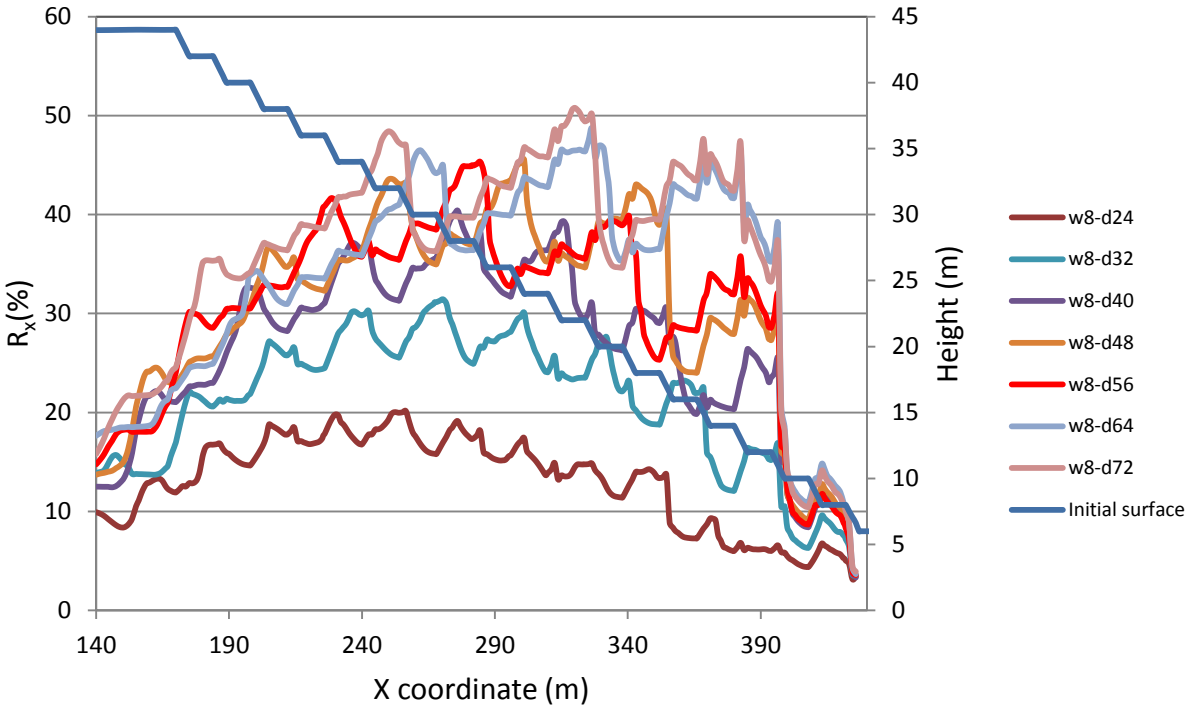

Figure D46: The value of R_x in along the slope of the impoundment within consolidated tailings ($(N_1)_{60} = 11$, blows/30 cm) due to E_5-north earthquake record (Northridge) for inclusions with width of 8 meters. In the legend in the right top of the figure, first number is the width of inclusions, second number is center-to-center spacing, and third number in some cases is time that the model was stopped due to bad geometry in a zone

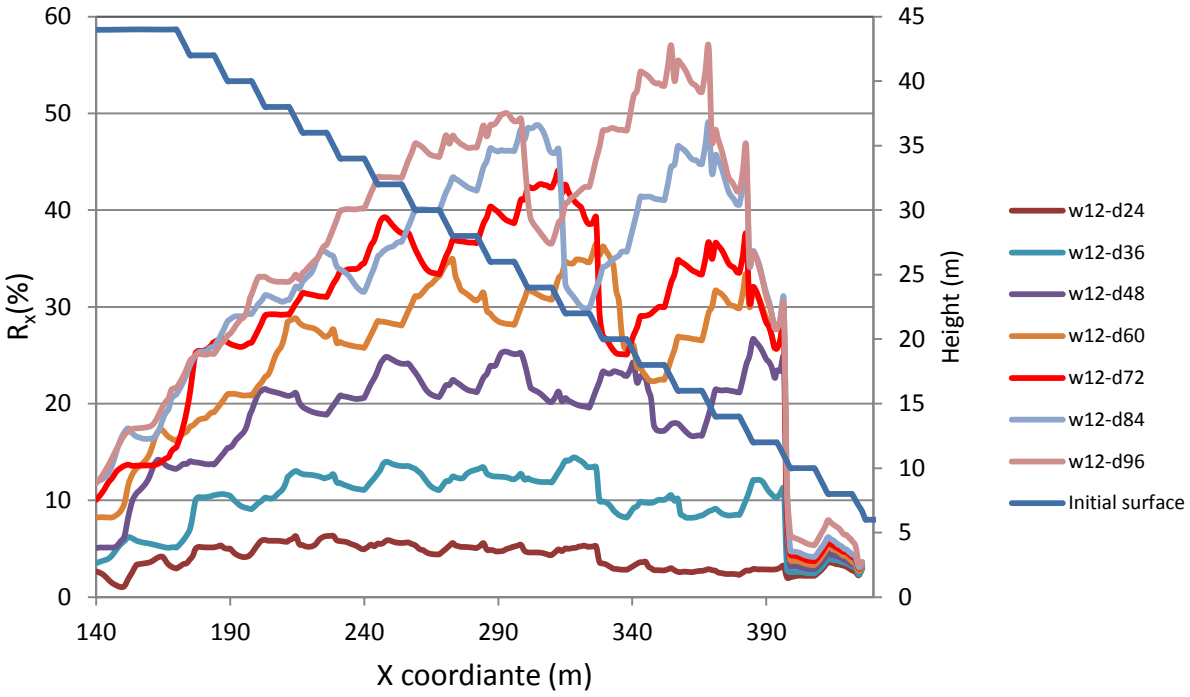

Figure D47: The value of R_x in along the slope of the impoundment within consolidated tailings ($(N_1)_{60} = 11$, blows/30 cm) due to E_5-north earthquake record (Northridge) for inclusions with width of 12 meters. In the legend in the right top of the figure, first number is the width of inclusions, second number is center-to-center spacing, and third number in some cases is time that the model was stopped due to bad geometry in a zone

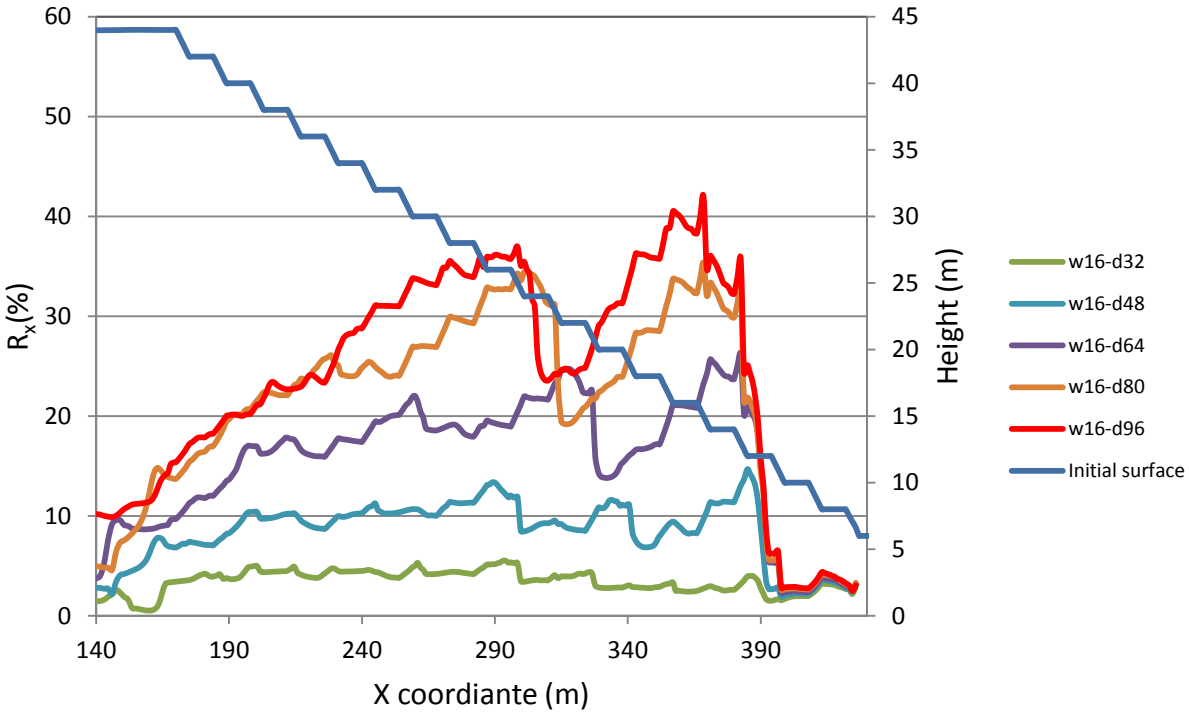

Figure D48: The value of R_x in along the slope of the impoundment within consolidated tailings ($(N_1)_{60} = 11$, blows/30 cm) due to E_5-north earthquake record (Northridge) for inclusions with width of 16 meters. In the legend in the right top of the figure, first number is the width of inclusions, second number is center-to-center spacing, and third number in some cases is time that the model was stopped due to bad geometry in a zone

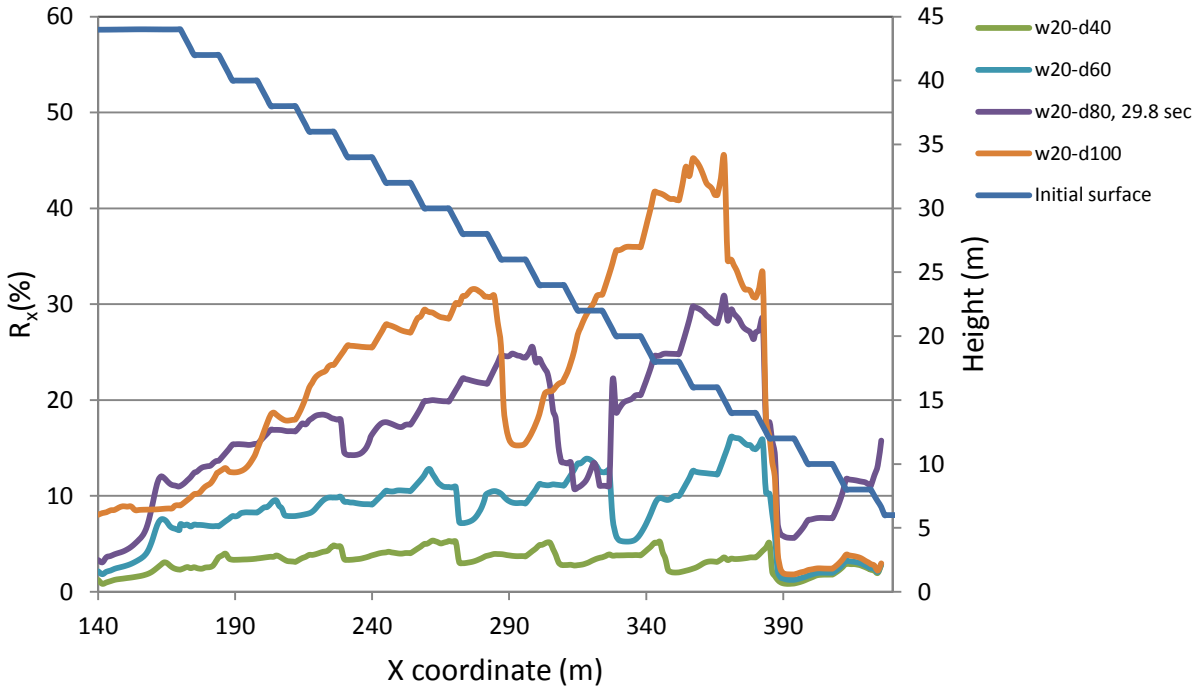

Figure D49: The value of R_x in along the slope of the impoundment within consolidated tailings ($(N_1)_{60} = 11$, blows/30 cm) due to E_5-north earthquake record (Northridge) for inclusions with width of 20 meters. In the legend in the right top of the figure, first number is the width of inclusions, second number is center-to-center spacing, and third number in some cases is time that the model was stopped due to bad geometry in a zone

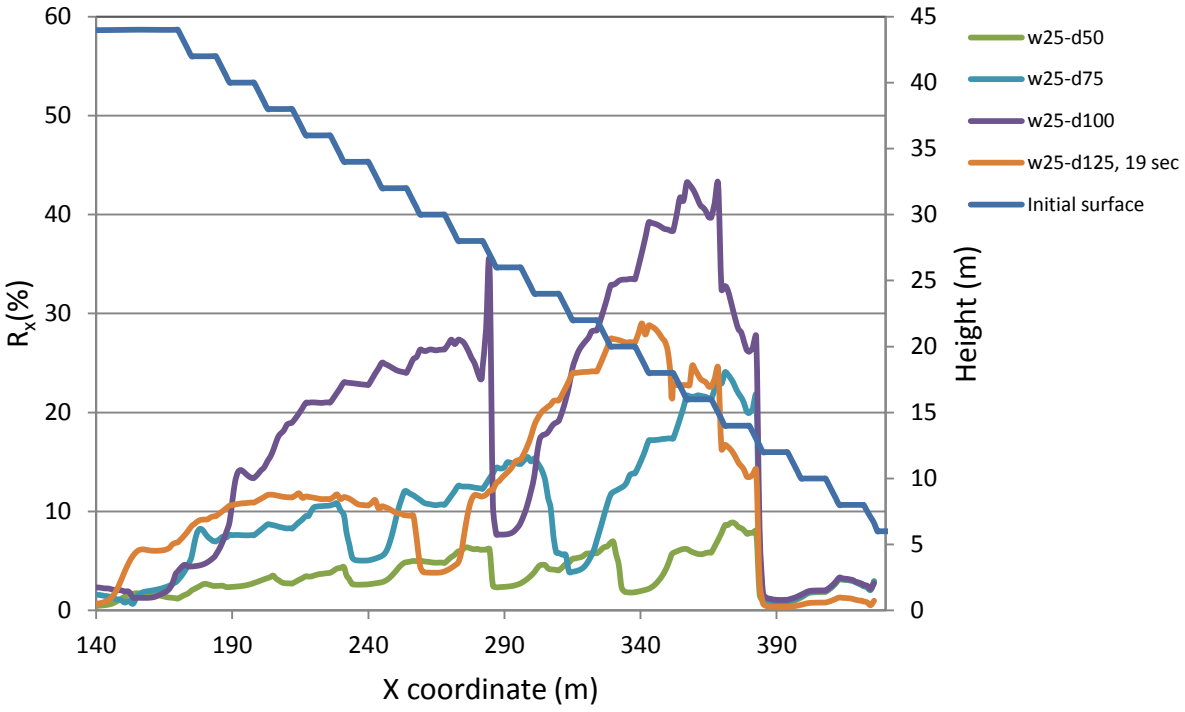

Figure D50: The value of R_x in along the slope of the impoundment within consolidated tailings ($(N_1)_{60} = 11$, blows/30 cm) due to E_5-north earthquake record (Northridge) for inclusions with width of 20 meters. In the legend in the right top of the figure, first number is the width of inclusions, second number is center-to-center spacing, and third number in some cases is time that the model was stopped due to bad geometry in a zone

D1.2 Evaluation of the effect of inclusions configuration on the performance of the tailings impoundment

Figures D51 to D56 shows graphs of average normalized horizontal displacements AR_x of the slope of the impoundment and WRI as a function of the total width of the WRI used in the impoundment for unconsolidated tailings ($(N_1)_{60} = 3$, blows/30 cm) due to E_1-sag, E_3-sag, E_4-sag, E_1-north, E_3-north, and E_4-north earthquake records. The black and gray bars show the average values of normalized horizontal displacements of the slope of impoundment and the WRI (AR_x) respectively. In horizontal axis, first number is total width of inclusions, first number inside of parenthesis is width of single inclusion and second number is center to center spacing of inclusions.

As shown in Figure D1, the AR_x total and WRI are less than 2% for all the configurations except the configuration 25-100 that its AR_x total is 8%. It shows that when the spacing of WRI increases from certain amount, the WRI lose their positive effect. This graph also shows that all the configurations can improve the seismic performance of tailings impoundment against E_1-sag ground motion record.

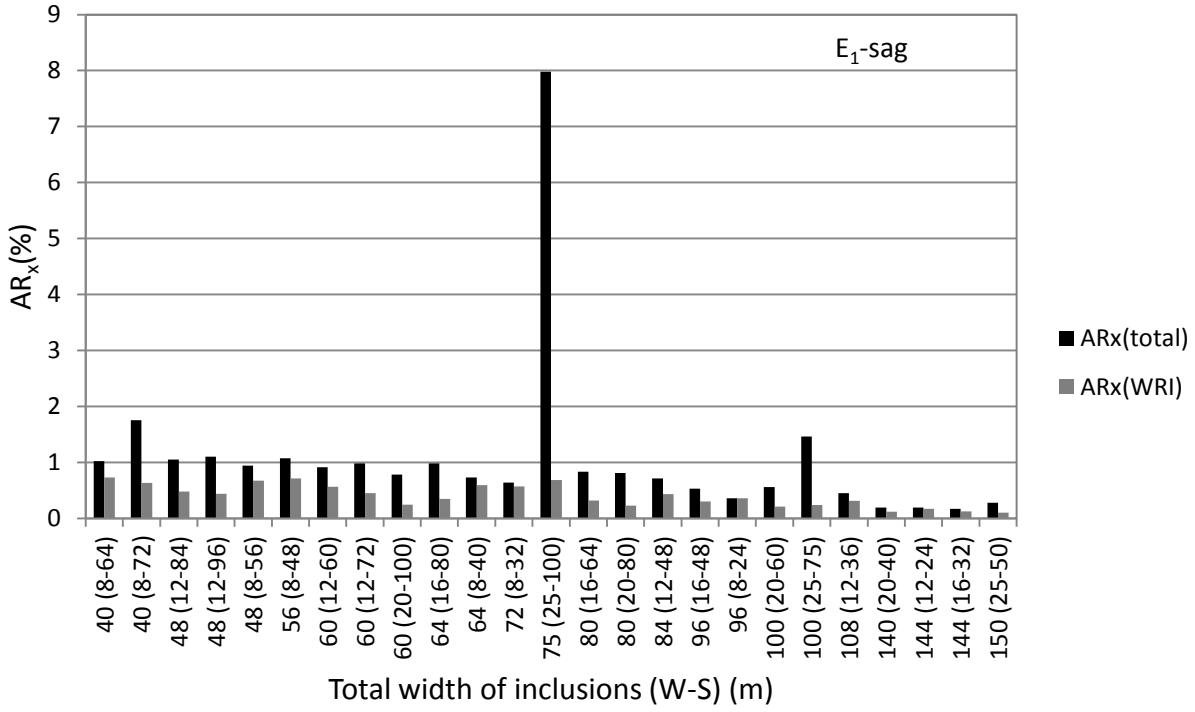

Figure D51: Average normalized horizontal displacements AR_x of the slope of the impoundment and of the WRI as a function of the total widths of the inclusions in the impoundment for unconsolidated tailings ($(N_1)_{60} = 3$, blows/30 cm), due to the E_1-sag earthquake record (S16T). Along the horizontal axis, the first number is the total width of the inclusions; the first number inside the parenthesis is the width of each single inclusion and the second number is the center to center spacing. Black and Gray bars represent the average normalized horizontal displacements of the slope of the impoundment and of the WRI, respectively

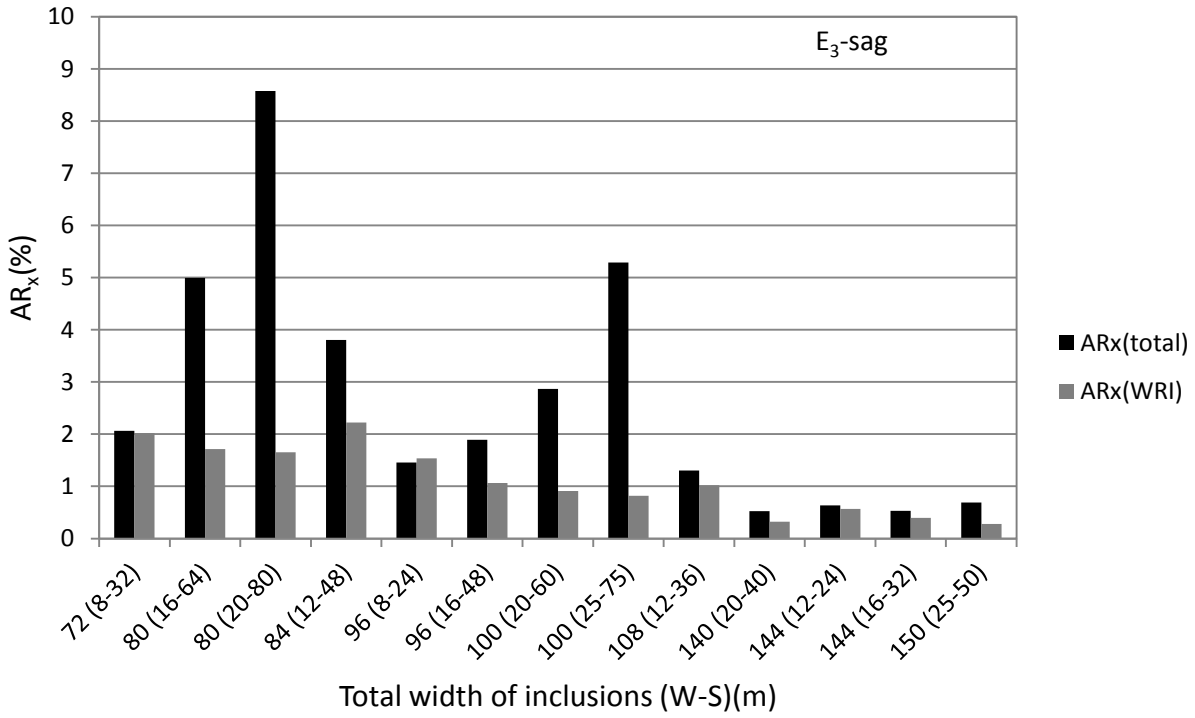

Figure D52: Average normalized horizontal displacements AR_x of the slope of the impoundment and of the WRI as a function of the total widths of the inclusions in the impoundment for unconsolidated tailings ($(N_1)_{60} = 3$, blows/30 cm), due to the E_3-sag earthquake record (S16T). Along the horizontal axis, the first number is the total width of the inclusions; the first number inside the parenthesis is the width of each single inclusion and the second number is the center to center spacing. Black and Gray bars represent the average normalized horizontal displacements of the slope of the impoundment and of the WRI, respectively

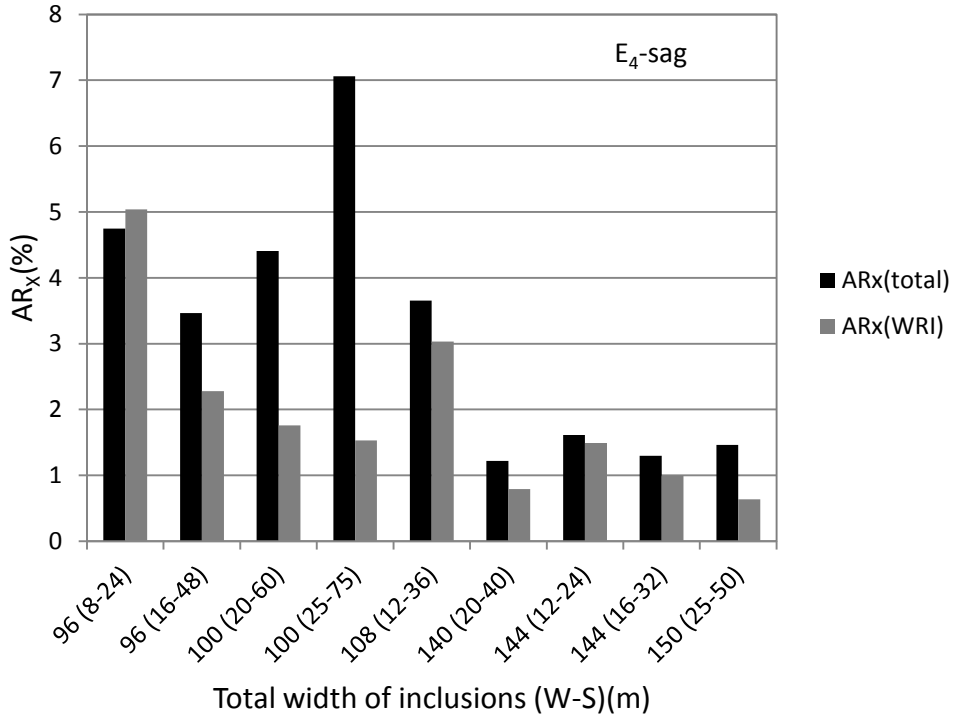

Figure D53: Average normalized horizontal displacements AR_x of the slope of the impoundment and of the WRI as a function of the total widths of the inclusions in the impoundment for unconsolidated tailings ($(N_1)_{60} = 3$, blows/30 cm), due to the E_4-sag earthquake record (S16T). Along the horizontal axis, the first number is the total width of the inclusions; the first number inside the parenthesis is the width of each single inclusion and the second number is the center to center spacing. Black and Gray bars represent the average normalized horizontal displacements of the slope of the impoundment and of the WRI, respectively

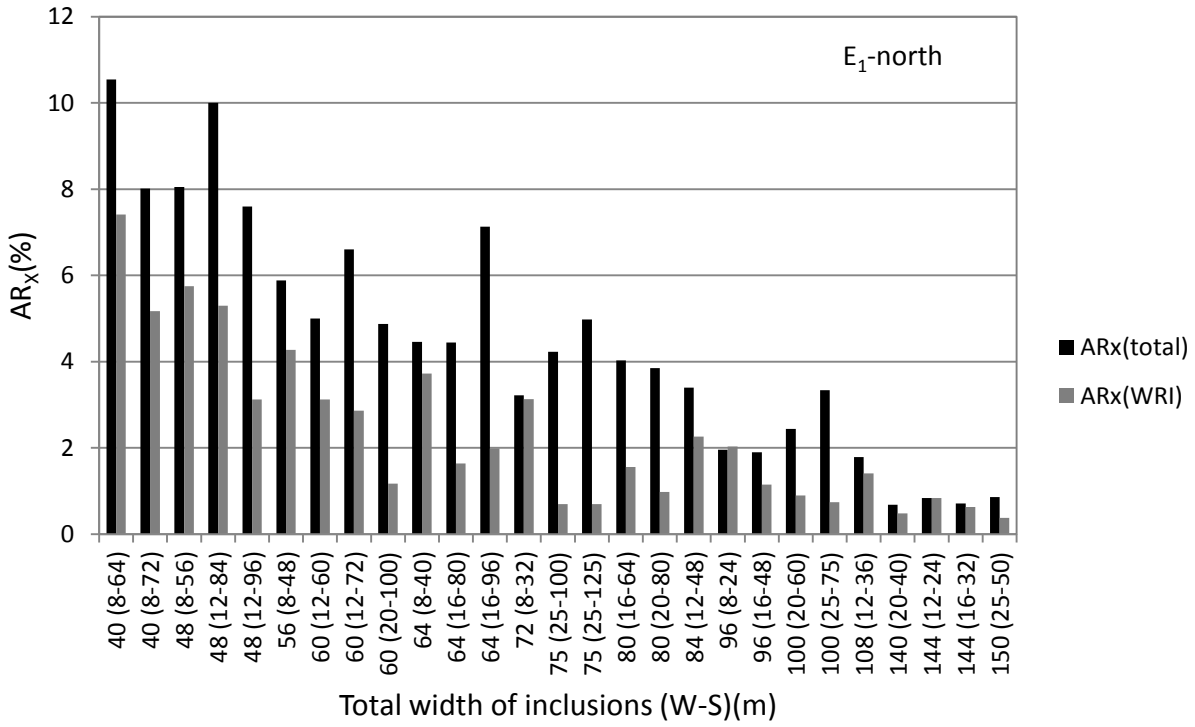

Figure D54: Average normalized horizontal displacements AR_x of the slope of the impoundment and of the WRI as a function of the total widths of the inclusions in the impoundment for unconsolidated tailings ($(N_1)_{60} = 3$, blows/30 cm), due to the E_1-north earthquake record (Northridge). Along the horizontal axis, the first number is the total width of the inclusions; the first number inside the parenthesis is the width of each single inclusion and the second number is the center to center spacing. Black and Gray bars represent the average normalized horizontal displacements of the slope of the impoundment and of the WRI, respectively

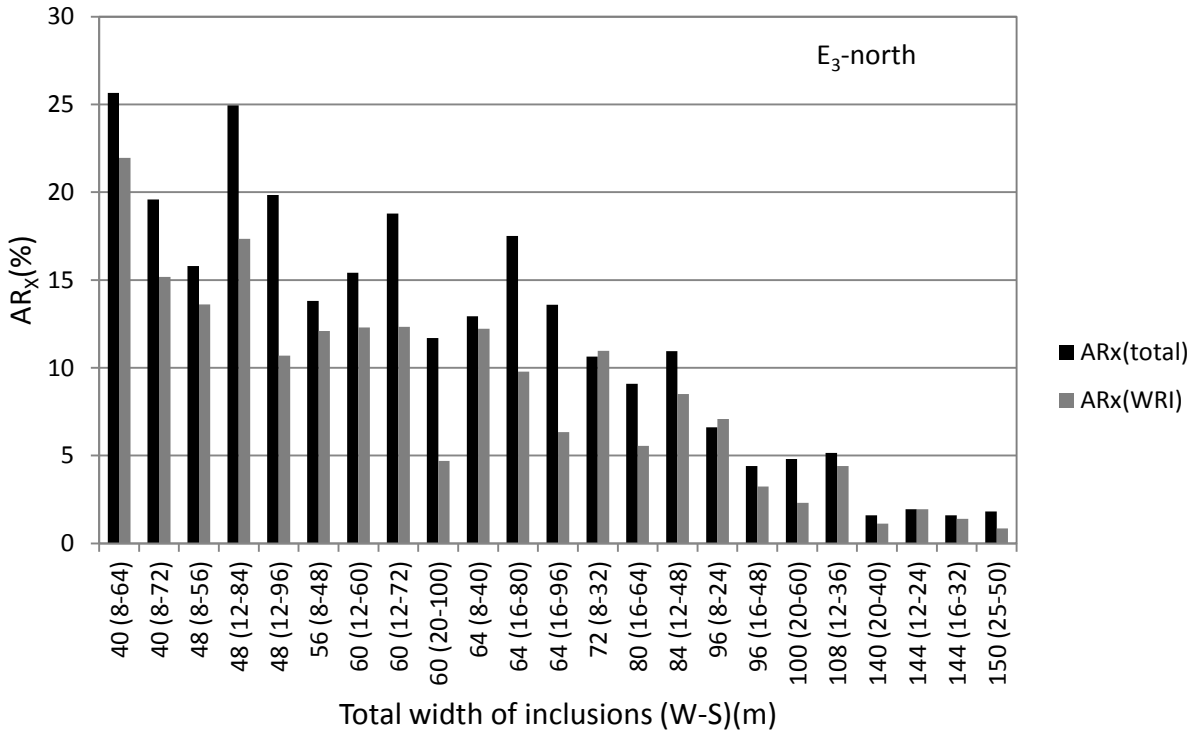

Figure D55: Average normalized horizontal displacements AR_x of the slope of the impoundment and of the WRI as a function of the total widths of the inclusions in the impoundment for unconsolidated tailings ($(N_1)_{60} = 3$, blows/30 cm), due to the E_3-north earthquake record (Northridge). Along the horizontal axis, the first number is the total width of the inclusions; the first number inside the parenthesis is the width of each single inclusion and the second number is the center to center spacing. Black and Gray bars represent the average normalized horizontal displacements of the slope of the impoundment and of the WRI, respectively

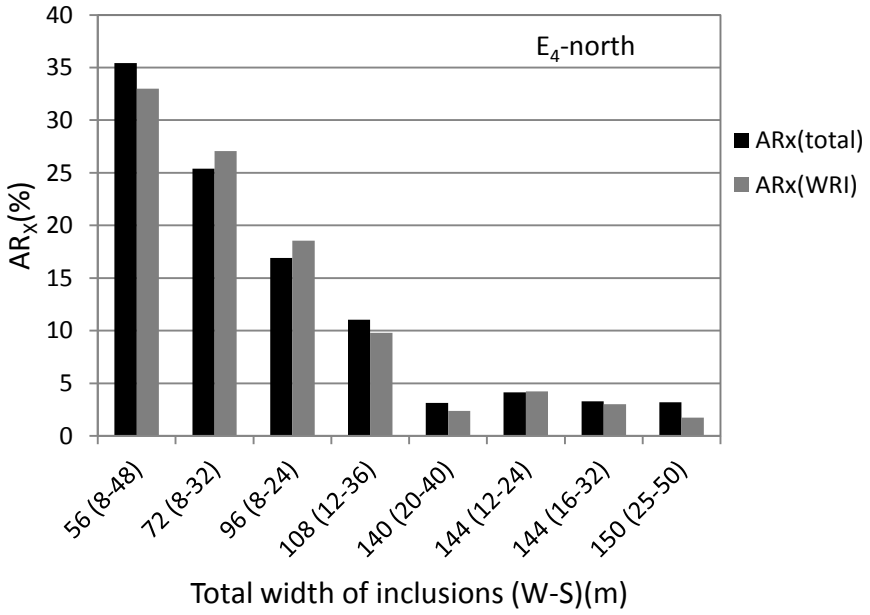

Figure D56: Average normalized horizontal displacements AR_x of the slope of the impoundment and of the WRI as a function of the total widths of the inclusions in the impoundment for unconsolidated tailings ($(N_1)_{60} = 3$, blows/30 cm), due to the E_4-north earthquake record (Northridge). Along the horizontal axis, the first number is the total width of the inclusions; the first number inside the parenthesis is the width of each single inclusion and the second number is the center to center spacing. Black and Gray bars represent the average normalized horizontal displacements of the slope of the impoundment and of the WRI, respectively

D1.3 Average normalized horizontal displacement of the downstream slope of the impoundment for various configurations of WRI

The calculated values of AR_x for the downstream slope (AR_x total) and for the WRI only (AR_x WRI) are presented for unconsolidated tailings impoundment in Tables D1 and D2, for the modified Saguenay and modified Northridge ground motions, respectively.

These results indicate that the deformation of the downstream slope (as interpreted from the AR_x values) generally tend to decrease with an increasing inclusion width, increase with an increasing inclusion spacing and increasing seismic loading. The displacements are usually more significant for the Northridge than for the Saguenay ground motions.

In 50 of the 162 simulations conducted, excessive deformation of individual elements near the surface of the impoundment led to an execution error ("bad geometry") that halted the simulation before the specified duration. These incomplete simulations are marked with an asterisk (*) in Tables D1 and D2.

Table D1: Average normalized horizontal displacement AR_x of the downstream slope of unconsolidated tailings impoundment and WRI alone for various configurations, due to modified Saguenay motions

Arrangement		E_1-sag		E_3-sag		E_4-sag	
Width (m)	Spacing (m)	AR_x total (%)	AR_x WRI (%)	AR_x total (%)	AR_x WRI (%)	AR_x total (%)	AR_x WRI (%)
8	24	0.36	0.36	1.45	1.57	4.74	5.04
	32	0.64	0.57	2.06	2.02	21.53*	22.56*
	40	0.73	0.59	4.46	3.57	30.98*	30.12*
	48	1.07	0.71	22.43*	18.29*	33.04*	29.19*
	56	0.94	0.67	24.33*	19.91*	-	-
	64	1.02	0.73	35.58*	29.8*	-	-
	72	1.075	0.63	36.66*	28.47*	-	-
12	24	0.19	0.16	0.63	0.57	1.61	1.49
	36	0.45	0.31	1.30	1.02	3.65	3.03
	48	0.71	0.43	3.80	2.22	22.40*	18.48*
	60	0.91	0.56	9.56*	10.77*	9.54*	7.47*
	72	0.98	0.45	18.20*	9.37*	24.72*	17.35*
	84	1.05	0.48	20.69*	12.93*	36.90*	27.96*
	96	1.10	0.44	21.7*	11.16*	-	-
16	32	0.17	0.125	0.53	0.39	1.29	1.0
	48	0.52	0.298	1.88	1.06	3.46	2.28
	64	0.83	0.319	4.99	1.71	9.77*	6.08*
	80	0.98	0.345	5.24*	1.52*	14.72*	8.83*
	96	4.28	0.717	11.73*	3.42*	39.72*	25.64*
20	40	0.19	0.11	0.52	0.32	1.22	0.79
	60	0.56	0.20	2.87	0.91	4.40	1.76
	80	0.81	0.22	8.57	1.65	7.47*	2.16*
	100	0.78	0.24	6.27*	0.95*	15.69*	5.31*
25	50	0.28	0.1	0.69	0.27	1.46	0.63
	75	1.46	0.23	5.28	0.82	7.05	1.53
	100	7.98	0.68	11.87*	1.12*	12.48*	1.61*
	125	0.931*	0.15*	23.63*	3.96*	18.50*	2.23*

* Analysis was stopped because of bad geometry in some elements

Table D2: Average Average normalized horizontal displacement AR_x of the downstream slope of unconsolidated tailings impoundment and WRI alone for various configurations, due to modified Northridge motions

Arrangement		E_1-north		E_3-north		E_4-north	
Width (m)	Spacing (m)	AR_x total (%)	AR_x WRI (%)	AR_x total (%)	AR_x WRI (%)	AR_x total (%)	AR_x WRI (%)
8	24	1.96	2.03	6.6	7.08	16.9	18.56
	32	3.22	3.13	10.63	10.97	25.39	27.06
	40	4.46	3.72	12.94	12.22	27.78*	27.43*
	48	5.88	4.27	13.81	12.09	35.43	33
	56	8.05	5.75	15.80	13.60	35.21	32.75
	64	10.54	7.41	25.65	21.95	43.27*	41.02*
	72	8.01	5.17	19.59	15.17	33.45*	28.39*
12	24	0.84	0.84	1.94	1.95	4.14	4.23
	36	1.79	1.41	5.15	4.4	11.03	9.80
	48	3.40	2.26	10.95	8.5	21.45*	18.44*
	60	5.0	3.12	15.41	12.29	29.21*	26.33*
	72	6.60	2.86	18.78	12.33	26.67*	20.67*
	84	10.0	5.30	24.95	17.35	34.44*	27.33*
	96	7.60	3.12	19.84	10.69	34.57*	24.74*
16	32	0.71	0.63	1.6	1.4	3.29	3.02
	48	1.9	1.15	4.4	3.23	9.67*	8.81*
	64	4.02	1.56	9.08	5.56	15.03*	10.90*
	80	4.44	1.64	17.51	9.78	25.37*	19.35*
	96	7.13	1.99	13.59	6.34	35.51*	23.31*
20	40	0.68	0.48	1.59	1.13	3.13	2.38
	60	2.44	0.90	4.8	2.3	8.41*	5.62*
	80	3.85	0.98	8.15*	3.71*	11.39*	5.11*
	100	4.87	1.17	11.69	4.7	15.10*	6.62*
25	50	0.86	0.38	1.82	0.85	3.2	1.74
	75	3.34	0.74	6.76*	2.73*	8.0*	2.88*
	100	4.23	0.70	13.23*	3.51*	10.40*	2.33*
	125	4.98	0.70	21.38*	3.50*	13.74*	1.29*

* Analysis was stopped because of bad geometry in some elements

D1.4 Damping parameters of bedrock

Rayleigh damping was assigned for bedrock. The damping ratio for Rayleigh damping for high and low frequency earthquake records was obtained by trial and error in such way that acceleration record at the top of the bedrock was same as input acceleration record. Figure D57 shows comparison between the input acceleration and the acceleration at the top of the bedrock for 0.2 seconds. As shown in this figure, there is very good agreement between the input acceleration and the acceleration at the top of the bedrock. Therefore, the Rayleigh damping ratios for bedrock according to high and low frequency earthquake input motions were obtained 0.03 and 0.02, respectively.

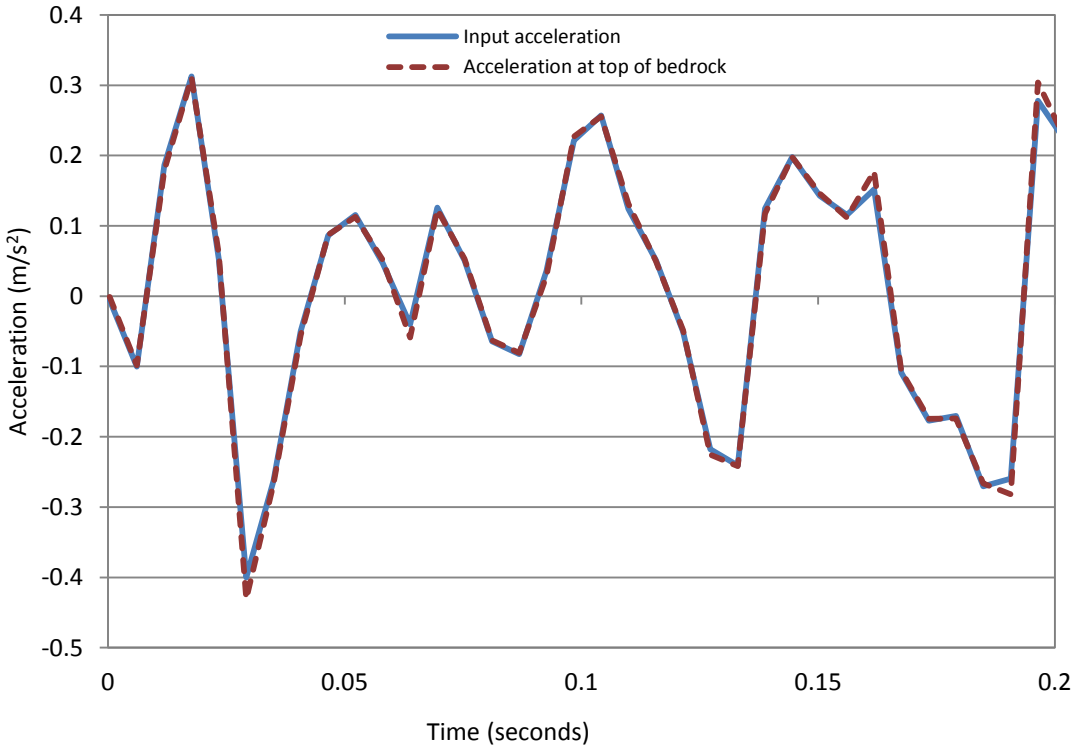

Figure D57: Comparison between input acceleration and recorded acceleration at the top of the bedrock.

D1.5 Pore water pressure ratio (r_u)

Figures D58 and D59 show the pore water pressure ratio (r_u) distribution inside the reinforced (unconsolidated) tailings impoundment (with WRI) for configuration 12-36 due to E_4-sag and E_4-north ground motions, respectively. As indicated by the large values of r_u values (> 0.8) in these figures, the tailings between the WRI can be expected to have liquefied at the end of shaking. The simulations indicate that the WRI would not reduce significantly the generation of excess pore water pressures in these tailings (except for locations very close to the inclusions), but would rather serve to prevent their deformation and flow due to liquefaction.

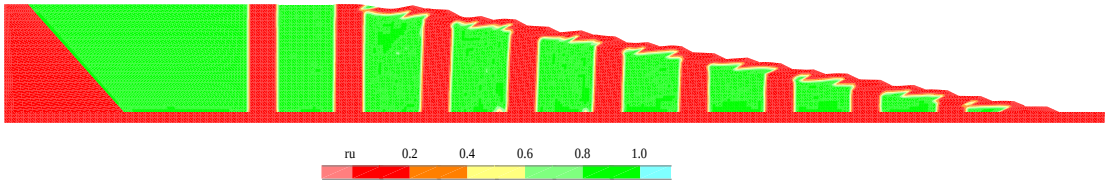

Figure D58: Distribution of the pore water pressure ratio (r_u) due to E_4-sag earthquake record (at end of shaking) in the reinforced tailings impoundment (with WRI) for W = 12m and S = 36m for unconsolidated tailings

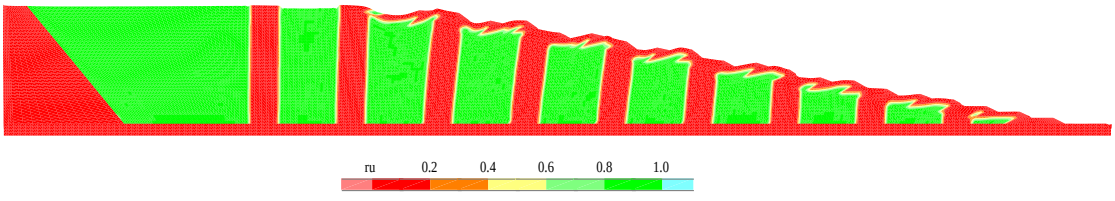

Figure D59: Distribution of the pore water pressure ratio (r_u) due to E_4-north earthquake record (at end of shaking) in the reinforced tailings impoundment (with WRI) for W = 12m and S = 36m for unconsolidated tailings

Figure 60 shows the pore water pressure ratio (r_u) distribution inside the reinforced (consolidated) tailings impoundment (with WRI) for configuration 12-36 due to E_4-sag ground motions. As indicated by the large values of r_u values (> 0.8) in these figures, the tailings between the WRI can be expected to have liquefied at the end of shaking. The simulations indicate that the WRI would not reduce significantly the generation of excess pore water pressures in these tailings (except for locations very close to the inclusions), but would rather serve to prevent their deformation and flow due to liquefaction.

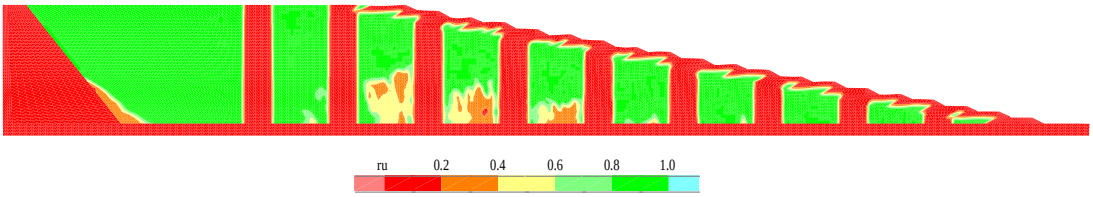

Figure D60: Distribution of the pore water pressure ratio (r_u) due to E_4-sag earthquake record (at end of shaking) in the reinforced tailings impoundment (with WRI) for W = 12m and S = 36m for consolidated tailings